THE

American Journal of

ANATOMY

VOLUME 116

JANUARY MARCH, MAY 1965

PUBLISHED BY

THE WISTAR INSTITUTE OF ANATOMY AND BIOLOGY
PHILADELPHIA PA

CONTENTS

No. 1 JANUARY 1965

No 2 MARCH 1965

No. 3 MAY 1965

The Time Dimension in Histology[1]

C. P. LEBLOND
Department of Anatomy, McGill University
Montreal, Canada

When we look back on the history of the Anatomical Sciences, we find at least three periods when important discoveries were made in an atmosphere of enthusiasm.

One was the Renaissance. Advances in Gross Anatomy at that time were due not only to anatomists such as Mondino and Estienne, but also to Italian artists such as Leonardo da Vinci, Raphael and Michael Angelo. These two currents of craft and art converged into the monumental work of the Flemish Anatomist, Vesalius who with simple tools (fig. 1) and a synthetic mind made Anatomy into the first modern science.

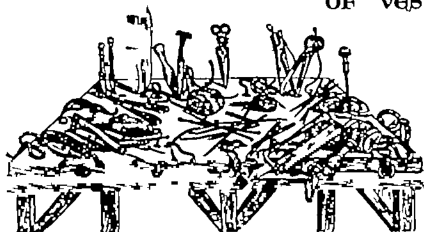


Fig. 1 Woodcut from the first edition (1543) of Vesalius *De Humani Corporis Fabrica* depicting instruments used for dissection, with long legend beginning thus:

> "In the present figure we have placed a board such as we employ in vivisections, resting on a table. On this board we have arranged almost everything which could be used in the administration of dissections."
> (translated in "The Illustrations from the Works of Andreas Vesalius," J. B. de C. M. Saunders and Charles D. O'Malley, 1950.)

The next exciting period was the second half *of the nineteenth century. Under the* impulse of Johannes Müller, a brilliant school of German histologists made full use of the light microscope, by then endowed with achromatic lenses (fig. 2). Organ after organ, structure after structure were described. Thus histology in its *turn became an organized science.*

Then around the turn of the century the enthusiasm tapered off. It is not easy to say why. Some anatomists felt that the limit of what could be done with the light microscope had been reached. Also little or no progress was made in trying to understand the nature of structures, perhaps because structures were looked upon as being essentially static. Indeed around 1900, even biochemists believed that the

---

[1] *Presidential address before the Diamond Jubilee* meeting of the American Association of Anatomists held under the auspices of Georgetown University, Washington, D. C., on April 9–11, 1963. Accepted for publication in October 1963.

body was something like that symbol of the XIXth century the steam engine It was thought that food is to the body what coal is to the engine as the value of food was measured only by the number of cal ories provided The organs were like so many cogs in the engine If biochemists were happy with such theories can we blame the anatomists for taking structures to be chemically static and the component cells to be fixed in position once and for all?

Then a few years after the Second World War came a third period of intense activity which has been deeply felt at the meetings of our Association Those who shown to change position with time so that structures which look static in stand ard histological slides are now shown by radioautography to be the site of intense activity Today I wish to illustrate several types of migrations of molecules and whole cells using examples that are familiar to me. And I thus hope to show that *radioautography gives histology a fourth dimen sion time*

The technique of radioautography is simple enough Lacassagne and co-workers started it in '25 by placing sections of radioactive tissues in contact with a photographic plate. Results were interesting but not precise as resolution was poor In 46

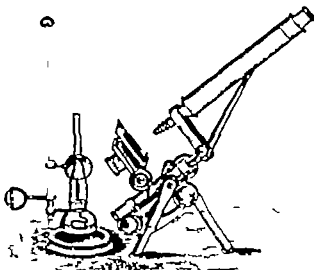


Fig 2 Microscope and lamp from the 1870'

use a new tool the electron microscope (fig 3) make up a large group of en thusiasts. Another devoted group is reinterpreting structures with the help of histochemical analysi In contrast to the time when an eosin tain did not mean much more than the pink color used for British countries on the map today each dye each reagent each enzyme has become another tool in their hands

Even radioelements are being used These may be made part of biological substances which may then be injected into an animal and traced in sections by means of *radioautography* With this technique molecules may be traced and shown to be on the move Even whole cells may be at McGill Leonard Bélanger and I both of us just back from military service used a different approach Sections containing radioactive material were coated with melted photographic emulsion (fig 4) The coated slides were exposed in the dark and developed by the usual photographic procedures A darkening appeared over radioactive sections (as in figs 5–11) which under high power could be assigned to the presence of black silver grains in the emulsion (fig 12) This technique provided a close contact between emulsion and section and thus allowed for the first time a high resolution. With this tool we could examine whether changes took place in the components of histological sections

The substances making up histological sections are mainly large molecules: *proteins, nucleic acids and carbohydrates*. Glucose is known to be taken up in tissues for the synthesis of complex carbohydrates and its breakdown products are utilized in the synthesis of proteins and nucleic acids. Hence if we inject *radioactive* glucose into an animal, radioactivity will be found in those various substances inasmuch as they are synthesized at the time.

Tiny baby rats, three days old, received an injection of glucose labeled with carbon[14] and were sacrificed at various time intervals thereafter (Kumamoto '56). Several organs were placed in a block and cut and the sections were exposed to the emulsion. After development and fixation, it could be seen with the naked eye that the sections of all tissues obtained soon after injection (fig. 5) appeared black, that is exhibited a strong radioautographic reaction. (The sections by the way were not stained, so that the dark outlines in figs. 5–11 are due exclusively to the reaction.)

One might have assumed that, since the animals were growing, the newly-synthesized carbohydrates, proteins and nucleic acids would be built up in the tissues and stay there. Yet in time the reactions decreased from the peak intensity at three hours (figs. 6 and following). After two or six months the labeled substances were largely gone. But there were a few persisting reactions over the lens (fig. 9) perhaps due to retention of labeled carbohydrates, as well as weak reactions in dentin (fig. 10) and bone (fig. 11) attri

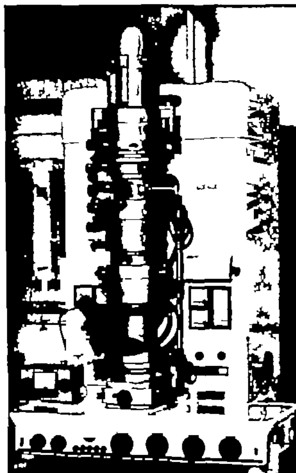


Fig. 3 One of the electron microscopes of the Department of Anatomy, McGill University (Siemens Elmskop 1)

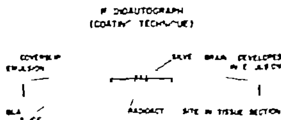


Fig. 4 Diagrammatic representation of a radioautograph prepared by the coating technique

buted to a labeled protein collagen. Briefly of the multitude of carbohydrates proteins and nucleic acids that were being synthesized in the young *most* disappeared with time Only a few exceptionally stable substances such as collagen and lens material remained. Now the substances that disappear must be replaced. They turn over

The turnover of proteins and nucleic acids may be examined using radioactive precursors labeled with the hydrogen isotope tritium (H) which emits soft rays producing sharply limited reactions in radioautographs

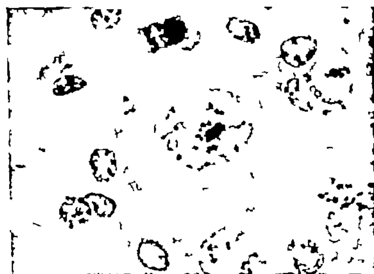
---

Figs 5–11 Photograph of whole histological slides bearing unstained radioautographs, from three-day-old rats given 30 μc of glucose-C^1 intragastrically and sacrificed t rious time i terval af er thi injection varying from three hours to six month A series of organs and ti sues were excised and fixed in Orth fluid. U tained 6-μ thick histological section were oated with NTB3 fluid emulsion Exposure w equal in all cases.

At three hours after injection (fig. 5) an intense blackening i seen, which i haped like the ariou organ and ti sues This reaction rev al the presenc of bstances of large molecula weight labeled with the C^1 of glucose At one day after injection (fig 6) there is slight decre se in the in ens ty f the reaction due to dep rture of labeled material ttributable to secretion or turnover At la er interval (figs 7 nd follow ing) the intensity of the reaction progres i ly decre ses A 14 days (fig 9) the reaction are w ak except for black pot indicating the presence of adioactivity in the len a tructure in which table ma erial i present At two month (fig 10) very little radioactivity i retained in org ns and ti ues ex ept for material howing wavy lines (due to radioactiv material in the matrix of dentin nd traigh lines (bone) A six month (fig 11) the reactions of dentin and bone are barely vis ble The decrease in dentinal reactions is due t he w ar of the ooth rfac nd in bone reaction to resorption processes (*not to true turnover*)

Thus except for few table bstances in lens and hard tissues he bstances synthesized from glucose in young rat (rbohydr tes, proteins, nucleic acid) how pid turnover

Reproduced from Kamamoto, 1954



(Reproduced from Leblond and Amano, 1962)

Fig. 12 Sites of RNA synthesis in the cell of spinal ganglion H and E stained radioautograph of DNAase treated section of spinal ganglion cell from mouse sacrificed 20 minutes after cytidine H^3 injection. The DNAse treatment is required because cells which synthesize DNA also take up cytidine-H^3 It is possible to remove DNA effectively by the method of Amano ('62) × 1,500

As precursor of ribonucleic acid (RNA) the nucleoside cytidine H^3 has been used as precursor of protein an amino acid such as leucine-H^3 and as precursor of deoxyribonucleic acid (DNA) the nucleoside thymidine-H^3 In these three cases the detection of the sites of synthesis is based on the same principle the labeled precursor remains in the tissue for about one hour or at most a few hours after injection Any nucleic acid or protein synthesized during that time acquires the label of the precursor When after the animal is killed the tissues are processed for histology the unused precursor is washed out but the labeled nucleic acid or protein is retained and will therefore be in the sections where it can be detected by radioautography

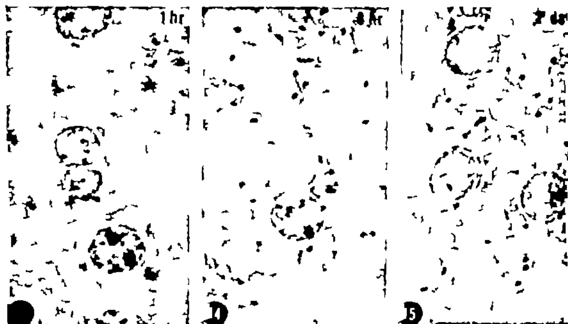
Let us first survey the turnover of RNA then of protein and finally of DNA using data obtained in this laboratory with adult, fully grown animals

RIBONUCLEIC ACID

The *behavior of ribonucleic acid* — RNA — is perhaps the most dramatic, as it is the simplest (Leblond and Amano '62) Immediately after injection of labeled cytidine there is no radioactivity in the cytoplasm. Radioactivity is restricted to the nuclei, as shown for instance in ganglionic cells (fig 12) where it occurs in nucleolus and chromatin. Thus, RNA is synthesized only in the organelles of the nucleus.

In smaller nuclei synthesis is less active but definite as shown by the presence of fewer grains (fig 12) As a matter of fact, the nuclei of nearly all the cells of the body that we have examined synthesize RNA (Amano et al '65)

Thus in liver the reactions appear again over nucleolus and chromatin, with none in the cytoplasm (fig 13) At later time intervals we can trace the new RNA migrating away from the site of synthesis Thus by eight hours after injection, silver grains appear over the cytoplasm (fig 14) By two days, most of the grains are over the cytoplasm (fig 15) It is concluded that the RNA made in the nucleus migrates to the cytoplasm rapidly Let us pause for a moment. While I am speaking to you and you are listening to me, RNA is being synthesized in nuclei throughout our bodies, and from all the nuclei RNA is flowing to the cytoplasms



(Reproduced from Leblond and Amano, 1962)

Figs. 13 14 15 RNA metabolism i liver cells. H and E stained radioautographs fter DNAse treatment of liver section from mice sacrificed one hour (fig. 13) eight hours (fig 14) and two days (fig. 15) after injection of cytidine-H³ ×1,500

The reactions t arly time intervals, are found only over nuclei (fig. 13) With time more and more grains ppear over cytopl sm (figs. 14 and 15) while the reaction over nuclei become weak (fig 15) Hence the RNA ynthesized i the nucleus migrates to cytoplasm.



Reproduced from Leblond and Amano, 1962)

Fig 16 Protein ynthesi in Purkinje cells of the cerebellum. H and E tained radioa to graph of Pu kinje cell from t sacrificed four hours after leucine-H injection (Photograph w taken by Dr J Carneiro using the two-exposure technique of H A. Graham) 1,500

The Purkinje cell occupying most of the field shows silver grains over the cytopl sm (C) nd over some of the hrom tin ma ses sc ttered in the nucleus (N) Th dark mas in center consi t of the ucleolus (left n) and perinucleolar hromatin neither of which shows radioacti ity here although protein ynthesis i now known to take place in both





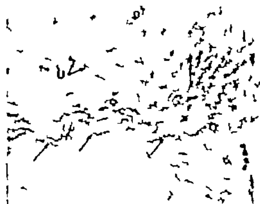
(Reproduced from Droz and Leblond, 1963)

Figs. 17 and 18 Protein synthesis and migration in ganglionic cells. H and E stained radioautographs of semilunar ganglion of 80-g rat given single injection of leucine-H³ and sacrificed after seven minutes (fig. 17) and four hours (fig. 18) × 1,000.

At seven minutes (fig. 17) the silver grains are scattered over nucleus (N) and cytoplasm (P) with the exception of the axon hillock (H) A few grains may be seen over satellite cells (S) At four hours (fig 18) the silver grains also extend to the axon hillock (H)

Hence, proteins synthesized in the cell body soon migrate into the axon hillock.

A word on what happens. You may remember that we have seen RNA synthesized in the chromatin of the nucleus. Now chromatin contains the genes each one with its own DNA The genes may be responsible for the production of the three types of RNA in the nucleus (Amano et al. '65) and particularly for that of distinctive RNA molecules, which may act as messengers and carry to other parts of the cell the *information received from the* genes. The messenger RNA s are then used in protein synthesis, their role being to direct the sequence of amino acids being built into each new protein.

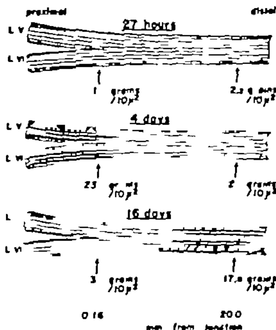


(Reproduced from Droz and Leblond, 1963)

Fig. 19 Protein migration in axons of spinal cord. H and E stained radioautograph of cross-section of the lumbar spinal cord of 250-g rat sacrificed one day after injection of leucine-H³ Labeling is seen on longitudinally cut axons (oblique arrows) coming from the ventral horn (outside the field at left) and going to the ventral root (far right) Silver grains may also be seen over individual axons in the ventral root (vertical arrow) whereas the axons seen in cross-section in the white matter are unlabeled (U)

PROTEIN

The *sites of protein synthesis* may be examined after injection of leucine-H³ for instance in Purkinje cells (fig. 16) Reactions are visible over these and other cells within minutes after injection and are found in both cytoplasm and nucleus.



Reproduced from Droz and Leblond, 1962)

F g 20 Diagrams representing the junction of the L_5 nd L_6 roots (t left) from which arises the sciatic nerve (right) The he vy black line seen in the second diagram (4 days fter injection of leucine-H) nd hird diagram (16 days fter injection) indicate the location of the axonal radioactivity observed at these two time intervals. Grain count were made on trans erse section of the nerv 1.6 mm nd 20 0 mm from the j nction. The grain count were xpressed per 10 μ of axon and given below each diagram.

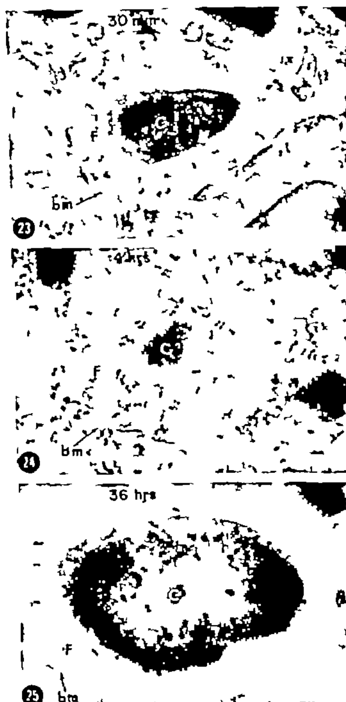
1 may be seen th axonal radioactivity is not significant at 1 1 day ppears t the junction four days nd in more d tal region t 16 d ys fter injection of leucine-H³



Reproduced from Droz and Leblond, 1962

Fig 21 nd 22 Demonstration of protein migr tion in axon H nd & t ined r dioautogr ph t 1 1 day and 16 days fter the first of multiple injection of leucine H Axon are indic ted by the letter A 1,,00

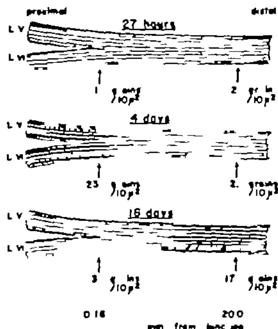
Sciatic nerv of 45-g t observed at 20 mm from the junction of the L_5 and L_6 br nches of the lumbar plexus. The axon re unreacti at one day (left) but trongly reactive t 16 day (righ (Reaction seen t both times over Schw nn cell cytopl m S)



(Reproduced from Nadler, Young, Leblond and Mitmaker 1964)

Figs. 23, 24 and 25 Protein migration in thyroid follicle viewed in light microscope as shown in H and E stained radioautographs of thyroid follicle t 30 minutes (fig. 3) 4 hours (fig. 24) and 36 hours (fig. 25) after injection of 2.5 μc of radioactive leucine into 200-g rats. × 1,200

Each picture represents follicle enclosed in its basement membrane (bm) with the deeply stained colloid ( ) and the surrounding follicular cells (f) At 30 minutes, radioactivity is distributed throughout the cytoplasm of follicular cells, but not significantly in the colloid At four hours the radioactivity tends to accumulate t the apex of follicular cells By 36 hours much of the radioactivity is in the colloid.



(Reproduced from Droz and Leblond, 1962)

Fig 20 Diagrams representing the j nction of the L_5 and L_6 root (t left) from which arises the sci tic nerv (right) The heavy black line seen i the second diagr m (4 days fter injection of leucine-H) and third diagram (16 d ys after injection) indicate the loca tion of the axon l radioactivity observed t these two time intervals Grain counts were made on trans erse section f the nerv t 1.6 mm nd 20 0 mm from the j nction. The grain cou t were expressed per 10 of axon nd gi en below ach diagram

It m y be seen tha axonal radioactivity i not significant t 1 1 d y ppe rs t the junc tion four d ys nd in more dist l region t 16 days fter injection of leucine-H

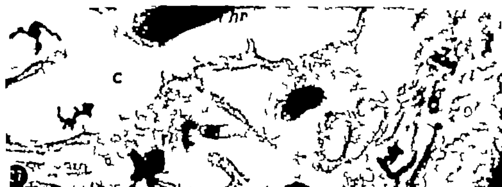


Reproduced from Droz nd Leblond, 1962)

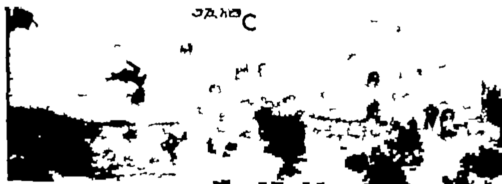
Figs 21 and 22 Demonstr tion of protein migr tion in axon H nd S stained adio utogr ph 1 1 day and 16 day fter the firs of multiple injection of leucine H A ons are ind ted by the letter A 1,500

Sciatic nerv of 43-g rat observed t 20 mm from the junction of the L_5 nd L_6 br nches of the lumbar plex The axon re unreactive t one d y (left) but trongly reacti t 16 day (right (Reaction are seen t both times over Schwan cell cytopl m S)









(Reproduced from Nadler, Young, Leblond and Mitmaker 1961)



(Reproduced from Warshawsky, Leblond and Droz, 1963)

Figs. 30–32 Protein synthesis and migration i the acinar cell of the pancre H nd E stained dioautograph of acinar cell in i I jected with leucine-H 1,000

A tw min tes (fig. 30) the reaction are confined t the basophilic ergastoplasm (e) At 30 min tes (fig. 31) slightly he ier reaction is seen over the ergastoplasm ( ) than at the pre ious time interval However the most intense reaction is now over the proximal portion of the region f zymogen granules where lusters of grains are di tinct (g) while the central portic of thi region ( ) how no reaction Later (4 h fig. 32) the reaction xtend to the whole zymogen region ( )

to the Golgi zone (fig 31 g) and later to the zymogen gr nules themselves (fig 32) Finally the labeled material appears in the ducts (fig 33) thu showing release of the protein as pancreatic secretion

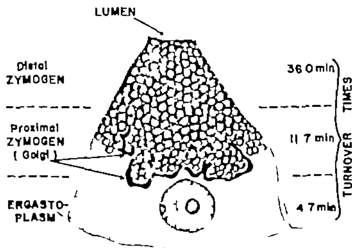
A remarkable feature is the speed with which proteins are secreted (Nadler '63) The approximate time it takes to replace an amount of protein equal to that present that is the *turnover time* is about five minutes for the proteins of the ergastoplasm (fig. 31) In other word every five minutes the proteins of thi region are replaced Then the proteins migrate to the Golgi zone where they are mad into zymogen granules in about 12 minutes Then it takes 36 minutes for the zymogen granules to migrate to the lumen About one hour in all!

Thus we have seen three types of cell that export proteins to the outside Neurons send off proteins to the axon th roid cells send thyroglobulin to the colloid and the acinar cells send pancreatic enzymes to the ducts All these proteins have a short turnover time (table 1) It m y be added that these cells also build up protein that remain sedentary that i stay within the cells and have a much longer turnover time



(Reproduced from Warshawsky Leblond and Droz, 1963)

Fig. 33 Migration of protein in pancreas H nd E stained radioautograph of excretory ducts and surrounding pancreatic acini of the rat four hours after leucine-H³ injection. × 500. The material within the lumen of the duct is radioactive. Hence by that time the proteins synthesized in acinar cells have passed into the ducts. (The reactions over the surrounding acini are mostly distributed over the entire zymogen granule region.)



(Reproduced from Warshawsky Leblond and Droz, 1963)

Fig. 34 Diagrammatic drawing of pancreatic cinar cell of the rat, as stained by the osmium tetroxide zinc iodide method for the Golgi pparatus. The ergastoplasm (homogeneous gray) containing the ucleus, is seen at the base of the pyramidal cell. Most of the osmiophilic laments of the Golgi pparatus are located at the junction between ergastoplasm and zymogen granules, with some between the granules. The zymogen granules making up the remainder of the cell extend to the apical lumen. The division of the cell into ergastoplasm, proxim l and distal zymogen regions is indicated t the left of the figure. A rough estimat f the turnover times of the exportable proteins in each region is shown t the right of the figure

TABLE 1

Approximate turnover time of proteins
(Calculated by Dr N J Nadler)

	Exportable	Sedentary
Neurons	1 day (axonal proteins)	2 weeks
Thyroid cell[a]	6 hours (thyroglobulin)	3 weeks
Pancreas cell[b]	1 hour (pancreatic enzymes)	3 days

Droz and Leblond, '63. *Nadler et al., '64.* *Warshawsky et al. '63.*

The important conclusion is that the static appearance of many cells in histological sections hides extensive migrations of molecules In the case of RNA we *observe migration from nucleus to cytoplasm* but never beyond the cell membrane Proteins however may migrate into extensions of the cells such as the axon or go outside as in thyroid and pancreas

DEOXYRIBONUCLEIC ACID

The synthesis of new DNA almost invariably indicates formation of new cells. But space has to be found for the new cells and space is at a premium in the adult organism Hence cell migrations often follow DNA synthesis

A case in point is the intestine Histology textbooks *mention* the presence of mitosis in the crypts of Lieberkuhn but not on the villi (figs 35 36) The presence of mitoses was explained by the old German histologists as a regeneration to correct the damage produced in the epithelium by enzymes and bacteria.

However there is usually no sign of *damage in the epithelium lining the sides* of the villi even though mitoses are abundant. The only irregularity is seen at the villus tip where cell streamers may be exfoliated or rather extruded (fig. 38) This region may be called the extrusion zone. Extrusion zones are found all along the gastrointestinal tract even where there are *no villi, as for instance in the colon* (fig 37)

To find out if damage produced by enzymes elicits mitotic activity an experiment was made in which the animals were starved since in this case digestive enzymes disappear (table 2) The number of mitoses per crypt hardly changed at all nor did the number of extrusion zones (Hooper and Blair '58) To rule out the role of bacteria, rats were given penicillin and germ-free animals were examined. Again no changes. Therefore *mitotic activity and extrusion zones* are both normal features of the intestine Since crypt mitoses are seen at all times of day there is continuous cell production And the extrusion zone at the villus tip points to the site of cell loss Presumably the cells arising in the crypts move out to become part of the villus epithelium and from there glide towards the villus tip where they are lost to the lumen (Leblond and Stevens 48)

It is possible to go a step further Knowing the number of cells of the epithelium and the number of mitoses the time required to produce a number of cells equal to that present that is the *turnover time* of the epithelium may be calculated approximately This was estimated to be less than two days for the rat duodenum When Miss Stevens reported this at the 47 meeting of the American Association of Anatomists the comment of an old Canadian anatomist no longer among us was "This is too silly for words

TABLE 2

Effect of starvation on intestinal epithelium
(Hooper and Blair '58)

	N of mitoses per crypt	% villi [illegible] extrusion zone
Control	7.3 ± 0.6	[illegible]4 ± 2.7
Starved	6.4 ± 0.6	58.0 ± 3.3



Figs. 35 and 36 Mucosa of small intestine from the end of the rat duodenum, fixed in Helly (fig. 35) or in Bouin (fig. 36) The distinction between crypts and villi (arrow placed at the junction) is quite clear after Helly fixation. A few crypt mitoses are shown by oblique arrows in the Bouin fixed preparation (fig. 36) ×135.

We had to confirm our conclusion. And this was done by radioautography We tried phosphate-P^{32} which is taken up by DNA in the course of its synthesis (but also by many other substances) Furthermore P^{32} emits strong beta-rays so that the radioautographic reactions were fuzzy yet they could be localized over the crypts at two hours after injection (fig 39) indicating cell formation there Later at 18 hours, a fuzz over the cells half way up the villi gave a crude but decisive demonstration of migration (fig. 40) And by two days all the epithelium seemed to be more or less labeled (fig. 41)

It took several years before a DNA precursor with less strong beta-rays than P^{32} became available. It was adenine labeled with carbon[14] (Walker and Leblond '58) Unstained preparations of the ileum from



Fig 27 Colon dult moose (I Warshawsky) 500 The crypt show goblet (light) and hief cell (grey w ll mitoses (oblique rrow) C ll mig f om the zone of mi otic ac ivit the ex ru ion zones on the urface



Fig. 38 Extrusion zone t the tip of duodenal villus of rat. Several cells seem to be pushed above the regular row of cells and almost separated from them. × 400

mice given adenine-C^{14} show early reaction in the crypts (fig 42) confirming cell formation there By 24 hours, the cells are inching their way up the villi (fig. 43) By three days, many have arrived at the ex trusion zone (fig 44) Perhaps some have already fallen into the lumen

And finally after another couple of years we had a still better DNA precursor namely thymidine labeled with tritium, which has even less strong beta-rays than carbon[14] and, therefore provides sharper pictures. Soon after injection (Leblond and Messier '58) labeled cells are seen in the crypts confirming that new cells are being formed there (fig 45). These labeled cells are later seen on the walls of the villi and reaching the tips (fig. 46) At that time labeled cells appear in the lumen (fig. 47) A similar migration of the epithelial cells of colon takes place from the crypts to the extrusion zone of the surface (Messier and Leblond, '60) Hence,







(Reproduced in part from Leblond, Stevens and Bogoroch, 1948)

Figs. 39–41 Migration of cells of intestinal epithelium as seen with phosphate-P^{32} H and E stained radioautograph of duodenum of rats sacrificed at various time intervals after injection of P^{32} phosphate. Approx. × 100.

At two hours after injection (fig. 9) dark fuzz is seen over the crypts (the upper limit of which is indicated by arrow) At 18 hours (fig. 40) the reaction extends nearly two-thirds of the way up the villi. At two days (fig. 41) the whole epithelium is radioactive.

It is concluded that the cell formed in the crypt migrate to the tip of the rat duodenum in bout two days.



F[illegible] 3[illegible] Co[illegible] [illegible] d[illegible]lt mouse [illegible] W[illegible] [illegible]shewsky [illegible] The crypt [illegible] show [illegible] (light) and [illegible] [illegible] mitoses [illegible] oblique arrow [illegible] C[illegible] [illegible] of mi[illegible] [illegible] the extru[illegible] zones [illegible] on the surfac[illegible]

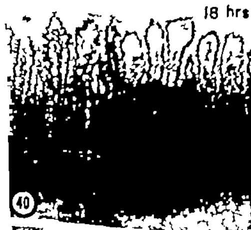


Fig. 38 Extrusion zone at the tip of duodenal villus of rat. Several cells seem to be pushed bove the regular row of cells and almost separated from them × 400.

mice given adenine-C show early reaction in the crypts (fig. 42) confirming cell formation there By 24 hours the cells are inching their way up the villi (fig. 43) By three days many have arrived at the ex trusion zone (fig 44) Perhaps some have already fallen into the lumen.

And finally after another couple of years, we had a still better DNA precursor namely thymidine labeled with tritium which has even less strong beta-rays than carbon[14] and therefore provides sharper pictures. Soon after injection (Leblond and Messier '58) labeled cells are seen in the crypts, confirming that new cells are being formed there (fig. 45) These labeled cells are later seen on the walls of the villi and reaching the tips (fig 46) At that time labeled cells appear in the lumen (fig. 47) A similar migration of the epithelial cells of colon takes place from the crypts to the extrusion zone of the surface (Messier and Leblond '60). Hence,







Figs. 39-41 Migration of cells of intestinal epithelium as seen with phosphate-P^{32} H and E stained radioautograph of duodenum of rats sacri ficed at various time intervals after injection f P^{32} phosphate. Approx. × 100

At two hours after injection (fig. 9) d rk fuzz is seen over the crypts (the pper lim of which is indicated by arrow) At 18 hours (fig 40) the reaction extends nearly two hirds of the way up the villi. At two days fig 11) the whole epithelium is rad oactive.

It is concluded th t cells formed the crypt migrate to the tip f the rat du denum in about two d ys.

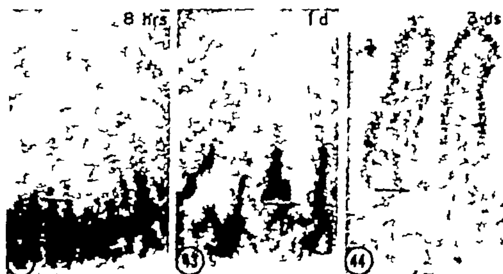
the static picture of the intestinal epithelium hides a continuous motion of its cells

The magnitude of the cell loss in the small intestine of a 3-month old rat was *estimated at about 1.3 billion cells per day* (Enesco and Altmann, '63) This figure may be compared to the total number of cells in the body of a rat of the same age 64 billions — a number not quite as large as the United States annual budget. Now if 1.3 billion cells come out of the epithelium of the small intestine each day and we add what comes out from the epithelia of pharynx, esophagus stomach and large intestine the total number of cells lost each day may approach two or even three billions that is about *one-twentieth or one-thirtieth of the total number of cells in the body* In other words the loss of cells from the digestive tract over a 20–30 day period is equal to the total number of cells in the body

Why is there such an apparent waste of cells? Some answer to this question may be given by a comparison with the lighting system of a department store today Fluorescent bulbs are all on evenly You may remember the days not so long ago when there were always a few of them flickering Then someone would climb up and replace the worn out bulb Today however all bulbs are replaced when they have about reached their half life that is before there is a chance of serious breakdown. Something similar occurs in the intestine By providing a continuous flow of new cells, a cell that is ailing will be swept away before the damage takes on serious proportions.

Mechanisms of cell renewal

As new cells arise in the epithelium of the adult intestine, there are also cells that are lost to the lumen. Since the histological appearance remains about the same at all times in the adult there must be a balance between cell production and cell loss. This must also be true of the proliferating cell populations of epidermis esophageal epithelium testis, blood forming organs etc. When this condition was first realized (Leblond and Stevens 48)



(Reproduced from Walker and Leblond, 1958)

Figs. 42–44 Migration of cell of intestinal epithelium, seen with adenine-C[14] Unstained rad. autographs of jejunum t 8 24 and 72 hours after injection of adenine-C[14] into mice The junction of crypts and villi is shown by arrows The early reactions (fig 42) are arranged in parallel bands corresponding to the nuclei of the crypt epithelium At one day (fig 43) the reaction extend part way up the side of the villi and at three days (fig 44) they predominate on the upper half and tip of the villi × 107

ing DNA prior to mitosis) Briefly the basal layer is the site of production of new cells

Superficial to the basal layer is the *spinous layer* composed of large cells with a spherical, light nucleus, then the *granular layer* with keratohyaline granules, and finally a few *keratinized layers* (fig. 48) If the cells labeled with thymidine-H³ are followed with time, they are found to migrate to the spinous layer and later to the granular layers. From what has just been said, steady state requires that for every cell that moves out of the basal layer to become a spinous cell, there be on the average one cell added by mitosis to the basal layer

The simplest way for Nature to achieve this aim would be that, of the two daughter cells of mitosis one moves out to become a spinous cell and one remains a basal cell that is each division would be a differential or asymmetric mitosis (fig. 50) Many authors, for instance Rolshoven in Germany ('51) and Mercer in England ('62) have assumed that the basal cells of stratified epithelia renew themselves by this type of mitosis.

If this is so then each time a cell divides, one of the daughter cells would stay in the basal layer and the other move to the spinous layer Let us therefore examine the daughter cells of the mitoses of basal cells. To be sure to recognize the two daughter cells of mitosis, maps were made from serial radioautographs of the esophagus at 48 hours after thymidine-H³ injection (Pereira and Leblond '63). Paired daughter cells were identified by physical proximity and comparable grain counts.

While a few pairs are composed of a basal and a spinous cell (in accord with the differential mitosis concept) numerous pairs consist of two basal cells (fig 51) or two spinous cells (fig. 52) These results eliminate the differential mitosis theory but rather suggest that two daughter cells of a mitosis come out independently and at random Thus in the diagram (fig 53) it may be seen that the division of a basal cell may give two basal, or one basal and one spinous, or two spinous cells. The critical step is the coming out of the basal layer After that, the evolution of the cell is irreversible up to keratinization and



Fig. 49 Coated radioautograph of esophageal epithelium (post-stained with hematoxylin) from an adult mouse sacrificed one hour after injection of 2.5 μc of thymidine-H³ per gm body weight. The lettering is the same as in figure 48. × 875.

Labeled nuclei are found in the basal layer (Cameron and Greulich, unpublished.)

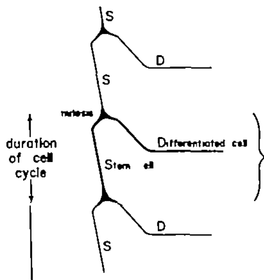


Fig. 50 Diagram illustrating the concept of differential mitosis. Each such mitosis of stem cell would produce a new stem cell and differentiated cell.

However no evidence in support of the existence of differential mitoses was found in renewal systems.


(Reproduced from Leblond and Messier 1958)

Fig 47 H and E stained radioautograph of the jejunum and adjacent lumen from the same mouse as in figure 48 The upper region of the villi is at the bottom of the picture ( ) and free cells are seen in the lumen above 600
Of the free cells seen in the lumen some are labeled (l) and others are not (u)



Reproduced from Leblond Greulich and Pereira 1963

Fig 48 Esophageal epithelium of 700 g male rat Bouin fixation H F stain 875
From the base up note the dermis (D) the basal layer with crowded cells and nuclei usually perpendicular to the surface (B) the spinous layer with fairly large cells, light nuclei and prominent nucleoli (S) the granular layer (G) and keratinized layers (K) At m, there is a metaphase and a cell believed to be squeezed out of the basal layer to enter the spinous layer



(Reproduced from Leblond and Clermont, 1952)

Fig. 54 Seminiferous epithelium of the rat, t stage VII of the cycle (PA-Schiff hematoxylin) showing from the base up, the basement membrane, the first layer of cells composed of two type A spermatogonia (A) and many resting spermatocytes (small, with dark chromatin, R) second layer composed of pachytene spermatocytes (P) and finally step 7 sperm tids with their head cap and few elongated, poorly seen step 19 spermatids.

shedding Why all cells divide regularly (every second day or so) in the basal layer and never do so in the spinous layer we do not know

The diagram is a bit *rigid*. In reality mitoses do not occur at the same time but at random However the diagram shows that for a given number of mitoses — three per cycle in the diagram —there will be three new basal cells and three that differentiate into spinous cells. Thus there is no change in the number of cells of the epithelium and the steady state of the cell population is maintained.

But a diagram is easy to do How can the epithelium do it? The paradox is that the migration of a cell is not the im mediate consequence of the mitosis from which the cell comes. And yet steady state requires that the number of migrating cells be equal to the number of mitoses The key to this paradox seems to be that the addition of new cells by mitosis tends to increase population pressure in the basal layer Indeed cells leaving this layer are often altered to a racket shape (fig. 48 s) as if squeezed out by pressure Presumably a cell added by mitosis can be accom modated only by forcing out one neighbor ing cell on the average. Thus the steady state would be maintained.

In the *testis* cells differentiate as they transform from spermatogonia (fig 54 A) to spermatocytes (R,P) spermatids (7 19) and spermatozoa, while approaching the lumen of the seminiferous tubule It is possible to time the migration accurately Two periods may be considered.

First spermatogonia have to divide in such a way that their stock is maintained while spermatocytes are produced. In fig ure 55 the stem spermatogonia — known as type A — are shown to divide three times by mitosis. Here each series of mitoses truly occur at about the same time Of the eight new cells arising from the last series of type A cell mitoses one remains a type A cell (left hand side) but the seven

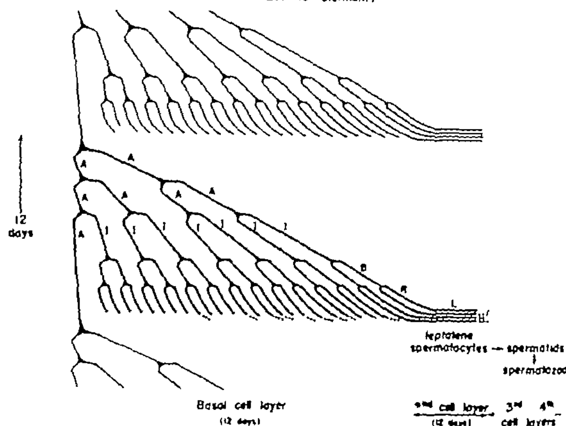


Fig. 55 Diagram of the most probable pattern for the development of spermatogonia (Stem Cell Renewal Pattern of Clermont and Leblond '53; recently modified by Clermont, '62)

At left the stem cell, also called dormant type A, undergoes three successive divisions the third one of which yields eight cells, of which one remains type A cell and the others become intermedi te type cells (I) The latter divide to give type B cell (B) which in turn divide to give the resting sperm tocytes (R) already seen in figure 54

This series of phenomena encompasses one cycle of the seminiferous epithelium lasting approximately 12 days

others (I) gradually acquire new features (Clermont and Leblond '53 Clermont '62) This is the *critical step* From here on, differentiation goes on in a series of complex but irreversible changes type B cells resting spermatocytes etc

The various steps of the differentiation may be timed if thymidine-H is injected The resting spermatocytes become labeled and their fate may then be traced. In figure 56 the labeled young spermatocytes are seen three days after injection Twelve days later the cells have become pachytene spermatocytes and a further 12 days later spermatids (fig 57) By this approach it has been possible to time all events of spermatogenesis (Clermont et al '59) Thus it takes about 12 days from the first division of each stem cell (fig. 55) to the *production of resting spermatocytes* From the stem cell to the free spermatozoon in the lumen it takes a total of about 48 days

In man it takes somewhat longer 64 days (Heller and Clermont, '63) From the testis the spermatozoon is on its own and it will take another few days before it makes its way through the epididymis and sees the light.

This last example was to make you aware of the time dimension in histology As for myself I am so convinced of it that when I had to have a new clock in my



(Reproduced from Clermont, Leblond and Messier, 1959)

Figs. 56 and 57 H and E stained radioautographs of seminiferous epithelium t stage XIII of the cycle, from rats sacrificed three days or 27 d ys after injection of thymidine-H³

At three days, the young, zygotene spermatocytes are labeled (fig. 56, arrow) At 27 days, the so-called step-13 spermatids are labeled (fig. 57 arrow) It is concluded that for cell to go from the first to the third cell layer of stage XIII, it took 24 d ys. Hence, the time required to change from the cells of one layer to those of the next one is 12 days. This is the duration of the cycle of the seminiferous epithelium.

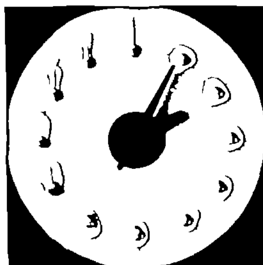


Figure 58

office I decided to indicate the hours by the 12 stages in the development of the human spermatid (Clermont and Leblond '55) The young spermatid appears at 1 o clock, produces the head cap by 5 o clock and at midnight, becomes the full fledged spermatozoon raring to go (fig. 58)

Of course the feeling of time has been present all along in anatomy As early as the Renaissance structural changes with time were traced during embryological development by Coiter and Fabricius. During the latter part of the Nineteenth Century as well as at the beginning of this century

when most anatomists were considering any structure as being static there were some particularly those interested in endocrinology (Bouin Evans and many others) who observed rapid structural changes produced by hormone injection and extirpation of endocrine glands More recently moving pictures of cultured cells have vividly shown movement for instance during mitosis.

But radioautography shows movement under physiological conditions and thus ideally introduces the time dimension in anatomy Histological sections of organs that we used to consider static are shown by radioautography to be the sites of rapid syntheses and migrations Thus the protein arising in the ergastoplasm of pancreatic cells manages within the space of an hour to enter the Golgi zone to become dressed up into a zymogen granule and finally to leave the cell in the pancreatic juice

Within the space of two days the cells arising from mitosis in the intestinal epithelium manage to climb to the tip of the villi and drop to their death in the lumen.

Thus with time we discover movement and movement gives a feeling of life In fact when we consider the whole body we become conscious of *a tremendous swarming of molecules and cells. And yet one sees that order reigns and the organization is massive* Thus in concluding it may be appropriate to look with a kind of reverence at the mysterious movements of Life in Nature

ACKNOWLEDGMENTS

The work reviewed in this article was done with the support of grants from the Medical Research Council of Canada and the National Cancer Institute of Canada. While it is not possible to acknowledge the help of the many co-workers several of whom are mentioned in the bibliography it must be pointed out that the quality of the radioautographs is largely due to Dr Beatrix Kopriwa the quality of the sections to Mr Hans Torunski and recently Miss Ritha Paradis Photographs are by Mr A Graham and drawings by Mrs Margot Oeltzschner Much of the burden of organization was carried by the senior secretary Mrs. F E. Streit

LITERATURE CITED

Amano, M. 1962 Improved techniques for the enzym tic extraction of nucleic cid from tissue sections. J Histochem. Cytochem., 10 204–212.

Amano, M C P Leblond and N J Nadler 1965 Radioautographic analysis of nuclear RNA in mouse cell revealing three pools with different turnover times. Exp. Cell Res. (in press).

Bélanger L. F and C. P Leblond 1946 A method for locating radioactive elements in tissues by covering histological sections with photographic emulsion. Endocrinology 39 8–13

Clermont. Y 1962 Quantitative analysis of spermatogenesi of the rat A revised model for the renewal of spermatogonia. Am. J Anat 111 111–129

Clermont, Y., and C. P Leblond 1953 Renewal of spermatogonia in the rat testis. Am. J Anat 93 475–502.

——— 1955 Spermiogenesis of man, monkey ram nd other mammals shown by the "periodic acid-Schiff" technique Am. J Anat 96 229–254

Clermont, Y C P Leblond and B. Messier 1959 Durée d cycle de l'épithélium séminal du rat. Arch. An t. microsc 48 bis 3 –55.

Droz B and C. P Leblond 1962 Migration of proteins along the axons of the sciatic nerve Science 137 1047 1048.

——— 1963 Axonal migration of protein in the central nervou system nd peripheral nerves as shown by radioautography J Comp Neur 121 325–346.

Enesco, M. and G. Altmann 1963 Size of cell population and number of cell extruded daily in the mall intestine of the adult rat Anat Rec (Proc) 145 226–227

Heller C G., and Y Clermont 1963 Spermatogenesis in man An estimate of it duration Science 140 184–186.

Hooper Catherine Stevens, and Mon Blair 1958 The effect of tarvation f epithelial renewal in the rat duodenum. Exp Cell Res 14 175–181

Kumamoto, Y 1956 Radioautographic and histological studies of young rat tissues with particular attention to dentin. Ph D thesis, McGill University Montreal Canada.

Lac ane A. J Lattes, nd J Lavedan 1923 Etude xpérimentale des effet biologiques du polonium introduit dans l'organisme J de Radiol et Elect 9 1 14 67–82

Leblond C P and M. Am no 1962 Synthetic ctivity in the nucleolus compared to that in the rest of the cell. J Hi tochem Cytochem 10 162 174

Leblond C P nd Y Clermont 19 2 Spermiogenesi of rat mouse hamster and guinea pig a revealed by the Periodic Acid Fuchsin Sulfurous Acid technique Am J Anat 90 167 214

Leblond, C P nd B Mes ier 19 8 Renewal of hief cell nd goblet ll in the small intestine a shown by radioautog phy after injection of thymidine H int mic Anat Rec 132 247 2–9

Leblond, C. P and C. E. Stevens 1948 The constant renewal of the intestinal epithelium in the albino rat. Anat. Rec., *100* 357–378.

Leblond, C. P., R. C. Greulich and J P M. Pereira 1964 Relationship of cell formation and cell migration in the renewal of stratified squamous epithelia. Proc. Sympos. on Wound Healing. In Advances in Biology of Skin, *5* 39–67

Leblond, C. P C. E. Stevens and R. Bogoroch 1948 Histological localization of newly formed desoxyribonucleic acid. Science, *108* 531–533.

Mercer G H. 1962 The cancer cell. Brit. Med. Bull., *18* 187–192.

Messier B and C. P Leblond 1960 Cell proliferation and migration as revealed by radioautography after injection of thymidine-H³ into male rats and mice. Am. J Anat., *106* 247–285.

Nadler N J 1963 Calculations of the turnover times of proteins in each region of the acinar cells of the pancreas. J Cell Biol., *16* 24–27

Nadler N J C. P Leblond and J Carneiro 1960 Sites of formation of thyroglobulin in the mouse thyroid as shown by radioautography with leucine-H³ Proc. Soc. Exp Biol. Med., *105* 38–41

Nadler N J B A. Young, C. P Leblond and B. Mitmaker 1964 Elaboration of thyroglobulin in the thyroid follicle. Endocrinology *74* 333–354

Pereira, J P M., and C. P Leblond 1963 Mode of renewal of epithelial cells in the esophagus of the adult rat. Anat. Rec., (Proc.) *145* 257

Pinheiro P C. P Leblond and B. Droz 1963 Synthetic capacity of reticulocytes as shown by radioautography after incubation with labelled precursors of protein or RNA. Exp. Cell Res., *31* 517–537

Roosen-Runge (Bolshoven), E. 1951 Ueber die Reifungsteilungen bei der Spermatogenese mit einer Kritik des bisherigen Begriffes der Zellteilungen. Verh. d. Anat. Ges., *49* 189–197

Walker B. E., and C. P Leblond 1958 Sites of nucleic acid synthesis in the mouse visualized by radioautography after administration of C¹⁴ labelled adenine and thymidine. Exp. Cell Res., *14* 510–531.

Warshawsky H., C. P Leblond and B. Droz 1963 Synthesis and migration of proteins in the cells of the exocrine pancreas as revealed by specific activity determinations from radioautographs. J Cell Biol., *16*. 1–23.

A Comparative Study of the Fine Structure of the Trophoblast in Several Hemochorial Placentas [1]

ALLEN C. ENDERS
Department of Anatomy, Washington University School of Medicine, St. Louis, Missouri

ABSTRACT Portions of the labyrinth or villi of placentas from late pregnancy from nine species in four orders of mammals were examined with the electron microscope. Pronounced patterns of layering of the trophoblast were found in these placentas which were all of the hemochorial type. The laboratory rat, laboratory mouse, hamster and deer mouse have three layers of trophoblast between the maternal blood space and fetal vessels (*hemotrichorial*), the rabbit two layers (*hemodichorial*), the guinea pig and chipmunk one layer (*labyrinthine hemomonochorial*), and the human and armadillo one layer (*villous hemomonochorial*).

The outer layer of trophoblast of the hemotrichorial placentas (the layer next to the maternal blood) is cellular, but the next two layers are apparently syncytial and are closely apposed to one another. The outer layer of the rabbit placenta is syncytial, while the inner layer contains some pockets of cells. In all of the hemomonochorial placentas examined, the continuous layer of trophoblast was syncytial. It was found that the surface layer of trophoblast of all the placentas studied is rich in granular endoplasmic reticulum, whereas in subsequent layers this element is less abundant. All of the placentas show both surface and basal modifications of trophoblast, but caveolae (pinocytotic vesicles) were found to be most commonly located in crypts, pockets, or other regions somewhat removed from the surface. It is suggested that an area of relative stasis of maternal plasma may be important for absorption of some substances by the placenta.

The Grosser system of classification of placentas is based on the tissue layers intervening between the maternal and fetal blood vascular systems in the chorioallantoic placenta (Grosser, '27). In application the specific category applies to the region of the late placenta with the most intimate association between the two vascular sysems. In the 1950's, rather strenuous objections to the continued use of this system of classification were raised (Wislocki, '54). These objections were based on a number of grounds. First, the Grosser system considered the placenta essentially as a filter, whereas physiological studies have indicated the large extent to which active transport is responsible for passage of substances across the placenta. Second, the Grosser system, based as it was on one region of the chorioallantoic placenta, tended to divert attention from other important regions of the placenta which exhibited different relationships. In addition, at the time that these objections were raised, the cytology of the chorion was beginning to be explored by electron microscopy, with indications that the trophoblast was often organized in a manner not discernible by light microscopy. It should be noted also that many textbook diagrams of the Grosser schema were so oversimplified as to be decidedly misleading (no fault of the system per se). Despite these objections to the classification it has, as Wimsatt ('62) recently pointed out, continued in common usage, in part because of the lack of an acceptable substitute. The future usefulness of such a system depends on our being thoroughly aware of its limitations. It may also be that by refining the categories, the efficacy of the classification may be extended. It is the purpose of this paper to describe some of the variations in the organization of the trophoblast among several placentas all included within a single large group from Grosser's classification, that of the hemochorial placenta.

MATERIALS AND METHODS

In all cases, small pieces of placenta were fixed in either Caulfield's ('37) buffered osmium plus sucrose, or glutaraldehyde. In the latter instance, 1 mm vertical

[1] Supported by National Science Foundation grant GB-1164.

slices through the placenta were fixed in 3% glutaraldehyde in 0 1 M phosphate buffer at pH 7.3 for two hours the appropriate area cut out in phosphate buffer under a dissecting microscope and then post fixed in 2% osmium tetroxide in phosphate buffer for two hours. Following rapid dehydration in cold ethyl alcohol the tissues were embedded in araldite 502 epoxy resin The sections were stained with the lead citrate method of Reynolds (63) and examined in an RCA EMU 3G electron microscope

Since classification of placentas is based on the structure of the mature placenta, late placentas were used The placentas used in this study were from the following animals five rats (*Rattus norvegicus*) day 19 to term six mice (*Mus musculus*) day 13 to term five hamsters (*Cricetus auratus*) day 13 to term one deer mouse (*Peromyscus maniculatus*) late pregnant (field caught) three chipmunks (*Eutamias quadrivittatus*) late pregnant (field caught) ten rabbits (*Oryctolagus cuniculus*) day 19 to term five guinea pigs (*Cavia porcellus*) 29 days to term six human four at term, one at seven weeks and one at five weeks gestation six armadillos (*Dasypus novemcinctus*) one in the placental expansion stage five late pregnant

DESCRIPTION

Layers of trophoblast

Both labyrinthine and villous hemochorial placentas can be grouped according to the number of layers of trophoblast In this manner placentas with three layers of trophoblast are designated hemotrichorial, those with two layers of trophoblast hemodichorial and those with one layer of trophoblast hemomonochorial

Hemotrichorial. The rat and mouse (murid) and hamster (cricetid) myomorph rodents have essentially the same organization of the trophoblast in the labyrinth Indeed, the rat and mouse labyrinths are practically indistinguishable There are three layers of trophoblast throughout the labyrinth (hemotrichorial) an outer middle and inner layer separating the maternal blood spaces from the fetal blood vessels and other extraembryonic connective tissue elements (fig 6)

The outer layer of trophoblast, which encloses the maternal blood spaces, is cellular with cell boundaries present at all times Distinct desmosomes are present not only between this layer and the middle layer (fig 7) but also occasionally between cells of the layer itself In late pregnancy the cells forming the outer layer are attenuated and irregular with some areas reduced to a thin flange Structures that are apparently pores are seen in these attenuated areas (fig 7) In a few places projections of the middle layer through the outer layer are seen Occasionally vesiculated projections from the surface of this layer protrude into the maternal blood space The surface of the outer layer which faces on the maternal blood space has irregular projections which only rarely have sufficient regularity to be designated microvilli. Such projections over thicker regions of the cells, for example the nuclear region tend to be somewhat more regular and microvillous in appearance In addition to the irregular projections and pore areas occasional caveolae can be seen. Except where desmosomes are present the outer layer is only loosely applied to the middle layer

The middle layer of trophoblast also shows variation in thickness being thin in some regions and thicker in the area of the nucleus However in general it is the thickest of the three layers of trophoblast. There are projections on the maternal side that delimit spaces which apparently communicate with vesicular channels passing two-thirds or more of the way through the middle layer Many of the folds on the outer side are irregular More often there are pockets with folds projecting into them from the margin of the invaginations (fig 7) Caveolae with the characteristic acinar shape are situated at the margins of the invaginations

In marked contrast to the loose association of the middle layer with the outer layer is the close apposition of the middle

The term caveolae is used in this paper to designate small acinar invaginations of the surface membrane Most of the invaginations seen in the endothelial cells are simple acinar structures identified in other tissues as pinocytotic vesicles (Bruns, Marchesi and Florey, '62) The invaginations seen in the trophoblast are usually larger have [illegible] denser region of the membrane and are often surrounded by a dense region of cytoplasm. These latter [illegible] similar to the pit described by Roth and Porter (64) in the developing mosquito oocyte

layer to the inner layer The junction between the middle and inner layers is a series of undulations of rather large dimension, with secondary irregularities superimposed. The two plasma membranes are closely apposed throughout their extent. Although distinct desmosomes are not present, in many regions some thickening of the inner leaflet of the membranes is apparent. In other places where the unit membranes can be discerned, the trilaminar arrangement typical of a tight junction is seen In the majority of instances all that can be determined is that in numerous places the two plasma membranes are more closely apposed (less than 160 A) than ordinary cell boundaries (figs. 7 and 9) No cell membranes extending between the two surfaces of the middle layer can be found, and in appropriate montages of electron micrographs cytoplasm can be traced around several blood spaces with continuity of cytoplasm between the widely dispersed nuclei observed. Consequently this layer in contrast to the outer layer is syncytial.

The common border of the inner trophoblast layer and middle layer has already been described The basal border of this inner layer fronts on the basement membrane separating it from the fetal connective tissue. Since the general contour of the fetal connective tissue area is less irregular than the junction between the inner and middle layers the overall arrangement is one of a sheet of protoplasm which has an undulating contour on the outer side and a smooth contour on the inner side On the inner surface are numerous, short stubby microvilli. Neither the distribution of the microvilli nor their shape is regular The basement membrane is frequently rather loosely associated with this layer and extends into only some of the clefts formed by the microvilli. Caveolae are quite rare in this layer

The cytoplasm of the inner layer can be traced for extensive distances and over several fetal vessels without interruption, despite the fact that folds from the outer (apical) surface frequenly extend near to the clefts between the microvilli on the inner (basal) surface Although it cann t be stated with certainty th l yer like e middle layer is probably syncytial (It should be noted that even if occasional cell membranes were to persist in the middle and inner layers the combined layers would be functionally syncytial in that the tight junctions between them would prevent lateral diffusion in the intercellular spaces.)

The layering of the trophoblast in the hamster placentas (fig. 11) and deer mouse placenta was essentially similar to that in the mouse and rat, except that some regions of the labyrinth were especially thin. In these regions the inner layer of trophoblast in particular was reduced in thickness. The relationship of the layers in the hemotrichorial placenta is depicted schematically in figure 1

Hemodichorial. In the rabbit (lagomorph) there are two layers of trophoblast separating the maternal blood spaces from the fetal vessels and other extraembryonic connective tissue elements in the labyrinth (figs. 12 and 14) The outer layer of trophoblast has regular thick and thin regions. (It is the thick regions of this layer that are apposed to trophoblast from the opposite side of the maternal blood space, forming "tubules from the enclosed space) Where the trophoblast of the two sides of the maternal blood spaces meet, desmosomes are found. There are also desmosomes where the cell membranes of outer and inner layers of trophoblast are closely apposed. The nuclei of the outer trophoblast are situated in the thick portions of this layer The cytoplasm extending across the thin regions is quite attenuated, and in some instances in late pregnancy shows apparent pore areas. However one can follow the cytoplasm in montages across several thin areas without coming to a partitioning cytoplasmic membrane. Therefore this layer is syncytial. There are irregular projections from the outer layer of trophoblast into the maternal blood spaces but the microvilli, which are short and blunt, are sparsely distributed (fig. 12) Where the outer layer of trophoblast is extremely attenuated it is close to the inner layer of trophoblast but only discontinuously adherent to it. In many places these thin flanges of cytoplasm are less than one-half the thickness of a mitochondrion in width. Caveolae can be seen at both surfaces of the

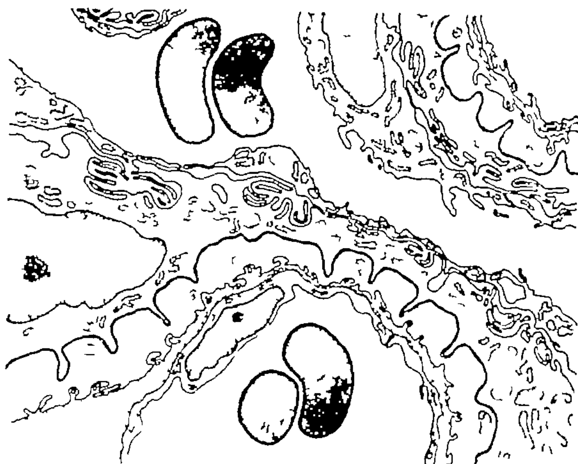


Fig 1 A schematic representation of the layering of the trophoblast in the hemotrichorial placenta. A maternal blood space cut across the picture from the upper left corner to the middle right *Fetal capillaries are seen in the middle of the bottom and the upper right corner Note* that between the two blood streams are the fetal endothelium basement membranes (cross-hatched), inner middle and outer layers of trophoblast.

outer trophoblast layer but are more common on the outer surface

The inner trophoblast layer is much less conspicuous than the outer layer It is quite thin over much of its extent with rather broadly spaced nuclear regions (fig. 13) Generally it is especially thin in the same regions where the outer layer is thin but it does not seem to have demonstrable pore regions. This layer of trophoblast does not present a smooth surface on either side but the outer surface lacks microvilli. Periodically along the inner surface however there are a few simple folded projections The basement membrane that is apposed to this layer is tenuous but is consistently present In places even in rabbit placentas from late in pregnancy two or three cells with distinct membranes separating them may be seen together in the inner layer In some of the placentas from earlier in pregnancy mitotic figures were also seen in this layer Nests of individual cells are most often found near the trophospongium There are therefore some cells in the inner layer but since flanges can ordinarily be seen extending for considerable distances and on occasion between at least two nuclei the trophoblast of this layer must be in the form of multinucleate cells or have syncytial regions. The relationship of the layers in the hemodichorial placenta of the rabbit is depicted schematically in figure 2

Labyrinthine hemomonochorial The guinea pig (histricomorph) has only a

single layer of trophoblast present in the labyrinth. This trophoblast is devoid of any evidence of cell boundaries, forming a continuous layer of syncytium varying greatly in thickness and having microvilli both on the free surface and on the basal surface (fig 16) The microvilli on the free surface (maternal blood spaces) are unevenly distributed with large numbers of long relatively uniform diameter microvilli in folds or narrowed portions of the maternal blood spaces In some places the microvilli are sufficiently numerous and extensive to suggest that they form spaces in which the maternal plasma is relatively stagnant. Although the trophoblast may be quite thick where the nuclei are situated in other places it is as thin as the diameter of a single microvillus, and indeed in these places is probably the thinnest of all of the hemochorial placentas examined. The microvilli facing the fetal side are approximately the same diameter as those of the maternal side but are largely situated in pockets and do not project as far from the surface (fig 16) The basement membrane beneath the trophoblast extends over these pockets but does not enter them. The relationship of the layers in the labyrinthine hemomonochorial placenta of the guinea pig is depicted schematically in figure 3

Preliminary observations on placental labyrinths from three chipmunks (*Eutamias quadrivittatus*) the only sciuromorphs examined show that the trophoblast in late pregnancy forms a single syncytial layer enclosing the maternal

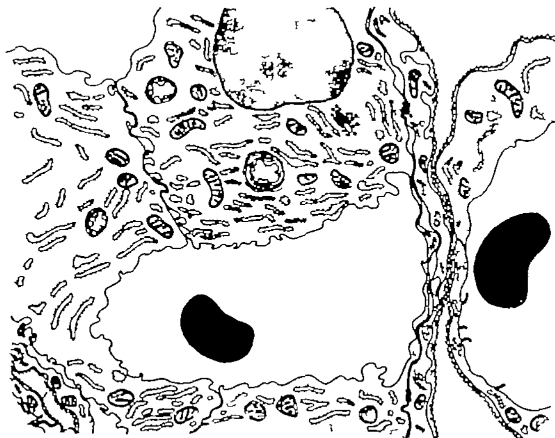


Fig. 2 A schematic representation of th[illegible] layering of the trophoblast in the hemodichorial placenta of the rabbit. A fetal capillary is [illegible] ng and maternal blood space in the lower center Note that between the fetal and mater[illegible] blood [illegible] eams are fetal endothelium basement membranes (cross-hatched) and inner [illegible] nd outer troph[illegible] last.

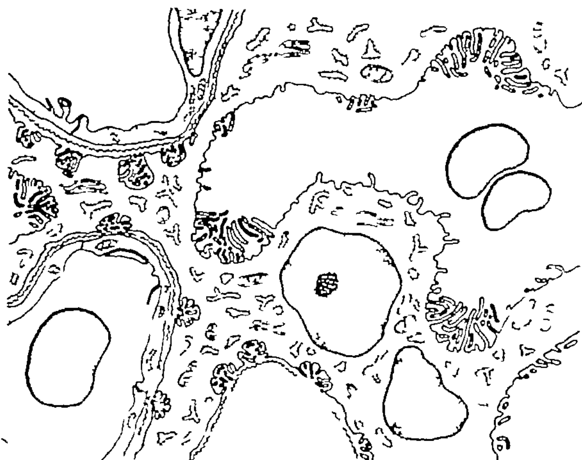


Fig. 3 A schematic representation of the layering of the trophoblast in the labyrinthine hemomonochorial placenta of the guinea pig. Fetal capillaries are seen in the upper and lower left corners. A maternal blood space is in the middle and right. Note that between the two blood streams are fetal endothelium, basement membranes (cross-hatched) and a single layer of syncytial trophoblast.

blood spaces. There are peculiar subsurface spaces under the numerous microvilli on the maternal surface of the syncytium (fig. 17). A filamentous material is present in these spaces which are in communication with the maternal blood spaces at intervals. Caveolae are present at the margins of these spaces as well as between the surface microvilli. In numerous places individual trophoblast cells are situated between the syncytium and the basement membrane. The fetal vessels are not as closely associated with the trophoblast in the labyrinth of the chipmunk placenta as they are in the guinea pig placenta.

Villous hemomonochorial. It has now been thoroughly established that the trophoblast of the villi of the late human placenta constitutes a single layer of syncytium with only scattered Langhans cells beneath it. The microvilli are numerous but short with a slightly bulbous distal end and are often branched (figs. 18 and 19). Caveolae are found at the bases of the microvilli. The trophoblast for the most part is rather thick, and the nuclei are unevenly distributed, frequently being in clusters. In some regions the trophoblast is thin, especially over vessels which may project slightly into the region of the trophoblast. The basal infoldings are not evenly distributed but tend to be grouped in clusters (fig. 19) without, however, the regularity seen in the guinea pig placenta.

The basement membrane is thick and for the most part does not extend into the invaginations.

The Langhans cells and the syncytium are usually loosely associated, except at the desmosomes formed in conjunction with the association of these two elements of the trophoblast (fig 18) The Langhans cells themselves are relatively undifferentiated. However intermediate stages of differentiation between Langhans cells and syncytium are seen, especially in young placentas. In term placentas isolated desmosomes with short fragments of membrane can occasionally be found. Even in the early placentas examined, the Langhans layer is discontinuous with processes of the syncytium reaching to the basement membrane at intervals of several Langhans cells The relationship of the layers in the villous hemomonochorial placenta of the human is depicted schematically in figure 4

The villi of the armadillo placenta are covered by a single layer of syncytial trophoblast with widely spaced, evenly distributed nuclei. At no time is there a Langhans cell layer although there are knots of cytotrophoblast (cell columns) at the tips of the growing villi in early stages. The surface of the syncytium has numerous microvilli which tend to be slightly longer especially in the early stages, and more branching than the microvilli of the human placenta (fig 20) In contrast to previous observations (Enders '60) caveolae could be seen at the bases of these microvilli (fig. 21) The trophoblast of

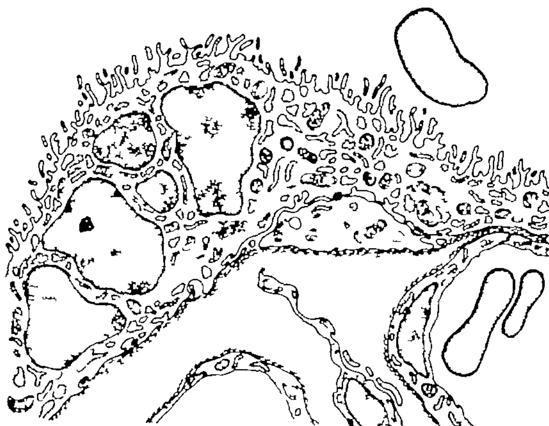


Fig. 4 A schematic representation of the layering of the trophoblast in the villous hemomonochorial placenta of the human. A fetal capillary is in the lower right. The maternal blood space is across the top. A portion of Langhans' cell seen beneath the syncytium in the middle of the picture. Note that between the fetal and maternal blood streams are fetal endothelium, basement membranes (cross-hatched) and one layer of syncytial trophoblast.

the armadillo placenta has few attenuated areas and is not ordinarily indented by fetal vessels. Infoldings of the basal plasma membrane form branching channels of small diameter which extend into the trophoblast over its entire inner surface in the later stages of pregnancy (fig 20) The basal infoldings greatly increase the surface area the amount of membrane surface appearing comparable on both sides of the trophoblast. The basement membrane is thick in later stages as in the human and in marked contrast to earlier stages. Although isolated desmosomes are found in the syncytium in early stages of pregnancy no such traces of formation of syncytium from cytotrophoblast are found in the late placenta. The relationship of the layers in the villous hemomonochorial placenta of the armadillo is depicted schematically in figure 5

Cytoplasmic organelles

Endoplasmic reticulum One of the striking features of hemochorial placentas is the abundance of granular endoplasmic reticulum particularly in whichever layer is most intimately associated with the maternal blood. In the myomorphs studied the cisternae of the endoplasmic reticulum are most abundant in the outermost layer (figs. 8 and 10) They frequently contain a moderately dense substance in the lumina of the cisternae (fig 10) The middle layer also has cisternae enclosed by ribosome-studded membranes but such cisternae are less abundant than in the outer layer There is a

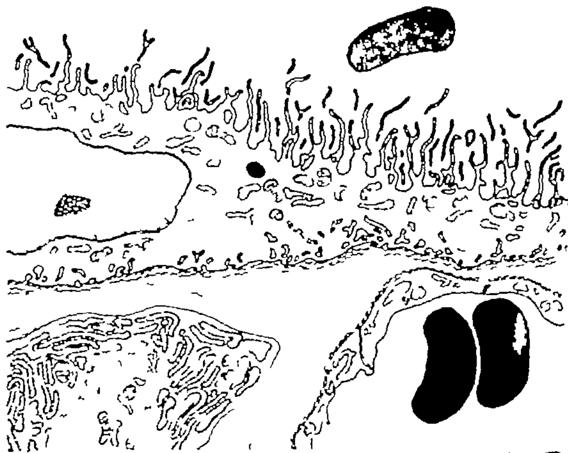


Fig. 5 A schematic representation of the layering of the trophoblast in the villous hemomonochorial placenta of the armadillo A fetal capillary is in the lower right. The maternal blood space is across the top. Note that between the two bloodstreams are fetal endothelium, basement membranes (cross-hatched) and one layer of syncytial trophoblast. A modified fibroblast, peculiar to the villi of the armadillo, is seen in the lower left

paucity of endoplasmic reticulum in the inner layer except near the nuclei and in occasional regions in which agranular endoplasmic reticulum fills the cytoplasm largely excluding other organelles.

In the rabbit also the outer layer is rich in granular endoplasmic reticulum, while it is much more sparsely distributed in the inner layer. The cisternae in the outer layer of trophoblast of the rabbit are heavily studded with ribosomes, and are frequently oriented parallel to one another often being in a plane normal to the free surface (fig. 14). There are a few strands of agranular endoplasmic reticulum in this layer also and in addition the lipid droplets are usually surrounded by agranular membranes (fig. 13). Ribosomal clusters not obviously associated with membranes are also found in the outer layer of the rabbit trophoblast.

The guinea pig, with its single layer of trophoblast, has abundant, partially dilated cisternae of endoplasmic reticulum (figs. 15 and 16). Only occasionally is a particular orientation of the cisternae of the endoplasmic reticulum apparent.

In the human, elongated cisternae of the endoplasmic reticulum with associated ribosomes are a conspicuous feature even in the term placenta (fig. 19). These cisternae are not usually well developed in the Langhans cells, but are abundant throughout the syncytium. The long axes of these cisternae are most commonly in the plane of the syncytium, but various orientations are found. In less well preserved material, the endoplasmic reticulum tends to break up forming more vesicular profiles. Some clusters of apparently free ribosomes are also present, although not as numerous as ribosomes associated with membranes. In preparations in which there is little dilation of the endoplasmic reticulum, a small amount of dense substance is present within the cisternae.

In the armadillo placenta, long strands of granular endoplasmic reticulum are present in the syncytium. Although this element is not as abundant in the armadillo as in the human, the tortuous cisternae can be followed for appreciable distances (fig. 20). The middle zone of the syncytium contains most of the endoplasmic reticulum. Cisternae here are irregular in outline but frequently course roughly parallel to the plane of the syncytium. The ribosomes along the membranes show a distinct spacing and are consequently individually discrete. The cells of the cell columns in younger placentas have numerous clusters of free ribosomes but less abundant cisternae of the endoplasmic reticulum. These cisternae are often relatively devoid of ribosomes. The armadillo trophoblast has less granular endoplasmic reticulum than the other species examined, but it should be noted that the armadillo placenta, unlike the others, has a modified fibroblast element in late pregnancy which is packed with cisternae of the endoplasmic reticulum.

Golgi. In hemochorial placentas Golgi membranes and vesicles are found throughout the cytoplasm, not just in the proximity of the nuclei. Typically four or five pairs of Golgi membranes with a few associated vesicles are found occupying an area about 2½ µ long. Dilations are frequently present at the ends of the cisternae. In the myomorphs examined such clusters of Golgi membranes and vesicles are found in all three layers of trophoblast (figs. 7, 8, 9) and may be present either superficial or deep to the nucleus, in addition to isolated areas well away from the nuclei. Although orientation of the axis of the cisternae parallel to the surface is most common, other orientations are also frequent. In the inner layer of trophoblast, Golgi membranes are rather rare, but may on occasion occupy most of the cytoplasm between the inner and outer membranes of this layer. One cannot therefore attribute a secretory polarity to the myomorph trophoblast, according to the position of the Golgi.

In the rabbit, clusters of Golgi membranes and vesicles are rarely more than 1 µ in diameter and, in contrast to the endoplasmic reticulum and lamellae-surrounded lipid, are a rather inconspicuous feature (fig. 14). Even in the inner trophoblast layer where endoplasmic reticulum is less abundant, the Golgi is inconspicuous.

In contrast to the other forms studied, the Golgi membranes of the guinea pig

trophoblast (fig 15) are extensive They tend to be arranged in linear fashion along the course of the trophoblast. Each set of Golgi membranes consists of five or six pairs of cisternae Although the membranes are slightly dilated, no dense substance is seen within the cisternae and Golgi vesicles are not particularly abundant Frequently the Golgi membranes are basally situated being between the endoplasmic reticulum and the basal microvilli

Golgi membranes are a common feature of the syncytium of the human term placenta However such regions are generally small clusters of membranes with a great abundance of vesicles (fig 18) Unlike in other species, some Golgi regions in the human appear to have more vesicles than cisternae In a number of Golgi regions dense granular material can be seen in association with one or more of the membrane pairs and in vesicles near the Golgi zone (fig 19) In other regions only small vesicles are found. Golgi membranes and vesicles may be found in any region of the syncytium but are more common basally than apically

The Golgi membranes and vesicles are somewhat more conspicuous in the Langhans cells due apparently to the lesser density of the background cytoplasm in these cells. In addition the cisternae seem more dilated in the Langhans cells

The individual clusters of Golgi membranes and vesicles in the syncytial trophoblast of the armadillo are slightly larger than in the other species (fig 20) but are not as linearly extensive as in the guinea pig The membrane pairs may number more than five and the associated vesicles are usually similar in diameter to the width of the cisternae Although fairly large clusters may be formed, associated granules are rather rare (fig 21) In general the Golgi is found in the central layer in which the endoplasmic reticulum is located or towards the basal side of this layer Only small relatively inconspicuous Golgi zones are present in the cells of the cell columns

Mitochondria The mitochondria of the trophoblast of hemochorial placentas are rather ordinary Unusual sizes and shapes such as are found in the uterus are lacking in the placenta. For the most part the mitochondria are moderately small with granular and short rod shapes predominating although branching forms are quite common The mitochondria generally have a fairly dense matrix The cristae are numerous but not tightly packed, and may be oriented in almost any direction (fig 8) Angular processes are seen on many of the cristae In the trophoblast of labyrinths of myomorphs the mitochondria of all three layers are approximately the same size Mitochondria are quite sparse in the inner layer and only moderately abundant in the middle and outer layers. A few more elongated forms are found in the outer cellular layer than in the two syncytial layers In the more elongated mitochondria of all three layers there is a tendency for the cristae to be at right angles to the long axis.

In the rabbit trophoblast mitochondria are spherical Those in the inner layer tend to be somewhat smaller as well as more sparse than in the outer layer However where there are pockets of relatively undifferentiated cells in the inner layer the mitochondria are larger The mitochondria in the guinea pig trophoblast are somewhat more elongated than in the other species There is a pronounced tendency for the cristae to be oriented at right angles to the long axis but they are generally not tightly packed.

The mitochondria of the human placenta are more numerous than in the other types studied (fig 18) The abundant mitochondria in the syncytium are small with a dense matrix and very irregular cristae which frequently course parallel to the external membrane of the mitochondrion. The mitochondria of the Langhans cells both in the early and later stages are larger and sparser than those of the syncytium and have more regular cristae The mitochondria of the armadillo syncytium are quite irregular having both round and elongated forms with short cristae which may be oriented in any direction There tends to be a zonation of the mitochondria with the largest numbers being found a short distance under the maternal surface of the syncytium (fig 20) Where the syncytium is thick a secondary less obvious concentration of mito-

chondria is found at the basal surface. In early pregnancy when cells of the cell columns are present, the mitochondria in these cells are sparsely distributed.

Microtubules are abundant in the syncytial trophoblast of all the placentas and in the cytotrophoblast of the outer layer of the hemotrichorial placentas. In some instances the microtubules are clustered, particularly where they are highly abundant in the first and second layers of the hemotrichorial placenta. However no centrioles are found in association with the clustered microtubules. Indeed the paucity of centrioles is a striking feature of the trophoblast. One centriole was seen in the syncytium of the human placenta. Another centriole was found in the outer layer of trophoblast in the rabbit placenta, and one in the syncytium of the chipmunk labyrinth, but none were seen in the other placentas.

Inclusions

As might be expected from a tissue such as the placenta which in the course of its transient existence, performs such a wide number of functions, almost all types of reported inclusions can be found at one time or another. Myelin figures multivesicular bodies crystalloid structures etc., were seen. However only those inclusions whose occurrence was sufficiently consistent to have an observed specific distribution are included here.

Lipid inclusions. In all the myomorphs examined there are large lipid droplets of a uniform, rather light intensity in the inner layer of trophoblast (a feature previously reported in the rat by Wislocki and Dempsey '55a). These droplets, in late pregnancy are several microns in diameter (fig. 9). A few fine droplets may be found elsewhere in the mouse and rat. In the hamster lipid droplets that are generally denser than those in the inner layer are found irregularly distributed in the middle layer of trophoblast (fig. 11). In the rabbit the lipid droplets are a conspicuous feature of the outer layer of trophoblast (fig. 13). They may show evidence of extraction in some instances and are commonly surrounded by agranular membranes.

Lipid droplets are not a conspicuous feature of the guinea pig trophoblast. Although some fine lipid droplets can be found in the guinea pig placenta, myelin figures and droplets with areas of differential density or fine dark granules, are more common (fig. 15). The latter inclusions resemble the lipid pigments which have been identified in other organs. Such granules are not as abundant in the trophoblast of the other placentas examined.

The distribution of lipid droplets has already attracted attention in the human placenta, in which they are very abundant in the syncytium during early stages of pregnancy and decrease in abundance in the later stages (Wislocki and Dempsey '55b Terzakis, '63 Lister '64). This change in abundance of lipid was also observed in comparing villi from the first trimester with those from term placentas. There is very little lipid visible in the armadillo trophoblast, although high levels of progesterone may be extracted from the placenta.

Glycogen. In the myomorphs, the distribution of glycogen in the labyrinth is somewhat uneven, but when present in the trophoblast it is most abundant in the middle layer (fig. 11) with some deposits in the inner layer. Neither the guinea pig nor the rabbit show appreciable glycogen in the trophoblast (exclusive of the trophospongium).

Glycogen is not abundant in the later villous placentas although it is found in the cytotrophoblast of both the human and the armadillo in the earlier placentas. It is never abundant in the syncytium of these placentas.

Filamentous structures. Filaments are found in the trophoblast in small groups associated with desmosomes, and in larger aggregations which cannot be associated directly with desmosomes. In the myomorphs a few short filaments are found in association with the desmosomes between the middle and outer layers. Larger aggregations of filaments are present in the outer layer of trophoblast where groups of filaments having the same general direction form large bundles (fig. 10). Such groups of filaments, although common, are not seen in all micrographs of this region.

Most of the filaments present in the trophoblast of the rabbit placenta are as-

sociated with the numerous desmosomes. The filaments seem to be particularly abundant in association with the desmosomes between the two layers In the guinea pig trophoblast small branching bundles of filaments are present in the syncytium. Since desmosomes are not present such filaments cannot be associated with these structures In general the filaments are found in thicker portions of the trophoblast coursing at slight angles to the surface *No particular region of the cytoplasm appears particularly prone to have filaments*

In the human fine filaments are associated with the desmosomes between the Langhans cells and the syncytium (fig. 18) Such filaments occur in long slender groups. When isolated desmosomes are found in the syncytium, fine filaments are often seen associated with them. Thin groups of filaments are also present in regions of the syncytium where no cell membranes or desmosomes are found In the armadillo placenta larger aggregates of filaments are present particularly in the midregions of the syncytial trophoblast. The bundles of filaments are branching and confluent in the cytoplasm at the nuclear level in some regions of the villi (fig. 22) Since there are no desmosomes in the older villi, such large filamentous bundles cannot be associated with these structures.

A peculiar fibrous structure was present in the middle layer of trophoblast in several of the rat and mouse placentas (fig 9) The coiled nature and definite spacing of this material made it appear to be a linearly arranged molecular aggregate

Fetal blood vessels Caveolae are found in endothelial cells of the fetal capillaries of all placentas They are more abundant in some places than in others but no particular correlation between abundance and position or other structural feature was observed. The largest number of vesicles per stretch of endothelial cell cytoplasm was found in the capillaries of the hamster placenta. In all three of the myomorphs examined sieve areas are found in some of the endothelial cells In many instances a thin central membrane could be seen cutting across individual pores. Frequently caveolae and sieve areas are seen within the same short stretch of endothelium. Irregular folds projecting into the lumen of the capillaries, especially at the junctions between endothelial cells, are abundantly present in the myomorph placentas. Such folds are also present in capillaries of other placentas but are not as extensive in nature

The endothelial cells of the rabbit and guinea pig placentas are frequently quite attenuated, but do not contain sieve areas. The endothelial cells of the villous placentas are not especially thin and although they have caveolae do not have sieve areas.

DISCUSSION

Indications of complex layering of trophoblast that can be seen by electron microscopy have been reported in individual studies on different species ever since Wislocki and Dempsey ('55a) first observed the wealth of cell membranes in the rat placenta The observations of these authors were extended by Schiebler and Knoop ('59) and more recently by Jollie ('64) who has described changes which occur in the rat placenta during the gestation period indicative of increased permeability and who designated the layers from maternal blood to fetal mesenchyme trophoblast I trophoblast II and element III Early studies on electron microscopy of the human placenta (Wislocki and Dempsey '55b Boyd and Hughes '54 Bargmann and Knoop '59 Rhodin and Terzakis '62) showed clearly the presence of Langhans cells at term While later studies have been more concerned with the cytology of the trophoblast (Terzakis '63, Lister '63a, '63b '64) the method in which Langhans cells may contribute to the syncytium remains a point of interest (Carter '64 Enders 64) Studies on the rabbit placenta (Larsen, '63a '63b Luse '57) and guinea pig yolk sac and subplacenta (Dempsey '53 Davies et al., '61) have not dealt specifically with the labyrinth although Wislocki and Dempsey in the previously mentioned paper on the rat did present evidence that the rabbit labyrinth was hemochorial rather than hemoendothelial. Despite the wealth of information concerning the structure of the trophoblast added by these studies the na

ture of the layering in species other than the human has remained somewhat obscure.

One of the most striking features of this study was the consistent nature of the patterns of layering observed. The hemochorial class of placentas is very large and the examples reported here cannot be considered comprehensive. While we therefore cannot be certain that other examples of hemodichorial placentas will be found, certainly we can expect there to be many more examples of the hemotrichorial placenta and probably the labyrinthine hemomonochorial placenta also It is interesting that no example of a cellular hemomonochorial placenta has yet been found. In both the labyrinthine and villous hemomonochorial placenta the only continuous layer of trophoblast is syncytial. It is also interesting that in myomorphs there are two apparently syncytial layers sufficiently closely apposed to form tight junctions, which nevertheless do not fuse. The origin of this trilayered pattern is not yet known, but Dr Mossman ('64) has suggested that these layers may represent the three sources of trophoblast in the rodent placenta — the giant cells, the trager epithelium, and the true chorionic epithelium. Should this suggestion prove to be the case a number of variations in layering might be expected to be found within the myomorphs

The possibility that an area of relative stasis of the maternal plasma may be important for absorption is definitely suggested by a comparison of the morphology of the different placentas. In all of the placentas the caveolae are situated principally in areas less directly associated with the maternal blood than many other regions of the surface membrane of the trophoblast.

In the hemotrichorial placenta the area with the greatest number of caveolae is the second layer The space between the first and second layer would be expected to be an area of relatively slow exchange with the maternal blood spaces In the labyrinth of the rabbit placenta, two possible areas of stasis are present one, where the two folds of surface trophoblast come together and another between the outer and inner layers of trophoblast Caveolae are most abundant in the former location. In the guinea pig placenta, groups of large microvilli projecting from the trophoblast into the maternal blood spaces form areas in which the flow of plasma would probably be slowed. In the chipmunk, the presence of an area of relative stasis is particularly striking There are subsurface spaces in the trophoblast of this species in which the rate of flow of maternal plasma would be severely reduced, since these spaces are joined to the surface only by narrow communicating channels.

The villous placentas with their less ordered arrangement of maternal blood spaces, tend naturally to have more static regions than do labyrinthine placentas in which a counter current flow is believed to exist (Mossman '26 '37) In the human placenta the blood both enters and leaves through the basal plate (Ramsey '62) Consequently relatively static areas would definitely be expected. In addition, however the microvilli are bulbous at their distal tips and are frequently branching and irregularly arranged which features would tend to produce localized regions of interference with the flow of plasma. It is at such regions that caveolae are most abundant. In the armadillo the path of maternal blood flow is more unidirectional, since the blood enters beneath the residual endometrium and exists through the myometrium (Enders, '60) In this species the branched and extensive microvilli along the surface of the trophoblast form numerous pockets where most of the caveolae are found.

In all of the placentas examined, the layer of trophoblast in closest association with the maternal blood showed highly developed granular endoplasmic reticulum This was true whether there were one two or three layers of trophoblast. The situation of these cells, which can be assumed to be protein producing, in close proximity to the maternal blood would naturally decrease the diffusion distance for respiratory exchange and thus increase the efficiency of energy utilization in the process of protein synthesis. In the hemotrichorial placenta and probably the hemodichorial placenta the products of such synthetic activity would have more ready access to the maternal blood than the fetal blood.

sociated with the numerous desmosomes. The filaments seem to be particularly abundant in association with the desmosomes between the two layers In the guinea pig trophoblast small, branching bundles of filaments are present in the syncytium. Since desmosomes are not present, such filaments cannot be associated with these structures. In general the filaments are found in thicker portions of the trophoblast, coursing at slight angles to the surface. No particular region of the cytoplasm appears particularly prone to have filaments.

In the human fine filaments are associated with the desmosomes between the Langhans cells and the syncytium (fig 18) Such filaments occur in long slender groups. When isolated desmosomes are found in the syncytium fine filaments are often seen associated with them. Thin groups of filaments are also present in regions of the syncytium where no cell membranes or desmosomes are found. In the armadillo placenta, larger aggregates of filaments are present, particularly in the midregions of the syncytial trophoblast. The bundles of filaments are branching and confluent in the cytoplasm at the nuclear level in some regions of the villi (fig. 22) Since there are no desmosomes in the older villi, such large filamentous bundles cannot be associated with these structures.

A peculiar fibrous structure was present in the middle layer of trophoblast in several of the rat and mouse placentas (fig 9) The coiled nature and definite spacing of this material made it appear to be a linearly arranged molecular aggregate

Fetal blood vessels Caveolae are found in endothelial cells of the fetal capillaries of all placentas. They are more abundant in some places than in others but no particular correlation between abundance and position or other structural feature was observed. The largest number of vesicles per stretch of endothelial cell cytoplasm was found in the capillaries of the hamster placenta. In all three of the myomorphs examined, sieve areas are found in some of the endothelial cells. In many instances a thin central membrane could be seen cutting across individual pores. Frequently caveolae and sieve areas are seen within the same short stretch of endothelium. Irregular folds projecting into the lumen of the capillaries especially at the junctions between endothelial cells, are abundantly present in the myomorph placentas. Such folds are also present in capillaries of other placentas, but are not as extensive in nature

The endothelial cells of the rabbit and guinea pig placentas are frequently quite attenuated, but do not contain sieve areas. The endothelial cells of the villous placentas are not especially thin and, although they have caveolae do not have sieve areas.

DISCUSSION

Indications of complex layering of trophoblast that can be seen by electron microscopy have been reported in individual studies on different species ever since Wislocki and Dempsey ('55a) first observed the wealth of cell membranes in the rat placenta The observations of these authors were extended by Schiebler and Knoop ('59) and more recently by Jollie ('64) who has described changes which occur in the rat placenta during the gestation period indicative of increased permeability and who designated the layers from maternal blood to fetal mesenchyme trophoblast I, trophoblast II and element III Early studies on electron microscopy of the human placenta (Wislocki and Dempsey '55b Boyd and Hughes, '54 Bargmann and Knoop '59 Rhodin and Terzakis '62) showed clearly the presence of Langhans cells at term. While later studies have been more concerned with the cytology of the trophoblast (Terzakis '63 Lister '63a, '63b '64) the method by which Langhans cells may contribute to the syncytium remains a point of interest (Carter '64 Enders '64) Studies on the rabbit placenta (Larsen '63a, '63b Luse '57) and guinea pig yolk sac and subplacenta (Dempsey '53 Davies et al., '61) have not dealt specifically with the labyrinth, although Wislocki and Dempsey in the previously mentioned paper on the rat did present evidence that the rabbit labyrinth was hemochorial rather than hemoendothelial. Despite the wealth of information concerning the structure of the trophoblast added by these studies, the na-

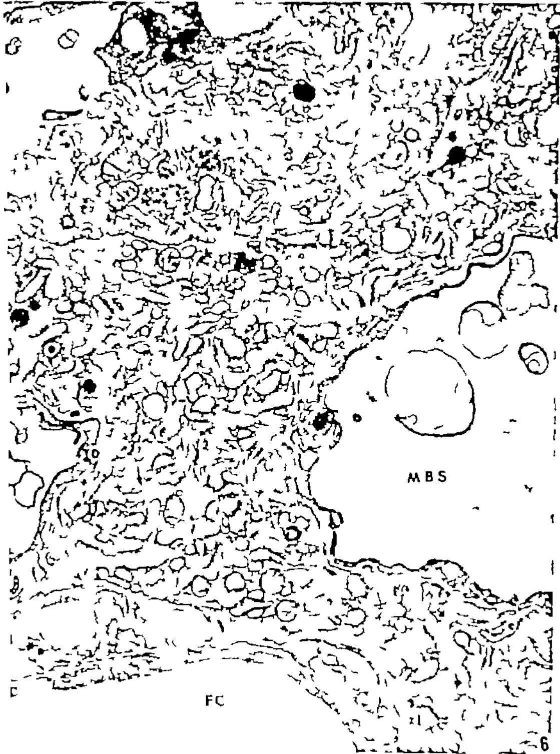

MBS
FC
6

PLATE 2

EXPLANATION OF FIGURE

7 In this section of the rat labyrinth, both the thin outer layer of trophoblast and middle layer have caveolae (small arrows) There is an pparent pore in the outer layer of trophoblast (large arrow) Note the desmosome to the right of the pore. The outer surface of the middle layer is folded (upper left) ER, endoplasmic reticulum; G Golgi; Gly glycogen; L, lipid; M, mitochondrion. × 31,000.


MBS
ER
G
FC

PLATE 3

EXPLANATION OF FIGURES

8 Portion of an outer trophoblast cell from the mouse placenta. Note the abundance of granular endoplasmic reticulum, the well developed Golgi, and the microtubules (large arrows). N nucleus × 28,000

9 The inner layer of trophoblast (S) at the left and the middle layer at the right in this picture of the labyrinth of the rat. Note how closely apposed the cell membranes of these two layers are. They probably form a tight junction to the right of the lipid droplet (L). In the upper right corner is an accumulation of a peculiar fibrous material seen in many of the rat and mouse placentas. G Golgi. × 60,000.

N

8

L

9

PLATE 4

EXPLANATION OF FIGURES

10 A junction between outer trophoblast cells is seen t the left of this picture of the rat labyrinth. At the top of the cell in the center a bundle of filaments may be seen in longitudinal section. A cross section of series of filaments is seen in the lower right of this cell. The slightly dilated endoplasmic reticulum seen here is quite commonly found in this layer × 28,500.

11 The layers of trophoblast of the hemotrichorial placenta of the hamster are seen in this picture. Note the folding of the surface of the middle layer and the caveolae (arrows) Lipid droplets like the large one in the middle of the picture are often found in this layer of the hamster placenta. The large granules to the right in the middl layer are glycogen. × 26,000.

10

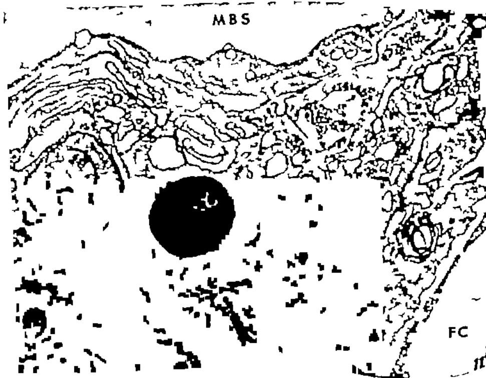


PLATE 5

EXPLAN TION OF FIGURE

12 A portion of the labyrinth of the hemodichorial placenta of the rabbit. Note the inner layer of trophoblast extending along the left side of the picture, and that thin flange of outer trophoblast extends over it at the bottom. The outer trophoblast from the two sides of the maternal blood space comes together t the top of the picture. The two cell membranes are indistinct where they are cut tangentially in this rather thick section. Note the numerous caveolae one of which is indicated (arrow) near the junction of the outer layers of trophoblast. G Golgi. × 28,500.


M.B.S.
FC
12

PLATE 5

EXPLANATION OF FIGURE

12 A portion of the labyrinth of the hemodichorial placenta of the rabbit. Note the inner layer of trophoblast extending along the left side of the picture, and that thin flange of outer trophoblast extends over it at the bottom. The outer trophoblast from the two sides of the maternal blood space comes together t the top of the picture. The two cell membranes are indistinct where they are cut tangentially in thi rather thick section. Note the numerous caveolae, one of which is indicated (arrow) near the junction of the outer layers of trophoblast. G Golgi. × 28,500.

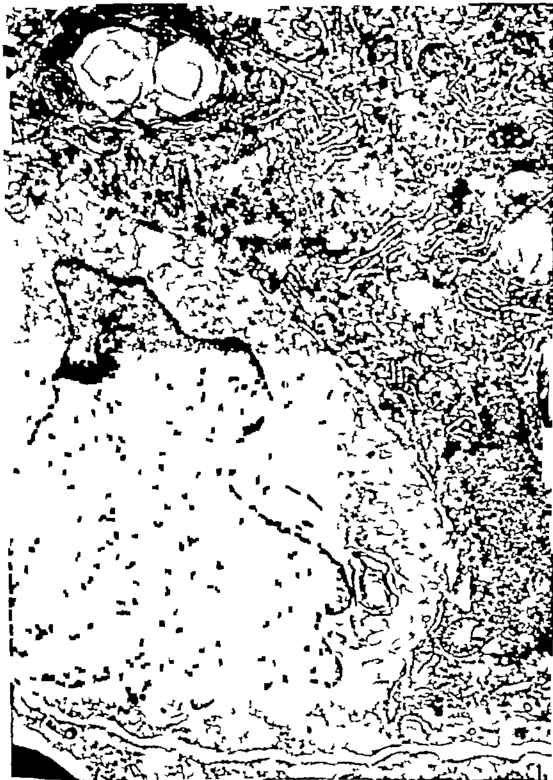


PLATE 7

EXPLANATION OF FIGURES

14 A region of apposition of the outer trophoblast from the two sides of the maternal blood space of the labyrinth of the rabbit. The parallel array of endoplasmic reticulum at right angles to the surface of the trophoblast seen here is common. G, Golgi. × 28,000

15 A portion of the syncytium of the labyrinthine hemomonochorial placenta of the guinea pig. Note the abundance of filamentous material and dark lipid pigment granules. There are numerous caveolae around the maternal blood space both in communication with it (arrows) and seen as isolated vesicles in section. The Golgi (G) is frequently even more extensive than it appears in this picture. × 20,000.

FC
14

MBS
FC
15

PLATE 8

EXPLANATION OF FIGURE

16 Portion of the labyrinth of the hemomonochorial placenta of the guinea pig. Note the pockets containing microvilli in the trophoblast adjacent to the basement membrane as well as the numerous microvilli in the two maternal blood spaces. The abundance of granular endoplasmic reticulum seen in this picture is typical of the guinea pig placenta, but it is unusual to see a stretch of cytoplasm this extensive without Golgi membranes. A myelin figure is seen at the left. × 20,500


FC
MBS
MBS
FC
16

PLATE 9

EXPLANATION OF FIGURE

17 A section of the labyrinthine hemomonochorial placenta of the chipmunk. There are extensive subsurface spaces containing filamentous material beneath the microvilli. An apparent point of continuity with the maternal blood space is seen at the large arrow. Numerous caveolae, such as that indicated by the small arrow, are present both off the subsurface spaces and at the base of the microvilli. The fetal capillary (FC) shows some evidence of distortion by swelling of the endothelial cells. Note the folding of the basal surface of the syncytium on the basement membrane. × 21,500.


FC

PLATE 10

EXPLANATION OF FIGURE

18 A portion of villus of the hemomonochorial placenta of the human is seen here Note the filaments associated with the desmosomes at the junction between the Langhans cell and the syncytium. Note also the many Golgi vesicles in the Golgi zones (G) Caveola (arrows) × 25,000.


MBS
G

PLATE 11

EXPLANATION OF FIGURE

19 A portion of villus of the hemomonochorial placenta of the human. Note the association of granules with the Golgi zones (large arrow) The infolding of the basal cell membrane seen here is typical, as i the bundance of granular endoplasmic reticulum. × 27,000.


MBS
V
11

PLATE 12

EXPLANATION OF FIGURE

20 A portion of villus from the hemomonochorial placenta of the armadillo. The zonation of the syncytium is clearly seen in this slightly tangential section. The tubular infoldings of the basal cell membrane, although exaggerated in extent by the angle of the section, are typical of the armadillo placenta. × 28,000.


MBS
20

PLATE 13

EXPLANATION OF FIGURES

21 A portion of a villus from the hemomonochorial placenta of the *armadillo. Caveolae (arrows) are common in pickets formed by the* microvilli. Note the abundance of endoplasmic reticulum. × 26,000.

22 A section parallel to the surface through the mid region of the syncytium of the hemomonochorial placenta of the armadillo. Note that the bundles of filaments branch and rejoin. Two Golgi zones are seen in face section at the left of the picture. N nucleus. × 43,000

MBS

21

22

Stereotaxic Localization of Supraoptic Ventromedial and Mamillary Nuclei in the Hypothalamus of Weanling to Mature Rats [1]

LEE L. BERNARDIS AND FLOYD R. SKELTON
Department of Pathology State University of New York at Buffalo, Buffalo New York

ABSTRACT Bilateral symmetrical electrolytic lesions were placed in the supraoptic, ventromedial and mamillary areas in groups of albino rats weighing 50, 100, 150, 200 250 and 300 gm.

The localization of the lesions was correlated with the coordinate setting used with the stereotaxic instrument.

The diagrams presented contain the data for the antero-posterior lateral and dorso-ventral coordinates plotted against the body weight of the respective groups and allow the extrapolation of coordinates for other hypothalamic structures.

The great interest in the role of the hypothalamus in homeostasis and the extensive use of the rat in this field of research has led to the preparation of anatomical atlases of the rat diencephalon (Gurdjian '27; Massopust, '56 De Groot, '59 Massopust, '61) and of the rat hypothalamus (Krieg, '32)

Literature on the anatomy of the rat hypothalamus is not voluminous (Gurdjian, '28 Krieg, '32 Clark, '39) and shows a conspicuous poverty of data regarding the change of stereotaxic coordinates for the localization of nuclei for rats of various body weights and ages.

The loci of hypothalamic nuclei and fiber tracts of rats above 250 gm body weight are regarded as constant. This is not the case in rats of lower body weights. When anatomical atlases of the rat diencephalon and hypothalamus do consider body weights, they usually consider rats weighing about 200 gm (Krieg 46; De Groot, '59 Massopust, '59 '61) Data which would allow one to use exact coordinate settings on the stereotaxic instrument are not given for animals below 100 gm body weight.

The purpose of the present study was to determine such coordinate settings for the hypothalamus of albino rats between 50 and 300 gm body weight. Rather than fine details of histological structure workable data are presented for use with modified Horsley-Clarke stereotaxic instruments

Three hypothalamic areas have been chosen as landmarks the supraoptic, the ventromedial and the mamillary This choice was made because previously reported work by this and other authors (Endröczi et al., '57 Hinton and Stevenson, '59 Bernardis et al., '63) demonstrated the control that these structures exert on growth and metabolism.

MATERIALS AND METHODS

Seventy-one male albino rats of the Charles River strain (SD) were divided according to body weight into six groups so that the mean weight of each group was about 50 100 150 200 250 and 300 gm respectively All animals received bilateral symmetrical lesions with the aid of a modified Horsley-Clarke stereotaxic instrument (Baltimore Instrument Co., Model S., Head Holder 63 11 01) A direct current of 1.5 mA flowed for 10 seconds from the bared tip of an enamel coated sewing needle (0 48 mm diameter) which served as anodal electrode. Attempts were made to place lesions as precisely as possible in the supraoptic ventromedial and mamillary nuclei.

After 2 to 3 weeks the brains were removed from the fixative and trimmed with a razor blade to obtain the hypothalamic blocks. After dehydration and paraffin em-

[1] This investigation was supported by Public Health Service Research Grant no. HE-06975, from the National Heart Institute.

bedding sections were cut at 12 μ mounted and stained with cresyl violet. Using a microprojector the sections were projected and the extent of the hypothalamic de struction outlined in schematic drawings of coronal sections of the hypothalamus taken from Krieg ('32) Two of these diagrams are presented in figures 1 and 2. The six coronal planes are located in the following antero-posterior levels: (1) optic chiasma, (2) paraventricular nuclei, (3) median eminence (ventromedial nuclei),

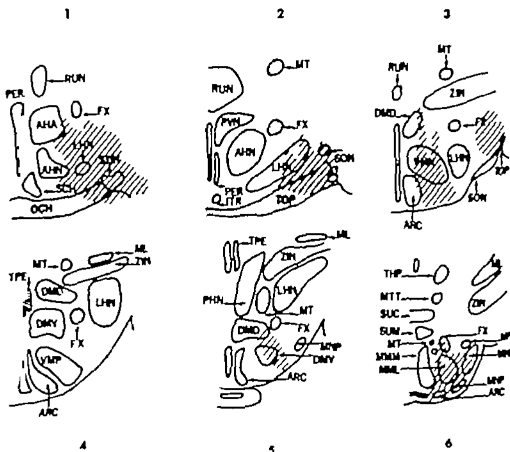


Fig. 1 Localization of lesions in the supraoptic, ventromedial and mamillary nuclei in rats of ?? gm body weight.

Abbreviations

AHA, Anterior hypothalamic area
AHN Anterior hypothalamic nucleus
ARC, Arcuate nucleus
DMD Dorsomedial hypothalamic nucleu (dorsal)
DMV Dorsomedial hypothalamic nucleus (ventral)
FX, Fornix
ITR, Infundibular tract
LHN Lateral hypothalamic nucleus
ML, Medial lemniscs
MMM, Medial mamillary nucleus (medial part)
MML, Medial mamillary nucleus (lateral part)
MNL, Lateral mamillary nucleus
MNP Prelateral mamillary nucleus
MPE, Mamillary peduncle
MT Mamillo-thalamic tract
MTT Mamillo-tegmental tract
OCH Optic chiasm
PER, Periventricular nucleus (ant. region)
PHN Posterior hypothalamic nucleus
PVN Paraventricular nucleus
RUN Nucleu reuniens hypothalami
SCH, Suprachiasmatic nucleus
SON Supraoptic nucleus
SUC Supramamillary commissure
SUM, Supramamillary nucleus
TPE, Periventricular tract
THP Habenulo-peduncular tract
TOP Optic tract
VMN Ventromedial nuclei
VMP Ventromedial nucleus (posterior)
ZIN Zon incerta

(4) ventral dorsomedial nuclei, (5) dorsal dorsomedial nuclei, (6) mamillary nuclei.

The stereotaxic coordinates are given with reference to the following zero planes: AP (antero-posterior)-intraaural line passing thru the external auditory meati, i.e. the ear bars of the head holder DV (dorso-ventral) — distance of tip of electrode from vertex of brain, ventrally towards the base. RL (lateral) distance from the mid-sagittal line, i.e. the mid-sagittal sinus.

RESULTS

Figure 3 shows the stereotaxic coordinates for the supraoptic ventromedial and mamillary nuclei in rats from 50 to 300 gm body weight. It has been found that the localization of these nuclei for rats of any body weight between 50 and 300 gm can be obtained by simple extrapolation from these graphs.

Figure 1 shows the actual localization of lesions in rats of 50 gm body weight, and figure 2 shows the same for rats of 300 gm body weight.

DISCUSSION

In the few anatomical descriptions of the rat hypothalamus that are available little specific mention is made of the weight and the age of the animals used. Gurdjian ('26 '27) did not state weight and age. De Groot ('59) used rats of 200 to 300 gm body weight for his atlas of the rat diencephalon. Only Massopust ('56) prepared scaled coordinates of the rat brain which took into consideration the different sizes of the rats used (100 to 300 gm) In another study ('61) Massopust used

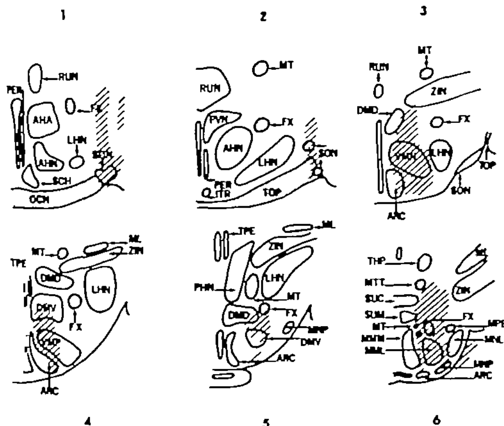


Fig. 2 Localization of lesions in the supraoptic, ventromedial and mamillary nuclei in rats of 300 gm body weight.

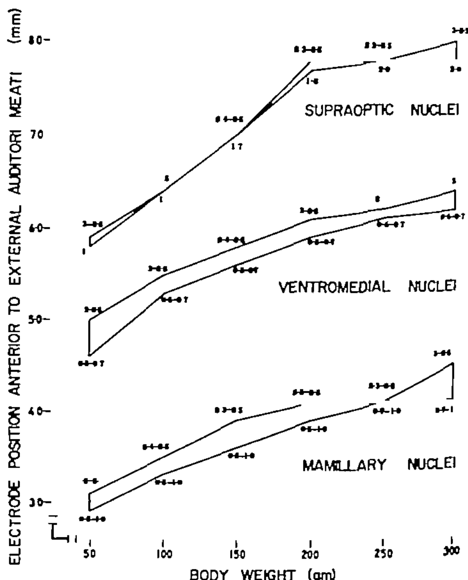


Fig. 3 Antero-posterior (ordinate) dorso-ventral and lateral stereotaxic coordinates for the supraoptic, ventromedial and mamillary nuclei of the hypothalamus of male rats from 50 to 300 gm body weight (abscissa) The figures on top of the curve indicate the dorso-ventral coordinates, the figures below the curve denote the lateral coordinates (see Materials and Methods)

rats of 200 gm body weight and emphasized the importance of correction factors for rats of this and lower body weights These atlases have proved adequate and it was not intended to repeat the work of these authors. The present investigation deals specifically with the localization of the supraoptic ventromedial and mamillary nuclei and has been prepared for use with rats of a wide weight and age range These nuclei have been chosen for two reasons First, they represent characteristic landmarks within the hypothalamus by virtue of their most anterior medial and most posterior position, respectively Second, these nuclei have been shown to affect key roles in homeostasis. The supraoptic nuclei have been demonstrated to be

the formation site of antidiuretic hormone (ADH)(Hild and Zetler '54) and have been shown to affect somatic growth (Hinton and Stevenson, '59 Bernardis et al. '63). The ventromedial nuclei are involved in the control of feeding behavior (Brobeck et al., 46 for review see Anand, '61) and the mamillary nuclei appear to be involved in the response to stress (Porter '53) Apart from the importance of locating these nuclei in rats of various ages for developmental studies the present coordinates allow some measure of extrapolation as to the location of other hypothalamic structures.

ACKNOWLEDGMENTS

The authors gratefully acknowledge the assistance of Mrs. Luisa Bohacek and Mr Richard Brennan. The photography was done by Mr. Emanuel Kaufman. They are thankful to Dr Donald G. Montemurro University of Western Ontario Institute of Cancer Research, London, Canada, for many helpful suggestions.

LITERATURE CITED

Anand, B. K. 1961 Nervous regulation of food intake. Physiol. Rev 41 677–708

Bernardis, L. L., B. M. Box and J A. F Stevenson 1963 Growth following hypothalamic lesions in the weanling rat. Endocrinology 72. 684–692.

Brobeck, J R. 1946 Mechanisms of the development of obesity in animals with hypothalamic lesions. Physiol. Rev., 26: 541–559

Clark, G. 1939 The use of the stereotaxic instrument in the rat. Science, 90 92.

De Groot, J 1959 The rat forebrain in stereotaxic coordinates. Verhandelingen der Koninklijke Nederlandse Akademie van Wetenschappen. Afd. Natuurkunde, Twede Reeks, Deel 17 no. 4, N. V Noord — Hollandsche Uitgevers Maatschappij Amsterdam, pp. 40.

Endröczi, E., S. Kovacs and G. Szalay 1957 Einfluss von Hypothalamusläsionen auf die Entwicklung des Körpers und verschiedener Organe bei neugeborenen Tieren, Endokrinologie, 34 168–175.

Gurdjian, E. S. 1926 The hypothalamus in the rat. Anat. Rec., 32 206.

——— 1927 The diencephalon of the albino rat. J. Comp. Neur., 43: 1–114.

Hild, W., and G. Zetler 1953 Experimenteller Beweis fuer die Entstehung der sogenannten Hypophysenhinterlappenhormone im Hypothalamus. Pflügers Arch., 257 169–201.

Hinton, G. G., and J A. F Stevenson 1959 The effect of hypothalamic lesions on the growth of young rats. Fed. Proc., 18 69.

Krieg, W J S. 1932 The hypothalamus of the albino rat. J Comp. Neur., 55 19–89

Massopust, L. C., Jr. 1956 The rat brain in stereotaxic coordinates. Anat. Rec., 124 463–464.

——— 1961 Stereotaxic atlases. A. Diencephalon of the rat. In El. Stimulation of the Brain. D. E. Sheer, Ed., Hogg Foundation Research Series, Univ of Texas Press, Austin, 1961 pp. 182–202.

Porter R. W 1953 Hypothalamic involvement in the pituitary adrenocortical response to stress stimuli. Amer. J Physiol., 172 515–519.

Reichlin, S. 1960 Growth and the hypothalamus. Endocrinology 67 760–773.

Innervation of the Pulmonary Artery Bifurcation of the Cat [1]

M. ANTHONY VERITY TREVOR HUGHES AND JOHN A. BEVAN
Departments of Pathology and Pharmacology The Center for the Health Sciences University of California, Los Angeles California

ABSTRACT The gross and microscopic innervation of the bifurcation and extrapulmonary portion of the pulmonary artery in the adult cat is described. Morphopharmacologic studies indicated that the major efferent and afferent innervation is contributed by the right recurrent cardiac nerve a branch of the recurrent laryngeal.

A morphologic description of the adventitial nerve bundles, preterminal axon plexus and medial, fine unmyelinated neurites as seen in methylene blue and Bielschowsky silver preparations is given. Rare, classical, pressoreceptor arborizations of de Castro type II were identified, but evidence was presented of degenerative and regenerative neural activity in the adventitial and pre-terminal plexus manifested by irregular axonic swellings, myelin ellipsoids with vacuolation, terminal growth cones and collateral sprouting. In these degenerative zones, the plexus assumed more discontinuous organization showing features very suggestive of simple pressoreceptor system composed predominantly of de Castro type I terminations.

The *in vitro* pharmacologic studies using the isolated pulmonary artery-nerve preparation confirmed the existence of effector vasoconstrictor adrenergic sympathetic fibers in the recurrent cardiac nerve. Small unmyelinated perivasal and perivasal collateral fibers disappear or show severe degenerative changes following bilateral sympathectomy and are considered to represent the sympathetic autonomic component.

Since Hering's ('25) description of the carotid sinus reflex the neuroanatomy of specialized sensory endings and afferent nerve fibers in the walls of the great vessels has received increasing attention The morphologic observations of de Castro ('28) delineated the characteristic patterns of specialized afferent nerve terminations in the carotid sinus and provided further impetus for anatomical (Sunder Plassmann, '30 Abrahám '53) and physiological studies (for review see Heymans and Neil, '58) Subsequently other specialized vascular reflexogenic zones, containing a predominance of pressoreceptor (baroreceptor) endings have been identified in the cat and include the aortic common carotid, coronary and brachiocephalic trunk areas.

Recent evidence has suggested that changes in pulmonary artery pressure are capable of inducing respiratory (Kinnison, '63) and systemic cardiovascular (Aviado et al. '51 Coleridge and Kidd, '60 '63) reflexes. Moreover the similar identity of the afferent system mediating the lobeline induced Bezold-like reflex (Bevan and Verity '61) and the pressure induced respiratory reflexes from the pulmonary artery bifurcation has recently been suggested from experiments in cats and dogs Bevan and Kinnison, '65)

While the physiologic evidence in the mammalia appears conclusive histologic studies of the presence of specialized afferent endings within the pulmonary artery are meager and conflicting The presence of myelinated and non-myelinated fibers associated with the extrapulmonary portion of the pulmonary artery was originally described by Stirling (1875) and confirmed by the investigations of v Schumacher ('02), Perman ('24) and Tello ('29) Takino ('33) and Takino and Watanabe ('37) concluded that the extrapulmonary portions of the pulmonary arteries received a rich sensory supply and described the presence of nodules fine nerve networks and diffuse arborizations in the walls. However the presence of specialized endings of the pressoreceptor type within the pulmonary artery of the cat was denied by Nonidez ('41) Recently Bianconi and Green ('59) and Coleridge et al. ('61) have provided some histologic and detailed electrophysiologic evidence for the pres-

[1] Supported by USPHS grants H-6730 and HE 06539-01.

ence of pressoreceptor in the pulmonary artery of the cat and dog respectively

The studies reported here were undertaken to re-examine the innervation of the extrapulmonary portion of the pulmonary artery in the adult cat in the light of the recent physiologic and pharmacologic observations. Special attention was devoted to examining the distribution of special receptors and patterns of innervation throughout the artery defining the major afferent and efferent pathways contributing fibers to the region, determining the existence of an efferent system and examining the effect of bilateral sympathectomy on the pattern of innervation.

A brief account of some of these observations has been published elsewhere (Verity and Bevan, '62 Bevan and Verity '62, '63)

MATERIAL AND METHODS

More than 50 adult cats of both sexes were used in the study The material consisted of portions of the pulmonary artery commencing at the pulmonary valve ring and extending to the origin of the lobar branches at the hilum. In many instances h aortic arch and/or origin of the brachiocephalic trunk was removed for comparative studies of pressoreceptor morphology Gross detailed dissections of the innervation of the pulmonary bifurcation were carried out in 15 adult cats. Some dissections were performed under physiologic saline with the aid of a dissecting microscope The nomenclature of Mizeres ('55) will be adopted in the description of the origin and components of the cardiosympathetic and cardiovagal nerves associated with the bifurcation.

Staining techniques

The innervation of the pulmonary artery was studied in transverse oblique and tangential sections. Various staining procedures used included

1 Modified Bielschowsky method following fixation in 10% neutral formalin for 2–3 weeks.

2. *Osmium tetroxide* (Maillet '59)

3 *Cholinesterase method.* (Coupland and Holmes '57)

4 *Methylene Blue Techniques:*

(a) Intravital perfusion Animals were anesthetized with sodium pentobarbital and overventilated through a tracheal cannula. The chest was opened and the descending aorta retrogradely perfused with 500 ml of 0.3% methylene blue HCl over a ten minute period. The tissue was excised and maintained in air on saline soaked gauze for 30 minutes.

(b) Supravital staining: Tissue was rapidly removed from the anesthetized animal and immersed for 15 minutes in gently oxygenated 0.3% methylene blue containing 146 mM NaCl and 5 mM $MgCl_2$ maintained at 37 C in a pharmacological tissue bath. The subsequent treatment of tissue from (a) and (b) was similar The dye complex was fixed *in cold saturated* (NH_4) MoO_4 overnight. The artery was opened and pinned onto Teflon mats, washed for 20 minutes rapidly dehydrated in n-butyl alcohol, cleared in methyl salicylate and serially sectioned at 20 μ after rapid paraffin embedding *in vacuo*

Denervation

Bilateral stellatectomy and upper thoracic sympathectomy was carried out in five animals. Following pentobarbital anesthesia the stellate ganglia were removed with sterile precautions through an extrapleural approach between the first and second rib in the mid-axillary line Paralysis of the nictitating membrane was used as a criterion of immediate successful denervation, and subsequently confirmed *post mortem.*

Pharmacology

The pathways and pharmacological characteristics of the motor innervation of the pulmonary artery of the cat were investigated using an *in vitro* technique similar to that previously described for the rabbit (Bevan '63) The animals were anesthetized with pentobarbital, bled and the pulmonary artery from the pulmonary valve to just beyond the bifurcation was rapidly removed together with its right vagal and sympathetic innervation including the upper half of the thoracic sympathetic chain The vessel with its nerve

of supply was mounted in Krebs bicarbonate solution equilibrated with 95% O_2 and 5% CO_2. The isometric contractions of the circular muscle were recorded on an Offner dynograph following electrical stimulation of the nerve or muscle. Under these conditions the vessel remained viable for at least 12 hours. Repetitive stimulation with supramaximal pulses frequency 25/sec, duration 1 msec for periods of 5–8 seconds were employed. Drugs were added directly to the tissue bath.

OBSERVATIONS

Nerve supply of the pulmonary bifurcation

The pulmonary artery bifurcation and adjacent portions of the right and left pulmonary arteries receive a rich innervation. On the right side the most constant nerve trunk to the bifurcation is the *right recurrent cardiac* nerve. The fibers arise from the vagus or the recurrent-laryngeal nerve as it loops around the subclavian artery immediately caudad to its origin from the brachiocephalic trunk. The nerve proceeds medially and caudally passing dorsal to the superior vena cava and lateral to the origin of the brachiocephalic trunk. The fibers ramify at the bifurcation by dividing into antero-lateral and postero-lateral branches which communicate with fine fibers from the pulmonary plexuses. During its course it communicates with one or more *right vagal cardiac* nerves, usually of very small size, and branches from the stellate ganglia or ansa subclavia. These latter branches are thought to contribute the efferent component. Minor variations in the mode of origin from the receeurrent laryngeal nerve were noted. In more than half the dissections the nerve arose as a separate trunk from the loop of the recurrent laryngeal and was joined by a *cardiosympathetic* branch from the adjacent stellate ganglion (fig. 1a). The recurrent cardiac nerve rarely arises from the angle of origin of the recurrent laryngeal (fig. 1b). In three animals the major portion of the nerve appeared to arise directly from the vagus as the vagal cardiac nerve also receiving a small filament from the recurrent laryngeal (fig. 1c). The contribution to the innervation of the pulmonary artery from the left side is similar to that of the right, but also receives invariably a small, direct contribution from the vagus in the form of the *ventro-medial cervical cardiac* nerve. This nerve arises from the vagus by a variable number of roots, usually two, and proceeds caudally passing over the aortic arch to ramify over the ligamentum arteriosum, pulmonary bifurcation and left pulmonary artery. The *superior cranio-*

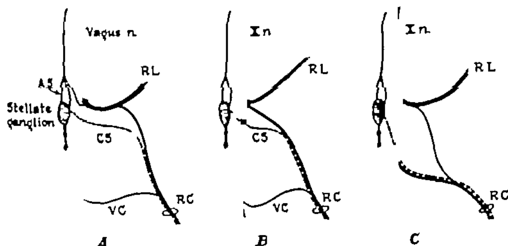


FIG. 1. Diagrammatic representation of the variable origin of the right recurrent cardiac nerve (RC) from the recurrent laryngeal (RL) and vagus nerves. The sympathetic contribution (CS) is seen arising from the stellate ganglion and ansa subclavia (AS). Vagal cardiac nerve (VC).

vagal root usually receives a direct branch from the left stellate ganglion. The bifurcation and left pulmonary artery receive a small inconstant branch from the *recurrent laryngeal* nerve as it passes under the aortic arch. In a few animals descending branches arise from the ascending portion of the recurrent laryngeal nerve to terminate around the bifurcation.

Neurohistologic observations on the innervation of the pulmonary artery

An extensive complex pattern of innervation exists throughout the extrapulmonary arteries. A diffuse network of myelinated and non-myelinated nerve fibers permeate the adventitia. Many of the primary nerve trunks supplying the adventitial plexus contain axons with irregular axoplasmic clumping small pale digestion chambers occasional collateral sprouts and terminal end bulbs (plate 1 figs. 1–5) These changes were more evident in the larger axons and were highly suggestive of regenerative and degenerative nerve fiber activity (Coërs and Woolf '59) The adventitial plexus contains axons 2–5 μ in diameter loosely organized in variably sized bundles (plate 1 fig. 6) A characteristic feature of the adventitial plexus the presence of round palely stained occasionally metachromatic nuclei. These are thought to represent Schwann cell nuclei. They are often situated at the junctional regions of the plexus (plate 1 fig 6) but not exclusively so occurring also singly and in close linear arrays (plate 1 fig 8) The adventitial plexus appears attenuated as it approaches the adventitiomedial junction where there is a loss of the close parallel organization with increasing neurite separation Schwann nuclei are less frequently seen but when present are elongated and often situated equidistantly from junctional regions (plate 2 fig 1) From here the fibers penetrate and ramify throughout the outer media Of note is the close relationship of the fibers to the penetrating vasa vasora. The neurites associated with the intramural vasa partially account for the increase in density of neural elements at the bifurcation of the pulmonary artery (Verity and Bevan '62) Sobin et al ('62) moreover described a rich arteriolar and venular confluence on the anterior surface of the pulmonary artery bifurcation in adult rabbits.

The innervation pattern within the media appears to consist of three separate patterns of neural organization which are capable of definition only in well stained methylene blue preparations.

(a) The predominant medial innervation is a highly plexiform organized pattern of small diametered unmyelinated and rarely myelinated (plate 2, fig. 2) nerves partially associated with the penetrating vasa around which they assume a spiral pattern. Only very rare Schwann cells are evident. Myelinated and unmyelinated fibers pass between the perivasal zones of innervation thus contributing to the plexiform pattern. Results of bilateral sympathectomy (*vide infra*) experiments indicate that this perivasal system is predominantly efferent in nature but does contain some small fibers resistant to stellatectomy

(b) A less frequent observation was the finding of small compact and rarely diffuse terminal arborizations throughout the media and adventitia (plate 2, figs. 3–5). The superficial arborizations are in continuity with unmyelinated branches of the adventitio-medial plexus and appeared comparable in some respects with the organization in the adventitia of the subclavian pressoreceptor zone (plate 1 fig 7) Small diffuse forms of terminations were apparent in the deeper layers of the media, even within the subendothelial zone The adventitiomedial arborizations consisted of compact fine axonic coils surmounted by irregularly sized swellings of variable staining density The subendothelial terminations were more diffuse (plate 2 fig. 6 7) and characterized by large pale axonic swellings terminal rings and intervening thickening of the axoplasm The subendothelial pre-terminal axons rarely showed terminal retraction (Coërs and Woolf '59)

(c) A very fine less than 1 μ in diameter single fibered widely spaced system is present throughout the media These neurites often arise from the perivasal plexus and ramify in a tortuous, occasionally varicose manner parallel to the smooth muscle but showing acute varia-

tions in course (plate 3 figs. 4 5) No Schwann nuclei or interstitial elements of Cajal accompany these fibers. Occasional branchings and rare fine plexiform pat terns are noted in some portions of their course Terminal rings, degenerative axoplasmic swellings or arborizations are not apparent, but in preparations stained optimally with methylene blue, small regular evenly stained fusiform swellings approxi mately 0.5–1 0 μ in diameter are present but are not related to any particular segment of the neurite or adjacent smooth muscle membrane.

Comparative neurohistologic studies of the aortic depressor subclaviobranchiocephalic and pulmonary reflexogenic zones

Neuromorphological studies of the aortic depressor area confirmed the presence of a special afferent receptor zone (Nonidez, 41 Abrahám, '53) Within the adventitia and outer media there is great variation in the mode of termination and attempts at classification into morphologic types appeared unwarranted a view supported by Abrahám ('53) for the nerve terminations in the carotid sinus Many variably sized axons branch and terminate in reticular enlargements (terminal menisci of de Castro) and show various pleomorphic swellings, neurofibrillary expansions, and ing formation along their preterminal course (plate 3 fig. 2) Occasionally fine neurites and discrete axonic coils issue from the preterminal axons and bizarre terminal menisci. The satellite cells (de Castro 40) localized in groups near the terminal menisci are only occasionally seen in the methylene blue preparations but when present are consistent with a Schwann cell origin. Similar arborizations are seen in the subclaviobrachiocephalic area (plate 3, fig. 3)

In both subclavian and aortic special afferent areas, portions of a myelinated and unmyelinated adventitial plexus are evident This plexiform organization merges imperceptibly into the regions of specialized terminal arborization. Some segments of the plexus show focal evidence of regenerative and degenerative neural activity (plate 1 fig 7) features which are indistinguishable from foci in the axons of the terminal arborizations.

The infrequent, small terminal arborizations described in the pulmonary artery (b) show manifestations of degenerative and regenerative neural activity comparable to that described in the established pressoreceptor zones. Compared to the aortic depressor arborizations those found in the pulmonary artery appear simple, diffuse more variable in morphology and situation and are composed of fine predominantly unmyelinated axons. Terminal menisci, neurofibrillary expansions and axonic swellings with rare focal collateral sproutings are however common to both areas.

In vitro pharmacologic observations on the innervation of the pulmonary artery

Contractile responses of the cat pulmonary artery were obtained following electrical stimulation of the thoracic sympa thetic chain near the stellate ganglion and the recurrent cardiac nerve (fig 2). Stimulation of the vagosympathetic trunk using a variety of stimulation parameters produced no response except when the elec trodes were placed near the ansa subclavia. The resultant contraction was 5–10% of that following recurrent car diac nerve stimulation. Destruction of the inferior cervical ganglion and the ansa subclavia reduced the response to stimulation of the chain near the stellate gan glion by 10–20%

After the addition of hexamethonium chloride (100 μg/ml) a ganglion block ing agent, the ratio of the response to stimulation of the recurrent cardiac nerve and of the vagosympathetic chain near the ansa to that to direct muscle stimulation was unchanged (fig. 3) The response to stimulation of the sympathetic chain was markedly reduced. There remained a small response about 5% of the original, which was not abolished by high doses of ganglion blocking agents.

This evidence suggests that the preganglionic motor fibers to the pulmonary artery synapse mainly in the stellate but also in other upper thoracic ganglia. Some post-ganglionic fibers to the artery probably loop rostrally in the vagus before

tions in structure in the age group 52–90 years. J Anat., 96 25.

Sobin, S. S., W G. Frasher and H. M. Tremer 1962 Vasa vasorum of the pulmonary artery of the rabbit. Circ. Res., 11 257

Stirling, W 1876 The nervous apparatus of the lung. Brit. Med., J 2: 401.

Swan, A. A. B., and D Whitteridge 1956 Abstr XX int. Physiol. Congress 867

Sunder Plassmann, P 1930 Untersuchu ger über den bulbus carotidis bein mensch. und tier im hinblick auf die sinusreflexe nach H. E. Hering; ein nergleich mit anderen gefässtrecken; die histopathologie des bulbus carotidis; das glomus caroticum. Z. Ges. Anat. Entwgesch., 93 666.

——— 1933 Über neuro-vegetative rezeptorenf lder im kreislauf-regulationsmechanismus nd durch deren sechaltung experimentell erzeugte morphologisch fassbare veränderun gen in sympathischen nervensystem. Z. ges. Neurol. Psychiat., 147 414

Takino, M. 1933 Über die innervation der lungengefässwand, besonders über das vorkommen, der ganglienzellen an der gefässwand de venae pulmonales und über die verbindungzustände der lungenblutgefässengwen bei de Fledermans. I. Mitteilung. Acta Sch. Ed Univ Kioto, 15 303.

Takino, M., and S. Watanabe 1937 Über die bedeutung des ligamentum arteriosum bzw de ductus botalli und der ansatzstelle desselben an der pulmonalwand (A. pulm.) als blutdruckzügler bei verschiedenen tierarten. Arch Kreislauf Forsch., 2: 18.

Tello, J F 1924 Genèse des terminaisons motrices et sensitives II. Terminaisons dans le poils de la souris blanche Trab. Lab. Invest. Biol. Univ Madrid 22: 257

Thaemert, J C. 1963 The ultrastructure and disposition of vesiculated nerve processes in smooth muscle. J Cell. Biol., 16 361.

Verity M. A., and J A. Bevan 1962 Distribution of nerve endings in the pulmonary artery of the cat. Science, 135 783.

von Schumacher S. 1903 Zur frage der herz innervation bei den säugetieren. Anat. Anz. 21 1

Unless otherwise indicated all photomicrographs are of methylene blue preparations. The scale represents 20 µ.

PLATE 1

EXPLANATION O FIGURES

1 Large prim ry medullated nerve bundle in pulmonary artery adventitia containing numerou nerve fibers some axons of which show large irregular fusiform swellings suggestive of early axonal degeneration.

2 Multiple, irregular axoplasmic swellings of one nerve in small adventitial nerve bundle. A normal nerve fiber lies to the left. A pale, elongate Schwann nucleus bordering on unmyelinated axon is seen in the lower right corner

3 A large medullated nerve fiber shows a fusiform axonic swelling with central pallor The pale outlines of the swollen myelin sheath (rrows) are seen. Pulmonary artery

4 Twi ted axi cylinder within a myelin ellipsoid. There is no evidence of gr nul r a onic debris but the outlines of the myelin sheath re tained. Early terminal sprouting s ggestive of regenerative collateral activity i present t the left of the ellipsoid. A Schwann nucleu i prese t (rrow)

5 A myelin ellipsoid with acuolation and axoplasmic fragmentation (digestive ch mbe of Cajal) i seen on the left i continuity with diff se termi al growth cone showing extensive collateral branching nd on coiling Pulmon ry artery

6 Syncyti l rr ngement of fine unmyelinated neurit bundles within the adventiti of the pulmonary artery Numerou Schwann nuclei present

7 Segme t of dventitio-medial nerve pl xu i th subcl vian pressoreceptor zon howing disconti uity d development of irregular tbori tio with onic welling nd coiling of the terminal neurites Bielschowsky

8 Portion f dve ti ial nerve ple t pulmonary artery bif rc tion nit i i g nume ou my lin ted on ccompa ied by multiple round d tri g i Schw n nuclei

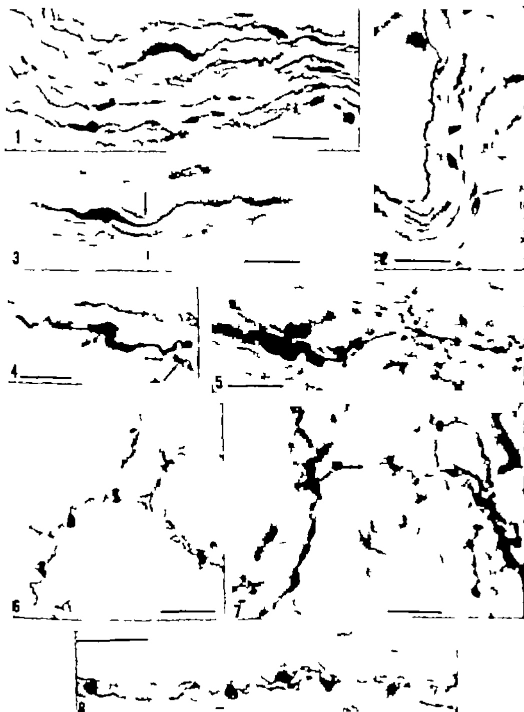

1
2
3
4
5
6
7
8

PLATE 2

EXPLANATION OF FIGURES

1 Three fusiform Schwann nuclei situated equidistantly from the convergence f three neurite bundles located within the pulmonary artery adventitia.

2 Tangential section of adventitio-medial junction in pulmonary artery A small myelinated fiber (arrow) enters the preterminal network. No Schw nn nuclei are apparent at this level of neuronal organization.

3 Example of rare classical, de Castro Type II pressoreceptor within the adventitio-medial zone of the pulmonary artery of an adult c t. The terminal is composed of a central axon with fusiform swellings and numerous collateral branches with axoplasmic retraction termi nation in fine meshwork of axonic coils. A small daughter terminal rborization is seen in the upper right corner Bielschowsky

4 Small, compact afferent termination within the media of the right di ision of the pulmonary artery The terminal neurites end in round and oval menisci uggestive of retraction f the terminal axoplasm (Coers and Woolf '59)

5 A more complex compact adventitial afferent termination in the pulmonary artery The termination arises from fine unmyelinated axons.

6 Fine unmyelinated subendothelial axon terminating in imple "flower-spray ending characterized by numerous small terminal menisci of Caj l.

7 Sub-endothelial termination resembling de Castro Type I endi g containing numerous fusiform aricosities along the course of the pre-terminal neurites

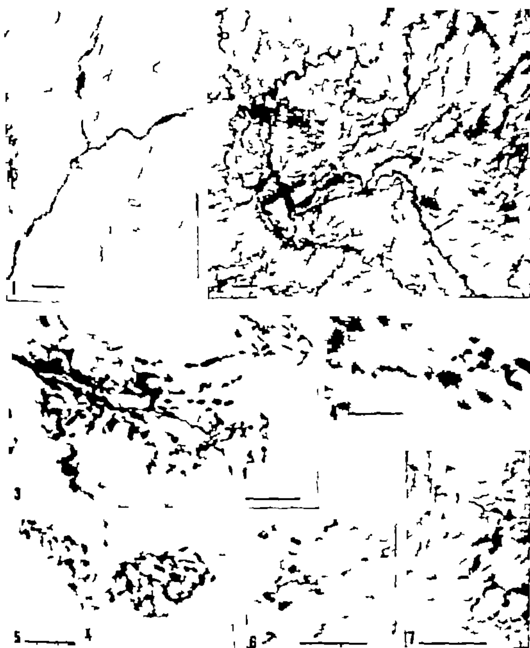

1
3
5
4
6
7

PLATE 3

EXPLANATION OF FI URES

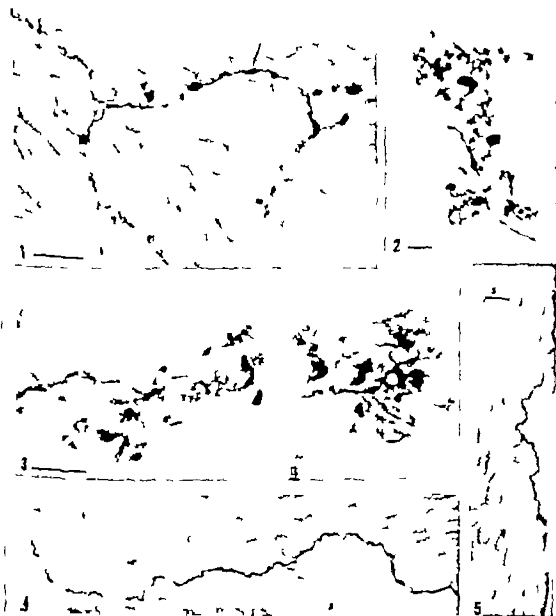
1 Portion of pulmonary adventitio-medial preterminal plexus of unmyelinated nerve fibers with a segment of the plexus showing early degeneration including axonal neurofibrillary hanges (arrow)

2 Terminal arborization (de Castro Type II) in the aortic depressor zone of an adult cat. Axon swelling coils with large irregular terminal expansions collateral branching and myelin lipoids suggestive of degenerative and *regenerative activity are seen.*

3 High power magnification of pressoreceptor termination (de Castro Type II) in the subclaviobrachiocephalic depressor area Axoplasmic retraction and swelling with terminal menisci and ring forms are organized around a central, myelinated axon.

4 Fine unmyelinated axon within the media of the pulmonary artery Note acute vari tions in course nd length with no attempts at branching.

5 Similar to figure 4 with small branch and occasional delicate fusi form swellings along the length of the primary axon.


1
2
3
4
5

The Blood Supply of the Bovine Hypophysis [1]

J F CUMMINGS AND R. E. HABEL
Department of Anatomy New York State Veterinary College Cornell University Ithaca, New York

ABSTRACT The rete mirabile cerebri and the hypophysial vascularization were studied by various injection and staining techniques. The rostral hypophysial arteries arose bilaterally from the arterial circle f the cerebrum, while the caudal hypophysial arteries arose from the rete mirabile on the dorsal and caudal surfaces of the gland. The ramifications of the rostral hypophysial arteries supplied the vascular structures in the hypophysial stalk, which were classified on the basis of their structure into three groups arborization forms, spike forms, and capillary loops. These structures drained into large portal vessel leading to the pars distalis. The pars distalis received sec ond smaller group of portal vessels from the capillary bed of the lower infundibular stem. The small group of portal vessels was limited in its extent by well-developed *hypophysial cleft. No direct arterial supply to the pars distalis could be demonstrated.* The findings f this study support the view that the blood in the hypophysial portal system flows distally from the hypophysial stalk to the pars distalis.

Evidence strongly suggests that the hy pophysial portal system forms a route for hypothalamic control over pituitary func tion (Harris '55 Greep '63) Direct neural control of anterior lobe secretion in the ox seems unlikely since Gilmore Peterson, and Rasmussen (41) were unable to find nerve fibers in the pars distalis The orig inal description of the hypophysial portal system in man by Popa and Fielding ('30) was followed by studies of pituitary circulation in many species (Romeis 40 Diepen, '62) The existence of a portal system and its functional implications have stimulated interest in the study of hypophysial vascularization.

The arterial supply to the bovine hypoph ysis arises from the rete mirable cerebri. This extensive arterial plexus which sur rounds the pituitary has perplexed anatomists since the time of Galen.

Ask-Upmark ('35) reviewed the early theories *on the physiologic significance of* the rete He postulated that the rete may operate mechanically in maintaining cere bral arterial pressure at a convenient and constant level. Zhedenov ('37) described the pre- and postnatal formation of the rete and the regression of the internal carotid artery in the ox. He believed that the rete functioned as a regulating reser voir Legait (44) reported highly innerv ated arteriovenous anastomoses between the arterioles of the rete and the cavernous sinus in the calf These anastomoses were most numerous in the region of the posterior hypophysial arteries and he concluded that they undoubtedly influence the hypophysial circulation. Barnett and Marsden ('61) studied retial function in two de capitated sheep By using constant and alternating pressure perfusion into the common carotid arteries and measuring venous pressure in the jugular veins, they concluded that the pulsation of the retial arteries assisted intracranial venous return.

In his comparative study of 1951 Green noted that the hypophysis of ungulates had not been studied from the point of view of vascularization. Bačić ('56) described the hypophysial portal system of the ox and drew functional conclusions. Daniel and Prichard described the hypophysial circulation in the sheep ('57a,b) and goat ('58)

The present study was undertaken to describe the blood supply to all lobes of *the bovine hypophysis. The work includes* a description of the rete mirabile cerebri, the rostral and caudal hypophysial arter ies the hypophysial portal system and the interlobar vascular connections.

MATERIALS AND METHODS

Eleven calf heads obtained shortly after death, were perfused with physiological saline solution via the common carotid

[1] This stud was supported in part by Research Fellowship from the American Veterinary Medical Association

arteries The heads were flushed until all traces of residual blood disappeared from the perfusate issuing from the jugular veins. Colored latex was injected bilaterally through cannulated common carotid arteries In most cases the latex was injected under a pressure of 200 to 300 mm of mercury from a pressure bottle apparatus. Several specimens were injected with a 50 ml syringe. Prior to injection hemostatic forceps were placed on the vertebral vessels and the jugular veins. When the vessels were filled the common carotid arteries were ligated After the latex hardened a block of tissue containing the optic chiasma hypophysis hypothalamus portions of the sphenoid and occipital bones and the associated vessels was removed with a band saw These blocks were fixed in 10% formalin and subjected to complete or partial corrosion

Complete corrosion was accomplished by submerging the tissue blocks in concentrated hydrochloric acid until the vessel casts were well defined. Remaining fatty debris was removed in 10% potassium hydroxide Partial corrosion in hydrochloric acid was employed in conjunction with dissection with the aid of a microscope

Five calf heads were injected with vinylite chloride using a pressure bottle apparatus at 300 mm of mercury The procedure followed was identical to that used with the latex preparations The tissue blocks were totally macerated in concentrated hydrochloric acid Latex and vinylite casts were used to visualize the gross arterial configurations surrounding the hypophysis

The heads of 14 calves were injected with India ink injection masses described by Green ('51) Shortly after death the heads were perfused via the common carotid arteries with physiological saline solution to which 0 2% sodium nitrite had been added (Lillie '54) The ink mass *was injected with a 50 ml syringe The* plunger of the [illegible]inge was depressed in 5–10 ml interval [illegible] n attempt to simulate an arterial p[illegible] A block of tissue containing the h[illegible] ysis and its surroundings was rem[illegible] nd submerged in 10% formalin Af[illegible] the block had hardened the adhe[illegible] portions of the sphenoid and occipita[illegible] s were removed from below with bone forceps The hypophysis was cleared in benzyl benzoate with or without preliminary dissection Ink preparations provided visualization of the finer vessels supplying the gland (fig. 14)

The blood content of the hypophysial vessels of nine adults and six calves was stained by the benzidine technique A tissue block, similar to that described above was removed and placed in 10% formalin for 24 hours. The hypophysis was extracted from the sella turcica without destroying its connections with the hypothalamus and replaced in 10% formalin for 6 to 7 days The blocks were cut by hand in horizontal, sagittal, or transverse planes The sections were included in a gelatin mass and cut at 50 µ on the freezing microtome (Carleton and Drury '57) The blood was stained by the method of Lepehne-Pickworth as given by Lillie ('51).

The pituitary glands of eight calves were embedded in paraffin and transverse and sagittal sections were made at 8 µ. Four were stained by Crossmon's modification of the Mallory trichrome method (Crossmon '37) the other four were stained with hematoxylin and eosin Two adult glands were stained by the trichrome method

The structures surrounding the hypophysis

The hypophysis of the calf was locked in the sella turcica so that it was extremely difficult to remove the brain and pituitary intact by a dorsal approach The fossa hypophysialis on the dorsal surface of the sphenoid bone accommodated the ventral portion of the gland The steep rostral wall of the sella was formed ventrally by the basisphenoid and dorsally by the presphenoid Caudodorsally the gland was limited by the dorsum sellae and the processus clinoideus caudalis The diaphragma sellae formed a strong dural roof over the dorsum of the gland

The caudodorsal portion of the diaphragm was tightly adherent to the gland In this region the cartilaginous caudal clinoid processes of the calf were anchored in the diaphragm Rostrally the diaphragm

The Latex was obtained from the Ceramics Company Inc 336 Canal Street, New York 13, New York
Vinylite chloride was obtained from Union Carbide Plastics, 270 Park Avenue New York 17 New York.

became attenuated and presented a foramen for passage of the hypophysial stalk. The diaphragm was elevated caudal to the foramen for the stalk, so that the arachnoid around the stalk extended for a variable distance between the diaphragm and the lower infundibulum (Boyd '60)

The cavernous sinus and the rete mirabile bordered the gland laterally

General morphology

The body of the calf's hypophysis was generally oval with its long axis directed rostrocaudad. The hypophysial stalk joined the rostrodorsal pole

The general nomenclature for the parts of the hypophysis is that proposed by Rioch, Wislocki, and O'Leary as reported by Green and Harris ('47) The neurohypophysis consisted of the median eminence of the tuber cinereum, the infundibular stem, and the neural lobe The infundibular stem was subdivided into upper and lower parts according to Xuereb Prichard, and Daniel ('54) The upper infundibular stem a continuation of the median eminence was surrounded by pars tuberalis. The lower infundibular stem devoid of pars tuberalis continued caudad to merge with the neural lobe. The lower stem lay in a groove formed by the dorsal surface of the adenohypophysis. The recessus infundibuli extended through the median eminence and terminated in the upper infundibular stem. Within the median eminence the ependyma-lined walls were folded into the lumen of the recess

The pars tuberalis formed an epithelial investment about the median eminence and the upper infundibular stem The pars tuberalis was best developed on the rostral surface of the infundibulum. Ventrally it was continuous with the pars distalis.

The pars distalis the largest portion of the gland, contributed to the formation of the rostral, ventral, and lateral walls of the organ. Dorsally the pars distalis was grooved to accommodate the posterior lobe.

The pars intermedia was applied to the ventral and lateral surfaces of the lower infundibulum and neural lobe. The hypophysial cleft (cavum hypophysis) limited the regions of contact between pars intermedia and pars distalis. In sagittal sections a small area was seen rostral to the cleft where the two portions were in direct contact. The pars distalis also joined the pars intermedia for a very short distance behind the cleft. On transverse sections the cleft appeared as a V-shaped space separating the pars distalis from the pars intermedia except in the dorsolateral regions where the cleft was nonexistent.

The central pars intermedia presented a light-colored conical projection which microscopically resembled the cellular structure of the pars distalis. This structure, the lobe of Wulzen ('14) was usually visible grossly The lobe projected from the pars intermedia into the cleft and the adjacent portion of the pars distalis showed a corresponding indentation.

The arteries surrounding the hypophysis

The hypophysis was surrounded by the rete mirabile cerebri. Zhedenov ('37) divided this arterial network into two contiguous components rete mirabile rostrale and rete mirabile caudale. The rostral rete corresponds in the main, to the rete mirabile of other authors.

The rete mirabile rostrale consisted of an arterial plexus on each side of the hypophysis (figs. 1 and 15) The lateral plexuses were connected by communicating branches rostral and caudal to the gland. Small arterial rami ran forward from the rostral communicating branches to the dura on the ventral surface of the optic chiasma where they converged ventrally with the extracranial extensions of the rostral rete and dorsally with the branches from the rostral cerebral arteries — if the latter were present.

In two calves an arterial branch arose from each rostral cerebral artery Right and left branches joined on the dura on the dorsal surface of the optic chiasma, forming a rete which communicated with the rete on the ventral surface of the chiasma through the notch formed by the divergent optic nerves. Baldwin ('64) found these branches in one of his calves.

As previously described by Schmidt ('10) there was an extracranial retial extension, consisting of intertwined arteries,

which ran out from the foramen orbitorotundum and re-entered the cranium through the optic canal. It ran toward the brain on the ventromedial surface of the dural sheath of the optic nerve and joined the fine rami of the rostral communicating branches to form the ventral rete on the dura of the chiasma.

The rete mirabile sent small arterial branches to the ventral surface of the hypophysis. This ventral retial extension, while constantly observed, seemed variable in its degree of development. One or two arterial twigs arose from this extension pierced the dura underlying the gland, and entered the foramina in the fossa hypophysialis It was not determined whether these rami were afferent or efferent in relation to the rete.

The rete mirabile received arteries from the internal maxillary The arteries joining the rostral pole of the lateral plexus entered the skull via the foramen orbitorotundum; the artery supplying the caudal pole entered via the foramen ovale. Zhedenov ('37) called both rostral and caudal arteries, arteriae pro rete mirabile To differentiate the rostral and caudal arteries the terms arteriae distales pro rete mirabile and arteria proximalis pro rete mirabile are suggested

The distal arteries for the rete mirabile varied from three to seven in number The external ophthalmic artery which also arose from the internal maxillary artery at this level occasionally contributed retial arteries. The proximal artery for the rete was a large branch of the internal maxillary artery The main trunk ramified in the caudolateral region of the rete but some smaller branches ramified on the dura around the mandibular nerve

In the calf the internal carotid artery joined the caudal portion of the rostral rete It entered the lateral plexus caudomedially and coursed rostrad in the substance of the rete beside the hypophysis (fig. 2) In the rostral portion of the rete it bent sharply dorsad and pierced the diaphragma sellae lateral to the hypophysial stalk. The artery received branches within the rete and increased in size as it coursed rostrad. It was considerably larger when it emerged from the rete to supply the brain through the arterial circle of the cerebrum (circulus arteriosus cerebri)

The rete mirabile caudale was formed by the condyloid and vertebral arteries. It consisted of three or four tortuous but anastomosing arteries, which joined the rostral rete and contributed to the formation of the caudal hypophysial arteries and the ventral retial extension.

The hypophysial arteries

Two or three hypophysial arteries arose from the arterial circle of the cerebrum. The medially directed hypophysial arteries ramified and joined the contralateral arteries in the formation of an arterial annulus around the median eminence (fig. 3) The arterial annulus of the hypophysis and its parent arteries issued branches to the optic chiasma and hypothalamus and to the pars tuberalis at the level of the median eminence. Other branches ran distally and penetrated the pars tuberalis of the upper infundibular stem (fig. 4). The annulus gave off a caudoventrally directed branch that ran along the lateral surface of the hypophysial stalk. Arriving at the lower infundibular stem it passed to the dorsal surface and anastomosed with the contralateral vessel to form a plexus (fig 5) Branches from the plexus ran to the lower infundibulum the pars intermedia, and the connective tissue septum between these regions. Fine twigs from the plexus ran caudad under the diaphragma sellae and joined the small terminations of the caudal hypophysial arteries on the dorsal surface of the gland. Branches from the rostral hypophysial arteries joined branches from the caudal hypophysial arteries within the substance of the lower infundibular stem.

The caudal hypophysial arteries consisted of extensions of the rostral and caudal retia on the dorsal and caudal surfaces of the gland. The most conspicuous component of the caudal hypophysial arteries was the large transverse anastomotic artery which connected the lateral plexuses on the dorsal surface of the gland. The transverse anastomosis and its branches were located in the dura of the diaphragma sellae Branches from the rostral border of the anastomotic artery were distributed to the rostral part of

the neural lobe the pars intermedia and the septum between these regions. Long branches from the anastomotic artery continued rostrally on the lower infundibular stem. Some branches from the rostral border of the tranverse artery ran to the diaphragma sellae and others joined the arteries of the lateral plexuses. Branches from the ventral and caudal borders of the tranverse artery supplied the neural lobe, the pars intermedia, the connective tissue septum, and the diaphragma. Some of these branches anastomosed ventrally with a caudal communicating branch of the rostral rete.

The hypophysial portal system

The hypophysial portal system consisted of three contiguous parts the vascular bed of the pars tuberalis and infundibulum, the portal vessels and the sinusoidal capillary bed in the pars distalis.

The rostral hypophysial arteries supplied the vascular structures of pars tuberalis and infundibulum. These vascular structures have been divided into three types on the basis of their morphology and distribution.

In the infundibulum, the most conspicuous formation was the arborization (figs. 8 and 9) These vascular trees were composed of the following; (1) an arteriole derived from the rostral hypophysial arteries, (2) a branching complex of capillary loops (3) a venule leading to a portal vessel. The arborizations generally penetrated perpendicularly into the deeper regions of the infundibulum. Although these trees were similar in their morphology and distribution, they varied in size complexity and depth of penetration The majority of the arborization forms originated from the rostral and lateral regions of the pars tuberalis.

The second type of vascular complex penetrating into the infundibulum resembled the spikes described by Daniel and Prichard ('57) Interposed between the afferent and efferent limbs was an elongated helical capillary network. A few spikes, like those described in the sheep were found in the median eminence but the majority were seen below this level in the calf. The spikes penetrating into the region of the median eminence were directed perpendicular to the long axis of the infundibulum.

The spike forms originating from the pars tuberalis below the median eminence pursued a dorsomedial course deep within the upper infundibular stem and often extended well into the median eminence. These longer helices ran parallel to the long axis of the infundibulum (figs. 10 and 11) They often had lateral branches which were arranged as capillary loops.

In addition to the spikes and arborizations smaller capillary loops originated from the capillary bed of the pars tuberalis. The loops were most numerous in the rostral and lateral regions of the infundibulum. They ran perpendicularly into the external regions of the median eminence and upper infundibulum, being more numerous in the latter These capillaries while easily recognized by their small size and short course showed variation in complexity Some were simple loops others were aggregates of loops

The vascular structure of the infundibulum was such that the external regions were supplied with loops from the capillary bed of the pars tuberalis, while the internal regions received loops from the arborizations and spikes.

The portal vessels linked the vascular structures of the infundibulum with the large capillary bed of the pars distalis (fig 12) They were grossly visible as they arose at various levels of the median eminence and the upper infundibular stem. They ran distally in the pars tuberalis, mostly in the rostral and lateral parts. In the pars distalis they ramified in the second capillary bed of the portal system. A few portal vessels from the lateral regions of the pars tuberalis supplied the dorsolateral parts of the pars distalis, but most of them supplied the vascular medulla described by Jubb and McEntee ('55) The greater vascularity of the medulla compared to the cortex was visible grossly (fig. 6)

The vascularization of the various parts of the hypophysis

The vascular bed of the pars tuberalis contained arterioles capillaries and

portal vessels The portal vessels reached their greatest diameter in the distal regions of the pars tuberalis. The pars tuberalis appeared to be the most vascular portion of the hypophysis.

The portal vessels draining the stalk were the main blood supply to the pars distalis. The capillary bed of the rostral portion of the lower infundibular stem was supplied by the caudoventral branches from the annulus of the rostral hypophysial arteries. In this rostral region where the hypophysial cleft was absent, a second small group of portal vessels united the capillary bed of the lower infundibulum with that of the rostrodorsal region of the pars distalis (fig. 7)

The pars distalis also received capillaries via the pars intermedia. These capillary connections were limited to the dorsal regions of the gland where the hypophysial cleft did not separate the pars intermedia from the pars distalis. These links were most apparent in the rostral region where the pars intermedia was supplied by branches of the rostral hypophysial arteries. These branches ramified in the capillary bed of the pars intermedia and some capillaries continued to the adjacent areas of the pars distalis.

The median eminence and the upper infundibular stem contained the arborizations spikes and capillary loops derived from the rostral hypophysial arteries. The lower infundibular stem was supplied by both rostral and caudal hypophysial arteries. The caudal hypophysial arteries supplied the neural lobe

The pars intermedia was the least vascular part of the gland The most rostral portion was supplied by the caudoventral branches from the arterial annulus of the hypophysis; the caudal part received branches from the caudal hypophysial arteries. The lobe of Wulzen was the most vascular portion of the pars intermedia. Its dense capillary bed was supplied by branches from the caudal hypophysial arteries which ramified near its base. The great vascularity of the lobe sharply contrasted with the adjacent area of the pars intermedia (fig. 13)

Figure 16 diagrammatically illustrates the vascularization of the various parts of the hypophysis.

DISCUSSION

The results of the gross study of the structures surrounding the calf's hypophysis were in general agreement with the previous studies of the ox by Koller ('22), Boyd ('60) and Glóez ('62)

The nomenclature applied to the rete mirabile cerebri and its branches is confusing Outlined below are some synonyms for the terms used in this paper.

Rete mirabile rostrale (Zhedenov '37)
Rete mirabile
Carotid rete
Rete mirabile caudale (Zhedenov '37)
Rete mirabile basile (Bruni and Zimmerl, '51)
Basi-sphenoidal arterial plexus (Daniel, Dawes, and Prichard '53)
Basi-occipital plexus (Baldwin and Bell, '63)
Arteriae distale pro rete mirabile
Distale Retebäste or Reteäste durch das Foramen orbitorotundum (German authors)
Le arterie genetrice della rete ammirabile (Bossi et al., '09)
Arteria anastomotica (Daniel, Dawes, and Prichard, '53)
Arteria proximalis pro rete mirabile
Proximaler Retaast or Reteast durch das Foramen ovale (German authors)
A meningea media (Bossi et al., '09)
A. generatrice prossimale della rete mirabile (Bruni and Zimmerl, '51)
Ram anastomoticus (Daniel, Dawes, and Prichard, '53)

Some authors have not differentiated the retial branches of the internal maxillary artery (Zhedenov '37) Sisson and Grossman ('38) mention that all arteries which concur in the formation of the rete may be called arteriae retis mirabilis cerebri" and they apply the same term to the external ophthalmic rete

The numerical variability of the distal arteries to the rete has been verified by the results of previous investigations. Zhedenov found one or more while Bruni and Zimmerl reported that there were ten. The 2 to 8 reported by Schmidt ('10) and the 3 to 8 of Ellenberger and Baum ('32) approximated the results of this study

In the adult ox, the internal carotid artery is represented by a connective tissue strand. In the calves examined in the present investigation the internal carotid artery was patent and it joined the rostral rete Legait (44) described the course of this artery in the rete of the calf but he called it the occipital artery

Schmidt ('10) described an extracranial vascular plexus arising in the region of the *foramen orbitorotundum*, which ran to the ventral surface of the optic nerve and eventually joined the contralateral plexus on the dura of the ventral surface of the chiasma. In two fetuses and a young calf Schmidt also found an intracranial retial extension which ran from the rostral rete to the dura of the chiasma. At the chiasma this extension joined the plexus formed by the extracranial vessels. He called this plexus, rete mirabile ophthalmicae internae. He concluded that in fetal life the internal ophthalmic artery is a direct branch of the internal carotid artery. Later the direct connection via the rostral rete is lost so that only the extracranial extension remains. In the present study the intra- and extracranial extensions were consistently demonstrable.

An arterial plexus was also evident on the dura on the dorsal surface of the optic chiasma. In two calves this plexus supplied by a small branch from the rostral cerebral artery. Thus the internal ophthalmic rete was present on the dura of both dorsal and ventral surfaces of the chiasma.

Schmidt ('10) reported a break in the retial extension on the ventral surface of the calf hypophysis. Pictures often show the ventral surface of pars distalis free of arteries in the adult (Ellenberger and Baum, '32 Martin and Schauder, '38) and the calf (Daniel Dawes and Prichard, '53) In the present study the rete was often complete around the ventral surface of the hypophysis.

The ventral retial extension was joined by one or two arteries from the foramina in the fossa hypophysialis. Franck (1894) reported branches which penetrated the sphenoid bone and emptied into the sella turcica. These arteries and the ventral retial extension would constitute an added problem in hemostasis in hypophysectomy via a parapharyngeal approach. Hill et al. ('35) and Cowie and Tindal ('61) have used this approach successfully in the goat.

In the ox, van Vuuren assumed that branches from the arterial circle of the cerebrum ran to the stalk and supplied the pars nervosa, the transitional part (pars tuberalis) and the pars intermedia. Martin and Schauder ('38) stated that the rich capillaries of the pars distalis were derived from approximately 20 branches of the internal carotid artery or the arterial circle of the cerebrum and that the caudal lobe was supplied by pial arteries. In the ox, Jubb ('62) described up to 20 small arterioles that arose from the arterial annulus which surrounded the proximal end of the hypophysial stalk. According to Jubb the arterioles lose their muscular coats upon entering the pars tuberalis and develop into large sinusoids which are continuous with the sinusoidal circulation of the pars distalis It is probable that Legait ('44) recognized the caudal hypophysial arteries because he mentioned a network of arteries on the pars nervosa derived from the carotid rete. Bačić ('58) made no mention of the rostral hypophysial arteries, but described ramifications of the arteries of the rete mirabile which penetrated the capsule of the gland and supplied the pars distalis directly

Daniel and Prichard studied the vascular supply of the hypophysis in the sheep ('57a and b) and goat ('58) Some differences can be noted between the arterial pattern of the calf and that of sheep and goats. The arterial annulus of the hypophysis in the calf differed from that of the sheep and goat in that it sent right and left caudoventrally directed branches to the lower infundibular stem. The dorsal branch of the caudal hypophysial artery described in the sheep corresponded to the transverse anastomotic artery on the dorsal surface of the calf's gland. The ventral branch of the caudal hypophysial artery of the sheep apparently has been replaced by the most caudal portion of the ventral retial extension. The transverse anastomotic artery and the ventral retial extension were supplied by both rostral and caudal retia. There is no caudal rete in the sheep and the ventral retial extension is absent. The artery of the lower infundibular stem, a branch of the dorsal branch of the caudal hypophysial artery in the sheep has been replaced by the caudoventral branches from the arte-

rial annulus and by the branches from the rostral border of the transverse anastomotic artery

In the present study it was noted that the rostral hypophysial arteries contributed to the formation of the arborizations spikes, and capillary loops that penetrated the infundibulum. Bačić ('56) grouped the arborizations and spikes under the classification of *gomitolo* after Fumagalli ('41) He subdivided the capillary loops into simple (*anse simplice*) and complicated types (*anse complicate*) after Morin ('39) Dellmann ('60) reported two types of vessels penetrating the infundibulum *kurze* and *lange Spezialgefässe* The short vessels were more numerous and terminated in the external infundibulum (zona externa infundibuli) as vascular arcades or anastomoses. The long vessels ran either parallel or transverse to the long axis of the infundibulum and reached the internal regions (zona interna infundibuli) Presumably the short vessels correspond to the capillary loops while the spikes and arborizations noted in the present study are subdivisions of the long vessels.

Bačić ('56) found 16–20 portal vessels in the ox. The majority of the portal vessels supplied the vascular medulla of the pars distalis. Aside from the vascular demarcation there was also a difference in the distribution of types of cells in the pars distalis (Jubb and McEntee '55)

In addition to the hypophysial portal system interlobar vascular connections have been described in different species (Morato '39 Holmes and Zuckerman '59 Duvernoy and Koritké '60) In the sheep Daniel and Prichard ('57a and b) found short portal vessels draining the capillary bed of the lower infundibular stem to the adjacent region of the pars distalis In the calf short portal vessels drained the capillary bed of the rostral part of the lower infundibular stem to the adjacent pars distalis Some of these vessels passed through the rostral part of the pars intermedia. This system was less developed than that demonstrated in the sheep The well-developed hypophysial cleft in the calf was considered to be the major factor limiting the extent of the second portal system.

A structure similar to the lobe of zen has been described by De Beer ('2[illegible]) in the pig and by Ganfini ('22) and W... ('53) in the sheep. House ('43) previously noted that the caudal hypophysial arteries supply this lobe in the ox. He believed that the development of the lobe was related to the vascularity of the primordia in the embryo Ganfini, who described the pre- and postnatal development of the *lobulo intermedia* in the sheep also observed numerous and relatively large vessels in this area.

The direction of blood flow in the hypophysial portal system has been the subject of considerable debate. The original concept of proximal flow i.e. toward the hypothalamus was presented by Popa and Fielding ('30) Wislocki and King ('36) concluded that the blood flowed distally from the stalk to the pars distalis. Some investigators have postulated that the direction of flow in the portal system is capable of fluctuation (Romeis '40 Spanner '52; Tanaka '61) In vivo studies have shown that the blood flows toward the pars distalis in the rat (Green and Harris '49 Barrnett and Greep '51; Daniel and Prichard '56) and the mouse (Worthington '55) Török ('54) found that in the living dog and cat the blood in the stalk was directed from the pars tuberalis to the anterior lobe He found small vessels on the caudodorsal surface of the pars distalis in which the blood flowed proximally

Daniel and Prichard described a distal blood flow in the vessels of the hypophysial stalk of the sheep ('57a,b) and goat ('57) Bačić ('56) held that a purely distal blood flow in the portal system of the ox was beyond consideration. He concluded that blood in the portal vessels flows proximally from the adenohypophysis to the infundibulum and pointed out that there may be certain functional phases during which the flow direction is reversed. Bačić based this conclusion on the content of the portal vessels. He noted the presence of cells allegedly liberated from the pars distalis by holocrine secretion, in the ramifications of the portal veins in the infundibulum Presumably these cells were swept into the infundibulum as result of the proximal blood flow in the portal vessels

Badić cited, as additional evidence for a proximally directed portal system, the existence of arterial ramifications from the rete mirabile which supplied the pars distalis directly

The present study failed to confirm the existence of cells from the pars distalis in any of the vascular structures of the stalk. No arterial ramifications of the rete mirabile were observed to supply the pars distalis directly

The morphology of the bovine hypophysial portal system indicated that distal blood flow was probable. The following observations lead to this conclusion. (1) The rostral hypophysial arteries supplied the afferent limbs of the vascular structures of the hypophysial stalk. (2) The efferent limbs of these structures were collected by portal vessels. (3) India ink injection via the common carotid artery filled the vessels of the stalk and the rostral part of the pars distalis but in some cases failed to reach the more caudal regions of the pars distalis. (4) Vascular connections between the hypophysial stalk and the hypothalamus were slight. Superficially the rostral hypophysial arteries sent proximally directed branches to the hypothalamus. Internally some of the capillary apices of the spike forms reached the ventral extremity of the hypothalamus. (5) There was no direct arterial supply to the pars distalis.

LITERATURE CITED

Ask-Upmark, E. 1935 The carotid sinus and the cerebral circulation. An anatomical, experimental and clinical investigation, including some observations on rete mirabile caroticum. Acta psychiat. (Kbh.) Suppl., 6 1–374

Badić, V 1956 O portalnom sistemu hipofize goveda. Vet. Arhiv (Zagreb) 26 254–266.

Baldwin, B. A. 1964 The anatomy of the arterial supply to the cranial regions of the sheep and ox. Am. J Anat., 115 101–117

Baldwin, B. A., and F R. Bell 1960 The contribution of the carotid and vertebral arteries to the blood supply of the cerebral cortex of sheep and calves. J Physiol., 151 9P–10P

Barnett, C. H., and C. D. Marsden 1961 Functions of the mammalian carotid rete mirabile. Nature, 191 73–74.

Barnett, R. J and R. O Greep 1951 The direction of flow in the blood vessels of the infundibular stalk. Science, 113: 185.

Bosi, V G. B Caradonna, G. Spampani, L. Varaldi and U Zimmerl 1909 Trattato di Anatomia Veterinaria, Vol. II, Angiologia, Casa Editrice Vallardi, Milano, 158–160.

Boyd, W H. 1960 The meningeal relations of the hypophysis cerebri. Anat. Rec., 137 437–451.

Bruni, A. C., and U Zimmerl 1951 Anatomia degli Animali Domestici. Seconda Edizione, Vol. II. Casa Editrice Vallardi, Milano. Chap V 330–331; 319

Carleton, H. M., and R. A. B Drury 1957 Histological Technique for Normal and Pathological Tissues and the Identification of Parasites, Third Edition. Oxford University Press, London. Chap. 4 72.

Cowie, A. T and J S. Tindal 1961 Hypophysectomy of the goat. J Endocrin., 22 313–320.

Crossmon, G 1937 A modification of Mallory' connective tissue stain with a discussion of the principles involved. Anat. Rec., 69 33–38.

Daniel, P M., J D K. Dawes and M. M. L. Prichard 1953 Studies of the carotid rete and its associated arteries. Proc. R. Soc. London, Series B 237 173–208.

Daniel, P M., and M. M. L. Prichard 1956 Anterior pituitary necrosis. Infarction of the pars distalis produced experimentally in the rat. Quart. J Exp. Physiol., 41 215–229.

——— 1957 The vascular arrangements of the pituitary gland of the sheep Quart. J Exp. Physiol., 42 237–248.

——— 1957b Anterior pituitary necrosis in the sheep produced by section of the pituitary stalk. Quart. J Exp. Physiol., 42: 248–254.

——— 1958 The effects of pituitary stalk section in the goat. Am. J Path., 34 433–469

De Beer, G. R. 1926 The Comparative Anatomy Histology and Development of the Pituitary Body Oliver and Boyd, London.

Dellmann, H.-D. 1960 Histologische Untersuchungen über den Feinbau der Zona interna des Infundibulum beim Rind. Acta morph. neerlando-scandin., 2 1–30.

Diepen, R 1960 Der Hypothalamus. In: Handbuch der mikroskopischen Anatomie des Menschen. begründet von Möllendorff, fortgeführt von Bargmann. Springer Berlin. Bd 4/7 325.

Duvernoy H., and J G. Koritké 1960 Sur la vascularisation de l'hypophyse. J Méd. Lyon, 41 476–488.

Ellenberger W and H. Baum 1932 Handbuch der vergleichenden Anatomie der Haustiere. Siebzehnte Auflage, Julius Springer Berlin. Chap. IV 665.

Franck, L. 1894 Handbuch der Anatomie der Haustiere mit besonderer Berücksichtigung des Pferdes. Schickhardt und Ebner, Stuttgart. Part II, 54–55.

Fumagalli, Z. 1941 La vascolarizzazione dell' ipofisi umana. Z. Anat. Entwickl-Gesch., 111 286–306.

Ganfini, C 1922 Su uno speciale lobulo dell' hypophysis cerebri in embrioni di pecora sul suo significato. Arch. ital. Anat. Embriol., 19 85–121.

Gilmore L. O., W E. Peterson and A. T Rasmussen 1941 Some morphological and functional relationships of the bovine hypophysis. Minn. Ag. Exp. St. Tech. Bull., 145 1–65.

Glósz, L. 1962 Die Schädelhöhlenkonfiguration des Basisphenoids unter besonderer Berücksichtigung der Sella Turcica. Acta vet. Acad. Sci. hung., 12: 213–233.
Green, J D 1951 The comparative anatomy of the hypophysis, with special reference to its blood supply and innervation. Am. J Anat., 88 225–312.
Green, J D and G. W Harris 1947 The neurovascular link between the neurohypophysis and adenohypophysis. J Endocrin., 5 136–146.
——— 1949 Observation of the hypophysio-portal vessels of the living rat. J Physiol., 108 359–361
Greep, R. O 1963 Architecture of the final common pathway to the adenohypophysis. Fertil. and Steril., 14 153–179
Harris, G W 1955 The function of the pituitary stalk. Johns Hopk. Hosp. Bull., 97 358–375.
Hill, R. T C. W Turner A. W Uren and E. T Gomez 1935 Hypophysectomy of the goat. Missouri Agr Exp. St. Bull., 230 1–18.
Holmes, R. L., and S. Zuckerman 1959 The blood supply of the hypophysis in Macaca mulatta. J Anat., 93 1–8.
House, E. L. 1943 The development of the hypophysis of the ox. Am. J Anat., 73 1–25.
Jubb, K. V 1962 Comparative Neuropathology by J R. M. Innes and L. Z. Saunders. Academic Press. New York and London. Chap. VI, The Hypophysis, 247
Jubb, K. V., and K. McEntee 1955 Observations on the bovine pituitary gland. II. Architecture and cytology with special reference to basophil cell function. Cornell Vet., 45 593–641.
Koller R. 1922 Zur vergleichenden Anatomie der Hypophysenumgebung. Z. An t. Entwickl. Gesch., 65: 163–203.
Legait, M. E. 1944 Anastomoses artério-veineuses au niveau du réseau admirable carotidien chez le veau. Ann. Endocr (Paris) 5 89–90.
Lillie, R. D 1954 Histopathologic Technic nd Practical Histochemistry The Blakiston Co. Inc., New York and Toronto.
Martin, P and W Schauder 1938 Lehrbuch der Anatomie der Haustiere. III. Band, Anatomie der Hauswiederkäuer. Schickhardt und Ebner Stuttgart, 401
Morato, M. J X. 1939 The blood supply of the hypophysis. Anat. Rec., 74 297–320.
Morin, F 1939 Ricerche sulla vascolarizzazione dell' ipofisi della sostanza nervosa contigu Anat. Anz., 88 369–380.
Popa, G., and U Fielding 1930 The vascular link between the pituitary and the hypothal... areas. Lancet, 219 238–240.
Romeis, B 1940 Die Hypophyse. In: Handbuch der mikroskopischen Anatomie des Menschen, von Möllendorff. Springer, Berlin. B... VI/3.
Schmidt, K. 1910 Die arteriellen Kopfgefässe des Rindes. Internat. Monatsschr. f. Anat. Phys., 27 187–264.
Sisson, S., and J D. Grossman 1953 The Anatomy of the Domestic Animals, Fourth Edition, Revised. W B Saunders Co., Philadelphia and London. Angiology 793.
Spanner R. 1952 Die Bedeutung der Hypophysenpfortadern für die Blutströmungsmöglichkeiten zwischen Hypophyse und Hypothalamus im Hypophysenkreislauf. Klin. Wschr., ... 32: 721–725.
Tanaka, F 1961 The apparatus in the blood vessels of the hypophysis regulating the blood flow Arch. Histol. Jap., 21 221–237
Török, B 1954 Lebensbeobachtung des Hypophysenkreislaufes an Hunden. Acta morph. Acad. Sci. hung., 4 83–89.
van Vuuren, H 1928 Bijdrage tot de Kennis der macroscopische Anatomie van de Hypophysis cerebri der Huisdieren. T Diergeneesk., 55 481–488; 529–537; 595–602.
Waage, S. 1953 The morphology of the hypophysis in some Artiodactyla. Kgl. Fysiog. Sällsk. Förhandl., Lund, 23 13–17
Wislocki, G. B and L. S. King 1936 The permeability of the hypophysis and hypothalamus to vital dyes, with a study of the hypophyseal vascular supply Am. J Anat., 58: 421–472.
Worthington, W C. 1955 Some observations on the hypophyseal portal system in the living mouse. Johns Hopk. Hosp. Bull 97 343–357
Wulzen, R. 1914 The morphology and histology of a certain structure connected with the pars intermedia of the pituitary body of the ox. Anat. Rec., 8 403–414
Xuereb, G. P M. M. L. Prichard and P M. Daniel 1954 The arterial supply and venous drainage of the human hypophysis cerebri. Quart. J Exp. Physiol., 39 119–217
Zhedenov B. H. 1937 On the question of the obliteration of the internal carotid artery in cattle. (Russ., title transl.) Arkh. Anat. Gistol., Embriol. 16 490–508.

PLATES

PLATE 1

EXPLANATION OF FIGURES

1 Ventral view of the rete mirabil injected with latex; calf apr arteria proximalis pro rete mirabile; adr arteriae distales pro rete mirabile; n5 ophthalmic and maxillary divisions of trigeminal nerve; ic, internal carotid artery; ror rete mirabile arteriae ophthalmicae internae; lp lateral plexus of rete mirabile rostrale; oc, optic chiasma; on, optic nerve; pd pars distalis; rcb, rostral communicating branches; rmc rete mirabile caudale; vo ventral retial extension. 2.5 ×

2 Ventral view of the rete mirabile injected with latex; calf On the left the rete was dissected to expose the internal carotid artery The pars distalis was removed pr arteria proximalis pro rete mirabile; n5, ophthalmic and maxillary divisions of trigeminal nerve; ic inter nal carotid artery; lis lower infundibular t m; lp lateral plexus of ret mirabil rostrale; nl neural lobe; oc optic chiasma; rmc rete mirabile caudale 3 ×


on
c
n5
Pd
apr
1
oc
n5
ic
lls
nl
apr

PLATE 2

EXPLANATION OF FIGURES

3 The rostral surface of the median eminence viewed after injection with India ink; calf. Note the branches of the rostral hypophysial arteries (rha) joining the median eminence at the top of the picture. The large superficial vessels running down the median eminence are injected portal vessels within the pars tuberalis. 12 ×

4 The lateral surface of the median eminence (the expanded upper portion) and the upper infundibular stem (the tapered lower portion) viewed after injection with India ink; calf. The right side of the picture is rostral; the top of the picture is dorsal. cvb, caudoventral branch of the rostral hypophysial arteries; rha, rostral hypophysial arteries. 15 ×

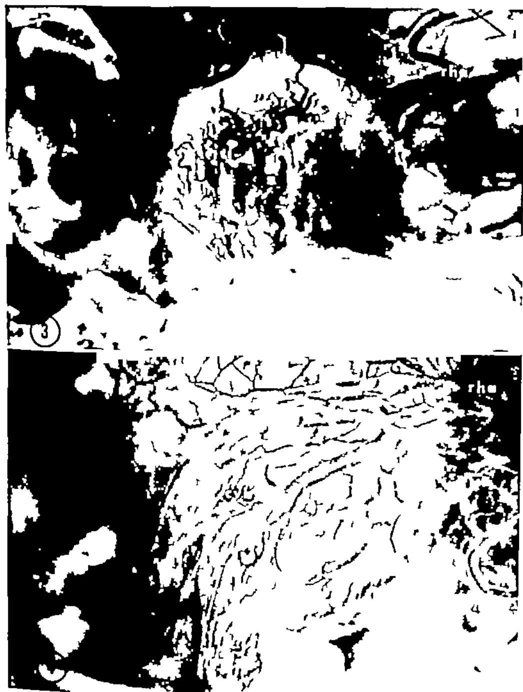

rha
3
rha
4
4

PLATE 3

EXPLANATION OF FIGURES

5 The caudal surface of the infundibulum viewed from above; calf. The vessels were injected with India ink. cvb, caudoventral branch of the rostral hypophysial arteries; ds, diaphragma sellae; lis, lower infundibular stem; me, median eminence. The caudoventral branch of the rostral hypophysial arteries on the left was interrupted in the course of dissection. 15 ×

6 A sagittal section cut through the rostral portion of an uninjected hypophysis; calf. The right side of the picture is ventral; the top of the picture is rostral. cor, cortex of pars distalis; ds, diaphragma sellae; lis, lower infundibular stem; med, medulla of pars distalis; pt, pars tuberalis; ri, recessus infundibuli; uis, upper infundibular stem. 7 ×

7 A sagittal section cut through the rostral part of the hypophysis; calf. The vessels were injected with India ink and the section cleared in benzyl benzoate. The left side of the picture is rostral; the top of the picture is dorsal. cvb, caudoventral branch of the rostral hypophysial arteries; lis, lower infundibular stem; pd, pars distalis; pi, pars intermedia; sps, second portal system. 65 ×


me
scv
lis
5
ds
is
cor
cor
lis
6
scv
lis
pi
pd

PLATE 4

EXPLANATION OF FIGURES

8 A section cut from the upper infundibular stem including the pars tuberalis; calf The vessels were injected with India ink and cleared in benzyl benzoate. The vascular area at the bottom f the picture is the pars tuberalis. The larg vascular complex arising from the pars tuberalis on the right is an arborization form. The smaller vessels to the left are capillary loops 235 ×

9 A section cut from the upper infundibular stem including the pars tuberalis; calf The vessels were injected with India ink and cleared in benzyl benzoate. The vascular region at bottom of the picture is the pars tuberalis. The large vascular complex projecting from the pars t beralis is an arborization form The smaller vascular complex to the right f the arborization form and partially concealed by it is a capillary loop 285 ×

10 Spike form injected with India ink; calf This section was taken from the upper inf ndibular tem and cleared in benzyl benzoate Note the capillary ramification from the lower half of the spike 290 ×

11 A section cut from the upper infundibular stem including the pars tuberalis; calf. The vessels were injected with India ink and cleared in benzyl benzoate. At the bottom of the picture are the fragmented vessels of the pars tuberalis. The elongated vascular complex projecting up and to the right is spike form. The smaller vessel complex emerging from the pars tuberalis at the right f the spike is a capillary loop 340 ×


8


9


10


11

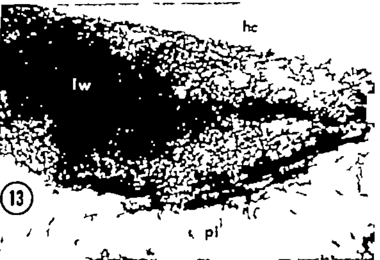
PLATE 5

EXPLANATION O FIGURES

12 A transverse section of 50 μ thickness cut through the upper infundibular stem and the rostral portion of the pars distalis; calf. The blood was stained by the benzidine method. pd, pars distalis; pt, pars tuberali ; pv portal vessels entering the pars distalis; ri, recessus infundibuli; uis upper infundibular stem. 30 ×

13 A sagittal section of 50 μ thickness through the lobe of Wulzen in which the blood was stained by the benzidine method; cow The left side of the picture is rostral; the top f the picture is dorsal. hc, hypophysial cleft; lw lobe of Wulzen; pi, pars intermedia. 140 ×

14 Lateral view f calf hypophysis injected with India ink and cleared in benzyl benzoate. cm, corpo mammillaris; ds, diaphragma sellae; hc, hypophysial cleft; me, median eminence; nl, neural lobe; oc, optic chiasma; pd, pars distalis; pi, pars intermedia. 5 ×


13
lw
hc
hc
pl

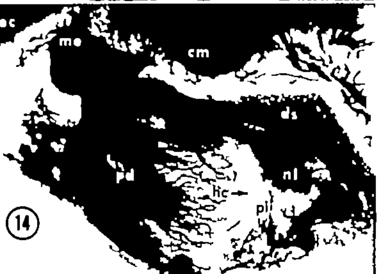

14
oc
me
cm
ds
pd
nl
hc
pl

PLATE 6

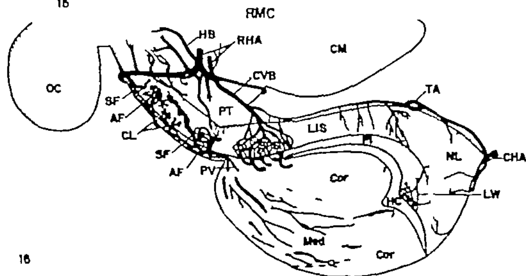
EXPLANATION OF FIGURES

15 A semidiagrammatic representation of the ventral surface of the rete mirabile cerebri; calf. APR, arteria proximalis pro rete mirabile; ADR, arteriae distales pro rete miabile; AS artery from the sphenoid bone; ERE, extracranial retial extension; IC internal carotid artery; IOR, rete mirabile arteriae ophthalmicae internae; LP lateral plexus of rete mirabile rostrale; ON optic nerve; PD pars distalis; RCB rostral communicating branches; RMC, rete mirabile caudale; VRE, ventral retial extension.

16 A diagrammatic representation f the blood supply to the hypophysis viewed from the left; calf The shaded area has been cut out t allow visualization of the distribution of vessels within the gland. AF arborization form (enlarged); CHA, caudal hypophysial arteries; CL, capillary loop (enlarged); CM, corpus mammillaris; Cor cortex of pars distalis; CVB caudoventral branch of the rostral hypophysial arteries; HB hypothalamic branch of the rostral hypophysial arter ies HC hypophysial cleft; LIS lower infundibular stem; LW lobe of Wulzen; Med, medulla of pars distalis; NL, neural lobe; OC, optic chiasma; PI, pars intermedia; PT pars tuberalis; PV portal vessel; RHA rostral hypophysial arteries; SF spike form (enlarged); SPS, second portal system; TA transverse anastomosis of the caudal hypophysial arteries.

ERE
IOR
ON
ADR
LP
PD
LP
VRE
AS
APR
IC
RMC

15



16

ltrastructure of Developing Muscle Cells the Chick Embryo [1]

E. RAWORTH ALLEN AND FRANK A. PEPE
Department of Anatomy The University of Pennsylvania School of Medicine Philadelphia

ABSTRACT Sectioned as well as negatively stained preparations of developing myotomal cells from the chick embryo were studied with the electron microscope. The application of these two techniques to similar material made it possible to observe developing muscle cells in successive stages of differentiation and at the same time visualize some of the isolated components making up these cells.

The thick and thin filaments observed in the embryonic muscle were morphologically indistinguishable from those bserved in adult muscle. The thin filaments found randomly dispersed in the cytoplasm of the early cells, were present in large concentrations before the first ppearance of thick filaments. The first observed thick filaments had lengths of 1.5 μ, equal to that f adult thick filaments. The appearance of large polyribosomes was correlated with the first appearance of the thick filaments. Single and small groups of ribosomes were always present. Early formed thick and thin filament aggregates were found in the same hexagonal array that is typical to the organization of myofilaments in adult myofibrils. Non-striated myofibrils, associated with periodic transverse tubular system, were found before striated myofibrils could be observed. Some preliminary observations were made concerning the appearance of glycogen particles.

Myofibrillar origin has been one of the ost controversial aspects of muscle dif rentiation. Almost every cellular com nent has been thought, at one time or nother to be the precursor of the con ctile elements. The association of mito ondria with myofibrillogenesis has been e of the most widely accepted concepts. me early workers proposed a direct ansformation of elongated mitochondria to myofibrils (Meves '07; Duesberg, '10 d Levi and Chevremont, 41) whereas hers believed in an indirect association e theories advocating a direct transfor ation of mitochondria to myofibrils were sed on the fact that all developing mus cells contain elongated mitochondria igned parallel to the cell axis. Prior to e development of electron microscopy is phenomenon was observed before yofibrils could be seen. Cowdry ('26) lieved that differentiation takes place as result of a surface film reaction between e mitochondria and the cytoplasm. Ear r Regaud ('11) had stated that the mito ondria induce some other cytoplasmic mponent to form myofibrils. Weed ('36) ld that these induced components were nall granules. Still othe workers have ated that myofibrils form as a result of the linear aggregation and fusion of the cytoplasmic granules (Godlewski, '02 Haggquist, '20 and McGill, '10) Moscona ('55) suggested a direct relationship between the appearance of myofibrils and decrease in the number of polysaccharide and ribonucleoprotein containing granules. Holtzer et al. ('57) proposed the entirely different idea, that the formation of myofibrils occurs in association with the cell surface Electron microscopic studies of myogenesis have not adequately clarified the subject (Van Breeman '52 Hibbs '56 Bergman, '62 and Shafiq '63) In Shafiq's ('63) recent investigations of muscle development in the fruit fly he found a close association between the cell membrane and first formed myofilaments, but *this was not the case with myofilaments* formed later in development. These latter filaments usually appeared near the tips of growing myofibrils.

Although myogenesis has not been adequately clarified in electron microscopy the fine structure of adult skeletal muscle has been extensively investigated (Hall et al 46; Huxley '57 Sjostrand and Ceder

[1] This investigation was supported by USPHS Training Grant 5T1 GM 351 and USPHS Research Grant AM-04806

gren, '57 Knappeis and Carlsen, '62; Pepe '63; and many others) It has been shown that muscle is composed of two types of filaments. Many studies not only *confirmed the presence of these filaments*, but also gave information concerning their individual protein content. Thick filaments found only in the A bands, contain myosin. Thinner ones found in the I band and the lateral portions of the A band, contain actin. The exclusive use of sectioned material may present some difficulties and inadequacies in interpretation. Thin sections do not always enable visualization of a complete structure since parts of the structure may extend out of the *plane of the section. In addition, problems* arise concerning the sampling of material and concerning possible artifacts produced during preparation. In order to obviate some of these difficulties, an entirely different method of preparation, utilizing homogenization and negative staining, may be used. Huxley ('61 '63) developed this method which enabled him to visualize important structural characteristics of filaments isolated from adult muscle.

In this investigation with respect to myofilaments, four major questions were asked

(1) Do thick and thin filaments appear simultaneously?

(2) Do the filaments change in dimension during development?

(3) Does any correlation exist between a particular sub-cellular element and the appearance of myofilaments?

(4) Can the initial organization of myofilaments into myofibrils be observed in myogenic cells?

With respect to the sub-cellular elements it was found that the changes in appearance of ribosomes and polyribosomes were quite drastic These particles are believed to be concerned with protein synthesis (Porter '54 Warner et al '62 Rich '63). Because of the drastic changes in these particles, it was possible to ask questions concerning their correlation with myofilament formation. In addition the first appearance of glycogen could be followed in this system and some preliminary observations were made

MATERIAL AND METHODS

A. Sectioned material

Fertile eggs from white leghorn chicks were incubated at 38.5 until the desired stages of development were reached. Embryos were staged throughout according to the series of Hamburger and Hamilton ('51) At various time intervals, stage 14 16 18 20 24 and 28 embryos were removed from eggs and placed in Simms balanced salt solution (Parker '30) With the aid of small sharp tissue knives and a dissecting microscope, they were stripped of membranes heads, hearts and lateral plate mesoderm. The trunks were placed in a fresh salt solution and the intermediate mesoderm, when *present*, was removed. Transverse sections of the trunk were made between the nineteenth and twentieth pair of somites and between the twenty-fifth and twenty-sixth pair of somites. The areas anterior and posterior to these cuts were discarded, leaving uniform trunk segments consisting of a spinal cord, notocord and five contralateral pairs of somites. There were only 22 pairs of somites present in stage 14 material, and therefore, segments 20 to 22 inclusive were used in this stage. The older material was usually bisected and cut transversely into halves or thirds without damaging the somites.

One of the eggs was incubated for days and the chick allowed to hatch. After 12 hours, a lethal dose ($1\ cm^3$) of sodium nembutal was injected intraperitoneally. Soon after the last muscle twitch was detected (approximately 15 minutes after administration of the nembutal) a thin strip of muscle was excised from the right midlateral breast. The tissue was put in Simms salt solution and cut into small pieces approximately 2 mm long and 1 mm in diameter

The small pieces of tissue were removed from the salt solution and fixed in a pre-cooled 1% osmium tetroxide solution in veronal buffer pH 7 4 for one-half hour. The fixed material was washed in Simms solution and dehydrated by bringing it through 20 40 60 80 95 and 100% ethanol solutions for five minutes each and allowed to remain in 100% ethanol for one hour with two changes. The br

hange of alcohol was replaced with an raldite solution consisting of equal vol mes of dodecenyl succinic anhydride and raldite 502. Vials containing the tissue nd the Araldite solution were placed on n electric rotary type mixer and left over ight at room temperature (approximately 7 hours) The Araldite mixture was re- laced with one containing an accelerator 0.2 cm benzyl dimethyl amine per 10 ml raldite mixture) The vials were re urned to the rotary mixer and left at room emperature for three hours before placing hem in a 40 C oven. Continual stirring was maintained in the oven for an addi ional three hours. The small pieces of issue were individually transferred to o. 000 gelatin capsules and the capsules were filled with fresh Araldite solution containing accelerator The capsules were eturned to the 40 C oven for three days of polymerization. The gelatin capsules were easily removed with light scraping under warm, running water

The hard resin blocks were sectioned with glass knives or with a diamond knife in a Porter Blum microtome Sections showing gray silver or slightly gold inter ference colors were picked up on uncoated 300 mesh copper grids.

Electron micrographs were obtained from unstained sections as well as from sections stained with phosphotungstic acid or lead tartrate. Staining techniques were as follows:

Phosphotungstic acid staining

A 1% solution of phosphotungstic acid was prepared in 95% ethanol. The grids were immersed in this stain for one min- ute, followed by two successive one min ute rinses in separate containers of 95% ethanol.

Lead tartrate staining

A solution of lead tartrate was prepared according to Millonig ('61) The grids were stained by floating them in an in verted position on several drops of the staining solution for eight minutes. Wash ing was accomplished by constant agita tion of the grids for one minute in ion-free water

An Hitachi HS, electron microscope was used for scanning this material. Most of the final micrographs, however were ob- tained in a Siemens Elmiskop I.

Hitachi HS

A 50 μ condenser and 30 μ objective aperture were used with an accelerating voltage of 50 kv Pictures were taken at a variety of magnifications (usually 5,000 × to 15,000 ×)

Siemens Elmiskop I

A 200 μ condenser and a 50 μ objective aperture were used. An accelerating volt age of 60 kv was used at a magnification of 10,000 × and 80 kv was used at 40,000 × magnification.

B Homogenized material

The material for these experiments cor responded to that used for sectioning. In addition, trunk segments were obtained from stage 17 and 30 embryos. Also breast muscle from 10 12, 14 and 18 day incubated embryos was used. Tissue trim- ming was done in a standard salt solution composed of 0 06 M phosphate buffer 0 009 M KCl, 10^{-4} M $MgCl_2$, and 10 M EDTA, pH 7.0 Solutions were kept in a coldroom (approximately 2 C) until im- mediately before use The solutions were then placed in small lowform preparation dishes which were immersed in ice. The trimming was done on ice with the aid of a dissecting microscope.

After trimming, the solution was re moved with a bulb pipette and replaced with a small volume of a similar solution to which an additional 3.5×10^{-4} M ATP was added (relaxing medium) Homog enization was accomplished by drawing the tissue repeatedly into a 1 ml syringe (without a needle) After most of the material was suspended it was transferred into 3 ml vials and placed in a Servall refrigerated centrifuge maintained at 0 C. The suspension was centrifuged at 400 g for five minutes. The supernatant was drawn off and saved. The residue was resuspended in an equal volume of relax ing medium and again centrifuged at 400 g for ten minutes. The residue was discarded and the two supernatants were combined. This combination was mixed with a fresh solution (2 or 3 ml) of relax ing medium and the final suspension was

used for negative staining The techniques for negative staining were based on methods described by Huxley and Zubay ('60)

Parlodian-coated 200 mesh copper grids were covered with a thin sheet of carbon. A drop of the suspension was placed on these grids and washed immediately with five or six drops of standard salt solution This was followed by a few drops of 2% aqueous solution of uranyl acetate (pH 4 0) which was allowed to remain for three seconds and drained as completely as possible with filter paper The grids were dried in air and observed in the electron microscope A Siemens Elmiskop I electron microscope was used exclusively for obtaining micrographs of this negatively stained material.

RESULTS

Sectioned material

Myotomal cells from the trunk somites of stage 14 chick embryos are morphologically similar to undifferentiated mesenchymal cells. Electron microscopic observations of these presumptive muscle cells reveal relatively rounded mononucleated cells The nuclei are centrally located spherical, and contain one or often two granular nucleoli. Typical nuclear membranes with nuclear pores can usually be observed. Mitochondria which are predominantly oval but occasionally elongated are found in the cytoplasm along with moderate number of free ribosomes No filamentous material is ever detected in these cells. By stage 16 most of the myotomal cells have become considerably elongated and contain oblong nuclei. In addition, in stage 16 many elongated mitochondria are seen that appear to be assuming positions parallel to the long axis of the cell. Single or small clusters of ribosomes which are not associated with any membranes give the cytoplasm a granular appearance Occasional, randomly dispersed, wavy filaments of 55 to 65 A diameters and variable lengths are found in the cytoplasm Lengths exceeding 1 μ however are not seen. These filaments are clearly visible when the sections are stained with phosphotungstic acid as shown in figure 1 and slight bulges with no distinct periodicity are often seen along their lengths.

By stage 18 the number of wavy thin filaments in the cytoplasm of the elongated cells has increased (fig. 2) Thick filaments with a diameter of 110 to 120 A and a 1.5 μ length are occasionally seen at this stage. They are never observed singly but only in aggregates of thin and thick filaments. These aggregates are shown in figure 3 Small, lateral projections are seen on the surface of the thick filaments when phosphotungstic acid stained sections are observed at high magnification (fig 3) At this stage, large polyribosomes first appear in the cytoplasm They appear to be arranged in a helical configuration Small cytoplasmic clusters of glycogen also first appear at this stage of development. These are much more visible by lead tartrate staining of the sections

Cells similar to those described in stage 18 are observed in stage 20 material. However there is an increase in the aggregations of the thin and thick filaments into early myofibrils. Helical arrangements of ribosomes, or polyribosomes, and large and small clusters of glycogen are seen in abundance in figures 4 and 5. Elongated mitochondria are again commonly aligned parallel to the cell axis.

After four days of development (stage 24) myotomal cells can be found representing every previously described stage of development. In addition, small myofibrils most of which measure approximately 0 5 μ in width are seen (fig. 6). Since the section seen in figure 6 was stained with lead tartrate rather than phosphotungstic acid the thin filaments in the background are not very apparent. There are no distinct I bands or Z lines present in these early myofibrils. At approximately 1 5 μ intervals tubules surround groups of filaments within fibrils as well as entire myofibrils (figs. 6 7) In several instances a dense material resembling a typical Z line is found in place of the tubule There is no sign of an M line or an H zone in the early myofibrils. In a few instances cross sections of small aggregates of thick and thin filaments may be seen (fig 6). These aggregates show the typical hexagonal array At this stage also glycogen, elongated mitochondria, ribosomes, and polyribosomes are all present in abun-

lance. The glycogen is often found in close proximity to a single membrane. There is always a clear space between the glycogen granules and the membrane This is easily seen in figure 5

. The typical banding patterns of mature myofibrils are seen in stage 28 material (fig. 8) The 1.5 µ A bands and the very Z lines are always present at this stage. The I bands vary in length from 0 to 0 4 µ depending on the state of contraction. A scarcely visible H zone bisected by a prominent M line is often seen in the center of the A band. The previously described tubular system is occasionally visible associated with the dense Z line. This is especially apparent in figure 8. The sarcomeres of the myofibrils, side by side, are generally in register. The sarcoplasm of these five-day embryonic cells contains an abundance of polyribosomes and elongated mitochondria. Many vesicles, some with a diameter as large as 0.8 µ are scattered throughout the cytoplasm.

The myofibrils found in breast muscle of 12 hour posthatched chicks are structurally similar to those observed in five-day embryonic myotumes. However they are present in larger numbers. Large vesicles are now often found in close proximity to the Z lines. In figure 9 a small tubular connection can be seen between these vesicles and the tubules surrounding the myofibrils. Thin filaments are occasionally seen scattered at random in the sarcoplasm. More cristae are observed in the elongated mitochondria of this muscle In many instances small vesicles are seen associated with the inner surface of the cell membranes An amorphous coat (base membrane) can often be seen associated with the exterior surface of post hatched chick muscle cells.

B Homogenized material

Thin filaments A small number of filaments with a beaded appearance are present in negatively stained preparations of stage 16 material. These filaments possess a fine structure identical with the thin ones described in 1963 by Hanson and Lowy ('63) No filamentous material is present in stage 14 and when preparations of stages older than 16 are observed, a much larger number of the thin filaments is observed. Representative filaments obtained from material of stages 16 18 and 28 are shown in figures 10 11 and 12 respectively The lengths of these filaments are extremely variable often measuring about 0.5 µ. None are seen with lengths exceeding 1.0 µ Their diameters range between 63 to 75 A. The filament itself is composed of two tightly wound strands, crossing over one another at 350 A intervals. The strands consist of approximately 50 A spherical units.

Thick filaments The thick filaments are structurally the same as those obtained from the adult muscle (Huxley '61 63) The filaments are 1.5 µ long and 105 to 120 A in diameter They are first seen in preparations from stage 18 embryos and whenever observed they always have the same dimensions. Figure 13 a, b and c show samples from three different stages. The thick filaments always have tapering ends. Broken filaments are easily recognized because of the lack of such a taper at both ends. The filaments have a rough surface except for a smooth central portion approximately 0 15 to 0.20 µ in length.

Other sub-cellular particles Ribosomes measuring 230 A in diameter are seen in all embryonic stages. In stages 16 and 17 they occur singly and in small clusters of not more than 6 to 8 closely associated particles. In stage 18 material large polyribosome chains are first seen. The long chains may contain as many as 70 to 75 ribosomes (figs. 11 14 and 16) In figure 15 small threads approximately 10 to 12 A in diameter can be seen connecting the ribosomes.

With the exception of stage 14 smooth surfaced glycogen granules are seen in all of the experimental material. The diameter of these granules varies from 150 to 450 A. The glycogen particles usually occur singly but small clusters are occasionally seen.

DISCUSSION

In order to be able to compare successive stages of muscle development, the same numbered somites from each embryo were used. There is a definite cephalo-caudad progression of development in the chick embryos. For this reason, the

muscle differentiation of the more cephalad somites was necessarily more advanced than that of the somites caudal to them. Table 1 illustrates the number of embryos used, the number of experiments performed and the total number of somites examined in each experiment.

In sections of the developing muscle thin filaments were seen two stages before thick filaments. This was confirmed using homogenization experiments and the respective thick and thin filaments were shown to be morphologically indistinguishable from myosin and actin filaments found in adult muscle (Huxley '61; Hanson and Lowy '63). The appearance of *the filaments will be discussed in more detail subsequently.*

The first unbroken thick filaments to be observed possessed lengths of 1.5 μ. Measurements were made from negative stained preparations of homogenized material. Broken filaments were easily detected because of the lack of tapering ends common to all thick filaments. No unbroken filaments of lengths shorter than 1.5 μ were seen in the early material. This suggests that thick filaments are rapidly assembled into their full lengths and do not slowly grow in the cytoplasm. If shorter lengths were often present they should have been detected since myosin filaments are insoluble in the solutions used for this separation. A similar solution was used by Huxley ('63) to grow artificial thick filaments from a purified myosin solution. The artificial filaments were identical to those naturally occurring in adult muscle, except that there were many which were longer or shorter in length. All the filaments, normal and artificial, had the same diameters, a smooth central zone of constant dimensions, rough surface and tapering ends. The fact that no thick filaments possessing lengths longer or shorter than 1.5 μ were present in this investigation also suggests that they could not have been formed as a result of the experimental procedures used.

Bergman ('62) described an association between free ribosomes and myofilament *differentiation. Correlations reported by earlier workers between various cellular* elements and myofibrillogenesis were never observed. Elongated mitochondria were found aligned parallel to the cell axis but no suggestion of a transformation into myofibrils was seen. Likewise, a fusion of cytoplasmic granules to form myofibrils was never seen. At times, some of the aggregates of thick and thin filaments were found in close association with the cell surface, but they were more abundantly found randomly dispersed in the interior of the cell. This random dispersion is not in agreement with the sarcolemmal end-plate idea suggested by Holtzer et al. ('57) but is in accord with Bergman ('62).

When actin filaments were present at the time preceding the first appearance of

TABLE 1

Number of embryos studied, number of experiments performed, and number of somites per experiment

Stage	Sectioned material	Homogenized material		
	No. of embryos studied	No. of experiments	No. of embryos in each experiment	Total no. of somites examined
14	1	1	4	24
16	2	3	6, 6, 7	60, 60, 70
17	—	1	5	50
18	2	3	5, 5, 5	50, 50, 50
20	2	—	—	—
24	4	1	6	60
28	8	2	6, 3	60, 30
30	—	1	5	50
10 day	—	1	3	—
12 day	—	1	3	—
14 day	—	1	2	—
18 day	—	1	2	—
Post hatched	1	1	1	—

filaments, single ribosomes and polyribosomes (3 to 6 or 8 ribosomes) were present. Observed simultaneously with the thick filaments were long polyribosomes. These elements were observed at the same time both in sectioned and homogenized material. Polyribosomes were first described by Warner et al. ('62). Helical arrangements of ribosomes were recently reported in the cytoplasm of differentiating muscle cells (Waddington and Perry '63) however no significance was given to their presence. By comparison of figures 16 and 11 it can be seen that the ribosomal chains found in sectioned material were like those found in homogenized and negatively stained preparations. In order to synthesize a protein the size of myosin (molecular wt. = 420,000) a group of many ribosomal units might be expected. Indeed 70 to 75 ribosomes are counted in some of the large polyribosomes. A chain having a diameter of 10 to 12 A, as described for messenger RNA (Rich '63) is occasionally seen interconnecting the ribosomes in a single chain.

The first appearance of glycogen in negatively stained preparations of stage 16 embryos and in lead tartrate stained sections of stage 18 embryos could not be correlated with the observations on myofibrillogenesis. The significance of the relationship of a single membrane associated with a large aggregate of glycogen seen in sectioned material is not clear.

The earlier appearance of thin filaments provides a high concentration of actin with respect to the first myosin filament to be formed. Considering that the thin filaments interact with the cross bridges of the thick filaments (Huxley '57) a hexagonal array of thin filaments around each thick filament is the most stable configuration. Any other configuration would result in steric hindrance of the interacting filaments and thus an increase in the number of non-utilizable reactive sites. In addition, if the two filament types were bound together by only one site of interaction, the torques resulting from the filament lengths would probably lead to easy breakage of the bond. Any other configuration is thus less probable than one in which one thin filament is connected to one thick filament along its entire length through many bonds.

Small aggregates of thick and thin filaments became aligned by some unknown mechanism and formed what appeared to be loosely connected, nonstriated myofibrils. Tubules were found at 1.5 μ intervals along early myofibrils forming segments comparable in length to a thick filament and an A band, or both. Electron micrographs of this material showed that the segments consisted of a hexagonal arrangement of thick and thin filaments. The fact that nonstriated myofibrils appeared before striated is in agreement with many earlier workers in light microscopy (Godlewski, '02 Duesberg, '07; Haggquist, '20 Weed, '36 Holtzer et al., '57; and Holtzer '61). Holtzer ('61) suggested that there is a period of several hours in the history of every myoblast in which it contains a fine nonstriated longitudinal myofibril. In addition, he suggested that new nonstriated sarcomeres are added meristematically at the tips of already cross striated myofibrils. The lining up of myofibrillar units observed in this work is similar to this meristematic growth. Some workers, both in light and electron microscopy stated that the Z line is the first cross striation to appear (Weed, '36; Van Breeman '52 Hibbs '56 and Shafiq '63). Van Breeman ('52) who performed the first studies of myogenesis in electron microscopy stated that a constriction at the site of the future Z line was the first banding pattern. Hibbs ('56) from electron microscopic studies of developing cardiac muscle concluded that Z bands appear concurrently with, or shortly after the first formation of myofilaments into myofibrils. In the most recent electron microscopic studies of developing muscle Shafiq ('63) could find no time during development at which myofibrils did not contain a Z band. As pointed out by Holtzer ('57) caution should be taken when interpreting such a sequence because contraction bands often form a pattern simulating Z line material. In the present investigation a tubule was found at regular intervals along the early myofibril. In this instance the tubular system was the first indication of a banding pattern (stage 20), and four stages later (stage 24) a dense

osmiophilic substance (Z line) was sometimes noticed associated with the myofibrils at the level of these tubules. Later in development, the Z lines were always dense and distinct. I bands were seen only after the Z lines were definitely present (occasionally in stage 24 often in stage 28) Also seen at this time were the H zones and M lines. Considering the sliding filament model proposed for muscle (Huxley '57 Huxley and Hanson '60) it appears logical that H zones were found only when I bands were present and vice versa. It also seems plausible to assume that no I bands would be formed until Z lines were present. Only then would there be an anchor point for the attachment of thin filaments and thus the formation of I bands.

ACKNOWLEDGMENT

The authors gratefully acknowledge the helpful comments and typographical assistance of Rae P Allen, which were instrumental in the completion of this paper

LITERATURE CITED

Bergman, R. A. 1962 Observations on the Morphogenesis of Rat Skeletal Muscle. Bull. of the Johns Hopkins Hosp., *110* 187–201.

Cowdry E. V 1926 Surface film theory of the function of mitochondria. Am. Naturalist, *60* 157—165.

Duesberg, J 1910 Les chondriosomes des cellules embryonnaires du poulet et leur role dans la genese des myofibrilles avec quelques observations sur le developement des fibres musculaires striées. Arch. Zellforsch, *4* 602–671.

Godlewski, E. 1902 Die Entwicklung des Skelet-und Herzmuskelgewebes der Saugethiere. Arch. mikr Anat., *60*: 111–156.

Hagquist, G. 1920 Uber die Entwicklung der querstreiftigen myofibrillen beim frosche Anat. Anz., 52. 389–404

Hall, C C A. Jakus and F O. Schmitt 1946 An investigation of cross striations and myosin filaments in muscle. Biol. Bull., 90 32–50.

Hamburger V and H. Hamilton 1951 A series of normal stages in the development of the chick embryo. J Morph., *88* 49–92.

Hanson J and J Lowy 1963 The structure of F-Actin and of actin filaments isolated from muscle. J Mol. Biol *6* 46–60.

Hibbs, R. C. 1956 Electron microscopy of developing cardiac muscle in chick embryos. Am. J Anat., *99* 17 52.

Holtzer H 1961 Aspects of chondrogenesis and myogenesis. Synthesis of Molecular and Cellular Structure 19th Growth Symp. Ed. by Dorothea Rudnick, Ronald Press Co., New York.

Holtzer H., J Marshall and H Finck 1957 An analysis of myogenesis by use of fluorescent antimyosin. J Biophys. and Biochem. Cyt., 3 705–724

Huxley H. 1957 The double array of filaments in cross striated muscle. J Biophys. and Biochem. Cytol., 3 631–648.

Huxley H. E. 1961 The contractile structure of cardiac and keletal muscle. Circulation, 24 328–335.

——— 1963 Electron microscopic studies on the structure of natural and synthetic protein filaments from striated muscle. J. Mol. Biol., *7* 281–306.

Huxley H. E., and J Hanson 1960 The molecular basis for contraction in cross striated muscles. *Structure and Function of Muscle* Ed. by G. H. Bourne Vol. *1* 183–227 N Y Acad. Press.

Huxley H. E., and G. Zubay 1960 Electron microscopic observations on the structure of microsomal particles from escherichia coli. J Mol. Biol., *2*: 10–18.

Knappeis, C., and F Carlson 1962 The ultrastructure of the z disc in skeletal muscle. J Cell Biol., *13* 323–335.

Levi, G., and M. Chevremont 1941 Transformations structurales de elements des muscles squelettiques pendant leur croissance in vitro Arch. de Biol., 52 523–551

Meves, F 1907 Uber mitochondrien bzw chondriokonten in dem zellen junger embryonen. Anat. Anz., *31* 399–407

McGill, C. 1910 The early histogenesis of striated muscle in the oesophagus of the pig and the dogfish. Anat. Rec., *4* 13–47

Millonig, G. 1961 A modified procedure for lead staining of thin sections. J. Cell Biol. *11* 736–739

Moscona, A. 1955 Cytoplasmic granules in myogenic cells. Exp. Cell Res., *9* 377–380

Parker R. C. 1950 Methods of Tissue Culture 2nd. Ed., p. 80, Ed. by Paul Hoeber Inc N Y

Pepe F 1963 Possibilities for the use of antibody staining techniques in electron microscopy Techniques in Endocrine Research Ed by Eckstein and Knowles, London Ltd Acad Press. p. 43–55.

Porter K. R. 1954 Electron microscopy of basophilic components of cytoplasm. J. Histochem. and Cytochem., *2*: 346–373.

Regaud, C. 1911 Les mitochondries organes du protoplasma considerées comme les agents de la fonction electique pharmacopexique des cellules. Rev Med., *31* 681–699.

Rich, A. 1963 Polyribosomes. Scientific Am 209 44–53.

Shafiq S. A. 1963 Electron microscope studies on the indirect flight muscles of drosophila melanogaster J Cell. Biol., *17* 363–373.

Sjostrand, F S., and E. Andersson-Cedergren 1957 The ultrastructure of the skeletal muscle myofilaments at various states of shortening J Ultrastructure *1* 74–108.

Van Breemen, V L. 1952 Myofibril development observed with the electron microscope An t. Rec., *113* 179–195

Waddington, C. H and M. M. Perry 1963 Helical arrangements of ribosomes in differentiating muscle cells. Exp. Cell Res 30 599–6[illegible]

Warner, J. R., A. Rich and C. E. Hall 1962 Electron microscopic studies of ribosomal clusters synthesizing hemoglobin. Science, 138: 1399–1403.

Weed, I. G. 1936 Cytological studies of developing muscle with special reference of myofibrils, mitochondria, golgi material, and nuclei. Z. Zellforsch mikr. Anat., 25: 516–590.

PLATE 1

EXPLANATION OF FIGURES

1 Electron micrograph of stage 16 material. Note filamentous material present only in scanty amount (arrows) Many single and small clusters of ribosomes are seen in the cytoplasm of the elongated cells. Section stained with PTA. 40,000 ×

2 Electron micrograph of stage 16 material. A high concentration of thin filaments is seen in the cytoplasm of two cells. N thick filaments are seen in these particular cells. Section stained with PTA. Polyribosome (P) 50,000 ×

3 Electron micrograph of filament aggregates in stage 18. Many thin filaments are seen interspersed with the thick filaments. Tubules may be forming between aggregates (arrows) Section stained with PTA. 144,000 ×

change of alcohol was replaced with an Araldite solution consisting of equal volumes of dodecenyl succinic anhydride and Araldite 502. Vials containing the tissue and the Araldite solution were placed on an electric rotary type mixer and left over night at room temperature (approximately 17 hours) The Araldite mixture was replaced with one containing an accelerator (0.2 cm^3 benzyl dimethyl amine per 10 ml Araldite mixture) The vials were returned to the rotary mixer and left at room temperature for three hours before placing them in a 40 C oven. Continual stirring was maintained in the oven for an additional three hours. The small pieces of tissue were individually transferred to no. 000 gelatin capsules and the capsules were filled with fresh Araldite solution containing accelerator The capsules were returned to the 40 C oven for three days of polymerization. The gelatin capsules were easily removed with light scraping under warm, running water

The hard resin blocks were sectioned with glass knives or with a diamond knife in a Porter Blum microtome. Sections showing gray silver or slightly gold interference colors were picked up on uncoated 300 mesh copper grids

Electron micrographs were obtained from unstained sections as well as from sections stained with phosphotungstic acid or lead tartrate Staining techniques were as follows:

Phosphotungstic acid staining

A 1% solution of phosphotungstic acid was prepared in 95% ethanol. The grids were immersed in this stain for one minute, followed by two successive one minute rinses in separate containers of 95% ethanol.

Lead tartrate staining

A solution of lead tartrate was prepared according to Millonig ('61) The grids were stained by floating them in an inverted position on several drops of the staining solution for eight minutes. Washing was accomplished by constant agitation of the grids for one minute in ion-free water

An Hitachi HS, electron microscope was used for scanning this material. Most of the final micrographs however were obtained in a Siemens Elmiskop I.

Hitachi HS

A 50 μ condenser and 30 μ objective aperture were used with an accelerating voltage of 50 kv Pictures were taken at a variety of magnifications (usually 5 000 × to 15,000 ×)

Siemens Elmiskop I

A 200 μ condenser and a 50 μ objective aperture were used. An accelerating voltage of 60 kv was used at a magnification of 10,000 × and 80 kv was used at 40,000 × magnification.

B Homogenized material

The material for these experiments corresponded to that used for sectioning In addition, trunk segments were obtained from stage 17 and 30 embryos. Also breast muscle from 10 12 14 and 18 day incubated embryos was used. Tissue trimming was done in a standard salt solution composed of 0.06 M phosphate buffer 0 009 M KCl 10 M $MgCl_2$, and 10^{-4} M EDTA, pH 7.0 Solutions were kept in a coldroom (approximately 2 C) until immediately before use. The solutions were then placed in small, lowform preparation dishes which were immersed in ice. The trimming was done on ice with the aid of a dissecting microscope

After trimming, the solution was removed with a bulb pipette and replaced with a small volume of a similar solution to which an additional $3.5 \times 10^{-}$ M-ATP was added (relaxing medium) Homogenization was accomplished by drawing the tissue repeatedly into a 1 ml syringe (without a needle) After most of the material was suspended it was transferred into 3 ml vials and placed in a Servall refrigerated centrifuge maintained at 0 C. The suspension was centrifuged at 400 g for five minutes. The supernatant was drawn off and saved. The residue was resuspended in an equal volume of relaxing medium and again centrifuged at 400 g for ten minutes. The residue was discarded and the two supernatants were combined. This combination was mixed with a fresh solution (2 or 3 ml) of relaxing medium and the final suspension was

used for negative staining. The techniques for negative staining were based on methods described by Huxley and Zubay ('60)

Parlodian-coated 200 mesh copper grids were covered with a thin sheet of carbon. A drop of the suspension was placed on these grids and washed immediately with five or six drops of standard salt solution. This was followed by a few drops of 2% aqueous solution of uranyl acetate (pH 4.0) which was allowed to remain for three seconds and drained as completely as possible with filter paper. The grids were dried in air and observed in the electron microscope. A Siemens Elmiskop I electron microscope was used exclusively for obtaining micrographs of this negatively stained material.

RESULTS

Sectioned material

Myotomal cells from the trunk somites of stage 14 chick embryos are morphologically similar to undifferentiated mesenchymal cells. Electron microscopic observations of these presumptive muscle cells reveal relatively rounded mononucleated cells. The nuclei are centrally located, spherical, and contain one or often two granular nucleoli. Typical nuclear membranes with nuclear pores can usually be observed. Mitochondria which are predominantly oval but occasionally elongated are found in the cytoplasm, along with a moderate number of free ribosomes. No filamentous material is ever detected in these cells. By stage 16 most of the myotomal cells have become considerably elongated and contain oblong nuclei. In addition in stage 16 many elongated mitochondria are seen that appear to be assuming positions parallel to the long axis of the cell. Single or small clusters of ribosomes, which are not associated with any membranes, give the cytoplasm a granular appearance. Occasional, randomly dispersed, wavy filaments of 55 to 65 A diameters and variable lengths are found in the cytoplasm. Lengths exceeding 1 μ, however, are not seen. These filaments are clearly visible when the sections are stained with phosphotungstic acid as shown in figure 1 and slight bulges with no distinct periodicity are often seen along their lengths.

By stage 18 the number of wavy thin filaments in the cytoplasm of the elongated cells has increased (fig. 2). Thick filaments with a diameter of 110 to 120 A and a 1.5 μ length are occasionally seen at this stage. They are never observed singly but only in aggregates of thin and thick filaments. These aggregates are shown in figure 3. Small, lateral projections are seen on the surface of the thick filaments when phosphotungstic acid stained sections are observed at high magnification (fig. 3). At this stage, large polyribosomes first appear in the cytoplasm. They appear to be arranged in a helical configuration. Small cytoplasmic clusters of glycogen also first appear at this stage of development. These are made more visible by lead tartrate staining of the sections.

Cells similar to those described in stage 18 are observed in stage 20 material. However, there is an increase in the aggregations of the thin and thick filaments the early myofibrils. Helical arrangements of ribosomes or polyribosomes, and large and small clusters of glycogen are seen in abundance in figures 4 and 5. Elongated mitochondria are again commonly aligned parallel to the cell axis.

After four days of development (stage 24) myotomal cells can be found representing every previously described stage of development. In addition small myofibrils, most of which measure approximately 0.5 μ in width, are seen (fig. 6). Since the section seen in figure 8 was stained with lead tartrate rather than phosphotungstic acid, the thin filaments in the background are not very apparent. There are no distinct I bands or Z lines present in these early myofibrils. At approximately 1.5 μ intervals tubules surround groups of filaments within fibrils as well as entire myofibrils (figs. 6, 7). In several instances a dense material resembling a typical Z line is found in place of the tubule. There is no sign of an M line or an H zone in the early myofibrils. In a few instances cross sections of small aggregates of thick and thin filaments may be seen (fig. 6). These aggregates show the typical hexagonal array. At this stage also glycogen, elongated mitochondria, ribosomes, and polyribosomes are all present in the

-tance The glycogen is often found in close proximity to a single membrane. There is always a clear space between the glycogen granules and the membrane. This is easily seen in figure 5

The typical banding patterns of mature myofibrils are seen in stage 28 material (fig. 8) The 1.5 µ A bands and the very dense Z lines are always present at this stage. The I bands vary in length from 0 to 0 4 µ depending on the state of contraction. A scarcely visible H zone, bisected by a prominent M line is often seen in the center of the A band. The previously described tubular system is occasionally visible associated with the dense Z line. This is especially apparent in figure 8. The sarcomeres of the myofibrils located side by side are generally in register. The sarcoplasm of these five-day embryonic cells contains an abundance of polyribosomes and elongated mitochondria. Many vesicles some with a diameter as large as 0.8 µ, are scattered throughout the cytoplasm.

The myofibrils found in breast muscle of 12 hour posthatched chicks are structurally similar to those observed in five-day embryonic myotomes. However they are present in larger numbers. Large vesicles are now often found in close proximity to the Z lines. In figure 9 a small tubular connection can be seen between these vesicles and the tubules surrounding the myofibrils. Thin filaments are occasionally seen scattered at random in the sarcoplasm. More cristae are observed in the elongated mitochondria of this muscle In many instances small vesicles are seen associated with the inner surface of the cell membranes An amorphous coat (basement membrane) can often be seen associated with the exterior surface of posthatched chick muscle cells.

B Homogenized material

Thin filaments A small number of filaments with a beaded appearance are present in negatively stained preparations of stage 16 material. These filaments possess a fine structure identical with the thin ones described in 1963 by Hanson and Lowy ('63) No filamentous material is present in stage 14 and when preparations of stages older than 16 are observed, a much larger number of the thin filaments is observed. Representative filaments obtained from material of stages 16 18 and 28 are shown in figures 10 11 and 12 respectively The lengths of these filaments are extremely variable, often measuring about 0.5 µ. None are seen with lengths exceeding 1.0 µ. Their diameters range between 63 to 75 A. The filament itself is composed of two tightly wound strands crossing over one another at 350 A intervals. The strands consist of approximately 50 A spherical units.

Thick filaments The thick filaments are structurally the same as those obtained from the adult muscle (Huxley '61 '63) The filaments are 1.5 µ long and 105 to 120 A in diameter They are first seen in preparations from stage 18 embryos and whenever observed they always have the same dimensions. Figure 13 a, b and c show samples from three different stages. The thick filaments always have tapering ends. Broken filaments are easily recognized because of the lack of such a taper at both ends. The filaments have a rough surface except for a smooth central portion approximately 0 15 to 0.20 µ in length.

Other sub-cellular particles Ribosomes measuring 230 A in diameter are seen in all embryonic stages. In stages 16 and 17 they occur singly and in small clusters of not more than 6 to 8 closely associated particles. In stage 18 material, large polyribosome chains are first seen. The long chains may contain as many as 70 to 75 ribosomes (figs. 11 14 and 16) In figure 15 small threads approximately 10 to 12 A in diameter can be seen connecting the ribosomes.

With the exception of stage 14 smooth surfaced glycogen granules are seen in all of the experimental material. The diameter of these granules varies from 150 to 450 A. The glycogen particles usually occur singly but small clusters are occasionally seen.

DISCUSSION

In order to be able to compare successive stages of muscle development, the same numbered somites from each embryo were used. There is a definite cephalo-caudad progression of development in the chick embryos For this reason the

PLATE 1

EXPLANATION OF FIGURES

1 Electron micrograph of stage 16 material. Note filamentous material present only in a scanty amount (arrows) Many single and small clusters of ribosomes are seen in the cytoplasm of the elongated cells. Section stained with PTA. 40,000 ×

2 Electron micrograph of stage 18 material. A high concentration of thin filaments is seen in the cytoplasm of two cells. No thick filaments are seen in these particular cells. Section stained with PTA. Polyribosome (P) 50,000 ×

3 Electron micrograph of filament aggregates in stage 18. Many thin filaments are seen interspersed with the thick filaments. Tubules may be forming between aggregates (arrows) Section stained with PTA. 144,000 ×





3

0.2

1

2

PLATE 1

EXPLANATION OF FIGURES

1 Electron micrograph of stage 16 material. Note filamentous material present only in a scanty amount (arrows) Many single and small clusters of ribosomes are seen in the cytoplasm of the elongated cells. Section stained with PTA. 40,000 ×

2 Electron micrograph of stage 18 material. A high concentration of thin filaments is seen in the cytoplasm of two cells. N thick filaments are seen in these particular cells. Section stained with PTA. Polyribosome (P) 50,000 ×

3 Electron micrograph of filament aggregates in stage 18. Many thin filaments are seen interspersed with the thick filaments. Tubules may be forming between aggregates (arrows) Section stained with PTA. 144,000 ×


N
Gg

PLATE 3

EXPLANATION OF FIGURE

5 Electron micrograph of stage 20 material. A cl ster of glycogen (Gl) is shown in close proximity to an early myofibril, but more often there is no close association seen. *Polyribosomes (P) are present in* the background. Thin filaments are again present in abundance but difficult to see. Stained with lead tartrate. Golgi (Go); mitochondria (m); Nucleus (N) 40,000 ×


N
m
Go
Gl
P
P
m
5

PLATE 4

EXPLANATION OF FIGURE

6 Micrograph of a longitudinal section of stage 14 material. Tubules (T) are seen at approximately 1.5 μ intervals along the early myofibril. Stained with lead tartrate. Nucleus (N); golgi (Go); glycogen (Gl); polyribosome (P); cross-section of myofilaments (F). 40,000 X


F
N
G
T
T

PLATE 5

EXPLANATION O FIGURE

7 Micrograph of stage 24 material T bules are seen surrounding filament within the myofibril as well s the entire myofibril. Stained with lead tartrat Glycogen (Gl) 144 000 ×


G
7
0.2 μ

PLATE 6

EXPLANATION OF FIGURE

8 Micrograph of stage 28 material. Typical banding patterns (A I H, M Z) are often seen. The association between the tub les (T) and the Z line is apparent. Note polyribosomes (P) in the background Unstained sections. 40,000 ×

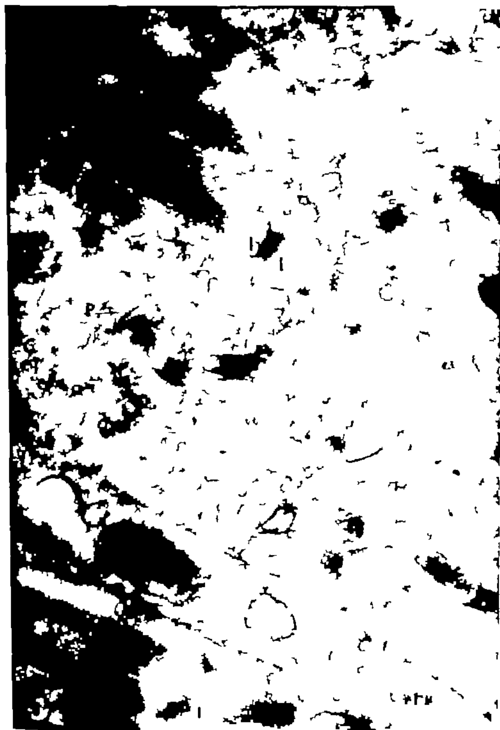

P

PLATE 7

EXPLANATION OF FIGURE

9 Micrograph of posthatched chick breast muscle. Myofibrils are contracted. Note connections between cytoplasmic vesicles (V) and tubules associated with Z lines (arrows). The interior of the sarcolemma possesses many vesicles and the exterior has an amorphous coat (Ac). Randomly dispersed ribosomes and glycogen particles are seen. Stained with lead tartrate. 38,000 ×.

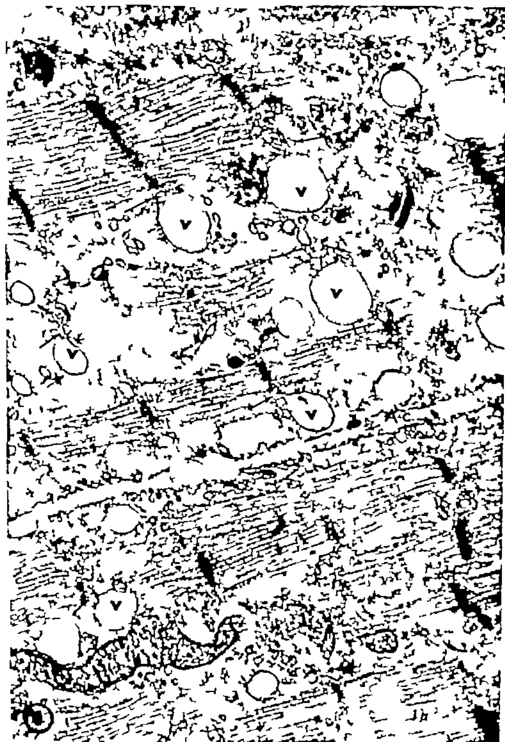
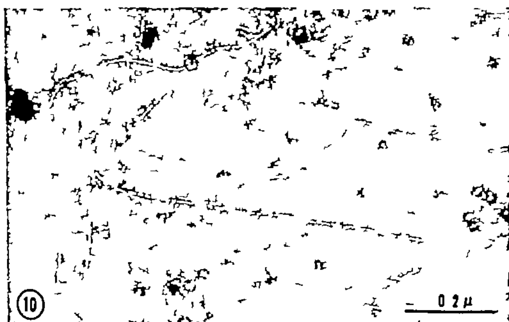

V
V
V
V
V
V

PLATE 8

EXPLANATION OF FIGURES

10 Micrograph of a negative stained preparation of stage 16 material. Thin filaments and fragments of thin filaments are seen. Single and small clusters of ribosomes are visible. 137,000 ×

11 Micrograph of negative stained preparation of stage 18 material. Two large polyribosomes are included with clump of thin filaments. 144,000 ×



11

PLATE 9

EXPLANATION OF FIGURE

12 Micrograph of negative stained preparation of stage 28 material. Thin filaments, single and small groups of ribosomes and glycogen particle (G) can be seen. 160,000 ×

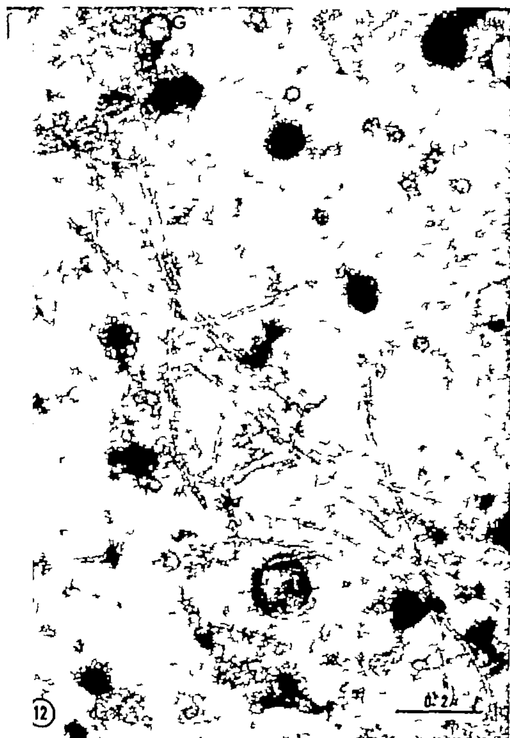

G
12
0.2 μ

PLATE 10

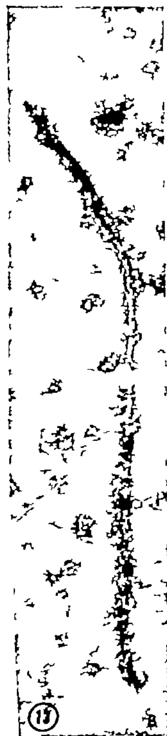
EXPLANATION OF FIGURES

13a Micrograph f a thick filament and part of another from stage 18 material. Note the tapering ends, relatively smooth central core and the otherwise rough surface found on this filament and those present in b and c. 152,000 ×

13b Micrograph of negative stained preparation of tage 1 One broken thin filament, ribosomes, and glycogen particles are seen in the background. 144,000 ×

13c Electron micrograph of stage 30 material. A thick filament is shown together with a broken thin filament. Ribosomes and some unidentifiable small granules are present in the background. 144,000 ×


A


17
B

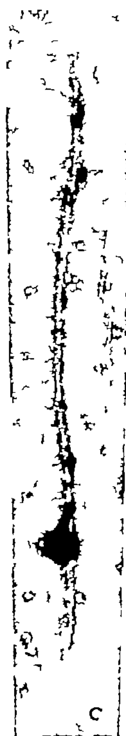

C

PLATE 11

EXPLANATION OF FIGURES

14 Micrograph from material pre-incubated for ten days. A polyribosome containing 70 to 75 ribosomes can be seen. Single and small clusters of ribosomes can be seen in the background along with glycogen. 123,000 ×

15 Micrograph from a negative stained preparation of stage 18. Small 10 to 12 A. threads (arrows) are seen interconnecting ribosomes of two polyribosomes. 137 000 ×

14

0.2 μ

15

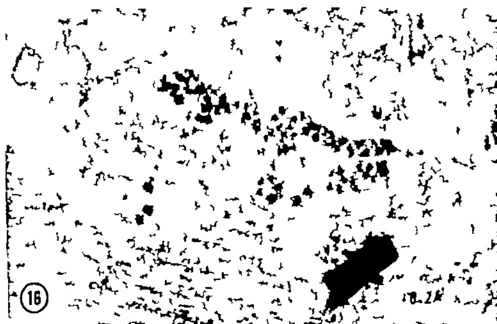
0.2 μ

PLATE 12

EXPLANATION OF FIGURES

16 Micrograph of section from stage 24 material. A polyribosome containing approximately 70 ribosomes is present adjacent to an early myofibril. Thin filaments, glycogen particles and ribosomes are seen in the background. Stained with lead tartrate 144 000 ×

17 Micrograph of stage 24 material. Many thin filaments are randomly dispersed in the cytoplasm surrounding an early myofibril. On the right side of the field, one thick filament can be seen paralleled and surrounded by many thin filaments. Section stained with PTA 144,000 ×



17

0.2 µ

'he Arterial System of the Head and Neck of the lhesus Monkey with Emphasis on the .xternal Carotid System [1]

WALTER A. CASTELLI AND DONALD F HUELKE
Department of Anatomy The University of Michigan, Ann Arbor Michigan

ABSTRACT The arterial plan of the head and neck of 64 immature rhesus monkeys (*Macaca mulatta*) was studied using four techniques — dissection, corrosion preparations, cleared specimens, and angiographs. In general, the arterial plan of this area in the monkey is similar to that of man. However certain outstanding differ ences were noted. The origin, course, and distribution f all arteries is described as well as the vascular relations to pertinent structures.

As has been mentioned previously Dyrud, 44 Schwartz and Huelke '63) ie rhesus monkey is useful for many ypes of medical and dental investigations, et its detailed gross morphology is virtu lly unknown. Although certain areas of he monkey have been studied in detail — rachial plexus facial and masticatory musculature subclavian axillary and cor nary arteries, orbital vasculature and ther structures (Schwartz and Huelke 33 Chase and DeGaris, 40 DeGaris and Glidden '38 Chase '38 Huber '25 Weinstein and Hedges, '62; Samuel and Warrick, '55 Eyster 44; Wagenen and Catchole '56 Tokarski, '31 Kennard, 41) ther areas have been virtually overlooked r have received but passing attention. he literature on the arterial supply of the rimate head has been adequately summarized by Dyrud (44) Very few investigators however have used *Macaca ulatta* specimens and more importantly 1 most of the articles only brief descriptions have been presented with many of ie pertinent morphological details not aving been stated or overlooked Addi onally only a few specimens have been sed in the majority of these works. It is ur purpose to present the arterial plan of ie head and neck, especially that of the xternal carotid arterial system

MATERIALS AND METHODS

Sixty four immature rhesus monkeys *Macaca mulatta*) were used for this study ll of the animals were embalmed with 10% formalin except 17 which were unembalmed. Four different techniques were used for the study of the arterial distribution (1) dissections — 27 specimens (2) corrosion preparations — 6 (3) cleared specimens — 15 (4) angiographs — 16 heads (11 unembalmed and 5 embalmed) The arterial system of the specimens used for dissection was injected with vinyl ace tate red latex, or with a red-colored gelation mass. For the dissection of smaller ar teries, the smallest of 150 μ in diameter the binocular dissection microscope was used The corrosion specimens were pre pared by injecting the arteries with vinyl acetate followed by maceration of the soft tissue with potassium hydroxide (3–10%) for 24 to 72 hours. The dye selected for injection of the cleared specimens was Teichmann s paste (Teichmann '52) colored with cinnabar These specimens were decalcified in 4% nitric acid and then cleared by the Spalteholtz method. The radiopaque material for the angiographs was the modified Schlesinger s mass (Reiner and Rodriguez, '57) the main components being mercury and barium sulfate

The head and neck was removed from the animal at the level of the clavicles or in some cases, a V-shaped section was made with the apex extending down to the arch of the aorta. Both common carotid

[1] This investigation was supported (in part) by USPHS research grant DE-00880 from the National Institute of Dental Research, National Institutes of Health, Bethesda, Maryland

Present address Department of Anatomy University of Concepcion, Concepcion, Chile.

arteries or the left common carotid artery and the brachiocephalic arterial trunk were cannulated depending on the individual situation paraffin (Castelli '63) or dental stone was applied to the cut surface to provide adequate vascular resistance so that the injected material would pass through the arterial channels and not seep out through the exposed tissue Photographs of all stages of dissection were taken as well as of many of the corrosion and cleared specimens.

OBSERVATIONS

Common carotid arteries Minor variations as to the origins of the common carotid arteries were found Most often a trunk, averaging 7 mm in length arises from the apex of the aortic arch and is the origin to the left common carotid artery and the brachiocephalic artery At times a very short common trunk is found however on sectioning the aorta, it is noted that both vessels have independent openings separated only by a thin septum. Of 32 specimens studied, the left common carotid artery and brachiocephalic trunk arose separately from the aortic arch in only one animal (figs 1 and 2)

The common trunk passes anterior to the left side of the trachea between the superior vena cava on the right and the left subclavian artery left vagus nerve and left phrenic nerve (fig 2)

The *brachiocephalic artery* has an oblique upward course across the front of the trachea and averages 16 mm in length It is covered by the left brachiocephalic vein or the superior vena cava, and by adipose tissue of the superior mediastinum. The brachiocephalic artery terminates in the thorax by bifurcating into the right common carotid and right subclavian arteries (fig 2)

The *right common carotid artery* has a short intrathoracic course (8 mm) ascending along the right side of the trachea (fig 2) Close to [illegible] f the thorax it is covered by th[illegible] f the sternohyoid and sternothyr[illegible]

The *left com[illegible] d artery* passes directly upward [illegible] e thorax medial to and slightl[illegible] the left vagus nerve adjacent t[illegible] t lung. It is covered by the adip[illegible] s of the superior mediastinum and as it leaves the thoracic cavity it is crossed by the left brachiocephalic vein

At the base of the neck, the common carotid arteries are less than 1 cm apart They diverge from one another throughout their course in the neck and, at the level of the carotid bifurcation they are 3 cm apart The common carotid artery is covered by the sternomastoid muscle and lies medial to the internal jugular vein with the vagus nerve behind and between them At approximately the mid-neck level the common carotid artery is crossed by the omohyoid muscle and the artery is tightly bound to the posterior surface of the lateral lobe of the thyroid gland. The common carotid artery divides into the external and internal carotid arteries approximately 1 cm above the angle of the mandible (fig 3) The bifurcation of the common carotid artery is 4 to 5 cm above the level of the sternoclavicular joint.

External carotid artery At the carotid bifurcation the external carotid artery is anterior and only slightly lateral to the internal carotid artery The internal carotid artery is tightly applied to the lateral wall of the pharynx by the posterior digastric muscle The external carotid artery runs parallel to the internal carotid artery for approximately 1 cm then passes between the stylohyoid and posterior digastric muscles. Above the posterior digastric muscle it swings laterally and passes obliquely upward through the parotid gland toward the posterior border of the ramus of the mandible reaching it slightly beneath the condylar neck. Here the external carotid artery continues forward medial to the ramus as the maxillary artery. Sometimes at this point a very small superficial temporal artery is given off (fig 3)

1 The *superior thyroid artery* is the first branch of the external carotid artery arising a few millimeters beneath the lingual facial trunk, or as a branch of this trunk. The superior thyroid artery is [illegible] inferior to the hypoglossal nerve and the posterior digastric muscle The artery is extremely short (approximately 5 mm in length) and fans out into several branches One a superior laryngeal branch passes horizontally deep to the thyrohyoid muscle



Fig. 1 The common arterial stem (1) of the brachiocephalic trunk (2) and left common carotid artery (3) overlying the trachea (4) (Dissection preparation.)

nd perforating the thyrohyoid membrane, supplies the upper part of the larynx. Another branch continues downward to supply other infrahyoid muscles. A terminal branch passes to the medial side of the thyroid lobe and from it very small branches arise to supply the isthmus of the thyroid gland and the upper part of the trachea. One or two small thyroid terminal branches are given off at the level of the apex of the lateral lobe. One of these passes downward on the lateral border of the lobe; the other on the posterior aspect of the lateral lobe (fig. 3)

2. The *lingual-facial trunk* arises from the anterior part of the external carotid artery 1 or 2 mm beyond its origin. The trunk passes forward and slightly upward deep to the posterior digastric muscle near its origin the hypoglossal nerve is lateral to the trunk and further on the nerve passes deep to the trunk to reach the tongue. The vessel continues forward for a distance of approximately 1 cm and di-



Fig 2 The large arteries in the upper mediastinum. The common arterial stem (1), brachiocephalic trunk (2); right subclavian artery (3); right common carotid artery (4); left common arotid artery (5); left subclavian tery (6); phrenic nerve (7); vagus nerve (8) (Dissection preparation)

vides into two main branches the lingual and facial arteries (figs 3 and 4)

The *lingual artery* appears to be a direct continuation of the common trunk. It passes deep to the hyoglossus muscle continuing to the tip f the tongue where it terminates. It gi t three main branches: dorsal lin p lingual and sublingual arteries (

The dorsal lingual branches are ple vessels arising from the lingual before it divides into the larger deep sublingual arteries The dorsal branches are distributed mainly to the posterior of the tongue the adjacent ual mucosa, the glossoepiglottic fold, the tine tonsil, and muscles of the area muscular branches from the lingual

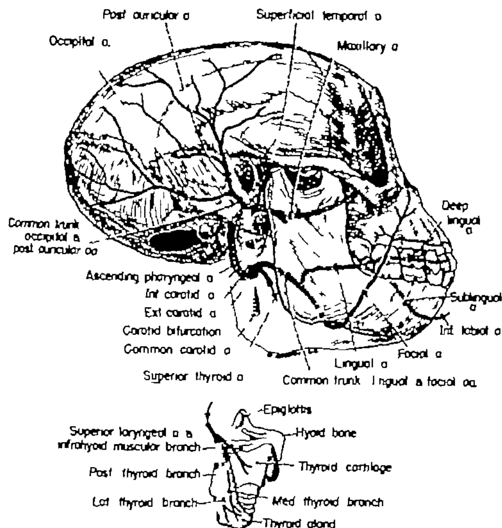


Fig. 3 Schematic drawing showing the course of the main branches of the external carotid artery

s downward to supply the hyoglossus d the thyrohyoid muscles (fig 4)

The deep lingual artery is the principal sel of the tongue and much of the vascularization of the horizontal portion of e tongue is dependent upon it. Ascend g branches arise from it which parallel ch other in their course towards the sur e of the tongue Before reaching the ngue mucosa they branch profusely and astomose with each other to form an terial network which is apparent roughout the entire dorsal surface of the ngue in the cleared specimens From this vascular network yet another smaller net work is formed by parallel arterioles which branch off toward the submucosa (fig. 4)

The sublingual artery passes towards the symphysis of the mandible in a deeper plane through the tongue frequently it is double Numerous branches to the sublingual gland arise from it, the largest of which arises from the lingual artery behind the origin of the main sublingual ar tery The sublingual branch as it passes anteriorly is in contact with the lateral aspect of the genioglossus muscle Throughout its course the artery supplies

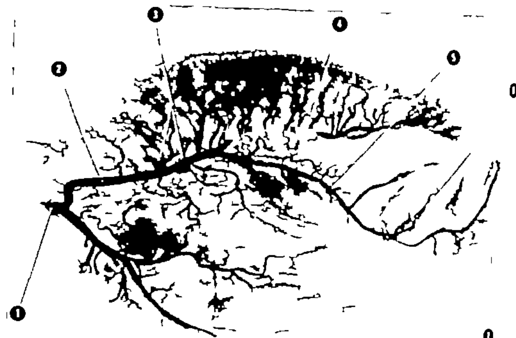


Fig. 4 The distribution of the lingual artery. Lingual-facial trunk (1); lingual artery (2 ... al lingual branches (3); deep lingual branch (4). Note the sublingual branch (5) passing ... the incisive area of the mandible (6) and into the lower lip (7). (Teichmann's paste ... decalcified and cleared preparation.)

the genioglossus and geniohyoid muscles and it anastomoses with mylohyoid and submental branches of the facial artery. Additionally it supplies the lingual alveolar mucosa, the attached and free gingiva. At the symphysis medial to the geniohyoid attachment, and directly on the midline either the right or left sublingual artery continues through a symphyseal foramen into the lower lip. As the artery passes through the mandible it supplies branches to the pulp periodontal membrane and supporting bone tissue of the central and lateral incisors (fig. 4). In the lip the artery passes vertically upward toward the free border. It bifurcates into right and left branches which distribute to the lower lip labial mucosa and gingiva. The sublingual branches in the lip anastomose with small branches of the facial artery forming an arterial network around the mouth (fig. 5).

The *facial artery* passes downward and forward lateral to the hypoglossal nerve and the thyrohyoid muscle. Laterally it is in contact with the low r part of the medial pterygoid muscle. The artery then curves around the inferior border of the mandible where it contacts the upper ... of the submandibular gland. It passes ... the face in front of the anterior ... the masseter muscle.

In its cervical course the facial ... has five major branches. The ... palatine artery arises near the ... of the lingual facial trunk. This ... courses posteriorly upwards and ... passing between the styloglossus and ... pharyngeus muscles which it supplies ... vessel terminates on the lateral ... geal wall at the level of the palatine ... The submandibular artery is an ... vessel which arises from the facial ... when it is in contact with the medial ... goid muscle. It is the main supply of ... submandibular gland. Numerous ... muscular arteries supply the medial ... goid and masseter muscles near their ... tion in the area of the angle of the ... ble. A small submental branch ... the inferior border of the mand... tributes mainly to the anterior ... and platysma muscles. As the facial ...

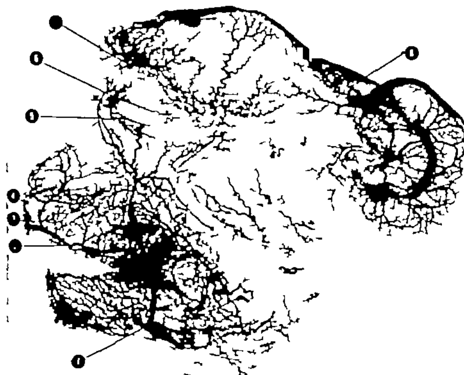


Fig. 5 General distribution of the arterial vessels of the face and part of the scalp Facial artery (1); superior labial (2); septal branch (3); lateral nasal branch (4); inferior palpebral branch (5); superior palpebral branch (6); supraorbital branch (7); parietal and frontal branches (8) (Teichmann's paste injection, cleared preparation.)

...sses the inferior border of the mandible ...mylohyoid branch arises from it to pass ...to the lateral surface of the mylohyoid ...uscle. The vessel then continues for...ard, parallel to the base of the mandible, ...d supplies the anterior digastric mus...es (fig. 6)

The facial artery as it passes in front ... the insertion of the masseter muscle is ...terior to the facial vein. It continues al...ost vertically upward to the area of the ...fraorbital foramen where it gives off its ...rminal branches (fig. 5) On the side ... the face it is *deep to the buccal pouch* ...d platysma muscle, adjacent to the base ... the mandible. The vessel then traverses ...e muscular mass about the corner of the ...outh Above the corner of the mouth, ...e facial artery is more superficial being ...vered only by the zygomaticoorbital mus...e complex. On the side of the face and ...ose to the insertion of the masseter mus...e two main buccal pouch branches pass posteriorly spreading out on the medial and lateral walls of the buccal pouch, where they form an intricate vascular network. The largest branch of the facial artery the superior labial branch, arises about 1 cm behind and slightly above the angle of the *mouth It passes horizontally through the* upper lip very close to its free border It then courses upward to the area beneath the ala of the nose At times this artery appears to be the continuation of the facial, for above its origin, the facial artery is small In cleared specimens it can be seen that this branch is the principal supply of the very rich arterial network of the upper lip. The superior labial artery has two principal branches the lateral nasal branch which passes upward beneath the external naris and around the ala of *the nose to supply the lateral surface of the* ala and a septal branch which courses upward adjacent to the midline to the nasal

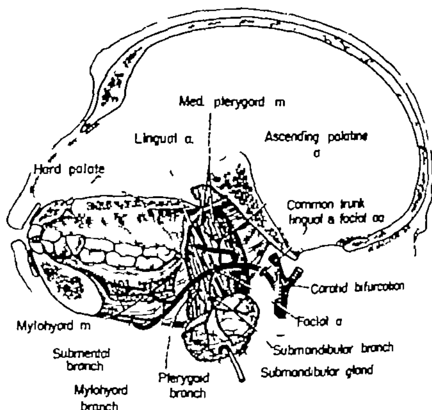


Fig. 6 Schematic drawing of the proximal part of the facial artery

septum and the skin of the lobe of the nose These branches anastomose around the external nares (fig. 5)

) At the level of the infraorbital foramen the facial artery terminates by sprouting into a variable number of smaller branches. Consistently there are anastomotic branches which join with terminals of the infraorbital artery Laterally a branch passes along the infraorbital rim to supply the musculature and lateral parts of the lower eyelid. A medial branch frequently double passes upward towards the inner canthus of the eye It passes beneath the orbicularis oculi muscle supplying it as well as the medial half of the lower eyelid the lateral side of the bridge of the nose and the most medial portion of the upper eyelid. At the inner canthus it anastomoses with very small arteries passing through the orbital septum (fig 5)

3 The *occipital and auricular arteries* most frequently arise by a common stem from the external carotid artery as it passes above the posterior digastric [illegible] cle The common trunk passes posteri[illegible] medial to the posterior digastric mu[illegible] and following its fibers. The length of [illegible] common trunk is variable in some cas[illegible] reaches the level of the external acou[illegible] meatus before dividing into occipital [illegible] auricular branches (figs. 3 and 7) [illegible] occipital artery sometimes double pa[illegible] lateral to the upper part of the poster[illegible] digastric muscle being covered by [illegible] splenius capitis and longissimus cap[illegible] muscles. It then continues posteriorly [illegible] upward along the bone to terminate [illegible] branches which supply the muscles [illegible] tached to the posterior aspect of the [illegible] and to the overlying scalp. Constantly [illegible] gives rise to a branch which perforates [illegible] skull by passing through a foramen [illegible] proximately 2 cm posterior to the exter[illegible] acoustic meatus. This is the post[illegible] meningeal artery the main supply of [illegible] posterior lateral portion of the dura [illegible] (fig 8)

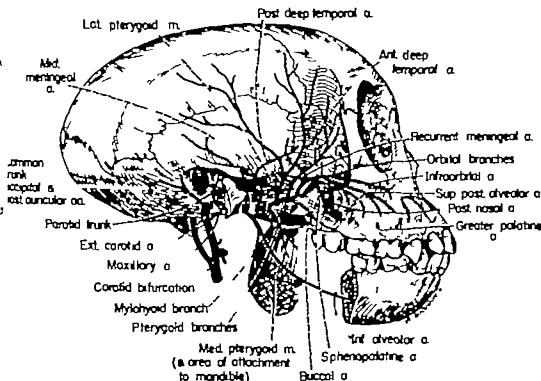


Fig. 7 Schematic drawing showing distribution of the maxillary artery

The auricular artery is a short trunk which passes upward behind and beneath the lower part of the auricle of the ear where it almost immediately divides into multiple branches. Some of these continue upward along the attachment of the auricle and supply its posterior surface. Others pass over the attachment of the sternomastoid muscle and distribute there. The auricular branches supply adjacent musculature the lateral and the posterior area of the scalp and the auricle (fig. 5) The branches to the auricle form rich anastomoses in the form of concentric vascular arches From these arches vessels sprout off to form yet smaller vascular networks which are located close to the free edge of the auricle (fig 5) The artery also gives rise to a small branch which passes through the stylomastoid foramen and accompanies the facial nerve

4. The *ascending pharyngeal artery* is a very thin branch arising from the superior medial side of the external carotid artery immediately above the lingual facial trunk (fig. 3) It passes vertically upward lying on the longus colli muscle In its upward course the vessel is crossed laterally by the stylopharyngeus and the styloglossus muscles. Near the base of the skull it divides into several terminal branches one of which passes through the jugular foramen to supply the meninges in the area of the sigmoid sinus. Other branches pass slightly forward and upward to be distributed to the musculature and mucosa of the upper portion of the pharynx. Continuing upward and forward along the base of the skull, the ascending pharyngeal artery supplies the membranous portion of the nasal septum behind the posterior edge of the vomer and behind the hard palate Small branches from it pass into the soft palate (fig 9)

5. The *maxillary artery* arises about 1½ cm beneath the external acoustic

In the Macacus rhesus, the nasal septum is continued behind the posterior border of the vomer by triangular-shaped membranous septum which extends backward for about 1½ cm along the base of the skull. Its inferior attachment is to the soft palate.

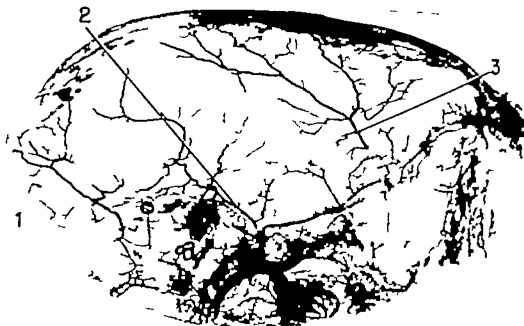


Fig. 8 Disposition of meningeal arteries. Posterior meningeal (1); middle meningeal (2); an rior meningeal (3) (Teichmann paste injection, decalcified and cleared preparation.)

Fig. 9 The arterial uppl f he asal septum. The septal branch of ascending pharyn artery (1) nasopalatine br nch 2 septal branch of internal nasal artery (3) (Vinyl acet injection, dissection prepar tion

eatus and less than 1 cm behind the mus of the mandible at the level of the ck of the condyle. As a direct continua n of the external carotid artery it passes rizontally forward medial to the neck the condyle toward the pterygopalatine ssa. Passing slightly medial and upward roughout this course the artery is in con-ct with the lower lateral surface of the teral pterygoid muscle In the pterygopal ine fossa the vessel terminates by divid-g into numerous branches. The main anches of the maxillary artery are 12 in umber several of which arise by common igins (fig. 7)

Very near the point of origin of the axillary artery the first branch arises It a short parotid trunk which soon divides ito six or seven secondary branches. hese *parotid gland branches* spread out in the parotid gland tissue and also supply the adjacent structures (figs 7 10 and 11) One of these a large *massetric artery* passes forward along the lateral side of the subcondylar portion of the ramus of the mandible to enter the deep head of the masseter muscle It supplies most of this muscle and anastomoses along the front edge of the ramus with other branches from the maxillary artery Near the angle this artery joins with branches of the facial artery which also supply the inferior part of the masseter muscle (fig 10) A *transverse facial artery* likewise is one of these branches which pass horizontally forward approximately ½ cm beneath the zygomatic arch It joins branches of the facial artery at the lateral inferior margin of the orbit. A very small ascending branch the zygomaticoorbital artery



Fig. 10 The main arterial vessel of face, temporal fossa and occipital regions. Occipital and posterior auricular arteries (1) posterior deep temporal artery (2) facial artery (3) submandibular branches (4); masseteric branch (5) and capsular arteries (6) (Vinyl acetate injection, corrosion preparation.)

courses obliquqely forward to anastomose with the arteries about the orbit It supplies the skin on the side of the cal varium and anastomoses at the side of the orbit with lateral branches from the facial as well as supraorbital branches from the ophthalmic artery (fig 5)

Several small *temporomandibular capsular branches* arise from the maxillary artery as the vessel passes adjacent to the medial side of the condylar neck. These ascending branches have a very short course, and pass into the medial aspect of the temporomandibular capsule and adjacent tissue. Additionally articular branches arise from the posterior deep temporal artery near its origin and from the parotid branches (fig 11)

The *tympanic and middle meningeal arteries* arise from a common trunk near the beginning of the maxillary artery medial to the condylar neck (fig 11) The trunk passes around the inferior border of the lateral pterygoid muscle to run medially inward toward the petrotympanic fissure. Near the base of the skull the vessel divides into its two named branches (figs 7 and 8) The tympanic artery is very small and passes posteriorly into the petrotympanic fissure towards the middle ear The meningeal artery passes through the lateral end of the foramen ovale to enter the middle cranial fossa. It grooves the inner table of bone at the base of the middle cranial fossa immediately above the roof of the glenoid cavity Here it divides into

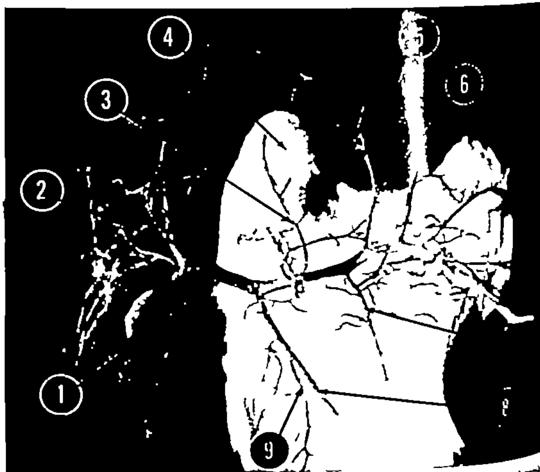


Fig 11 Vessel in rel tion to the temporomandibula area. Maxillary artery (1); parotid gland (2); tympanic-middle meningeal trunk (3); condyle (4) posterior deep temporal artery (5) masseteric branch (6) buccal branch (7); inferior alveolar artery (8); and mylohyoid branch (9) (Vinyl acetate injection; corrosion preparation.)

wo main branches which run anteriorly nd posteriorly The anterior branch asses on the inner aspect of the squamous portion of the temporal bone towards he tip of the lesser wing of the sphenoid one where it anastomoses with the meningeal branch of the ophthalmic artery he posterior branch is much smaller and uns over the petrosquamous suture to anastomose with meningeal vessels of the osterior auricular and occipital arteries. n general, the meningeal artery is quite mall and in half of the cases most of the edial side of the cranial vault is supplied y a meningeal branch of the ophthalmic rtery and by meningeal branches of the ccipital and posterior auricular arteries ig. 6) The middle meningeal artery also as anastomotic connections with its fellow of the opposite side by means of short ansverse communications which pass cross the top of the skull above the superior sagittal sinus.

A *posterior deep temporal artery* ascends ertically from its origin in front of the apsule of the temporomandibular joint asses over the lateral pterygoid muscle hich it supplies, and continues upwards o supply the deeper fibers of the temporalis muscle (fig. 18) Here it divides to two or three secondary branches which spread out in a fan-shape manner owards the origin of the temporalis muscle (figs. 7 and 10)

Near the origin of the posterior deep temporal artery small masseteric and capsular arteries arise which pass downward and posteriorly to their area of supply The masseteric branch passes through he mandibular notch to supply the upper deep portion of the masseter muscle. It is much smaller vessel than is the masseteric artery which arises with the parotid ranches and is a minor arterial supply of he masseter muscle. The capsular branch ften multiple, fans out as it passes backward to supply the anterior part of the capsule of the temporomandibular joint figs. 11 and 12)

The *inferior alveolar artery* arises medial to the neck of the condyle from the lower surface of the maxillary artery It passes obliquely downward and forward close to the medial pterygoid muscle and the interpterygoid fascia. Before entering the mandibular canal, the inferior alveolar artery usually gives rise to a small mylohyoid branch which distributes to the posterior part of the mylohyoid muscle Within the mandible the inferior alveolar artery supplies the dental pulps, periodontal membranes interdental and interradicular septa base of the mandible and the area of the angle of the mandible (figs 7 11 12 and 13) A mental artery emerges through the mental foramen and supplies the soft tissue of that area.

Pterygoid arteries supply both the medial and lateral pterygoid muscles The area of origin of the medial pterygoid muscle receives its blood supply from arteries arising from the tympanic middle meningeal trunk. These vessels distribute mainly to the area of the pterygoid fossa. The middle portion and mandibular insertion of the medial pterygoid muscle is supplied by branches arising from the inferior alveolar artery and by small branches arising directly from the maxillary artery The lateral pterygoid muscle receives small arteries which come directly from the maxillary artery additionally the posterior deep temporal artery sends small branches to it.

The *buccal artery* accompanied by the buccal nerve passes downward through the anterior portion of the temporalis muscle to reach the posterior portion of the buccinator muscle to which it distributes The ascending and lateral branches of the anterior deep temporal arteries also supply the buccinator muscle by small branches which end in the upper posterior portion of the muscle The main portion of the buccinator is supplied by branches of the facial artery Anastomosis between all of these vessels occurs within the muscle (figs. 15 and 11)

Three or four *anterior deep temporal arteries* arise from the maxillary just before it passes into the pterygopalatine fossa (fig 7) Some ascend into the most anterior fibers of the temporalis muscle while others descend into the fibers which attach to the temporalis crest of the ramus of the mandible

A few orbital branches arise from the maxillary artery at the pterygopalatine fossa and pass through the inferior or

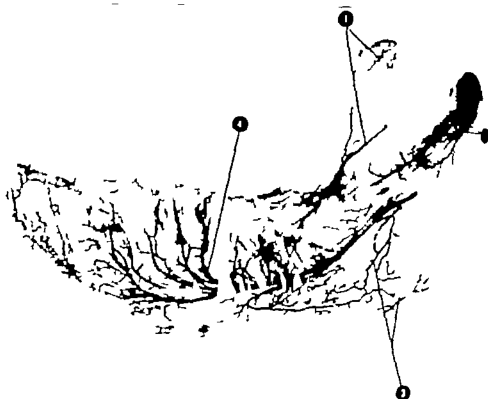


Fig. 12 Differential vascular supply of a mandible with permanent dentition. Arteries of the coronoid proces (1) coming from the temporalis muscle. The arteries of the condylar process (2) arise from those of the capsule of the temporomandibular joint and l teral pterygoid muscle. Vessel of the angle region (3) arising from the inferior alveolar artery and from the vessels supplying the muscles attached to it. Branching arrangement of the al eolar dental arteries (4). (Tei mann s paste injection decalcification and cleared preparation.)

bital fissure to supply the tissues at the apex of the orbit (fig 14)

The *recurrent meningeal artery* is extremely small and follows the maxillary nerve passing posteriorly into the middle cranial fossa where it supplies the area of the trigeminal ganglion (fig 7)

The *posterior superior alveolar artery* arises from the maxillary artery at the pterygopalatine fossa. It passes forward for a very short distance along the floor of the orbit anterior and medial to the inferior orbital fissure where it enters a small foramen near the anterior end of the fissure (fig 14) It continues forward in the maxilla above and lateral to the maxillary sinus Throughout its course alveolar-dental branches are given off which supply the teeth and supporting tissues as far forward as the cuspid tooth Each alveolar-dental artery divides into secondary branches which supply the dental pulps the periodontal membranes [illegible] the interradicular and interdental [illegible] (fig. 14) The *infraorbital branches* [illegible] either from the posterior superior [illegible] artery or from the sphenopalatine [illegible] They are small branches which pass [illegible]ward along the infraorbital nerve [illegible]ralling around and paralleling the [illegible] throughout its course (fig 14) [illegible] at the infraorbital foramen these [illegible] terminate by distributing in the [illegible]bital area and anastomosing with branches of the facial artery

The *sphenopalatine artery* appears [illegible] a direct continuation of the [illegible] artery It passes through the [illegible]tine foramen and after a short [illegible] gives rise to posterior nasal and [illegible]ing palatine arteries (fig 15)

The posterior nasal arteries suppl[illegible] most all of the lateral nasal wall [illegible] superior and inferior branches The [illegible]

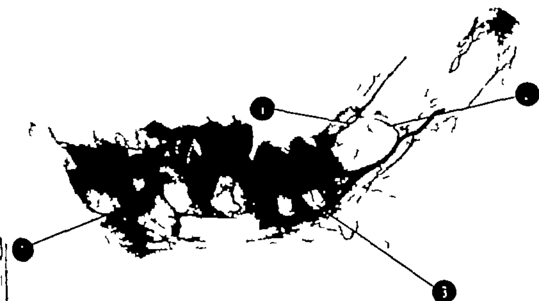


Fig. 13 Arrangement of the vessels in mandible with mixed dentition. Vascular supply to the second molar tooth bud has two sources from the vascular system of the temporalis muscle (1) and from the inferior alveolar artery (2); single vessel from the inferior alveolar artery is supplying the pulp tissue of the developing first molar (3) The inferior alveolar artery ends at the level of the canine tooth (4) (Schlesinger injection media; arteriograph preparation.)

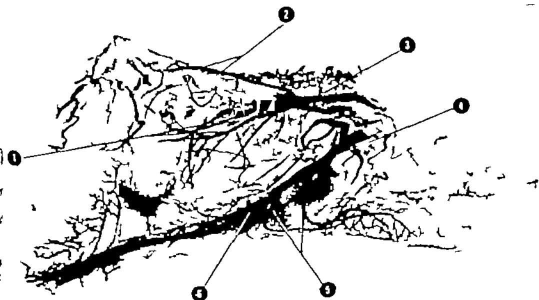


Fig. 14 Distribution of arterial vessels in the maxilla. Posterior alveolar artery (1) infraorbital arteries (2) orbital branches (3) descending palatine artery (4) lesser palatine arteries (5) and greater palatine artery (6) (Teichmann paste injection decalcified and cleared preparation)



Fig. 15 The sphenopalatine artery (1) branching into the posterior nasal artery (2) with its superior nasal branch (3) and inferior nasal branch (4) and the descending pala-tine artery (5) spreading out on the palate. (Vinyl acetate injection; corrosion preparation.)

rior branch is distributed to the middle concha and meatus, and the maxil lary sinus. The inferior nasal branch supplies the inferior concha and meatus and the floor of the nasal cavity (fig. 15) The posterior nasal artery also gives rise to a branch which supplies the roof of the nasal cavity and to a *nasopalatine artery* which passes to the nasal septum and runs obliquely forward and downward toward the incisive canal through which it passes. Here it anastomoses with the anterior palatine artery (fig 9) On the nasal septum the vessel also anastomoses with branches of the posterior and anterior arteries of the septum

The *descending palatine artery* passes downward and forward through the ptery gopalatine canal emerging at the greater palatine foramen (figs 14 and 15) As it passes through the pterygopalatine canal it gives rise to one or two small posterior collateral branches the lesser pala- arteries (fig 14) The greater pala- artery is the main supply of the pal- and it is the direct continuation of th- descending palatine trunk. It passes fo- ward following the curvature of the up- arch, medial to the teeth towards the i- cisive foramen (fig 16) Lateral to th- incisive foramen branches of the grea- palatine artery pass upward thr- small foramina in the maxilla, behind th- anterior teeth. As small thin vessels th- surround the apex of the upper ce- and lateral incisors. These branches s- ply the dental pulp periodontal m- branes and supporting bone tissue of th- anterior teeth (fig 17) Throughout it- palatal course the greater palatine art- distributes to adjacent tissue by m- and lateral branches. The medial branch- pass toward the midline to anasto- with vessels of the opposite side Late-

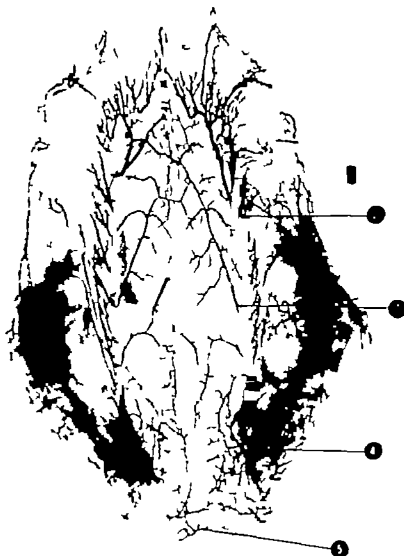


Fig. 16 General distribution of greater palatine artery Short vessels from the greater palatine artery (1) supply the gingiva and alveolar mucosa (2); palatal vascular arches anastomosing with those of the opposing side (3); lesser palatine artery (4); and arterial plexus in soft palate (5) (Teichmann paste injection decalcified and cleared preparation.)

branches are much thinner and supply the alveolar mucosa gingiva, and alveolar bone (fig. 16)

The *lesser palatine arteries* distribute mainly to the soft palate Usually one or two arteries are present and they anastomose with vessels from the opposite side near the midline of the soft palate (figs. 14 and 16)

Internal carotid artery From its point of origin the internal carotid artery passes toward the base of the skull arching slightly forward and medialward (fig 18)

It is posterior to the external carotid artery which it parallels for 1 cm The artery is compressed between the posterior digastric and the longus colli muscles the sympathetic trunk is closely bound to its



Fig. 15 The sphenopalatine artery (1) branching into the posterior nasal artery (2) with its superior nasal branch (3) and inferior nasal branch (4) and the descending palatine artery (5) spreading out on the palate. (Vinyl acetate injection; corrosion preparation)

rior branch is distributed to the middle nasal concha and meatus, and the maxillary sinus. The inferior nasal branch supplies the inferior concha and meatus, and the floor of the nasal cavity (fig 15) The posterior nasal artery also gives rise to a branch which supplies the roof of the nasal cavity and to a *nasopalatine artery* which passes to the nasal septum and runs obliquely forward and downward toward the incisive canal through which it passes Here it anastomoses with the anterior palatine artery (fig 9) On the nasal septum the vessel also anastomoses with branches of the posterior and anterior arteries of the septum

The *descending palatine artery* passes downward and forward through the pterygopalatine canal emerging at the greater palatine foramen (figs 14 and 15) As it passes through the pterygopalatine canal, it gives rise to one or two small posterior collateral branches the lesser palatine arteries (fig 14) The greater palatine artery is the main supply of the palate and it is the direct continuation of the descending palatine trunk. It passes [illegible] ward following the curvature of the [illegible] arch medial to the teeth towards the [illegible] cisive foramen (fig 16) Lateral to the incisive foramen branches of the greater palatine artery pass upward through small foramina in the maxilla, behind the anterior teeth. As small thin vessels the[illegible] surround the apex of the upper [illegible] and lateral incisors These branches [illegible] ply the dental pulp periodontal [illegible] branes and supporting bone tissue of the anterior teeth (fig 17) Throughout [illegible] palatal course the greater palatine [illegible] distributes to adjacent tissue by [illegible] and lateral branches. The medial branches pass toward the midline to [illegible] with vessels of the opposite side [illegible]

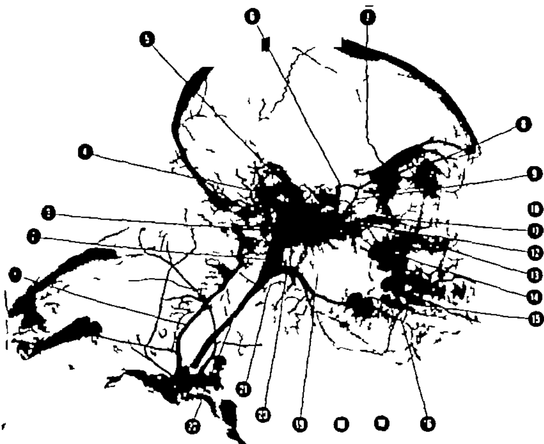


Fig. 18 Arteriograph of head and neck. Principal arteries have been numbered. (Formalin embalmed specimen injected with Schlesinger radiopaque media.)

1. Vertebral artery
2. Internal carotid artery
3. Common trunk for occipital and posterior auricular arteries
4. External auditory meatus
5. Middle meningeal artery
6. Ophthalmic artery
7. Anterior meningeal artery
8. Supraorbital artery
9. Posterior deep temporal artery
10. Anterior deep temporal artery
11. Posterior superior alveolar artery
12. Sphenopalatine artery
13. Posterior nasal artery
14. Descending palatine artery
15. Facial artery
16. Sublingual artery
17. Deep lingual artery
18. Lingual artery
19. Inferior alveolar artery
20. Superior thyroid artery
21. External carotid artery
22. Common carotid artery

principal lateral branches close to the free border of the lower lip

The structure of the nasal septum in the Macaque has revealed an additional nutrient source which is not seen in humans. The nasal septum projects backward as a membranous wall that divides the roof of the nasopharynx into two lateral compartments (Geist '61) This membranous septum is close to the roof of the pharynx and is supplied by the ascending pharyngeal artery The vascularization of the septum then is supplied by three main arterial sources — the nasopalatine artery the septal branch of the sphenopalatine artery and the septal branch of the ascending pharyngeal artery

The skin and subcutaneous tissue over the temporal fossa and part of the frontal and parietal areas in the human is sup-

plied by the superficial temporal artery In the Macaque however this area is supplied by small branches arising from neighboring arteries — posterior deep temporal, posterior auricular and parotid branches This arterial disposition may account for the fact that in the Macaque the superficial temporal artery is represented by a very small vessel with limited distribution or is completely absent.

The distribution of the middle meningeal artery in the cranial cavity of the Macaque is somewhat different from that found in the human Its anterior branch is much reduced in size and distribution In the Macaque a large meningeal branch of the ophthalmic artery is distributed to the lateral wall of the anterior and middle cranial fossa, the area of supply of the anterior branch of the middle meningeal artery in the human

Lineback ('61) described the middle meningeal artery as the largest branch of the maxillary artery We found as did Dyrud ('44) that the posterior deep temporal artery is the largest branch arising from the maxillary artery

When cleared preparations of the parotid gland are studied a variable number of arterial branches arising from a common trunk, are seen traversing the glandular tissue These vessels radiate outward toward the external surface of the gland The major part of these vessels supply the parenchyma and stroma of the gland. Some of these vessels extend beyond the gland to supply adjacent structures. One artery supplies the masseter muscle and is its main vessel Others are distributed to a limited area of the face distributing as do the zygomaticoorbital and transverse facial arteries in the human.

The distribution of the vessels supplying the mandible and maxilla have been thoroughly studied in the cleared specimens. In general the mandible in the Macaque has the same arterial pattern as in the human (Castelli '63 Cohen '59) the condyle of the mandible receives its nutrition by means of perforating arteries which come from vessels of the capsule of the temporomandibular joint and from those which supply the lateral pterygoid muscle Likewise the origin and the disposition of the vessels which supply the coronoid process and the area of the [illegible] is similar to that found in the [illegible] they arise from those vessels which [illegible] the temporalis muscle and from those [illegible] the masseter and medial pterygoid [illegible]cles respectively

Since the incisive area of the [illegible] is primarily supplied by the [illegible] artery the distribution of the inferior [illegible]veolar artery is therefore limited to [illegible] body of the mandible for as [illegible] above the condyle coronoid process [illegible] incisive area are all supplied by other [illegible]sels. The inferior alveolar arterial [illegible]bution and its ascending alveolar [illegible] branches are quite similar to that [illegible] in the human mandible. [illegible] these vessels branch into thin [illegible] to the interalveolar and [illegible] septa to the periodontal membrane [illegible] to the pulp of the teeth. It was [illegible] that one or two arterial branches [illegible] into the pulp tissue of each dental [illegible] This finding is in agreement with [illegible] found in humans (Provenza, '59) and [illegible] cats (Castelli '62)

As far as the supply of the periodon[illegible] membrane is concerned several [illegible] (Orban '53 Schubach and Goldman [illegible] Bernick '60) have suggested that [illegible] of gingival origin also contribute to [illegible] nutrition of the membrane. In fact, [illegible] presence of these vessels was not [illegible] firmed as an additional vascular [illegible] other than those given by the alveolar [illegible]tal branches; the only vessels which [illegible] found in that area were venous and [illegible]lary networks from the periodontium [illegible] gingiva at the level of the dental [illegible]

In the Macaque the participation of [illegible] greater palatine artery in the nutrition [illegible] the intermaxillary bone and superior [illegible]cisors is not like that found in the [illegible] The study of the cleared maxillae in [illegible] Macaque shows the absence of the [illegible]rior superior alveolar artery The [illegible] of distribution of the anterior [illegible] alveolar artery was supplied by the [illegible]sion of the greater palatine artery [illegible] into the anterior part of the [illegible] bone

LITERATURE CITED

Bernick, S 1960 Blood supply to [illegible] teeth Anat. Rec 137 141 145.
Castelli, W A 1962 Vascular [illegible] dental pulps in [illegible] J Dent Res 41 [illegible]

——— 1963 Vascular architecture of the human adult mandible. J Dent. Res., 42: 796–792.

[illegible] R. E. 1938 The coronary arteries in 200 hearts of rhesus monkey Am. J Phys. Anthrop., 23 299–320.

[illegible], R. E., and C. F DeGaris 1940 On the brachial plexus in macaca rhesus, compared with man. Am. J Phys. Anthrop., 27 223–254.

[illegible], L. 1959 Methods of investigating the vascular architecture of the mandible. J Dent. Res., 38 920–931.

DeGaris, C. F and E. M. Glidden 1938 Branches of the aortic arch in 153 rhesus monkeys. Anat. Rec., 70: 251–262.

[illegible], J. 1944 The external carotid artery of the rhesus monkey (macaca mulatta) Anat. Rec., 90 17–22.

[illegible] A. B. 1944 The cavernous sinus in macacus rhesus monkey Anat. Rec., 90 37-40.

[illegible], D. F 1961 The anatomy of the rhesus monkey Edit. by G. C. Hartman and W L. Straus, Jr Hafner Publishing Co., New York. Chapt. IX, 180–209

[illegible], E. 1925 Ein M. Mandibulo-Auricularis Bei Primaten, Nebst Beitragen Zur Kenntnis Der Phylogenese Ohrmuskulatur Anat. Anz., 60: 11 21

[illegible], M. A. 1941 Abnormal findings in 264 consecutive autopsies on monkeys. Yale J Biol. Med., 13 701–702.

[illegible], P 1961 The anatomy of the rhesus monkey Edit. by G. C. Hartman and W L. Straus, Jr Hafner Publishing Co., New York. Chapt. XII, 248–268

[illegible], B. 1953 Oral histology and embryology Edit. by C. V Mosby Co., St. Louis, p. 183

Provenza, D. V 1959 The blood vascular supply of the dental pulps with emphasis on capillary circulation. Cir. Res., 6. 213–216.

Reiner L., and F Rodriguez 1957 An injection mass f maximal radiopacity for postmortem angiography J Mount Sinai Hospital, 24 1139–1145.

Samuel, E. P and R. Warwick 1955 The origin of the phrenic nerve in the rhesus monkey J Comp Neur., 102: 557–563

Schubach, P L., and H. Goldman 1957 A technique of radiographic visualization of the vascular system of the periodontal tissues. J Dent. Res., 36. 245–248.

Schwartz, D. J and D F Huelk 1963 The morphology of the head and neck of the macaca monkey The muscles of mastication and the mandibular division of the trigeminal nerve. J Dent. Res 42: 1222–1233.

Teichmann, L. 1962 Cited by Schwering: Anatomische Trocken-Feucht und Knochenpraparate. Springer Verlag, Berlin, p. 79

Theile W 1852 Die Arteriensystem of Siminia Innua. Archiv Fur Anatomie, Physiologie und Wissenschaftliche Medicin, 419–428

Tokarski, S 1931 Les Variations de L'Artère Maxillaire Interne Chez L'Homme Expliquées par les Variations Chez les Primates. Comp. Rendus, 25 507–510

Wagenen, G., and H. R. Catchpole 1956 Physical growth of the rhesus monkey (macaca mulatta) Am. J Phys. Anthrop., 14 245–273.

Weinstein, J D and T R. Hedges 1962 Studies of intracranial and orbital vasculature of the rhesus monkey (macaca mulatta) Anat. Rec 144 37–42.

Structural Orientation and Density in Cetacean Humeri [1]

WILLIAM J. L. FELTS AND FRANCIS A. SPURRELL
Department of Anatomy, School of Medicine, Minneapolis Campus, and Department of Veterinary Surgery and Radiology, St. Paul Campus, University of Minnesota.

ABSTRACT The cetacean humerus is a short, robust bone without an open medullary cavity. It lies in the base of the resilient, streamlined pectoral limb (flipper) between the only free articulation (the glenohumeral) and approximately the body contour. The humerus is acted upon by muscles of the shoulder complex and receives loadings from the flattened distal portion of the limb as this hydroplane acts against body inertia and water resistance in control of body attitude.

This study is an analysis of development and structure of the humerus in terms of the unique functional role of the flipper of finback, beluga and pilot whales. Gross external and internal architecture are depicted by photographs and by whole bone and frontal section radiographs. Structural density (bone/unit volume of humerus, with mineral content known to be constant) is analyzed indirectly by photodensitometry of standardized radiographs of sawed sections. Results are shown in graphic reconstructions of sections and of the whole bone. By comparison of radiodensity with the actual weight/volume of excised samples, sections are also reconstructed in terms of absolute density distribution.

It is found that the spongy cetacean humerus, from its origin, is without central resorption and that its definitive structure is produced primarily by differential concentration of bone along endorected gradients of porosity. Thus, the greatest concentration of bone is on medial and lateral sides while bone only half as dense fills the anterior and posterior sides and underlies the most dense regions. The core region is extremely porous. Within the biological context, this is a most reasonable approximation of the engineered box-beam as employed in some aircraft wings. Whole bone and frontal section radiographs show that, within this overall density pattern, the distribution of bone trabeculae resembles the classic illustrations of trajectories in the loaded beam.

The ontogenetic and phylogenetic factors with possible bearing on this type of bone development and structure are discussed.

This paper is concerned with the distribution of bone in humeri of three species of cetaceans. It is the first of a projected series of publications on whale limb bone structure and development, as well as on other items of comparative bone structure and mechanics. In order to place our methods and results in correct perspective it is necessary, therefore, to make some rather detailed introductory remarks on the particular research area and on the unique character of the whale limb.

The overwhelming majority of studies on orientation, density and the mechanical significance of bone structure have dealt with tubular bones of terrestrial mammals, especially those of man and other primates (classic examples: Koch, '17; Weidenreich, '23; Benninghoff, '25; Murray, '36). Such an emphasis is both understandable and profitable, yielding a very substantial amount of fundamental information. This has been true particularly in recent years, during which materials-testing methods and other quantitative techniques have been applied to questions of physical strength, mechanical organization, volume, density and the proportions of organic and inorganic material in bones and bone tissue (e.g., Dempster and Liddicoat, '52; MacFarland, '54; Bell, '56; Evans, '57; Baker and Schrarer, '58; Trotter and Peterson, '62). At the same time, however, there has been scant advance along similar lines in comparative skeletal structure (except in the area of comparative bone histology, e.g., Enlow and Brown, '56, '57, '58 and Enlow, '62; Meister, '51, '56, '62; Pratt, '59; Smith, '60; Smith and Walmsley, '59) and some

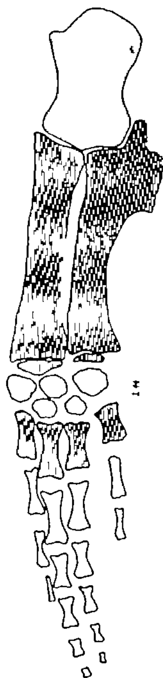
[1] Supported by National Science Foundation, Grant no. G-13146.

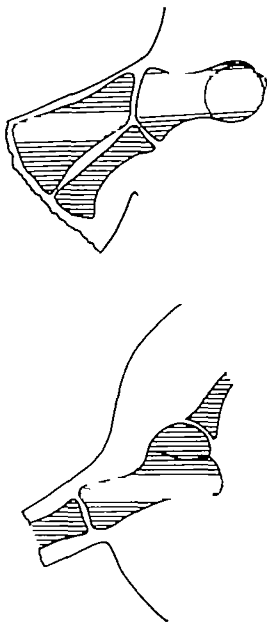
tests of bone physical properties cited by Bell, '56 and Evans '57) This disparity is critical for the comparative approach is necessary in order to distinguish species specific from more general structural characteristics and to develop some insight into common mandatory relationships which must exist between function size gross and microstructure and density composition and physical strength of skeletal elements.

As a preliminary approach to some of these aspects of comparative skeletology we have studied the pectoral limb (flipper) skeleton of some of the more available types of whales. The project was undertaken because cetaceans whether large or small possess characteristics of body limb and skeleton that afford maximum contrast with terrestrial forms. In the limb skeleton the proportions internal architecture and some features of growth and development of individual bones all contribute to a pattern quite unlike that encountered in the more commonly studied, weight-bearing bones of land mammals Roux (1893) Schmidt (1899) and Murray ('36) have figured and briefly discussed the gross mechanical organization of dolphin limb bones, with limited information and considerable oversimplification of structure These publications will be discussed in the final section of this paper The material in our study is from the large mysticete finback whale (*Balaenoptera physalus*) (Slijper '58) and two relatively small odontocetes the pilot whale (*Globicephala malaena*) (Sergeant, '62) and beluga (*Delphinapterus leucas*) (Vladykov 44) As an ancillary project, visits were made to marine aquaria to observe captive animals such as *Tursiops truncata* the dolphin.

From some of the observations of Howell ('30) Budker ('58) and Slijper ('58) supplemented by our own in field and laboratory the essential characteristics of the cetacean flipper may be summarized. The limb of course does not support body weight rather it is subjected to varying transverse forces due to water resistance and body inertia in acting as a stabilizer dive-plane and secondary direction control (The essential propulsive organ is the horizontal tail fluke and the prime rudder is the flattened caudal region.) In all cetaceans the limb is without significant musculature beyond the lower humerus The scapulohumeral joint is freely movable but articulations distal to it are limited by cartilage butt-ends, capsules, ligaments and the dense fibrous tissue which fill in the outline of the streamlined hydroplane. Only with a difficulty proportional to thickness can one bend the distal regions of the tough, resilient flipper when freshly removed from the body Therefore all deliberate movements — adduction, abduction, extension, flexion and rotation of the extremity — occur at the shoulder The flipper of an unconscious or fresh-killed small odontocete (fig. 2) may be abducted approximately 90 to sagittal plane adducted to about 30 (with rest or glide position in the range of 40–45) extended or carried forward approximately 90 to the body axis, and flexed and rotated to be flat against the body with trailing edge dorsal In the abduction adduction plane the flipper may be rotated about its longitudinal axis approximately 75 in either direction Appropriate scapular movement is apparent in the extremes of abduction, adduction and rotation This general statement for the beluga pilot whale and the dolphin is reasonable when compared with the movements of the latter in aquaria For obvious reasons of size and mass, the very large whales cannot be handled or easily retained in observation tanks and their flipper movements are less well documented. However there is nothing in their configuration or musculoskeletal anatomy suggesting movement patterns significantly different from those of smaller cetaceans.

With the humerus surrounded by muscles in the root of the flipper and the elbow but slightly beyond body contour the free extremity is virtually all antebrachium and manus. Of these the latter dominates with a shape varying greatly among the species. In the broad spatulate flipper of the beluga, the relatively long digits are spread apart in the manner of an open hand with adducted thumb the intervening spaces are occupied by extremely dense fibrous tissues continuous with the deep subcutaneous layer In those species





. 1 Right, lateral view of the skeleton of ectoral limb of 28 3 meter female spec en of *Balaenoptera physalus* (finback whal) ed on overlapping radiographs of intact limb e scale for one foot or 30 5 cm

Fig. 2 Orientation of humerus and radius and ulna in body and flipper base. Upper dorsolateral view of left extremity lower anterior iew of right extremity Based on anatomy of dolphin, *Tursiops truncata*.

with narrow and straight flippers (e.g. finback whale) and falciform ones (e.g. pilot whale) the digits are quite parallel and even more elongated. The static posterior angle of the flipper characteristic of some whales is due as much to the carpal antibrachial angle as to curvature of the digits.

The cetacean limb has the essential mammalian component of bones with some striking modifications and additions in keeping with overall adaptation of the member. The humerus is short and robust and in nearly all species is shorter than the radius and ulna with which it articulates end-on. The flattened antibrachial elements are bound firmly together by fibrous tissues and form the semistreamlined core of the free extremity. These bones are flattened and broad in the odontocetes but more slender in the mysticetes or whale bone whales. In both groups the radius is the larger anterior element. The number of carpals varies with the species; in various odontocetes there are either five or six but in other whales the number is either highly variable or not definitely ascertained (Eales '55). The odontocetes and some mysticetes have five digits; in the rest of the species there are four. The digits consist of metacarpals and a phalangeal complement varying between species, possibly varying with the individual and quite likely differing between fetus and adult (Eales '55). In the fetus of the beluga these number (from first to fifth digit) 2–3, 7–8, 6–7, 5 and 4; in the pilot whale fetus, 4, 15, 10, 3 and 2; in the finback fetus (4 digits only) 4, 8, 8 and 4. (These numbers are based on 6 beluga, 12 pilot whale and 2 finback embryos and fetuses studied in our laboratory.) In the cleared fetal limbs interphalangeal lines are not always easy to distinguish and irregular shapes among nearly continuous terminal elements add to the difficulty.

In individual bone development and structure the cetaceans exhibit peculiarities shared with the only other fully aquatic mammals, the Si ema (manatee, dugong) (Fawcett '42) and with penguins (Meister '62). All whal limb bones are without open medull cavities, being composed of spongy porous bone throughout their inter. The strongest indication that this somehow is a to full aquatic adaptation is the fact that the bones of the partly-terrestrial sea lions, seals and walruses have some internal cavitation. Distinction must be made, however, between the heavy solid bones of the manatee and penguin and the rather lighter spongy bones of cetaceans. In cetaceans the basic mammalian pattern of appearances and fusions of primary and secondary ossification centers persists but the entire sequence is retarded as compared with terrestrial mammals. (This is a major reason for confusion and doubt concerning numbers and positions of bones in mascerated skeletons.) Maturation of carpal centers is especially irregular and secondary bipolar phalangeal centers rarely are complete even in the adult beluga and pilot whales. In bringing fresh-killed specimens, flexibility of the flipper beyond the radius and ulna is due more to a high proportion of resilient cartilage than to to any factor of mechanical organization.

In this investigation we have concentrated on the humerus of three species having common basic characteristics but with a very considerable range in adult size and flipper type. Preliminary examination showed that of the three major limb bones the humerus would contribute most to the immediate goals, to define the characteristics of such bone at microscopic and organic inorganic levels and to investigate the relationship of bone structure and density to limb function. (The microscopic structure of the humerus will be treated in a separate publication on growth and remodeling in whale humeri, radii and ulnae.) The size and internal structure of the finback whale humerus (the second largest one extant (only that of the blue whale *Balaenoptera musculus*, being larger) was a great advantage in that it permitted analytical techniques not readily applicable to smaller bones of either cetacean or other groups of mammals. In addition, size differences between finback and the small odontocete humeri have afforded some insight into the relationship of size to bone structure and density. For these reasons, data on the finback whale humerus comprise the major part of this report.

MATERIALS AND METHODS

Materials for this investigation (and concomitant ones of whale limb structure and skeletal development) have been from several sources. The right flipper of a 6 meter female finback whale was obtained through the British Columbia Packers Ltd. from their whaling station at Coal Harbour B C This was received frozen and was dissected and macerated without chemical fixation. A series of formalin fixed limbs of finback and other odontocete fetuses was received from Dr ... Truex, Department of Anatomy Hahnemann Medical College Philadelphia. Whole preserved fetuses of beluga and pilot whales were supplied by Dr David E. Sergeant, Arctic Unit, Fisheries Research Board of Canada Montreal. Finally a limited number of fetuses and a good developmental series of whole limbs of postnatal beluga and pilot whales were collected at, respectively Churchill Manitoba, and Dildo Trinity Bay Newfoundland. Our gratitude is acknowledged to the contributors and to the personnel of the Adanac Whale and Fish Products Ltd., Churchill, and the Arctic Fisheries Products, Ltd. and the Fur Farmers Feed Co-op ..., Dildo whose far more than tolerant attitude made possible our field study

The fetal limbs were removed and processed for routine histological sections or prepared as whole mounts. In the latter alternative specimens were treated in 5% KOH to which alizarin Red S was added for staining of calcified centers. After clearing in glycerin the preparations were studied in conjunction with sections of the opposite limb This material and radiographs of immature postnatal specimens supplied information on early development of the humerus and related skeletal elements.

Processing of flipper skeletons of the finback and smaller whales consisted of a schedule of radiography measurement, stripping or dissection, defatting and drying. As soon as received in the laboratory the beluga and pilot whale flippers were radiographed to record extent of ossification and permit measurement of the intact skeleton. Throughout this study radiography was carried out with a diagnostic Westinghouse 125 KVP 200 Ma machine utilizing a Machlett Super Dynamax rotating tungsten anode tube with 1 mm focal spot. Such whole limb radiographs were generally useful but of less than optimum resolution due to tissue density and secondary radiation from intraskeletal and extraskeletal fat. Specimens next were either dissected or simply stripped, then macerated in a constant temperature hot water bath (96 C) After 24 to 72 hours depending on specimen size the bones had loosened from fibrous tissue and cartilage and could be cleaned with a soft wire brush. Their high fat content required that the bones be treated in warm zylene and benzene for as long as a week or ten days. They then were washed in hot water and detergents and allowed to dehydrate partially at room temperature before the process was completed in an 80 C oven. After unfused secondary centers were cemented in position final photographs and radiographs were taken and selected specimens were prepared for sectioning.

The great size of the finback flipper and its individual bones required some modifications in processing The initial radiograph was made in an overlapping series of films which were photographically reduced and assembled in a composite (fig 1) Tissue density and secondary radiation prevented good resolution of all the bones. The particular thickness of the humerus made appraisal of internal structure impossible The flipper was dissected and disarticulated into large units which were macerated in a large hot water tank at 97 C until bones could be brushed clean Although some of the vast amount of residual fat was removed in solvent baths final cleaning was accomplished only after the humerus was bandsawed into thick sections. Before sectioning, another attempt was made to radiograph the intact bone; the results were hardly better than in preliminary mapping.

In photography radiography and sectioning, the humeri were positioned in accordance with standard planes and axes. These and the topography of the humerus were defined in terms of skeletal orientation in the glide or rest position in smaller cetaceans in aquaria (fig. 2) In this sense (fig. 3) the medial (or inferomedial) surface of the finback humerus extends

distad from the tubercle the lateral (or superolateral) surface extends from the stubby neck and head while anterior and posterior margins begin between head and tubercle and terminate at the concave mar*gins of the distal articular surface* *As will* be described in a later section each species has small deviations from this stereotype (fig 4) For most photographs and all whole bone radiographs humeri were placed with medial surfaces down and distal ends supported so as to hold anterior and posterior margins parallel to and equidistant from the table or cassette For bandsaw sectioning the bones were placed in this position within a wooden box, the long axis of which coincided with the median or sagittal plane of the bone. The box then was filled with a mixture of saw dust and acetate cement When this matrix had hardened the whole unit was placed on guides and moved into the band saw (variable speed with one-[illegible] an inch thick blade) in serial passes. Before bone sections were removed from the matrix, reference lines or points were placed for orientation in photographs, *radiographs and reconstructions.*

The finback humerus was cut first into two-inch thick sections. It was possible to complete cleaning and drying of these without warping. The thick sections were cut twice again so that the humerus was reduced to 41 sections. Disregarding the first and forty-first because they did not have two plane surfaces there were [illegible] sections with a thickness as close to 1[illegible] as was practical Over 10% of the [illegible] was lost in saw waste. Subsequent [illegible] complete analysis of the finback humerus similar sections were made of beluga and pilot whale humeri. In obtaining such scale thickness sections of these lower proportionally more was lost to saw [illegible]

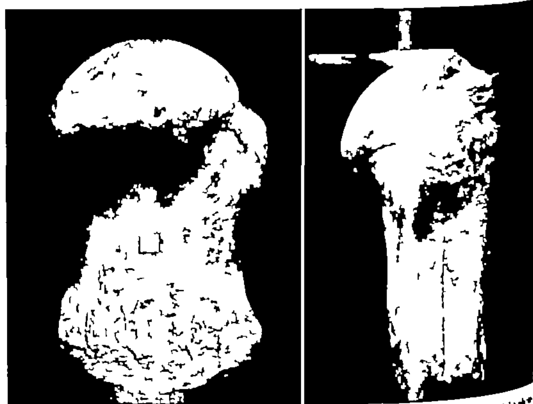


Fig. 3 Views of l[illegible] surface (left photograph) [illegible]nd posterior surface or margin (right photograph) of humerus [illegible] k whale White pat[illegible]h is one inch square. Vertical scribed lines are the employed in orientatio[illegible] tion for density reconstructions. Slightly less than one-[illegible] size

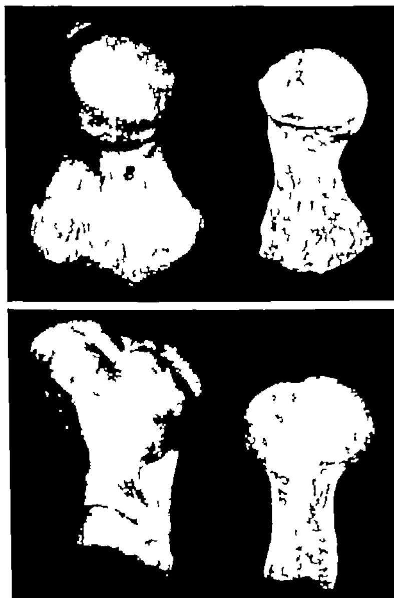


Fig. 4 Views of left humeri of the beluga (*Delphinapterus leucas*) (right) and pilot whale (*Globicephala melaena*) (left) Upper row lateral surfaces lower row anterior surfaces or margins. Approximately one-half natural size

Sections were radiographed on Eastman dustrial Type M film in no-screen hold and with an aluminum foil filter be een subject and cassette For each cies the most desirable exposure was termined by trial Definitive radiographs the 12 mm finback sections were made 100 KV and 350 MaS Bel g1 and pilot whale sections 3 5 mm thick, were ex posed at 100 KV and 200 MaS An alumi num step-wedge was placed on all films and the standardization of exposure and development was checked by photodensitometric comparison of wedge images

To produce a set of data permitting graphic reconstruction and some degree of

quantitative analysis the serial finback radiographs were read systematically for optical density on a MacBeth Quantalog photodensitometer. A transparent acetate sheet ruled off in centimeter squares was superimposed on the reference points of each radiograph. The optical density of the center of each square then was assayed by the 3.5 mm diameter light beam of the photodensitometer. (A smaller diameter would have approached pore-size in some regions while a larger beam would have missed subtle changes in density.) Some 14,200 points were read actually accounting for radiodensity in 1,215 cm^3 of bone but representing or sampling slightly more than 92% of the area of the sections. The remaining area of the sections was lost through omission of incomplete squares (i.e. of less than three quarters useful area) or of those with tapered edges, along the periphery of sections. After all readings were collected, the range between the highest and lowest individual O.D. values (representing, respectively the lowest and highest radiodensities) was divided to establish deciles to which all readings then were assigned. These deciles numbered in order of increasing optical density (or decreasing radiodensity) have been used in graphic reconstructions of single sections or planes (fig. 11) and in plots of all points of a single decile visible in medial-lateral and anterior posterior outlines of the whole bone (fig. 12). The first decile is poorly represented due to its occurrence in the peripheral band where incomplete squares or edge taper precluded readings. This dense bone category would have been represented more completely had the photodensitometer beam been smaller, especially had the thin surface layer of the head been registered.

Because our exposures were within the linear portion of the curve for response of the particular film to x radiation, radiograph optical density is simply the proportional inverse of bone section radiodensity. To establish the relationship of absolute density (i.e. weight volume) and mineral proportion to optical density of the radiograph a 1 cm (inside diameter) core-drill was used to remove standard test cylinders from representative sections and in all deciles. These were recleaned and [illegible] until weight loss was complete, then weighed. From known volume of the cylinder and its dry fat-free weight, [illegible] density was calculated. Samples then were ashed in a muffle furnace for 24 hours at 600 C. Comparison of weights before and after ashing established the mineral proportion of the samples.

When the work with the finback humerus was completed, a more simple analysis was made of beluga and pilot whale humeri. Serial radiographs were read for optical density only along lines which [illegible] graphic reconstructions represented medial-lateral planes through the bones (fig. [illegible]). The exposure data for these sections were given earlier. Decile ranges were established from maximum and minimum densitometer readings found in scanning the obviously dense and rarified regions of all sections then applied to values encountered only in the indicated plane.

OBSERVATIONS

The anatomical materials and techniques of this investigation have yielded several categories of information. *Gross structure and development* of finback, beluga and pilot whale humeri are presented for their own value and to create background and frame of reference for the qualitative and quantitative evaluation of humeral internal architecture. The *radiographic appearance* and the graphic *reconstruction* of humeral architecture and density constitutes the main thrust and most substantial contribution.

1. Gross configuration of cetacean humeri. In the sense of classic comparative anatomy the finback, beluga and pilot whale humeri deserve formal description. Only certain features of each and [illegible] however contribute to understanding of the radiographs density reconstructions and bone structure comprising the remainder of the report. Because of the difficulty in describing the humerus as positioned in the base of the flipper it will be oriented here as illustrated in figures 3 and 4, [illegible] in medial-lateral and anterior-posterior aspects with the longitudinal axis vertical.

In table 1 overall lengths and the ratios of principal diameters to length are shown for the single finback humerus and [illegible]

TABLE 1

Dimensions of cetacean humeri

Specimen	Length	Proximal a-p	Proximal m-l	Midshaft a-p	Midshaft m-l	Distal a-p	Distal m-l	Volume	Density
		Mean ratio of diameters to length of humerus							
	cm							cm³	gm/cm³
Finback (1)	68	0.63	0.63	0.44	0.32	0.55	0.26	19,200	0.52
Pilot whale (means of 4)	14.2	0.53	0.73	0.44	0.42	0.71	0.32	503	0.67
Beluga (means of 4)	11.0	0.49	0.61	0.25	0.28	0.49	0.33	210	0.69

NOTE Volume of small humeri determined by displacement of water without vacuum; volume of finback specimen established from section area (saw waste accounted for) after cleaning. Density is that of mineral structure, intertrabecular space included; calculated from dry, fat-free weight and the volume of the beluga and pilot whale humeri, and from dry fat-free section weight and calculated volume (section area thickness, saw waste accounted for) for finback specimen.

pical, mature humeri (4 each) of the luga and pilot whales. Axes for the ameters are in accord with the orientation of the odontocete humerus depicted in figure 2, and the surfaces (medial and lateral) and margins (anterior and posterior) defined in Materials and Methods nd shown in figures 3 and 4 Finback fig 3) beluga and pilot whale humeri fig. 4) are quite similar albeit with several individual characteristics in one respect or another From the tabular data nd the photographs it is obvious that the humeri are short, robust bones having relatively very large articular surfaces and eminences for muscular attachment. As group they are at their proximal ends broad as or broader in the medial-lateral direction (i.e., across the opposed head nd tubercle) than in the anterior posterior direction (i.e along the major axis the elbow articulation) Approximately the proximal half of each consists of a road metaphysis terminating in a short, thick neck, massive head (hemispherical somewhat less) and large tubercle In our single finback humerus the tubercle is immature, the removal of a large mass of cartilage having revealed the rough surface shown by figure 3 The tubercle is squared-off and nearly as large s the head in the pilot whale while in the beluga it is rather smaller and sloped posteroinferiorly The expansion of the distal end of the bone in the anterior posterior plane is greatest relative to length in the pilot whale and finback. In all forms the distal articular surface is beveled in the anterior posterior plane and concave in the medial-lateral one the end-on articulation with radius and ulna is, therefore rather more complex than would appear at first examination. The distal surface of the finback humerus has an extension or additional facet on the posterior margin for articulation with the large ulnar process (fig. 1) characteristic only of the mysticetes.

The head, located on the lateral and superior aspect of the humerus is directed superiorly and somewhat posteriorly with both angles varying among the three species. A thick buttress beneath the head extends far down the lateral or posterolateral surface this feature is a most prominent ridge in the pilot whale more rounded in the beluga and is of broad gentle contour in the finback humerus. Its position relative to the midshaft has much to do with the proportion of anterior posterior and medial-lateral diameters to overall length. In all three species a pronounced fossa, wherein inserts the deltoid muscle, is immediately anterior to the lower extent of the neck buttress The tubercle is the superior and rather anterior continuation of the entire flattened medial surface in each of the humeri From lateral view a portion of the tubercle is visible anterior to the head in finback and pilot whale humeri but in this view of the beluga the tubercle is hidden almost completely by the head (fig 4) In dissection of pilot and beluga whales it has been observed that with the flipper in glide position (p 172 and fig 2) the tubercle is

nearly in firm contact with the edge of the scapular fossa.

The shaft is difficult to define in cetacean humeri. That of the finback humerus (fig 3) comprises approximately a quarter of overall length It is hour-glass shaped in lateral view smoothly tapered to the anterior view and elliptical to oval in cross-section (fig 7) The shaft in pilot whale and beluga humeri is little more than the region of merger of proximal and distal expansions Cross-section shape is roughly that of a triangle the base of which is at the root of the tubercle and the apex on the buttress of head and neck (figs 9 and 10)

Surface texture of cetacean humeri is noteworthy The surface of the head in the three species in this study as well as in various museum specimens has a texture best described as pebble-grain. In addition, the head of the finback humerus is marked by a large number of rounded protuberances (± 5 mm in diameter and height) in an irregular distribution central in its posterior half In none of our specimens is this unexplained roughness reflected in the contour of overlying articular cartilage The surface of the tubercle has areas of rough and smooth texture characteristic of this type of muscle attachment the arrangement of muscles here and elsewhere on the humerus is in agreement with the descriptions of Murie (1873) and Howell ('30) The distal half of the humerus is of very rough texture, and the alignment of the multitudinous small tubercles and depressions corresponds to the fiber orientation in the ligamentous layer which attaches thereon and is continuous over the elbow synchondrosis to the similar surfaces of radius and ulna.

2 Development of the cetacean humerus The pertinent question in cetacean limb development concerns the origin of its spongy structure and its lack of a narrow cavity In this respect, as well as others in histogenesis and maturation, the beluga, finback, and pilot whale embryonic and fetal specimens display common characteristics The following is based on microscopic sections and cleared preparations from all three species For documentation features of pilot whale development are shown in figure 5.

The cartilage models of the major skeletal elements as well as those of most of the phalanges are completely formed by the time calcification and ossification take place in the humerus. The cavity of the shoulder joint is evident in the youngest specimen available (a 40 mm beluga embryo) but the elbow joint is united by fibrous tissue from the earliest stages The gradient of cartilage maturation from middle toward either end is not as distinct or as organized as in common land mammals In particular the zone of flattened cells indicative of rapid longitudinal growth (Streeter 49) is absent. In addition, at no time in embryonic and early fetal periods are there regular rows of hypertrophic cells in the central region or adjacent to the advance of endochondrial ossification.

A striking feature of pre-osseous cartilage models is the extent and intensity of calcification in their central region. Were a superficial examination of alizarin-stained cleared specimens not supplemented by histological sections, the impression would be that limb bone ossification proceeds from deep centers. The lag in time between calcification of cartilage formation of perichondral osseous spicules and subsequent endochondral ossification is extended. In the absence of data on embryonic age dating of these events is impossible the lag in sequence is illustrated however in one phase of the proximal-distal gradient of the pilot whale flipper in which most phalanges possess [illegible] alizarin-stained nodules while only the metacarpal is ossified.

By the time of origin of the perichondral osseous sheath (fig 5) the calcified region of the humeral cartilage is [illegible] shaped, its blunt end directed distad [illegible] at its widest point is the calcified cartilage superficial. Perichondral ossification begins around this narrow exposure on the humeral midpoint and increases in length as the calcified region enlarges and further extends to the surface. Endochondral invasion, deep to the middle of the bony sheath, produces a cavity containing large irregular remnants of cartilage matrix surrounded by bone. The intervening os-





FIG. 5 Photomicrographs of the humerus of 37 cm fetus of the pilot whale (*Globicephala malaena*). Section is well lateral to the true anterior-posterior plane of the humerus. It exposes the open glenohumeral articulation, the conjunction of humerus, radius and ulna at the elbow and lateral trabeculae of the ossified shaft as well as the expanded regions of endochondral ossification proximal nd distal to it. Not the curvilinear chondro-osseous junctions, fully trabecular composition of ossified shaft, and absence of medullary cavitation. Lower enlargement details the endosteal sequence of finer trabeculae (within area delimited by dashed lines in upper photomicrograph). These features are discussed in text. Magnification of whole bone section × 7 of enlargement, × 21

nective tissue is highly vascular but without hematopoiesis. Rather than proceeding along a regular front, cartilage erosion and replacement continues in an irregular meandering fashion.

The first perichondral ossification is in the form of a flattened array of trabeculae about the superficial exposure of calcified cartilage In further development within the thick periosteum (fig 5) trabeculae are laid down at angles to the cartilaginous surface As seen in the photomicrograph the greatest angle nearly perpendicular is at the middle of the shaft and the least at its ends (i.e against the cartilage) Osteogenesis proceeds along all faces of this trabecular structure (which appears as a woven honey-comb in surface view of cleared specimens) but the greatest activity is peripheral. As development progresses successive generations of trabeculae arise at the ends of earlier ones. This circumferential and longitudinal growth of the ossified shaft is not paralleled by internal resorption. Osteoclasts are found in eroding cartilage and in small number on central endochondral spicules however they are rare among the periosteal trabeculae.

The lack of material from late fetal periods precludes study of remodeling in the endochondral regions and of the relative compacting of peripheral bone the general developmental trend, however is obvious from the pattern established in the earliest phases. It is possible to project humeral length width and the angle of periosteal bone to cartilage surfaces in the embryo and arrive at the essential proportion of the adult bone without considering either internal or external modeling resorption. It is clear enough therefore that the adult humerus can be accounted for on the basis of virtually equal and constant longitudinal and transverse growth trabecular periosteal osteogenesis about a slightly remodeled core of endochondral bone, and lack of massive internal resorption.

With the exception of the proximal humeral the secondary ossification centers in the whale limb skeleton are all of postnatal origin Beluga and pilot whale radiographs suggest that the sequence of centers in the three major bones is most likely: proximal humerus, distal humerus and proximal radius and ulna, and distal radius and ulna. The time distinction at the elbow is very slight. The distal radius and ulna are out of turn compared with other mammals (i.e. they should ordinarily appear before the proximal ones The sequence of epiphyseal fusion is more certain: distal humerus, proximal radius and ulna, proximal humerus, and (after a long interval) distal radius and ulna. The overall classic mammalian pattern of early appearance and late fusion at shoulder and wrist, therefore generally is retained The appearance of the distal radial and ulnar centers after the proximal ones and the delayed closure at the wrist may be related regionally to irregular ossification in the carpal centers and very slow ossification in the digits.

3 *Radiographic appearance of internal structure* While structural density in whale humeri can be appreciated in transverse sections (figs. 6, 7 8 9 and 1 only longitudinal sections adequately depict the overall pattern of structural orientation. Radiographs of such sections of beluga and pilot whale humeri are shown in figure 13 Transverse sectioning of the single finback humerus precluded similar appraisal of its internal architecture however comparison of finback sections with transverse sections of the smaller humeri and correlation of the latter with longitudinal sections confirms that the finback humerus has the same basic structural orientation. The following commentary should, therefore, be applicable to all three species

The regions of greatest radiodensity (except for the thin surface layer of the head and distal face) are the thick medial and lateral walls of the shaft and metaphyses (fig 13) In all three forms, a trabecular pattern can be traced from the medial and lateral walls superiorly into the head and and tubercle. Trabecular lines from the upper medial wall pass directly up into the tubercle, while those from progressively lower origins curve superiorly and laterally into the upper neck and the upper thirds of the head From the upper lateral wall trabecular lines lead into the lower head region from lower origins they curve across into the tubercle The angular

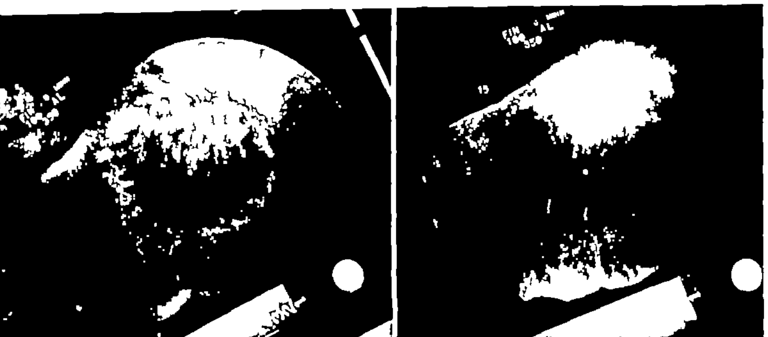
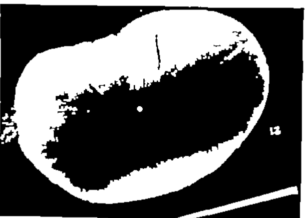


Fig. 6 Radiographs of 12 mm thick transverse sections of humerus of finback whale *Left*, through *head and tubercle*; right through *proximal metaphysis*. Slightly more than one-fourth natural size. See text for methods of sectioning and radiography



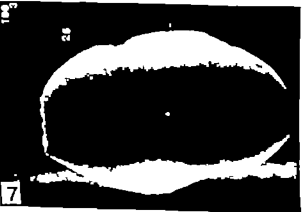






Fig. 7 (left) and figure 8 (right) Radiographs of 12 mm transverse sections of humerus of finback whale. Exposure and printing [illegible] in figure 6.

Fig. 7 Upper proximal level of [illegible] half [?] lower midshaft level (as in fig. 17).

Fig. 8 Upper just proximal [illegible] distal epiphyseal line; lower level of [illegible] distal epiphyseal line [illegible] secondary [illegible]. Slightly more than one-fourth natural size.

tionship of these lines as they intersect ch other and the central axis of the bone essentially the same as in the classic end of the femur (Koch, 17 hin, '35) and in the photographic rep sentation of the dolphin humerus by urray ('36) An additional set of tra cular lines in the pilot whale humerus tend from a thick, dense point between ad and tubercle and fan out in the upper ad region. This feature is less obvious the beluga humerus.

At progressively lower levels in the merus, the angle of trabeculae arising om the dense regions decreases until at e narrowest point in the shaft the orien tion is nearly horizontal and the texture ite irregular Below the least diameter nother arciform pattern of trabeculae can traced from the dense bone to the distal ticular surface. This disposition is more vious in the beluga than in the pilot hale where it is partly obscured by a orizontal array of fine trabeculae The gions immediately deep to the distal ticular surface and that of the head nsist of a large number of fine short abeculae

Serial sections of finback humerus The ction radiographs (figs. 6 7 and 8) and ctions themselves (figs. 17 and 18) re al that, in addition to the lack of an open edullary cavity the finback humerus is ithout a uniform, compact wall and that consists largely of spongy bone with only rtain regions of a more dense structure t almost all sections the central region less dense than the periphery with the adient varying greatly according to level the humerus and, in many sections ffering along anterior posterior and me al-lateral axes as well. In the center of me sections pore diameter is as great 3 to 5 mm, while ½ to 1 mm is typical. ven in the most dense regions, porosity ranging up to 0 1 mm) is discernible to e naked eye The least dense regions are ade up of interspersed trabeculae and rforated platelets while more dense ongy bone consists of tubes and short lls or chambers with fenestrated walls hereafter referred to as tubes) The boun aries of such spaces of course appear trabeculae in long section

The only suggestion of a central canal in the finback humerus is the large (± 1.0 cm) irregular vascular labyrinth near the center of the three smallest midshaft sec tions (fig. 7). From this cavity channels of lessening diameter can be traced through proximal and distal sections radiating at considerable angle toward the surface of the shaft and metaphyses and the epiphy seal line Below this magnitude the vas cular pattern is lost in the interstices of spongy bone

In terms of porosity and structural or ganization, the proximal secondary center comprising the head and upper tubercle, is the most uniform portion of the humerus. The proximal epiphyseal line arches in both medial-lateral and anterior-posterior planes so that the metaphysis of the pri mary center intrudes into sections through the head and tubercle (fig 6) No special ized tracts are seen in transverse sections of the head, but a general radial disposi tion of trabeculae immediately deep to the articular surface as well as a more obscure circumferential pattern, can be identified. A similar arrangement appears in some sections of the tubercle but the overall disposition within this immature protuberance is vertical, or nearly so and only the most superficial trabeculae are aligned perpendicular to the irregular surface

On either side of both proximal and distal epiphyseal lines, but especially on the metaphysial ends there are numerous relatively thick-walled vascular channels. The complex ends of primary and second ary centers are faced off with terminal plates approximately as thick as the articu lar surface on the head. In our particular specimen the proximal line had only a few points of fusion in the distal end fusion was almost complete

The upper level of the proximal me taphysis (fig. 6) has the thinnest surface layer in the entire humerus sections through this region consist largely of bone tubes aligned in the medial-lateral direc tion centrally and in the vertical periph erally These in section are the vertical and arching trabecular lines seen in figure 13 The only dense region is a thick, broad one on the medial side as in the longi tudinal section the medial wall thickens

and is dense at a higher level across from the laterally situated head. In successively lower sections this region increases in thickness and width and is paralleled by a similar concentration on the lateral side. In the same range of sections the anterior and posterior marginal regions become more dense relative to the center but are less dense and to a lesser depth than the medial and lateral walls By the twentieth section (approximately the boundary between metaphysis and shaft) there is a notable difference between the two surfaces two margins and the center of the humerus At this level the medial-lateral disposition of bone in the central region is replaced by a predominantly vertical one again, this correlates well with the longitudinal sections (fig. 13)

In the shaft and distal metaphysis there is a sharp regional distinction in structural density and orientation. The centers of these sections are the most porous or rarified in the humerus being made up of thin trabeculae and perforated plates. Most of the rest of the sections consist of *bone tubes aligned vertically or nearly so* This condition points up the strong similarity to the pilot whale humerus as seen in longitudinal section (fig. 13) The density of the medial and lateral regions increases as that of the central region decreases with the greatest differentiation in sections immediately below the narrowest point in the shaft. From this level distad there is in addition a strong transverse pattern of trabeculae extending from medial to lateral. This feature again as in the pilot whale is most obvious in the distal metaphysis (fig 8) A localized pattern of similar distribution is found deep to the large pit on the lateral surface where the deltoid muscle inserts. From the thick, dense wall of this depression, a bone tract sweeps broadly in medial, anterior posterior and less obviously in proximal and distal directions Comparison with the vertical tions suggests that the proximodistal nt of this pattern is lost in the text of cross-sections. Throughout the sh nd distal metaphysis the moderat nse anterior and posterior marginal r s consist of vertical tubes which m o may not be grouped in rows paralleling the curved surfaces.

Immediately proximal to the distal epiphyseal line the medial and lateral regions of higher density are of greater depth and the narrow central band of very porous bone stands out in sharp contrast. The *vertical orientation of bone tubes indicates* a trabecular system similar to that in the lower end of the pilot whale humerus. The distal secondary center consists of moderately dense bone orientated approximately perpendicular to the epiphyseal line and to the distal articular surfaces.

Serial sections of pilot whale and beluga humeri. The humeri on which this description is based are fully mature. Their epiphyseal lines are fused and unrecognizable in either longitudinal (fig 13) or transverse sections (figs. 9 and 10). In overall external appearance (fig. 4) and in major dimensions (table 1) the pilot whale humerus most resembles that of the finback whale The beluga humerus differs from the other two chiefly in its relatively narrower midshaft region. These similarities and contrasts are reflected in *internal architecture.*

Correlated examination of longitudinal and transverse sections shows that the interior of the proximal half of the *pilot whale humerus* consists primarily of trabecular lines arching from medial and lateral surfaces of the shaft and metaphyses *In addition to this major pattern* there are certain lesser ones: perpendicular trabeculae deep to the surface of the head, vertical trabecular lines (from the medial metaphysis) in the tubercle and trabecular lines passing into the upper head from an origin in the superior surface of the neck. *Throughout* the head most of the short neck, and the top and sides of the tubercle the surface layer is thin uniform and of a radiodensity not much in excess of the trabeculae within the head In contrast, the uppermost limit of the medial surface on the tubercle, is somewhat thicker *and is more* radiodense than any other point in the bone (figs. 9 and 13) (about as dense as the entire surface of the head in the beluga humerus in figs. 10 and 13) The medial and lateral concentrations of bone begin respectively high on the tubercle

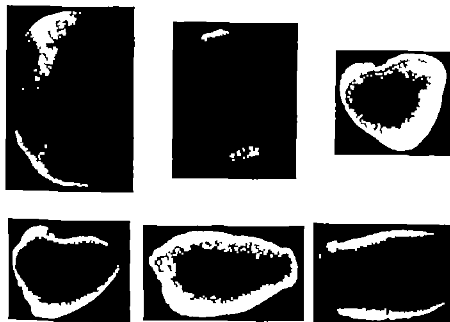


Fig. 9 Radiographs of 3 mm sections through humerus of pilot whale. *Upper left to lower right:* through head-tubercle, proximal metaphysis, shaft proximal to narrowest point, midshaft, distal metaphysis and immediately proximal to distal articular surface. Approximately four-fifths natural size.

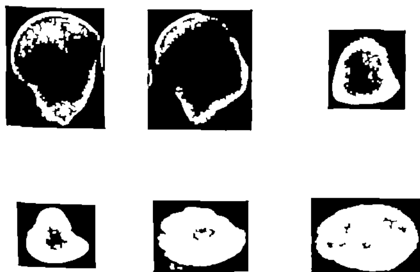


Fig. 10 Radiographs of sections through humerus of beluga whale. Section thickness, exposure, printing and section levels parallel those in figure 9 Approximately four-fifths natural size

below the head increasing in thickness distad toward the midshaft point.

In the third quarter of its length cross-section shape of the pilot whale humerus (fig. 9) is roughly triangular the base being the medial surface and the apex the lateral surface on the buttress of the neck. Throughout this region the base and apex of the triangle are dense and thick while the sides of the triangle are as dense but to a lesser depth In approximately the upper half of this region trabeculae are directed medially and laterally in a continuation of the pattern seen in the upper half of the humerus progressively downward, this orientation is replaced centrally by a more open and irregular one grouped about the central vascular labyrinth. This level (fig. 9) is comparable to the smallest midshaft section of the finback whale humerus (figs. 7 and 17)

In the lowest quarter of its length (fig. 9) the pilot whale humerus progresses from oval through elliptical to essentially rectangular cross-section Here there is a rather homogeneous pattern of transverse and vertical trabeculae The medial and lateral walls remain dense while becoming progressively thinner; the anterior and posterior margins are quite uniform without a dense surface zone Structural density rises immediately deep to the distal articular surface which is approximately as thick and dense as that of the head

Except for the especially radio-dense thin articular surface of the head (fig 13) the upper third of the *beluga humerus* does not differ greatly from that of the finback and pilot whales. In the remainder of the humerus however comparison is striking. The constricted middle region (fig 10) triangular in cross-section through most of its extent, is almost uniformly dense in a thick peripheral zone The interior both relatively and absolutely is very porous. Demarcation between outer and inner zones is by way of a short density gradient. This lack of distinction between medial lateral and anterior-posterior planes is in marked contrast to the situation in the other species To a l rge degree a similar density distribution prevails throughout the remainder of the beluga humerus In the oval to elliptical sections of the distal expansion (fig 10) the dense thin peripheral zone is but slightly reduced at the immediate anterior and posterior margins. From just below midshaft, porosity of the central zone increases and persists until the distal epiphysis is reached

4 *Graphic reconstruction of density distribution in the humerus* Although the whale humerus has the definite, complex internal architecture just described, it is obvious that a great deal of its apparent mechanical organization has to do simply with density of structure. The general pattern of density can be visualized in serial radiographs however anything more than subjective examination requires a method which yields a concise picture of the size shape and position of density bodies (per se and relative to trabecular patterns) allows comparison within and between bones and permits evaluation of the influence of mineral content on the radiographic image. Toward this end optical density reconstructions allow us to schematize and quantitate what is seen in radiographs and they may be compared between bones. However certain factors (explored in detail in a later section) must be considered in viewing such reconstructions Optical density of the radiograph or radiodensity of the bone section, is dependent upon the amount of bone (absolute or structural density) and its incorporated or mineral content. Ash tests for the finback humerus (p 193) have demonstrated the absence of a gross regional pattern of mineralization. Therefore optical density (or radiodensity) is a function of absolute density to which it bears the log relationship revealed in figure 14 Optical density reconstructions consequently do not represent equally spaced intervals of absolute density and high optical densities are more closely grouped in weight per unit volume than are low ones. Interpretation of absolute or structural density from such reconstructions is not however difficult.

Three types of reconstructions, each with advantages and disadvantages, may be made from opti al density data The *first* type the single-section map, is produced by conversion of photodensitometer readings to optical density deciles It is both highly informative in *itself* and is the source of data for the other reconstructions

ns. The individual complexity and the mber of such maps however prohibits tical reconstruction of more than a v deciles and levels. Illustration of these impractical. The *second* type of reconstruction involves plotting medial-lateral and anterior-posterior views of the distribution of single OD deciles within the outlines of the entire bone. The results are in a sense perpendicular views of a three-

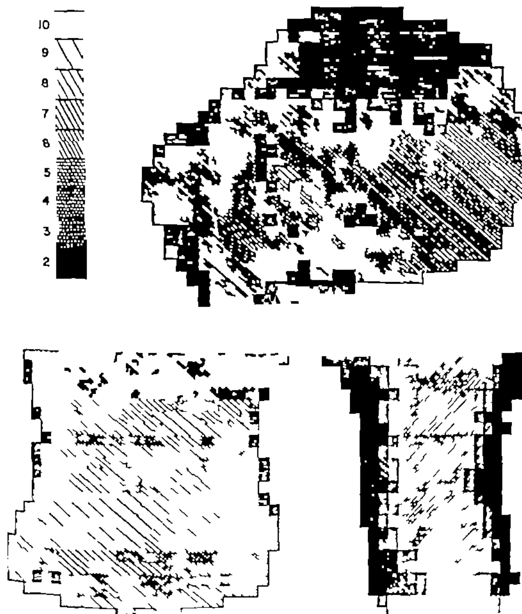


Fig. 11 Graphic reconstructions of sections through humerus of finback whale based on distribution of radiograph optical density. The bar at upper left indicates the code used to depict optical density deciles 2 to 10 (decile 1 not being encountered in these sections). See p. 178 for technique. Upper right, section through head and tubercle (same as in fig. 6). *Lower left*, an anterior-posterior plane through distal half of humerus. *Lower right*, medial-lateral plane through distal half of humerus.

dimensional transparent humerus in which only one decile at a time is visible as a complex of dots in the appropriate positions in each section. Such reconstructions are most useful in depicting vertical and transverse dispositions of each decile relative to whole-bone configuration but one must depend on other methods for some details of interior relationships. The single-decile distributions for the finback humerus are shown in figure 12. The *third* type of reconstruction is the vertical section showing all deciles as they are distributed along fixed planes passing through all the single-section maps. These have been used with the distal half of the finback humerus (fig. 11) and the full vertical extent of beluga and pilot whale humeri (fig 13) Where density distribution is not such as to warrant vertical plane reconstruction the single-section map may suffice as in the case of the proximal end of the finback humerus in figure 11 The frequency distribution for optical density readings for the entire sample is shown in figure 15 and for selected levels in figure 16 The structure of bone from the individual deciles of the finback humerus is shown by photomacrographs in figure 18.

The finback humerus. Structure of the finback humerus as reflected in optical density of radiographs, is, for convenience and with anatomical justification, treated in two major divisions: (1) the generally symmetrical shaft and distal expansion and (2) the proximal mass consisting of head incomplete tubercle and abbreviated neck. Separation is made (between sections 16 and 17 in reconstruction) through the proximal metaphysis. There is obvious continuity between these regions but their overall density patterns are nearly as distinctive as the related differences in external configuration.

Section radiographs of the shaft and distal expansion display an ordered sequence of optical density in both mediolateral and anteroposterior planes. In general this consists of a progression of dominant densities somewhat intermixed with the higher or lower densities on either

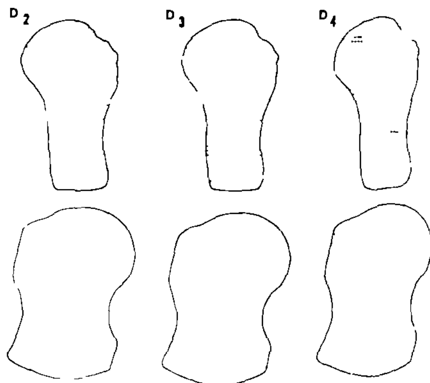


Figure 12 (Part 1)

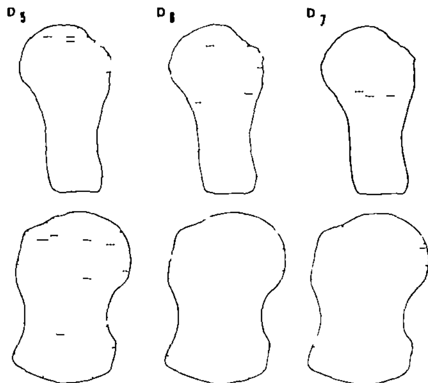


Figure 12 (Part 2)

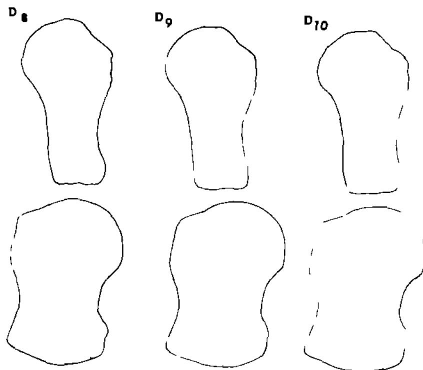


Figure 12 (Part 3)

Fig. 12 The distributions of individual deciles of radiograph optical density in anterior posterior (upper row) and medial-lateral (lower row) outlines of the finback humerus. From decile 2 to decile 10 radiograph density increases and bone structural density decreases. The *few* cases of decile 1 encountered are shown (for convenience) as small circles along with decile 10 See page 192 in text.

side rather than a precise step-wise gradient. This is obvious in frontal and sagittal vertical plane reconstructions (fig. 11) and is inferred in the medial-lateral and anterior-posterior views of single-decile distributions (fig. 12). The following description is based on a correlated examination of these two types of reconstructions as well as of all the unillustrated single-section maps. The highest and lowest optical densities in the entire humerus are at nearly the same levels in the shaft. The greatest concentration of bone, *Decile 2* (with which are found the few recorded points of *Decile 1*, p. 178) is localized on the medial and lateral surfaces; a few points of this range are found far down on the medial surface of the distal epiphysis but the general distribution is in the ten midshaft sections of least diameter. *Decile 3* is distributed irregularly in the D2 concentration but generally is disposed deeper and occupies peripheral zones proximal and distal to the more dense bone. *Decile 3* also extends toward the edges of the curved anterior and posterior margins. *Decile 4* is intermixed with D3; however, it is more plentiful and extends farther in all directions including that toward the anterior and posterior margins. At the other end of the scale the lowest bone concentrations, *Deciles 9 and 10*, are found only in the center of the lower and middle levels of the shaft and in the distal epiphysis. Although there is some irregularity, the second lowest decile generally overlaps and surrounds the lowest and has a greater vertical extent. The interruption of this density group at the level of greatest distal width is due to the more dense bone at and on either side of the epiphyseal line. The next higher density, *Decile 8*, has a broader anteroposterior disposition and, extending into more proximal and distal levels, surrounds the lower densities and is intermixed irregularly with them. In contrast with the limited distributions of the three (four if D1 is included) highest and the three lowest optical density ranges, the intermediate *Deciles 5, 6 and 7* underlie the dense medial and lateral bone, surround the more rarified central region, and (irregularly in the case of D7) occupy peripheral zones along the anterior and posterior margins of the [illegible]

The proximal mass of the [illegible] humerus, although relatively more [illegible]enous than the shaft, exhibits a [illegible] endoectad increase in density and [illegible] differences in peripheral density [illegible] to configuartion of head, neck and [illegible]cle. (In the following, it should be [illegible] in mind that the head is directed [illegible] lateral and the tubercle [illegible]) The lowest density is in *Decile 8*, [illegible] in appreciable amounts only in the [illegible] levels of the mass, in the base of the tubercle and in the root of the neck [illegible] treas beneath the head. Higher than [illegible] D8 is encountered irregularly in the [illegible] *and tubercle. Decile 7* is distributed [illegible] in the center of the mass and out [illegible] lower portion of the head, but is [illegible] only deep in the base of the [illegible]. Where present, D7 is intermixed with [illegible] and D6; however, it is scarce in the [illegible] proximal levels. *Deciles 5 and 6* are [illegible] most common density ranges in the [illegible] metaphysis, tubercle and head-neck. [illegible] D6 which fills in where D7 is lacking [illegible] the tubercle. In general, D5 and D6 [illegible]plete the upper anterior and posterior [illegible]gins in a pattern continued from the [illegible]. *Decile 4* is broadly dispersed among [illegible] and D6 in the more medial and lateral [illegible]gions of the proximal mass and with [illegible] under the curvature of the head. [illegible] is quite restricted in distribution; [illegible] on the medial face of the upper [illegible]ysis in the upper region of the [illegible] under the head, in the lower region of the head proper and on the superior [illegible] of the neck. *Decile 2* is present [illegible] superior surface of the neck and [illegible] points only in the curvature of the [illegible]

For the finback humerus as a [illegible] radiograph optical density, or [illegible] radiodensity distribution may be [illegible]marized as follows: *Deciles 10, 9 and* [illegible] comprising approximately 10% of [illegible] volume (figs. 15 and 18) are located [illegible] the central shaft, extending from the [illegible] of the tubercle and neck down to the [illegible]tal epiphysis. This density range [illegible] major and minor axes of the bone [illegible]tions is greater in anteroposterior than [illegible] mediolateral extent, but nowhere occupies a peripheral position. The intermediate

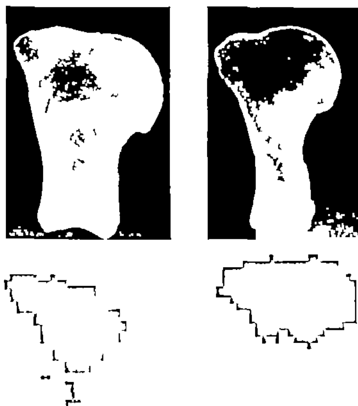


FIG. 13 Radiographs and graphic reconstructions of density of sagittal sections of pilot whale (left) and beluga (right) humeri. Shaded areas represent low bone densities (optical density deciles 10 9 and 8); solid black dots depict high bone densities (o.d ds 4, 3, 2 and 1) The clear white areas and the small circles delimiting them represent intermediate bone and radiograph densities (o.d ds 7 6 and 5) See page 178 for description of method and page 195 for discussion.

sity range D7 6 *and* 5 constituting roximately 68% of total volume occu s nearly all the proximal mass and a d share of the distal mass surrounds core of lesser density and (except for) makes up most of the anterior and terior margins of the humerus. The st dense bone is in the medial and lat l surfaces of the central shaft, but a ry concentration (D4 3 *and* 2 and ttered instances of D1) typifies almost entire medial and lateral regions of humerus. This range makes up ap ximately 22% of the volume of the merus. The graphic reconstructions d this general summary of distribution are a considerable quantitation of what is observed in section radiographs however the log relationship of radiodensity to absolute density requires that analysis of the latter characteristic be made before the mechanical nature of the humerus is appreciated fully

If radiodensity or optical density of the radiograph is to reflect simply absolute density (i e the amount of bone structure encountered by the x-ray beam) the mineral composition of the humerus must be constant throughout. The ratio of pre ashing to post-ashing weights in a series of 54 standard core-samples of the finback humerus was 0 66 with a range of 0.64

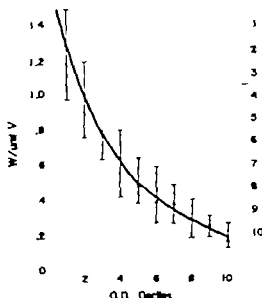


Fig. 14 The relationship of weight per unit volume (absolute density) of 154 1 cm diameter core-drill samples of 12 mm thick finback humerus sections plotted against the optical density of 3 mm points on radiographs of the samples. Optical density is expressed in deciles of the entire range encountered in the humerus. Vertical lines indicate weight range encountered in the approximately 15 samples of each decile. See page 178 for description of technique and page 194 for discussion.

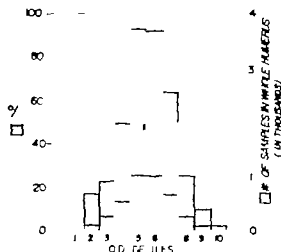


Fig. 15 The percentage occurrence (left scale) and absolute numbers (right scale) of each of the optical density deciles based on 14,200 readings of radiographs of serial cross sections of the finback whale humerus. See page 192 for a discussion of these distributions

to 0.68 Not the slightest trend ... optical density deciles was observed. ... may assume, therefore that in both O.D. and A.D reconstructions of this ... the determinate factor is the quantity ... structure

The relationship of absolute dens... (weight/volume) of 154 standard 1 c... core-drill samples to optical density of the central 3.5 mm of their radiographs ... shown in figure 14 The appearance ... such bone samples is represented by fig... 18. The fragility of bone of the low... densities precluded cutting samples of the same diameter as the photodensitometer light beam. Consequently figure 14 ... ally relates absolute density of a 0.94 c... (1 cm × 1.2 cm) cylinder to the ... density of a 0.085 cm cylinder ... Density variations in the unread portion ... the larger cylinder as well as the ... introduced by grouping O.D. readings ...

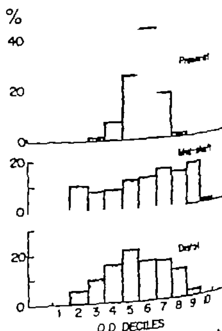


Fig. 16 The percentage occurrence of each ... the radiograph optical density deciles at th... levels in the finback whale humerus. The p... ... is through the head and tubercle, the ... through the midshaft region, and the ... through the expansion just proximal to the ... epiphyseal line. Each level is represented ... the means of three successive sections. See p... 195 for discussion of these distributions

-tiles, are sufficient to account for the shown in the graph.

The relative positions of optical density ciles on the weight/volume scale are n best in a comparison of absolute deny (A.D.) means (fig. 14) The most ne bone O.D. decile 1 in the medial and eral walls of the midshaft, has an A.D. an of 1.28 gm/cm³ nearly 6.5 times t of bone in O.D. decile 10 Taken in group O.D. deciles 1 2, 3 and 4 have ans of from 1.28 to 0 62 gm/cm plac g them in the second fourth sixth, and venth deciles of absolute density The re of the humerus O.D. deciles 8 9 and ranges in mean weight/volume from 28 to 0 17 gm/cm³ within the tenth and rt of the ninth decile of absolute density e intermediate optical density deciles 5 and 7 corresponding to the proximal ex nsion, pericentral zone, anterior and terior margins and much of the distal pansion, are in the eighth and ninth solute density deciles with means of m 0 48 to 0.35 gm/cm Based on the rcentages of each O.D. decile (fig. 15) d the A.D. means for each of the groups (fig. 14) the most radiodense 22% the humerus has a mean absolute deny of approximately 0 95 gm/cm³ the termediate 68% 0 41 gm/cm³ and the st dense 10% approximately 0.22 gm/ . This distribution of absolute density demonstrated by a three dimensional aph on a single section (no. 25 in mid aft) is shown in figure 17

The distribution of bone density at criti levels in the finback humerus is repreted by figure 16 which is constructed m means of the O.D. decile distribuns in the three largest sections (nos. 9 and 11 through head and tubercle) ree smallest sections (23 24 and 25 in idshaft) and three largest sections in the stal expansion (33 34 35) These levels proximate the radiographs in figures 6 and 8. On the optical density decile ale the mean position of the nine sec ns is at 5 7 virtually that for the entire umerus (5 5 fig. 15) In terms of abso te density the means of each of the ree sets of sections fall in the eighth D decile 1e between approximately 44 and 0 55 gm/cm The large proxial sections, having an O.D.D. mean of 5 8 consist 90% of bone registering in the fifth, sixth and seventh O.D. deciles, with 45% in the sixth decile alone. The midshaft sections with an O.D. decile mean of 6 0 consist 40% of intermediate density bone, 32% more dense and 28% less dense (fig. 17) The distal sections have an O.D. decile mean of 5 4 and are 55% intermediate, 31% high and 15% low density Thus while there is a gener alized endoectad (radio and absolute) density gradient through most of the humerus there are definite regional differ ences in its slope and, in nearly all levels, a slope difference in the anteroposterior and mediolateral plane. On the other hand, the density differences within a given level tend to balance out, so that mean section density along the length of the humerus does not depart drastically from the mean for the entire bone.

The beluga and pilot whale humeri. Graphic reconstructions and radiographs of sagittal sections through beluga and pilot whale humeri are shown in figure 13 Reconstructions are based on the same high, low and intermediate optical density decile groupings used in discussion of the finback humerus and they represent virtually the same sections as in the accompanying radiographs. This method together with examination of transverse section radiographs (figs. 9 and 11) reveals several points of comparison and contrast between the large and small humeri.

In the finback humerus (figs. 11 and 12) the least dense bone is disposed centrally in the middle and lower shaft, but the concentration of low density (O.D. deciles 10 9 and 8) is almost entirely in the proximal end of beluga and pilot whale humeri. The most dense bone in the *beluga* humerus is in the surface of the head except for a small area on the medial face of the tubercle, that process has a surface layer less dense than on the head but as dense *as any region of the shaft.* Within this shell the head and tubercle consist of very low density bone this concentration ex tends down to the upper metaphysis. The definite but sparse pattern of trabecular lines does not influence the overall density characteristic, at least at our magnitude of analysis In the *pilot whale* humerus the

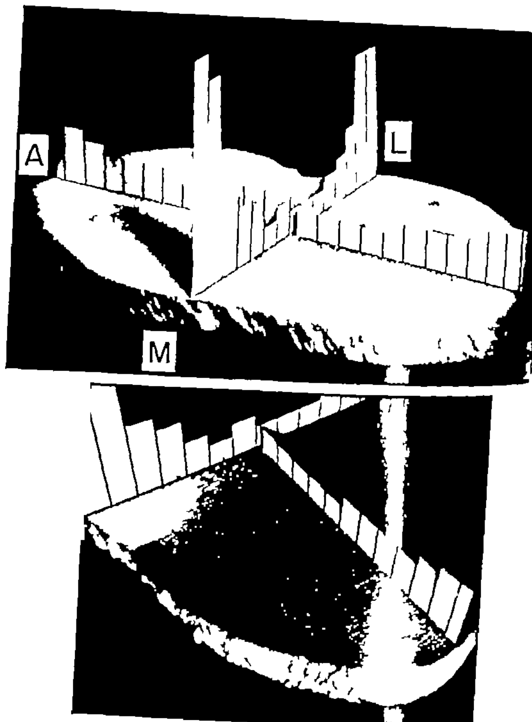


Fig. 17 A three-dimensional plot of weight per unit volume (absol. to density) on [illegible] tion of the finback whal[illegible] humerus. Bone density data in medial-lateral (M-L) and [illegible] (A-P) planes were derived from the relationship of optical density to absolute density [illegible] figure 14 [illegible]pplied to radiograph density along indicated lines. See page 195 for [illegible]

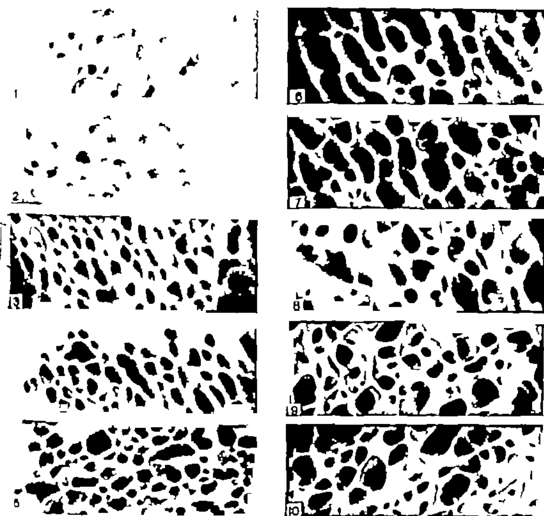


Fig. 18 Photomacrographs of bone from the section illustrated in figure 17 Numbers 1 to 10 indicate the optical density of radiographs at points from which bone was removed. Magnification, X 12.

surface layer of head and tubercle is not as dense nor as thick as in the beluga bone The low density concentration within is more restricted to the center of the proximal mass but does extend to the surface in the upper tubercle and is prolonged downward into the core of the metaphysis. The distribution of density bone (O D D 7 8 and 5) in the proximal nd of the pilot whale humerus is almost a perfect reconstruction of the well-defined pattern of trabecular lines extending from the upper shaft into the tubercle nd head and from the upper surface of the neck into the head. Similarly the concentration of high density bone (O D D 1 2, 3 4) under the articular surface of the head represents the converging and crossing of trabecular lines of intermediate density

In spite of the lack of a large concentration of low density in the central shaft of either beluga or pilot whale humeri, the presence of some loci of this range in a core of intermediate density flanked by a thick zone of high density creates a sharp endoectad gradient in the sagittal plane. It should be borne in mind how

ever that the high density zone in the shaft wall is almost continuous (but is thinner on anterior and posterior margins) in the pilot whale and is completely cir cumferential in the beluga humerus (figs. *9* and *10* and page *188*) Clearly too there is a sharper districtión between peripheral and core regions (especially in the beluga) than exists in the large finback humerus this fact would have been obvious even if individual deciles rather than groupings had been used in reconstructions

Cleared fetal specimens and radiographs of postnatal beluga and pilot whale humeri were examined for evidence of development of regional density and inter nal architecture The overall endoectad gradient can be accounted for by the peri osteal and endosteal processes described earlier Medial and lateral concentrations of bone appear first centrally on those surfaces in the circumnatal humerus then spread to the definitive extent during the first year of life Development of internal structural orientation parallels that observed by Wolff (1892) in the proximal end of the human femur that is trabecu lar orientation in the shaft metaphysis, head and and tubercle bases becomes apparent as osteogenesis progresses proxi mally and distally but is evident in the secondary centers only as those ossicles approach definitive size and near fusion with the primary center Total adult alignment of trabeculae follows fusion of pri mary and secondary centers

DISCUSSION

As indicated in the Introduction the cetacean flipper is a hydroplane adjusta ble at the shoulder and only semiflexible beyond In a rather broad range of move ments it is subjected to transverse loading from body inertia and water resistance Because of the streamlined cross-sectional shape of the flipper loading in the anterior posterior plane in either the rest ing or moving limb must be insignificant compared with that in the medial-lateral plane as the limb is moved or when it affords lateral stability in fast turns Maxi mum loading occurs at higher speeds when the flipper is rotated for diving and surfac ing, for use as an anterior rudder or for full braking action, and when rotation is coupled with abduction or adduction to roll the body on its long axis.

The humerus located immediately distal to the only free articulation and quite rigidly joined with the skeleton beyond obviously has a key role relative to the functional load on the flipper. In the aquatic medium, the mass of the limb bones themselves is a less significant load factor than one might at first consider, but *the actions of shoulder* muscles and the loads carried by the broadly disposed antebrachial elements transmit a predictable (if unmeasured) set of forces into the substance of the humerus. This bone experiences therefore alternating tensions and compressions on its medial and lateral sides and far lesser but similar loads on anterior and posterior sides. In addition to these forces transmitted by muscles and by the connective tissues spanning the brachium and antebrachium, there would be localized tensions, compressions and shearing forces at, and adjacent to, the articular surfaces Considering the location and proportions of most cetacean humeri, torque would seem relatively less critical than in the long tubular bones of land animals

Structural density and orientation in the humerus match well its functional environment. Our findings in this report have been anticipated in brief by Murray ('36) Apparently *without* experience with captive animals or limb dissections, Murray stated the essentials of the limb function and the forces acting on the humerus. He reviewed Roux s (1893) and Benninghoff's ('27) drawings of the dolphin radius and ulna and *Schmidt's* (1899) photograph of a single logitudinal section of the dolphin humerus. Schmidt and Murray had the correct impression of trabecular orientation and gross regional density as revealed by their limited material (Murray however erroneously compared the internal organization of the humerus with that of the radius it will be shown in a subsequent paper that the figures of Roux and Benninghoff on which Murray's comparison was based were unrealistic) In essence, ours has been a whole-bone quantitative extension of this preliminary examination.

Had our study been restricted to longitudinal sections (fig. 13 and Schmidt's photograph) or to transverse sections of only the finback and pilot whale humeri (figs. 6 through 9) an unequivocal statement could have been made concerning basic structure. In such sections humeral density is disposed along the lines of a box beam. An engineered box beam compares with an I-beam, the center column of which has been divided and carried laterally to produce a structure resistant to considerable torque as well as single-plane (superior-inferior) bending while the I-beam is designed essentially to counter the latter. Within the biological context of living tissues and the continuing processes of growth and maintenance the degree to which humeral density distribution approaches the engineering ideal is striking. We have seen that, in the finback humerus the most dense quarter of all bone substance lies in medial and lateral sides in a concentration that is thickest in its midlength and thins out toward the head and tubercle at one end and the distal articular surface at the other. Bone approximately half as dense, but constituting two-thirds of volume, underlies the more dense bone, fills in the expanded ends and completes the anterior and posterior margins. The remaining tenth of humeral volume is the rarified core of the shaft and distal expansion and it is but a fourth as dense as the medial and lateral sides. Employed as the main spar in some aircraft wings (and supplanted by equivalent unitized construction in more modern craft) the box-beam mainspar has thicker top and bottom than side walls, and a hollow center. Although static and continuous flight loading is not paralleled in the water-borne cetacean, intermittent and variable loading of the flipper is strongly comparable to conditions in the wing and it involves similar structural organization. Rather than being made up of plates of uniform material in calculated thicknesses and at prescribed distances from the neutral axis of the hollow center the amedullary humerus consists of appropriate endosteal gradients of porous but quite evenly mineralized bone. Although the humerus differs from the engineered beam again in its complex of articular surfaces and processes and depressions for muscle attachment, the distribution of bone substance along the length of its irregular configuration is fairly consistent.

Although the longitudinal (sagittal) section (fig 13) and many transverse sections of the beluga humerus (fig. 10) strongly resemble those of the finback and pilot whale the anterior-posterior constriction and thick wall of the midshaft region are departures from the box-beam concept. In view of the overall commonness of other features of internal and external morphology it appears that the thick, continuous wall and contrasting rarified core are advantageous within a relatively small, rounded midshaft, as is the case in most shaft levels in most terrestrial long bones (for only those of great relative length e.g. primate limb bones, have clear tubular walls). The anterior posterior and medial lateral differences (to one degree or another) in deep and peripheral density conversely appear advantageous only within relatively broad flattened shafts. The beluga has the shortest, broadest flipper of the three species in our study but one might expect torque as a determinant of tubularity to be of greater magnitude in other forms (e g the pilot whale) in which the elongated antibrachium and manus extend at an angle behind the humeral axis. The humerus of the grossly similar narwhal, incidently is virtually identical to that of the beluga on the other hand, the dolphin and pilot whale are quite similar in body and humeral configuration but differ in relative breadth of flipper. It seems therefore that the proportions of the beluga humerus and its particular midshaft structure are part of a group of musculoskeletal adaptations not ascribable to a single load factor such as torque or to flipper shape alone.

Within the modified box-beam density distribution of bone in the humerus, structural orientation is complimentary. As Murray ('36) has pointed out the Schmidt (1899) photograph of the longitudinally sectioned dophin humerus suggests a trabecular pattern mimetic of the distribution of tension and compression trajectories in a loaded cantilever beam (Koch 17) Our radiographs reveal considerably more detail in such sections and demonstrate that

here as in the case of density distribution the shape and functional relationships of the humerus compromise the engineering model. As we have shown trabecular lines in the proximal end of the humerus are directed superiorly and centrally from medial and lateral sides to intersect those from the opposite side at an angle very near 90 (and the longitudinal or neutral axis of the humerus at 45) The right angle intersection also exists in the tuber cle where lines from the medial side meet those passing across from the upper part of the tubercle toward the head. Short subarticular trabeculae within the head obscure what is apparently a similar inter section of lines entering from the tubercle and upper lateral shaft. The overall tra becular pattern in the proximal humerus therefore closely approximates that in the basal neck and major trochanter in the human femur or the entire proximal end of a short-necked femur lacking that distinctive human trait of dense compression trabeculae extending from the metaphysis and lower neck to the upper region of the head (Tobin '35) The lack of dominance of compression over tension lines is in keeping with the non weight-bearing role of the whale humerus. Structural orientation instead is directed toward the generalized support of head and tubercle and the carrying of their loadings into the deep substance of the proximal end of the bone and into the more dense regions of the shaft. At the more simple distal end of the humerus the articular surface is backed by a correspondingly simple pattern of nearly perpendicular trabecular lines passing up into the more dense regions of the shaft. In total the humerus, as a modified box-beam supplemented by a meaningful arrangement of medium and low density spongiosa carries flipper loadings into the supporting and attitude-determining complex of the shoulder In spite of its particular nearly tubular mid shaft construction the beluga humerus in its other parts and and in its internal architecture generally fits this characterization

In the development of the concept of mechanical trajectories in the structural orientation of bone (e g von Meyer 1867 Koch, 17 Benninghoff '25) there has been the assumption that compacta and spongiosa are more than spatially related, the theory demands trajectorial unity throughout the load-bearing structure. In cetacean humeri there is a suggestion of structural compliance to such a requirement. In transverse sections and in radiographs of longitudinal sections there is obvious vertical linearity of bone and spaces In longitudinal sections one may trace linearity from proximal to distal spongiosa through the more dense bone of the shaft. Whether or not this is taken as anatomical evidence of trajectorial continuity through compacta depends upon whether one considers cetacean humeri to have a special compacta or simply a regional concentration of spongiosa. We would suggest that these limb bones (in total perhaps more akin to short bones such as the calcaneus than to terrestrial long bones) are but another example of skeletal adaptation to function and not the material with which to solve a basic question of terrestrial limb bone architecture.

Cetacean humeri, in spite of the lack of an open medullary cavity have relatively low overall density Actually in this they compare closely with human humeri (0 66 to 0 72, varying with sex and race Trotter et al. '60) Zangerl ('35) pointed out that in early fossil forms of marine mammals and reptiles the limb bones were very dense (pachyostotic) but that this condition was succeeded by a decreased density in later members of the same lines In the present-day manatee (Fawcett '42) and penguin (Meister '62) humeri are extremely pachyostotic, having but slight amounts of very heavy spongiosa surrounded by thick, dense compacta The density of the penguin humerus, at 0 6 is approximately twice that of our single finback humerus and slightly less than one and one half times that of the mean for beluga and pilot whale humeri. Zangerl, Fawcett and Meister agree with Napo ('23) that pachyostosis would be an a vantageous characteristic in the early stages of secondary marine adaptation, for a dense skeleton would aid in increasing the specific gravity of the body in le water

Fawcett (42) proposed hypothyroidism as a direct causative factor in the correc

achyostosis of the manatee. The poorly eveloped thyroid and high-iodine vegeta le diet of this sluggish animal, together ith retarded osteogenesis and a lack of esorption comparable to that in experimental and clinical hypothyroidism, makes his proposal reasonable and attractive etacean limb bones lack central resorption and have an embryonic and later development strongly resembling that of the manatee. On the other hand the degree f reorganization implicit in the functional rientation of the highly porous adult pongiosa of the cetacean appears to rule ut at least such a degree of endocrine nvolvement as apparently exists in the manatee.

The spongy structure and apparent evolution of the cetacean humerus pose an nteresting area of speculation. If ceta eans are a highly successful and advanced secondary marine adaptation from terrestrial mammal related also to the ungulates (Howell, '30 Slijper '58) then ne can assume the primative humerus to ave been a reasonable approximation of he tubular equivalent in extant land orms. Indeed, the Archaeocetes (e.g. *Basilosaurus cetoides*) available in the fossil record, *had a relatively* long, rounded humerus and a rather typical mammalian lbow configuration (Slijper '58 and display in U S. National Museum) Assuming further that pachyostosis was an early trend, in the cetacean line transient skeletal adaptation to marine existence this requires no significant alteration in osteogenesis other than a suppression of inter nal resorption (coincident with or actually linked to a reduction in rate of longitudinal growth a function of cartilage rather than bone) The vast increase in density can occur in a bone otherwise little departed from terrestrial form, for the humerus of the manatee is of more or less conventional shape and has free shoulder and elbow articulations. The subsequent reversal of the pachyostotic trend and the development of a spongy structure (a phrase preferable to the word osteoporosis with its implications in geriatric pathology) must, therefore have been preceded by those alterations in body dimensions and extra-skeletal tissue composition that negated the problem of bouyancy and would have been concomitant with the acquisition of those characteristics of body and limb now distinguishing the ceta ceans from the less adapted but marine *Sirenia* and from the amphibious seals and walruses. There would seem to be no reason to expect, either on the basis of logic or the processes of osteogenesis that the decrease in density would have taken the form of a return to tubularity One could oversimplify and suggest that the cetacean humerus is a very short "long bone with virtually no diaphysis and with conjoined metaphyses It is however more in keeping with all direct and indirect evidence to conclude that the humerus is the product of an evolutionary opening-up of the vascular spaces of a pachyostotic form, in a manner selective for the conditions in the evolving flipper of the several cetacean forms. In successive generations, of course this phylogenetic trend would be manifested by progressively lesser depositions on formed trabeculae for as indicated earlier the embryonic manatee and cetacean bones are quite similar

The difference in density in the prox mal expansion of the humerus of the pilot *whale and especially the beluga as com*pared with the finback whale may well be part of a species difference in the evolution from the pachyostotic condition. Certainly there is insufficient evidence to permit more than the suggestion that it may also be related to simple humeral size difference. Total volume difference between the humerus of the large mysticete and the two small odontocetes is of the order of the magnitude seen in small primates and in the rodents where we have observed (unpublished and continuing studies) that that amount and relative fineness of the proximal and distal spongiosa decreases and the relative thickness of the adjacent compacta increases as bone and animal size decrease. The size dif ference between beluga and pilot whale humeri, however appears to be too slight for this to be the only factor involved.

The relationship of the aims, techniques and results of this study to those in other areas of skeletal research merits some comment. Compartive structural and density studies of whole bones present prob-

lems in morphological considerations and technical applications far more difficult than are encountered in, for example population studies of bone mineralization in which standard lines through a chosen bone are scanned and analyzed In the latter of course structure is rendered virtually a constant in comparative analyses on the other hand, structure varies with species and with size and it is a requirement that, as in current work in quantitative light or electron microscopy the researcher consider the range of structure to be "seen by the apparatus This problem is obvious in the projected extension of our study to other large and small forms

The great size of the finback humerus the diameter of the photodensitometric light beam and the size of the core samples used in weight and ash-weight determinations all contributed to a particular level of appreciation of structure and density distribution. Each of the 0 085 cm cylinders assayed by the light beam and each of the 0 94 cm^3 cylinders excised, weighed and ashed were only 2.25×10^{-4} and 2.04×10^{-4} parts, respectively of the total volume of the humerus. These are on the other hand very appreciable quantities when compared with entire bones of common laboratory animals or with sizable fractions of those of common domestic animals or man. Actually the proportionality of the photodensitometric scan to bone size (i.e. section area) was very high in the smaller cetacean bones and the reconstructions were nearly at the limit of application of the "big bone technique It is clear that an analysis of any of the bones of the wide range of smaller animals at the level of appreciation employed with the finback whale would involve very small macroscopic or frank microscopic samples

While the individual readings and weights from the whale bone sections illustrate the proportion of bone tissue and space (mineralization being uniform in the sample size used) these data really are integrations of the sort of microregional variations in structural and mineralization revealed in thin-section microradiographs from smaller species (Vincent '55 Engstrom, '56 and Lacroix. 58) The fact that the ratios of pre-ash to post-ash weights of core samples of the finback humerus grouped so closely about a typical higher mammalian value (Trotter and Peterson, '62 Seale '63) indicates the mineralization variations average out even well within samples that are absolute quite large but, relative to whole bone are quite small. This being true our studies of density distribution could have been based on serial integrations of partial continuous microphotodensitometric scans of microradiographs of a sufficient number of well-distributed thin bone sections. This alternative with a bone the size of the finback humerus or even the smaller cetacean humeri or the limb bones of the horse or of man, would be laborious to the point of impracticability The technique of choice for larger bones, therefore is a continuous recording, mechanically driven photodensitometer scanning high resolution radiographs with a light beam appropriately proportional to size Such an adaptation now has been made to the gross densitometer used in this study

The extension of radiographic magnification procedures to smaller bones (e.g., those of shrew mouse rat, rabbit and dog) requires considerable selection of the anatomical level to be recorded or interpreted regionally film type and exposure and tion to be used (i.e., macro- or micro-radiography) and possibly photographic reduction or enlargement to render large and small species equivalent. Necessary too is the use of a recording microdensitometer There are, in final analysis, certain species differences that render some direct comparisons of equivalent accuracy virtually if not literally impossible For example scans of true-size sections of shrew and human limb bones with proportional light beams (or of enlarged bones with a constant light beam) would be dominated in the first case by lacunae and cement lines (the minute shrew bone having no vascular channels) and in the second by the complexity of haversianized bone in the vastly larger organ.

LITERATURE CITED

Baker P T., and H Schraer 1958 The estimation of dry skeletal weight by photometry of roentgenograms. Human Biology 30 17–[illegible]

…, G. H. 1956 Bone as mechanical engineering problem. In The Biochemistry and Physiology of Bone. Ed. by G. H. Bourne. Academic Press, Inc., N Y

…oningshoff, A. 1925 Spaltlinien am Knochen, eine Methode zur Ermittlung der Architektur platter Knochen. Anat. Anz., 60 169–206.

…dker F 1968 Whales and Whaling. George G. Harrap and Co., Ltd., London.

…arpenter W T and R. T Liddicoat 1952 Compact bone as non-isotropic material. Am. J Anat 91 331–362.

…les, N B. 1955 The manus of the Narwhal, Monodon monoceros L. Proc. Zool., Soc. Lond., 124: 201 211.

…gstrom, A. 1956 Structure of bone from the anatomical to the molecular level. In Ciba Foundation Symposium on Bone Structure and Metabolism. Ed. by G E. W Wolstenholme and C. M. O'Connor Little, Brown and Company Boston.

…ilow D. H. 1962 The functions of the Haversian System. Am. J Anat 110 289–308.

…ilow D. H and S. O. Brown 1956 A comparative histological study of fossil and recent bone tissues. Part I. Tex. J Sci., 8 405–443.

—— 1957 A comparative histological study of fossil and recent bone tissues. Part II. Tex. J Sci., 9 186–214

—— 1958 A comparative histological study of fossil and recent bone tissues. Part III. Tex. J Sci., 10: 187–230.

…vans, F G. 1957 Stress and Strain in Bones. Their Relation to Fractures and Osteogenesis Charles C Thomas, Springfield, Ill.

…awcett, D. W 1942 The amedullary bones of the Florida manatee. Am. J Anat., 71 271 308.

…owell, A. B 1930 Aquatic mammals; their adaptations to life in the water. Charles C Thomas, Springfield, Illinois.

…och, J. C. 1917 The laws of bone architecture. Am. J Anat., 21 177–298.

…acroix, P 1956 The histological remodeling of adult bone. In Ciba Foundation Symposium on Bone Structure and Metabolism. Ed. by G. E. W Wolstenholme and C. M. O'Connor Little, Brown and Company Boston.

McFarland, W 1954 Evaluation of bone density from roentgenograms. Science, 119 810–811.

…eister W 1951 Changes in histological structure of the long bones of birds during the molt. Anat. Rec., 111 11–21

—— 1956 Changes in histological structure of the long bones of the white-tailed deer (Odocoileus virginianus) during the growth of the antlers Anat. Rec., 124 709–721

—— 1962 Histological structure of the long bones of penguins. Anat. Rec., 143 377–388

Meyer H. 1867 Die Architecture der Spongiosa. Reichert und Dubois-Reymond's Archiv 615–628.

Murie, J 1874 On the organization of the Caaing whale. Trans. Zool. Soc. Lond., 8 235–301.

Murray P D F 1936 Bones. A study of the development and structure of the vertebrate skeleton. Cambridge University Press.

Nopcsa, F 1923 Vorlaufige Notiz ber Pachyostose und Osteosclerose einiger mariner Wirbeltiere. Anat. Anz., 56 353–359.

Pratt, C. W M. 1959 Postnatal changes in the shaft of the rat femur J Anat., 93 309–322.

Roux, W 1893 Das Esetz der Transformation der Knochen. Berliner Klin. Wochenschr., 30 509–511

Schmidt, R. 1899 Vergleichend-anatomische Studien uber den mechanischen Bau der Knochen und seine Vererbung. Zeitschr. Wiss. Zool., 65 65–97

Seale, R. 1963 Personal communication regarding ash weights of rhesus monkey skeleton.

Sergeant, D. E. 1962 The biology of the pilot or pothead whale (Globicephala melaena) (Traill) in Newfoundland waters. Bull. Fish. Res. Board, Canada, No. 132.

Slijper, E. J 1958 Walvissen. D. B Centen Uitgeversmaatschappij Amsterdam.

Smith, J W 1960 Collagen fiber patterns in mammalian bone. J Anat., 94 329–344

Smith J W and R. Walmsley 1959 Factors affecting the elasticity of bone J Anat., 93 503–523.

Streeter, G. L. 1949 Developmental horizons in human embryos (fourth issue) A review of the histogenesis of cartilage and bone. Contr Embryol. Carnegie Inst., 33 149–166.

Tobin, W J 1955 The internal architecture of the femur and its clinical significance. The upper end. J Bone and Joint Surg., 37-A: 57–71.

Trotter M., and R. R. Peterson 1962 The relationship of ash weight and organic weight of human skeletons. J Bone and Joint Surg., 44-A: 669–681

Trotter M., G. E. Broman and R. R. Peterson 1960 Densities of bones of White and Negro skeletons. J. Bone and Joint Surg., 42-A. 50–58.

Vincent, J 1955 Recherches sur la constitution de l'os adulte. Editions Arscia, Brussels.

Vladykov V D 1944 Etudes sur les mammiferes aquatiques. III. Chasse, biologie et valeur economique du Marsouin Blanc ou Beluga (Delphinapterus leucas) du fleuve et du golfe Saint Laurent. Department of fisheries, Province of Quebec, Quebec, Canada.

Weidenreich, F 1923 Knochenstudien Z. Anat. Entwicklungs 69 382–466, 558–597

Wolff, J 1892 Das Gesetz der Transformation der Knochen Berlin.

Zangerl, R. 1935 IX. Pachypleurosaurus edwardsi, Cornalia sp. Osteologie, Variationsbreite — Biologie. In B Peyer Die Triasfauna der Tessiner Kalkalpen. Abh. Schweiz. Pal. Ges., 56 1–80.

...inal Cord Segments

GROSS STRUCTURE IN THE ADULT MONKEY

CAROLYN EYSTER THOMAS AND C. MURPHY COMBS
Department of Anatomy Northwestern University Medical School, Chicago Illinois

ABSTRACT Dorsal and ventral roots were dissected bilaterally on spinal cords of adult monkeys six rhesus, six irus and three baboons. Measurements made were the distance between the uppermost cord attachments of successive nerve roots (segment length); the distance between the uppermost and lowermost fila within each root (root attachment length); and the distance between the lowermost fila of one root and the uppermost fila of the subjacent root (interroot length) Segment lengths, dorsally and ventrally are essentially alike within each species. In rhesus the average at various levels ranges from 4¼ mm in cervical and sacral to 12½ mm in lower thoracic; in irus, from 4 mm in cervical and sacral to 10 mm in lower thoracic; in the baboon, from 5¼ mm in cervical and sacral to 19 mm in lower thoracic. Within each species the dorsal and ventral root ttachment lengths are similar as are the interroot lengths, except in the lower thoracic levels. There dorsal interroot lengths range up to 3 mm longer than ventral. Cross sectional areas of the various levels were planimetrically determined. Within each species the largest areas are at lower cervical and lower lumbar levels. Individual segment volumes were calculated. In rhesus and irus these vary only about 60 mm³ from the largest to the smallest segment, excluding sacrocaudal levels. In baboon this difference is as much as 260 mm³

In an earlier report (Thomas and ...mbs, '62) on the gross structure of ...inal cord segments in the adult cat, it ...as noted that no precise data existed on ...is subject for the primate Although ...lling (1859) Lüderitz (1881) Donald...n and Davis ('03) Hovelacque ('27) and ...eek ('35) reported on various aspects ... gross spinal cord structure, no one of ...e studies has given detailed data on the ...anner in which dorsal and ventral roots ...tach to the spinal cord in a primate. ...e to the common usage of certain mon...ys in the research laboratory such in...rmation is needed. In addition, some ...ther fundamental conclusions regarding ...rd structure and development reached ... the above investigators should be ...ecked in other species. The present ...udy has used three types of monkeys.

MATERIALS AND METHODS

Complete bilateral dorsal and ventral ...ot dissections were done in six Macaca ...esus, six Macaca irus and in three ...aboons (*Papio papio*) All were adults. ...he animals were lethally anesthetized ...nd immediately after death the entire vertebral column with intact spinal cord and associated structures was removed and immersed in 10% formalin for several weeks. For beter differentiation between small arteries and rootlets certain animals within each species were injected through the heart with colored latex at the time of death.

The dissections were performed under a 10 × or 20 × dissecting microscope and were essentially like those described before for the cat (Thomas and Combs '62) In the present study the various rostrocaudal measurements determined were the root attachment length, that is the length of cord surface to which the rootlets of each root are attached the interroot length, that is the length of cord surface devoid of rootlets lying between the attachment of adjacent roots the segment length, that is, the distance between the rostralmost attachment of one spinal nerve and the rostralmost attachment of the caudally adjacent spinal nerve The general appearance of the roots was recorded and

Supported by Grant NB03700(03), U S P.H.S., N I N D B and Research Career Development Award (GM231347), Division of General Medical Sciences, U S P.H.S.

for each of the three types of monkeys a complete drawing was made which typified the dorsal and ventral root patterns.

Typical cross-sectional areas at all except the lowest cord levels were determined in four rhesus and in four irus monkeys as well as in the three baboons. The technique used was similar to that described for the cat (Thomas and Combs '62) Segment volume was calculated by multiplying the average cross-sectional area by the corresponding average dorsal segment length

RESULTS

The cords as a whole The total lengths in millimeters of the cords studied were: rhesus — 175 209 234 237 256 280 irus — 180 190 202 202, 207 227; and baboon — 311 330 334 In all specimens the caudal tip of the cord was found near the level of the fourth to the sixth lumbar vertebra.

The numbering of the various nerves presents somewhat of a problem due to the variation in the number of thoracic and lumbar vertebrae particularly in the baboon In a study of 216 macaques Schultz ('61) found an average of 12.1 thoracic and 6 9 lumbar vertebrae In the same report ('61) he noted in 66 baboons an average of 12.5 thoracic and 6 4 lumbar vertebrae. For simplicity in reporting the results of the present study all of the monkeys have been considered as having 12 thoracic and 7 lumbar vertebrae.

Segment lengths In this study the rostrocaudal distance between the uppermost attachments of successive nerve roots is defined as the segment length This measurement was obtained by adding the length of cord occupied by each set of rootlets to the length of whatever caudally adjacent space devoid of rootlets was present

Figures 1 and 2 show graphically the results obtained from the ventral and dorsal cord surfaces. In these and all subsequent graphs of length measurements the single intermediate line indicates the average length, while the upper and lower step-like lines show the full range of all the lengths seen, either on the right or on the left side in individual animals Since detailed data can be derived readily from each graph only certain points require comment or emphasis.

Ventral segment length measurements (fig 1) in the baboon show that segments T7 through L1 are distinctly the longest averaging between 13.5 and 18 mm in length Cephalically the shortest segments are C8 through T3 which show an average length of about 6 to 6.5 mm. It is notable that C1 averages only 6.5 mm in length in this species. Caudally beginning at L2 the segment lengths progressively decrease until the average sacral and caudal measurements are between 5.5 and 7.5 mm.

In the rhesus (fig. 1) the longest average ventral segment lengths appear from T6 through L2 averaging between [illegible] and 12 mm. Little variation exists between C1 and T2 with the average ranging between a low of 3.5 mm at C1 and a high of 6 mm at C3 and C6. The decrease in length caudally is somewhat gradual, beginning at L3 until the shortest segments 4.5 mm are found at S2 and S3.

In the irus (fig 1) the longest mean ventral segment lengths occur between [illegible] and L3 where they average from 7 to [illegible] mm. From C1 to T4 the lengths vary between 3.5 mm and 5.5 mm. Caudal to L3 the lengths range from 6 to 4.5 mm.

Figure 2 comprises the data obtained from measurements of dorsal segment lengths in the various monkeys. In all three species the ranges and the averages are essentially the same as those taken from the ventral cord surface. In the baboon certain differences appeared in the cervical region where dorsally the longest segment is at C4

General characteristics of rootlets Figures 3 and 4 are drawings of the typical arrangements found for ventral and dorsal root attachments in the monkeys studied. Because the cords of the different species used differed mainly in size and in the proportions of the various lengths measured this one set of figures is sufficient to show the general appearance of the rootlets for each The overall features are much the same as those described previously for the cat (Thomas and Combs '62) thus only certain points deserve special comment.

The presence or absence of a dorsal root at C1 could not be determined with certainty in all of the monkeys. In the irus

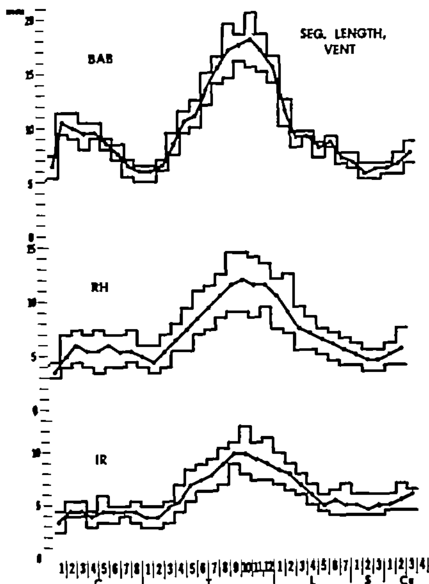


FIG. 1 Ventral segment lengths. In this and all figures indicating length measurements, the upper and lower steplike lines denote the full range of all the lengths seen in individual animals while the intermediate line shows the average of the lengths. Spinal cord levels are represented on the horizontal line and lengths in millimeters are indicated on the vertical. Abbreviations in this and all figures BAB baboon RH, rhesus; IR, irus C, cervical; T thoracic; L, lumbar; S, sacral; Ca caudal.

present bilaterally in one animal, unilaterally in one other and absent bilat ly in the other four specimens. In the rus it was absent bilaterally in three es, but in the other three no determina- n could be made because of damage in region at the time of cord removal In the baboon, dorsal C1 was present bi laterally in two animals, but, in the other the area had been too traumatized for any valid conclusion to be drawn.

Root attachment lengths. These data were obtained from measurements made between the uppermost and lowermost fila

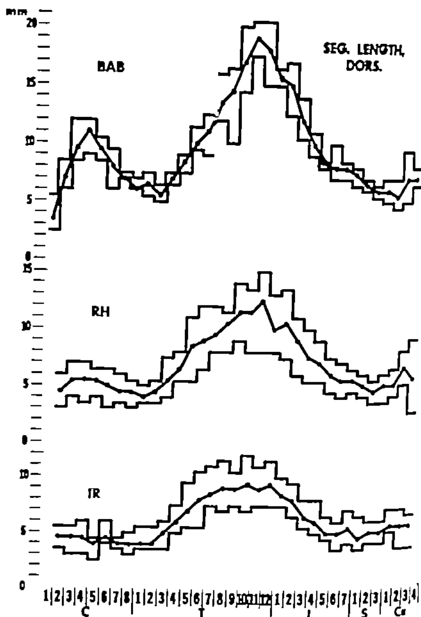


Fig. 2 Dorsal segment lengths. See legend for figure 1.

within each root. The averages and ranges for the lengths of ventral and dorsal root attachments are shown in figures 5 and 6

In the baboon, the graphs of ventral and dorsal lengths show a striking similarity to those of the respective ventral and dorsal segment lengths both in contour and in absolute lengths. In the rhesus the ventral root attachment lengths are much the same as the ventral segment lengths but dorsally from T2 to L5 the root attachment lengths are from one to 3.5 mm less than the corresponding segment lengths. These differences are most pronounced between T5 and L1. In the irus the ventral root attachment lengths are similar to the ventral segment lengths, except that the root attachment lenghs are from 0.5 to 2 mm shorter at corresponding levels. Dorsally from T3 to L2 the root attachment lengths

VENTRAL

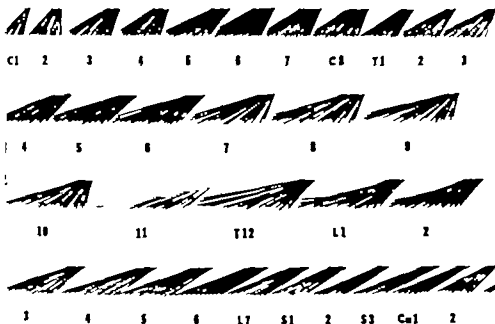


Fig. 3 Pattern of ventral root attachments. See legend for figure 1. These were taken from rhesus monkeys but serve for the general pattern in all three species. See text.

DORSAL

C2 3 4 5 6 7 C8 T1 2 3 4

5 6 7 8 9 10

11 T12 L1 2 3 4

5 6 L7 S1 2 S3 C 1 2 3

Fig. 4 Pattern of dorsal root attachments. See legend for figure 1. These were taken from the same monkeys but serve for the general pattern in all three species. See text.

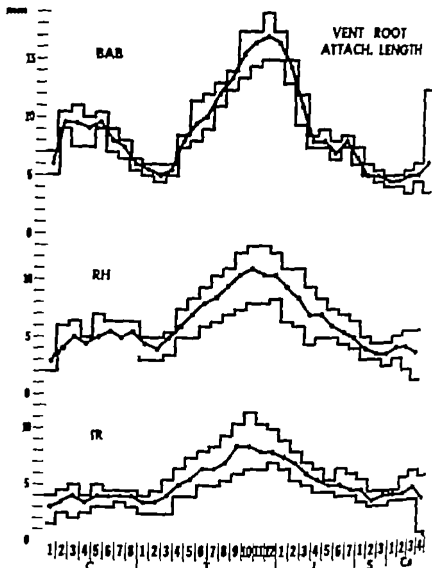


Fig. 5 Ventral root attachment lengths. See legend for figure 1.

are from 1 to 3 mm shorter than the corresponding segment lengths.

Interroot lengths The averages and ranges for the length of cord surface if any devoid of rootlets lying between the attachment of adjacent roots are shown in figures 7 and 8 In all three species the averages of the ventral lengths are small measuring usually between zero and 1 mm in length.

Dorsally the interroot lengths vary more between the species and from one cord level to another within each species than they do ventrally In the baboon, the average dorsal lengths measure from zero to one mm except at T7 T9 and T11 where they reach 2 mm. In the rhesus, on the other hand, at C2 and from T4 through L2 lengths from 2 to 4 mm are found dorsally At lower cervical and lower lumbar levels the averages of the lengths vary from 0 to 0 5 mm. In the fox the pattern is much like that of the rhesus except that the averages of the lengths in the former are about 1 mm less. Ventrally the interroot lengths comprise an insignificant part of the segment lengths. Dorsally between T4 and T12 in both these

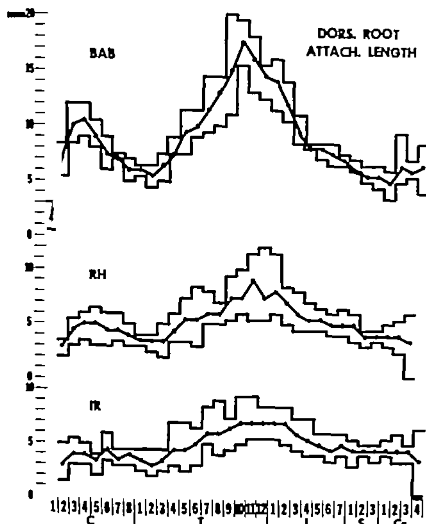


Fig. 6 Dorsal root attachment lengths. See legend for figure 1

d from the interroot length comprises up one-third of the segment length. How r in the baboon the interroot length ver makes up more than one-eighth of segment length.

All of the above data were collected and ulated separately for the right and left es of each animal. Generally the sides re similar but variations up to 2 to 3 n were common.

Because the averages and ranges of the rious measurements taken do not necesarily represent the actual characteristics any individual specimen, graphs of root attachment and interroot lengths were made for all of the individual cords and compared to the group graphs. In all cases the individual graphs displayed a general contour which was similar to that of the average. It should be emphasized however that from one segment to another the individual graphs showed much fluctuation above and below the average. This feature is shown in the ranges which have been presented with each average. It remains though that the graphs of the averages suffice for predicting the overall pattern of root attachment, although, they

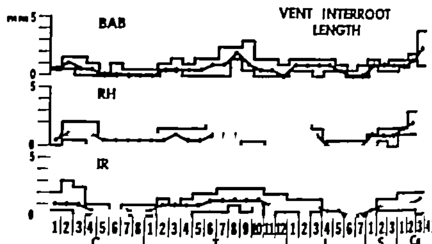


Fig. 7 Ventral interroot lengths. See legend for figure 1.

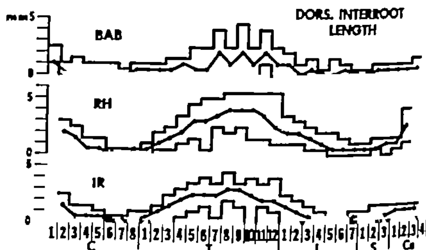


Fig. 8 Dorsal interroot lengths. See legend for figure 1

are inadequate for foretelling the appearance which might be encountered at a specific cord level in a given animal.

Cross sectional areas The averages of the results from the three baboons four rhesus and four irus monkeys used in this part of the study are presented in figure 9 In the baboon the cord enlargements are prominent at C6 through C8 and L2 through L7 where the greatest areas are respectively 53 mm and 37 mm The smallest non-sacral area is 17 mm at level T10 The remarkable size of C1 60 mm should be noted.

In the rhesus the cord enlargements appear at C5 through T1 and L2 through L7 where the greatest areas are 36 … at C7 and 29 mm at L6. The small… non-sacral area is 15 mm² at T6 through T11 In these animals C2 has a cross sectional area of 34 mm²

In the irus the enlargements are … from about C4 through T1 and L3 through L7 where the greatest areas are 30 … at C4 through C7 and 20 mm² at L… through L6 The smallest non-sacral … is 10 mm² at T8 through T12.

Measurements within individual … ments rostral and caudal to the … used for the cross-sectional … showed no variations worthy of … Graphs for individual animals were …

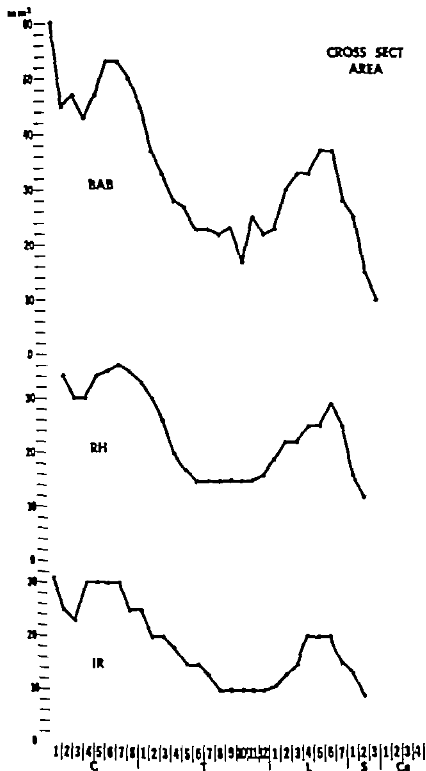


Fig. 9. Cross-sectional areas. See text for explanation.

pared for comparison with the average and were essentially the same

Segment volume The data for this were obtained by multiplying the averages for cross-sectional areas by the corresponding average dorsal segment lengths The results are given in figures 10 11 and 12. In each of these figures the graphs for segment length and cross-sectional area for each animal have been added in order to emphasize how strikingly they differ from each other

In the baboon the greatest volume is seen at C4 where the value is 463 mm³ From here, caudally the curve rapidly declines to 210 mm at T2. From this level a gradual increase occurs until a maximum, 450 mm³ is found at T11. Below this the volume remains relatively large until L5 is reached, after which it rapidly tapers off into sacral regions.

In the rhesus the largest rostral volume, 195 mm³ is found at C5. Caudal to this *level a decrease occurs until a low at* [illegible]

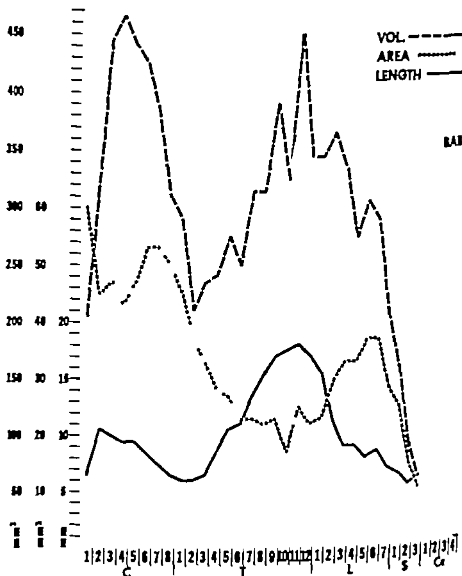


Fig. 10 Comparison of segment volume, area and length in the baboon.

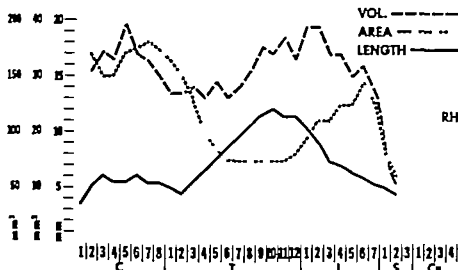


Fig. 11 Comparison of segment volume, area and length in the rhesus monkey

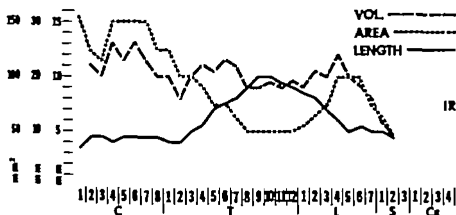


Fig. 12 Comparison of segment volume, area and length in the irus monkey

mm³ is seen at T4 and T8. From this region the volume increases until it reaches 95 mm³ at L1 and L2. At L6 a value of 60 mm³ occurs, but caudally a rapid decrease is evident.

In the irus the greatest volume 130 mm³ is at C4 and C6. Caudal to this a gradual decrease is seen until a low of 80 mm³ is found at T2. It is noteworthy that an immediate increase appears caudally so that T4 through T7 vary between 105 and 115 mm³. From T8 through L1 the volumes vary from 90 to 95 mm. After a rise to 120 mm³ at L4 they sharply decrease into lower lumbar and sacral areas.

DISCUSSION

The relevant findings of Stilling (1859) Lüderitz (1881) Donaldson and Davis ('03) and Hovelacque ('27) all of whom were interested primarily in human cord structure have been discussed in a previous study of gross spinal cord structure in the adult cat (Thomas and Combs, '62) The general results of these investigations particularly those of the cat, will be compared with the present observations in the monkey

In the cat, variations in length from one segment to another are similar to those described for the human, except that the

longest segments are the lower thoracic and upper lumbar instead of the mid-thoracic as in the human The curve for the averages of the segment lengths in the baboon is strikingly like that for the cat. Similarly the rhesus and irus show greatest segment lengths in lower thoracic and upper lumbar regions however little or no variation occurs between C1 and T2. This contrasts with the marked increase in length seen from C2 through C5 in the cat and baboon

Dorsal and ventral segment length patterns are essentially alike in the cat and apparently so in the human. This similarity is also found in the three species of monkey used in the present study On the other hand notable differences between dorsal and ventral measurements for root attachment and interroot lengths certainly occur in the cat. In this animal the dorsal interroot length may comprise almost one-half the segment length in lower thoracic levels whereas ventrally the interroot lengths are considerably shorter In the baboon the dorsal and ventral root attachment lengths are remarkably alike and show only slight differences from the segment lengths. This correlates with the relatively inconsequential sizes of the interroot lengths The root attachment patterns in rhesus and irus are more like that in the cat In these two types of monkey the interroot lengths are quite small ventrally but dorsally comprise up to one third of the segment lengths

In all the monkeys studied the cross-sectional cord areas exhibited proportions similar to those previously described in the human and in the cat. In all of these the greatest areas are at lower cervical and lower lumbar segments with the former being the greater In the cat and monkey an increase in area occurs in the uppermost cervical levels as the cord reaches the brain stem

Lassek ('35) reported volumetric data for spinal cord segments in various animals including cat and monkey Thomas and Combs ('62) confirmed his findings about total segment volumes in the cat. On the other hand, his graph for the valu[illegible] in the macaque differs in several wa[illegible] from the present results in rhesus and ir[illegible] Lassek ('35) found a maximum value of 120 mm³ at about C5. Caudal to th[illegible] a sharp decline occurred until a low [illegible] about 45 mm³ appeared at T2 and T3 Be[illegible]tween T7 and L2 the range was fr[illegible] about 70 to 95 mm³ At L3 through L[illegible] segment volumes of 90 to 105 mm³ we[illegible] seen Caudally the amounts sharply de[illegible]clined into sacral areas. In the prese[illegible] study the general contours of the graph[illegible] of rhesus and irus resemble those de[illegible]scribed by Lassek ('35) but differ con[illegible]siderably in the degree of variation fro[illegible] one level to another For example, Las[illegible]sek's greatest segment volume, which oc[illegible]curred at a cervical level, was about t[illegible] times that at T2, whereas in the prese[illegible] study the greatest value, also in the cer[illegible]ical region, is only about one and one-h[illegible] times as great as those found at upp[illegible] thoracic levels. If Lassek ('35) used on[illegible] one specimen, it could be that our resu[illegible] are not closely comparable because th[illegible] present data were compiled from averag[illegible] of measurements taken from a number [illegible] animals. The present results emphasi[illegible] again the major role played by segment[illegible] length in determining segmental volu[illegible]

LITERATURE CITED

Donaldson, H. H., and D J Davis 1903 A de[illegible]scription of charts showing areas of the cro[illegible] sections of the human spinal cord at the lev[illegible] of each spinal nerve. J Comp. Neur [illegible] 19–40

Hovelacque A. 1927 Anatomie des Nerf[illegible] Craniens et Rachidiens et du Système Gra[illegible] Sympathique chez l'Homme. 2 vols Gaston Doin et Cie., Paris, vol. 1 [illegible]–297

Lassek, A. M. 1935 A comparative volumetric study of the gray and white substance of the spinal cord. J Comp. Neur 62 361–376

Lüderitz, C. 1881 Über das Rückenmarksegment. Ein Beitrag zur Morphologie und Histologie des Rückenmarks. Archiv f Anat u Entwickel. Anat. Abtheil, pp. 423–[illegible]

Schultz, A. H 1961 Vertebral column and thorax. Primatologia, vol. 4 Lieferung [illegible] 66. S Karger Basel, Switzerland.

Thomas, C. E., and C. M. Combs 1962 Spinal cord segments. A. Gross structure in the adult cat. Am. J Anat 110: 37–48.

ectron Microscopic Observations on Primary ecidua Formation in the Rat [1]

WILLIAM P JOLLIE
Tulane University School of Medicine New Orleans, Louisiana

SERGIO A. BENCOSME
Queens' University Kingston, Ontario, Canada

ABSTRACT Cytological changes in uterine stromal cells of the rat during induced primary decidua formation have been examined electron microscopically Decidua forming stroma was examined at daily intervals for the five days during which the reaction reaches maximal hypertrophy and hyperplasia and was compared with pseudopregnant, non-decidual (control) endometrium. Stromal cells of control stroma resemble embryonic fibroblasts. They appear to be of two types, depending on whether they contain rough – or smooth-surfaced endoplasmic reticulum. As the decidual reaction progresses, the cells enlarge and become binucleate; cells which contain exclusively rough surface endoplasmic reticulum no longer are evident. Glycogen and fat become abundant, the former in association with smooth-surfaced membranes of the endoplasmic reticulum. Mitochondria become more numerous, smaller and show evidence of rearrangement in internal organization. There is pronounced increase in fine intracytoplasmic fibrillar component; and a spectrum of "microbodies" and lysosomes appears. At the height of the reaction, the stroma appears epithelioid. The possible functional significance of these changes is discussed.

Implantation of the mammalian blastocystic vesicle is considered the result of interreaction between endometrium d trophoblast. The precise role of each ring implantation, however remains orly understood (Eckstein, Shelesnyak d Amoroso '59) Tissue relationships ring implantation have been studied to vantage in rodents where embryonic d uterine contributions to this process readily dissociated (Loeb '07; Krehbiel, '; Shelesnyak, '57 Jollie '61) The ini l maternal contribution is the transmation of the uterine stroma into pri ury decidua at the site of implantation. Although the decidual reaction has been idied extensively descriptions of the se ential histologic features of the process the site of implantation have been re icted by the limits of light microscopy e decidual cells described at an ultra uctural level in the rat (Wislocki and mpsey '5.) are not the primary decid l cells dealt with in this paper The fine ucture of human decidual cells has been scribed (Hamperl, '58 De Palo and Stop lli, '60) and a comparison made with n-decidual stroma (Dubrauszky and hmitt, '58) Because of differences in modes of implantation, however homologies between human decidual cells and pri mary decidual cells of the rat are uncer tain

The purpose of the present investiga tion is to describe at an electron microscopic level the changes in stromal cells which accompany decidual cell forma tion at the site of implantation in the rat. In order to eliminate extrinsic structural changes in the forming decidua imposed by trophoblast, we have confined the investigation to an examination of induced decidua formation during pseudopreg nancy

When the cervix of a virgin rat in estrus is stimulated electrically the action of coitus is duplicated in that, through a re flex pathway to the hypothalamus,, pitui tary luteotropin is released, thereby establishing progesterone secreting corpora lutea (Corner and Allen, '29· Greep and Hisaw 38) This physiologic state constitutes pseudopregnancy During a four day period following cervical stimulation, the endometrium becomes sensitized by

This investigation was supported by Research Grant from the National Institutes of Health (HD 00530-03) and by the Medical Research Council of Canada.

progesterone This period is equivalent to the preimplantation period in a true pregnancy (De Feo '62) If trauma is applied to the antimesometrial uterine mucosa four days after stimulation this sensitized endometrium subsequently undergoes decidual cell formation thus simulating the uterine response to the implantation process. A description of the ultrastructural changes in the cells of the stroma which accompany this response we feel may help clarify the uterine contribution to the nidation process.

MATERIALS AND METHODS

Nineteen sexually mature virgin female Sprague-Dawley rats weighing from 200 to 250 gm, were used Animals in estrus as determined by vaginal lavage, were made pseudopregnant by electrical stimulation of the uterine cervix with a Colmar Model 104 A Laboratory Stimulator Stimulation consisted of 50 impulses of 25 volts at a frequency of 2 per second and a duration of 0 4 second. In order to induce maximal decidua formation four days after stimulation the uteri of one group of animals (15 specimens) were mechanically traumatized by drawing a burred hypodermic needle inserted at the tubo-uterine junction along the antimesometrial length of the lumen (Velardo Dawson, Olsen, and Hisaw '53) These animals were autopsied at one two three four and five days following trauma, three animals for each day To serve as controls a second group (four animals) was killed four days after cervical stimulation without uterine trauma. Sections of the antimesometrial subepithelial stroma from both groups were taken for light and electron microscopy

Under nembutal anesthesia, the uterus was exposed by a ventral incision. Entire uterine segments were excised and transferred immediately to a drop of fixative viz. either phosphate buffered glucose-osmium (Millonig '61a) or phosphate buffered glutaraldehyde (Sabatini, Bensch and Barrnett, 63) Under a dissecting microscope the antimesometrial endometrium of each segment was excised with a razor blade and cut into blocks approximately 1 × 1 × 3 mm. The long axis of each block (against which sections later were cut) was perpendicular to the long axis of the uterus. These were fixed further in the refrigerator for one hour. Glutaraldehyde fixed tissues were post fixed in phosphate buffered 1% osmium for two hours. Tissues were then dehydrated rapidly in ethanol and embedded in butyl araldite (Richardson, Jarett and Finke '60)

Adjacent to the area of the uterus which was used for electron microscopy several segments were taken and fixed in Helly Zenker formol and 3% neutral buffered glutaraldehyde and were embedded in paraffin. All paraffin embedded tissues were cut at 5 μ. Zenker-formol fixed tissues were stained either with hematoxylin and eosin or with a tetrachrome. Glutaraldehyde fixed tissues were either impregnated with silver after the method of Gömöri ('37) for differentiation of reticular and collagenic fibers, or were stained with alcian blue-PAS.

Blocks of araldite embedded tissue were cut on a Porter Blum ultramicrotome with glass knives Thick sections (0.5 μ) were stained with borax-toluidin blue for final orientation of the block. Thin sections were stained with lead hydroxide (Millonig, '61b) and examined under an RCA EMU-3G electron microscope

OBSERVATIONS

The pseudopregnant stroma before trauma

The mucosa of the antimesometrial aspect of the uterus, (i.e. the region in which decidua will form if trauma is applied) in the pseudopregnant uterus before trauma (day 0) exhibits regional structural differences when compared either with mesometrial, and paramesometrial endometrium, or with more deeply situated, (i.e., juxtamuscular) antimesometrial stroma. Basal aspects of the luminal epithelial cells exhibit highly irregular often branched extensions; a distinct subepithelial basement membrane precisely parallels the plasmalemma (figs. 1 2, and 3). S... such projections (figs. 1 2, and 3). Subepithelial stromal cells at this stage are disposed as loosely and irregularly arranged stellate or fusiform elements (fig. 1) Interstitial material of the sub...

lial stroma appears as a sparse, floc ent material of medium electron den- occasionally individual reticular rs can be identified (fig. 1) fascicles of lagen are absent. Occasionally cyto- smic extensions of stromal cells come o close relationship with luminal epi lium (figs. 1 2 and 3) The subepithe- l basement membrane appears always to rvene between stromal and epithelial ls, however At certain points the stro- l cell extensions may approach the mbrane to a distance equal to that be- een subepithelial basement membrane d epithelial basal plasmalemma viz., 0 Å (fig 2) Mitochondria both in epi elial and in stromal cells, appear to be ncentrated within such approximating tensions (fig. 2)

Individual stromal elements in the sub- thelial, antimesometrial area resemble roblasts of mice (Kajikawa, Tanii and nono, '59) and rats (Schulz, '58) else- ere in the body (figs. 1 and 3) Adja nt cells rarely abut, but where they , juxtaposed plasma membranes are ooth and although they not always are rallel, apposed membranes are unmodi- d (fig. 1) The ovoid nucleus has an ner nuclear membrane surfaced inter lly with fairly regularly disposed chro- atin clumps. The outer nuclear mem- ane is sparsely studded with ribosomes d is frequently seen to be in continuity th membranes of endoplasmic reticu- m (fig. 1) These latter membranes are undant and in any given stromal cell pear as either one of two types viz. rrow somewhat tortuous cisternal tu- les which are rough-surfaced which ap- ar filled with a homogeneous material low electron density which occasionally tach, and which often parallel the long ds of the cell; or dilated vacuolar cister e which are smooth-surfaced and which, ve for a sparce flocculent material, ap- ar optically empty (fig. 1) In all stro- al cells at this stage free ribosomes are undant.

The Golgi complex at day 0 is juxtanu- ear compact and disposed, in relation to e centrosome, toward one pole of the ll. Mitochondria appear as long rods ith regular ladder-like cristae mitochon- iales. The mitochondrial matrix is of medium electron density and contains small osmiophilic granules (figs. 2 and 3) Besides mitochondria, stromal cells at day 0 contain other bodies of similar size, but of varying internal structures (fig. 3) These appear to be of three varieties: lipo- somes myeloid figures and "microbodies" i.e., homogeneous bodies which approxi mate mitochondria in size but which are enclosed by a single unit membrane (Rouiller and Bernhard, '56 Ashford and Porter '62 Porter and Bonneville '63)

Cells of the fully decidual stroma

In contrast to the stromal cells de- scribed above subepithelial cells of the antimesometrial stroma in the fully deci dual uterus (day 4 or 5) resemble tightly packed often binucleated epithelioid ele ments (figs. 9 through 12) There is an increase in nuclear size, and the nuclear outline tends to be irregular often deeply scalloped The outer nuclear membrane generally appears smooth and is continu- ous with membranes of the endoplasmic reticulum Throughout the cytoplasm these latter membranes are abundant, forming an extensively ramifying smooth-surfaced tubular system the system appears to be filled with a flocculent material which is less concentrated (i.e., of less density) than interstitial material and comparable to blood serum. Rough-surfaced endo- plasmic reticulum also is present, though less conspicuous

Golgi elements are dispersed and ap- pear as isolated clusters of smooth sur faced vacuoles, a few smooth parallel membranes and microvesicles (fig 9) Mitochondria are numerous small, and ovoid or spherical in shape. The matrix is homogeneous, and cristae mitochondriales are regular; mitochondrial granules have not been identified at day 4 or 5 Various inclusions are evident; liposomes are very abundant; in addition to these to "micro- bodies, and to myeloid figures, lysosomes have been identified (fig. 9)

Glycogen is abundant in fully formed decidua and appears as individual gran- ules which are irregular in shape, but ap- proximately 100 Å in diameter (figs. 9 10 and 11) These are revealed in high con- trast with lead hydroxide staining Rather than being segregated into glycogen-rich

areas of the cytoplasm, the granules appear to be diffusely scattered (figs 9 and 10); occasionally where particularly abundant, accumulations of granules appear related to cisternae of endoplasmic reticulum (fig 11)

A fibrillar material which consists of wavy filaments 50 to 70 A in diameter is particularly abundant in fully differentiated decidual cells. Individual filaments show no periodicity Frequently this material is so abundant that cytoplasmic organelles appear displaced and relatively large areas of the cells appear fibrillar (fig 10)

The cell surface of decidual cells shows extensive modification. Free intercellular space is limited in extent. Where plasma membranes of adjacent cells abut, they frequently interdigitate or form desmosomes (fig 12) The latter lack the contact plaques of true desmosomes (i.e maculae adhaerentia) and consequently more closely resemble zonulae adhaerentia (Farquhar and Palade '63) Occasionally limited areas of apposed plasma membranes separate to delimit a small enclosed intercellular space (fig 12) Such spaces appear to contain material optically similar to that seen in cisternae of smooth surfaced endoplasmic reticulum

Sequential changes during primary decidual cell formation

Except for the features noted above there is little change in fine structure of interphasic nuclei during the decidual reaction.

Cisternae of the endoplasmic reticulum *in most stromal cells appear markedly dilated* at day 1 unattached ribosomes in rosettes, are abundant throughout the cytoplasm (fig 4) By day 2 dilatation has progressed to a point where the cells appear vacuolated (figs 5 and 6) The distended cisternae typically are smooth-surfaced. Many stromal cells at day 2, however still exhibit narrow rough-surfaced tubules of endoplasmic reticulum (fig 6)

After day 2 the cells becomes more epithelioid (fig 7) and stromal cells which contain exclusively rough-surfaced endoplasmic reticulum are no longer seen. As the decidual reaction proceeds endoplasmic reticulum of the smooth-surfaced variety becomes more abundant [illegible] increasingly irregular in arrangement [illegible] contents of the dilated cisternae appear [illegible] remain of fairly constant density throughout the reaction, consisting at all stages (even in certain cells at day 0) – [illegible] light, mottled, flocculent material which [illegible] similar in appearance to intercellular [illegible]stance Occasionally small, rough-[illegible] faced membranous profiles are seen [illegible]terspersed among profiles of [illegible] cisternae

At day 1 mitochondria are similar [illegible] mitochondria of non-decidual (i.e [illegible]trol) cells. By day 2 mitochondria [illegible] spherical the cristae are less regular, [illegible] matrix shows areas of focal rarefaction [illegible] no longer contains osmiophilic granules (figs. 5 and 6) Profiles of such ballooned mitochondria often are accompanied [illegible] profiles of inclusions intermediate between mitochondria and myeloid figures (fig [illegible] By day 3 mitochondria are again of re[illegible]lar appearance (i.e. contain ladder-like cristae mitochondriales) although they [illegible]main large and ovoid (fig. 7) Both [illegible]chondria and liposomes appear to [illegible] in numbers to day 5.

Lysosomes first appear at day 2 and [illegible]come increasingly numerous until day [illegible]

Glycogen granules have not been [illegible]fied before day 4 at which time they [illegible] numerous and diffusely scattered throughout the cytoplasm even in the [illegible] areas of the cell (fig. 10) This fibrillar material appears first on day 1 as [illegible] gathered fascicles of fine filaments [illegible] 50 to 70 A in diameter (fig 4) [illegible] *creases in amount* during days 3 and [illegible] during which time thick bundles of [illegible]ments are seen to traverse the cytoplasm randomly (figs 8 and 10), displacing [illegible]cal cytoplasmic organelles. These [illegible]ments apparently are not in relation [illegible] desmosomes.

As the stroma undergoes decidual [illegible]formation the gross outline of the cell becomes more irregular large cytoplasmic extensions reaching into the intercellular space. The greatest irregularity is seen [illegible] day 3 after which time the hypertrophied cells have become more polyhedral [illegible] packing Desmosomes are first seen [illegible] day 2 (fig 6) Both interdigitation and

l modification of the plasma ma are at a peak on day 5

DISCUSSION

nduction of decidual cell formation in ents in the absence of an embryo was t described more than half a century (Loeb '07) However by calling the ue masses so produced deciduomata, a hological nature was implied to an es tially normal process It has been ablished that deciduoma formation is an unorganized tumorous reaction, but her a correlated regional differentia n of the uterine stroma which precisely ulates the maternal response to im ntation (Shelesnyak, '59)

In the antimesometrial implantation a of the pseudopregnant stroma before uma, non-decidual cells resemble fibro sts. Endoplasmic reticulum is seen to disposed in these cells in either of two tinct arrays (1) as rough-surfaced cis nae, which are relatively narrow and ed with a homogeneous electron dense terial and (2) as smooth-surfaced cis nae which are relatively distended and tain a finely flocculated material. In eudopregnant, non-traumatized stroma d in early decidua viz., up to day 2, only e type of endoplasmic reticulum is nd in any one cell After day 2 all de dual cells appear to contain predomi ntly the smooth-surfaced variety often, wever scattered profiles of rough-sur ed cisternae remain It is interesting to te that the dilated smooth-surfaced cis nae which are more characteristic of lly formed decidual cells, are also evi nt in stromal cells in the pseudopreg nt uterus before trauma. They are not en in juxtamyometrial stroma, nor in of the uterus other than the anti mesometrial region It is tempting to con de that this particular variety of endo asmic reticulum is characteristic of cidual cells and that cells showing such lated smooth-surfaced cisternae before uma are pre-decidual i.e selected" ements which are hormonally sensitized undergo deciduogenesis.

It is known that smooth-surfaced endo asmic reticulum is associated with gly gen synthesis (Millonig and Porter '60 rter and Bonneville '63) In our study a marked build-up of glycogen by day 4 is evident. The relationship between accumulated glycogen granules and smooth-surfaced cisternae which is sometimes seen on this day consequently may be a morphological manifestation of such synthetic activity An abundance of glycogen is interpreted to subserve the function of nourishing an embryo

Although stromal cells in non-decidual and early decidual stages resemble fibroblasts they appear most like those of the embryo (Schulz, '58) In embryonic fibroblasts endoplasmic reticulum is abundant, roughly parallels the axis of the cell and is in continuity with the outer nuclear membrane furthermore the condition seen here in which free ribosomes are very abundant and diffusely scattered throughout the cytoplasm is thought to characterize differentiating embryonic tissues in general (Slautterback and Fawcett, '59) It is perhaps of some significance that stromal cells of the pseudopregnant uterus, which have a high capacity for differentiation and a high metabolic potential, have an appearance suggestive of embryonic tissue.

In their capacity for differentiation and high metabolic potential, these cells might also be likened to cells of the blastema of regenerates In this regard, the relationship of stromal cell to luminal epithelium which has been observed in our study calls to mind the relationship of blastema to epidermis in the regenerating limbs of amphibia and barbels of cat fish. It is well established that blastema will not differentiate into regenerative elements without contact by overlying wound" epithelium (Rose 48 Thornton '58 Goss, '56) Electron microscopic studies on differentiating blastema indicate an intimate relationship between differentiating blastemal cells and the basal aspect of the epithelial cells (Hay '60 Salpeter and Singer '60) In many ways this relationship appears comparable to that which we have described and illustrated in early decidualization, e.g., the relationship between differentiating stroma and epithelium. Furthermore since mitochondria are regarded as sites of cytochrome oxidative enzyme systems (Watson and Siekevitz, '56) localization of these organelles in approximat

ing extensions of both stromal and epithelial cells may signify a build-up of metabolic energy reserves under the hormonal sensitization of pseudopregnancy in preparation for decidua formation. A positive correlation between the capacity of the cytochrome system — i.e metabolic potential — and numbers of mitochondria has been demonstrated elsewhere (Mattisson and Birch Anderson, '62)

The initial response to decidua inducing trauma involves (1) an increase in amount and a complexity of arrangement of endoplasmic reticulum (2) a ballooning of mitochondria and (3) a synthesis of a fine fibrillar material. The irregularities observed in mitochondrial structure particularly at day 2 may indicate increased mitochondrial function and/or rapid mitochondrial multiplication in the face of augmented energy requirements of cells which are undergoing hypertrophy hyperplasia and differentiation. Elaboration of endoplasmic reticulum can be interpreted as precedent to glycogen synthesis glycogen being first observed at day 4 It is difficult however to establish the functional significance of the fibrillar material As regards its functioning in the production of intercellular fibrils we have not observed any indication of an extrusion of these intracellular filaments to the exterior of the cell. Occasionally at day 0 single fibrils 80 A thick which exhibit the 40–60 A periodicity which is characteristic of reticulum are seen immediately outside of the cell membrane. However it is well established that the number of fibers decreases during the decidual reaction in rats (Wolfe and Wright 42 Fainstat, '63) whereas we have observed a pronounced increase in intracellular fibrils during the first three days of the reaction We have never observed any evidence of phagocytosis of reticulum or collagen by stromal cells as has been suggested elsewhere (Dubrauszky and Schmidt '58 Luse and Hutton '64) Nor are the intracellular fibrils found here comparable to the "Kollageneinschlüsse of Wessel ('59) since they are not separated from the surrounding cytoplasm by a unit membrane They appear however comparable to the protofibrils observed elsewhere as follows (1) in embryonic fibroblasts (Schulz, '58) (2) in atypically proliferating fibroblasts (Iikizume '59) and (3) in "redifferentiating" blastemal cells (Hay '58). Whether they are comparable to the tonofibrils (keratin filaments) observed in a variety of cells, particularly cells of stratified squamous epithelium (Baradi and Jollie, '61) and stratified cornified epithelium (Hibbs and Clark '59) remains a question which can be answered only when the chemical nature of the filaments has been determined Their presence may be solely a morphological expression of alterations in consistency of the "back-ground" cytoplasm during a sol-gel transformation which accompanies such rapid differentiation and growth During implantation in a typical pregnancy such filaments collectively may function to support both hypertrophic decidual tissue and an enlarging embryo as concomitantly the collagen content of the uterus becomes markedly reduced.

The appearance of lysosomes in decidual cells until day 5 suggests impending autolysis Indeed in induced decidua formation, atrophy begins on day 6 (Velardo Dawson Olsen and Hisaw '53) these days are comparable to the ninth and tenth days post coitum in a typical implantation a stage at which the embryo undergoes pronounced enlargement at the expense of surrounding decidual endometrium at this time trophoblast is most active in phagocytosis both of decidual debris and of extravasated maternal blood cells Consequently the fact that a peak in abundance of both glycogen and lysosomes is reached at a stage when autolysis is imminent appears timed to subserve an embryonic nutritive function. The microbodies identified as early as day 1 are interpreted as being developmental forms of lysosomes (Porter and Bonneville '63)

We cannot state with certainty however how many of the changes which we have noted are functionally significant exclusively in decidual formation. Undoubtedly some changes may be associated with the rapid mitotic rate which is known to accompany the reaction and a resultant lack of typical interphasic cytoplasmic organization Such changes would be likely to be characteristic as well for

owth and differentiation elsewhere in the body Tentatively one might suggest that an increase in endoplasmic reticulum, a shortening of mitochondria (mitochondrial replication?) and the dispersal of Golgi elements may result from this condition.

LITERATURE CITED

...ford, T P and K. R. Porter 1962 Cytoplasmic components in hepatic cell lysosomes. Cell Biol., 12: 198–202.

...cadi, A. F and W P Jollie 1963 Electron microscopic observations on cell surface modifications in gustatory epithelium. Acta Anat., 50 306–311.

...rner, G. W and W M. Allen 1929 Physiology of the corpus luteum. II. Production of a special uterine reaction (progestational proliferation) by extracts of the corpus luteum. Am. J Physiol., 88 326–339.

...Fee, V J 1962 Comparative effectiveness of several methods for the production of deciduomata in the rat. Anat. Rec., 142. 226 (abstract)

... Palo, A., and I. Stoppelli 1960 The submicroscopic structure of human decidua. Minerva Ginec., 12. 633–647

...rowsky V und H. Schmitt 1958 Mikroskopische und elektronmikroskopische Untersuchungen am Gitterfasersystem der Corpusmucosa während des Cyclus und der Gestation. Arch. Gynäk 191 212 223.

...kinda, P M. C. Shelesnyak and E. C. Amoroso 1959 A survey of the physiology of ovum implantation in mammals. In Implantation of Ova, Memoirs of the Society for Endocrinology N 6 3–12.

...inaat, T 1963 Extracellular studies of uterus. I. Disappearance of the discrete collagen bundles in endometrial stroma during various reproductive stages in the rat. Am. J Anat 112: 337–370.

...rquhar, M. G., and G E. Palade 1963 Junctional complexes in various epithelia. J Cell Biol., 17 375–412.

...mbri, G. 1937 Silver impregnation of reticulum in paraffin sections. Am. J Path 13 993–1001

...s, R. T 1956 An experimental nalysis f ...tate barbel regeneration in the catfish J Exp. Zool 131 27–49

...erp, R. O., and F L. Hisaw 1936 Pseudopregnancies from electrical stimulation of the cervix in the diestrum. Proc Soc. Exp. Biol and Med., 33 359–360

...rmperl, H 1958 Über Kollagenneuschilbuse ...m Deciduazellen. Klin. Wschr 36 939–940.

...hkimura T 1959 Studies on the fine structure of the cells in typical proliferation with special reference to fibrillogenesis within the cytoplasm. Acta Pathol. J pon 9 133–140.

...y E. D 1958 The fine structure of blastema cells and differentiating cartilage cells in regenerating limbs of Amblystoma larvae J Biophys. Biochem. Cytol 4 583–591

——— 1960 The fine structure of nerves in the epidermis of regenerating salamander limbs. Exp. Cell Research, 19 299–317

Hibbs, R. G., and W H. Clark 1959 Electron microscope studies of the human epidermis the cell boundaries and topography of the stratum malpighii. J Biophys. Biochem. Cytol., 6 71–76.

Jollie W P 1961 The incidence of experimentally produced abdominal implantation in the rat. Anat. Rec., 141 159–166.

Kajikawa, K., T Tanii and R. Hirono 1959 Electron microscopic studies on skin fibroblasts of the mouse with special reference to the fibrillogenesis in connective tissue. Acta Pathol. J pon. 9 61–80

Krehbiel, R. H. 1937 Cytological studies of the decidual reaction in the rat during early pregnancy and in the production of deciduomata. Physiol. Zool., 10 212–233.

Loeb, L. 1907 Über experimentelle Erzeugung von Knoten von Deciduagewebe in dem Uterus des Meerschweinchens nach stattgefundener Copulation. Centralbl. f. allg. pathol. und Pathol. Anat., 18 563–565.

Luse, S., and R. Hutton 1964 An electron microscopic study of the fate of collagen in the post-partum rat uterus. Anat. Rec., 148 308 (abstract)

Mattisson, A. C. M., and A. Birch-Andersen 1962 On the fine structure of the mitochondria and its relation to oxidative capacity in muscles of various invertebrates. J Ultrastruc ture Res., 6 205–228.

Millonig, G. 1961 Advantages of phosphate buffer for osmium tetroxide solutions in fixation. J Applied Phys., 32 1637 (abstract)

——— 1961b A modified procedure for lead staining of thin sections. J Biophys. Biochem. Cytol., 11 736–739.

Millonig, G and K. R. Porter 1960 Structural elements of rat liver cells involved in glycogen metabolism In Proceedings of the European Regional Conference on Electron Microscopy Delft pp. 655–659.

Porter K. R., and M. A. Bonneville 1963 In An Introduction to the Fine Structure of Cells and Tissues Lea and Febiger Philadelphia.

Richardson, K. C L. Jarett and E. H Finke 1960 Embedding in epoxy resins for ultrathin sectioning in electron microscopy Stain Technology 35 313–323.

Rose, S. M 1948 Epidermal dedifferentiation during blastema formation in regenerating limbs of Triturus viridescens J Exp. Zool., 108: 337–361

Rouiller C., and W Bernhard 1956 Microbodies and the problem of mitochondrial regeneration in liver cells. J Biophys. Biochem Cytol., 2 (Suppl.) 355–359

Sabatini, D D K. Bensch and R. J Barrnett 1963 Cytochemistry and electron microscopy The preservation of cellular ultrastructure and enzymatic activity by aldehyde fixation J Cell Biol 17 19–58

Salpeter M. M and M. Singer 1960 Differentiation of the submicroscopic adepidermal membrane during limb regeneration in adult Triturus. Anat. Rec., 136 27–39

Schulz, H. 1958 In Die Submikroskopische Anatomie und Pathologie der Lunge, Springer Verlag, Berlin-Göttingen — Heidelberg.

Shelesnyak, M. C. 1957 Some experimental studies on the mechanism of ova-implantation in the rat. In Recent Progress in Hormone Research 13 296–317

——— 1959 Histamine and the nidation of the ovum In Implantation of Ova, Memoirs f the Society for Endocrinology 6 84–93.

Slautterback, D B., and D. W F wcett 1959 The development of the cnidoblasts of Hydra. An electron microscopic study of cell differ entiation. J Biophys. Biochem. Cytol., 5: 441–452.

Thornton C. S. 1956 Epidermal modification in regenerating and non-regenerating limbs of anuran larvae. J Exp. Zool., 131 373–393.

Velardo, J T A. B. Dawson, A. G Olsen and F L. Hisaw 1953 Sequence of histological changes in the uterus and agina of the rat during prolongation of pseudopregnancy [illegible] sociated with the presence of [illegible] Am. J Anat., 93: 273–306.

W tson, M. L., and P Siekevitz [illegible] lation and analysis of [illegible] brane fraction. J Biophys. Biochem. C[illegible] 2 (Suppl.) 379–383.

Wessel, W 1959 Die menschlichen [illegible] zellen und ihre Kollagen[illegible] im E[illegible] tronenmikroskop. Virchows Arch. path. [illegible] 332: 224–235.

Wislocki, G. B and E. Dempsey [illegible] tron microscopy of the placenta of the [illegible] Anat. Rec., 123 33–63.

Wolfe, J M., and A. W Wright [illegible] brous connective tissue of the [illegible] duced maternal placenta in the rat [illegible] ticular reference to the relationship [illegible] reticulum and collagen. Am. J Path., [illegible] 431–461

PLATE 1

EXPLANATION OF FIGURE

1 Subepithelial endometrial stroma in the pseudopregnant, non-traumatized terus (Le t day 0) Note that some cells contain smooth-surfaced endoplasmic reticulum; others contain the rough-surfaced variety In the former (which appear most bundant in this particular figure) there are points of continuity between dilated, smooth-surfaced cisternae and the outer membranes of nuclear envelopes. The basal portions of luminal epithelial cells are seen at the extreme top of the figure. A basement membrane appears always to parallel precisely the basal plasmalemma of each of these cells. Epithelial basal projections approximate extensions from subepithelial stromal cells. × 15,000

Abbreviations

ep luminal epithelium
en, endothelium
cl, capillary lumen
bm, basement membrane
d, desmosome
f, fibrillar material
m, mitochondrion
li, liposome
mb, microbody
my myeloid figure
ly lysosome
G, Golgi membranes
g glycogen
s–er smooth-surfaced endoplasmic reticulum
–er rough-surfaced endoplasmic reticulum
N–ep; N–O; N–1; & c., epithelial cell nucleus, nucleus of stromal cell at day 0; nucleus of tromal cell t day 1; & c.

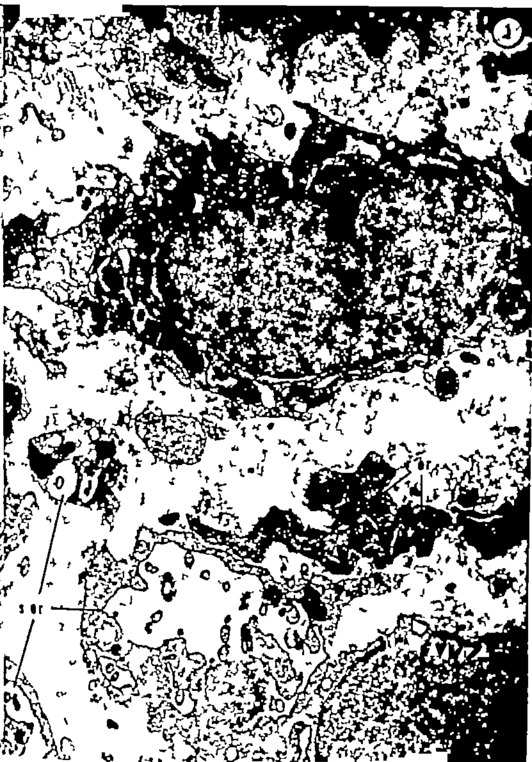

1
S ER

PLATE 2

EXPLANATION OF FIGURES

2 Stromal-epithelial cell relations at day 0. Epithelium is toward the top of the figure. Note that, even at points of closest approximation (arrows) basement membrane consistently intervenes between epithelium and cells of the stroma. Epithelial mitochondria appear to be concentrated basally into those projections which approach stromal cells, conversely stromal mitochondria often are concentrated int those portions of the stromal cell which approximate the epithelium. × 22,000.

3 Stromal cell-epithelial relations t day 0. Epithelium is toward the top. Featured within the stromal cell is a localized Golgi apparatus, which is characteristic for this day and various microbodies. × 22,000.

4 Stromal cells at day 1 (i.e., the day following traumatization of the pseudopregnant uterus) Within hypertrophying cells a fibrillar material is evident t this day Apposed plasma membranes still appear unmodified. × 22,000.


m


3



PLATE 3

EXPLANATION OF FIGURES

5 Epithelial-stromal cell relations at day 2. Note the complex looping of the adepithelial basement membrane. Hypertrophying decidual cells exhibit increasingly abundant fibrillar material, variety of cytoplasmic inclusions and Golgi apparatus (arrows) which is becoming highly ramified throughout the cell and/or fragmented. × 17,500.

6 Portions of three stromal cells at day 2. The cell at the left appears to contain predominantly endoplasmic reticulum of the rough-surfaced variety. The cell at the center of the figure exhibits smooth-surfaced endoplasmic reticulum. Free ribosomes are abundant in all three cells. Desmosomal contiguities between cells, such as between the one in the center and the one at the right, are first apparent on this day. Note also a disorganization in mitochondrial structure which is especially prevalent in stromal cells at this stage. × 13,500.

5

6

PLATE 4

EXPLANATION OF FIGURES

7 Relation of a three-day decidual cell to a stromal capillary. A basement membrane separates endothelium from decidual cell; where this membrane is cut in grazing section, it is seen to be fibrillar (arrows). Note the general epithelioid appearance of the decidual cell at this day. × 10,000

8 An enlarged area of cytoplasm of three-day decidual cell, showing displacement of typical organelles by an accumulation of fibrillar material. × 28,000

PLATE 5

EXPLANATION OF FIGURE

9 Several decidual cells four days following trauma are seen in relation to a stromal capillary. Decidual cells exhibit the characteristics which typify stroma at the height of the decidual reaction, viz numerous profiles of smooth-surfaced endoplasmic reticulum, highly dispersed Golgi elements, abundant fibrillar material, numerous lysosomes and accumulations of glycogen granules. An erythrocyte and a lymphocyte are seen within the capillary lumen. × 14,500.



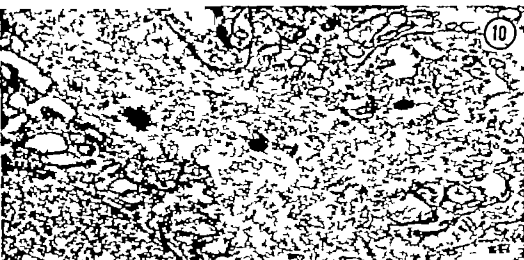
PLATE 6

EXPLANATION OF FIGURES

10 A portion of a four-day decidual cell. A cytoplasmic area which is rich in fibrillar material (and which, conversely shows paucity of typical organelles) is pictured. Note the abundance of glycogen in this region. × 22,000.

11 A portion of a four-day decidual cell. Note the abundance of smooth-surfaced endoplasmic reticulum. Frequently (as at arrows) there seems to be relationship between these membranes and accumulations of glycogen granules. × 22,000.

12 Primary decidua five days following uterine trauma. Portions of three cells are illustrated; note the interdecidual cell junctions. Desmosomes, which here appear in a linear array lack the intercellular contact placques of maculae adhaerentia and are interrupted by areas of the cell surface where apposed membranes diverge to enclose small, irregular intercellular space. × 22,000.


10


11


12

'he Shape of Rat Kidney Tubular Cells

RUTH ELLEN BULGER

Department of Anatomy Harvard Medical School, Boston, Massachusetts

ABSTRACT Many cells specialized for ion transport have complex shapes. The cells of the nephron are no exception. Besides the well-documented lateral processes seen in the basal region of many tubular cells, two further specializations are found in rat kidney tubular cells which serve to increase the lateral cell membrane area. These are an interdigitation of processes confined to the apical region, and an interdigitation of more extensive processes that extend the full height of the cell.

Many mammalian renal tubular cells xhibit extreme complexity in shape. Light iicroscopists of the nineteenth and early wentieth centuries saw and recorded the resence of these extraordinary elabora- .ons of cell form. Before 1900 Heidenain (1874) Schachowa (1876) Lanuer (1895) and Zimmermann (1898) .oted the irregular and complicated lateral rocesses extending from the cells of the roximal convoluted tubule, ascending nick limb of the loop of Henle and the istal tubules. Zimmermann (1898 '11 15) identified the complex shape of the ells of the thin limb and visceral glomerlar epithelium. The application of elec- 'on microscopy to the kidney reaffirmed nd in some cases extended our under tanding of the configuration of the cells 1 certain regions of the nephron. Attenion has been focused mainly upon elabora .ons of the basal surface of the epitheum.

In this study electron micrographs have een obtained which indicate that cell hapes in certain regions of the rat kidney re more complex than has been reported eretofore by electron microscopists. A escription is offered of two further comlexities in the shape of the cells of the enal tubule which serve to increase the rea of lateral cell membrane. These are ateral projections in the apical region of he cells and lateral projections that exend the full height of the cells. These ndings are in substantial agreement with bservations already recorded in the earlier terature of light microscopy but they reuire reiteration because they have been verlooked or largely ignored by contempoary students of renal fine structure.

MATERIAL AND METHODS

Kidneys of ten adult rats of the Charles River strain were fixed by three methods: immersion, perfusion, or dripping on the surface of the organ in the living anesthetized animal. The fixative used was 1 3% OsO buffered with s-collidine (Bennett and Luft, '59) In some cases calcium chloride was added to the fixing fluid. Only the superficial regions could be studied in the kidneys processed by dripping fixative on the surface. Perfusion was accomplished by injecting cold fixative into the abdominal aorta after clamping the vessel both above and below the level of the renal artery A vein was cut to allow fluid outflow The kidneys to be fixed by immersion or after preliminary perfusion were cut into thin pie-shaped pieces with the papilla at the apex and then divided into six regions parallel to the base which were fixed separately to maintain orientation as to the location of the tubules under study After one hour of fixation, the tissues were rapidly dehydrated in ethanols and embedded in epoxy resin (Luft, '61) The sections were cut on a Porter Blum microtome stained with saturated uranyl acetate and Millonig s lead tartrate ('61) and viewed with RCA-3E and 3F microscopes.

OBSERVATIONS

The complex apical outline of the rat proximal convoluted tubular cell can be seen in a light micrograph of a 1 μ thick section (fig 1) The terminal bars appear as undulating lines which outline the

Present address Department of Pathology, University of Washington Medical School, Seattle, Washington 98105.

apical interdigitation of the cells in that part of the nephron In addition to small secondary irregularities or extensions larger lateral processes can be seen. These correspond to the specializations in cell shape that are the subject of this study of rat kidney tubular cells.

The first consists of an extensive inter locking of fine processes that extend ra dially from the cell apex. In electron micrographs small cytoplasmic compart ments are frequently observed at the lu minal border of the epithelium (figs. 2 3) These enclaves of cytoplasm are bounded by a continuous plasma membrane and joined to neighboring cells by typical junc tional complexes. They are interpreted as cross sections of the lateral processes that extend radially from the apical portion of the epithelial cells and evidently corre spond to the fine processes whose inter digitations are seen as the fine irregulari ties of the boundary contour in views from the luminal surface with the light micro scope. In sections of proximal convoluted tubules that pass tangential to the lumen the continuity of these processes with the cell body can be seen and the complexity of this apical interdigitation can be more fully appreciated (fig 4) These apical interdigitating processes are most numerous in the proximal convoluted tubule and the upper portion of the thin limb of the loop of Henle They are less abundant in the ascending thick limb and the distal tubule. Such apical extensions have been seen in the proximal convoluted tubule of dog cat, gerbil and human (Bulger unpublished observation) The emphasis in previous electron microscopic studies has been upon amplification of surface at the cell base The apical interdigitation seen in these species serves to increase the area of lateral cell membrane in the apical region of the cells.

The second category of surface specialization to which we wish to draw attention is lateral compartments of varying width that are not confined to the apical region, but extend the full height of the epithelium from lumen to base. They seem to be radial processes similar in all respects to those already described for the squamous cells of the loop of Henle (Rhodin '58a,b) They are connected to neighboring cells by junctional complexes and differ from the apical processes described above and from the basal lateral processes of Clark ('57) and Rhodin ('58a,b) only in that they extend from lumen to base. They are most numerous in the first part of the ascending thick limb and in the thin limb (Rhodin, '58a b) but occur also in the proximal convoluted tubule and in limited numbers in the cortical part of the ascending limb and distal convoluted tubule. An electron micrograph is presented in figure 5 of the proximal part of the ascending thick limb in the inner stripe of the rat medulla. Many compartments are seen bounded by lateral cell membranes that have junctional complexes near the luminal border. In this region of the nephron, the compartments are often only wide enough to hold one mitochondrion. A similar region is shown in figure 6 Processes of the cell at the bottom of the figure can be seen to alternate with processes of other cells that extend from base to lumen hence indicating a similar pattern of lateral interdigitation.

A low power electron micrograph of the proximal tubule (fig. 7) demonstrates both of these categories of surface elaboration. The long arrows on the figure mark junctional complexes where the cell membrane is seen to run directly to the basal surface — hence would normally be interpreted as lateral boundaries of cells. The large number of these membrane pairs far exceeds the number of cells comprising the cross section of the tubule and hence gives some measure of the abundance of slender lateral processes that extend from base to lumen The shorter arrows mark junctional complexes where the cell membranes run from the lumen into the cell for a short distance and return to the surface — demarcating small lateral processes that are confined to the apical region of the cell. A schematic three-dimensional representation of the rat proximal convoluted tubular cell is presented in figure 1 showing apical interdigitation, lateral interdigitation and basal-lateral interdigitation.

The two specializations described here along with the well-documented lateral processes of the basal region of the cell

...rease the area of lateral cell membrane ...tact.

...lements of the smooth-surfaced endo...smic reticulum are very commonly in ...e apposition to the lateral cell mem...nes, and because this relationship may ...e some functional significance in rela...n to the amplification of lateral cell sur...e, it will be described here. This special...ization of the smooth-surfaced mem...nes was first noted in an abstract by ...son et al. ('63) It was visualized by ...se authors as a continuous tubular sys...n extending from the apical region to ...e middle and basal parts of the rat proxi...al convoluted tubular cell. In our prep...tions, the smooth-surfaced profiles ...pear as an anastomosing system of ir...ularly shaped elements (fig. 9) This ...tem can be seen along all the lateral ...l membranes: those bounding apical ...partments those running from the ...en to base and those surrounding the ...ral processes seen in the basal cyto...sm. The system is most highly devel...d along the membranes in the apical ...t of the cell although it can extend ...oughout the height of the cell The ...lgi apparatus often lies close to the ...ooth surfaced membranes described ...ve. This may reflect some functional ...ociation between the two but, on the ...er hand it should be kept in mind that ...large number of lateral interdigitations ...the proximal convoluted tubular cells ...rease the probability of seeing the ...ooth-surfaced membranes in close spa...l relation to the Golgi apparatus

DISCUSSION

The remarkable elaboration of cell out...es in the renal epithelium which is now ...mmonly included among the contribu...ns of electron microscopy was actually ...arly established by the work of several ...cerning light microscopists from 1874 ...1942. In 1874 Heidenhain found that ...cytoplasm of the mammalian proximal ...nvoluted tubule ascending thick limb of ...loop of Henle, and the distal tubules ...tained a large number of little rods ...ich he called "Stäbchen. Isolated cells ...m the dog proximal convoluted tubules ...re depicted by him as having large arms ...cytoplasm that extend laterally and give off small secondary processes. Schachowa (1876) discussed the complicated lateral borders of the basal portion of dog kidney tubular cells. Although these interdigitating grooves and furrows varied in shape and number they were seen in the cells of the proximal convoluted tubule, thick ascending limb and distal tubule. Similar flutings of the lateral cell surface were seen in several mammalian species (including human) by Landauer (1895) He established that the radiating processes existed in the uppor portion of the cell as well as at the base. Using cat and dog kidneys Zimmermann (1898 '11 '15) confirmed the earlier studies. He stressed the transition between the complex apical outline of the pars convoluta and the simple apical outline of the pars recta. The extremely complex form of the cells of the thin limb and the visceral glomerular epithelium were identified and beautifully illustrated by Zimmermann. A comprehensive review of these and additional investigations was written by von Mollendorff in 1930

Graffiin and Foote ('38 '39) and Foote and Graffiin ('42) studied the two segments of the proximal tubule in the cat and dog nephron by silver impregnation of the highly complicated cell boundaries. The cells of the first segment of the proximal tubule of the cat were found to be extraordinarily interdigitated at the surface less complex in the intermediate region and again extremely irregular near the basement membrane. Those of the second segment of the proximal tubule were essentially rectilinear at the luminal surface but usually interdigitated in variable degree near the basement membrane. In the first segment of the proximal tubule of the dog nephron, the cell shapes were reported to be far more irregular than those of the cat and no significant differences in the complexity of their outline could be detected at the luminal intermediate and basal levels of the cells. Chrome-silver preparations of the second segment of the dog proximal tubule are similar to those described in the cat but the simple rectilinear cell outline seems to be present from lumen to basement membrane.

Early electron microscopic studies of the kidney in some cases extended but ...

others actually confused the understanding of cell shapes in the nephron. Pease and Baker ('50) regarded the fine processes on cells of the visceral layer of Bowman's capsule as ridges of the basement membrane instead of cellular processes. In sections subtangential to the tubular lumen they showed the interlocking of the basal regions of the proximal tubular cells. In transverse sections however cutting the cells from basement membrane to lumen the numerous cell membranes at the base of the proximal and distal tubular epithelia were not clearly resolved and were interpreted as condensations of cytoplasm forming tubular sheaths around the mitochondria. In 1951 Dalton recognized that the cells of the visceral layer of Bowman's capsule have fine cytoplasmic processes. He also pointed out the tortuous lateral cell membranes in a proximal tubular cell but then failed to appreciate the implications of the irregularity of outline for interpretation of sections in the other plane and simply described basally located intracellular filament like structures" in both proximal and distal tubular cells.

Sjöstrand and Rhodin ('53) noted the basal cytoplasm of the proximal tubules of mice to be divided into open compartments by well-defined intracellular double membranes. The compartments were thought to be closed basally opening into the perinuclear or intermediate zone of cytoplasm. In 1954 Rhodin proposed that the intracellular membranes seen in thin sections of the basal region of the cytoplasm represented a complicated system of infoldings of the basal cell membrane. According to this interpretation, the folds of cell membrane delimit narrow parallel compartments of the overlying cell that are open to the cell body above and extend downward to the basement membrane. Pease ('55a,b '56) in his later papers agreed that the basal region of the cells of the proximal convoluted tubule was subdivided by "infoldings or intussusceptions" of the plasma membrane. He drew attention to the fact that this specialization was even more elaborate in the distal tubule Ruska et al. ('57) noted that the infolded" cell membranes rarely if ever return directly to the cell base The membranes generally return to the basement membrane at a distance from the point of infolding [illegible] enclose portions of cytoplasm. They [illegible] scribe a labyrinthine system of inter[illegible] municating potential spaces between the paired membranes at the base of the [illegible] thelium.

As a result of studies of ferentiation in the kidneys of mice, Clark ('57) seems to have a clear understanding of the shapes the cells. He found that cell membrane was relatively simple contour while the lateral cell was often tortuous and interlocking. The formation of the basal striations which be- gins after birth was interpreted to be the result of progressive flutings of the [illegible] umnar cells. In two extensive papers [illegible] lished in 1958 Rhodin concluded that the basal parts of the proximal and distal [illegible] voluted tubular cells are provided with [illegible] multitude of radially disposed thin [illegible] like cytoplasmic processes that interdigitate with those of neighboring cells like the meshing of cogwheels. The sides of the upper portion of the proximal tubular [illegible] were said to be smooth contoured without any radiating lamellar processes. In later reviews Rhodin ('62, '63) continued diagram the cells of the proximal luted tubule with rectilinear cell in the apical part of the cell.

Many electron microscopic studies [illegible] focused attention on specializations of the basal cell membrane in epithelia special[illegible] ized for ion transport. Pease ('56) noted the vast increase and postulated that such a modification might increase the area of active surface for ion transport. Similar modifications were discovered that [illegible] creased the membrane area on the lateral surface of cells in many of these transport[illegible] ing tissues (Millen and Rogers, '56, [illegible] well and Pease, '56; Pease, '56; Pappas [illegible] Smelser '58 '60 '61; and Munger, [illegible] Some tissues such as gall bladder ([illegible] mada, '55 and Hayward, '62a,b) [illegible] membrane specializations almost [illegible] on the lateral surface

From recent work, including that [illegible] Clark ('57) and Rhodin ('58a, b) it [illegible] become increasingly apparent that [illegible] of the structures first identified as [illegible] infoldings are in fact interdigitating [illegible] eral processes occupying corresponding [illegible]

esses in adjacent cells. Parks ('61) rediscovered that the basal region of the cells of the striated duct of mouse parotid gland has leaf-like processes which fit into grooves on adjacent cells. While studying the ciliary epithelium of the adult albino rabbit, Tormey ('63) found that the "infolded plasma membranes described by previous workers were cell membranes covering projections or interdigitations from adjacent cells. By studying serial sections, he showed that the apical (embryologically basal) and lateral interdigitations appear to be two aspects of the same structure. Hence many surface specializations which were formerly thought to be mechanisms for increasing the basal cell membrane area, in fact, increase the area of lateral cell surface.

Various amounts of lateral interleafing exist between cells of non-mammalian organs involved in the movement of ions. The dogfish rectal (salt-secreting) gland consists of cells with apical interdigitations and lateral projections (Bulger '61 '63). Christensen ('63) has shown that the distal tubular cells of the salamander kidney (*Batrachoseps attenuatus*) have thin lamellae which interdigitate with adjacent cells. The cells of the nasal salt secreting gland of the lizard (*Dipsosaurus dorsalis*) have lateral infolded processes (Philpott and Templeton, '64). Extreme complexities in cell shape have been reported in the nasal gland of marine birds by Doyle ('60a,b) and in the calciferous gland of the earthworm (*Lumbricus terrestris*) by Ellis ('63).

The cells throughout the rat nephron tend to have a branching, star-shaped form. In some regions of the tubules, the irregular outlines frequently extend the entire height of the cell as in the proximal convoluted tubule, the squamous thin limb cells, and the first part of the ascending thick limb. In other regions the branching form involves mainly the basal region of the cells as in the latter part of the thick ascending limb and the distal convoluted tubule. The visceral epithelium of the glomerulus also has many radiating and branching processes giving rise to the familiar pedicels.

It is difficult and probably premature to attempt to assign any specific function to the complex shape of the rat kidney cells. However certain observations seem appropriate. The form of the kidney cells leads to an increase in the lateral cell surface area, an increase in the intercellular space and an increase in area of cell to cell contact. Since much of the kidney tubule is involved in ion transport processes, it is probably safe to assume that the complex cell shape is related to these processes. This is further substantiated by the fact that cells with complex shapes are found in other organs specialized for ion transport in mammalian and non-mammalian species. However, some doubt is cast on this interpretation by the fact that the branching cell shape is found in two regions of the nephron not thought at present to be involved with active ion transport the visceral epithelium of Bowman's capsule (podocyte) and the descending thin limb of the loop of Henle. The interleafing processes of the podocyte may offer support while giving rise to a large number of filtration slits. Although it has been postulated that the cells of the ascending portion of the loop of Henle (including the thin limb cells) contain an active pump which moves sodium into the interstitium of the papilla thus setting up the countercurrent multiplier system, the descending limb is thought to play only a passive role. No distinct morphological differences have been demonstrated between the cells of the ascending and descending limbs in spite of the seemingly different physiological roles.

The smooth-surfaced anastomosing system of membrane limited elements found along the lateral cell membrane may be functionally related to the lateral cell membrane. Ericsson et al. ('63) postulated that the part of the endoplasmic reticulum associated with the lateral cell membranes may represent a transport system connecting the apical cytoplasm with the intercellular space and the Golgi-cytosome region. Although as yet there is no physiological data to support this hypothesis, the close morphological association of these elements is at least circumstantial evidence for some functional interaction between the cytoplasmic and surface membranes.

PLATE 1

EXPLANATION OF FIGURES

1 Light micrograph of a 1 μ thick Epon section, stained with toluidine blue, of a rat proximal convoluted tubule cut obliquely. The terminal bars can be seen as undulating lines that outline the complex interdigitations of the cells in this part of the nephron. There are large processes as well as smaller irregularities. × 2,400.

2 Electron micrograph of the apical region of a proximal convoluted tubular cell of the rat. Small cytoplasmic compartments are seen, bounded by continuous plasma membrane and joined to neighboring cells by junctional complexes, which are interpreted as lateral extensions of the apical region of neighboring cells. × 21,600.

1

2

PLATE 2

EXPLANATION OF FIGURES

3 Electron micrograph showing three compartments in the apical cytoplasm. *The lateral* cell membrane dividing the two cells has a tortuous course. × 19,400

4 The pical interdigitating processes can be followed in this somewhat tangential section. The cell t the lower left can be seen to abut on the lumen in four places. × 16,800.



PLATE 3

EXPLANATION OF FIGURES

5 Electron micrograph of early part of the ascending thick limb located in the inner stripe of the rat medulla. Many compartments are seen separated by lateral cell membranes which are interpreted as profiles of lateral processes that extend for the height of the cell. Examples of lateral compartments in the apical region of the cell can also be seen. × 12,500.

6 Electron micrograph of early part of the ascending thick limb located in the inner stripe of the rat medulla. The dense areas identify terminal bar regions. The cytoplasm of the cell on the bottom can be seen to interdigitate with the lateral processes of what are presumed t be other cells. × 9,200


(5)
(6)

PLATE 4

EXPLANATION OF FIGURE

7 Electron micrograph of a rat proximal convol ted tubule. The long arrows mark junctional complexes where the cell membrane seems to run directly to the basal surface — hence should be lateral boundaries of cells. The large number of these lateral boundaries indicate lateral processes which extend from base to lumen. The short arrows mark junctional complexes where the cell membranes run into the cell for short distance and return to the urface — demarcating small lateral processes in the apical region of the cell. × 5,600.

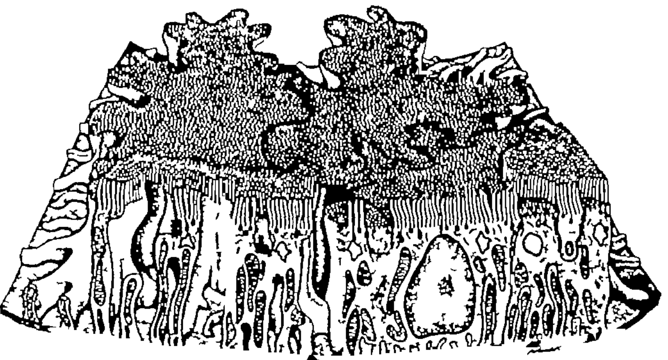


PLATE 5

EXPLANATION F FIGURE

8 A diagram of rat proximal convoluted tubular cells showing three types of l teral interdigitating processes those in the pical region those in the basal region, and those extending for the height of the cell.

Ruth Ellen Bailey



(8)

PLATE 5

EXPLANATION OF FIGURE

6 A diagram of rat proximal convoluted tubular cells showing three types of lateral interdigitating processes those in the apical region, those in the basal region, nd those extending for the height f the cell.

Histochemical Study of the Hamster Ovary

SARDUL S. GURAYA AND GILBERT S. GREENWALD
Department of Obstetrics and Gynecology University of Kansas Medical Center Kansas City Kansas

ABSTRACT The hamster ovary has been studied histochemically for various lipids. The granulosa cells of normal follicles contain lipid bodies of various sizes composed mainly of phospholipids. Some lipid bodies also contain triglycerides cholesterol and its esters. The theca cells contain lipid granules consisting of phospholipids. At the onset of atresia, the granulosa stores lipids bundantly which consist of triglycerides, cholesterol and its esters and slight amount of phospholipids. The theca of atretic follicles, also stores lipids consisting of phospholipids first, and then in sequence phospholipids and triglycerides and finally phospholipids, triglycerides, cholesterol and its esters. The theca hypertrophies and persists to form the interstitial gland whereas the granulosa cells, with their lipid droplets, regress and disappear The interstitial gland in the hamster ovary occurs as patches of various sizes and these are derived from the theca of atretic preantral and antral follicles. Most of the lipid droplets of the interstitial gland, are mobilized within the preovulatory ovary The replenishment of lipid droplets begins on day 1 of the cycle (metestrus) On day 2, the interstitial gland is gain filled with lipid droplets which are rich in cholesterol and its esters, triglycerides and phospholipids.

In ovaries treated with pregnant mare serum (PMS) on each of the days of the estrous cycle, numerous large preantral follicles having 4–7 layered granulosa, are stimulated to ovulate Normally such follicles become atretic, indicating that a lack of sufficient *endogenous pituitary gonadotrophins prevents these follicles from matur*ing. Neutral lipids, especially cholesterol and its esters, could not be demonstrated in the normal granulosa in the PMS-treated ovaries. The follicles, which were atretic at the time of injections, were not affected by exogenous hormones. Human chorionic gonadotrophin (HCG) did not conspicuously ffect the growth of follicles. Both PMS and HCG caused mobilization of lipid droplets from the interstitial gland

Knigge and Leathem ('56) studied the tochemistry of growth and atresia of licles in the hamster ovary but did not ect lipid bodies in the normal granulosa ls. They reported that the granulosa ls of atretic preantral follicles, undergo pertrophy and are the source of inter tial tissue whereas the granulosa cells atretic vesicular follicles degenerate and appear They overlooked the transfor tion of the theca of atretic follicles into erstitial tissue described by the present thors in the ovary of different mammals uraya and Greenwald, '64a, '64b)

Greenwald ('61 '62a) found that the mster ovary develops approximately ten ge follicles on day 1 of the estrous le but has an additional 25 follicles reserve that can be stimulated if preg nt mares serum (PMS) is injected. The llicles developing under the influence of IS are termed reserve follicles

In the present study of the hamster ary experiments were designed to find possible explanation for the following interrelated problems (1) the histochemical nature of normal and atretic follicles of the estrous cycle, (2) the nature and fate of the reserve follicles in normal ova ries as well as in ovaries treated with gonadotrophins on different days of the cycle (3) the relationship between the reserve follicles described by Greenwald and the luteinizing preantrum follicles of Knigge and Leathem (4) and finally the origin and changes of the interstitial gland in the normal and treated ovaries.

MATERIAL AND METHODS

Sexually mature golden hamsters were used in the present experiments The stages of the estrous cycle were deter mined by vaginal smears the postovula tory thick discharge was especially helpful in determining the various days of the cycle. The morning of metestrus recog nized by a thick vaginal discharge, was designated as day 1 the morning before the next expected ovulation as day 4 Pre-ovulatory and postovulatory periods were

determined by removing one ovary between 7 and 12 P M on day 4 Subsequently the females were caged with fertile males and the vaginae checked the next morning for spermatozoa Hamsters which had two consecutive four day cycles were divided into various groups The ovaries in the first group were from untreated animals killed on different days of the estrous cycle Other animals were injected sc with 60 I u pregnant mares serum (PMS) on day 1 and killed on days 2 3 4 or on days 1 and 2 of the next cycle The animals in the third group were given 60 I.u PMS on day 4 at 9 A M and killed at 10 P M of the same day or on days 1 2, 3 or 4 of the next cycle or on days 1 2 or 3 of the third cycle The animals in the fourth group were not given PMS but were injected with 20 I u human chorionic gonadotrophin (HCG) on day 2 Some of the hamsters were killed 10 hours after the injection of HCG and others killed on day 3 The histochemical techniques for lipids previously reported (Guraya and Greenwald '64a '64b) were also employed in the present study

OBSERVATIONS

a *Follicular development in the normal ovary*

The histological details of follicular development will be omitted as they are similar to previous observations (Greenwald '62a) The current report will be concerned mainly with the histochemistry of normal and atretic follicles of all sizes Frozen gelatine sections colored with Sudan black show both preantral and antral follicles containing various amounts of lipids From the amount and nature of lipids follicles can be distinguished as normal and atretic follicles.

Normal follicles Normal preantral follicles possessing one or many layers of granulosa cells are present in large numbers on all days of the estrous cycle Some of the large preantral follicles begin to increase in size on the night of day 4 and develop antra on day 2 of the next cycle The antra further grow in size during days 3 and 4 Such vesicular follicles which thus appear from days 2 to 4 are the cyclic developing follicles

The granulosa cells of the normal pr[illegible] antral and antral follicles contain lipi[illegible] in the form of granules, rods, spheres a[illegible] heterogeneous bodies of different [illegible] (figs 2, 3 and 9) The histochemical r[illegible] actions of the lipid bodies are the same [illegible] reported for the lipids of normal granulo[illegible] in rat, bat, cat, dog and opossum (Gur[illegible] and Greenwald, '64b) They consist [illegible] phospholipids However some lipid bodi[illegible] of normal granulosa in the hamster ar[illegible] also stain violet in Nile blue indic[illegible] ing the presence of neutral fats Su[illegible] lipid bodies also color intensely in Sud[illegible] III Sudan IV Fettrot and oil red [illegible] methods described by Pearse ('60) Th[illegible] indicates that some of the lipid bodies [illegible] contain triglycerides. Such lipid bodi[illegible] also stain blue-green after the Schultz re[illegible] used according to Gomori ('52) The blu[illegible] green color fades away after some [illegible] This reaction further reveals the [illegible] and its esters in some of the lipid bodi[illegible] The histochemical reactions of lipid bodi[illegible] in normal granulosa indicate that th[illegible] consist of mainly phospholipids with [illegible] amounts of triglycerides, and cholester[illegible] and its esters. Cholesterol and its est[illegible] were not demonstrable in the granulosa [illegible] normal preantral and antral follicles [illegible] ing preovulatory and postovulatory peri[illegible] when the interstitial tissue is also deple[illegible] of cholesterol and its esters.

The theca of preantral follicles (wit[illegible] many layered granulosa) is well develop[illegible] but it is not as hypertrophied as in se[illegible] follicles The sudanophilic lipid bodi[illegible] which are sparsely distributed in the the[illegible] of all follicles, stain positively in a[illegible] haematein followed by a negative reac[illegible] in control material extracted with p[illegible] dine. This indicates that the lipid gran[illegible] of the theca consist of phospholipids [illegible] the Nile blue technique they stain [illegible] revealing the acidic nature of the phos[illegible] lipids. However some lipid granules [illegible] the theca of antral follicles stain viole[illegible] Nile blue suggesting as well the pres[illegible] of neutral lipids. These lipid granules [illegible] color more intensely in red Sudan [illegible] than the rest of the lipid granules, [illegible] demonstrating traces of triglycerides [illegible] addition to phospholipids. The lipid gr[illegible] ules of the theca give a negative reac[illegible] for cholesterol and its esters. No [illegible]

differences have been found in the ferentiation and development of theca follicles in the same size range. The id bodies of both granulosa and theca completely dissolved after pyridine ex as determined from negative re ion in Sudan black.

Atretic follicles. Atresia affects follicles all sizes. Preantral follicles become on all days of the estrous cycle ile the antral follicles, show the first of atresia on day 3.

With the start of atresia, dramatic anges occur in the amount and nature lipids (figs. 1, 2, 3–6 and 10–13). The osa of atretic preantral and antral becomes heavily loaded with su- lipid droplets of various sizes, hich react positively with Nile blue rious red Sudan dyes and Schultz test. e positive reaction with acid haematein comes weaker during progressive stages atresia. The various histochemical re tions indicate that atresia leads to ex ssive storage of neutral fats (triglycer es) and cholesterol and its esters, and to decrease in the amount of phospholipids e latter mostly constituted the lipids in e normal granulosa. The granulosa of e preantral follicles is slightly more re- stant toward atresia than that of antral llicles which show a rapid regression and sintegration. The granulosa and its lipid cumulations in both preantral and an al follicles gradually degenerate and dis- pear.

The regressive changes in the granulosa both preantral and antral follicles are osely accompanied by specific changes in e theca which gradually hypertrophies figs. 1, 3–6 and 10–13). Coarse lipid ac umulations formed by necrosis of the anulosa can be observed in the center of ch hypertrophied thecae which also start oring fine lipid granules consisting of st phospholipids and then triglycerides. nally when the granulosa and its lipid cumulations have disappeared the cells the hypertrophied theca closely resem- the interstitial cells of the ovary simul their lipids also react positively cholesterol and its esters. The hyper d thecae of atretic preantral folli form patches which are loaded with danophilic lipid droplets and resemble the preantral follicles in size as the thecal cells now have occupied the space vacated by the gradual resorption of granulosa cells.

The vesicular follicles which escape from atresia on day 3 ovulate on the night of day 4 and give rise to cyclic corpora lutea which are fully differentiated on day 1 of the subsequent cycle. On days 1 and 2, the cyclic corpora lutea show sudano- philic lipid droplets which give positive reactions for phospholipids and triglycer ides. On day 3, the corpora lutea contain increasing numbers of lipid droplets some of which also indicate the appearance of cholesterol and its esters. Further in- crease in lipids on day 4 is due to the stor age of more triglycerides and cholesterol and its esters (fig. 7) as the reaction for phospholipids becomes very weak. In the subsequent cycle the cyclic corpora lutea of the previous cycle are reduced to small scars, the central parts of which are filled with abnormal lipid accumulations con- sisting of mainly triglycerides and choles- terol and its esters.

Interstitial gland. The interstitial gland is well developed in the hamster ovary. It occupies all of the ovary except for the follicles and corpora lutea. Connective tis- sue divides the interstitial gland into patches of different sizes (figs. 1 and 2). In ovaries removed on days 2, 3 and 4 the interstitial gland is loaded with sudanophilic lipid droplets consisting of phospholipids, triglycerides, and choles- terol and its esters (figs. 1 and 8).

In the hamster ovary follicular atresia is closely related to the formation of inter stitial gland which originates by hypertro- phy of the theca of atretic preantral and antral follicles as already described. The granulosa of these follicles stores lipid droplets but ultimately disappears without contributing to the interstitial gland.

The lipid droplets of the interstitial gland do not show any change in their amount on the different days of the es- trous cycle with the exception of the pre- ovulatory and postovulatory periods. Dur ing the preovulatory period (7–12 p.m. on day 4) the lipid droplets are mobilized from the interstitial gland and this is ac companied by increasing vascularity of the interstitial gland. Complete depletion of

the lipid granules did not occur which may be attributed to partial mobilization as well as formation of new lipid granules. The postovulatory ovaries (4–11 a.m. on day 1) also show less lipids especially cholesterol and its esters. On day 1 the lipids are gradually restored in the interstitial gland and on day 2 the tissue is loaded with lipid droplets consisting of phospholipids, triglycerides and cholesterol and its esters. The lipid accumulations due to degeneration of granulosa and corpora lutea do not show any change in their amount and histochemistry as they continue to give positive reactions for neutral fats and cholesterol and its esters.

b. *Effects of PMS and HCG on the hamster ovary*

Follicles. Ovaries removed from hamsters which were given 60 I.U. PMS on day 1 and killed on days 2 and 3 contained more than the normal number of vesicular follicles (fig. 2). Correspondingly the normal preantral follicles of medium and large size which were present in large numbers in the untreated ovaries at a similar stage were missing. The granulosa of normal follicles in the PMS-treated ovaries seems to contain less lipid bodies than in the untreated ovaries. The Schultz reaction also becomes more or less negative. This indicates that after PMS-treatment the lipid metabolism of the granulosa is slightly stimulated.

The atretic preantral follicles of various sizes, which were already present in the ovaries at the time of PMS injection, *did not show any change in their development* and histochemistry (fig. 2). They continued to contain lipid droplets composed of triglycerides, cholesterol and its esters and sparse phospholipids. Some of the vesicular follicles in the PMS-treated ovaries also became atretic on day 3 as described in the untreated ovary and showed the same stages of regression accompanied by degeneration of granulosa cells and hypertrophy of theca. Numerous follicles from the ovaries treated with PMS on day 1 ovulated by midnight of day 4 of the same cycle or day 1 of the subsequent cycle. Some preantral follicles which had a single-layered granulosa at the time of treatment, were also stimulated in the PMS-treated ovaries as a number of follicles having 1 to 4 layered granulosa appeared on day 3. The corpora lutea formed from follicles stimulated by PMS showed the same histochemical changes in lipids as described for the cyclic corpora lutea.

Ovaries treated with PMS on days 2 or 3 revealed the same changes in the follicular apparatus as described in the ovaries of hamsters given PMS on day 1. However, the normal preantral follicles, which were stimulated by PMS, did not attain the large size of the vesicular follicles present at the time of injection. The numerous follicles, which were stimulated by PMS between days 2 and 3, lengthened the estrous cycle as they ovulated between days 2-3 of the subsequent cycle. This revealed that the follicles stimulated by PMS require a definite time for maturation before they can be ovulated. The vesicular follicles developing at the time of PMS injection on day 2 or 3 became atretic. Further details of follicular development in PMS-treated ovaries are the same as described by Greenwald ('62a).

In the ovaries of hamsters injected with HCG at day 2, no conspicuous effects on the follicles were noticed. Normal and atretic follicles of all sizes, were observed.

Interstitial gland. The interstitial gland in the ovaries of hamsters injected with either HCG or PMS on days 2 or 3 showed a conspicuous reduction in the amount of sudanophilic droplets (figs. 2, 3 and [illegible]); this was also accompanied by a corresponding decrease in the Schultz reaction for cholesterol and its esters. Complete depletion of lipid droplets from the interstitial gland was not achieved due to the fact that new lipid droplets originated at the same time as mobilization. Both HCG and PMS treatments caused considerable luteinization and hypertrophy of the interstitial gland.

DISCUSSION

The histochemical techniques for lipids differentiate normal and atretic follicles of all sizes in the hamster ovary. The granulosa of normal follicles contains lipids consisting of mainly phospholipids; small amounts of triglycerides and cholesterol and its esters also occur in some lipid bodies. The phospholipids require both

um ions and postchroming for adequate ...ation. Such lipid bodies consisting of ...osphollpids were described in the gran... ...losa of normal follicles in other mammals ...uraya, '64a; Guraya and Greenwald ...4b). However Knigge and Leathem ...56) did not observe lipid bodies in the ...anulosa of normal hamster follicles. The ...pid bodies of normal granulosa in mam...mals correspond to the multivesicular ...odies described by electron microscopists ...Guraya '64a).

The significance of the sparse triglycer...ides and cholesterol and esters present in ...e normal granulosa of hamster follicles ...ld not be determined. They are not ...ound in the normal granulosa of rat bat, ...t, dog and American opossum (Guraya ...d Greenwald '64b) whereas they appear ...uring follicular atresia in these species. ...is possible that utilization of triglycer...ides and cholesterol and its esters in the ...ormal granulosa of hamster follicles is a ... process thus resulting in their accu...ation. Their storage is slightly re...uced after the injection of PMS. Choles...l and its esters also disappear from the ...nulosa of all normal follicles during the ...reovulatory and postovulatory periods ...ost likely because of the high levels of ...onadotrophins during this time. Simi...arly cholesterol and its esters are de...leted from the interstitial gland at this ...tage.

Cholesterol and esters appear in the ...yclic corpora lutea of the hamster at day ... after which regression occurs very rap...idly simultaneously the corpora lutea ac...cumulate triglycerides. Cholesterol and ...sters were not observed in the current ...yclic corpora lutea of the rat (Deane '52 ...uraya, '64b). However the corpora lutea ...f the previous two cycles in the rat show ...holesterol and its esters. The differences ...i lipid activity between the cyclic corpora ...a of the rat and hamster appear to be ... to the rapid degeneration of luteal ... in the hamster. It is perhaps of sig...ificance that the regression of the corpora ...tea at day 3 of the hamster estrous cycle ...oincides with the onset of atresia in some ...f the larger developing follicles (Green...ld, '62b).

Many normal large preantral follicles ... present on all days of the hamster estrous cycle. They were stimulated to ovulate in animals injected with PMS on different days of the cycle. These follicles undoubtedly represent the so-called "reserve follicles" of Greenwald ('62a) who also stated that they were smaller than 267 μ at the time of PMS treatment and normally would have existed in this size range during the ensuing estrous cycle. The current study as well as the previous investigation of Greenwald, indicate that the hamster ovary develops numerous follicles during the first phase of follicular growth, which are potentially capable of development. The biphasic pattern of follicular growth, which is the result of some physiological differences is now well recognized (references in Knigge and Leathem). In the current study it was not determined why the hamster ovary develops more follicles during the first phase than the ten follicles that ultimately form an antrum during the second stage of follicular growth. Treatment with PMS suggests that large preantral follicles do not normally enter the second phase of growth because of the lack of endogenous gonadotrophins which are only sufficient to stimulate ten follicles per ovary to undergo further growth. The role of pituitary gonadotrophins in antral formation has been reported in a number of previous studies. Smith ('30) and Swezy ('33) believed that follicular development proceeds to antrum formation in the absence of the hypophysis whereas Williams ('44) and Paesi ('49) felt that gonadotrophins may be involved to some degree. Hisaw ('47) has suggested a system of self-contained organizers which account for early follicular growth. If Hisaw's suggestion is followed then there seems to be an imbalance between the organizers, which differentiate numerous follicles during the first phase, and the pituitary FSH content which stimulates only ten follicles during the second phase.

Beside the normal follicles atretic follicles of various sizes are present at all stages. They can be distinguished from the normal follicles by the large amounts of triglycerides cholesterol and its esters and some phospholipids in their granulosa cells. Knigge and Leathem also stated that atretic preantral follicles stain with Su-

dan black B Nile blue sulfate and show positive reactions for cholesterol and phospholipids. In the PMS-treated ovaries, the atretic follicles were not affected and continued to show their neutral fats, cholesterol and its esters and little phospholipids This indicates that once atresia begins, the follicle cannot revert to its normal course of growth

During atresia, the granulosa and its lipids degenerate leaving behind the theca which hypertrophies and persists. Similarly the granulosa of atretic follicles in rat bat, cat, dog and opossum regresses but the theca remains intact (Guraya and Greenwald, 64b) Numerous types of atresia were identified in the hamster ovary in the histochemical studies of Knigge and Leathem According to them in atresia type I (occurring in preantral follicles) the granulosa is luteinized and persists while in type 2 (occurring in vesicular follicles) the granulosa degenerates and disappears. The luteinizing preantral follicles of Knigge and Leathem are identical with the "reserve follicles described by Greenwald which become atretic as a result of lack of endogenous gonadotrophins. The current study did not reveal the aberrant types of atresia observed by Knigge and Leathem.

The present study suggests that the cause of atresia in the large preantral follicles is due to insufficient FSH The cause of atresia in the vesicular developing follicles between days 3 and 4 could not be determined It occurred even in ovaries treated with PMS Hisaw (47) suggested that atresia occurs because of (1) a failure of proper differentiation of theca interna and (2) inadequate stimulation by LH On the other hand Burrows (49) believes that the ovulatory release of LH is mainly responsible for the atresia of small follicles. Knigge and Leathem observed the transformation of granulosa of preantral follicles into interstitial cells but according to them, the thecal cells do not give rise to interstitial tissue This is contrary to the present observations which clearly show that *only* the theca takes part in the formation of interstitial cells. Since Knigge and Leathem did not follow the different stages of atresia the large patches of interstitial tissue [illegible] the preantral follicles in size possibly [illegible] led them in assuming the transformation of granulosa into interstitial tissue. [illegible] similar histochemical nature of lipid droplets in the atretic granulosa and interstitial tissue also contributed to their interpretation. In the ovaries of rat, bat, cat, [illegible] and opossum the interstitial tissue [illegible] mostly derived from theca and [illegible] stromal cells of atretic follicles (Guraya and Greenwald '64b) In the dog [illegible] the germinal epithelium also takes part [illegible] the formation of interstitial tissue (Guraya and Greenwald '64b)

The interstitial gland, which is well developed in the hamster ovary is filled [illegible] sudanophilic lipid droplets of various [illegible] consisting of phospholipids, triglycerides and cholesterol and its esters. Such lipid droplets have also been described [illegible] the interstitial gland of other mammals (Guraya and Greenwald). Previous workers also reported lipids and cholesterol in the interstitial tissue of some mammals ([illegible] erences in Guraya and Greenwald [illegible] and '64b) With the techniques used [illegible] the current study it is difficult to determine the role of the interstitial lipid droplets in the endocrine physiology of the hamster The droplets were mobilized during the preovulatory period similar to that observed in the rat (Deane '33 Guraya and Greenwald '64b) They were also depleted from the ovaries of hamsters treated with HCG and PMS Depletion of lipid droplets containing cholesterol and its esters was also observed in rabbits injected with HCG (Guraya and Greenwald [illegible] The depletion of lipid droplets during the preovulatory period in rat, hamster and rabbit suggests the formation of some [illegible] sential steroids The lipid droplets of the interstitial gland have been suggested [illegible] precursors in the formation of estrogens androgens and progestins (for references see Guraya and Greenwald, '64b) [illegible] rect evidence for the formation of [illegible] steroids was presented in earlier studies However some indirect evidence for progesterone production by the interstitial cells of rabbit and rat ovaries has been recently presented by Taylor ('61) [illegible] et al ('59) and Hilliard et. al ('63)

ACKNOWLEDGMENTS

The senior author (S.S.G.) was a post fellow of the Population Council w York. This investigation was supported by research grant HD 00596-02 to lbert S. Greenwald from the United Public Health Service

LITERATURE CITED

rrows, H. 1949 Biological Actions of Sex ... 2nd. ed. Cambridge University Press, Cambridge.

...ne, H. W. 1952 Histochemical observations in the ovary and oviduct of the albino rat during the estrous cycle. Am. J. Anat., 91 363–413.

...man, G. 1952 Microscopic histochemistry. University of Chicago Press, Chicago

...eenwald G. S. 1961 Quantitative study of follicular development in the ovary of the intact or unilaterally ovariectomized hamster. J. Reprod. Fertil., 2: 331–361.

——— 1962a Analysis of superovulation in the adult hamster. Endocrinology 71 378–389

——— 1962b Temporal relationship between unilateral ovariectomy and the ovulatory response of the remaining ovary. Endocrinology 71 664–666.

...uraya, S. S. 1964a Histochemical studies on the yolk nucleus in the oogenesis of mammals. Am. J. Anat. 114 283–291.

——— 1964b Lipid changes in the corpora lutea in rat with some observations on the full term human corpus luteum. Anat. Rec., 148 374 (Abstract)

Guraya, S. S., and G. S. Greenwald 1964a Histochemical studies on the interstitial gland in the rabbit ovary. Am. J. Anat., 114 495–519.

——— 1964b A comparative histochemical study of interstitial tissue and follicular atresia in the mammalian ovary. Anat. Rec. 149 411–434

Hilliard, J. D. D. Archibald and C. H. Sawyer 1963 Gonadotropic activation of preovulatory synthesis and release of progestin in the rabbit. Endocrinology 72: 59–66.

Hisaw F. L. 1947 Development of Graafian follicle and ovulation. Physiol. Rev. 27 95–119

Knigge, K. M., and J. H. Leathem 1956 Growth and atresia of follicles in the ovary of the hamster. Anat. Rec., 124 679–707

Levy H. H. W. Deane and B. L. Rubin 1959 Visualization of steroid 3 β-ol-dehydrogenase activity in tissues of intact and hypophysectomized rat. Endocrinology 65 932–943

Paesi, F. J. A. 1949 The influence of the pituitary gonadotropins and of mixtures of pituitary and chorionic gonadotropins on the follicles in the ovary ? the hypophysectomized rat and normal mouse. Acta Endoc., 3 156–172.

Pearse A. G. E. 1960 Histochemistry. J. and H. Churchill Ltd. London.

Smith, P. E. 1930 Hypophysectomy and replacement therapy in the rat. Am. J. Anat., 45 205–273

Swezy O. 1933 Ovogenesis and its relation to the hypophysis. Science Press

Taylor F. B. 1961 Histochemical changes in the normal and experimentally treated rats. Acta Endocr. 36 361–374

Williams, P. C. 1944 Ovarian stimulation by oestrogens. Effects in immature hypophysectomized rats. Proc. Roy. Soc. B 132: 189–199

Figures 1–14 are photomicrographs from frozen gelatine sections of hamster ovary fixed in formaldehyde-calcium, postchromed in dichromate-calcium and colored with Sudan black. Gelatine sections were cut at 10 µ.

PLATE 1

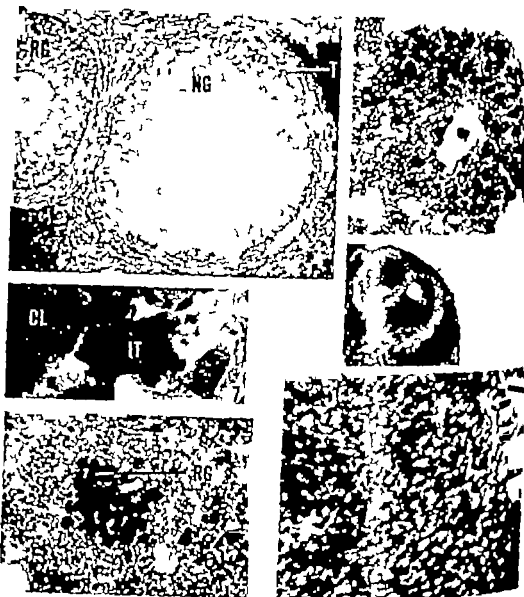
EXPLANATION OF FIGURES

1 A portion of untreated day 2 morning ovary showing interstitial tissue (IT) filled with sudanophilic lipid droplets, and many preantral follicles. Regressing granulosa (RG) of atretic follicles show lipid accumulations. × 38.

2 A portion of day 2 evening ovary treated with 60 i.u. PMS on day 1, showing antral follicles which have sparsely scattered heterogeneous lipids in their granulosa. Many preantral follicles seen in figure 1 have been stimulated to grow by the PMS. Follicles having regressing granulosa (RG) at the time of injections have not been affected. Most of the lipid droplets of the interstitial tissue (IT) have been depleted. The lipid accumulations formed by the degeneration of granulosa and corpora lutea remain intact. × 66.


IT
RG
1


CL
NG
IT
RG
2



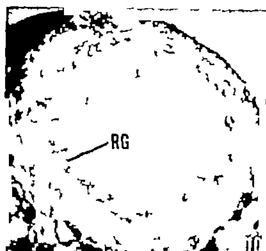
3 A section of normal and atretic preantral follicles, demonstrating the amount of lipids in the normal gran loss (NG) as well as regressing granulosa (RG). The atretic follicle illustrates the start of treala. The theca (T) contains sparsely scattered lipid bodies. × 250

4–6 Sections of atretic follicles demonstrating successive changes of atresia accompanied by the grad al regression of granulosa (RG) and hypertrophy of theca (T). Figure 4, × 86. Figure 5 × 165. Figure 6 × 250.

7 A portion of day 4 morning ovary demonstrating lipid material in the corpus luteum (CL) and interstitial tissue (IT) × 36.

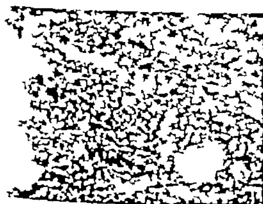
8 A higher powe view f interstitial tissue from day 2 ovary showing lipid droplets













9 A portion of normal antral follicle from day 3 ovary showing the lipid bodies in the granulosa (NG) and theca (T) × 280

10–13 Atretic antral follicles, illustrating the successive stages of atresia accompanied by gradual regression of granulosa (RG) and hypertrophy of theca (T). Figure 10, × 165. Figures 11–13, × 280.

14 A portion of interstitial tissue from day 3 ovary treated with 25 I.U. of human chorionic gonadotrophin. Animal killed 16 hours after injection of HCG. Note depletion of lipid material as compared with the untreated ovary shown in figure 8. × 440

hn Hunter on Spontaneous Intersexuality [1]

THOMAS R. FORBES
Department of Anatomy Yale University School of Medicine
New Haven, Connecticut

ABSTRACT Available information is assembled from published and unpublished accounts and pictures, and from study of surviving specimens, of cases of spontaneous intersexuality pseudohermaphroditism, and other reproductive anomalies in mammals and birds which were studied by John Hunter (1728–1793) An effort is made to interpret this information in terms of current endocrine theory

John Hunter (1728–1793) published) papers relating to spontaneous inter xuality in vertebrates one of them on) freemartin (1779) and the other on t reversal in the pheasant (1780) Both nd as classics. After nearly 200 years) observations of the great British bi ght are of continuing interest, even ugh a whole science of endocrinology s developed in the interval. A review of) studies on sex reversal seems in order search in London at the Library and interian Museum of the Royal College of rgeons of England disclosed not only e reproductive tracts of the freemartins ich Hunter described in print but other lated specimens prepared by or for unter as well as a number of unpubhed drawings of some of these animals d their organs.

The purpose of this paper is to describe unter's cases of spontaneous intersexual- r and related anomalies in birds and ammals in terms of the gross anatomy en in the available specimens and awings and to attempt to evaluate this aterial and Hunter's two published re- rts on vertebrate intersexuality (1779 '80) in the light of modern concepts of docrinology I am deeply indebted to ss Jessie Dobson Curator of the Hunrian Museum, and to Mr William R. Librarian, Royal College of Sur ons of England, for their unfailing kind advice and assistance and for to reproduce original drawings d records which illustrate this article.

MATERIAL

The reproductive tracts to be described dissected by or for John Hunter They are preserved in alcohol in sealed cylindrical glass jars some of them the original containers. The illustrations to be considered are, with one exception, on folio size sheets bound into Volume III of a collection in four volumes of original Illustrations of some of Hunter's specimens. These fine drawings, made for Hunter are the work of John Gilpin, William Bell, an artist named Roberts and possibly others. (Not all the drawings are signed.) Since the lines on the tissue paper overlays which label the original drawings are too faint for good reproduc tion, new outlines have been drawn and errors in identification of structures have been corrected.

The 1786 edition and Palmer's post humous 1837 edition of Hunter's Works were both illustrated by engraved reproductions of original drawings of Hunter's preparations. The drawings are clear but lack the vigor and interest of the originals. Plates 1–4 reproduce drawings which were copied as engravings. As far as I know none of the drawings which illustrate this paper have ever themselves appeared in print.

Catalogues of the specimens in the Hunterian Museum were prepared by William Home Clift (1775–1849) son of Hunter's youthful assistant and an early curator of the Museum (Clift, 1831) and by B. Thompson Lowne, a later curator (1872, 1893). I obtained helpful information from the catalogues and from legends to the plates in the 1786 and 1837 editions of Hunter's Works.

[1] This research was supported by grant ... from the National Science Foundation. The ... and its contents were ... aged by enemy action in May 1941.

OBSERVATIONS AND DISCUSSION

Cattle The freemartin has been known since antiquity (Forbes 46) but the fascinating natural experiment which results in this anomaly was not adequately elucidated until the classic studies of Lillie ('16 '17) and of Keller and Tandler (17) Lillie ('17) has succinctly described and explained this usually sterile female twin of a male co-twin:

> In such females, commonly known as free-martins, the internal organs of reproduction are usually predominantly male in character and the external organs are usually at least, of the female type; there are however considerable variations as will appear The conclusion was reached that the sterile free-martin is zygotically a female modified by the sex hormones of the male twin, which circulate in both individuals during foetal lif owing to secondary fusion of the chorions and anastomosis of the foetal circulation of the two individuals.

Lillie's interpretation, based on careful and very extensive observations, has been generally accepted. He reminds us that in the embryo the rudiments of the organs of both sexes are present. This, of course, is what makes possible the retention of heterosexual structures. Lillie was concerned with *fetal* freemartins the only postnatal specimen he studied was a seven week-old calf

The four bovine freemartins discussed by John Hunter (1779) were much older The first belonged to Charles Palmer Esq There is no drawing relating to this animal, and Hunter does not describe it. He does mention that, whereas the flesh of the freemartin is as tender as that of a spayed heifer or an ox, several of Palmer's neighbors found the meat from his animal "nearly as bad as bull beef The reproductive tract, preserved in the Hunterian Museum as specimen P 1543 is small and clearly that of a calf There are two testis-like gonads and two epididymides at the cephalic extremities of bilateral uterine tubes and vasa deferentia. The uterine fundus is slim. Attached near its caudal end are a pair of what seem to be seminal vesicles. The vasa deferentia open into the vagina near the cervix There are labia minora and a small clitoris. The urethra opens near the base of the latter The well developed masculine structures and the apparent toughness and strong [illegible] of the flesh suggest the effects of [illegible] large amounts of androgen.

"Mr Wright's Free-Martin was [illegible] years old and resembled an ox or spayed heifer rather than a bull or cow (plate [illegible] One of the two drawings of the reproductive tract, dissected by Hunter is reproduced as plate 2. Hunter called the [illegible] testes because:

> First, they were above 20 times larger than the ovaria of the cow and nearly the [illegible] the testicles of the bull, or rather of [illegible] of the ridgil, the bull whose testicles [illegible] come down. Secondly the spermatic [illegible] were similar to those of the bull, [illegible] of the ridgil. Thirdly the cremaster [illegible] passed up from the rings of the abdominal muscles to the testicles, as it does in the ridgil (Hunter 1779) [Richard Owen (Hunter 1837) suggested, "It is probable that these bodies were remains of the corpora Wolffiana."]

Grossly the gonads are unmistakably testicular in appearance (plate 2). The spermatic vessels are conspicuous because they have been injected with a reddish material. Each testis and its epididymis [illegible] still invested with tunica vaginalis [illegible] the back it is seen that the tunica has [illegible] opened and that half of one testis [illegible] been cut away on the long axis A [illegible] deferens extends a short distance [illegible] each epididymis and is then divided [illegible] ine tubes join the uterine horns, the [illegible] converge into the uterus. A large seminal vesicle is attached to each side of the uterus near its caudal extremity [illegible] uterine lumen appears very [illegible] Hunter says it ends blindly at the [illegible] The seemingly distended ducts of the [illegible] inal vesicles open with the vasa deferentia into the anterior vaginal wall, as does the urethra. The clitoris is small.

About 1909 microscopic sections of [illegible] least some of the sexual glands of Hunter's freemartins were prepared under the supervision of Sir Arthur Keith, the Curator of the Hunterian Museum (Berry Hart, '09) The exact origin of [illegible] of the sections of testis is not recorded but some of them came from the Wright and Arbuthnot (see below) freemartins Berry Hart states ('09):

Not the editor of an edition of [illegible] (Palmer, 1837).

> The special fact which emerges is that all) sexual glands are testes in Hunter ...es, that adjacent structures are epididy- ...and that in none of the sexual glands ...are present. *The characteristic testicular* ...is in the form of tubuli seminiferi, ...d in only one are spermatozoa present.

...le ('17 page 417) however doubts ...t masculinization of the gonad ever ...ceeds as far as the formation of sper ...zoa.

Mr Arbuthnot's Free-Martin was seven ...rs old. Hunter thought this animal ...s more entitled to the name of herma ...odite than the first [Mr Wright's] or the ...d [Mr Wells's] for it had a mixture of the parts, though all were imperfect. ...rawing of the live freemartin does not ...w teats or an udder but Hunter implies ...where that they were *present. He says* ...t the animal had both ovaries and ...tes he was mistaken about the former ...right gonad has been exposed by re- ... of its capsule or tunica vaginalis ...ate 3) The gonad is closely associated ...h an epididymis, is oval and about one ... inch long, and is one of those proven ...y to be a testis (Berry Hart, ...)

...by is another elongate dark body ...ich I cannot identify Hunter says of ...s and a similar but smaller mass on the ...t,

> Although I call these bodies testicles ...t they were only imitations of them, for ...when cut into they had nothing of the struc ...ure of the testicle; not being similar to any- ...thing in Nature, they had more the appear ...nce of disease (1779)

...e left body lies outside a tunica vagin- ...which envelops the left epididymis and ...p (1½ inches long) *testis.*

A well developed vas deferens extends ...each epididymis The seminal ves- ...are large and long and extend into ...mesometrium. The urethral opening is ...the anterior vaginal wall. The proximal ...of the uterine horns and all of the ...e fundus have been opened to show their lumina are extremely narrow

> "Mr. Wells' Free-Martin" was between ...and four years of age and looked more ...heifer than free-martins usually do. ...teats and udder were small compared ...h those of heifer but rather larger than ...ther of the former examples the begin- ...of the vagina was similar to that of ...cow but soon terminated little beyond the opening of the uterus, as in the first described. The vagina and uterus, to exter nal appearance, were continued, although not pervious, and the uterine part divided *into two horns, t the end of which were the* ovaria (Hunter 1779)

The ovaria are testes (plate 4) The left tunica vaginalis has been opened to expose the enclosed gonad and epididymis and a bristle demonstrates the lumen of the attenuated neck of the tunica. Ac tually the right tunica has also been opened, although this is not illustrated, and it is possible to see a right testis and epididymis. The vasa deferentia are inter rupted and fragmentary There are two large seminal vesicles The uterine horns and fundus are well formed. The body of the clitoris is attached along nearly all of its length. Its hypertrophy under the in fluence of fetal androgen has caused this organ *to acquire heavy transverse folds* (but not the sigmoid curvature shown by Hunter's artist in plate 4) The opened vagina shows the ostia of the vasa defer entia, major vestibular glands, and urethra (plate 5)

The volume of original drawings in cludes a side view of a fifth bovine free-martin that of Mr Lock (plate 6) Hunter's description *if* he wrote one of this animal seems not to have survived, and the reproductive tract is not now in the Museum, but Clift's catalogue (1831) refers to

> 242. The external and internal organs of generation of Free Martin. Mr Lock's. *See Museum Drawings. Hunterian.*

Hunterian means that the dissection was made by John Hunter himself. Presum ably this preparation was not described in his published article (Hunter 1779) be- cause the animal was a subsequent acqui- sition The dissected reproductive tract probably was lost when the Museum was bombed in 1941 The sketch of the animal itself, however is striking in its portrayal of a mixture of the external features of bull and cow

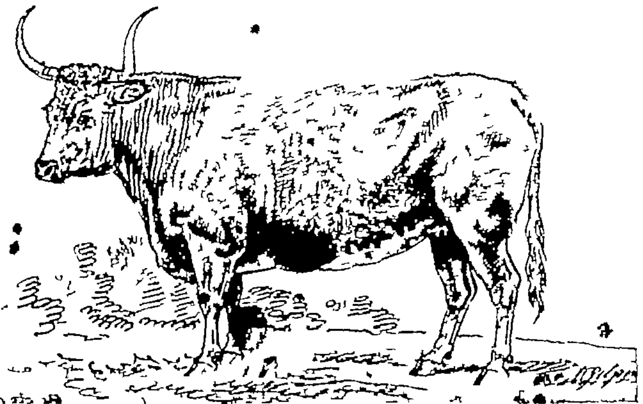
---

Probably as an example of the eighteenth century's cheerful disregard of spelling, this name appears as "Arbuthnot" in Hunter's paper (1779) and on a side view (not reproduced) of the freemartin, as "Arbuth- not" on the tissue paper overlay for the drawing of the free martin reproductive tract, and as "Albuth- not" on picture of the reproductive organs of [illegible] (plate 7).

PLATE 1

EXPLANATION OF FIGURE

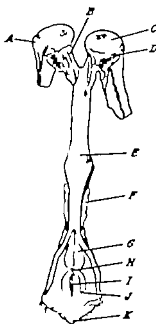
This fine drawing by John Gilpin of Mr Wright's freemartin shows body contours intermediate between those of the bull and cow Note also the well developed horns and rudimentary udder $\times$ 0.8.



Thomas H. Forbes

PLATE 2

EXPLANATION OF FIGURE



A, Epididymis
B Uterine horn
C Testis
D Probably heavily injected spermatic vessels
E, Uterine fundus
F Seminal vesicle

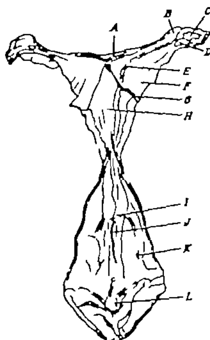
G Duct of seminal vesicle
H Bristles in orifices of vasa deferentia
I, Urethral meatus
J Opening of vestibular gland
K, Clitoris



Posterior aspect of the reproductive tract of Mr Wright' freemartin. The artist was William Bell. The posterior vaginal wall has been incised, and there are bristles in the orifices of the ducts of the seminal vesicle. The spermatic vessels have been injected. × 0.7

PLATE 3

EXPLANATION OF FIGURE



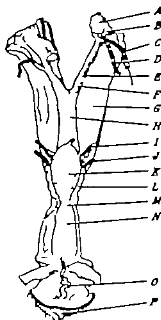
A, Uterine horn opened to show lumen
B Epididymis
C Testis
D Unidentified mass
E Vas deferen
F Mesometrium
G Cut edge of anterior layer of broad ligament
H Narrow lume of uterine fundus
I Openings of vasa deferentia
J Urethral opening
K, Opening of vestibular gland
L, Clitoris



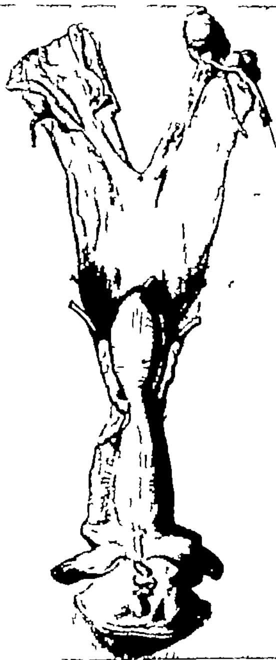
Posterior aspect f the reproductive tract of Mr Arbuthnot' freemartin, as drawn by William Bell. The vagina, the uterine fundus, the uterine horns, and one tunica vaginalis have been opened. × 0

PLATE 4

EXPLANATION OF FIGURE



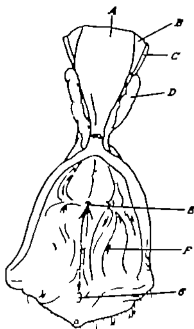
A, Testis
B Epididymis
C, Tunica vaginalis with bristle in lumen
D Spermatic vessels, probably injected
E, Segments of vas deferens
F Uterine horn
G Mesometrium
H Uterine fundus
I, Retrovesical canal
J Ureter
K, Bladder
L, Seminal vesicle
M Urethra
N Vagina
O Body of clitoris
P Glans clitoridis



Anterior aspect of the reproductive tract of Mr Wells' freemartin. Drawn by William Bell × 0·7

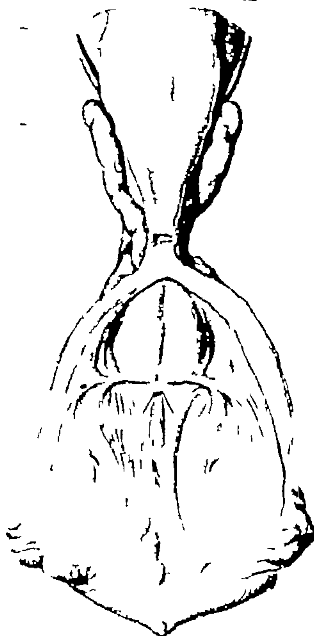
PLATE 5

EXPLANATION OF FIGURE



A Uterus
B Bladder
C Ureter
D Seminal vesicle

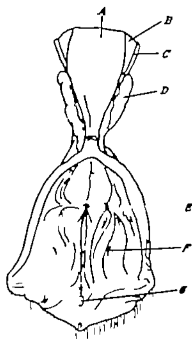
E, Bristles in ostia of vasa deferentia
F Ostium of major vestibular gland
G, Clitoris



Posterior aspect of part of reproductive tract of Mr Wells freemartin. The dorsal wall of the vagina has been incised [a]nd reflected, exposing the inner surface × 0.7

PLATE 5

EXPLANATION O FIGURE



A, Uterus
B Bladder
C Ureter
D Seminal vesicle

E, Bristles in ostia of vasa deferentia
F Ostium of major vestibular gland
G Clitoris

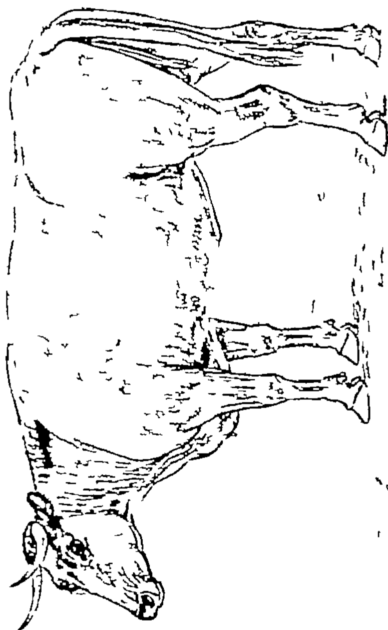


PLATE [illegible]

EXPLANATION OF FIGURE



A. "The terminations of the spermatic vessels pulled out of the Tunica Vaginalis which should be [illegible] ele from which the Gubernaculum is seen passing into the Vaginalis"

B. "Tunica vaginalis"

C. Epididymis, vas deferens, and spermatic vessels

D. "Are small interspersed bodies which may be either considered as [illegible] or Tubes, [illegible] in the Tunica or what is most probable ligaments [illegible] [sic] [illegible] edges of the Broad Ligament. Actually these are prob[illegible] rudimentary [illegible]

E. Fundus of bladder

F. Urethra

G. Seminal vesicle

H. "The orifice of the [illegible] urethra.

I. "The Common Tunic [illegible] [illegible] above [illegible]

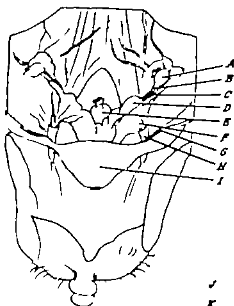
J. Glans clitoridis



Posterior view of reproductive tract of Mr Arbuthnot's hermaphrodite hog (see also foot note 4). Identification of some organs is quoted from tissue paper overlay of original. × 0.6.

PLATE 8

EXPLANATION OF FIGURE



A, Gonad
B Ovarian ligament
C, Uterine (Fallopian) tube
D Uterine horn
E, Rectum
F Round ligament
G Cut edge of abdominal musculature
H Processus vaginalis extending through inguinal canal
I, Bladder and body wall
J Prepuce
K, Glans



The internal reproductive organs of an intersexual donkey. "The Penis is dissected off from the Pubis and turne down. The Rings are dissected with Popart' [sic] Ligament which shew what is called the Gubernaculum in the Male or round Ligament in the Female passing through the ring and hollow for some way. The Bladder is turned out and over the Pubis for the better exposure of uterus or parts in the Pelvis. × 0.6.

PLATE 9

EXPLANATION OF FIGURE

No 9 The monstrous Lamb

Plate — Is a section of that Part of the skin of the Belly in which the Penis lays. The Scrotum, the Perinaeum, Anus and a little of the Tail, all of which gives us what are commonly called the external parts of Generation

A the cutting on of the Tail

B B the skin surrounding the anus not covered with wool with little [illegible] to the Anus

C the beginning of the imperfect canal where the urine flows out somewhat similar to the Female

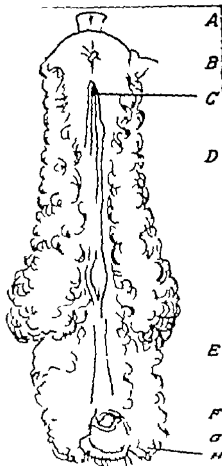
D D The continuation of the imperfect canal or groove as it passes along the Perinaeum

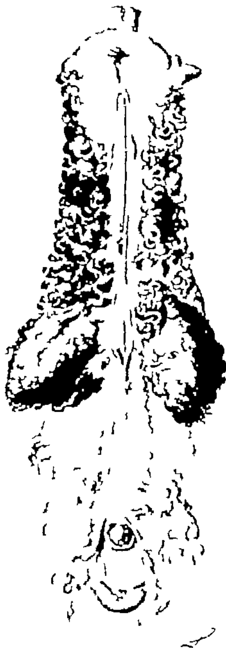
E The skin of the Belly covering the Penis not formed into a groove

F the Glans Penis

G The Prepuce

H H The split scrotum —

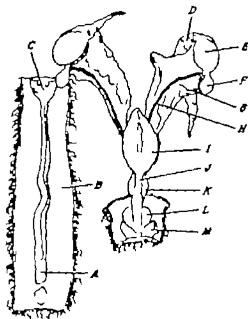




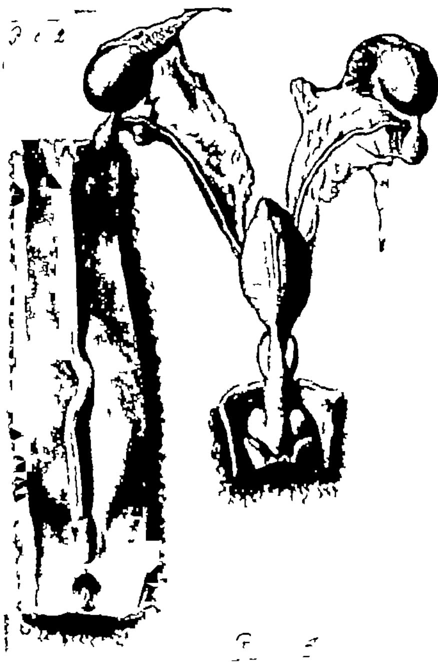
Original legend (× 0 6) copy of overlay and view of external organs of Mr Beadle lamb (× 0 6)

PLATE 10

EXPLANATION OF FIGURE



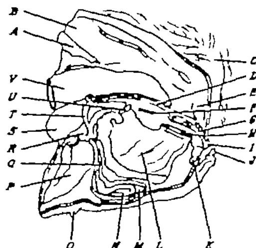
A, Glans of penis
B Deep surface of abdominal kin
C Union of crura of penis
D Epididymis
E, Testis
F Appendix testis (hydatid)
G Abdominal end of inguinal canal
H Persi tent paramesonephric (Müllerian) duct
I Bladder
J Membranous urethra
K, Prostate
L, Bulbourethral gland
M, Crus f penis



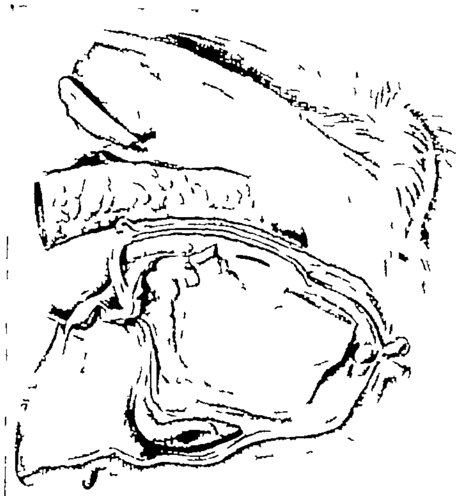
Mr Beadle lamb. On the left is the dorsal aspect of the penis and of the adjacent abdominal skin. On the right are the other reproductive organs. (The two portions of the tract were originally joined t C and M) × 0 7

PLATE 11

EXPLANATION OF FIGURE



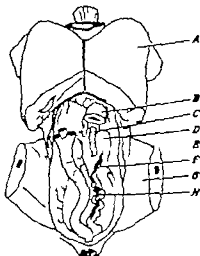
A, Sacrum
B Gl teal muscles
C, Tail, reflected dorsally
D Vagina and terus
E, Sphincter ani
F Urethra, opened. Bristle lies in urethral lumen and extends int upper vagin
G V gina
H, The cut urface of Iskium where it joined Ilium
I Orifice of vagina
J Clitoris
K, Cru of clitoris
L, The cut surface of the muscles arising from the Pubis, Ischium, & c.
M Head of epididymis
N Testis
O Nipple
P Peritoneum
Q Spermatic cord exposed by opening processus vaginalis
R, Internal inguinal ring
S Bladder
T Uterine horn
U The cut urface of the Pubis where it joined Ilium
V Rectum



Parasagittal section of pelvis of an adult "hermaphrodite" sheep. × 0 7

PLATE 12

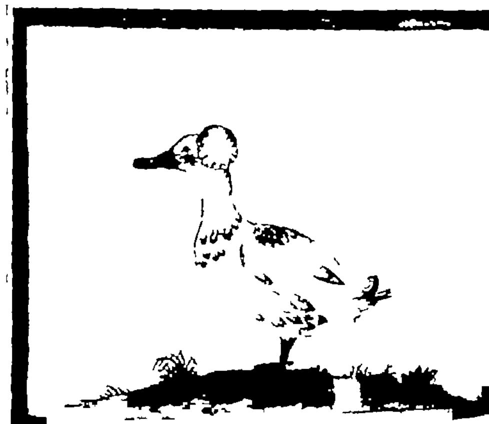
EXPLANATION OF FIGURE



A Pectoral muscles
B Upper digestive tract
C Left ovary
D Left kidney
E. Large intestine
F Fimbria of oviduct
G Thighs
H Oviduct



Ventral view of the reproductive organs of pheasant which had undergone transformation of its plumage from female to male Hunter says that the organs are those of normal female. × 0.8.



In an old Duck that had become a Drake in Feather I often observed that she made a noise like the Drake and at other times like the Duck as usual

This sketch of sex-reversed duck is ttributed to John Hunter The original is in watercolor I

Facsimile of note in Hunter' hand about this bird. In an old Duck that had become Drake in Feather I ften observed that she made noise like the Drak nd at other times like the Duck as usual. × 0 7

›ronary Arteries of Gallus Domesticus

FLORA E. F. LINDSAY AND HELEN J. SMITH
Anatomy Department, University of Glasgow Veterinary School, Glasgow Scotland

ABSTRACT The pattern of the coronary arteries of the domestic fowl is described. In the fowl heart the longitudinal sulci do not contain descending rami of the coronary arteries. The largest coronary vessels are the right and left deep coronary arteries, which early in their course come to lie on the ventral face of the I–V septum immediately below the endocardium. The circumflex arteries which occupy the corresponding coronary sulci are minor trunks. Differences in the relative distribution of the right and left deep coronary arteries allow recognition of three heart types
Heart Type Two i.e., right coronary artery dominance, is found to be the commonest;
Heart Type Three (left coronary artery dominance) and
Heart Type One (balanced coronary circulation) are less common.
Some details of the origin and course of the atrial, infundibular, conal and valvular arteries are given. The presence of homo-coronary and intercoronary anastomoses is noted.

The coronary vessels of the domestic wl receive little attention in the standard xt book. Kaupp ('18) gives a brief ther confusing description of the coronary arteries; Sturkie ('54) locates the ght coronary artery on the ventral surce of the heart and the left coronary on e dorsal surface and indicates that the rminal branches of these vessels anastoose freely Simons ('60) describes the ronary arteries as coursing over the surce of the heart.

Petren ('26) examined 139 hearts of fferent species of birds, including 64 wl hearts Myczkowski ('60) examined 7 hearts of several avian species and inuded 14 fowls in his survey The latter ro authors have described the ventricular teries in some detail, but disagree as to hether the superficial or deep rami contute the larger trunks. The atrial vessels em to have received less attention

Terminal anastomoses between right nd left circumflex vessels have been menoned by Petren ('26)

The histogenesis of the coronary arteries f the chick is described by Hughes ('42 3)

The present study was undertaken in ollaboration with colleagues using the omestic fowl in an investigation of atherotous conditions of the coronary vessels.

TOPOGRAPHICAL OBSERVATIONS

A general examination of the heart surface confirms that the circumflex coronary sulcus resembles that of the mammal and contains vessels surrounded by fat in the sub-epicardial connective tissue.

The longitudinal sulci, unlike those of the mammal, are not channels containing the descending rami of the coronary arteries, but shallow furrows marking the junction of septal and outer ventricular walls. Owing to the orientation of the heart *in situ* the left or ventral longitudinal sulcus courses obliquely on the ventral or anterior surface of the heart, crosses this surface above the apex, and becomes continuous with the right or dorsal longitudinal sulcus. The latter connects to the circumflex sulcus at a wide shallow depression which contains the termination of a large vena cordis media. The incisura apicis cordis does not necessarily correspond to the junction of left (ventral) and right (dorsal) longitudinal sulci (figs. 5 and 6)

In hearts fixed in systole the incisura occurs at about the junction of the lower and middle thirds of the right ventricular wall in those fixed in ventricular diastole it coincides with the lowest level of the right ventricular cavity and the longitudinal sulcus on the right border of the heart. In ventricular diastole the left

(ventral) longitudinal sulcus and the incisura apicis may be very poorly marked.

The aortic bulb shows three semilunar cusps and three sinuses aortae (valsalvae). *In situ* these sinuses are positioned as right and left anterior or ventral sinuses, and a posterior or dorsal sinus aortae.

The coronary arteries of the domestic fowl are usually described as being two in number a right or anterior and a left or posterior. Occasionally a third, more rarely a fourth vessel may be present. In the coronary vascular distribution a number of minor variations are common, but the main vessels seem to be arranged in one of three basic patterns. The difference lies mainly in the manner of distribution of the deep ventricular vessels and on the basis of recognition of this difference the terms Heart Type One Heart Type Two and Heart Type Three have been used.

In the following description the capital letters in brackets are the letters used to identify the principal vessels in the accompanying plates.

MATERIALS AND METHODS

Two hundred and ten hearts from adult birds of varying ages have been studied either by latex injection and subsequent dissection and/or erosion, or by radiographic preparations using Dionosil, Photogel or Micropaque alone, and as barium/gelatine mixtures the latter allowing for the "open heart" technique and dissection. Some specimens were prepared from separate hearts others by injection of the coronary vessels with the heart *in situ*. The injections were made via the sciatic artery the aorta, or one or both coronary arteries.

The methods used to "unroll" the [illegible] specimens are modifications of that [illegible] by Schlesinger ('38) differing in [illegible] interventricular septum is left intact. [illegible] serves to demonstrate radiographically [illegible] relationship of the larger arteries [illegible] interventricular septum.

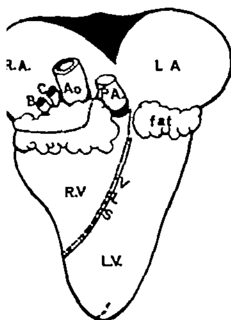
The manner of "unrolling" the heart [illegible] varied somewhat, depending upon [illegible] structures to be demonstrated. [illegible] the method used is to unwrap the [illegible] ventral) wall of the right ventricle [illegible] the rest of the heart. The left ventricle and sometimes the left atrium, are [illegible] opened and the heart gently flattened.

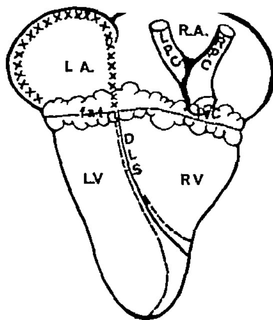
The first incision is begun behind the pulmonary artery and continued [illegible] the ventral wall of the right ventricle, [illegible] lowing the left or ventral longitudinal sulcus to the lower part of the right [illegible] dorsal longitudinal sulcus. The left [illegible] attachment of the right A–V valve is [illegible] rated. An incision along the right coronary sulcus, severing the right circumflex [illegible] "unwraps" the ventral wall of the right ventricle carrying the right circumflex artery with it. An incision is then made through the left ventricular wall [illegible] diately behind the upper part of the dorsal longitudinal sulcus and carried down [illegible] the apex of the heart. This incision can be extended up through the left atrial [illegible] or along the left coronary sulcus. The left ventricle is opened out (figs. 1 and [illegible]

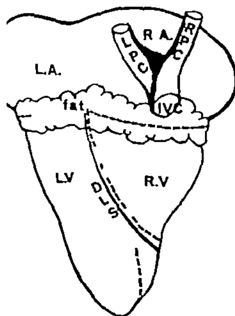
An alternative method, which makes [illegible] possible to leave the left attachment [illegible] the right A–V valve intact, is to begin the first incision through the right ventricle [illegible] the upper part of the dorsal longitudinal sulcus and continue parallel to the [illegible] tudinal sulci to just below the [illegible]

Abbreviations

A., Right coronary artery
A Right circumflex
A Right deep coronary
A Proximal ramus of A
A Distal ramus of A
A Ramus perforans of A
B., Left coronary artery
B Left circumflex
B[1] Left deep coronary
B[2], Interatrial ramus of B
A.O., Aorta
B.C., Brachiocephalic arteries
D.L.S., Dorsal (right) longitudinal sulcus
I.A.C., Incisura apicis cordi
L.A., Left atrium
L.V., Left ventricle
P.A., Pulmonary artery
R.A., Right atrium
R.A.V.V., Right atrioventricular valve
R.V. Right ventricle
S Sternum
S.S., Sinus septum
S.V. Sinus venosus
V.L.S., Ventral (left) longitudinal sulcus
V.V. Valvulae venosae
I.V.C., Inferior vena cava
L.P.C., Left precava
R.P.C., Right precava







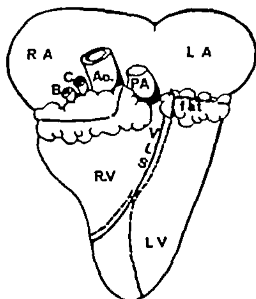


Fig. 1–4 Ventral and dorsal views of hen heart (semi-diagrammatic) Dotted lines – – – – indicate lines of incision in basic method of unrolling heart. × × × × Indicates one modification.

arteriosus severing the right septal attachment of the right A–V valve and thus allowing the "unwrapping" of the free wall of the right ventricle. The incision through the left ventricular wall is then begun behind and parallel to the upper part of the left or ventral longitudinal sulcus This is continued down to the apex of the heart and also partly along the left coronary sulcus (figs. 3 and 4)

The right coronary artery (A)

This trunk, 0 3 mm to 0.5 mm in length and 1 mm to 1.8 mm in diameter arises in the right (ventral) sinus aortae It divides into a smaller superficial or circumflex artery and a deep artery or ramus profundus.

The right circumflex artery (ramus superficialis dexter (A)) seldom exceeds 1 mm in length and has a diameter of 0.5 mm to 0 8 mm. It passes antero-ventrally between right auricle and conus arteriosus bifurcating as it reaches the coronary sulcus The smaller branch runs to the left, supplying the adjacent part of the right ventricular wall and terminates in two or three conal branches. The larger subdivision is the main continuation of the circumflex artery which takes a flexuous course in the right coronary sulcus toward the upper depression of the right (dorsal) longitudinal sulcus giving off atrial valvular and ventricular branches.

The atrial branches number five to seven, depending upon the number of major stems of musculi pectinati. They leave the circumflex artery and supported by the sub-epicardial fat of the coronary sulcus enter the overhang of the atrial wall and divide into ascending and descending vessels. The larger ascending branches are at first eccentrically placed in the musculi pectinati, then become more centrally placed and their divisions follow the pillars anastomosing with branches of the interatrial and left circumflex arteries they provide many interpectinate branches. The descending vessels supply the atrioventricular junction.

Ventricular branches — as many as eight to twelve of these are demonstrable They vary in calibre some being very fine tortuous vessels. All run ventrally parallel to the long axis of the heart, to supply the ventral (anterior) wall of the right ventricle. Usually they do not cross the left (ventral) longitudinal sulcus. (The blood supply to the most distal part of the ventral wall of the right ventricle is reinforced by vessels which pass upward over the ventral longitudinal sulcus, and which are derived from the deep coronary arteries right and left.)

The valvular branches are numerous and small, running distally into the distal muscular cusp of the right atrioventricular valve in the area of continuity with the anterior (ventral) wall of the right ventricle.

The right circumflex artery usually terminates by bifurcating into its last atrial and ventricular branches. The former may anastomose with the left circumflex artery — intercoronary anastomosis The last ventricular branch, or one of its subdivisions, quite frequently anastomoses with a branch of the ramus perforans of the right deep coronary artery — intercoronary anastomosis.

A variation of this arrangement may be found, in that either the right circumflex artery or its smaller left branch may arise independently from the aorta, alongside the right coronary artery in the right sinus aortae This probably constitutes the third coronary artery described by Petren ([illegible] as arising from the sinus aortae dexter in 12 of 49 specimens. In two of our specimens three divisions of the right circumflex artery were present, the middle one arising in common with the right deep coronary artery the others arose independently from the sinus aortae which consequently showed three orifices.

The right deep coronary artery (ramus profundus dexter (A)) is much longer than the circumflex division, being 7 to 16 mm in length and 1 to 1 4 mm in diameter It shows three patterns of distribution depending upon the heart type

Heart Type One that is a balanced circulation is less frequently found and will be described last. Heart Types Two (right coronary artery dominance) and Three (left coronary dominance) are the usually encountered and the description of these follows first.

In hearts of Type Two the right deep coronary artery supplies, as it does in the

e types, part of the anterior or ventral l of the right ventricle at its distal ler the right atrioventricular cusp and dorsal walls of both atria. In addition, his type it provides the major supply he I–V septum, the left ventricular and the apex cordis.

passes in a curve on to the right ven- face of the I–V septum, coming to lie subendocardial position in a furrow e junction of septum and aorta. Here minates by a bifurcation into a proxi- (A) and a distal (A) division. The trunk and the primary divisions are emely flexuous in hearts viewed in ricular systole these vessels straighten in ventricular diastole. The primary ions of the left coronary artery are st straight in both systole and diastole e ventricles.

fore dividing, the right deep coronary y gives off small branches to the sep- and to the right A–V muscular cusp valvular vessels enter the cusp at its extremity The septal branches anas- se freely with similar branches from left deep coronary vessels and the ular vessels bifurcate as they enter the , most of them running parallel to the axis of the cusp near its free margin. e proximal division (ramus proxi- s (A)) curves dorsally on the right r third of the I–V septum, to bifurcate l to the right septal attachment of I–V cusp; the ensuing branches divide arly and from here pass deeply and circling fashion into the dorsal wall e left ventricle. The terminals do not ally extend to the apex of the heart, area being supplied by the distal divi or in hearts of Type Three by the left coronary artery One branch of the r limb of the bifurcating proximal s has a rather different course and is ed here the ramus perforans (A) It trates the wall of the left ventricle pos- r to the right longitudinal sulcus pass- pward to divide into several branches, f which commonly anastomoses with minal of the left circumflex artery (coronary anastomosis) while another lly joins the last ventricular branch e right circumflex artery to form a coronary anastomosis. The ramus rans supplies the adjacent dorsal walls of both atria and the cusp of the right A–V valve via its right septal attachment. The valvular branches have a course and position similar to those derived from the main trunk of the right deep coronary with which they anastomose.

The distal division (ramus distalis (A)) runs toward the apex of the heart on the right ventral face of the I–V septum. It terminates as two or three major subdivisions left, middle and right, or it may take the form of a single trunk giving off side branches. The terminals supply a large part of the I–V septum and the left ventricular wall, including the apex or lower third, others pass upward into the lower part of the right ventricular wall.

Thus, in hearts of Type Two the deep division of the right coronary artery is well developed, providing many septal and left ventricular vessels the latter, passing deeply from the septum into the left (dorsal) ventricular wall and circling from right to left, constitute the major supply to the apex of the heart and the left ventricular wall.

In Heart Type Three the deep division of the right coronary artery is much reduced and the major supply to the left ventricular wall and the apex cordis is provided by the deep division of the left coronary artery

In a small number of the specimens examined in this series hearts of Type One were found, in which one cannot distinguish dominance of either left or right deep ventricular vessels a balanced circulation being established.

The left coronary artery (B)

This arises in the left sinus aortae and curves to the left and ventrally to arrive at the upper border of the left ventricle just to the left of the conus arteriosus Here it gives rise to deep branches (rami profundi) one to three in number and terminates as the left superficial or circumflex artery The trunk measures 0.8 to 1 4 mm in diameter and from 2 to 9 mm in length. It contributes several very small infundibular and conal branches directly Close to its origin there is given off a quite considerable vessel the interatrial artery Occasionally this vessel may arise

is noted in the fowl. This does not seem to have been recognized previously

ACKNOWLEDGMENTS

The authors wish to acknowledge the skill and patience of Mr A. Finnie in the preparation of the photographs, and to thank Miss J Nicol M.S.R. for many of the radiographs. Thanks are also due to Mr J Winning for some of the heart preparations.

Text figures by Miss S White, B V.M.S M.R.C.V.S

LITERATURE CITED

Baroldi, G O Mantero and G. Scomazzoni 1956 Collaterals of the coronary arteries in normal and pathologic hearts. *Circul. Res.*, *4* 223–229

Damodaran, S. 1959 Coronary arterial pattern in domestic animals. Indian Vet. Journal, *36* 249–300

Gregg, D E. 1950 Coronary Circulation in Health and Disease. Henry Kimpton, London. Chap 2, 26–27

Hughes, A. F W 1942/43 Histogenesis of the arteries of the chick embryo. J Anat., 77 282.

Kaupp B. F 1918 Anatomy of the Fowl. 206–209 W B. Saunders & Co., Philadelphia and London.

Marius, J 1889 Some observations on the development of the chick heart. Arch. Biol. (Paris) Vol. 9 403–418.

Moore, R. A. 1930 Coronary arteries of the [illegible] Am. Heart J 5: 743.

Myczkowski, K. 1960 Morphology of the coronary arteries of fowl and some wild [illegible] Folia morphologica XI, No. 1.

Petren, T 1926 Die coronararterien des [illegible] herzen. Morph. Jahrb., [illegible]

Pianetto, M. B. 1939 Coronary circulation of the dog. Am. Heart J 18: 403.

Quiring, D P 1933/34 [illegible] chick heart. J Morph., [illegible]

Reiner L., J Molnar, F A. [illegible] Freudenthal 1961 Interarterial coronary anastomoses in neonates. Arch. Path., [illegible] 134

Romanoff A. A. 1960 The Avian Embryo Chap. 8, 646. MacMillan Co., New York

Schlesinger M. J 1938 An injection plus dissection study of coronary artery occlusions and anastomoses. *Am. Heart J.*, *15* [illegible]

——— 1940 Significant variations in the anatomic pattern of coronary vessels. [illegible] Pub. No. 13 61.

Simons, J R. 1960 Biol. & Compar. Physiol. of Birds. Vol. *1* 353. Ed. A. J. Marshall, Academic Press, New York and London.

Spalteholz, W 1923 Arch. Entwicklungsmech. Organ, 52: 490–531.

Sturkie, P D 1954 Avian Physiology Chap. 4 63. Comstock Publishing Associates, New York.

Tonge, M. 1869 Trans. Roy Soc., [illegible] 412.

PLATE 1

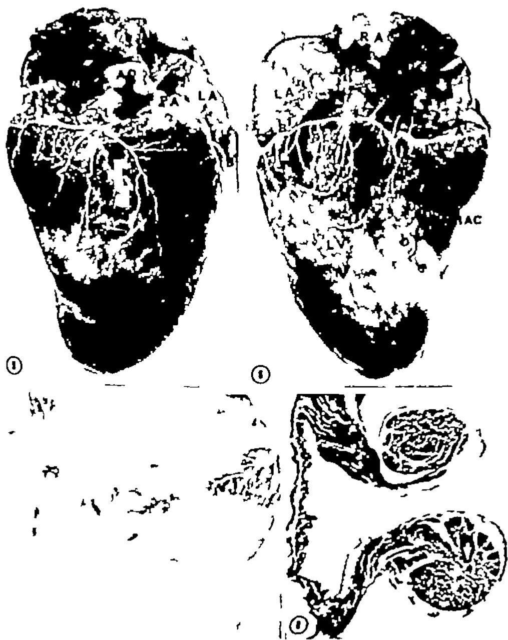
EXPLANATION OF FIGURES

5 Barium/gelatine injected specimen. Ventral view ▶ indicates atrial arteries.

6 Barium/gelatine injected specimen. Dorsal view ▶ indicates atrial arteries.

7 Barium/gelatine injected specimen. Dorsal close-up of coronary sulci. ▶ Indicates atrial branches of left circumflex to region of sinus venosus Dotted line - - - - encloses area of anastomoses between branches of B A and A

8 Section through musculi pectinati. H. and E. Arrow indicates large atrial artery


AO
PA
LA
RA
LA
AC
LV
1
2
3







9 Barium/gelatine injected pecimen. Ventral view of base of heart.

10 Barium/gel tine injected specimen. View of interventricular septum after the anterior wall of R.V has been freed and reflected round the longitudinal sulci. This shows the close relationship of A and B¹ t the septum. △ Indicates limit of interventricular septum.

11 Barium/gelatine injected pecimen. Right extremity of R.A.V.V. R.V = reflected wall of RV ▷ Indicates valvular artery of A ---- Indicates junction of I-V septum and LV wall.



Photoradiograph of barium gelatin injected and "unrolled" heart, Type Two (right coronary artery dominance) — — — D^1 outline of area of I–V septum. D^2 area of anastomosi between right and left circumflex and ramus perforans

PLATE 4

EXPLANATION OF FIGURE

13 Photoradiograph of barium/gelatine injected and partially "unrolled" specimen of Heart Type Three (left coronary artery dominance) R.V — its anterior wall cut and partly freed along the longitudinal sulci. L.V — opened out. × × × — Indicates the distal border of R.A.V.V. All other lettering explained in list of abbreviations on page 302.


AO
B1
B2
V
A
L
V
13



14 Heart Type One. Balanced coronary circulation.

ability and Differentiation of Human Trophoblast Organ Culture

TIEN WEN TAO AND ARTHUR T HERTIG
Department of Pathology Harvard Medical School, Boston, Massachusetts

ABSTRACT Organ culture of 15 immature human placentas — obtained at thera peutic abortion of 5–22 week gestations — was carried out in medium consisting of horse serum, 20%; NCTC 109 15%; and balanced salt solution, 65% to which was added 100 I.U. of penicillin per ml of culture medium. Minced placental fragments were placed on filter paper laid across glass beads within Petri dish; the medium barely covering the beads. Moist incubation was carried out t 35–36°C in mixture of 5% CO_2 and 95% O_2 for 4–6 weeks; the medium being changed every 2–3 days. Radioautographic techniques using 1–2 μc of methyl H^3-thymidine per ml of medium as well as routine histological techniques were employed. These showed that Langhans epithelium or cell masses — cytotrophoblast — differentiated or metamorphosed into new syncytiotrophoblast. Only cytotrophoblastic nuclei took up the radioactive thymidine which ppeared later in the new syncytiotrophoblast. Ordinary histologic preparations showed that the new" syncytiotrophoblast resembled the original syncytiotrophoblast by virtue of its position (between original cyto- and syncytiotrophoblast) together with its loss of cell boundaries and its acquisition of intracellular vacuoles nd cytoplasmic chromophilia. The cytotrophoblast remained viable for three weeks and then gradually decreased in amount with corresponding increase in the amount of new" syncytiotrophoblast. The latter was the predominant though necrotic tissue seen at six weeks. These techniques are tools for investigating the many aspects of growth, differentiation and endocrine function of human trophoblast.

lthough cells from the human placenta e long been studied in tissue and cell ture preparations (Guggisburg and Neu ler '28 Friedheim '28; Jones et al. 43 wart et al. 48 Thiede 61) organ ture appears to offer a more promising e for the investigation of the differentia n and endocrinology of the placenta ao and Hertig, '61; Tao '62) The great itation of these tissue and cell culture hniques is the morphological and func nal instability of many types of cells ring the course of cultivation (Parker h Levintow and Eagle '61) Thus, in e case of placental cultures, the cells lose st of their distinguishing morphological atures (Stewart et al. 48; Thiede '61 o '62) and also their ability to secrete nadotropic hormone (Tao '62) Organ lture on the other hand, maintains the tegrity and organization of the tissues d is generally more suitable for the servation of function This *in vitro* vironment, therefore p rmits analysis of llular growth and differentiation and eo secretory potential f the trophoblast

In the present report placental specimens obtained at 5 to 22 weeks of gestation were studied in organ culture for 4 to 6 weeks. Evidence is presented indicating a transformation of Langhans cytotrophoblast to syncytiotrophoblast based upon cytological changes and radioautographic studies with tritiated thymidine Morphological aspects of the viability of the var ious cellular elements are also described with special emphasis on trophoblast.

MATERIALS AND METHODS

Fifteen specimens of normal human placenta were obtained at the time of therapeutic abortion by curettage hyster otomy or hysterectomy for a variety of medical and psychiatric reasons. The gestational ages ranged from 5 to 22 weeks. Specimens were prepared under sterile conditions for organ culture usually within 1 to 2 hours after surgical removal.

The study was part of the researches in partial fulfillment of the requirements for the Degree of Doctor of Philosophy, Harvard University 1962. The work was supported by USPH Training Grant 2G-113, USPHS Research Grant C 3451 now designated as HD-00137

Through gross dissection the villi were isolated and minced into fragments of approximately 1 mm After washing in physiological saline to remove blood and debris the fragments were ready for organ culture. Random samples were taken for histological examination

For the preparation of organ culture a single layer of glass beads 4 mm in diameter was placed in a glass or plastic petri dish and barely covered by culture medium On top of the beads were laid strips of filter paper (Whatman filter paper no 1 or no 2) onto which the minced fragments were transferred (fig 1) Thus the tissues were in contact with but not immersed in the medium Incubation was carried out at 35 –36 C in an incubator gassed with a mixture of 5% CO_2 and 95% O_2 (The atmosphere was kept moist by the presence of a dish of water in the incubator) A gas mixture of 5% CO_2 and 95% air was also found to be satisfactory The culture medium was renewed every 2 to 3 days Two to four fragments were removed for histological examination daily during the first week, and then every 3 to 4 days throughout the rest of the cultivation period of 4 to 6 weeks duration. They were fixed in cold Rossman s fixative processed through paraffin embedding sectioned serially at 6 μ and stained in accordance with the periodic acid Schiff (PAS) procedure (Pearse '60)

For radioautographic studies, organ cultures were prepared in the same manner as described Methyl H³-thymidine was added to the culture medium in the concentration of 1 to 2 μc per ml of medium. Placental fragments were incubated in the radioactive medium for varying periods of time ranging from one hour to two weeks Some cultures after 6–24 hours of such incubation with H -thymidine were thoroughly washed with physiological saline and transferred for further cultivation into medium containing no isotope Fragments were removed periodically thereafter at 1 to 3 day intervals for 1 to 2 weeks All fragments for radioautography were fixed in Serra s fixative for one hour and processed through paraffin impregnation and embedding Mounted tissue sections, serially sectioned at 5 μ were stained in accordance with Feulgen s procedure for DNA (Swift, '55 Pearse '60) and [illegible] dried after water rinse. The slides were then dipped briefly in pre-melted [illegible] Nuclear Track emulsion NTB-3 in the [illegible] using the dipping technique described [illegible] Joftes and Warren ('55) After [illegible] the appropriate exposure time [illegible] be 2–3 weeks at approximately [illegible] best results) the slides were developed [illegible] 18 –20 C in Kodak Superkodalith [illegible] oper for three minutes washed in [illegible] Stop Bath SB-1a for 15 seconds [illegible] acid fixer for five minutes and then [illegible] in running water for 2 5 minutes [illegible] were counterstained with 0 1 [illegible] green dehydrated in graded alcohols [illegible] mounted in permount. The end result [illegible] a thin layer of photographic film [illegible] imposed on the tissue section. [illegible] tions of morphological structures and [illegible] ization of incorporated tritiated thymidine could thus be made simultaneously

RESULTS

Langhans cytotrophoblast

During the first 24 hours of cultivation no significant morphological changes [illegible] place except for the increased nuclear [illegible] sity of syncytiotrophoblast (compare [illegible] 2 and 3) Mitotic activity was reflected [illegible] the nuclear incorporation of tritiated thymidine into DNA (figs. 8 and 9)

Regional aggregation of some cytotrophoblastic cells started to appear [illegible] early as 24–48 hours in culture [illegible] cases however it became significant [illegible] abundant only after 5–6 days (fig [illegible] Intracellular vacuoles of various sizes [illegible] also seen as early as 24–48 hours [illegible] became more abundant and of [illegible] size in older cultures. Such vacuoles [illegible] was usually associated with the [illegible] altered cytotrophoblast as exemplified [illegible] figure 5 These vacuoles were neither [illegible] nor glycogen as judged from [illegible] ical examination of Sudan Black and [illegible] reactions

Some of the initially chromophobic [illegible] trophoblastic cells gradually acquired [illegible]

The culture medium was [illegible] 80% NCTC 109 15% [illegible] and 100 I U penicillin/ml [illegible]

Preliminary studies have shown [illegible] survive better when they are [illegible] mersed in the fluid medium.

Obtained from the New England [illegible] Boston, Mass Specific activity [illegible]

[illegible]ophilia during cultivation as shown in [fig]ure 6. This acquisition of chromophilia [wa]s more often demonstrated by the ag[gre]gated altered cytotrophoblast" (fig. 7) Such altered cytotrophoblast became [ag]gregated, vacuolated (fig. 5) and/or [ch]romophilic (fig. 6) It appeared to [mer]ge with the cytoplasm of the initial [syn]cytium during the course of cultiva[tio]n.

From radioautographic studies, different [cel]l types exhibited different degrees of [thy]midine incorporation. Langhans cyto[tro]phoblast showed active incorporation [wi]thin 3 to 24 hours of exposure to H³ [thy]midine (figs. 8 and 9) During the [sa]me period, however there was no label[in]g in the initial syncytium. After removal [of] the nutrient medium containing H³ [th]ymidine the same cultures were allowed [to] continue in nutrient medium containing [th]e isotope for another 1 to 2 weeks. Nu[cle]ar labeling was then seen not only in [ag]gregated altered cytotrophoblast" (fig. [...]) but also in the syncytial layer (figs. [...]12) Since there was no labeling in the [ini]tial syncytium but only in discrete cyto[tro]phoblastic cells when the isotope was re[m]oved from the culture the labeled nuclei [ap]pearing in the syncytial layer later in the [co]urse of cultivation could logically only [ha]ve been derived or have migrated from [th]e previously labeled cytotrophoblast.

Viability of the trophoblastic cells in the [La]nghans layer whether altered or not [al]tered, was maintained well for at least [2]-3 weeks as exemplified in figures 13 and [1]4. Such cytotrophoblastic cells started to [de]crease in number significantly only after [th]ree weeks in culture. A few scattered [ce]lls however could still be seen after six [w]eeks.

Cell column cytotrophoblast

This type of cytotrophoblast appeared [to] exhibit the most active mitotic activity [in] the placenta as reflected in the greatest [p]roportion of such labeled cells from radio[au]tographs (fig. 8) Even though no quan[ti]tative data are available on the ratios of [la]beled to non-labeled cytotrophoblastic [ce]lls of different types, the cell column [v]ariety seemed to be more heavily labeled. [It] also appeared to survive the longest *in [v]itro* as shown by its continuing presence after most of the other cellular elements in the villi had undergone necrosis (fig 15)

Syncytiotrophoblast

The nuclei of the initial syncytiotrophoblast became small and dense within 6–24 hours in culture as shown in all of the illustrations of cultured villi (compare any of the figures with fig. 2 which shows the morphology of the villi prior to cultivation) This phenomenon makes possible accurate morphological identification of initial syncytium, as distinguished from that syncytium formed during cultivation. Radioautographic studies showed that the former was not able to incorporate H³ thymidine whereas the latter was shown to contain labeled nuclei which were derived or migrated from the cytotrophoblast. Details of the transformation from cytotrophoblast to syncytiotrophoblast have already been covered in the section on Langhans cytotrophoblast.

The syncytium became irregular during the course of cultivation, thick at certain areas and thin at others (fig 14) It also appeared to increase greatly in quantity and thus is seen as the predominant tissue, even though necrotic after 4 to 6 weeks of cultivation (figs 16 17)

Mesenchymal core

Mitotic activity was shown by the cells in the mesenchymal core though to a much lesser degree than that shown by the cytotrophoblast (figs. 8 to 12) During the course of cultivation the blood vessels became necrotic (fig. 5) and ultimately disappeared. The core stroma became dense and compact with apparent thickening of basement membrane (figs. 7 15) After 4 to 6 weeks in culture only a few scattered mesenchymal cells could be seen in the dense and apparently fibrotic stroma (figs 15 16 17)

DISCUSSION

The results have clearly shown that the Langhans cytotrophoblast has the ability *in vitro* to develop some of the characteristics normally exhibited by the syncytiotrophoblast Such characteristics are a

---

The initial syncytiotrophoblast is defined as the cyncytium normally associated with the placental villi prior to cultivation.

Through gross dissection the villi were isolated and minced into fragments of approximately 1 mm After washing in physiological saline to remove blood and debris the fragments were ready for organ culture. *Random samples were taken for* histological examination

For the preparation of organ culture a single layer of glass beads, 4 mm in diameter was placed in a glass or plastic petri dish and barely covered by culture medium. On top of the beads were laid strips of filter paper (Whatman filter paper no 1 or no. 2) onto which the minced fragments were transferred (fig. 1) Thus the tissues were in contact with but not immersed in the medium Incubation was carried out at 35 –36 C in an incubator gassed with a mixture of 5% CO_2 and 95% O_2. (The atmosphere was kept moist by the presence of a dish of water in the incubator) *A gas mixture of 5%* CO_2 and 95% air was also found to be satisfactory The culture medium was renewed every 2 to 3 days. Two to four fragments were removed for histological examination daily during the first week, and then every 3 to 4 days throughout the rest of the cultivation period of 4 to 8 weeks duration They were fixed in cold Rossman's fixative processed through paraffin embedding, sectioned serially at 6 μ and stained in accordance with the periodic acid Schiff (PAS) procedure (Pearse '60)

For radioautographic studies organ cultures were prepared in the same manner as described. Methyl H^3-thymidine was added to the culture medium in the concentration of 1 to 2 μc per ml of medium. Placental fragments were incubated in the radioactive medium for varying periods of time ranging from one hour to two weeks. Some cultures after 6–24 hours of such incubation with H^3-thymidine were thoroughly washed with physiological saline and transferred for further cultivation into medium containing no isotope Fragments were removed periodically thereafter at 1 to 3 day intervals for 1 to 2 weeks. All fragments for radioautography were fixed in Serra's fixative for one hour and processed through paraffin impregnation and embedding Mounted tissue sections serially sectioned at 5 μ were stained in accordance with Feulgen's procedure for DNA (Swift, '55 Pearse, '60), and [illegible] dried after water rinse The slides were then dipped briefly in pre-melted [illegible] Nuclear Track emulsion NTB-3 in the [illegible] using the dipping technique described [illegible] Joftes and Warren ('55) After [illegible] the appropriate exposure time ([illegible] be 2–3 weeks at approximately [illegible] best results) the slides were developed [illegible] 18 –20 C in Kodak [illegible] oper for three minutes, washed in [illegible] Stop Bath SB-1a for 15 seconds, [illegible] acid fixer for five minutes and then [illegible] in running water for 3–5 minutes. [illegible] were counterstained with [illegible] green dehydrated in graded alcohols [illegible] mounted in permount. The end result [illegible] a thin layer of photographic film [illegible] imposed on the tissue section [illegible] tions of morphological structures and [illegible] ization of incorporated tritiated thymidine could thus be made simultaneously

RESULTS

Langhans cytotrophoblast

During the first 24 hours of culture [illegible] no significant morphological changes [illegible] place except for the increased [illegible] sity of syncytiotrophoblast (compare [illegible] 2 and 3) Mitotic activity was [illegible] the nuclear incorporation of tritiated thymidine into DNA (figs. 8 and 9)

Regional aggregation of some cytotrophoblastic cells started to [illegible] early as 24–48 hours in culture [illegible] cases however it became significant [illegible] abundant only after 5–6 days (figs. [illegible] Intracellular vacuoles of various sizes [illegible] also seen as early as 24–48 hours [illegible] became more abundant and of a [illegible] size in older cultures. Such vacuolization was usually associated with the [illegible] altered cytotrophoblast as exemplified [illegible] figure 5 These vacuoles were neither [illegible] nor glycogen as judged from [illegible] ical examination of Sudan Black and [illegible] reactions.

Some of the initially chromophobic cytotrophoblastic cells gradually acquired [illegible]

The culture medium was composed of [illegible] 50% NCTC 109 [illegible] balanced salt solution [illegible] and 100 I.U. penicillin/ml ([illegible])

Preliminary studies have shown that [illegible] survive better when they are not completely immersed in the fluid medium.

Obtained from the New England [illegible] Boston, Mass. Specific activity [illegible]

[illegible]gsberg, H., and W Neuweiler 1928 Über [illegible]-züchtungsversuche von Placenta und Decidua. [illegible]bl. Gynäk. 50: 1437–1438.

[illegible]ng, A. T and H. W Edmonds 1940 Gen[illegible]sis of hydatidiform mole. Arch. Path., 30 [illegible]60–291.

[illegible]ng, A. T and J Rock 1941 Two human [illegible]va of the previllous stage, having an ovula[illegible]on age of about 11 and 12 days respectively [illegible]arnegie Contrib. to Embryology 29 127–156

[illegible]m, D. L., and S. Warren 1955 Simplified [illegible]iquid emulsion radioautography J Biol. [illegible]photogr. Assoc., 23 145–150.

[illegible]ey, G. E. S., G. O. Gey and M. K. Gey 1943 [illegible]lormone production by placental cells main[illegible]ained in continuous culture. Johns Hopk. [illegible]losp. Bull 72: 26–38.

[illegible]hlow L., and H. Eagle 1961 Biochemistry [illegible] cultured mammalian cells. Ann. Rev Bio[illegible] 30: 605–640.

[illegible]sley A. R., J G. B Pierce, J G A. Dennen [illegible]nd J. R. G. Gosling 1963 Morphogenesis of [illegible]yncytiotrophoblast in vivo an autoradio[illegible]raphic demonstration. Science 141 349–350.

[illegible]rse, A. G E. 1960 Histochemistry Theo[illegible]etical and Applied. Little Brown and Co., [illegible]oston.

[illegible]wart, H. L., M. E. Sano and T L. Montgomery [illegible]1948 Hormone secretion by human placenta [illegible]rown in tissue culture. J Clin. Endocrin., 8 [illegible]175–188.

[illegible]reeter, G. L. 1926 The "Miller" ovum — the [illegible]oungest normal human embryo thus far known. Carnegie Contrib. to Embryology 18: 31–48.

Swift, H. 1955 Cytochemical techniques for nucleic acids. In The Nucleic Acids, ed. Davidson and Chargaff. p 51

Tao T W 1962 Tissue culture studies of normal immature human placentas with special reference to morphogenesis, endocrine function and reaggregation. Ph D Thesis, Harvard University

Tao, T W., and A. T Hertig 1961 Studies on morphology and hormonal secretion of human immature placentas maintained in organ and tissue cultures. Excerpta Med., Sec. 1, 15(7) 857

Thiede H. A. 1960 Studies of the human trophoblast in tissue culture. I. Cultural methods and histochemical staining. Amer J Obstet. and Gynec., 79 636–647

Wislocki G. B and H. S. Bennett 1943 The histology and cytology of the human and monkey placenta, with special reference to the trophoblast. Amer J Anat., 73 335–453.

Wislocki, G. B., and E. W Dempsey 1955 Electron microscopy of the human placenta. Anat. Rec., 123 133–167

Wislocki, G B and H A. Padykula 1961 Histochemistry and electron microscopy of the placenta. In Sex and Internal Secretion, ed W Young. 3rd ed. Vol. 2 883–957 Williams and Wilkin Co., Baltimore.

Wynn R. M., and J Davies 1964 Ultrastructure of transplanted choriocarcinoma and its endocrine implication. Amer J Obstet. and Gynec., 88 618–633

PLATE 1

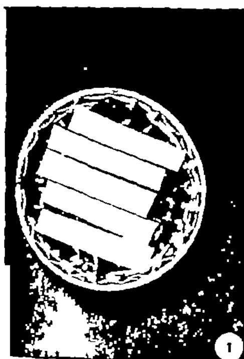
EXPLANATION OF FIGURES

1 The organ culture preparation as described in the text. × 1.5.

2 Human chorionic villus at 12 weeks of gestation showing mesenchymal core C; cytotrophoblast, Cy and syncytiotrophoblast, Sy. PAS-diastase. × 350.

3 One day culture of chorionic villi from the same specimen shown in figure 2. Note that the nuclei in the syncytium are small and dense, whereas the remainder of the tissues resembles that before cultivation as seen in figure 2. PAS-diastase × 350

4 A 12-day culture from a 12-weeks-old human placenta. Note the aggregated cytotrophoblastic cell — altered cytotrophoblast, A Cy occupying the intermediate position between syncytium, Sy and mesenchymal core C, or unaltered cytotrophoblast, Cy. Note further that the nuclei of these intermediately lying cells are of varying density PAS-diastase × 448


1


C
Cy
Sy
2


3


ACy
Cy
Cy
C
C
Sy
4

PLATE 2

EXPLANATION OF FIGURES

5 A three-day culture from five weeks-old human placenta showing the edge of a horionic villus. Not the presence of aggregated and vacuol ted altered cytotrophoblast, A Cy (paler and larger nuclei) some of which appears to merge with the initial syncytium, Sy (denser and smaller nuclei) without any intervening cell boundary PAS-diastase. × 560.

6 A four-day culture from a 11–12-weeks-old human placenta. Note the incorporation of chromophilic latered cytotrophoblast, A Cy into the cytoplasm of the initial syncytium Sy Unaltered Langhans cytotrophoblastic cells, Cy are also present. PAS-diastase × 720.

7 A four-day culture from five-weeks-old human placenta showing chromophilia of a layer of altered cytotrophoblast, A Cy now resembling syncytiotrophoblast in appearance Initial syncytium, S appears as a thin layer Discrete cytotrophoblastic cells, Cy often in masses, are also present. PAS-diastase × 560.

8 A culture from a six weeks-old human placenta, incubated for 4 hours in medium containing 1.5 μc H^3-thymidine/ml. Isotopic labeling, revealed as black granules, is localized to the nuclei of cytotrophoblast, Cy and tromal cells, S, whereas initial syncytium, Sy is not labeled. Feulgen and light green × 350.

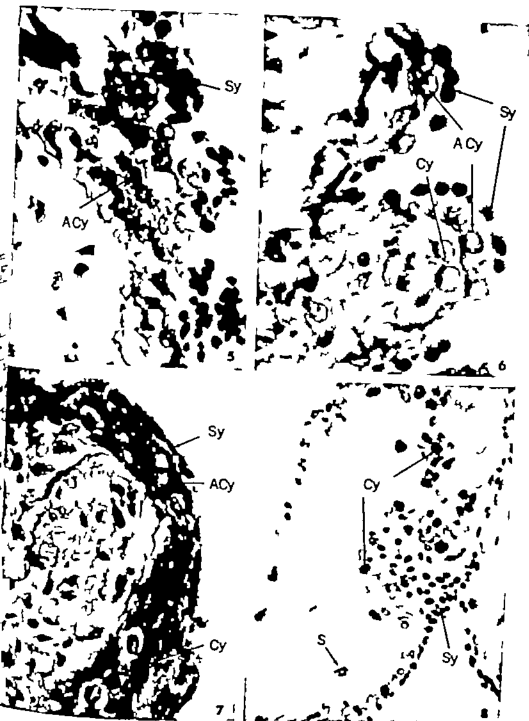

Sy
ACy
5
Sy
A Cy
Cy
6
Sy
ACy
Cy
7
Cy
S
Sy
8

PLATE 2

EXPLANATION OF FIGURES

5 A three-day culture from five-weeks-old human placenta showing the edge of a chorionic villus. Note the presence of aggregated and vacuolated altered cytotrophoblast, A Cy (paler and larger nuclei) some of which ppears to merge with the initial syncytium, Sy (denser and smaller nuclei) without any intervening cell boundary PAS-diastase. × 560.

6 A four-day culture from a 11–12-weeks-old human placenta. Note the incorporation of chromophilic, latered cytotrophoblast A Cy into the cytoplasm of the initial syncytium, Sy Unaltered Langhans cytotrophoblastic cells Cy are also present. PAS-diastase. × 720.

A four-day culture from a five-weeks-old human placenta showing chromophilia of a layer of altered cytotrophoblast, A Cy now resembling syncytiotrophoblast in appearance. Initial syncytium, Sy appears as a thin layer. Discrete cytotrophoblastic cells, Cy also in masses, are also present. PAS-diastase × 560.

8 A culture, from six-weeks-old human placenta, incubated for 24 hours in medium containing 1.5 μc H^3-thymidine/ml. Isotopic labeling, revealed as black granules, is localized to the nuclei of cytotrophoblast, Cy and stromal cells, S whereas initial syncytium, Sy, is not labeled. Feulgen and light green. × 350.


Sy
S
Cy
Cy
Sy
9


ACy
10


Sy
ACy
11


12


12a

PLATE 4

EXPLANATION OF FIGURE

13 A 19-day culture from a 12 weeks-old human placenta. Note the viability of cytotrophoblast, some of which appears aggregated. PAS-diastase. × 350.

14 Another section of the same culture shown in figure 13. Note that the syncytium is thick at places and thin at others. PAS-diastase × 350

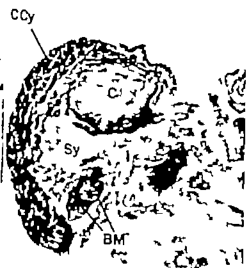
15 A 31-day culture from a 6.5 weeks huma placenta. Many cell column cytotrophoblastic cells, C Cy laden with glycogen, are seen in the peripheral position of the fragment. In contrast, there is great amount of necrotic syncytium, Sy Basement membrane BM, is thick and mesenchymal core, C appears fibrotic. PAS. × 140.

16 A 31-day culture from five-weeks human placenta. Note the large amount of necrotic syncytium which is better seen in higher magnification in figure 17 PAS. × 140

17 A higher magnification of the outlined area in figure 16, showing the syncytial nature of the necrotic mass. × 560


13


14


CCy
Cl
Sy
BM
15


16


17

urther Evidence for the Presence of Nigro-neostriatal opamine Neurons in the Rat

NILS-ERIC ANDÉN ANNICA DAHLSTRÖM, KJELL FUXE AND KNUT LARSSON

Department of Histology Karolinska Institutet, Stockholm Sweden and Department of Pharmacology nd Psychology University of Göteborg Sweden

ABSTRACT With the help of the highly specific and sensitive histochemical fluorescence method of Falck and Hillarp for the cellular demonstration of monoamines the catecholamine-containing cell-bodies within the brain stem have been studied after unilateral removal of large part of the neostriatum 1 to 28 days after the operation.

Most of the catecholamine-containing cell-bodies within the substantia nigra — but no other monoamine-containing cell-bodies — appeared to be distinctly increased in fluorescence intensity and somewhat swollen 2 to 4 days after operation while after 3 to 4 weeks they showed a marked to very marked decrease in fluorescence intensity together with marked degenerative changes. Parallel with the changes in the cell-bodies there occurred rapid and marked accumulation of catecholamines within very abundant swollen nerve fibers in the internal capsule. These nerve fibers were traced caudally via the retrolenticular part of the internal capsule down to the crus cerebri. These results together with those in previous paper (Andén, Carlsson, Dahlström, Fuxe, Hillarp and Larsson, '64) seem to provide conclusive evidence for the presence of nigro-neostriatal dopamine neurons.

Strong experimental evidence for the sence of dopamine neurons in the ro-neostriatal system has been given in revious paper (Andén, Carlsson Dahlöm, Fuxe, Hillarp and Larsson '64) this paper the changes in the dopamine ntents of the neostriatum (nuc. cauda putamen) were studied both biocheml ly and histochemically in the latter se using the fluorescence microscopical thod of Falck and Hillarp (Falck, Hilp Thieme and Torp '62 Falck, '62) er lesions made mainly within the subntia nigra. Important but preliminary ta on the changes in the intraneuronal techolamine distribution of these neuns after removal of the neostriatum re also obtained by means of the histoemical fluorescence method These dies have now bee completed. The sults in the present d previous paper em to provide conc' sive evidence that ere exists a pathw of dopamine neu ns originating in e substantia nigra cending in the int nal capsule and end g in the neostr tum with abundant rve terminals that contain very high ncentrations of opamine

MATERIAL AND METHODS

About 100 male albino rats (body weight 200–250 g) were used. In about 75 of the animals at large part (mostly about two-thirds) of the nuc caudatus putamen was removed on the right side by gentle suction with a fine glass cannula (a hole of about 2 mm in diameter having been drilled in the overlying bone and parts of the cerebral cortex sucked away first to expose the caput of the nucleus) The animals were killed 1 2, 4 7 21 and 28 days after the operation. The rest of the animals served as controls.

The animals were killed by decapitation under light ether anesthesia. The mesencephalon, diencephalon and right and left halves of the fore-brain except the part cranial to the nuc caudatus putamen were dissected out, freeze-dried treated with formaldehyde gas and embedded in [illegible] as described in detail previously (F[illegible] '62 Dahlström and Fuxe '64a) Serial sections (transverse horizontal and [illegible] tal) were made with a thickness of [illegible] Fluorescence microscopy and [illegible] tography were performed a [illegible] Dahlström and Fuxe ('64a) A [illegible] ber of sections were first [illegible]

and then stained with toluidine blue or Einarson's gallocyanin-chromalum for the identification of fluorescent structures.

The fluorescence method used has a high sensitivity and specificity and permits demonstration of even very low concentrations of primary catecholamines and 5-hydroxytryptamine in the cell bodies and axons belonging to monoamine neurons (cf Carlsson, Falck and Hillarp '62 Falck, 62 Dahlström and Fuxe 64a Norberg and Hamberger 64) The fluorescent products formed from these amines during the formaldehyde treatment exhibit under certain conditions a characteristic green (to yellow-green) and yellow fluorescence respectively

RESULTS

After the more or less complete removal of the neostriatum, very abundant swollen nerve fibers running towards the operated structures developed a strong green fluorescence. This was no doubt due to a very marked accumulation of a primary catecholamine (shown with the use of histochemical criteria for the specificity of the fluorescence reaction see Dahlström and Fuxe '64a) The fibers could be traced from fluorescent nerve bundles which ran from the crus cerebri through the retrolenticular part of the internal capsule and entered the neostriatum via the fibrae capsulae internae (figs. 1 2a,b) The amine accumulation was very marked to 7 days after the operation (fig 1) accumulation was found on the operated side) The accumulation



Fig. 1 Nuc caudatus putamen after [removal] of its major part two days before [killing] section. A large accumulation of [strongly] green-fluorescent material is observed within fibers in the capsula interna just in front of the chiasma opticum [in front of] the lesion. × 75.



Fig. 2a Neostriatum of normal rat. A strong, green fluorescence is present between the nerve cell bodies Th fibrae capsulae internae (A) are completely non fluorescent

Fig. 2b Nucleu odatus putamen two days after removal of its major part [before] section. A large accumul tion of trongly green-fluorescent material has occurred within fibers running in fibrae capsulae internae (→) × 120.

…pletely disappeared, however in the …als killed *21 and 28 days after the* …ation.

…e large groups of monoamine-con… …ing nerve cells were closely studied …cially those of the catecholamine type … present within the mesencephalon …ups A8–A10) see Dahlström and … ('64a) The cell bodies of these … normally show a medium green fluo… …ence due to the presence of low con… …rations of a primary catecholamine …o changes were observed within the …rescent cell bodies one day after operation. Two and four days after operation *a small but distinct* increase in fluorescence intensity had occurred within a fairly large number or perhaps the major ity of the nerve cells belonging to group A9 (figs 3a, b 4) which lie mainly within the zona compacta but are aslo present within the zona reticulata and pars lat eralis, on the ipsilateral side of the lesion. The processes of these cells were seen more distinctly than normally and the same was true of the fluorescent zone around the nucleus No such increase was observed within the fluorescent cells

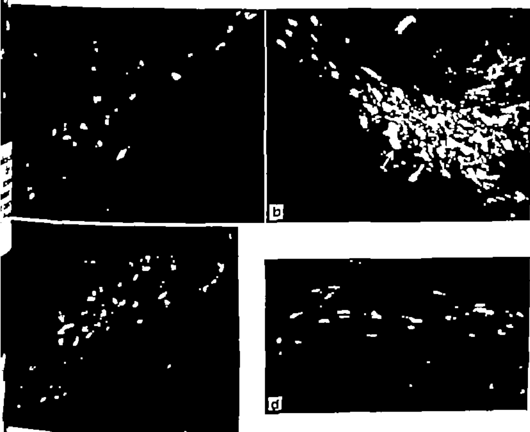


Fig. 3a Zona compacta of substantia nigra. Normal animal. Cross-section Oval cell-bodies … medium green fluorescence in their cytoplasm are observed. × 120.

Fig 3b Zona compacta of substantia nigra two days after removal of nucleus caud… …tum on the same side Cross-section. The fluorescence intensity has increased in most of the …echolamine cell bodies, some of which appear to be somewhat swollen (→) × 120.

Figs. 3c, d Zona compact of substantia nigra 28 days after removal … the …c …udatus …tum on the same side Cross-section. A large decrease in the fluorescence intensity ha… oc…red in most of the ca echolamine-containing cells, which are considerably shrunk and much …aller than in normal an…mals. A few cell-bodies still have normal fluorescence intensity (→) … 120.

of the other groups of monoamine-containing cell-bodies The cells within group A9 on the contra-lateral side of the lesion seemed to be unaffected. The Nissl-picture in the cells with an increased fluorescence intensity appeared to be normal, with coarse, intensely stained Nissl-granules

Twenty-one to twenty-eight days after operation a marked decrease in fluorescence intensity occurred within a large number of the cells (Group A9) localized to the same regions (figs 3c, d) as those that had shown an increase two and four days after operation (i.e. mainly within the zona compacta) The cell bodies showed a very weak green fluorescence and appeared also to be shrunk and much smaller than usual (figs 3c, d) They further showed a loss of stainability of Nissl-bodies. The other fluorescent cells within the substantia nigra appeared normal or showed an only slightly reduced fluorescence intensity The number of cells affected was clearly correlated to the extent of the damage done to the nuc caudatus putamen In the animals where a very large part of the nucleus had been removed most of the fluorescent nerve cells in group A9 showed a decreased fluorescence intensity especially in comparison with that observed two and four days after operation. In no case was any obvious decrease in fluorescence intensity observed within this group on the contralateral side nor within the cells ı the rest of the catecholamine-contai groups (A8 A10) in the mesencephal At no time after operation did the 5H containing nerve cells in the mesencep alon (B7–B9 see Dahlström and Fu '64a) show any certain change in t fluorescence intensity

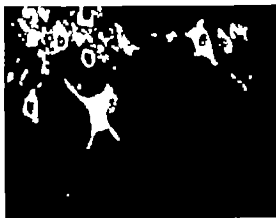


Fig. 4 Zona compacta of substantia nigra tw days fter removal of the nuc caudatus putamen on the same side Two multipolar cell-bodies with fairly large increase in their fluorescence i tensity are present 300.

A normal fluorescence microsc picture was observed in the medulla o longata and pons at all time interv studied after the operation

DISCUSSION

After the transection of the ax belonging to peripheral or central mo amine neurons, the amines accumul rapidly in the central part of the ne This provides a convenient method of visualizing the pathways of such ne (Dahlström and Fuxe '64c, d). In th central nervous system the accumul amines disappear within a few wee probably due to degenerative processes the affected neurons (Dahlström and Fuxe, '64b) The cell bodies of cent catecholamine neurons have been f to show an increased fluorescence in sity within a few days after axotomy i all probability due to increased conc trations of their catecholamines (Dahl ström and Fuxe '64b)

These methods have been used in the the present and previous studies (A Carlsson Dahlström Fuxe Hillarp and Larsson '64) on the existence of a neostriatal dopamine neurons Th seems now to be little doubt that the c nucleus of this neuron system is re sented by the large group (Group A9 of nerve cells in the substantia nigra, m within the zona compacta, which n mally show a medium specific fl cence due to the presence of pr catecholamines. It has been found in the present paper that these nerve cells — in contrast to all other catecholamine c in the lower brain stem — react a removal of the nuc caudatus p first with an increased fluorescence in sity and later on show a markedly d creased fluorescence and degen changes The increase was not p marked which may be due to the l

r only the terminal parts of the axons -- been destroyed.

Simultaneously with the increase in the -rescence intensity of the cell-bodies -e occurred a strong accumulation of -ary catecholamines within lesioned -ns which ran towards the neostriatum could be traced caudally via the in-al capsule and its retrolenticular part -n to the crus cerebri (mainly the cen- part) This accumulation disappeared r 3 to 4 weeks. By this time most of the bodies of group A9 showed a marked of fluorescence intensity and signs of -eneration. The accumulation of green -rescent fibers was present in the same -ts as where the cells of group A9 are -wn to send fiber bundles ascending -ugh the ventral part of crus cerebri, retrolenticular part of the internal -sule and the more dorsal and anterior -ts of the internal capsule entering the -ae capsulae internae and ending fi--ly in the neostriatum with abundant -ve terminals (to a large part sublight -roscopical) (see Fuxe, Hökfelt and -son, '64) containing very high con-trations of dopamine.

The nigro-neostriatal dopamine system -o doubt one of the best examples at -present time of how monoamine ter-nals can be connected with the mono-ine-containing axons and nerve cell -ies to which they belong, thus, making -ossible to study the entire monoamine -rons cell-body axon and terminals. -er examples are the bulbo-spinal nor-enaline and 5-hydroxytryptamine sys-s (see Dahlström and Fuxe, '64b)

ACKNOWLEDGMENTS

This work has been supported by a -lic Health Service Grant (NB 02854-) from the National Institute of Neuro-ical Diseases and Blindness and by -nts from the Swedish Medical Research -ncil, Stiftelsen G och T Svenssons -me, Knut and Alice Wallenberg Foundation and by the National Institute of Child Health and Human Development (HD 00344-04) U S Public Health Service. The research has also been sponsored by Air Force Office of Scientific Research, OAR (Grant AF EOAR 64-30) through the European Office of Aerospace Research, United States Air Force.

LITERATURE CITED

Andén, N -E., A. Carlsson, A. Dahlström, K. Fuxe, N -A. Hillarp and K. Larsson 1964 Demonstrating and mapping out of nigro-neostriatal dopamine neurons. Life Sci., 3: 523–530.

Carlsson, A., B Falck, K. Fuxe and N -A. Hillarp 1964 Cellular localization of monoamines in the spinal cord. Acta Physiol. Scand., 60: 112–119

Carlsson, A., B. Falck and N -A. Hillarp 1962 Cellular localization of brain monoamines. Acta Physiol. Scand., 56 Suppl. 196.

Dahlström, A., and K. Fuxe 1964a Evidence for the existence of monoamine containing neurons in the central nervous system. I. Demonstration of monoamines in the cell bodies of brain stem neurons. Acta Physiol. Scand., 62: Suppl. 232.

——— 1964b Evidence for the existence of monoamine containing neurons in the central nervous system. II. Experimentally induced changes in the intraneuronal amine levels. Acta Physiol. Scand., (in press)

——— 1964c A method for the demonstration of monoamine containing nerve fibres in the central nervous system. Acta Physiol. Scand., 60: 293–295

——— 1964d A method for the demonstration of adrenergic nerve fibers in peripheral nerves. Z. Zellforsch., 62: 602–607

Falck, B. 1962 Observations on the possibilities for the cellular localization of monoamines with fluorescence method. Acta Physiol. Scand., Suppl. 197

Falck, B N. -A. Hillarp G. Thieme and A. Torp 1962 Fluorescence of catecholamines and related compounds condensed with formaldehyde. J Histochem. Cytochem., 10: 348–354.

Fuxe K., T Hökfelt and O. Nilsson 1964 Observations on the cellular localization of dopamine in the caudate nucleus. Z. Zellforsch., 63 701–708.

Norberg, K.-A. and B. Hamberger 1964 The Sympathetic Adrenergic Neuron: Some characteristics revealed by histochemical studies on the intraneuronal distribution of the transmitter. Acta Physiol. Scand 63 Suppl 238.

promulgated by the National Society for Medical Research were observed.

The entire cecum and distal two inches of ileum were fixed in cold (4 C) calcium-sucrose-formol solution (Ca 1.27% formalin 10% sucrose 10%) following sacrifice of the animals by chloroform. Because of its excellent contrast and clear cellular outline in our experimental set-up the histochemical stain for reduced diphosphopyridine nucleotide (DPNH) diaphorase was utilized primarily (Burstone '62) This system involves nitro-blue tetrazolium nitro-BT) as electron accepto... with reduced DPN as subst... for 45 minutes or more at 3... tudinal muscle layer strip... muscle submucosa and... mounted whole in PVP (... No attention was paid to... enzymatic activity

Cell size was measure... brated Bausch and Lomb ... piece disk micrometer Th... reported is the sum of ... diameters perpendicular ... divided by two Complete ... urements were carried out ... from each specimen. In ... the possibility of mechanical [illegible] artefacts mesenteric as well as [illegible] enteric ganglia from the cecal pouch [illegible] used.

In the ileum, where the ganglia [illegible] large and cell uniformity is great, [illegible] consecutive neurons were counted [illegible] each specimen enough to render [illegible] vey statistically valid.

RESULTS

The diameters of the myenteric ganglion cells in the cecum of rats [illegible] ...

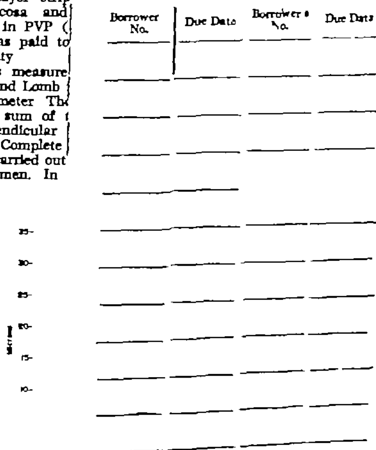


Fig. 1 The size of m... of the animal. Each column... standard error is shown above... column is given the mean neuronal size [illegible] the average body weight of the group and the number of cells measured.

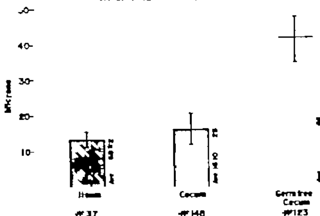


Fig. 2 The relationship between organ size and the dimensions of myenteric neurones in the ileum and cecum is depicted graphically The columns give the mean size of the nerve cells with one standard error above and below the top of each column. The exact values are written on the side of each column, below which we have indicated the organ and the number of cells counted.

While one should guard against loose interchange of terms such as area of innervation (a squared function) and organ circumference (linear concept) we feel that in this system the two appear to be determinants of cell size. Which one it really is has not been settled. However since most ganglia are located beneath the mesenteric attachment, it may be surmised that the area of innervation extends around the circumference of the bowel wall, rather than along it. Therefore volume as such is probably less important.

re times as large as in the conventional um. The organ circumference has in- ased approximately 2 to 3 times. Ileal rones in this group appeared smaller n those in the cecum, but proved not nificantly so after statistical analysis. ere is no size difference between the enteric neurones in the ileum of germ- e and conventional rats of the same , where no change in organ size has en place.

When young germfree rats are removed m their isolators and thus convention- zed the formerly enlarged cecum re- ns to normal size over a period of 1 to 2 eks (Gordon and Wostmann, '59) The enteric ganglion cells in the cecum re- ond by a return to conventional propor ns from 30.8 μ to 13 1 in small rats g. 3) Following this return to normal the neurones of the cecum grow at rate similar to those in the ileum, as the imal gains weight. In other words, the crease in neuronal diameter occurred in face of normal growth. At first the nglion cell sizes in the two organs over p however the growth curve for the cecal nerve cells is steeper than that for ileal nerve cells.

In the 300 gm Fisher rat the cecal cir cumference is considerably greater than that of the ileum, and the difference between their myenteric neurones is statistically significant (fig. 4) When the growth curve in figure 3 is extended to the point of full growth of the animal approximately such a difference might be expected.

A comparison of figures 2 and 3 calls attention to the fact that in spite of organ enlargement, body weight continues to be a factor in determining neuronal size. The neurones of the cecum are noticeably larger in medium sized than in small germfree rats.

DISCUSSION

The results presented here indicate a relationship between increasing body size and increasing diameter of ganglion cells within the peripheral parasympathetic nervous system of the rat. A similar correlation was reported for human sympathetic ganglia by Anraku ('33) Terni ('22) felt

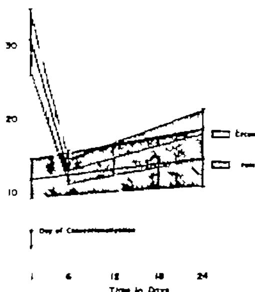


Fig. 3 In this table we have plotted a graph of neuronal size in the cecum and ileum against time. On day 1 the animal were germfree but had just been exposed to laboratory surroundings (conventionalized) Between day 6 and d y 12 the normal intestinal flora has become firmly established. By this time the cecum returns to normal size, as well. The ileum is no larger in germfree than in conventional animals. On day 1 th animals weighed 30 gm (3 weeks old) and grew in the course of the experiment to about 90 gm, at seven weeks of age. The area under the vertical and diagonal lines respectively includes two standard errors one on either side of the best straight line, which could be drawn from our calculations.

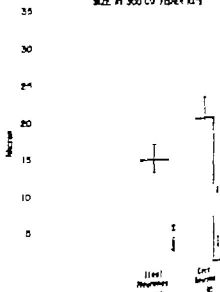


Fig. 4 The two columns represent the size of ileal and cecal myenteric neurones in large rats. The actual value in microns is given on the ... of each with standard error. One standard error is plotted above and one below the top of each column. The figures below the columns indicate the number of cells measured.

that sympathetic cells undergo continuous alterations in size and shape throughout the life cycle of man. Apparently the latter point, to some extent at least holds true in our experimental model, for we observed a definite correlation between increased organ size and neuronal enlargement in the germfree cecum. Gasparini ('52) noted greater cell volumes in the ganglia of the uterine cervix during pregnancy While he deals in volume and we in a linear function, this undoubtedly represents a good analogue to the situation in the germfree cecum. Unfortunately there can be no exact size comparison between the two sets of data, as no measurements were given by the author It would have been extremely interesting to attempt an answer to the old questions posed by Levi ('25) is there an end point of cell growth? What is the largest size of a ganglion cell compatabile with function?

A considerable body of evidence is pointing towards cell hypertrophy or enlargement as an anatomical feature of hyperfunction within the nervous system (Bachrach et al. '34 Nicholson, '31)

While it is doubtful whether electrical stimulation is capable of inducing morphological alterations in sympathetic ganglion cells (Eve 1896) excessive stimulation elsewhere in the nervous system has been associated with a considerable increase in cell volume (Edström, '57).

Benninghoff ('32) suggested that neuronal hypertrophy as well as hyperplasia took place when increased functional demands were placed on the myenteric plexus. Friede ('63) considered neuronal size proportional to the area of dendritic ramification which may be synonymous with area of innervation. An enlarged area of innervation presumably represents added functional load.

In the present experiment we have own that among other things body eight and organ size (here cecal diamer) are responsible for neuronal growth. ost myenteric neurones are located unr the mesenteric attachment, hence gan circumference might be expected to important in determining the area of nervation. The gradated increase of neunal sizes from ileum to cecum to germe cecum adds further support to this esis.

Function and structure are interrelated the neurovegetative periphery It is artling to consider such structural dy mism within a system commonly reed to as inert to pathological alterans.

ACKNOWLEDGMENT

The authors wish to thank Dr Albert hheber Chief, Department of Germfree search, for his kindness in making the rmfree animals used in this study availble to us.

LITERATURE CITED

-aikhosseini, S. F 1963 Über die Abhängigkeit der Nervenzellengrösse von der Körper grösse beim Hunde. Anat. Anz., 112: 32–38.

-araku, Y 1933 On the post-natal growth of the human sympathetic ganglion. Trans. Soc. Path. Jap 23 941–943.

-achrach, D K. Kovács, A. Traub, E. Horváth and B. Korpássy 1954 Histomorphological signs of hyperfunction in the magnocellular nuclei of the ant. hypothalamus of the rat. Acta Morph. Acad. Sci. Hung., 4 179–185.

-enninghoff, A. 1951 Vermehrung und Ver grösserung von Nervenzellen bei Hypertrophie des Innervationsgebietes. Z. Naturforschg., 6. 38–41.

-urstone, M. S. 1957 Polyvinyl pyrrolidone as mounting medium for stains for fat and for azo-dye procedures. Amer J Clin. P th., 28 429–430.

——— 1962 Enzyme Histochemistry Academic Press, New York.

Dupont, J R., H. R. Jervis and H. Sprinz 1965 Auerbach' Plexus of the rat cecum in relation to the germfree state. J Comp. Neur., in press.

Ebbesson, S. O E. 1964 A quantitative study of the superior cervical ganglion in primates with critical evaluation of histological counting techniques. Dissertation submitted to the faculty of the graduate school of the University of Maryland in partial fulfillment of the requirements for the degree of doctor of philosophy

Edström, J E. 1957 Effects of increased motor activity on the dimensions and the staining properties of the neuron soma. J Comp. Neur., *107* 295–304.

Eve, F C. 1896 Sympathetic nerve cells and their basophil constituent in prolonged activity and response. J Physiol., 20 334–353.

Friede, R. L. 1963 The relationship of body size, nerve cell size, axon length and glial density in the cerebellum. Proc. Nat. Acad. Sci. USA, 49 187–193.

Gasperini, F 1952 Morphologische Befunde an den Pyrenophoren des Ganglion cervicale uteri unter Berücksichtigung des Alters und des Funktionszustandes der Geschlechtsorgane. Acta Anat., (Basel) *15* 308–314.

Gordon, H. A., and B. S. Wostmann 1959 Responses of the animal host to changes in the bacterial environment Transition of the albino rat from germfree to the conventional state. Recent Progress in Microbiology VII. International Congress for Microbiology Symposium V Stockholm 1958; Almquist and Wiksells Uppsala, Sweden, pp. 336–339

Irwin, D A. 1931 The anatomy of Auerbach plexus. Am. J Anat., 49 141–166.

Lapicque, L. 1946 Cytoarchitectonique du ganglion sympathique en function du poids du corps. C. R. Acad. Sci. (Paris) 222 255–258.

Levi, G. 1925 Wachstum und Körpergrösse (Die structurelle Grundlage der Körpergrösse bei voll ausgebildeten und im Wachstum begriffenen Tieren) Ergebn. Anat. Entwicklungsgesch., 26 87–342.

Nicolosi, G. 1934 Sul comportamento delle cellule nervose dell'intestino soprastante ad una stenosi. Arch. Ital. Chir 37 707–733.

Terni, T 1922 Ricerche sulla struttura sull' evoluzione del simpatico dell'uomo. Monit. Zool. Ital., 33 63–72.

Tower D. B. 1954 Structure and functional organization of mammalian cerebral cortex The correlation of neurone density with brain size J Comp. Neur *101* 19–51.

ome Efferent Connections of the Nucleus ledialis Dorsalis

N EXPERIMENTAL STUDY IN THE CAT [1]

RIYAD R. KHALIFEH WILLIAM W KAELBER AND WALTER R. INGRAM
Departments of Anatomy and Neurology University of Iowa, Iowa City Iowa

ABSTRACT Single unilateral electrolytic lesions were placed stereotaxically at different loci in the nucleus medialis dorsalis of the cat. The modified Nauta-Laidlaw silver method for the study of degenerating axons was used. Five animals with satisfactory lesions and staining qualities form the basis of this report. The nucleus medialis dorsalis in the cat sends efferent fibers to gyrus proreus, orbitalis, sigmoideus anterior and genualis; also to the globus pallidus and putamen and to other thalamic nuclei. The findings indicated wider areas of projection of the nucleus medialis dorsalis to the frontal cortex than has been previously reported for this species. W were unable to confirm efferent connections from the nucleus medialis dorsalis to the caudate and hypothalamus as reported by others.

The advent of newer histological techques and the judicious use of older ones s renewed interest in the efferent conctions of the nucleus medialis dorsalis d its physiological significance. Nauta d Whitlock in 1954 used a modified Bielowsky silver impregnation procedure to ace degenerating fibers after producing sions stereotaxically Fibers from the ucleus medialis dorsalis were traced to e gyrus proreus and medial orbitofrontal rtex. Intrathalamic connections with the idline and paramedian cell groups were so seen. In addition, some degenerating bers were present in the dorsolateral part f the anterior hypothalamus. In 1958 howers,using the Swank Davenport modi cation of the Marchi method traced deenerating fibers from small stereotaxic sions in the nucleus medialis dorsalis cross the internal medullary lamina into e nuclei ventralis lateralis and ventralis osterior Degenerating fibers to the anrior nuclear group were believed to be resent but could not be demonstrated unquivocally Fascicles to the midline nuclei and the medial hypothalamic region were traced by way of the diencephalic eriventricular system. Fibers from the agnocellular portion of the nucleus medilis dorsalis were found to project to the audate and globus pallidus.

Johnson, in 1961 employing the Nauta ilver impregnation method, found efferent connections from the nucleus medialis dorsalis in the cat to the adjacent thalamic nuclei, the nuclei of the midline, the centromedian and the nucleus ventralis posterior. Some fibers were seen in the dorsal hypothalamic area. Rostrally fibers were reported to enter the antero-ventral and antero-dorsal nuclei, nucleus rhomboidalis and the anterior part of the nucleus reticularis. A few fibers were believed to enter the globus pallidus and a larger number to terminate in the head of the caudate nucleus. The putamen was free of terminal degeneration.

Nauta, in 1962, used the Nauta-Gygax and Albrecht Fernstrom techniques of silver impregnation in studying connections of the medial part of the nucleus medialis dorsalis of the *Macaca mulatta*. Fibers were traced to the nucleus reticularis thalami, dorsal hypothalamic area, lateral preoptic and hypothalamic regions, nucleus of the diagonal band substantia innominata, anterior perforated substance and olfactory tubercle A small number of degenerating fibers coursed through the substantia innominata to enter the amygdala near its rostral pole. No degeneration could be traced from the thalamic lesion to medial regions of the hypothalamus, although some fibers in the inferior thalamic

[1] This study was supported in part by the National Institutes of Health, United States Public Health Service, Grants 5T1 NB 5249 and MH 00473.

peduncle ended in the lateral hypothalamic area. No evidence was found of efferent fibers from the nucleus medialis dorsalis to the caudate which is in accord with a previous study on the cat (Nauta and Whitlock, '54) No degenerating fibers could be traced to the globus pallidus.

The connections of the nucleus medialis dorsalis with the hypothalamus are still controversial. Because of their functional implications, a separate review of the pertinent literature is devoted to them

LeGros Clark ('32) was able to follow degenerated fibers into the periventricular system as the result of a small localized lesion involving the nucleus medialis dorsalis in the rat. He was unable to trace them as far as the hypothalamus However he maintained that the "intimate connection between the nucleus and the periventricular system and the nuclei of the midline is an important fact, and there can be little doubt that through this system the nucleus can be brought into direct functional relation with the activities of the hypothalamus."

Murphy and Gellhorn in 1945 found that strychninization of the posterior hypothalamus fires the nucleus medialis dorsalis when cortical effects have not yet been produced Strychninization of the nucleus medialis dorsalis causes "firing" in the ipsilateral and then the contralateral cortex. Using the criteria of the comparative amplitude of response the time of appearance and the persistence of strychnine spikes Murphy and Gellhorn concluded that the following pathways form tracts of preferential discharge 1 *Hypothalamus to nucleus medialis dorsalis* 2. nucleus medialis dorsalis to cortex and 3 cortex to nucleus medialis dorsalis and hypothalamus. As was mentioned perviously Nauta and Whitlock ('54) Showers ('58) and Nauta ('62) found degenerating fibers in the hypothalamus after lesions in the nucleus medialis dorsalis.

From a review of the literature it is evident that there is little agreement on the subcortical efferent connections of the nucleus medialis dorsalis of the thalamus. While Nauta found no connection with the caudate in the cat (Nauta and Whitlock, '54) or monkey (Nauta, '62) such connections were seen in the cat by [illegible] ('61) and the monkey by Showers ('58). Nauta and Whitlock's ('54) and [illegible] ('61) results in the cat also differ with respect to connections with the globus pallidus.

The thalamohypothalamic connections remain a controversial subject. Although there has been much speculation about their functional significance they have not been unequivocally demonstrated, and the findings of different authors using the same histological techniques are inconsistent. Consequently this study was undertaken to investigate further the subcortical connections of the nucleus medialis dorsalis in an effort to resolve some of these discrepancies.

MATERIAL AND METHODS

Single unilateral electrolytic lesions were placed stereotaxically at different levels on the left side in the nucleus medialis dorsalis of the cat. The lesion was produced by passing an electric current of 1.5 ma for 10–12 seconds through a 26 gauge nichrome electrode insulated except at the tip (figs. 1 and 2) The electrode was directed perpendicularly down to the region of the nucleus through the cortex. The modified Nauta Laidlaw (Nauta '5[illegible]) silver method for the study of degenerating axons was used to trace the connections.

The animals were allowed to survive 9–12 days and then sacrificed under Nembutal anesthesia by opening the thorax and cannulating the innominate artery through an intracardiac approach. About 200–300 cm^3 of isotonic saline was used to perfuse *the brains followed* by about 500 cm^3 of 10% formol saline The brains were then removed and stored in 10% formol saline for a period of 12–16 weeks. Frozen sections were cut at 30 μ for staining by silver impregnation and 60μ for Weil and cresyl violet stains. Consecutive sections were taken 650 μ apart. Five animals with satisfactory lesions and staining qualities form the basis of this report.

RESULTS

For descriptive purposes the efferent connections are grouped into three categories: 1 Thalamocortical, 2. Thalamo-subcortical and 3. Intrathalamic.

1 *Thalamocortical.* Fibers, in thick ndles, left the nucleus medialis dorsalis the thalamus and coursed ventrolaterally nd rostrally across the internal medullary mina and the ventrolateral thalamic re on (fig. 6) to the anterior limb of the ternal capsule. For the most part these ere grouped in the region of the inferior alamic peduncle and most medial and ntral part of the internal capsule ventro-teral to the caudate nucleus (figs. 3 and) In more rostral transverse sections ey were scattered in the basal regions the brain among fibers of the internal psule, ending on cells in the granular yer of the gyrus proreus, gyrus orbitalis d the most ventral parts of the gyrus nualis and sigmoides anterior Preter inal degeneration was more abundant in e gyrus proreus as compared to the other rl.

In horizontal sections the fibers were en to fan out in the thalamus and de-end to the anterior hypothalamus, where ey then proceeded ventrolaterally and strally to that part of the internal cap-le located between the caudate medially d the putamen and globus pallidus later ly (figs. 3 5 and 7) On reaching the udal end of the head of the caudate cleus the fibers split into lateral and edial bundles. The lateral bundle curved ound the head of the caudate and the edial bundle passed into the region of the edial septal nucleus and medial islands Calleja. Some fiber fascicles passed into e caudate itself but retained their fascic ar arrangement and did not disperse nong the cells of this nucleus. All fas-cles, viz. lateral, medial and those pass-g through the head of the caudate met strally in the subependymal region of e lateral ventricle and proceeded to the ontal cortex (fig 5) Fibers that reached e ventral part of the gyrus genualis took slight dorsal curve at the rostral end of e head of the caudate.

2. *Thalamosubcortical connections* Fi-ers running in the most medial part of e internal capsule took a somewhat lat ral course to end in the globus pallidus nd in lesser numbers in the putamen fig 4) A few fibers appeared to end in he nucleus ansae lenticularis but their resence could not be confirmed in all sections at this level. Degenerating fibers were seen in the region of the medial septal nucleus medial islands of Calleja, anterior hypothamus preoptic region and substantia innominata, but there was no preterminal degeneration. In addition, there were fibers belonging to the internal capsule in the lateral region of the head of the caudate but with no preterminal degeneration.

In horizontal sections it was evident that thalamofugal fibers coursed ventrorostrally in the medial part of the internal capsule and fanned out in the basal region of the brain at the level of the anterior hypothalamic and preoptic areas. Some of them turned caudolaterally to end in the globus pallidus and putamen while the rest continued to the frontal cortex (fig 5)

3 *Intrathalamic connections.* Fibers leaving the lateral margin of the nucleus medialis dorsalis proceeded in different directions. Some appeared to terminate in the ventral and lateral nuclei of the thalamus particularly the ventralis posterolateralis and ventralis posteromedialis of the former and the lateralis dorsalis and lateralis posterior of the latter Other degenerating fibers were seen in the anterior midline and intralaminar groups of thalamic nuclei to varying degrees (figs. 3 5 8 and 9) Fibers to the midline nuclei and some of those to the intralaminar nuclei left the medial side of the nucleus medialis dorsalis Degenerating fibers were seen in the nucleus reticularis in all animals. On the side opposite to the lesion no degeneration was seen in the nucleus medialis dorsalis or other thalamic nuclei.

There was degeneration in the nucleus habenularis lateralis and medialis in all the animals which was attributed to the electrode passing through them and/or the striae medullaris thalami. This was probably true for degeneration found in the fornix and corpus callosum as well.

DISCUSSION

Thalamocortical fibers Phylogenetic studies have indicated a progressive enlargement and differentiation of the nucleus medialis dorsalis in parallel with the development and elaboration of the frontal lobes In the cat LeGros Clark and Boggon ('33) showed with Marchi studies that the

nucleus medialis dorsalis gave rise to fibers which run ventrally into the most medial fasciculi of the internal capsule passing in the basal surface of the brain to terminate in frontal lobe areas viz. prefrontalis orbitalis lateralis, intermedia and medialis. Nauta and Whitlock ('54) also traced degenerating fibers from the nucleus medialis dorsalis to the gyrus proreus and medial orbitofrontal cortex in the cat. Waller and Barris ('37) in the cat, found that the nucleus medialis dorsalis projected to more dorsal parts of the gyrus proreus. These three studies on the efferent fibers from the nucleus medialis dorsalis to the frontal cortex in the cat are in general agreement although the cortical areas to which the nucleus projects differ in extent.

In the present study we found that degenerating fibers from the nucleus medialis dorsalis passed ventrolaterally and rostrally across the internal medullary lamina to the anterior limb of the internal capsule ventrolateral to the caudate nucleus. In more rostral transverse sections they were scattered in the basal regions of the brain among fibers of the internal capsule. The course of these fibers to the frontal cortex was further elucidated by an examination of horizontal sections and their relationship to the caudate nucleus was of interest, viz. the manner in which they converged immediately rostral to this nucleus. The fibers made connections with cells in the granular layer of the gyrus proreus gyrus orbitalis and most ventral part of the gyri genualis and sigmoides anterior Since more abundant preterminal degeneration was seen in the gyrus proreus than the other gyri it was concluded that more fibers reach this area.

Fibers to the orbital gyrus reached it primarily on the medial side with a few going to the lateral part. This agrees with the previous studies of LeGros Clark and Boggan ('33) and Nauta and Whitlock ('54) Fibers passing to the most ventral parts of the gyri genualis and sigmoides anterior took a slight curve dorsally at the rostral end of the head of the caudate These fibers had not been previously described and were less abundant than fibers going to the gyrus proreus and orbitalis.

In higher primates and man the [illegible] medialis dorsalis projects to the [illegible] and orbital regions of the frontal [illegible] Although homologies are difficult to [illegible] the general scheme of projection [illegible] be similar in that the most ventral [illegible] rostral tip of the frontal lobe in the [illegible] ceives fibers from the nucleus [illegible] dorsalis.

Thalamosubcortical connections [illegible] present findings concerning [illegible] connections of the nucleus medialis [illegible] salis differed in some respects from [illegible] of previous studies (Johnson, '61 [illegible] and Whitlock, '54; Nauta, '62) Fibers [illegible] ning in the most medial part of the [illegible] capsule among the anterior thalamic [illegible] ations took a somewhat lateral course [illegible] end in the globus pallidus and to a [illegible] extent the putamen. The fibers were [illegible] in number and their interruption did [illegible] cause dense degeneration in the [illegible] nucleus Such connections, with the [illegible] pallidus were found by Showers ('[illegible] Marchi preparations in the monkey [illegible] Johnson ('61) with the Nauta silver [illegible] nique in the cat. Nauta and Whitlock ('[illegible] in the cat and Nauta ('62) in the [illegible] did not find connections between [illegible] dorsomedial nucleus and the globus [illegible] dus. The functional significance of [illegible] nections with the globus pallidus and [illegible] men is not clear It is possible, [illegible] that impulses from the frontal lobe [illegible] relayed to the basal ganglia through [illegible]

The absence of connections between [illegible] caudate and nucleus medialis dorsalis [illegible] this study was contrary to Showers ('[illegible] and Johnson's ('61) findings but [illegible] with those of Nauta and Whitlock ('[illegible] and of Nauta ('62) Some fibers [illegible] into the caudate in a caudorostral [illegible] to join other fiber bundles surrounding [illegible] in the subependymal region. The [illegible] that passed into the substance of the [illegible] date kept their fascicular arrangement [illegible] did not disperse among its cells Also [illegible] preterminal degeneration was seen [illegible] caudate. Thus it was inferred that [illegible] reaching the caudate did not make [illegible] nections with its cells but rather [illegible] through en route to the frontal cortex [illegible]

Connections between the dorso[illegible] nucleus and the hypothalamus reported [illegible] other workers were not confirmed [illegible]

crepancy could not be explained other by suggesting that impulses from the mo-medial nucleus may reach the hypothalamus along multisynaptic pathways er a relay in other thalamic nuclei.

Intrathalamic connections The nucleus medialis dorsalis has widespread and fuse intrathalamic connections with the terior lateral, ventral, midline and in-laminar groups of nuclei. It also sends ers to the reticular thalamic nucleus ese findings represent more diffuse in thalamic connections than have been orted previously (Johnson, '61 Nauta d Whitlock, '54 Nauta, '57; Showers 1)

Connections with the anterior nuclear oup found in the present study deserve ditional comment. The electrode was serted perpendicularly through the cortex and the needle track passed through cingulate gyrus. As it has been shown at the anterior nuclear group makes connections with the gyrus cinguli (Clark and ggon, '33 Walker '38) some of the er degeneration in the anterior nuclei ay be secondary to the needle track. The nctional significance of these intrathalamic connections is of interest, since they nnect the nucleus medialis dorsalis with e specific and the diffuse thalamic projection systems. These connections enable e nucleus medialis dorsalis to influence e activities of remote cortical and subrtical regions with which it does not tablish direct fiber connections.

ACKNOWLEDGMENTS

The authors wish to express their appreciation to Mrs. Gerald Kerr and Miss Doris Andersen for valuable technical assistance and to Mr Alan Hage for preparing the illustrations

LITERATURE CITED

Clark, W E. LeGros 1932 The structure and connections of the thalamus. Brain, 55 406–470.

Clark, W E. LeGros, and R. H. Boggon 1933 On the connections of the medial cell groups of the thalamus. Brain, 56 83–98.

——— 1933 On the connections of the anterior nucleus of the thalamus. J Anat., 67 215–226.

Johnson, T N. 1961 Fiber connections between the dorsal thalamus and corpus striatum in the cat. J Exp Neurol., 3 556–569.

Murphy J P and E. Gellhorn 1945 Further investigation on diencephalic-cortical relations and their significance for the problem of emotion. J Neuro-physiol., 8 431–447

Nauta, J H. 1957 New Research Techniques of Neuro-Anatomy Ed. by William Windle. Thomas, Springfield, Illinois, pp. 17–26.

——— 1962 Neural associations of the amygdaloid complex in the monkey Brain, 85 505–520.

Nauta, J H., and D. G Whitlock 1954 An anatomical analysis of the nonspecific thalamic projection system. In. Brain Mechanisms and Consciousness, A Symposium. Thomas, Springfield, Illinois.

Showers, M. J C. 1958 Correlation of medial thalamic nuclear activity with cortical and subcortical neuronal arcs. J Comp. Neur., 109: 261–315.

Walker A. E. 1936 An experimental study of the thalamo-cortical projections of the Macaque monkey J Comp. Neur 64. 1–39.

Waller H., and R. W Barris 1937 Relationships of thalamic nuclei to the cerebral cortex in the cat. J Comp. Neur 67 317–341

PLATE 1

EXPLANATION OF FIGURES

1 Photomicrograph of a transverse section through the thalamus showing the site of the lesion in the nucleus medialis dorsalis on the left side. Cresyl violet stain × 1½

2 Photomicrograph of a horizontal section showing the site of the lesion in the nucleus medialis dorsalis on the left side. Cresyl violet stain × 1½


1


2

Abbreviations (plates 2 and 3)

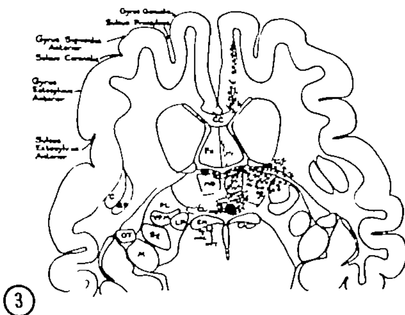
Aa, Area amygdaloidea anterior
AM, N Anterior medialis
CA Commissura anterior
CC, Corpus callosum
Cd, N Caudatus
Ch, Chiasma opticum
CI, Capsula interna
CL, N Centralis lateralis
Cl, Claustrum
CM N Centrum medianum
FX, Fornix
GL, Corpus geniculatum laterale
GP Globus pallidus
Hp Hypothalam s posterior
HPT Habenulo-peduncular tract
LD N Lateralis dorsalis
LI, N Lateralis pars intermedia
LP N Lateralis posterior
MD N Medialis dorsalis
MG Corpus geniculatum medialis
Mm Corpus mamillare
MLT T Mammillo-thalamic tract
NCM N Centralis medialis
NPc, N Commissura posterior
Npr N Prothalamicus
NR, N Ruber
N.Sept med N Septalis medialis
OT Optic tract
Ped, Peduncularis cerebralis
PVA, N Periventricularis anterior
Pv N Paraventricularis
Put, Putamen
R, N Reticularis
Re, N Reuniens
Rh, N Rhomboidalis
RPO Regio praeoptica
S Stria medullaris
Sch N Supra chiasmaticus
Sg, N Suprageniculatus
Sm, N S bmedius
SO N Supraopticus
Spt, Are septalis
Sth N Subthalamicus
VA N Ventralis anterior
VL, N Ventralis lateralis
VM, N Ventralis medialis
VPL, N Ventralis postero-lateralis
VPM, N Ventralis postero-medialis

PLATE 2

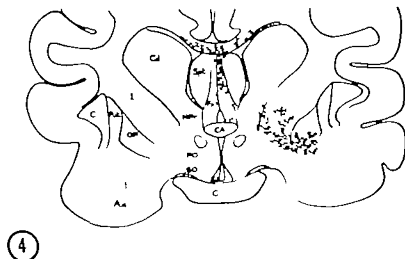
EXPLAN TION O FIGURES

3 A semi-diagramm tic illustration of horizontal section showing the rostro-lateral course of the degenerated fibers from the nucleus medialis dorsalI through the thal mus t the internal capsule. Some fibers make con ection with cell in the gyrus gen alis The black spot represents the lesion Circles indic t preterminal degeneration and dots indicate degenerating fibers of passage

4 A semi-di grammatic illustration of transverse section through the optic chiasm showing the course of degenerating fibers in the most medial nd ventral part of the terior limb of the internal capsule Note that some fibers end in the globu pallidus Circles indicate pre-termin l degeneration and dot indicate fibers passing through



3



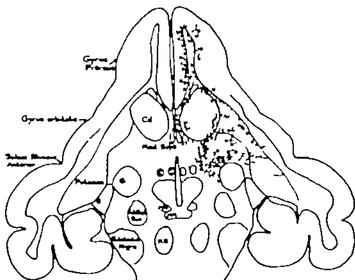
4

PLATE 3

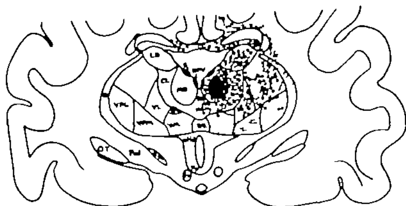
EXPLANATION OF FIGURES

5 A semi-diagrammatic illustration of a horizontal section more ventral than figure 3 showing degenerating fibers in the anterior limb of the internal capsule on their way to the gyrus proreus. Some fibers make a caudo-lateral turn to end in the globus pallidus and putamen. Note the course of the fibers in the caudate nucleus. Circles and dots signify as before.

6 A semi-diagrammatic illustration of a transverse section through the thalamus showing the intrathalamic spread of the degenerating fibers. Black spot represents the lesion.



5



6

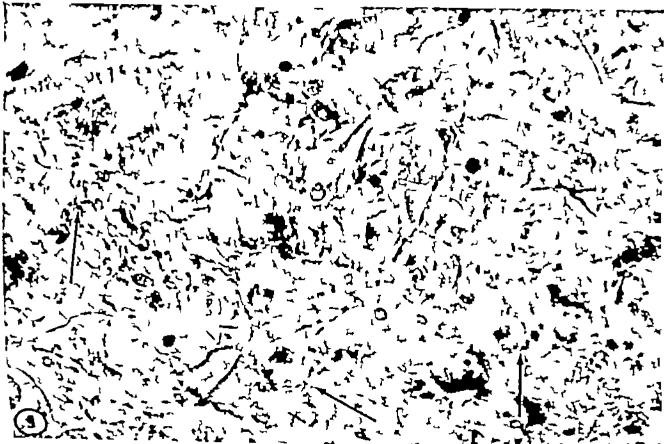
PLATE 4

EXPLANATION OF FIGURES

7 Photomicrograph illustrating degenerating fibers and preterminal degeneration in the gyrus proreus (arrows). A number of normal fibers are also present. Nauta stain × 600

8 Photomicrograph illustrating degeneration in the thalamus. Nauta stain × 300





Photomicrograph illustrating degeneration in he ha areus. Note he preterminal degeneration, N [illegible] at he × 600.

ne Pattern of the Microcirculatory Bed in the entricular Myocardium of Domestic Mammals

ROGER E. BROWN
Department of Veterinary Anatomy School of Veterinary Science and Medicine Purdue University W Lafayette Indiana

ABSTRACT Observations, as determined by injections of India ink through the coronary arteries of isolated and perfused beating hearts, were presented. Tissue blocks were removed from the right and left ventricular walls and the interventricular septum, sectioned and cleared for microscopic examination and photomicrography The term microcirculatory bed was defined as those vessels 100 μ and smaller in diameter. The descriptions were based on 76 normal adult hearts of both sexes of six domestic species.

The arterioles divided by dichotomous branching until the final division resulted in two daughter capillaries. At no time was capillary observed leaving an arteriole larger than 15 μ in diameter The arterioles had a modified type of end artery pattern. Arterial anastomoses were uncommon in the areas and species examined. A specific area of cardiac muscle fascicle was supplied by several arterioles whose capillaries intermeshed. The implications of this concept in relation to micro-embolism were explored.

Capillary anastomoses were frequent but the connecting vessel was only about 20 μ in length. Three types of capillary anastomoses were identified. Capillaries did not cross the muscle fascicles of the myocardium.

Collecting venules were often distinctive in their morphological pattern. "Turnip root" patterns were observed in all species and represented the local venous collection of muscle fascicle. A venule' capillary components were usually from several arteriolar sources.

Supported in part by research grant HE 04317-05 from the N tional Heart Institute, U S. Public Health Service.

This paper will present some observa ns on the morphological pattern of the icrocirculation in the ventricular myordium of adult domestic mammals. This ttern was determined by injections of dia ink through the coronary arteries of lated and perfused beating hearts.

The distribution and general pattern of e major arteries and veins has been lequately established for the human art and those of domestic mammals. In e past, the dissector has examined only e larger vessels because injection mate ls failed to penetrate the smaller chanls in the myocardium The microscopist s concentrated his attention on the mor ological features of the vessel walls and s neglected the definitive pattern of the icrocirculation.

The microcirculatory bed in different sues is assembled in an almost endless mber of variations and other than in e heart has been studied by numerous vestigators. A satisfactory method of sualizing the capillary bed was developed by Wearn ('28a) and used primarily for capillary/heart fiber ratio studies but the morphological pattern in the ventricular myocardium was not fully explored. Functional studies and pathological findings indicate that the larger coronary vessels are true end arteries. Extensive research now being conducted on circulatory diseases makes it imperative that the structural pattern of the microcirculation be investigated.

The descriptions that follow are based on 76 *normal adult hearts of both sexes* of six domestic species.

REVIEW OF THE LITERATURE

Literature describing the myocardial microcirculatory pattern in domestic mammals is sparse. Two reasons may be given for this. First, a satisfactory method of visualizing the capillary bed was slow in developing and secondly there are inher ent difficulties in reproducing this pattern by drawings or photomicrographs for wide spread use.

The first work to gain the attention of American investigators was that of Wearn ('28a) who succeeded in injecting the capillary bed of cat and rabbit hearts us ing both Berlin blue and India ink. The slides from these hearts formed the basis for his classical work on capillary/heart fiber ratio determinations. Wearn and co-workers ('37 '28b '36) continued work in this area and extended it to include hyper trophied hearts and the Thebesian system

Truex and Angulo ('52) investigated the microcirculation of the conduction system of the heart and furnished excellent descriptions of the venous portion of the vascular tree and its anastomotic channels

Reynolds and co-workers (58) gave an accurate description of a venule forming from venous capillaries in their work on the dog

The article by Provenza and Scherlis (59) contains a morphological description of the myocardial capillary bed in the dog although it was primarily concerned with the muscle components of the precapil laries.

Bennett s publication ('36) contains a detailed description of the developmental anatomy of the blood vessels of the pig heart. This is useful as a basis for explaining the presence of the group of vessels loosely called the Thebesian system.

MATERIALS AND METHODS OF STUDY

Injection materials

[1] Several methods for injecting the capil laries of the heart with various materials were employed in the course of this investigation One method in particular was satisfactory in giving a uniform and complete injection of the microvascular system of the myocardium Both the failures and successes will be described in some detail

In selecting materials for vascular injection it was necessary to choose substances that contain suspended particles of such diameter that they would enter the capillaries without difficulty Other requirements for the injection material were that it remain in the capillaries during sectioning show no extravasation or staining of adjacent tissues and withstand the processes of fixation freezing dehydration, clearing embedding and [illegible] The final product should lend [illegible] examination by conventional optic [illegible] recording by photomicrography

Preliminary injection studies were [illegible] on dog hearts to test the [illegible] thorium dioxide for visualizing the [illegible] This compound has excellent radio-[illegible] qualities making it suitable for x ray [illegible] croangiographic studies as well as [illegible] tional light microscopic examination. [illegible] problems limiting its usefulness [illegible] maintaining it in suspension and the [illegible] ability of this suspension to enter [illegible] completely outline the capillary [illegible] These limitations combined with the [illegible] nical difficulties of stereomicrograp[illegible] phy the radiation hazard and [illegible] producing potential of the compound caused its rejection as a suitable [illegible] after several months of effort.

The Crossman method ('40) for the selective staining of red blood cells [illegible] tried as a means of outlining the [illegible] circulation. This procedure results in [illegible] brilliant red staining of all erythrocytes [illegible] *situ* and renders the course of the [illegible] system visible. The technique [illegible] used effectively on sections over [illegible] thick which limits its usefulness for [illegible] lowing vessels over some distance [illegible] many instances the capillaries did [illegible] have sufficient red cells present to [illegible] quately outline the intricate branching patterns inherent in a capillary bed. The technique was also rejected as a [illegible] method for the type of project [illegible] plated.

India ink has been employed [illegible] for injecting blood vessels and in [illegible] vestigation proved to be the most [illegible] tory of the various substances [illegible] used for this purpose. Perfusion of the isolated beating heart when correctly [illegible] gave satisfactory and uniformly [illegible] ful injections. The procedure used [illegible] essentially that described by Wearn [illegible] with some modifications which [illegible] more effective and useful.

The perfusate used was [illegible] Locke s solution maintained at 3[illegible]°C [illegible] chemicals were of reagent quality [illegible] solved in distilled water and [illegible] Pyrex glass containers. [illegible]

---

[1] Higgins Ink Co. Inc Brooklyn 15, New Yo[illegible]

was used as it came from the bottle ...re being taken to decant it carefully ...ving any flocculated material behind. ... precluded the necessity of the diffi...lt task of filtering. Wearn had diluted ...e ink 50% with physiological saline ...lution but this was undesirable for this ...rk due to the decreased opacity and the ...rmation of a fine sediment. The pH of ...ggins India ink was 9 0 with the alka...dity apparently due to the presence of ...monium hydroxide which helps main...in the carbon in a colloidal state. India ...k also contains a surface acting agent ...r the same purpose and the dilution ...commended by Wearn seems to defeat ...e purpose of these additives. Late in ... course of this work, another brand of ... ink (Pelikin) was found which had pH of 7 6 This ink had less adverse ...ects on the vascular physiology and ...ntained its colloidal suspension of car...n particles thus preventing the forma...n of emboli which could plug the ...aller elements of the microcirculatory ...e. Just before the perfusion, commer... formalin (40%) was added to the ...dia ink to a concentration of 2% for ...alin without altering the colloidal prop... of the ink. This gave rapid fixation every portion of the heart and pre... autolysis.

Age numbers and species injected

Seventy-six animals of six domestic spe...– were examined during the course of ...is study Of these numbers four were ...eep aged three years, two were steers ... months old, two horses of nine and ... years of age four pigs aged seven ...ks, eight cats varying from 9 months 4 years of age and 56 dogs 1 to 3 years ...age. The sex ratio of the animals was ... in all species except cattle. Adult ...imals were used for the study as other ...k in progress indicates that the morpho...gical pattern of the capillaries in the ...art undergoes a radical change from ... to adulthood. To obtain a good in...tion of the capillary bed it was neces...ry to use completely healthy animals. ...ills from an animal colony sick with a ... disease were seldom successfully ...ected with India ink.

Injection methods

The animals were killed by a blow on the head. The heart was removed through a left thoracotomy and a cannula tied into the aorta (fig. 1) at a sufficient distance from the aortic valves to prevent blocking the openings of normal as well as anomalous coronary arterial channels. The valves were competent in all the species studied and prevented the escape of the ink into the left ventricle By cannulating the aorta both coronary arteries were injected simultaneously at the same pressure. Injection pressures were determined by the height of the perfusing fluids and this was adjusted ... approximate the systolic blood pressure of the various species.

Perfusion was started before beating ceased. If the contractions had stopped they were restored almost immediately after the perfusion was under way Hearts from anesthetized animals did not respond to the perfusion as regularly or as vigorously as animals killed by a blow on the head. Over 35 hearts were rejected as

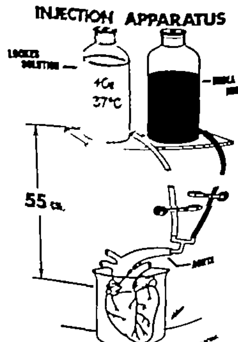


Fig 1 Perfusion and injection apparatus John Bouchet & Co ... Park Avenue, New York 16, New York.

poorly injected before this fact was recognized. The presence of air bubbles in the cannulas tubing and vessels was avoided at all costs. The most effective way to clear the system of air was to allow the perfusing fluid to flow freely into the aorta and out the stumps of the right carotid and brachiocephalic arteries while gently massaging the heart. This encouraged the air bubbles present to leave with the stream of escaping fluid. Hemostatic forceps were then applied to each of these vessels thus diverting the perfusing fluid to the coronary arteries The heart lost its deep red color and the surface veins were washed free of erythrocytes. Those hearts which blanched out evenly proved to inject properly Areas which retained a red color proved later to have received an incomplete ink injection When the heart was beating well as evidenced by its rate, rhythm and intensity the flow of Locke's solution was stopped and the flow of India ink begun. The ink entered the aorta and then by way of the coronary arteries flowed into the vessels of the myocardium with the heart injecting itself by its own action. It should be emphasized that no other method will fill the myocardial capillary bed It seems that the heart must assist or at least have its muscular elements in motion to accomplish this Many injections were tried on non-beating hearts with very poor results.

Immediately after the start of the ink injection the arteries filled first and appeared as black stripes on the heart during the first diastole. As the ink filled the capillary bed in the following diastole the entire heart became uniformly black. The ink then appeared in the veins on the epicardial surface The heart rate slowed immediately rapidly weakened and usually ceased within one minute. Several dog hearts in this series suddenly began to dilate following the ink injection and the contractions ceased immediately At a later examination these hearts proved to be the most perfectly injected of any examined during this investigation. Wearn ('28a) noted this dramatic enlargement in his work on cats with the resulting material being the best for his studies.

Tissue preparation

Following the injection a silk cord was tied firmly around the great vessels [illegible] to the atria and the heart was immersed in 5% neutral aqueous formalin for further fixation. After 24 hours the ligature was removed, the great arteries and veins were trimmed as close to the heart as possible and the chambers of the heart gently flushed with flowing water to remove blood clots and the excess India ink. The hearts were again immersed in 5% formalin for further fixation for 48 hours. The complex arrangement of cardiac muscle layers necessitated the selection of several planes of sectioning to give both a cross sectional and longitudinal concept for full visualization of the morphological pattern. Sagittal and transverse tissue blocks were removed from the areas indicated in figure 2. The regions selected represented the right and left ventricular wall and the interventricular septum.

The tissue blocks were washed in running water for several hours to remove the residual formalin since tissue containing this compound caused uneven freezing with subsequent tearing upon sectioning. The tissue blocks were placed on a [illegible] 130 mm freezing stage of a Zeiss [illegible] type microtome. Sections were cut at thicknesses of 40 60 80 120 and [illegible]. They were mounted on glass slides and racked in a horizontal plane in a specially designed holder until almost dry to [illegible]

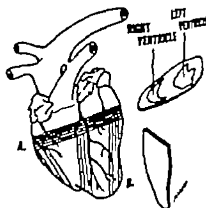


Fig. 2 Scheme of sectioning

[1] Fisher Scientific Co., Chicago, Illinois

gelatin mounting medium to harden. sections were dehydrated by an ascending series of alcohol, cleared in xylene and coverslipped with Permount.

Additional blocks of tissue from the same areas were washed dehydrated in alcohol, cleared and embedded in paraffin. Sections were cut from these blocks at 10 and 40 μ in thickness. The sections were mounted on glass slides and cover slipped after the paraffin had been removed with xylene. These histological preparations revealed that the India ink filled the lumina of the large and small vessels of the microcirculation. The range of thickness from 10 to 40 μ allowed study of the smallest vascular ramifications at magnifications of 100 to 430 × with the conventional light microscope. The arterial and venous trees were examined in the thicker sections under lower magnification with the dissecting microscope. At 30 to 150 magnifications carbon filled blood vessels could be followed through the various planes in the thick sections and their pattern of distribution accurately determined. Extravasation could be readily identified and were found in only a few of the preparations. The injected hearts prepared as described afforded an opportunity to study the microcirculatory architecture of the heart in more detail than had been possible with other materials and methods mentioned earlier

Optical and photographic equipment

The light microscope used in this study was a binocular monobjective Bausch and Lomb with optical combinations producing 100, 150 and 430 magnifications. The binobjective stereoscopic dissecting microscope was a Leitz with magnifications from 16 to 150 and a Bausch and Lomb with magnifications of 10 and 90. Illumination for the dissecting microscopes was provided with a Bausch and Lomb 100 watt microscope lamp with the sections being trans-illuminated. Drawings were made from observations in both of microscopes but the written description of the morphological pattern are mainly from studies with the dissecting

The photomicrographs were made with two instruments The first was a Carl Zeiss photomicroscope equipped with an automatic 35 mm camera. The second instrument was a Leica 35 mm camera with an Ipso one-third reducing adapter mounted on a Spencer A O microscope equipped with an Orthro-illuminator The photographic film used was Panatomic X[*] and Adox KB[**] developed in Kodak D-11 All film exposures were made at 40 magnifications of the prepared slide Each photomicrograph in this paper is accompanied by a micron scale and a line drawing of a cross section of the heart with the area marked where the photomicrograph was taken.

OBSERVATIONS AND DISCUSSION

General statement

Before presenting the data some of the terms used throughout this paper will be defined. The term microcirculatory bed refers to those blood vessels 100 μ and smaller in diameter This diameter has been selected as the beginning of the microvascular system since this is roughly the limit at which the arterial and venous vessels can be dissected without optical aid. Arterioles and venules are vessels having this diameter and decrease in size by branching to form capillaries. The capillaries are those vessels which connect the smallest ramifications of the arterioles and venules and serve as the site for the exchange of substances between parenchymal cells and blood. The term venous sinuses describes those vascular channels from the lumen of the heart which penetrate between the muscle trabeculae and present an extensive network which terminates peripherally in numerous blind recesses. Connections called "Thebesian vessels" are collateral channels between the lumen of the heart chambers and the coronary arteries veins and capillaries The term end artery implies an arterial blood vessel without connections with other arterial vessels. This concept refers to the absence of anastomotic connections between arteries of relatively large size which if present would provide blood to a

[*] Eastman Kodak Co Rochester New York.
[**] Adox Fotowerke, Frankfurt, Germany

given capillary field from several peripheral loci.

The term muscle fascicle is used to refer to a group of muscle cells of sufficient number to be seen by the naked eye and is separated from adjoining layers by connective tissue sheaths. The term muscle layer is used to represent the total of a number of fascicles that have the same directional orientation in the heart.

Unless specifically stated otherwise all descriptions of the microcirculation that follow were observed in all the domestic species examined (horse cow sheep pig dog and cat)

Arterioles

The following description is limited to those arterial branches of the microcirculation measuring 100 μ or less in diameter. These arterioles entered the myocardium in connective tissue septa with the accompanying veins. The arteries bifurcated and decreased in diameter in a dichotomous manner with the two daughter vessels being of equal size (fig 6) The rapidity with which the arterial caliber decreased varied with the different daughter vessels and their ultimate function. In those vessels which acted primarily to transport blood through the tissues the diameters decreased gradually In those which vascularized the adjacent area the diameters were reduced more rapidly as they terminated in their capillary network. The diameter of the arteriole at the level of the first capillary branching varies little in the different regions of the myocardium or in the domestic species studied At no time was a capillary observed leaving a vessel which exceeded 15 μ in diameter. The usual ending of a terminal arteriole was by division into two daughter capillaries (figs 5 9 10 11 12) These capillaries could pursue the same direction (figs 9 10 11 12) but often ran in opposite directions (fig 10)

The small arteries were found to lie in the spaces between and parallel to the muscle fascicles (fig 7) The arteriole pierced the muscle bundle usually diagonally or transversely (fig 7) and immediately arborized into capillaries which were parallel to and in contact with the muscle fibers. A specific area of a cardiac muscle fascicle was supplied by [illegible] arterioles whose capillaries [illegible]

Anastomotic communications between arterioles measuring less than 40 μ in diameter were found occasionally in [illegible] adult hearts (fig. 8) These [illegible] fine communications would be of [illegible] functional significance in [illegible] effects of sudden arterial occlusion. The arterial trees of the microcirculation were morphologically end arteries and were limited in their distribution to one [illegible] fascicle alone.

Arterial arcades the "Micro-[illegible]" of Saunders (57) are present in skeletal muscle, intestinal wall and the skin (9) The pattern was not observed in the depths of the myocardium but only on the [illegible] surface of the heart and then in a somewhat modified form.

No additional evidence can be [illegible] as to the number caliber and location of the larger anastomoses between the left and right coronary arteries. These [illegible] be studied with injection techniques differing from those employed here.

Capillaries

The arterioles penetrated the connective tissue of the muscle fascicles and distributed capillaries running parallel to each of the cardiac fibers. The great number of capillaries was apparent when the entire microcirculatory bed was completely injected with India ink. The sections taken parallel to the muscle fibers showed this interrelated mesh of capillaries [illegible] strikingly The capillaries were spaced between the muscle fibers in an approximate ratio of one capillary to one muscle fiber (fig. 16)

The daughter capillaries of a [illegible] arteriole branched extensively with [illegible] negligible change in caliber (figs 5 [illegible] 11) These branches had frequent anastomoses and formed a network with [illegible] gated meshes. The anastomoses were short (approximately 20 μ) and connected immediately adjacent capillaries (figs [illegible] 12 16) The anastomoses were of [illegible] types as illustrated in figure 3

When the tissue was fixed and [illegible] ded in such a way that shrinkage caused the muscle fascicles to become separated it was clear that the capillaries [illegible]

t fascicles and did not cross between .ir layers (figs. 7 9 13 14 17) It ght be postulated that the interplay of layers over each other could shear off apillary crossing between fasciculi.

The Purkinje system s capillary supply unit of area was found to be much less n that to the heart muscle and the ply decreased as the endocardium was roached (fig. 14) However the Pur je fibers had approximately the same mber of capillaries per fiber as the myo dial area. This agrees with the findings Wearn ('28a) As these specialized scle bundles spread through the myo dium, the capillary pattern was distinc and this system could be followed ough the myocardium without conven al histological staining procedures.

The complex arrangement of the muscle cicles at the junction of the ventricular lls and the interventricular septum re ted in the complex pattern of capillaries strated in figure 15

The length of the capillaries shown in res 5 10 11 12, 20 and 23 may ac nt for the high rate of oxygen extrac n from the coronary circulation as npared to other tissues and organs uhmer '61)

Venules

A collecting venule looked quite differ t from a terminal arteriole. The capil les came from all directions along the scle fibers made a sweeping curve to n with each other and rapidly formed venule (figs. 17 18 19 20 23 24) e term "turnip root was applied to this ginning venous tree as descriptive of its pearance under the dissecting stereo croscope. This structural pattern was served in all species studied and is well strated by figures 17 18 19 This all venule then extended along in the scle fascicle for a short distance or was usually the case, turned abruptly d crossed perpendicular to the fibers to ch the space between the muscle bun s (figs. 18 19) Each collecting venule tined a muscle fascicle thus gaining e and resulting wall strength before ssing the connective tissue space be ten fascicles. The interplay that must cur in movements of these fascicles over one another would dictate a vessel of some size to withstand the shearing action cre ated by the heart s contraction. The same line of reasoning would indicate that vessels crossing between muscle layers should be of even larger size and strength and this was verified by examination of the cleared sections.

Single capillaries were frequently observed joining a venule as large as 50 µ in diameter (fig. 21) This observation was made in all regions of the ventricular myocardium of all species studied and is in direct contrast to that of the arterial tree where capillaries originated only from arterioles 15 µ or smaller in size.

The venules of the cardiac microcirculation consistently showed a markedly oval shape on cross section of the vessel wall. This was not attributed to a fixation artifact but was considered a normal morphological feature. Their location between the cardiac muscle fascicles and layers combined with the high pressures present in the heart would offer a plausible explana tion for this oval shape. The morphologi cal pattern of a collecting venule in these observations agrees with the work of Reynolds et al. ('58) on the dog.

General discussion

The heart s location in the circulatory pathway is a most fortunate one The capillary bed of the lung acts as a filter for most of the emboli from the body s venous return before its passage through the coronary vessels Thus, macro-emboli associated with the coronary circulation are limited to those originating in the pulmonary veins, the left ventricular chamber and the coronary arteries themselves. Of greater concern in this investigation is the role of micro-emboli in the myocardial microcirculation. Because of the larger diameter of the lung capillaries (12 to 16 µ) as compared to those of the heart (6 to 8 µ) any emboli which pass through the lungs are of a diameter that will lodge in the microcirculation of the myocardium at the bifurcation of the smallest terminal arteriole. With this fact in mind the definitive pattern of the microcirculation assumes a major role. Figures 3 and 4 are provided to serve as a basis for discussing the implications of this pattern.

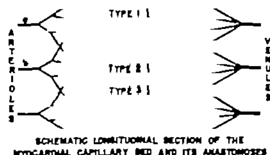


Fig. 3 Schematic longitudinal section of the myocardial capillary bed and its anastomoses.

The longitudinal representation (fig. 3) indicates that a specific area of a cardiac muscle fascicle is supplied by several arterioles whose capillaries are inter meshed. This observation was made in all the domestic mammalian species ex amined The exact manner or pattern of this intermeshing of capillaries appeared to be a random arrangement when ex amined by all the optical methods available Thus, the schematic nature of figures 3 and 4 must be emphasized and other patterns could have been included as well.

Figure 3 also illustrates the three types of capillary anastomoses observed in the six domestic species examined. Type 1 anastomosis, between the daughter capil laries of a terminal arteriole was the most frequent of those occurring in the myocardial capillary bed. Type 2 anastomoses were found second in frequency and oc curred between the capillaries of terminal daughter arterioles Type 3 anastomoses were the least common and occurred be tween the capillaries of arterioles origi nating from a more distant dichotomous branching

The schematic cross-sectional view (fig 4) illustrates some of the locations the capillaries of arterioles *a* *b* and *c* might occupy in relation to specific cardiac fibers. The possible circulatory impairments which may occur from an embolus plug ging the smallest terminal arteriolar branches of the myocardial microcircula tion is now evident. For instance if the embolus occurred at arteriole *a* the cardiac fibers nourished by its capillaries would not be endangered because of adjacent functional capillaries. In the case of an embolus occurring in arteriole *b*, the result might be more serious because the anatomic arrangement placed three of its capillaries about of cardiac fiber With the occurrence of an embolus in arteriole *c*, the death of the enclosed cardiac fiber surrounded by *c*'s capillaries would be possible. The concept is thereby proposed that any single cardiac fiber may be surrounded by capillaries from one, two, three or [illegible] terminal arterioles. This capillary pattern would suggest the possibility of scattered randomly located, micro-infarcts occurring in the heart. These infarcts would be characterized by a small diameter (one cardiac fiber) but of considerable length due to the extreme length of many of the myocardial capillaries. The resulting pathology would be insidious but the total accumulation over a period of time could be significant. Pathologists should not regard lightly the abnormal cellular appearance of a single cardiac fiber surrounded by normal myocardial tissue and assign this appearance to a fixation staining or dehydrating error which occurred in processing the section.

The influence of the previously described three types of capillary anastomoses in preventing the damaging effects of a shower of micro-emboli has not been investigated.

Figure 3 also shows that all of the capillaries of a terminal arteriole do not empty into the same beginning venule. It was very rare for this to occur Thus, the concept of an end artery as far as its arterial side is concerned and multiple outlets to its venous capillaries in the myocardial microcirculation is noted. The schematic nature of these drawings must [illegible]

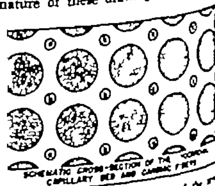


Fig 4 Schematic cross section of the myocardial capillary bed and cardiac fibers

...phasized. Frequently the daughter capillaries pursued a course in opposite directions and gained their venous returns into two comparatively widely separated venous ... The variations in the myocardial ...circulatory pattern at the capillary level were numerous. Whether this is due to a purely random arrangement, or ... arrangement specifically provided for the survival of the fittest, can only be material for some future investigation.

SUMMARY AND CONCLUSIONS

Some observations on the morphological pattern of the microcirculation in the ventricular myocardium of adult domestic mammals as determined by injections of India ink through the coronary arteries of isolated and perfused beating hearts have been presented in this paper. The descriptions are based on a study of 76 normal adult hearts of both sexes of six domestic species.

The method of visualizing the capillary bed was similar to the procedure of Wearn developed in 1928 for use in capillary/muscle fiber ratio studies. Tissue blocks were removed from the right and left ventricular walls and the interventricular septum, sectioned and cleared for microscopic examination and photomicrography. The term microcirculation was defined as those vessels 100 µ and smaller in diameter.

The arterioles divided by dichotomous ... until the final division resulted in two daughter capillaries. At no time was a capillary observed leaving an arteriole larger than 15 µ in size. The arterioles of the myocardium of the heart had a modified type of end artery pattern. Arteriolar anastomoses were uncommon in the ... and species examined. A specific ... of a cardiac muscle fascicle was supplied by several arterioles whose capillaries intermeshed. The concept was proposed that a single cardiac fiber could be ... by capillaries from one, two, ... or four terminal arterioles. The implications of this concept in relation to micro-embolism was explored.

Capillaries were notable for their length compared to those reported in other tissues of the body. This may be a factor in the high oxygen extraction ability of the heart as an organ. Capillary anastomoses were frequent but the connecting vessel was only about 20 µ in length. Three types of capillary anastomoses were identified. Capillaries did not cross between muscle fascicles of the myocardium.

Collecting venules were often distinctive in their morphological pattern. "Turnip root" patterns were observed in all species and represented the local venous collection of a muscle fascicle. A venule's capillary components were usually from several arterial sources.

Venous sinuses were observed penetrating to some depth of the myocardium in all species. Connections between the coronary circulation and these sinuses were not observed. Arterio-luminal, arterio-sinusoidal and Thebesian veins were not demonstrated in the areas examined. The methods used may not have been adequate for their identification.

This paper is submitted with the full realization that the mammalian heart is as yet incompletely explored with respect to the structure and form of the microcirculatory bed and that further work will necessitate modification or extension of the concepts here advanced.

LITERATURE CITED

Bennett, Henry Stanley 1936 The development of the blood supply to the heart in the embryo pig. Am. J. Anat., 60: 27–53.

Crossman, G. 1940 The selective staining of red blood cells. Stain Technol. 15: 155–157.

Provenza, D. Vincent, and Sidney Scherlis 1959 Coronary circulation in the dog's heart. Demonstration of muscle sphincters in capillaries. Circulation Research, 7: 318–324.

Reynolds, S. R. M., M. Kirsch and R. J. Bing 1958 Functional capillary beds in the beating, KCL-arrested and KCL-arrested perfused myocardium of the dog. Circulation Research, 6: 600–611.

Rushmer, Robert F. 1961 Cardiovascular Dynamics. W. B. Saunders Co., Philadelphia, pp. 100.

Saunders, R. L. de C. H., J. Lawrence, D. A. MacIver and N. Nemethy 1957 Part V. The anatomic basis of the peripheral circulation in man. Or the concept of the macromesh and micromesh as illustrated by the blood supply of muscle in man. Peripheral Circulation in Health and Disease. Walter Redisch and Francisco F. Tangco, editors. Grune & Stratton, New York, pp. 113–145.

Shipley, R. A., J. Shipley and J. T. Wearn 1937 The capillary supply in normal and hypertrophied hearts of rabbits. J. Exp. Med., 65: 29–44.

Truex, Raymond C., and Armand W Angul 1952 Comparative study of the arterial and *venous systems of the ventricular myocardium* with special reference t the coronary sinus. Anat. Rec., 113 467–492.

Wearn Joseph T 1928a The extent of the capillary bed of the heart. J Exper Med., 47 273–292.

——— 1928b The role of the [illegible] sels in the circulation of the heart. J [illegible] *Med.*, *47* 293–316.

——— 1936 Chapt. I. The [illegible] Coronary Vessels. Diseases of Coronary [illegible] and Cardiac Pain. Edited by R. L. [illegible] Macmillan Co., New York.

PLATE 1

EXPLAN TI N OF FIGURES

5 Terminal arteriole left ventricle sheep.

6 Terminal arteriole left ventricle dog.

7 Arteriole entering muscle bundle left ventricle dog.

8 Arterial anastomosis, right ventricl dog.

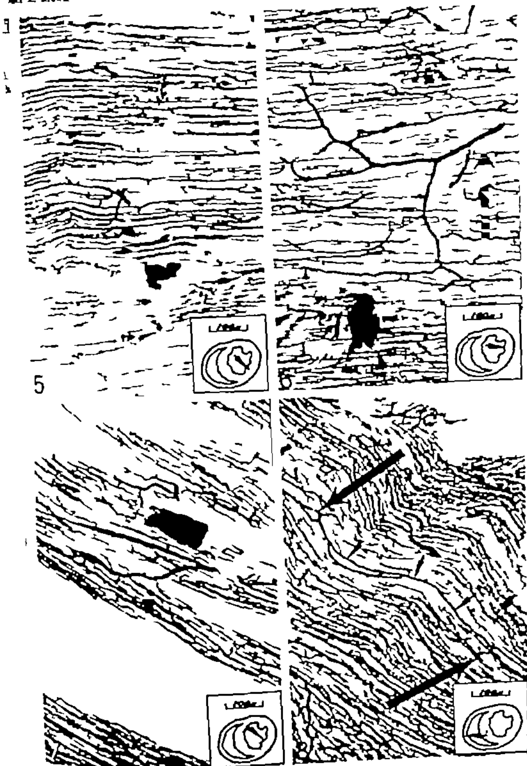

5

PLATE 2

EXPLANATION OF FIGURES

9 Terminal arteriole, right ventricle horse.

10 Terminal arteriole, right ventricle dog.

11 Terminal arteriole, left ventricle, cat.

12 Terminal arteriole right ventricle, pig.

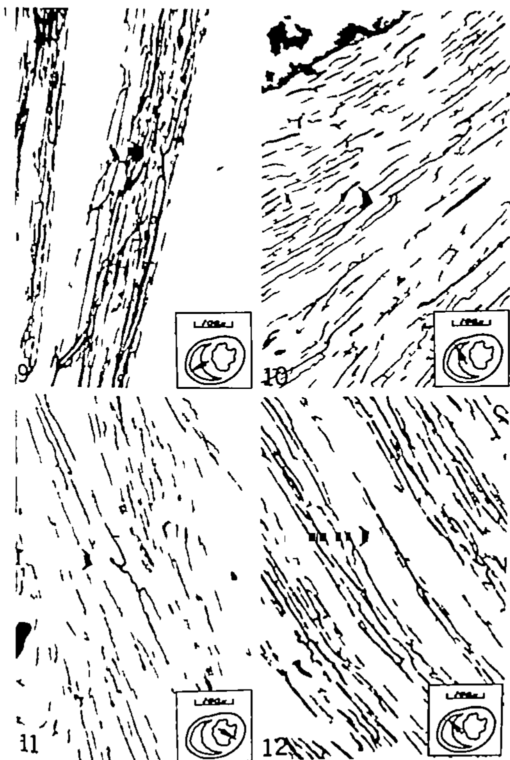


PLATE 3

EXPLANATION O FIGURES

13 Capillaries in muscl fascicles right ventricle, dog

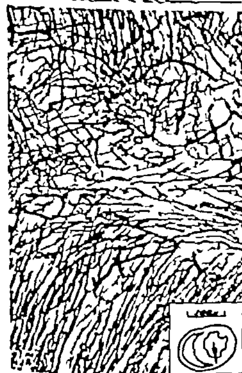
14 Capillaries, myocardial and Purkinje area, dog.

15 Capillary pattern, junction of walls and septum, dog

16 Capillaries, right ventricle, dog.







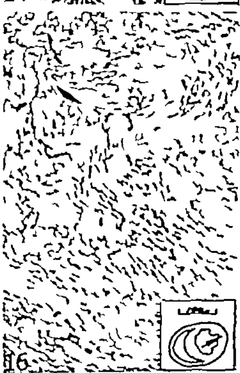



PLATE 4

EXPLANATION OF FIGURES

17 Venous pattern, right ventricle, horse.

18 Venou pattern left ventricle, dog.

19 "Turnip root" venous pattern, interventricular septum, dog.

20 Capillaries forming venules, right ventricle dog.




18


19

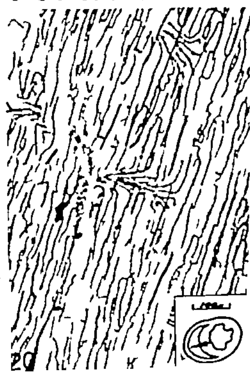

20

PLATE 5

EXPLANATION OF FIGURES

21 Venou pattern, left ventricle dog.

22 Venous pattern right ventricle, horse.

23 Venous pattern right ventricle, horse.

24 Venous pattern interventricular septum, sheep.


21


22


23


24

Fig 1 The cranio-cervical venous system f the dog. Diagram after Padget

Fig 2 Lateral view f dog head w b radio-opaque filling of the transverse sinus (sup dorsal erebral ein, internal m xillary m external jugula ein, and vertebral ein



Fig 3 Dorsoventral view of the dog head with radio-opaque filling of the transverse sinus, (superior) dorsal cerebral vein, internal maxillary veins, mastoid emissary vein, cranio-occipital vein, (external) jugular vein, left inferior petrosal sinuses, basilar veins and vertebral veins in the center



Fig 4 Tilted lateral view of dog head superficial temporal vein communicating with dorsal vein as demonstrated on the venogram

lar cavernous sinuses in this order of magnitude

When filling was made in a reverse direction through the (superior) dorsal cerebral vein, additional filling was noted towards the ethmoidal veins through the superior longitudinal sinus and to the orbital veins through the basilar sinuses. In both cases the greatest filling appeared in (1) the (superior) dorsal cerebral veins and (2) basivertebral veins (basilar sinuses and vertebral veins)

The schematic diagram of these details is presented in figures 1 2 3 and 5

Venous communication in the dog

In addition to the described main venous drainage pathways of the brain the following communications with extracranial venous channels were noted:

(1) Superficial and deep temporal veins with the (superior) dorsal cerebral vein and transverse sinus. Figure 4

(2) Paravertebral venous plexus (ventro-dorsal veins) with basilar plexus Figure 3

(3) Mastoid emissary vein to the occipital vein from the sigmoid sinus. Figure 1

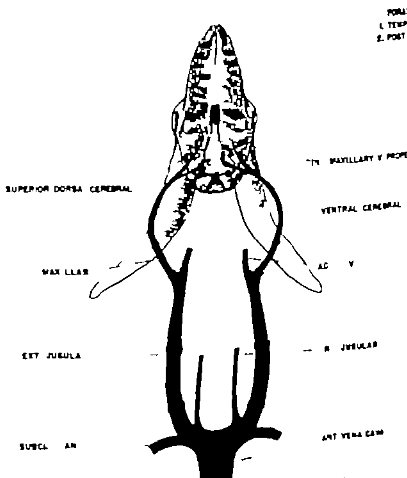
(4) Orbital veins and vena reflexa from the cavernous sinus to facial vein Figure 4

(5) Parietal emissary vein to the superficial temporal vein.

(6) Occipital emissary vein to the occipital vein from the transverse sinus

(7) Frontal emissary vein to supraorbital veins from the (superior) dorsal longitudinal sinuses.

(8) Pterygoid veins to the internal maxillary vein and vena reflexa from the cavernous sinus.



F g 7 Cranio-cervical venou ys em f the sheep

(9) Anterior ethmoid veins from the sal longitudinal sinuses to the angular ns.

(10) Anterior condyloid vein (hypo-sal) connecting the ventral cerebral n with the vertebral plexus.

(11) Diploic veins connecting frontal dxary veins with the transverse sinuses ough the diploic canal, bypassing the perior) dorsal longitudinal sinus.

Rhesus monkey

On rhesus monkeys the type of venous flow was found to be identical with that man; i.e. the presence of large internal gular veins leaving the skull through the gular foramen (part of foramen la rum) and being a continuation of the moid sinus. There is a constant small amen that actually corresponds to the nporal foramen and is described under mes postglenoid foramen (Batson, 44) and (Straus) foramen lacerum spurium (Van Gelderen, '24) This foramen drains cerebral blood from the inferior petrosal sinus. There is a small condyloid canal but no temporal foramen (fig. 6)

Sheep

In this species there is a large temporal foramen through which the dorsal cerebral vein passes. The superficial temporal vein, carrying extracerebral blood joins the large dorsal cerebral vein within a short bony canal before the latter vein leaves the skull.

There are two ventral occipital sinuses and the condyloid veins in the bony condyloid canal connect the dorsal and ventral cerebral venous systems (fig. 7)

Pig

This animal has a large internal jugular vein, leaving the skull through the jugular

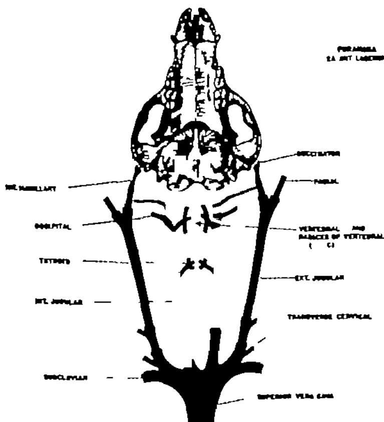


Fig 8 Cranio-cervical venous system of the pig

(lacerum) foramen. There is no temporal foramen. There is usually a condyloid canal connecting the dorsal and ventral cerebral venous systems (fig. 8)

Cat

Felines have internal jugular veins leaving the skull through the posterior part of the foramen lacerum. The initial part of the internal jugular vein corresponds to the (inferior) ventral cerebral vein.

A rudimentary temporal foramen is frequently present but the *size of it is variable.* Most frequently this foramen and the (superior) dorsal cerebral vein draining through it is very small (Harrison '56) and (Mivart 1895)

There is communication between the dorsal and ventral cerebral venous systems through a condyloid canal and vein (fig 9)

Rabbit

A very small internal jugular vein m[ay] leave through the posterior jugular fo[ra]men but there is a temporal foram[en] rather high above the external opening of the auditory meatus through which the dorsal cerebral vein drains the larger p[art] of the cerebral blood into the superficial temporal vein. The temporal foramen is situated between the squamosal and per[i]mastoid bones near the tip of the sq[ua]mosal process of the parietal bone (Bensley '23)

Communication between the dorsal and ventral sinus systems is through the condyloid canals containing the same vei[ns] (fig 10)

Horse

The internal jugular vein of the hor[se] does not contain cerebral blood but rathe[r]

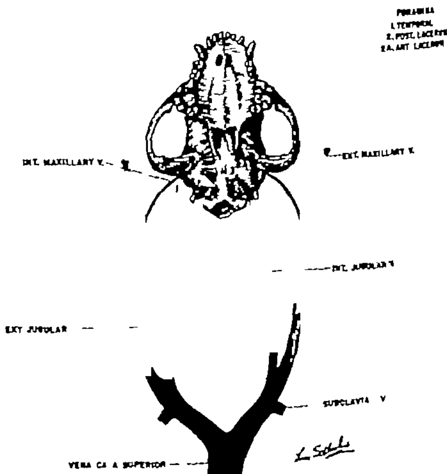


Fig 9 Cranio-cervical venou[s] system of the cat.

a admixture of blood converging from pharyngeal, esophageal and thyroid veins. There is a temporal canal and foramen emitting the (superior) dorsal cerebral vein as a continuation of the transverse sinus, and through the posterior part of the foramen lacerum the (inferior) ventral cerebral vein drains the ventral cerebral sinus system. The (superior) dorsal cerebral vein enters the superficial temporal vein, and the (inferior) ventral cerebral vein joins the cerebrospinal veins to form the occipital vein (Bolk et al. '31 and Martin, '15) (fig 11)

There is no condyloid canal and vein in the horse, but there is an extracranial communication between cavernous (i.e. ventral sinus system) and transverse (i.e. dorsal sinus system) sinuses through the rete mirabile (?) reflexa.

Ox

The bovine internal jugular vein, like that of the horse does not drain cerebral blood The ox possesses a temporal foramen or more precisely a fissure like opening of the temporal canal through which the (superior) dorsal cerebral vein drains. Superficial temporal veins and orbital veins enter the transverse sinus through a bony canal thereby emptying extracranial blood into it (Bolk et al '31 and Martin '15)

Connection between the transverse sinus and ventral cerebral sinus system is accomplished by the condyloid veins in the condyloid canals (fig. 12)

DISCUSSION

It is not the purpose of this paper to present the phylogenetic and embryologic aspects of the cranio-cervical venous system Still it would be an omission not to mention that the basic pattern of the cranio-cervical venous channels of a dog

Generally speaking, young animals with incompletely ossified cranial bones may have fissure-like structures instead of clear cut foramina on the base of skull.

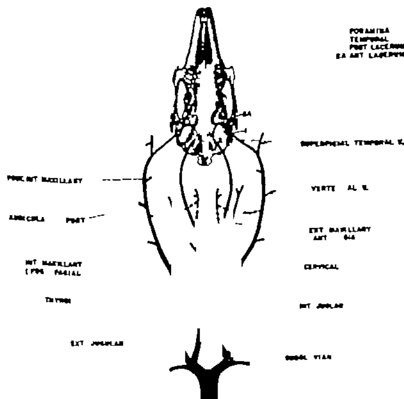
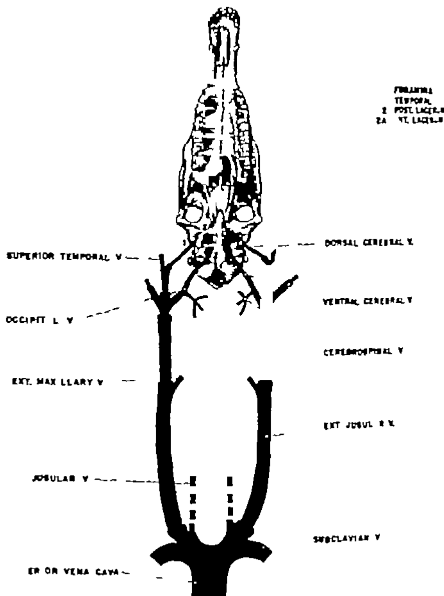


Fig 10 Cranio-cervical venous system of the rabbit



F g. 11 Cranio-cervical venous system of the horse

fetus is similar to that of the early human fetus (Padget, '37) Due to greater devel opment of the face nose mouth, ears (and horns) the external jugular vein as the continuation of the (superior) dorsal cerebral vein becomes predominant in many other mammals such as dog sheep rabbit ox and horse In man as well as in rhesus monkey pig and cat however the internal jugular vein remains predominant in the adult.

The relative size of the [illegible] veins would indicate the site for [illegible] drawal of cerebral venous blood [illegible] in species possessing a non-human [illegible] pattern drainage of extracerebral [illegible] into the temporal canal and into the [illegible] sal cerebral vein immediately after [illegible] emergence from the skull results in [illegible] ture of a large amount of extracer[illegible] blood. For this reason specimens of [illegible] obtained from the temporal foramen [illegible]

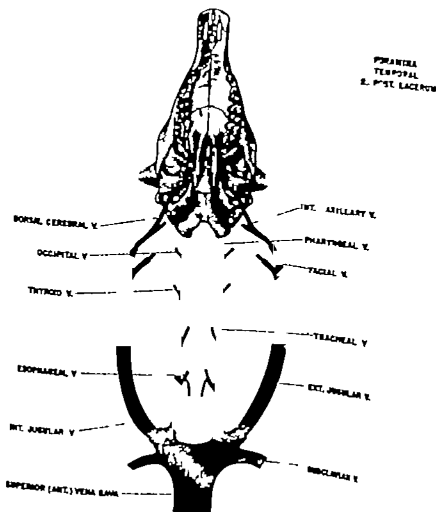


Fig. 12 Cranio-cervical enous system of the ox

annot truly be considered representative f cerebral venous blood.

All factors of anatomy considered, the osterior third of the (superior) dorsal si us is the most suitable site for withdraw ng cerebral venous blood samples in ex erimental animals.

The presence (+) absence (−) and legree of development (+ to +++) of the nain features of this tudy are summa- ized in table 1 The ease or difficulty of ccess to the dorsal lor gitudinal sinus was also considered.

In man and in rhesus monkey the best ite for withdrawal of cerebral enous blood is the jugula bulb through percuta- neous puncture as first recommended by Myerson (Nylin, '57)

In the non-primate group of mammals studied by us the dog is the choice species because of its proportionately larger brain size and because the posterior third of the dorsal longitudinal sinus can be ap- proached optimally through a bone-flap on the skull-top. This bone-flap interrupts the frontal and parietal emissary veins and the connecting diploic veins and thereby a small and constant contamin extracerebral blood through the ethmoidal veins will occur thus the experimental error

TABLE 1

Comparative anatomy of the cerebral venous return

Variables	Jugular (lacerum) foramen	Temporal foramen	Int. jugular vein	Dorsal cerebral vein	Condyloid canal and vein	Dorsal longitud. sinus	[illegible]
Man	+++	−	+++	−	+	+	
Rhesus Monkey	+++	+	++	+	+	+	
Pig	++	−	++	−	+	+	
Cat	+	±	+	±	+	+	
Dog	+	++	±	+++	+	+	
Sheep	+	++	−	++	+	+	+
Rabbit	+	++	±	++	+	+	
Ox	+	++	−	++	+	−	
Horse	+	++	−	++	−	+	—

Postglenoid foramen.
There is vein suspended in the falx, rather than typical sinus.
Lumen irregular
Foramen on the temporal squama.
Note Species with well developed temporal foramina have no true internal jugular veins and their main cerebral venous outflow is the (superior) dorsal cerebral vein through this foramen.

ACKNOWLEDGMENT

This study was greatly helped by the advice and encouraging criticism given by William L. Straus Jr Ph D Professor of Anatomy and Physical Anthropology of the Johns Hopkins University School of Medicine, Baltimore Maryland

The cooperation of the U S Army Chemical Center Edgewood Maryland is hereby gratefully acknowledged.

Technical assistance of Mary B Cahill R.N Lucile R. Gransky B.A. Nicholas A. Battistone the Radiology Department and Pathology Department of VAH Perry Point Maryland, is greatly appreciated.

The Medical Photography was contributed by Luther R Gilliam Chief of Medical Illustration Service VAH Perry Point, Maryland and the art work by Leon Schlossberg, Instructor of Art as Applied to Medicine at the Johns Hopkins University School of Medicine Baltimore Maryland

LITERATURE CITED

Batson, O V 1944 Anatomical problem concerned in the study of cerebral blood flow Fed. Proc., 3 139–144

Bensley Benjamin A 1923 Practical Anatomy of the Rabbit an Elementary Textbook i M mmalia An tomy 8th ed Blakiston Philadelphia

Bolk, Louis, Ernst Göppert, Erich Kallius and Wilhelm Lubosch 1931 H dbuch der Vergleichenden Anatomie der Wirbeltiere U ba and Schwarzenberg Berlin

Bradley O C., and T Grahame 1959 Topographical Anatomy of the Dog. 6th ed. Macmillan, New York.

Ellenberger Wilhelm, and Hermann Baum 19[illegible] [illegible] Anatomie des Hundes. Dietrich Text Leipzig.

Gelderen C. van 1924 Die Morphologie der Sinus Durae Matris. Zweiter Teil Die [illegible] chende Ontogenie der Neurokraniellen [illegible] der Vogel und Saugetiere Ztschr f. Anat. Entwicklungsgesch., 74 432–508

Gray Henry 1954 Anatomy of the Human Body 26th ed. Lea and Febiger Philadelphia

Harrison, Bruce M. 1958 The Dissection of the Cat. C B Mosby Co., St. Louis

Kety S S., and C F Schmidt 1948 [illegible] oxide method for quantitative determination of cerebral blood flow in man Theory procedure and normal values. J Clin. Invest 27 [illegible] 483.

Martin P ul 1915 Lehrbuch der Anatomie der H ustiere 2 Auflage 2. Hälfte Schickhardt and Ebner Stuttgart.

Mivart St. George Jackson 1895 The Cat [illegible] Scribner Sons, New York.

Nylin G 1957 Estimation of Cerebral Blood Flow and Cerebral Blood Pool by the [illegible] Labeled Erythrocytes. In book Wright [illegible] S., Millikan, C. H. eds. Cerebral Vascular Disease Second Princeton Conference

Padget, Dorca H. 1957 The Development of the Cranial Venous System in Man from the Viewpoint of Comparative Anatomy [illegible] tion of Carnegie Institution of Washington Vol XXXVI pp 79–140

She kin H A M. H. Harmel and S S Kety 1948 Dynamic anatomy of the cerebral circulatio Arch. Neurol. and Psych. [illegible] 240–252

Sisson, S and J D Grossman 1953 The Anatomy of the Domestic Animals 4th ed. [illegible] Saunders Co Philadelphia and London

Straus, William L. J Personal Communication

Osteolathyrism in Mice and Inhibition of the Endosteal Bone Reaction in Estrogen treated Mice by Aminoacetonitrile[1]

D J SIMMONS A. M. PANKOVICH AND A. M. BUDY

Radiological Physics Division, Argonne National Laboratory Argonne Illinois Department of Surgery (Orthopaedics) University of Chicago Clinics Chicago Illinois and Department of Physiology University of Chicago Chicago, Illinois

ABSTRACT The effect of aminoacetonitrile (AAN) on the skeletons of young mice injected with estrogen was studied histologically and microradiographically. AAN (0.5 2.5 5, 10 or 20 mg) was administered daily during the first week of treatment alone or in combination with a single injection of 1 mg estradiol valerate on the first day. The animals were sacrificed at intervals of seven days for a period of four weeks. The bone reaction leading to ossification of the marrow cavities as consequence of estrogen-treatment was diminished by 5–20 mg AAN and the effect was roughly proportional to the dose of the nitrile. The metaphyseal trabeculae (distal femur) of the AAN-treated mice developed a mosaic appearance. While administration of the nitrile alone induced the formation of periosteal hyperostotic and osteo-cartilaginous hyperostotic fiber bone tissue over the femoral shafts late in the post-treatment recovery period, combined treatment with estrogen potentiated these changes during the treatment period itself. The cortical bone tissue was also demineralized by combined treatment, and fused osteocyte lacunae regularly appeared as an apparent sequela of both cell enlargement and degradation of perilacunar matrix. Conversely estrogen completely protected the epiphyseal cartilages against degenerative changes (abnormal vascular invasion rents etc.) after low doses of AAN (0.5–2.5 mg) during the treatment period, but the hormone was only partially effective after higher doses of AAN It was suggested that aminoacetonitrile disrupts both the formation of new bone collagen and the integrity of collagenous structures deposited prior to treatment.

Estrogen administered to mice stimulates ossification within the medullary cavities of most of the skeletal elements (Gardner and Pfeiffer '38 Urist et al., '50) The endosteum becomes an actively proliferating tissue. New bone is formed centripetally and, if treatment is prolonged, the marrow cavity may become completely obliterated. Potentiation of the endosteal bone reaction has been ascribed to increased vascularization or to some unspecified local insult to the primitive connective tissue cells of the marrow These cells respond by modulating to osteoblasts (Urist et al. '50 Simmons '63) Although attempts have been made to inhibit this new bone formation with testosterone (Urist et al., '50 Suzuki, '58 Parker and Crossley '62) the results have been equivocal nor is the role of the pituitary growth hormone well-established (Gardner and Clouet '44)

An increasing number of reports indicate that non-endocrine agents such as β-aminopropionitrile (BAPN) and aminoacetonitrile (AAN) and their analogs are effective inhibitors of ground substance formation in connective tissues i.e., reduced hexosamine content of bone (Castellani and Castellani-Bisi, '58 Ponseti and Aleu, '58) and of collagen polymerization (Levene and Gross, '59 Van den Hooff et al., '59 Gross, '63 Martin and Goldhaber '63) It is less well-known whether these compounds or their metabolites disrupt collagen formed prior to administration, but they cause extensive multiple lesions of mesodermal tissues particularly in the skeletal and vascular systems. These include epiphyseal tearing and slipping, periosteal new bone formation, reduction of endochondral bone formation, kyphoscoliosis, dislocations de-

[1] Work performed under the auspices of the Atomic Energy Commission, and was partially supported by Research Fellowship DPD-12, 685, United States Public Health Service Grant A-6333 Met., and the Atomic Energy Commission (At(11-1)-787) awarded to Dr Franklin C. McLean, Physiology Department, University of Chicago, Chicago, Illinois.

generative arthritis and dissecting aneurysm of the aorta. Clinically the changes are known as osteolathyrism and the complete syndrome can be produced after inclusion of *Lathyrus odoratus* L. seeds in the diet or treatment with nitrilic compounds for prolinged periods In the rat, estrogen apparently inhibits the development of lathyrism (Ponseti and Shepard '54 Selye and Bois '56) and retards the regression of the skeletal lesions after temporary AAN treatment (Selye '57) In the rat, the hormone suppresses osteoclastic resorption only of bone of endochondral origin (Urist et al 48 Lindquist et al. '60) The present experiments have utilized the estrogen-treated mouse to observe the effect of AAN on both newly forming and old collagenous tissues, and to determine whether AAN will interfere with estrogen induced new bone formation.

MATERIALS AND METHODS

In a preliminary experiment 12 CF mice 30–35 days old were divided into four groups Group 1 received intraperitoneally a total of 1 0 mg estradiol valerate (Delestrogen) in 0.5 mg doses on the first and third day group 2 received 10 mg AAN intraperitoneally daily for six days; group 3 received both estradiol valerate and AAN group 4 served as controls. The nitrile was not neutralized prior the injection Three mice from each group were sacrificed on the seventh and fourteenth days. At autopsy the left femurs and tibias were removed and fixed in 95% alcohol and Susa solution respectively The remaining carcasses were eviscerated and stained with Alizarin red S to ascertain the gross effects of the agents upon the skeleton The femurs were embedded undecalcified in methyl methacrylate and cut longitudinally at 75–100 μ on a high-speed rotary saw The sections were microradiographed on Kodak Spectroscopic Plates 649-0 The tibias decalcified in Susa solution were embedded in paraffin, sectioned longitudinally and stained by the gentian violet technique described by Selye ('57)

Since the preliminary study indicated that AAN could suppress endosteal bone formation in mice a second and more extensive experiment was designed to establish the dose at which AAN was most effective. The experimental plan was similar to the preliminary one, except that groups were composed of six mice and estradiol valerate was administered in a single 0.5 mg dose subcutaneously on day 1 Control mice received sesame oil or water Other groups received an intraperitoneal injection of either 5, 1 or 20 mg AAN alone or 0.5, 2 5 5, 10, or 20 mg AAN daily for six days in combination with the single subcutaneous dose of estrogen. At autopsy at the end of the first, second, third and fourth weeks the mice were x-rayed. The femurs were fixed in 10% neutral formalin or 95% alcohol and sections were prepared for microradiography and histology as before. Paraffin embedded sections were stained with hematoxylin eosin and azure II. The lengths of the long bones were obtained from x rays

RESULTS

Preliminary experiment. The epiphyseal cartilages of the lower femurs of mice treated with AAN appeared somewhat thicker than the controls in the radiographs (figs. 1A, 1C). Combined treatment with AAN + estrogen appeared to suppress the endosteal bone reaction which was well-established at the end of the first week in the group receiving estrogen alone (fig. 1B 1D)

Dose-dependent changes

Control and estrogen-treated groups. After one week, the epiphyseal cartilage of the femurs of the estrogen-treated animals was thinner than that of the controls. The metaphyseal trabeculae were thicker and longer and the cortex exhibited a slight endosteal reaction. The undifferentiated mesenchymal cells of marrow were differentiating to osteoblasts and these cells lined the free surfaces of the trabeculae. At two weeks the endosteal reaction had spread proximally to the neck of the femur and long narrow trabeculae filled the distal third of the bone The growth cartilage was thinner than in the controls and the

Delestrogen was generously supplied by Dr. E. C. Rothenstein, Jr., Squibb Institute, New Brunswick, New Jersey

sification front was slightly irregular occasionally sites of epiphyseal-diaphyseal sion were observed. By the fourth week, endosteal reaction was much less in se. Fewer osteoblasts lined the older beculae, but heavy confluent deposits ying to remodeling filled the distal half the shaft and epiphyseal medullary aces.

Epiphyseal cartilages The epiphyseal rtilages of AAN-treated mice were someat thicker than those of the controls at three dose levels (figs. 2 3) Columns chondrocytes in the proliferating zones short, disoriented, and separated by de areas of acellular matrix. Removal the hypertrophic zone cells by invading taphyseal vessels was irregular and the sification front appeared discontinuous. ter 5 mg AAN the tissues may also have en disrupted by large tears and vascular aces (figs. 3 4) Partial bony fusion of e epiphysis and metaphysis occurred in few animals after 20 mg AAN Regression of these changes was generally aprent during the post-treatment recovery riods although occasional foci of vascular erosion were still seen at the end of the cond week after 5 mg AAN The cellurity and thickness of the cartilage were ss irregular by the fourth week. The ondrocytes and matrix in affected areas ntained granules of dark blue staining aterial which may represents calcium lts.

Estrogen preserved the cartilage after w doses of AAN + estrogen (AAN + E) ring the treatment period. Thickening the plate was slight after 5 mg AAN + but the foci of vascular erosion were aller and less severe than in mice eated with the nitrile alone The protecve influence of estrogen was not apparent after 10–20 mg AAN + E. While the rtilages were approximately as thick as ose of the mice treated with estrogen one owing to regressive changes during the post-treatment period, the damage to e plates was persistent and may be exaggerated. Small tears not found at one week, for example were present at two eeks after 2.5 mg AAN + E.

Slipped epiphyses Slipped epiphyses were not common in AAN-treated mice although the cartilage and metaphysis of one animal dead after receiving six injections of 20 mg AAN was irregularly dissected by bands of muscle and dense connective tissue which also appeared under the periosteum (fig. 5) Animals of the four week recovery period which were pretreated with 5 mg AAN + E seemed disposed toward an increased incidence of epiphyseal slippage. In several instances muscle fibers seemed to enter the bone along transverse tears in the periosteum and cartilage, perhaps following rotation of the epiphysis on the bony metaphysis.

Articular cartilage degeneration. Foci of degeneration apparent either as a simple loss of cartilage tissue or as fibrous invasion occurred on the joint surfaces after 5 mg AAN during the first week. No fur ther evidence of joint deterioration oc curred during the recovery period. The extent of damage after combined treat ment with AAN + estrogen was similar and not dose-dependent, although the tissue was sometimes replaced by bone trabeculae

Metaphyseal bone Demonstrable changes occurred in the metaphyses of the bone, and some of the effects of the nitrile were persistent throughout the period of obser vation The numbers of the osteoblasts in the zone of endochondral ossification and those lining the trabeculae did not seem to be reduced by AAN and, in fact, 5–10 mg AAN or AAN + E seemed to intensify modulation to osteoblasts at the ossification front. The trabeculae (fig 6) were thinner after AAN treatment and had a mosiac appearance (fig. 7) their distribution and form were also quite irregular at one week, but they became more massive than the controls at two weeks. At four weeks the distinction between the groups was slight with the exception of the fine structure of the bone. The dark blue staining granules observed in car tilage after AAN treatment were also observed in the cytoplasm of osteoclasts in mice injected with 20 mg AAN and a few were observed in osteoblasts and the osteogenic precursor population. The deposits were particularly dense after combined AAN and estrogen treatment.

While osteoblastic activity in the metaphysis was undiminished in the first week after 0.5–5 mg AAN + E, the ossification

front was discontinuous and there was ex tensive osteoclastic resorption. Osteoid deposition on calcified spicules of cartilage was delayed by 10–20 mg AAN + E. In all cases, the numbers of trabeculae were diminished by combined treatment and they were individually abnormal as noted above (fig. 7) short and relatively more massive than in the mice treated with estrogen. Large vesicular spaces occurred in subepiphyseal areas (fig. 8) The in tensity of the endosteal reaction was re duced atfer 2.5–10 mg AAN + E or re-stricted to areas where trabecular bone was already established after 20 mg AAN +E. Although most bones show masses of con-fluent trabeculae in the distal half of the *shaft, there are relatively more vascular* spaces and the most proximal and newly formed trabeculae are thinner than those in the estrogen controls.

Cortical bone

The shaft of the femur normally con-tains dense fully mineralized lamellar bone demarcated into zones of periosteal and endosteal growth by regular cement lines (fig. 10) The osseous lamellae al ways enclose a few small vascular spaces. While the lacunae of osteocytes are usu-ally elongated and narrow the cells in areas of tendon insertion along the neck and trochanters tend to be more ovoid and less precisely aligned along lamellae The periosteum over the neck of the femur in young mice may be somewhat thicker than in older animals

In the normal mouse, the endosteal *borders of the bone at the level of the mid-*shaft are smooth (fig 10) The endosteal lining is composed of spindle-shaped reti-cular cells which possess the ability to un-dergo cytomodulation to active osteoblasts. While estrogen treatment did not alter the appearance of the cortical bone tissue the hormones stimulated the rapid meta plasia or modulation of these potentially osteogenic cells within the endosteal lining to the osteoblast class. The new endosteal bone produced under the influ ence of estrogen (fig. 9) has a distinctly fibrous appearance and the lacunae en closing the osteocytes are ovoid

The histologic and microradiographic appearance of cortical bone was not usu *ally affected by AAN at the different dose* levels. However patches of enlarged confused lacunae with abnormal [illegible] nar matrix (fig 9) appeared at the end of the treatment period in the mid-shaft of bones of several mice which had received daily injections of 5 mg AAN The tissue in these areas was of low mineral density (fig. 11) This defect appeared even more frequently during the treatment and post-treatment recovery periods in mice which had received both AAN and estrogen. It seemed most likely that the tissue had been demineralized and that we were not dealing with a failure of newly formed bone to mineralize. The changes occurred deep within the mid-shaft cortex rather *than at actively forming* surfaces of bone and they appeared to be local manifestations frequently associated with developing periosteal hyperosteotic tissue

Periosteal hyperostoses. The periosteum thickened over the entire proximal half of the femur during the first week of treatment with 5–20 mg AAN Although the periosteal muscle attachments remained intact at this time the periosteum became less firmly bound to the bone Subsequent metaplasia of proliferating periosteal cells early in the post-treatment recovery period resulted in the formation of hyperosteotic fiber bone tissue (*callus*) after 10–20 mg AAN (figs. 10 12–14) Basophilic globules and granules were scattered throughout the developing callus tissue

The severity *of these changes* was [illegible] more marked during the treatment period [illegible] *per se* in the groups treated with AAN + E. Although the periosteum and its muscle attachments remained intact and apparently functional the periosteum thickened within seven days after the onset of treatment. Callus formation during treatment with 2.5 mg AAN + E was as great as that which had occurred with 5 mg AAN alone during the post-treatment recovery period The mid-shaft cortex of one animal contained a large vascular space which was at some distance from the nutrient canal Osteoclasts were conspicuous in the callus tissue Repair was not complete at the end of the experiment in mice treated with 5 mg AAN + E but the periosteum remained loosely attached to the shaft.

Osteo-cartilaginous hyperostosis Periosteal proliferation also formed osteo-cartilaginous hyperostotic fibrous bone (figs , 14) on the proximal third of the shaft a mouse during the recovery period ree weeks after injections of 20 mg AAN trogen, however potentiated this change ring the treatment period at this dose d in a few mice which had received mg AAN + E. The cartilage component, composed largely of disorganized pertrophic cells and a few discoid cells pical of the proliferating zone of epiphyseal cartilages was bound by a narrow ter band of fiber bone and a larger inner ne of irregular bone trabeculae

Studies by Hamre and Yaeger ('57 '58) ve provided convincing evidence that e active substance in L. odoratus seeds nnot by itself produce exostoses, but that can do so in the presence of intact functional muscles.

DISCUSSION

The effect of injected AAN on the skeleton of mice was dose-dependent and cer m of the anomalies have been manifest rats and other species after feeding lathyrogens for prolonged periods of time. The incipal skeletal involvements in these ice were enlargement and tearing of the owth cartilage in the proliferative zones tachment of ligamentous and tendinous sertions and subsequent growth of periosteal hyperostotic tissue (callus) and faulty nd/or delayed endochondral ossification nd mineralization patterns resulting from e disruption of epiphyseal cartilage structure. With the exception of degenerative ent changes, the incidence of slipped iphyses and periosteal hyperostotic and steocartilaginous hyperostotic tissue increased after combined treatemnt with strogen and with higher levels of AAN 5-20 mg) Akamatsu and Takahashi '64) failed to observe histologic alterations in epiphyseal cartilage plate struc and kyphoscoliosis in their studies nth mice fed BAPN and kyphoscoliosis t least, was not observed in our preliminary studies after whole mouse skeletons were stained with Alizarin red S How ver Dasler and Milliser ('57) indicate hat the skeletal effects of mice induced by the different lathyrogens are much more variable than in rats.

The prime target of lathyrogens in connective tissues is the ground substance — in particular the synthesis of chondroitin sulfate (Sobel et al., '56 Shintani and Taylor '62) Sulfated mucopolysaccharides were irregularly distributed in the bones of rats studied by Bélanger ('55) following the administration of nitrilic compounds. Cellular utilization of sulfate (S^{35}) was reduced in the cartilage plates of mice (Akamatsu and Takahashi, '64) and in the epiphyseal lesions of rats studied by Kennedy and Kennedy ('62) but not in adjacent histologically normal regions of the growth cartilage (Kennedy and Kennedy '62) The appearance of darkly basophilic granules in the matrix of the cartilage plate in the present studies, possibly representing acid mucopolysaccharides and/or calcium salts, confirm the observations of Borle et al. ('59) These granules were also present in the fiber bone of the developing hyperostotic callus tissue, and are comparable to the globules of strongly PAS positive material and amorphous metachromatic substance in the poorly calcifying zones of healing fracture callus (Storey and Varasdi, '58) in epiphyseal lesions produced by semicarbazide (Ramamurti and Taylor '59) and in the bones of lathyritic rats (Ponseti and Shepard, '54 Selye '58) and chicks (Dasler and Milliser '58) It is of some interest that the incidence of these granules and globules was exaggerated in the present study only after the severest changes to the bones were induced by combined treatment with AAN and estrogen. They possibly arise in response to the need of lathyritic connective tissues for stabilizing hexoses, but the biochemical data related to the hexosamine content of skeletal tissues is somewhat contradictory Cartilage plate hexosamine content and its synthesis was found to be reduced by Castelliani and Castelliani-Bisi ('58) and Pedrini and Pedrini Mille ('59) in lathyritic rabbits but these findings were unsupported by others (Karnovsky and Karnovsky '61) Lathyritic fracture callus was also reported to contain lower than normal hexosamine values (Bolognani, '61)

The appearance of bone cells was normal after nitrile treatment, although early senescence disappearance and modulation of osteoblasts to spindle-shaped cells has been reported in BAPN-treated suckling rats (Clemons and Angevine, 57) In this study AAN did not stimulate the modulation of cells to osteoclasts although this event was observed by Clemmons and Angevine ('57) in BAPN-injected rats and in rats fed a diet including *L. odoratus* L. seeds (Gardner '59) There is also little evidence to suggest that the functional activity of osteoblasts is impaired by AAN treatment. Periosteal fibrous hyperostotic tissue and endochondral trabecular formation continued at all dose levels although AAN reduced the numbers of trabeculae and partially inhibited the endosteal bone reaction after very high doses

It seems clear from this study that AAN is able to suppress partially the proliferation of endosteal bone in estrogen-treated mice the effect was greater when estrogen was administered intraperitoneally While the effect after the subcutaneous injection of 0.5–2.5 mg AAN + E was negligible progressively fewer trabeculae were formed with increasing doses of AAN Estrogen enhances collagen synthesis in bones of mice (Vaes and Nichols '62) Augmentation of the potentially mitotic osteoblast population has been demon-[illegible] with tritiated thymidine labeling in metaphyses of mice as early as six hours after a single dose of estradiol valerate (Simmons '63). The trabeculae which formed under the influence of AAN and AAN + E were abnormal and the fibrillar structure appeared loosely organized perhaps owing to disruption of the pattern of cross linking and polymer formation (Martin et al. '61) Current experiments favor the concept that lathyritic compounds prevent the normal aggregations of collagen fibers from native tropocollagen by interfering with the formation of chain pairs—intermolecular cross links — so that the conversion of soluble to insoluble collagen by fibril aggregation is blocked (Martin et al. '61 Martin and Goldhaber '63) Distorted endochondral trabeculae have previously been described in rats by Menzies and Mills ('57) and by Ponseti and his coworkers ('54) Some workers have compared the mosaic structure of rat lathyr[illegible] bone to a Pagetoid-like condition (Ponse[illegible] and Shepard, '54; Bean and Ponseti, '5[illegible] Wawzonek et al., '55· Amato et al. '5[illegible] Ramamurti and Taylor '59) but cement lines characteristic of this disorder were absent in mice.

There is also evidence that lathyrogenic compounds attack mature collagen. While this study showed that the effect of AAN on the osteocytes and matrix in the mid-shaft of the femur was negligible, combined treatment with estrogen combined[illegible] resulted in osteocyte enlargement, perilacunar matrix degradation and demineralization of bone. Owing to the fact that the low mineral densities occurred deep with-in the cortex, it is conceivable that the [illegible]ter and intramolecular defects produced in the structure of collagen owing to the administration of the nitrile might have ex-posed the collagenous fibers to the action of collagenolytic enzymes. Deterioration of collagenous structures would, as a consequence adversely affect the mineral content of the tissue. It has yet to be established if the changes in collagen at the molecular level are directly related to alterations in the solubility of collagen (Od[illegible] and Gross, '63) Focal lacunar enlargement ocurs in osteoporosis, and it has been suggested that osteocytes produce [illegible] sins to degrade perilacunar bone [illegible] (Little et al., '62) Lipp ('54) and [illegible] recently Bélanger et al. ('63) have com-mented that osteocytes possess some [illegible] characteristics usually attributed to osteo-clasts and that under certain cond[illegible] (parathyroid treatment) they may [illegible] intralacunar resorption. Osteoporotic-like bone resulting from lathyritic compound[illegible] has been described (Bean and Ponse[illegible] '55 Gardner '59) and in these [illegible] cortical tissue was additionally [illegible] by large vessels and remodeling of the bone in areas of periosteal hyperostotic tis-sue formation. These features are [illegible] to the condition in AAN + E-treated [illegible] described by Selye ('58) and, as [illegible] above might have resulted from the [illegible] ruption of lateral intramolecular [illegible] collagen (Levene '62)

LITERATURE CITED

—amatsu, Y and M. Takahashi 1964 Lathyrism of mice. Bony changes induced by β-aminopropionitrile feeding and autoradiographic study of bones using S35 Arch. Pathol., 78 61–66.

—nato, V P M. Sliema and R. Bombelli 1959 Early skeletal and vascular changes in rats fed on sweet pea (Lathyrus odoratus) seeds. J Bone and Joint Surg 41B 600–610.

—ker, D. J P and J N Crossley 1962 Effect of testosterone on oestrogen-induced bone formation in mice. Nature, London, 194 1098–1094.

—ux, W B., and I. V Ponseti 1955 Dissecting aneurysm produced by diet. Circulation, 12 185–192.

—inger, L. F 1955 Autoradiographic visualization of Ca45 intake by normal and pathological cartilage in vitro. Proc. Soc. Exper Biol. and Med 88 180–182.

—inger, L. F J. Robichon and D. H. Copp 1962 Alpharadiographic observations of demineralized dog bone after parathormone treatment and E.D.T.A. venoclysis. Anat. Rec., 145 208 only

—ck, A. B., J Karnovsky and G. Nichols, Jr. 1959 Changes in inorganic composition of tissues in experimental osteolathyrism. Am. J Physiol., 197 1224–1228.

—stellani, A. A., and C. Castellani Bisi 1958 decrease in hexosamine content of epiphyseal plates in experimental lathyrism. Proc. Soc. Exper. Biol. Med., 98: 318–320

—ermons, J. J and D. M. Angevine 1957 The occurrence of multiple fractures in suckling rats injected with β-aminopropionitrile (Lathyrus factor) Am. J Path., 33 175–187

—sler W and R. V Milliser 1958 Osteolathyrogenic action of mercaptoethylamine and of cystamine. Prod. Soc. Exper. Biol. and Med 99: 759–760.

—rdner, A. F 1959 The effects of various levels of sweet peas (Lathyrus odoratus) in the diet, with protein and amino acid supplementation, on the alveolar bone of young rats. Oral Surg., 12. 876–889.

—rdner W U and D. H. Clouet 1944 Osseous proliferation in estrogen treated hypophysectomized mice. Anat. Rec., 88 433 only

—rdner W U and C. A. Pfeiffer 1938 Skeletal changes in mice receiving estrogen. Proc. Soc. Exper Biol. and Med., 37 678–679

—ross, J 1963 An intermolecular defect of collagen in experimental lathyrism. Biochim. biophys Acta, 71 314

—re C. J and V L. Yaeger 1957 Influence of muscle section on exostoses of lathyritic rats. Arch. Pathol., 64 426–433.

—— 1958 Influence of denervated muscles on exostoses of rats fed sweet pea diet. Arch. Pathol., 65 215–227

—rnovsky M. J., and M. L. Karnovsky 1961 Metabolic effects of lathyrogenic agents on cartilage in vivo and in vitro J Exper Med., 113 381–403.

Kennedy J S and G. D C. Kennedy 1962 Autoradiographic studies in experimental lathyrism. J Path. Bact., 84 123–135.

Levene C. L. 1962 Studies on the mode of action of lathyrogenic compounds. J Exper Med., 116 119–130

Levene, C. L., and J Gross 1959 Alterations in state of molecular aggregation of collagen induced in chick embryos by β-aminopropionitrile (Lathyrus factor) J Exper. Med., 110 771–790.

Lindquist, B A. M. Budy F C. McLean and J L. Howard 1960 Skeletal metabolism in estrogen-treated rats studied by means of Ca45 Endocrinology 66 100–111

Little K., M. Kelly and A. Courts 1962 Studies on bone matrix in normal and osteoporotic bone. J Bone J t. Surg., 44B 503–519.

Lipp, W 1954 Neuuntersuchungen des Knochengewebes (Morphol. Histochem. und Beeinflussung durch das periphere vegetative Nervensystem durch Fermente und Hormone) II. Histologisch erfassbare Lebensäusserungen der Knochenzellen. Acta Anat., 22: 151–201

Martin, G. R., and P Goldhaber 1963 Action of aminoacetonitrile on bone collagen in tissue culture. Biochem. Biophys. Acta, 69 568–569.

Orloff, S. D and J Gross 1963 Experimental lathyrism in the chick embryo. J Exper Med., 117 1009–1018.

Pedrini, V., and A. Pedrini-Mille 1959 Decrease of enzymatic synthesis of hexosamine in epiphyseal plates of aminoacetonitrile-treated rabbits. Proc. Soc. Exper Biol. Med., 101 258–260.

Ponseti, I. V., and F Alen 1958 Fracture healing in rats treated with aminoacetonitrile. J Bone Jnt. Surg., 40-A 1093–1102.

Ponseti, I. V and R. S. Shepard 1954 Lesions of the skeleton and of other mesodermal tissues in rats fed sweet-pea (Lathyrus odoratus) seeds. J Bone Jnt. Surg., 36-A: 1031–1058.

Ramamurti, P and H. E. T ylor 1959 Skeletal lesions produced by semicarbazide and experimental analysis of the action of lathyrogenic compounds. J Bone Jnt. Surg., 41-B 590–599

Selye, H. 1958 Influence of various hormones and vitamin D preparation upon established bone lathyrism. Acta Anat., 33: 146–156.

—— 1957 Lathyrism. Rev Canad. Biol 16 1–82.

Selye, H and P Bois 1956 On the influence of various hormones upon the development of experimental lathyrism. Rev Canad. Biol., 15 281.

Shiotani, Y K., and H. E. T ylor 1963 The effect on ... of lathyrogens on the uptake of radiosulfate by epiphyseal cartilage Lab Investig 11 697 702.

Simmons, D J 1963 Cellular changes in the bones of mice as studied with tritiated thymidine and the effects of estrogen. Clin. Orthop., no. 26, 176–190

Sobel, A. E., M. Burger, B. C. Deane, ... Albaum and K. Cost 1957 Calcification XVIII Lack of correlation between ...

tion in vitro and glycolytic enzymes. Proc. Soc. Exper. Biol. and Med., 96 32–39

Storey E., and G Varasdi 1958 Fracture repair in the rat during aminoacetonitrile administration and following its withdrawal. Brit. J Exper. Path., 39 376–385

Suzuki, H. K. 1958 Inhibition of estradiol-induced endosteal bone formation after intrafemoral implantation of testosterone propionate into mice. J Bone Jnt. Surg., 40-A 435–445.

Urist, M. R., A. M. Budy and F C. McLean 1950 Endosteal-bone formation in estrogen-treated mice. J Bone Jnt. Surg., 32-A 143–162.

Vaes G and G. Nichols, Jr 1962 Metabolism of glycine-1-C^{14} by bone in vitro. effects of hormones and other factors. Endocrinology [illegible] 890–901

Van den Hooff, A., C. L. Levene and J. [illegible] 1959 Morphologic evidence for [illegible] changes in chick embryos treated with [illegible] propionitrile. J Exper. Med., 110 1017.

Wawzonek, S., I. V Ponseti, R. S. Shepard [illegible] L. G. Wiedenmann 1955 Epiphyseal [illegible] lesions, degenerative arthritis, and [illegible] aneurysm of the aorta produced by [illegible] triles. Science 121 63–65

PLATE 1

EXPLANATION OF FIGURE

1 Microradiographs of longitudinal sections of femurs from mice after one week of treatment. A — Control; B — Aminoacetonitrile-treated; C — Estrogen-treated; D — Aminoacetonitrile estrogen-treated. Note the absence of endosteal bone (EB) formation in the metaphysis of the mouse in D (50 ×)

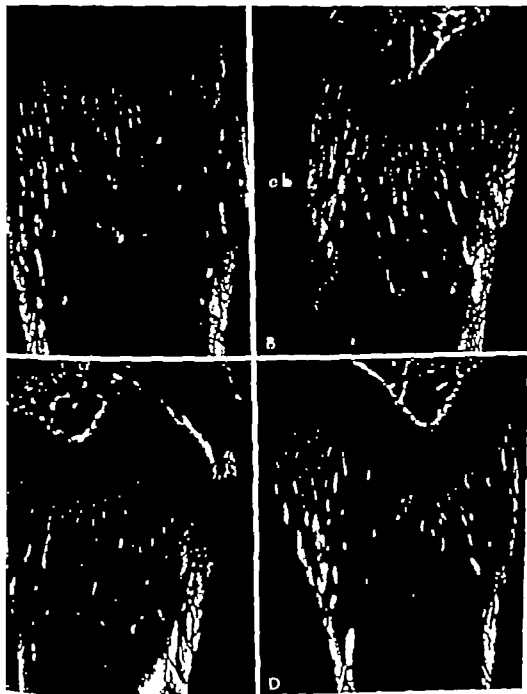

cb
B
D

PLATE 2

EXPLANATION OF FIGURES

2 Photomicrograph of the distal end of the femur from control mouse showing the normal structure of the epiphyseal cartilage. (200 ×)

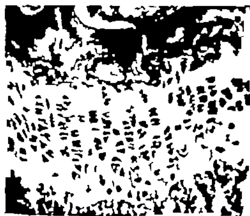
3 Photomicrograph of large rent in the proliferating zone of the thickened distal femoral epiphyseal cartilage from a mouse one eek after daily treatment with 5 mg AAN (100 ×)

4 Photomicrograph of vascular lesion in the proliferating zones of the epiphyseal cartilage from the distal femur of a mouse one week after daily treatment with 5 mg AAN Note the disorganization of the cell columns. (150 ×)

5 Photomicrograph showing slipped ep physis in the distal femoral epiphyseal cartilage from a mouse dead fter six injections of 20 mg AAN per day The cartilage and metaphysis is irregularly dissected by muscle bands (M) (75 ×)

6 Photomicrograph of normal endosteal bone trabeculae (T) in the distal femur from mouse which had received estrogen. (200 ×)

7 Photomicrograph f bnormal ndosteal bone trabeculae (T) in the distal femur from a mouse one week after treatment with 5 mg AAN per d y Note the mosaic structure of the trabeculae lined by numerous osteoblasts. (200 ×)





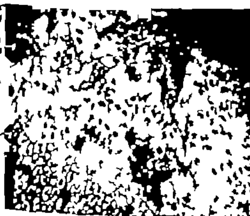








PLATE 3

EXPLANATION OF FIGURES

8 Photomicrograph of the distal end of the femur from a mouse one week after treatment with 20 mg AAN per day and estrogen. Note large vesicular spaces t the border between the cartilage and metaphyseal bone. (125 ×)

9 Photomicrograph of mid-shaft cortical bone from a mouse injected with 20 mg AAN per day and estrogen and sacrificed fter the third week post-treatment recovery period. Not the enlargement and apparent fusion of osteocytes plus the degradation of the perilacunar matrix (OF) An endosteal reaction is present (E) (150 ×)

10 Photomicrograph of mid-shaft cortical bone from a mouse injected with 10 mg AAN per day and estrogen and sacrificed after the first week post-treatment recovery period. Note the formation of periosteal hyperostotic fibrous bone (F) and the endosteal reaction (E). (125 ×)

11 Microradiograph of the mid-shaft cortex of femur from a mouse treated with 5 mg AAN per d y and sacrificed at the end of the tre tment period. Note the demineralized (low density) region in the middle of the thickness of the shaft bordered by fully mineralized periosteal and endosteal surfaces. (100 ×)

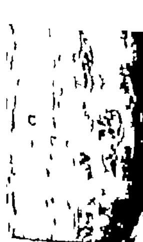
12 Microradiograph f mid-shaft cortical bone from mouse injected with 5 mg AAN per day and sacrificed after the first week post treatment recovery period Note the formation of periosteal hyperostotic bone (F) and destruction of the underlying cortical tissue (C). (175 ×)

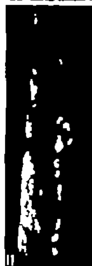
13 Photomicrograph f the proximal haft f femur from mouse dead after four daily injections of 10 mg AAN Note the formation of an osteocartilaginous periosteal hyperostosis. Limiting sheath of fiber bone (F); Medial zone of cartilage (C) Inner zone of trabecular bone (T); Cortex (B) (125 ×)

14 Microradiograph of the proximal shaft of femur from mouse injected with 20 mg AAN per day and estrogen and sacrificed at the end of one week. Note the formation of an osteocartilaginous periosteal hyperostosis and destruction of the underlying cortical bone (B) Cartilage (C); Trabecular bone (T) (175 ×)






C
F


11


F
T
C
12


B


C
T
B
14

of the tubule depends on the starting point chosen and on the species under consideration Some investigators consider mammalian spermatogenesis to begin with the appearance of new spermatogonial stem cells or type A spermatogonia (Ortavant, '56 Amann '62b) and others consider spermatogenesis to commence with the first of a series of spermatogonial mitoses leading to the formation of primary spermatocytes (Roosen Runge '51 Leblond and Clermont '52a Oakberg '56b Clermont Leblond and Messier '59 etc) Taking the appearance of the new stem cells as the onset of spermatogenesis Ortavant ('59) calculated that in the ram spermatogenesis extends over 4 68 cycles of the seminiferous epithelium Using the same starting point Amann ('62b) postulated spermatogenesis to take 4.5 cycles in the bull. Spermatogenesis extends over about four cycles in the rat (Leblond and Clermont, '52a) the mouse (Oakberg '56b) and in man (Heller and Clermont, '63) when the first of the series of spermatogonial devisions is considered as the onset of spermatogenesis. In the monkey six cycles of the seminiferous epithelium have been reported (Clermont and Leblond '59)

The duration of spermatogenesis has been determined in a number of mammals using techniques such as colchicine injections (Roosen-Runge '51) x-irradiation (Oakberg '56b) elevation of testicular temperature (Asdell and Salisbury 41) studies on sexually maturing animals *(Clermont and Perey 57 Hauser et al '52)* and isotope injections (Ortavant '56 Sirlin and Edwards '38 Foote and Koefoed-Johnsen '59 Clermont et al. '59 Koefoed-Johnsen '59 Heller and Clermont '63) Probably the best of these methods is the one employing a labeled precursor of desoxyribonucleic acid. After the label is incorporated into the germ cells the process of spermatozoa formation can be followed by isolating cell constituents chemically or by autoradiography at suitable intervals Using isotopes the duration of spermatogenesis has been estimated to be 48 days in the rat (Clermont et al '59) 49 days in the ram (Ortavant '56) and 64 days in man (Heller and Clermont '63)

Isotopes also have been used to measure total time from labeling to ejaculation and to time the rate of spermatozoa [illegible]sage through the epididymis and other [illegible] current ducts. The time from label[illegible] appearance of radioactive sperm [illegible] ejaculate has been reported to be [illegible] days for the ram (Ortavant, '59) [illegible] days for the bull (Koefoed-Johnsen, [illegible] Orgebin '61) 39–42 days in the [illegible] (Foote and Koefoed-Johnsen, '59 Koefoed-Johnsen, '59) and 39 days in the b[illegible] (Singh '62) Using P[illegible] the time [illegible] for passage of spermatozoa through [illegible] epididymis has been estimated to be [illegible] 14 to 20 days in the ram (Ortavant, [illegible] '59) 8–11 days in the bull (Orgebin [illegible] and 14 days in the boar (Singh, '62)

MATERIALS AND METHODS

Experimental animals

Fourteen healthy Dutch-belted male [illegible] bits averaging 2.21 kg in body weight [illegible] ranging from 1 to 2 years of [illegible] used in this study Eight bucks were [illegible] to time sperm formation in the test[illegible] six bucks were used to study sperm [illegible] port All had previous histories of [illegible] sperm production, and had been trained to serve the artificial vagina

Thymidine injections

Thymidine-methyl-H[illegible] was purchased [illegible] a sterile solution containing one [illegible] of tritiated thymidine per milliliter [illegible] different lots of isotope used had [illegible] activities between 6 6 and 9 6 curies per *millimole* Each animal received [illegible] travenous injection of thymidine-methyl[illegible] into a marginal ear vein at a rate of [illegible] millicurie per kilogram of body [illegible]

Design of experiment

After the thymidine-H[illegible] injections [illegible] ular biopsies and unilateral castr[illegible] were performed during a 42-day period [illegible] eight bucks in groups I and II ([illegible]) [illegible] study sperm formation time Group[illegible] II were essentially replicates, but the [illegible] tervals followed in the second [illegible] four males were altered slightly [illegible] first group in order to provide ad[illegible] information The order of testis [illegible] was randomized in group I and [illegible] in group II No surgery was done [illegible] *bucks assigned to group III.* Instead [illegible]

TABLE 1

ntervals between the injection of tritiated thymidine and testicular biopsies or removal of whole testes

Animal	Testis		Interval after injection of thymidine-H³
	Group I		
1	Biopsy	L testis	2 hrs
	Removal	L testis	1 day
	Biopsy	R testis	4 days
	Removal	R testis	5 days
2	Biopsy	R testis	13 days
	Removal	R testis	14 days
	Biopsy	L testis	15 days
	Removal	L testis	16 days
3	Biopsy	L testis	26 days
	Removal	L testis	28 days
	Biopsy	R testis	30 days
	Removal	R testis	32 days
4	Biopsy	R testis	36 days
	Removal	R testis	38 days
	Biopsy	L testis	40 days
	Removal	L testis	42 days
	Group II		
5	Biopsy	R testis	2 hrs
	Removal	R testis	1 day
	Biopsy	L testis	4 days
	Removal	L testis	5 days
6	Biopsy	L testis	12 days
	Removal	L testis	13 days
	Biopsy	R testis	14 days
	Removal	R testis	15 days
7	Biopsy	R testis	28 days
	Removal	R testis	29 days
	Biopsy	L testis	30 days
	Removal	L testis	31 days
8	Biopsy	L testis	36 days
	Removal	L testis	38 days
	Biopsy	R testis	40 days
	Removal	R testis	42 days

ucks were ejaculated for 63 days post njection to determine the time interval beween thymidine-H³ injection and the apearance of the isotope in the ejaculated emen. The remaining animal had one pididymis removed 35 days post injection nd the other one 38 days post-injection to elp time sperm transport. As long as hey remained on the experiment all bucks were ejaculated twice each Monday and wice each Thursday excepting on days 8 to 42, when one semen sample was ollected each day. The daily semen col ections coincided with the expected appearance of the first radioactive sperm in the ejaculate. At least 30 minutes and no more than 60 minutes was allowed be tween successive ejaculates on the same day On days 35 through 63 semen smears were prepared for autoradiography

Biopsy and castration procedures

The animals were anesthetized with ether and prepared for surgery as previously described (Swierstra, Whitefield and Foote '64) The biopsies were performed by making a scrotal incision and exposing the tunica vaginalis and the tunica albuginea. A relatively avascular area was located on the tunica albuginea at the lat eral part of the testis midway between the poles. The tunica albuginea was nicked" with a sharp pointed scalpel and slight pressure on the testis resulted in the protrusion of a small mass of seminiferous tubules. The mass of protruded tubules, averaging 11 mg, was removed with a pair of curved iris scissors Single sutures were placed in the tunica vaginalis and scrotum. Castrations were performed as previously described by Swierstra et al. ('64)

Autoradiographic procedures

Testicular tissue and pieces of the caput, corpus and cauda epididymis were fixed in three parts of 95% ethyl alcohol and one part of acetic acid (Carnoy's fixative) processed routinely and cut at 8 μ. The slides were stained with the Feulgen technique and coated with a thin layer of 0.3% celloidin Later the layer of celloidin was found to be unnecessary Semen smears were prepared by diluting one part of the ejaculated semen with nine parts of physiological saline Semen smears also were prepared from different parts of the epididymis. The smears were fixed in Carnoy's solution and stained with the Feulgen technique

All slides were coated with NTB 3 nuclear emulsion, spread by a stainless steel roller dried quickly and placed in light tight plastic boxes containing a small bag of "Drierite The slides were exposed for 50–55 days in the refrigerator at 5 C. At the end of the exposure period the slides were developed and fixed at 5 C in a refrigerated room (Belanger '61)

Histological analysis

The seminiferous tubules were classified into eight stages previously described by Swierstra and Foote ('63) It was planned to analyze all cell types present in two tubules of each of the eight stages in each piece of biopsy or whole testis. However this goal was not reached in all biopsies because they were relatively small and the eight stages were not always present. Excepting for the biopsy on *day 26* only sections from whole testes were used in the determination of the duration of spermatogenesis. All nuclei in the selected tubules were classified as labeled or not labeled, using the 100× oil immersion objective. Background per nucleus was less than one and was ignored. No attempt was made to count the exact number of grains lying above each nucleus

RESULTS

Two hours post-injection of thymidine H³

Biopsies taken two hours after the injection of the thymidine-H³ revealed that nuclei of the following cell types were labeled: Type A spermatogonia, intermediate type spermatogonia, type B spermatogonia, preleptotene and early leptotene primary spermatocytes The autoradiographs showed that no label was incorporated in primary spermatocytes more advanced than the early leptotene stage (stage 1) in secondary spermatocytes in spermatids and in spermatozoa (plate 1) Thus of all cell types that incorporated the thymidine-H³ the primary spermatocytes in the leptotene stage were the most advanced spermatogenic cells. Similar observations were made for the rat (Clermont et al '59) and the mouse (Monesi '62)

Longer intervals post-injection of thymidine H³

The evolution of the labeled spermatogenic cells determined from the material obtained according to the schedule given in table 1 is presented in figure 1 Four days post-injection the label had advanced from the leptotene primary spermatocytes in stage 1 to young primary spermatocytes in stage 4 Five days post injection the most advanced cells showing the label were the older primary spermatocytes in stage [illegible] At *day 13* these were the old primary spermatocytes in stage 2 of the next cycle, [illegible] *day 14* these were the old primary spermatocytes at the end of stage 3 at day [illegible] these were the secondary spermatocytes [illegible] stage 4 and at *day 16* the spermatids [illegible] the beginning of stage 6 (table 2).

Labeled spermatozoa had advanced [illegible] the middle of stage 4 at 26 days, to the middle of stage 6 at 28 days, to stage [illegible] 29 days and to the end of stage 8 at [illegible] days post injection. Labeled spermatozoa were first observed in semen smears of the caput epididymis at 31 days post-injection. In the group of five animals ejaculated regularly for 63 days labeled spermatozoa appeared for the first time in the semen from one animal at 39 days, and from four animals at 41 days post-injection.

Duration of spermatogenesis

The duration of one cycle of the seminiferous epithelium and the duration of the complete process of spermatogenesis were calculated by utilizing the relative frequency (duration) of the eight stages of the seminiferous epithelium. These relative frequencies for stages 1 through [illegible] were 27 7 13.4 7.3, 11.0 4 1 15 [illegible] and 8 6 respectively (Swierstra and Foote '63)

Two hours after the administration of the isotope the most advanced cells that were labeled were the leptotene primary spermatocytes in stage 1 At longer post-injection intervals the label progressed to more advanced cell types in spermatogenesis At 31 days post-injection the spermatozoa in the end of stage 8 were labeled Thus during this 31-day interval the label progressed from leptotene primary spermatocytes in stage 1 to spermatozoa [illegible] the end of stage 8. This interval equals 2.82 cycles of the seminiferous epithelium (fig 1) Based on this observation one cycle of the seminiferous is 11 0 days. Additional estimates of the duration of one cycle of the seminiferous epithelium (columns 6 and 7 table 2) were obtained by considering all possible intervals as given in table 2. The average of the 55 [illegible] possible was 10 9 ± 0 1 days. [illegible]

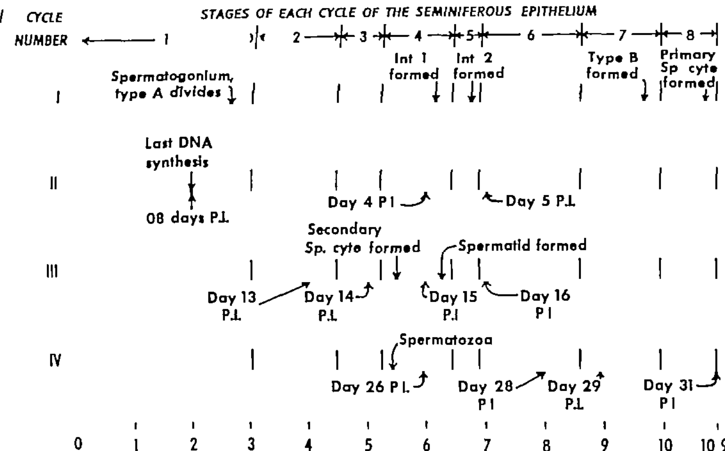


Fig. 1 The spermatogenic cycle in the rabbit. The four cycles of the seminiferous epithelium and the duration f the eight stages comprising each cycle are shown, along with the points at which the different spermatogenic cells arise. The most advanced labeled cells t various intervals post-injection are indicated by days P.I

TABLE 2

Estimates of the duration of one cycle of the seminiferous epithelium

Post-injection interval in days	Most advanced cell type labeled	Cycle and stage reached by the most advanced, labeled cell type	Interval since labeling as leptotene primary spermatocyte		Duration of one cycle in days	
			Time in days	Number of cycles traversed	Based on initial point of labeling	Based on intermediate points of labeling[1]
0.08	Prim. spermatocytes (leptotene)	II 1	0.00	0.00	—	—
4.0	Prim. spermatocytes (zygotene)	II-4	3.92	0.37	10 6	—
5.0	Prim. spermatocytes (pachytene)	II-6	4.92	0.46	10.7	11.1
13.0	Prim. spermatocytes (pachytene)	III-2	12.92	1.20	10 8	10 8 10 8
14.0	Prim. spermatocytes (pachytene)	III-3	13.92	1.29	10 8	10 8 10.8 11
15.0	Sec. spermatocytes	III-4	14.92	1.39	10.7	10 8 10.8 1[illegible] 10 0
16.0	Spermatids	III-6	15.92	1.48	10 8	10 8 10.8 [illegible] 10 5 11 1
26.0	Spermatozoa	IV-4	25.92	2.35	11.0	11 1 11 1 11 11.3 11.3 11
28.0	Spermatozoa	IV-6	27.92	2.54	11.0	11 0 11 0 11 11 2 11 3 11 10 8
29.0	Spermatozoa	IV 7	28.92	2.64	11.0	11 0 11 0 11 11 1 11.5 11 10 5 10 8
31 0	Spermatozoa	IV-8	30.92	2.82	11.0	11 0 11 0 11 11 1 11.2 11 10 6 10.7 11
			Mean duration		10.8	11 0
			Overall mean ± S.E.		10 8 ± 0 1	

[1] Each preceding point of labeling provided data for calculating cycle length.

ment was obtained among the various estimates.

DISCUSSION

Thymidine methyl H^3 appears to be exclusively incorporated into DNA and is firmly held by the DNA after incorporation. The thymidine-H^3 pool is of short duration and labeling occurs only during a short interval after administration of the isotope (Rubini et al. '60) Autoradiographs prepared from tissue containing tritiated thymidine have high resolving power due to the very low energy of the beta particles the average range in tissue being less than 1 µ. These characteris[tics] make thymidine-methyl-H^3 an ideal co[m]pound for studying spermatogenesis (Moneal '62)

In the rabbit labeled thymidine wa[s in]corporated in all three types of sperma[to]gonia (type A intermediate type and t[ype] B) and newly formed primary sperma[to]cytes (table 3) No label was incorpor[ated] in primary spermatocytes past early le[p]tene in secondary spermatocytes in s[per]matids and in spermatozoa. These res[ults] are in agreement with microspectroph[oto]metric DNA measurements carried out [on] the DNA content of type B spermatocy[tes]

TABLE 3

... Lifespan, incorporation of thymidine-methyl-H and amount of DNA in spermatogenic cells

Cell type	Cycle and stage of formation	Cycle and stage of division	Estimated lifespan in days	Incorporation of labeled thymidine	Amount of DNA: Just after formation	Amount of DNA: Prior to division
— spermatogonia	I-1	I-4	3.4	Stage 4	2N	4N
spermatogonia	I-4	I-5	0.6	Stages 4, 5	2N	4N
spermatogonia	I-5	I-7	2.8	Stages 6, 7	2N	4N
— spermatogonia	I 7	I 8	1 1	Stages 7 8	2N	4.40
...mary spermatocytes	I-8	III-4	16.5	Stage 8(I) Stage 1(II)	2.40	4 64
...ondary spermatocytes	III-4	III-4	0.8	N incorporation	1.84	1.84
...rmatids	III-4	undergo spermiogenesis	10 0	No incorporation	0.94	undergo spermiogenesis
...rmatozoa	IV-4	—	5.6	No incorporation	—	—

About four cycles of the seminiferous epithelium (I, II, III and IV) occur from the time that type A ...atogonia divide until the time that spermatozoa resulting from these type-A spermatogonia leave the ...is (fig. 1).

This 3 4 days is the estimated life span of the spermatogonia formed in stage 1 and dividing in stage ... of the same cycle. The life span of the stem cells is 10.9 days (one cycle of the seminiferous epithelium) ...longer in the table.

...in stages 2 and 3 were present in the biopsies taken two hours after the injection of the isotope. As ... no definite conclusions can be drawn as to whether or not type A spermatogonia in stages 2 and 3 ...porate labeled thymidine.

The amount of DNA present in one genome is denoted as N

Amount of DNA in arbitrary units as determined by microspectroph... (Swierstra, '62)

Spermatids are called spermatozoa when they reach stage 4 of cycle IV

...leptotene leptotene and pachytene pri...ary spermatocytes, and on secondary ...ermatocytes and spermatids (Swierstra, ...). Incorporation of labeled thymidine co...cided with DNA duplication. The micro...ectrophotometric measurements showed ...at the DNA content of newly formed pri...ary spermatocytes was about half that ...type B spermatogonia prior to division ...nthesis of DNA occurred rapidly in the ...ewly formed primary spermatocytes. ...oubling of the DNA content had taken ...ace before these cells approached the ...d of stage 1 These studies (table 3) ...rther showed that old primary spermato...tes had about twice as much DNA as ...e secondary spermatocytes and four ...mes as much as the spermatids. These ...ata are in accord with previous work ...wift, '50) and from this it was con...uded that all the DNA necessary for the ...o maturation divisions was synthesized ...n the preleptotene phase of the primary ...ermatocytes. Furthermore since no tri...ated thymidine was incorporated into ...condary spermatocytes, spermatids and spermatozoa at the time of the administration of the isotope it appears that there is no DNA exchanged or so-called "metabolic DNA in spermiogenesis.

Thirty-one days post-injection the label had advanced to spermatozoa leaving the testis (end of stage 8 plate 1) At this time 0.9% labeled spermatozoa also were present in semen smears from the caput epididymis. However histological sections from the caput epididymis prepared at the same time as the semen smears did not reveal labeled spermatozoa. This suggests that with a small fraction of the sperm cells labeled in the epididymis, semen smears are a better means of locating labeled spermatozoa than are histological sections.

The duration of one cycle of the seminiferous epithelium was calculated to be 10.9 days. This figure was derived by considering all possible intervals shown in figure 1 In general the most accurate time localizations can be made on cell types that have a short lifespan (e.g sec ondary spermatocyes) and in stages that

are of short duration (e g stage 3) In these studies the progression of the label appears to have been accurately localized in time since the estimates of cycle duration were similar Table 3 includes estimates of the lifespan of the different cell types.

Labeled spermatozoa first appeared in the ejaculate between 39 and 41 days post injection (table 4) Only a small number of spermatozoa were initially labeled and the grain count per cell varied. It is postulated that a few spermatozoa with low labeling were derived from primary spermatocytes which had nearly completed their DNA synthesis at the time the labeled thymidine was injected. Other spermatozoa were the most intensely labeled of any found at any time In subsequent ejaculates the proportion of spermatozoa labeled increased rapidly but the proportion of label cells with a maximum grain count decreased. This decrease in grain count is best explained by considering the pattern of spermatogonial divisions in the rabbit (Swierstra and Foote '63) Near the end of stage 1 type A spermatogonia divide (fig 1 table 3) Half of the newly formed type A spermatogonia remain to become stem cells and the other half divide to give rise to intermediate type spermatogonia (Int.) These newly formed intermediates subsequently divide to produce more intermediates (Int.) The latter undergo mitosis and give rise to type B spermatogonia. These cells in turn divide and produce preleptotene primary spermatocytes. According to this pattern one type A spermatogonium produces [illegible] primary spermatocytes. Each of the primary spermatocytes undergoes two ma[illegible]turation divisions and gives rise to fo[illegible] spermatozoa. By this scheme 64 sperm[illegible]ozoa theoretically are produced from [illegible] type A spermatogonium (Swierstra [illegible] Foote '63) and each spermatozoa cont[illegible] one sixty fourth of the original DNA [illegible] type A spermatogonium.

Based on these observations it is [illegible]pected that spermatozoa labeled origin[illegible] as preleptotene primary spermatocy[illegible] contain on the average twice as m[illegible] tritiated thymidine as spermatozoa label[illegible] as type B spermatogonia and four tim[illegible] as much as spermatozoa labeled as [illegible] spermatogonia (table 4) Also, it sh[illegible] be noted that spermatogenic cells wh[illegible] have nearly completed their DNA synth[illegible]sis or started DNA synthesis shortly [illegible] the time that the isotope was administ[illegible] are expected to incorporate less label th[illegible] similar cells in which thymidine-H³ [illegible]tion and DNA synthesis coincided. Th[illegible] observations explain the gradual decre[illegible] in the intensity of labeling of sperma[illegible] in the semen with time.

The absolute duration of each of th[illegible] eight stages of the cycle of the semin[illegible]erous epithelium was calculated by mu[illegible]ing the relative frequencies of the sta[illegible] and the observation that one cycle of th[illegible] seminiferous epithelium equals 10.9 d[illegible] (table 5) The estimate of the total d[illegible]tion of spermatogenesis in the rabbit d[illegible]pends on the point chosen as the com[illegible] of spermatogenesis. If spermatogonia [illegible]

TABLE 4

Time intervals between labeling of the various spermatogenic cells and the subsequent appearance of labeled spermatozoa at the head of the epididymis and in the ejaculated semen

Cell type in which the label was incorporated	Time interval: Labeling to head of epididymis	Time interval: Labeling to ejaculated spermatozoa	Expected intensity of labeling in the spermatozoa
	days	*days*	
Newly formed primary spermatocytes	31	39–41	100[1]
Type B spermatogonia	bout 33	41–43	50
Int. type spermatogonia	bout 34	42–44	25
Int. type spermatogonia	bout 37	45–47	12.5
Type A spermatogonia	about 38	46–48	6.25

Epididymal transport 8–10 days (see results).

[1] Assumed that the different spermatogenic cells incorporated initially the same amount of label. Intensity of initial label arbitrarily chosen as 100.

TABLE 6

Duration of the stages of the cycle of the seminiferous epithelium in the rabbit

Stage	Relative frequency	Duration
	%	*days*
1	27 7	3 0
2	13.4	1.5
3	7.3	0 8
4	11.0	1.2
5	4.1	0 4
6	15.7	1.7
7	12.2	1.3
8	8.6	0.9

nsidered to begin with the first of the ries of spermatogonial divisions leading the production of primary spermatoytes, then it takes about four cycles of e seminiferous epithelium or 4 × 10.9 43.6 days. However if one assumes at spermatogenesis starts with the for ation of spermatogonial stem cells and at the lifespan of these stem cells is one ycle of the seminiferous epithelium then permatogenesis would extend over about 75 cycles or 51.8 days.

Epididymal transport was eight days for he rabbit and ten days for four rabbits hus, depending on the point chosen as he onset of spermatogenesis the approxiate minimum total time for spermatoenesis and epididymal transport in the abbit is either 52 or 60 days.

ACKNOWLEDGMENTS

This investigation was supported in part y the Lalor Foundation and by Public ealth Research Service Grant GM10263 ational Institute of General Medical Sciences, Public Health Service The techical assistance of John Whitefield and hurston Dale is gratefully acknowledged.

LITERATURE CITED

mann, R. P 1962a Reproductive capacity of dairy bulls. III. The effect of ejaculation frequency unilateral vasectomy and age on spermatogenesis. Am. J. Anat., 110: 49–67

——— 1962b Reproductive capacity of dairy bulls. IV Spermatogenesis and testicular germ cell degeneration. Am. J Anat., 110 69–78.

ledell, S. A., and G. W Salisbury 1941 The rate at which spermatogenesis occurs in the rabbit. Anat. Rec., 80 145–153.

Belanger, L. F 1961 Staining processed radioautographs. Stain Tech., 36: 313–317

Clermont, Y 1954 Cycle de l'épithélium séminal et mode de renouvellement des spermatogonies chez le hamster. Rev Canad. Biol., 13 208–245

——— 1963 The cycle of the seminiferous epithelium in man. Am. J Anat., 112 35–51

Clermont, Y and C. P Leblond 1955 Spermiogenesis of man, monkey ram and other mammals as shown by the periodic acid-Schiff technique. Am. J Anat., 96: 229–251.

——— 1959 Differentiation and renewal of spermatogonia in the monkey (*Macacus rhesus*) Am. J Anat., *104* 237–274.

Clermont, Y., and B Perey 1957 Quantitative study of the cell population of seminiferous tubules in immature rats. Am. J Anat., *100* 241 260.

Clermont, Y., C. P Leblond and B. Messier 1959 Durée du cycle de l'épithélium séminal du rat. Arch. Anat. microsc. Morph. exp., *48* 37–55.

Curtis G. M. 1918 The morphology of the mammalian seminiferous tubule. Am. J Anat., 24 339–394.

Ebner V von 1888 Zur spermatogenese bei den Säugethieren. Arch. mikr. Anat., *31* 236–292.

Foote R. H., and H. H. Koefoed-Johnsen 1959 The use of adenine-8-C[14] for studying spermatogenesis in the rabbit. J Animal Sci., *18* 1553.

Hauser E. R., G. E. Dickerson and D. T Mayer 1952 Reproductive development and performance of inbred and crossbred boars. Mo. Agr Expt. Sta. Res. Bul. 503.

Heller C. G., and Y Clermont 1963 Spermatogenesis in man: An estimate of its duration. Science, *140* 184–186.

Koefoed-Johnsen, H. H. 1959 Saedopsamlingshyppighedens indflydelse på spermiernes dannelse — og transporttid hos tyren. Den kgl. Vet. Landbohøjskole Inst. Sterilitet, Aarsberetning, 253–264.

Leblond, C. P and Y Clermont 1952a Spermiogenesis of rat, mouse, hamster and guinea pig as revealed by the "periodic acid-fuchsin sulfurous acid" technique. Am. J Anat., *90* 167–216.

——— 1952b Definitions of the stages of the cycle of the seminiferous epithelium in the rat. Ann. N Y Acad. Sci., 55 548–573.

Monesi, V 1962 Autoradiographic study of DNA synthesis and the cell cycle in spermatogonia and spermatocytes of mouse testis using tritiated thymidine. J Cell Biol *14* 1–18.

Oakberg, E. F 1956a A description of spermiogenesis in the mouse and its use in the analysis of the cycle of the seminiferous epithelium and germ cell renewal. Am. J Anat., 99 391–413.

——— 1956b Duration of spermatogenesis in the mouse and timing of stages of the cycle of seminiferous epithelium. Am. J Anat., *99* 507–516.

Orgebin, M. C. 1961 Etude du transit épididymaire des spermatozoïdes de taureau marqués à l'aide de P-32. Ann. Biol. Anim. Bioch Biophys., *1* 117–120.

Ortavant, R 1954 Détermination de la vitesse de transfert des spermatozoïdes dans l'épididyme de Bélier à l'aide de [32]P C. R. Soc. Biol., Paris, *148* 866–868.

——— 1954b Etude des générations spermatogoniales chez le Bélier C. R. Soc. Biol., Paris, 148 1958–1961.
——— 1956 Autoradiographie des cellules germinales du testicule de Belier Durée des phénomènes spermatogénétiques. Arch. Anat. microsc. Morph. exp., 45 1–10.
——— 1959 Spermatogenesis and Morphology of the Spermatozoon. Reproduction in Domestic Animals, Vol. II, H. H Cole and P T Cupps, ed. Academic Press, New York, Chap. 1
Roosen-Runge, E. C. 1951 Quantitative studies on spermatogenesis in the albino rat. II. The duration of spermatogenesis and some effects of colchicine Am. J Anat., 88 163–176.
Roosen-Runge, E. C., and L. O. Giesel 1950 Quantitative studies on spermatogenesis in the albino rat. Am. J Anat., 87 1–30.
Rubini, J R., E. P Cronkite, V P Bond and T M. Fliedner 1960 The metabolism and fate of tritiated thymidine in man. J Clin. Invest., 39 909–918.
Singh, G. 1963 Durée de passage dans l'[illegible] idyme des spermatozoïdes de [illegible] u ^{32}P Ann. Biol. Anim. Bioch. [illegible] 2: 43–46.
Sirlin, J L., and R. G. Edwards [illegible] labeling of mammalian spermatozoa [illegible] radioactive tracers. J Exp Zool., [illegible]
Swierstra, E. E. 1962 The cytology and [illegible] of spermatogenesis in the rabbit, and [illegible] desoxyribonucleic acid content of sperm[illegible] genic cells. Ph.D Thesis, Cornell [illegible] Ithaca, New York.
Swierstra, E. E., and R. H. Foote 1963 [illegible] and kinetics of spermatogenesis in the [illegible] J Reprod. Fertil., 5 309–322.
Swierstra, E. E., J W Whitefield and R. H. Foote 1964 Action of amphetericin B [illegible] zone) on spermatogenesis in the rabbit. J Reprod. Fertil., 7 13–19.
Swift, H. H. 1950 The desoxyribose [illegible] acid content of animal nuclei. Physiol. Zool. 23 169–198.

PLATE 1

EXPLANATION OF FIGURES

Figures 2–7 are microphotographs of Feulgen-stained autoradiographs of rabbit testes removed at different time intervals after thymidine-methyl-H³ injection. All photographs × 990.

PL, primary spermatocyte in preleptotene; L, primary spermatocyte in leptotene; P primary spermatocyte in pachytene; D primary spermatocyte in diplotene; M, metaphase configuration; R. secondary spermatocyte; S spermatid and Z, spermatozoa.

2 Two hours post injection; stage 1 Leptotene primary spermatocytes in stage 1 are the most advanced labeled cells.

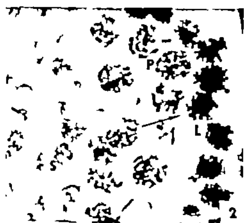
3 Four days post-injection; stage 4 Zygotene primary spermatocytes in stage 4 are the most advanced labeled cells.

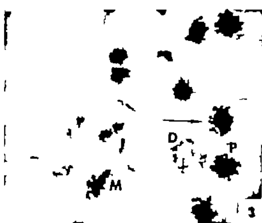
4 Fifteen days post-injection; stage 4 Secondary spermatocytes in stage 4 are the most advanced labeled cells. One cycle of the seminiferous epithelium later than in figure 3.

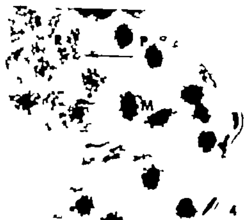
5 Twenty-six days post-injection; stage 4 Spermatozoa in stage 4 are the most advanced labeled cells. Two cycles of the seminiferous epithelium later than in figure 3.

6 Thirty-one days post injection; stage 8. Labeled spermatozoa are leaving the testes.

7 Thirty-one days post-injection. A few intensely labeled spermatozoa are present in semen smears from the head of the epididymis

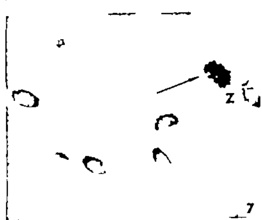

P
L
2


D
P
M
3


R
P
M
4


Z
M
P
M
5


PL
P
S
Z
6


Z
7

The Terminal Air Sacs and their Blood Supply in a 37-day Infant Lung [1]

EDWARD A BOYDEN
Department of Biological Structure University of Washington, Seattle Washington

ABSTRACT Wax models of terminal spray of peripheral air passages from the middle lobe of 37-day infant lung are presented in three views. Superimposed on drawings of the models are reconstructions of the arteries and veins. The spray begins with pre terminal bronchiole and ends in trifurcation of alveolar ducts, each giving rise to two clusters of saccules. The third duct and its clusters are markedly under developed. So far there is no evidence that new acini are being formed and the possibility of this seems less and less likely

Terminal arteries do not follow the rigid pattern of Miller ('37) namely that an artery accompanying an alveolar duct breaks up into as many branches as there are atria and each of these into as many branches as there are sacculi. Instead, the six clusters are partially supplied by two rami which branch irregularly and also supply adjacent clusters. Parts of cluster may be supplied by arteries from distant and alien sources. A long arterial ramus frequently takes short cut through saccules of other clusters. Conspicuous are numerous small adventitious branches arising from the main artery Often peripheral vein is continuous with pleural vein.

Recent estimates based upon random sampling methods, indicate that between birth and maturity the human lungs increase in *volume* from 0 2 of a liter to 5 5 liters, in the *number of alveoli* from 24 to 296 millions and in *air tissue interface* from 2.8 to 75 square meters (Dunnill, '62) How this is accomplished has long puzzled investigators. Is growth accompanied by the introduction of new blocks of tissue such as acini, or by the increase in number of non-respiratory branches, or is it primarily a matter of growth and differentiation of elements already present at birth?

The purpose of this study has been not only to bring new observations to bear on this problem but also to ascertain the vascular pattern in the respiratory margin of the infant lung so far as it is possible to do this from reconstruction of serially sectioned material. The specimen chosen for study is the middle lobe of a 37-day male infant. The latter had died following surgical repair of a congenital heart lesion. Following the autopsy the lobe was injected with Zenker-formol solution through a middle lobe vein (due to shortness of other tubes) and found to be perfectly preserved. The specimen had the further advantage of being spaced in time between two stages previously studied — those of a newborn and an infant of two months (Boyden and Tompsett '65)

I The terminal air sacs

The position of the terminal spray that was reconstructed by the wax-plate method is indicated by an arrow in figure 1 The spray lies near the tip of the middle lobe on its cardiac surface To obtain the total count of branchings the bronchus leading to the tip of the lobe (B a2) was dissected up to the point where the tissue block was cut out Then the block was serially sectioned and the bronchus reconstructed graphically The solid lines in the figure indicate that portion of the bronchial tree which is completely lined by cuboidal epithelium the dotted lines mark the beginning of respiratory bronchioles.

Figure 2 is a tracing of serial section no 637 which passes approximately through the middle of the spray indicated by the arrow in figure 1 Branch 29*b* (fig 2) is a respiratory bronchiole of the second order giving rise to three alveolar ducts

[1] Supported by Research Grant HD-00836, National Institutes of Health, U S Public Health Service
For complete reconstruction of this block of tissue, see figure 1, Boyden and Tompsett, '65 for orientation of bronchus B[a]2 in the middle lobe, see figure 41, Boyden, '55.

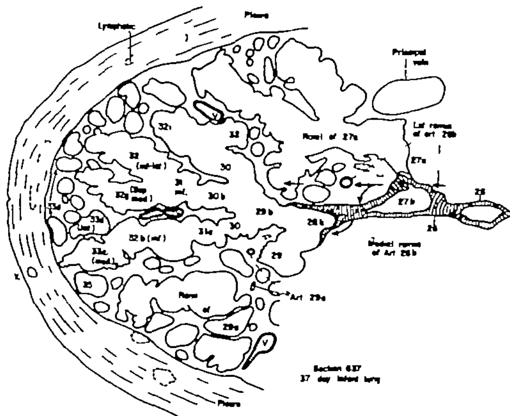


Fig 2 A tracing of Section no. 637 the most revealing section through the terminal spray of air sacs modeled in figures 3 to 8 (× 60) The section lies in the plane of the arrow shown in figure 1 Hence, the pleural surface of the spray will slope diagonally upwards. *Cross lined* areas indicate extent of cuboidal epithelium *numbers* the generations of branchings of the middle lobe bronchus, *arrows*, the course of artery 28b (cf figs. 10 and 12); *double line* veins *heavy line* arteries. The last respiratory bronchiole (29b) divides into three alveolar ducts (*30a*, *b*) The plane of this section is indicated by horizontal line in figures 3 to 6 and figures 10 to 12

(34b) and a pleural group (*34a*) which consists of superior (*35a*) and inferior (35b) saccules. To see the lateral group (33b) it is necessary to view the model from above (fig. 8B) In this view *33b* is seen to divide into a recurrent (*34d*) and a pleural group (*34c*) consisting of medial (35c) and lateral (*35d*) saccules

The inferior division (*32b* fig. 3B) divides into a larger inferolateral portion (33d) to be described below and a smaller superior-medial portion (*33c*) The latter splits into superior (*34e*) and inferior (34f) saccules The inferolateral portion (33d) gives rise to half the cluster From above (fig. 8B) it is seen to divide into a wedge-shaped medial portion (*34g*) and a larger lateral portion (*34h*) The medial portion (*34g*) splits into a superior (*35e*) and an inferior saccule (*35f*) The lateral portion (*34h*) divides into an inferior saccule (*35h*) and a superior group (*35g*) which consists of a medial (*36a*) and a lateral (*36b*) saccule (see also fig. 4B)

(b) *Cluster 31b* This lower cluster arising from alveolar duct *30a* (fig. 3B) is much the smaller of the two. In a lateral view of the model (fig 4B) it can be seen to divide into an undeveloped proximal portion (*32d*) and a distal expansion (*32c*) The latter gives rise to a small lateral saccule (*33f*) and a large medial group (*33e*) *33e* is best seen in figure 3B On the medial side it divides into superior (*34i*) and inferior (*34j*) portions The former (*34i*) splits into a superior (*35i*)

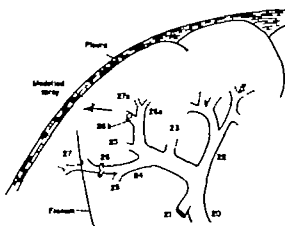


Fig. 1 A reconstruction of the tip of the cardiac surface of the middle lobe of a 37-day male infant (× 10) showing endings of bronchus B[4]a2. (For course of entire bronchus, see fig. 1 Boyden and Tompsett ('65).) *Arrow* indicates position of terminal spray of air sacs displayed in figures 3 to 8. *Solid lines* bronchioles lined with cuboidal epithelium; *dotted line* respiratory bronchioles lined by flat epithelium and patches of cuboidal epithelium 20–27 generation of branchings of middle lobe bronchus.

(*30a* *30b* and *30c*) Each of these in turn gives rise to two transitional ducts (*31a* to *31f*) each the short stem of a cluster of alveolar saccules Together the six clusters extend through 55 (20 μ) sections. The over all depth of the spray therefore is 1 1 mm The absolute distance in the fixed specimen, from the beginning of respiratory bronchiole *29b* to the pleura ranges from 0 7 to 1 3 mm At the level of section 637 it is approximately 1 0 mm. This section was the starting point from which two models were reconstructed The clusters were so complex that it was necessary to build up clusters *31a* and *b* first (figs 3 and 4) then the four remaining clusters (figs. 5 and 6) The proximal stems — those common to both sets of clusters — were thus reconstructed twice

Let us now look at the proximal stems of clusters *31a* and *b* as seen from the medial side (figs 3A and B) The diagram in figure 9 summarizes the mode of subdivision At the right side of figure 3B the pre-terminal bronchiole (*26b*) divides into two terminal bronchioles (*27a* and *27b*) Bronchiole *27b* divides into two respiratory bronchioles of the first order (*28a* and *28b*) Bronchiole *28b* bifurcates into respiratory bronchioles of the second order (*29a* and *29b*) (The dotted areas on the drawing indicate the distribution of cuboidal epithelium.) Secondary branch *29b* virtually trifurcates into three short ducts (*30a* *30b* and *30c*) In this model the last two ducts (*30b* and *c*) are represented by severed stumps, but in figures 5 to 8 they are fully modeled

Returning to figure 3 alveolar duct *30a* divides into transitional ducts (*31a* and *31b*) These are short stems, each giving rise to a cluster of alveolar saccules In the previous study they were termed "transitional ducts" because in these early stages one cannot know whether they will persist as definitive ducts or will be incorporated in the cluster At two months of age the latter seemed to be their fate (cf. B. and Tompsett '65, fig. 15) Also the term "cluster" is deliberately non-committal for it is premature as yet, to identify one or the pair of these with a primary lobule

At this point it is desirable to equate this study with the previous report on the changes that take place between the newborn and the infant of two months There it was shown that what had been the most distal respiratory bronchiole in the newborn — namely the last duct bearing patches of cuboidal epithelium on one side and flat epithelium on the other — had become transformed within two months into a definitive alveolar duct. This seemed to have been accomplished by the process of elongation and the new outgrowth of regularly spaced alveoli So also, in the 37-day infant the duct supporting the clusters (alv duct *30a* fig. 3B) is giving rise to alveoli and contains no trace of cuboidal epithelium Until still older stages are reconstructed, it will not be known how far centrally this process of conformation extends. With this introduction we may now proceed to the description of individual clusters.

(1) Alveolar duct 30a

(a) *Cluster 31a.* Let us begin with the transitional duct *31a* (fig 3B) This short stem divides into two main portions: a superior division (*32a*) and an inferior one (*32b*) *32a* splits into a medial (*33a*) and a far lateral portion (*33b*) The medial one (*33a*) divides into a recurrent ...

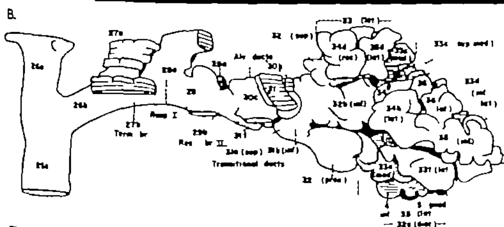
(b) *Cluster 31d.* This lower cluster of he two (*31d*, fig. 5) is larger than the pper cluster (*31c*) — the reverse of the ituation seen in figure 3 As viewed in gure 5B it divides into a larger *superior edial division* (*32g*) and a smaller in- or-lateral one (*32h*) *32g* splits into qual medial (*33k*) and lateral (*33l*) por ons. The latter is mostly hidden but can e seen passing behind the medial. The edial (*33k*) breaks up into a superior 35s) and an inferior saccule (*35t*)

The *inferior lateral division* (*32h*) — s seen in the lower right corner of fig re 6 — is virtually three-lobed. Above is superior horn (*33m*) Below are the me- ial and lateral horns which subdivide espectively into saccules *35w* and *x* and 35y and z. The relative positions of divi sions *32g* and *32h* are best seen in figure 8A (left margin)

(3) *Alveolar duct 30c*

This is the rudimentary appendage on the lateral side of duct *30b* (fig. 6) It seems to represent an attempt by a third pair of clusters (*31e* and *31f*) to share the terminal surface of the lung at this level. Such rudimentary outgrowths have been seen in the cast of a premature infant lung (fig. 13 Boyden and Tompsett, '65) in which the injection of plastic had been stopped just as it was entering the atria of the clusters. In this preparation it was not uncommon to see a smaller "ball try ing to share the top of the branch with a pair of larger ones. The interesting ques-





Figs. 4A and B Photograph of wax model (A) and explanatory drawing (B) of the branches of alveolar duct 30a as seen from the lateral side (× 60) Alveolar ducts 30b and and their branches have been removed, but their stumps are visible (30a itself is hidden in this view)

Figs. 5A and B Photograph of wax model (A) with explanatory drawing (B) of alveolar d... 30b and its branches (× 60) as seen from the medial side after removal of alveolar duct ... and its branches. The proximal bronchioles common to both 30a and 30b have been modeled ... Projecting below the main model is an abortive cluster (31f) which will be described in fig... 6 and 8 (For description of branches see text.)

tion is whether such rudimentary pairs will catch up in growth with the others and thereby form a substantial means of increasing respiratory surface

(a) *Cluster 31e* This is the larger of the two clusters It divides atypically (fig 6B) into three portions a pleural (*32l*) an inferior (*32j*) and a recurrent (*32k*) The pleural further splits into a distal (3... and a proximal (*33p*) saccule Two of the... three may be seen from above (fig ...

(b) *Cluster 31f* This is still ... rudimentary (fig 6B) It divides ... proximal (*32m*) and a distal (*32l*) b... the latter ending in a rudimentary ... (*33q*) and an inferior (*33r*) saccule

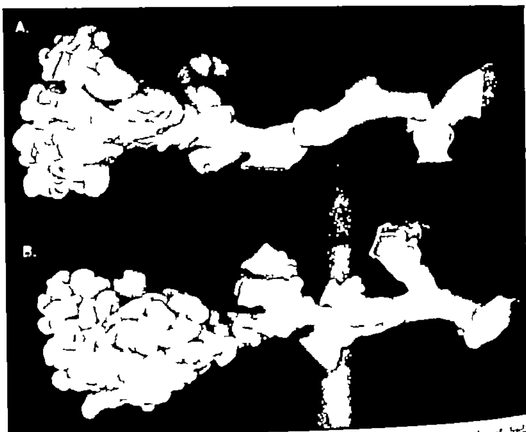
II The vascular pattern

The blood supply of the terminal spray is illustrated in figures 10–12. Arteries and veins were plotted graphically at the same magnification as the models then transferred to drawings of the models and corrected by inspection wherever necessary Since the fresh specimen was injected through a middle lobe vein, the veins are relatively larger and the arteries relatively smaller The veins can be followed all the way even into the pleura (fig 10) but the arteries are lost as soon as they break up into the smaller arterioles.

(a) *Arterial pattern* The subterminal bronchiole (*26b* fig 10) is paralleled on its lateral surface by a small artery having three or four layers of smooth muscle. This vessel (*Art 26b*) divides into lateral and medial rami. The lateral ramus stays on

B.

Fig. 8A and B Photograph of wax model (A) with explanatory drawing (B) of alveolar ducts 30b and 30c and their branches as seen from the lateral side (60) This view shows to best advantage the two abortive clusters *31* and *31f* derived from alveolar duct 30c (see text)



Figs. 7A and B Photograph of the two wax models from above (× 60) *A* branches of [illegible] ducts 30*b* and 30*c*; *B* branches of alveolar duct 30*a*. (For description see text and fig 8)

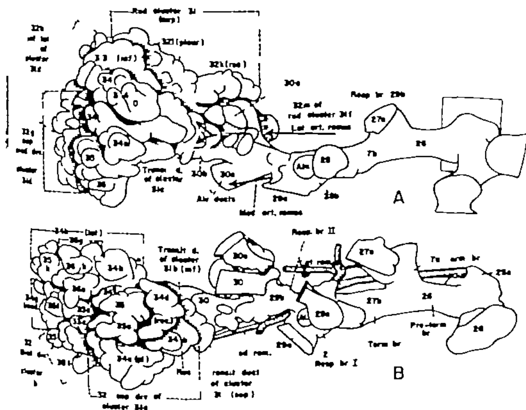
the same side of the bronchiole as the [illegible]rent artery (cf fig 2) but the medial [illegible] dips under the bronchiole to reach the medial side of alveolar duct *30a* (see also fig 8) As soon as it reaches this level it gives off a stout vertical branch (*Art. 29a*) which enters the territory of respiratory bronchiole *29a* and contiguous air spaces (figs 10 and 12) The medial ramus then divides into two main branches the lower of which follows *31b* (fig 10) but continues beyond this to supply adjacent distal air spaces of unknown origin The upper branch which is a more direct continuation of the medial ramus runs in a groove between clusters *31a* and *31b* but is closely applied to the medial side of *32b* to which it gives branches Distally it divides into an upper stem which disappears between saccules *33c* and *35l* and a lower stem which supplies *34l* and *34j* as well as air spaces of an adjacent cluster Strangely there is no visible branch to *32a* and its medial division [illegible] yet its lateral division *33b* (see left [illegible] portion of fig. 10) is supplied by a [illegible] nal branch of the lateral arterial [illegible] which has inserted itself between the [illegible] upper clusters of the spray (*31a* and *31* [illegible]) The lower lateral division of this [illegible] (*34h*) (see asterisk, fig. 8B) is supplied by another artery of unknown origin which ascends from below from an entirely [illegible] ent group of clusters (see asterisks [illegible] 10 and 12)

Similarly the lateral ramus of *Art* [illegible] (fig. 12) does not follow the exact [illegible] of the bronchiolar stem. After giving [illegible] major branches (*Art 27a*, *Art.* [illegible]) [illegible] bronchioles *27a* and *28a* it leaves the [illegible] chial tree to course between alien [illegible] until it reaches cluster *31c* There it [illegible] around both sides of the cluster On [illegible] way to this position it gives off a descend[illegible] ing branch to the peripheral air spaces of bronchiole *27a* which, surprisingly [illegible]

the flanks of cluster *31e* (cf fig. 2) But no arterial supply is detected for cluster *31f* (lower middle part of fig 12) nor for *31d* (right lower portion) nor for the previously mentioned *32a* (fig 10) Since these substantial portions of the terminal spray are fully supplied by a capillary network, one must infer that the arterioles supplying them are too small to be traced to their sources or that earlier arterioles have been converted into plexuses or that saccules can be supplied by capillary-sized vessels from adjacent clusters (see below)

In any case, it is obvious that the arterial pattern of this terminal spray does not fit the accepted description of the mode of branching of the pulmonary artery in the adult lung as described by Miller ('37) He writes (p. 71) "When the artery reaches a point distal to the *ductus alveolaris* it breaks up into as many branches as there are *atria* (fig 53) Each of the atrial arteries breaks up into as many branches as there are *sacculi alveolares*

This statment has been challenged also by K. K. Pump ('61) on the basis of fresh autopsy specimens of adult lungs injected with Vultex Moulage In a study of the circulation of the primary lobule of Miller he finds that "Distal to the alveolar duct there are no further vessels which can be identified as subdivisions of the pulmonary artery except the capillary network of the alveoli. Also in an as yet unpublished observation (personal communication) he finds that in the adult lung the artery ac



Figs. 8A and B Explanatory drawings of the models shown in figure 7 In this lung the two groups of clusters interdigitate the 33m and n group overlapping the 34g and h group. A — This top view of the model shown in figures 5 6 and 7A illustrates best the uppermost saccules of cluster 31c also the position of the alveoli on ducts 30b and 30c. Arrow indicate the course of the two main arterial rami (see figs. 10 and 12) B — This view of the model shown previously in figures 3, 4 and 7B illustrates best the position of the alveoli on duct 30a, the uppermost saccules of cluster 31a, the inferior lateral groups of 31 and the medio-lateral relation of the two arterial rami. Asterisk, the saccule supplied by the distant artery marked by an asterisk in figures 10 and 12.

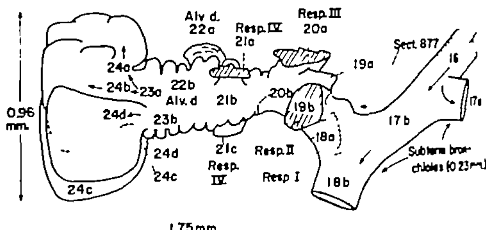


Fig. 15 Explanatory sketch of a peripheral spray of clusters in an infant lung of two months (after Boyden and Tompsett, Acta Anat., '65) *Dotted* areas indicate the distribution of cuboidal epithelium; *24a-d*, outlines of four terminal clusters branching via transitional ducts (*21*) from a histologically definitive alveolar duct (*22b*) Equally revealing is the origin of the first respiratory bronchiole (*18a*) from pre-terminal bronchiole. At earlier stage *18a* must have been a terminal bronchiole.

shows in diagram form the pattern of division of a primary respiratory bronchiole from another specimen. Incidentally this author would omit the term alveolar duct and substitute respiratory bronchiole on the ground that it is almost impossible to tell the hitherto designated "last respiratory bronchiole from the alveolar duct. In figure 13 the author indicates that there can be as many as five generations of alveolized ducts (i.e respiratory bronchioles) between the terminal bronchiole and the saccules (S) that the latter may even arise as sessile outgrowths and that trifurcation of ducts or of bronchioles is fairly common In fact the pattern seems to be more elaborate than the author conservatively admits Following R2B to the end in figure 13 one can make out a maximum of at least nine branchings instead of five divisions of the terminal bronchiole.

These figures of Dr Pump's strongly suggest to the writer some of the changes that may take place in the infant lung to produce the adult pattern As one looks at the clusters shown in figures 3 to 8 one is impressed by the frequency with which recurrent or proximal saccules occur If the clusters undergo elongation in later stages then saccules which now appear to be recurrent or proximal on a branch could be left behind as sessile or short stalked saccules

Another assumption that can safely be made is that in the first two months elongation of the elements that form the clusters has not yet become noticeable The changes that *are* taking place occur primarily in the stems proximal to the clusters In this 37-day lung, for instance, only two orders of respiratory bronchioles can be recognized but at two months (fig. 15) four orders are present and as alveoli are appearing centripetally respiratory bronchioles become transformed into alveolar ducts and terminal bronchioles become the first order of respiratory branches. Perhaps the most striking feature is the appearance of histologically definitive alveolar ducts (22) interpolated between transitional ducts (23) and the last respiratory bronchioles (21) Obviously it is too early to reach final conclusions but as more sprays are studied it seems less and less likely that the lung grows by the addition of new ... as suggested by Engel ('62) and others

LITERATURE CITED

Boyden, E. A. 1955 Segmental Anatomy of the Lungs. A Study of the Patterns of the Segmental Bronchi and Related Pulmonary Vessels. Blakiston Division, McGraw-Hill, New York, Toronto, London.

Boyden E. A and D. H. Tompsett 196? The branching pattern in the developing lung of the infant Acta Anat (in press)

Dunnill, M. S. 1962 Postnatal growth of the lung. Thorax, 17 329–333.

Elliott, F. M., and L. Reid 1965 (In press.)

Engel, S. 1962 Lung Structure. Charles C Thomas, Springfield, Illinois.

Kump, K. K. 1961 The circulation of the primary lobule of the lung. Dis. Chest, 39 614–621.

——— 1962 The circulation of the secondary lobule of the human lung. Dis. Chest, 41 364–371

——— 1964 The morphology of the finer branches of the bronchial tree of the human lung. Dis. Chest., 46 379–398.

Oxidative Enzymes of Intermediary Metabolism in Healing Bone Fractures

A HISTOCHEMICAL STUDY [1]

KAROLY BALOGH, JR. AND JOSEPH V. HAJEK

Department of Pathology, Harvard Medical School, Massachusetts General Hospital and Massachusetts Eye and Ear Infirmary Boston, Massachusetts

ABSTRACT The fibulae of young adult rats were cut at the mid-diaphysis with scissors and examined at various stages of repair. The distribution of enzymes participating in glycolysis, in the citric acid cycle, and in the hexose monophosphate shunt was studied histochemically in healing bone fractures.

Three days after the fracture there was marked proliferation and an increased enzyme activity in the osteoprogenitor cells in the inner layer of the periosteum along the entire diaphysis. Remarkable enzyme activity was also observed in the newly formed osteocytes. No qualitative differences were noticed among osteoprogenitor cells, osteoblasts, and osteocytes. Necrotic muscle fibers, periosteum, and bone cells failed to react.

Seven days after the fracture, a bulky cartilaginous callus developed. The proliferating osteoprogenitor cells of the periosteum and of the callus had similar enzyme pattern. As the fibroblast-like osteoprogenitor cells of the callus developed into chondrocytes, enzyme activity increased. This was especially striking for isocitric dehydrogenase and glucose-6-phosphate dehydrogenase. When the chondrocytes became hypertrophic, they gradually lost enzyme activity. Mononuclear and multinuclear osteoclasts, macrophages and foreign body giant cells showed marked activity of most demonstrated enzymes. Glucose-6-phosphate dehydrogenase activity was marked in foreign body giant cells, but appeared weak in osteoclasts.

At 14 days the enzyme pattern of the callus was essentially the same as at seven days.

At 30 days bone union was well established, but there was still considerable osteoblastic and osteoclastic activity.

The histochemical findings have been described in detail and discussed in correlation with pertinent morphological and biochemical data. Histochemically bone regeneration proved to be essentially recapitulation of normal bone growth.

A considerable body of knowledge has been acquired on various aspects of fracture repair but many fundamental questions concerning it remain unanswered. Despite the advent of modern research techniques in biochemistry reliable quantitative data on the metabolism of callus are hard to obtain due to obvious difficulties in sampling. Although the complex structure of the callus lends itself to the application of histochemical methods for the demonstration of enzyme activity this approach has not been adequately explored. Only alkaline phosphatase activity has been demonstrated in bone regeneration (Pritchard and Ruzicka, '50 Majno and Rouiller '51) but the role of this enzyme in calcification is not fully understood (Bourne '56). In the last decade, a number of histochemical methods were developed that localized the activity of oxidative and hydrolytic enzymes. We thought it possible to demonstrate changes in the intermediary metabolism of the callus during differentiation of the osteoprogenitor cells by using some of these techniques. The present paper reports a histochemical investigation of oxidative enzyme activity in the cells of healing fractures.

Inasmuch as the distribution of oxidative enzyme activity in growing cartilage and bone has been the subject of a previous study (Balogh et al. '61) normal skeletal tissues were considered only in connection with the reparative processes.

[1] This study was supported by Research Grant B 04185-03 of the National Institute of Neurological Diseases and Blindness, U. S. Public Health Service. [illegible] trainee ('63) under the National Institutes of Health Pathology Training Grant 2G-193(C3).

TPNH diaphorase, and TPN mediated iso- and glucose-6-phosphate dehydrogenase reactions. The outer layer of the periosteum was slightly edematous near the fracture. The fibroblasts of this layer [illegible] to be more numerous and showed a considerable increase of enzyme activity in comparison to the normal periosteum. The osteoprogenitor cells and osteoblasts of the periosteum showed marked proliferation which increased as the fracture site was approached. This was accompanied by a correspondingly intensified activity of all enzymes except succinic dehydrogenase. The osteoprogenitor cells and osteoblasts revealed strong activity of DPNH and TPNH diaphorase glyceraldehyde 3-phosphate lactic, dihydrolipoic and malic dehydrogenase and moderate activity of isocitric and glucose-6-phosphate dehydrogenase (fig 2). The endosteum was lined by relatively few osteoblasts, which reacted identically to those of the periosteum. One or two cell-layers deep under the periosteum young osteocytes revealed a remarkable oxidative enzyme activity (fig. 3). The cytoplasm of the younger osteocytes was filled with diformazan, whereas the older osteocytes exhibited considerably less enzyme activity. No qualitative differences in enzyme pattern were noted among osteoprogenitor cells, osteoblasts and osteocytes.

Close to the fracture sites and at the bone defects themselves the periosteum and endosteum were necrotic and failed to reveal any enzymatic activity (fig 1). Necrosis of the cortical bone extended for a variable distance from the fracture site. Dead bone was frequently covered by living periosteum which showed evidence of increased osteogenesis (fig. 3). Irregular areas of bone necrosis were also seen at the fracture ends and in isolated bone fragments. The cytoplasm of dead osteocytes did not contain any diformazan. In the areas of bone necrosis the cells in many Haversian canals maintained some enzyme activity.

Seven days

There was a large cellular callus, its bulk consisting of fibroblast-like osteoprogenitor cells and cartilage cells in various stages of differentiation (figs. 4 and 7). The osteoprogenitor cells and young blood vessels spread from the torn ends of the periosteum and endosteum into the space between the fracture ends of the fibula. The osteoprogenitor cells showed marked to moderate activity of DPNH and TPNH diaphorase glyceraldehyde-3-phosphate lactic, dihydrolipoic and malic dehydrogenase (fig 5). Demonstrable enzymatic activity became stronger as these cells differentiated into chondrocytes, and then gradually decreased as the enlarged cartilage cells underwent degeneration. Changes in enzymatic activity associated with cell differentiation were most impressive in the sections demonstrating the localization of isocitric and glucose-6-phosphate dehydrogenase activity. These enzymes were not demonstrable in the undifferentiated osteoprogenitor cells, but were quite active in young chondrocytes. Enzyme activity declined as the older cartilage cells became hypertrophic (figs. 4a, 6 and 7). New osteocytes were formed by the osteoprogenitor cells that invaded the cartilaginous ground substance. In some areas chondroclasts were active in removing the cartilage prior to bone formation. The chondroclasts were enzymatically similar to the osteoclasts. The latter were seen in large numbers on the surface of the newly formed periosteal and endosteal bone spicules and exhibited strong activity of DPNH and TPNH diaphorase glyceraldehyde-3 phosphate, lactic dihydrolipoic succinic malic and isocitric dehydrogenase (figs. 6 8 9). Since succinic dehydrogenase activity was hardly demonstrable in osteoblasts and osteocytes osteoclasts stood out sharply because of their marked succinic dehydrogenase activity (fig 8). Some mononuclear or binuclear cells that exhibited a qualitative enzyme pattern identical with that of the multinuclear osteoclasts were observed on consecutive sections in the vicinity of the

For the designation of various cell types in growing bone we have used the terminology of Young (93). Accordingly undifferentiated cells on or near the surface of bone or calcified cartilage were classified as osteoprogenitor cells. These are identical with the spindle and reticulum cells or mesenchyme cells of other authors. The progeny of these cells, osteoblasts, lined the surface of bone or calcified cartilage. Cells derived from osteoblasts and contained within bone lacunae were considered osteocytes. Multinuclear osteoclasts and chondroclasts were multinuclear cells on or near the surface of bone or calcified cartilage, respectively.

The *course of fracture healing has been* studied histologically by several investigators (Downs and McKeown '32 Urist *and McLean* 41; *Enneking* 48 Pritchard '52) Their detailed descriptions and the comprehensive reviews by Lauche ('37) *Weinmann and Sicher* ('55) *Ham* and Harris ('56) serve as a basis for the presentation of our results The sequence *of well known histologic changes observed* during fracture healing will be mentioned here for orientation or in reference to *some specific histochemical observations*

Previous studies have shown that certain oxidative enzyme systems can be demonstrated histochemically in tissues after decalcification with buffered, cold Versene (Balogh '62, '64) Other practical and theoretical aspects of these histochemical techniques have been discussed by Pearse ('60)

MATERIAL AND METHODS

Male Sprague-Dawley rats weighing 200–250 gm were anesthetized with ether and the lateral aspect of both hind legs was prepared with a depilatory agent and 70% ethanol. A skin incision, 0 5 cm long was made on both hind legs. The muscles were separated bluntly and the fibulae were cut through sharply with dissecting scissors in the mid-diaphyseal region. The periosteum was spared as much as possible. The fracture ends were left in a *position as normal as possible The skin* was closed with metal clips. The operation was done under semisterile conditions. No wound infection occurred. No attempt was made to immobilize the injured limbs. The animals were kept on a regular laboratory diet *ad libitum* and were sacrificed by decapitation at intervals of 3 7 14 or 30 days after the fracture. The fibulae were dissected and partially decalcified with *buffered cold* Versene overnight (Balogh, '62, '64) The tissue blocks were frozen on dry ice and *mounted* for cutting in a cryostat (−18 C) with a rotary microtome at 20 μ. The *diaphyses of the fibulae were sectioned* longitudinally the frozen sections were placed on coverslips thawed, and allowed to stand for 30 minutes at room temperature

After this the sections were incuba[illegible] aerobically for 30 minutes at 37°C [illegible] media designed for the histochemical de[illegible] onstration of the following oxidative e[illegible] zymes: DPNH diaphorase (Scarpe[illegible] et al., '58) TPNH diaphorase (Scarpe[illegible] et al. '58) glyceraldehyde-3-phosphate d[illegible] hydrogenase (Himmelhoch and Karn[illegible] sky '61) lactic dehydrogenase (Nachl[illegible] et al., '58a) dihydrolipoic dehydrogena[illegible] (Balogh '64) isocitric dehydrogena[illegible] (Nachlas et al., '58b) succinic dehyd[illegible] genase (Nachlas et al., '57) malic deh[illegible] drogenase (*Nachlas et al.*, '58a) a[illegible] glucose-6-phosphate dehydrogenase (Nach[illegible] las et al., '58b) Nitro-BT was used as a[illegible] *indicator of enzyme* activity in all rea[illegible] tions. Nitro-BT is a water-soluble, pale[illegible] ditetrazolium salt which forms a da[illegible] blue, finely granular diformazan on redu[illegible] tion by enzymes near their sites of activ[illegible] (Nachlas et al., '57 Pearse '60) In [illegible] instances, control sections to rule out no[illegible] specific reaction were incubated in med[illegible] which lacked only the individual su[illegible] strates. Enzymatic reactions were stopp[illegible] by fixing the sections in 10% neutral fo[illegible] malin for two hours at room temperatur[illegible] *Thereafter* the sections were mounte[illegible] with Kaiser s glycerol gelatin and observe[illegible] under the light microscope.

OBSERVATIONS

Diformazan deposits indicative of en[illegible] zyme activity were found in the cytoplas[illegible] only Cell nuclei and ground substanc[illegible] did not react. *All control* sections re[illegible] mained negative, ruling out nonspecif[illegible] histochemical reactions.

Three days

A large number of mesenchymal cell[illegible] were seen scattered between the damage[illegible] muscle fibers and were concentrated i[illegible] the granulation tissue around the fractu[illegible] site (figs. 1 and 2) These cells wer[illegible] round, ovoid, stellate, or tadpole-like an[illegible] displayed considerable activity of DPN[illegible] diaphorase dihydrolipoic lactic and mal[illegible] *dehydrogenase.* The relatively sma[illegible] round or ovoid cells were remarkable fo[illegible] their strong *succinic* dehydrogenase

DPNH, reduced diphosphopyridine nucleotide; TPN or TPNH, triphosphopyridine nucleotide [illegible] reduced form; Nitro-BT [illegible] diphenyl-3,3′-(3,3′-dimethoxy-4,4′-biphenylene) [illegible] [illegible] chloride.

of DPNH diaphorase and TPN-mediated isocitric and glucose-6-phosphate dehydrogenase reactions. The outer layer of the periosteum was slightly edematous near the fracture. The fibroblasts of this layer appeared to be more numerous and showed a considerable increase of enzyme activity in comparison to the normal periosteum. The osteoprogenitor cells and osteoblasts of the periosteum showed marked proliferation which increased as the fracture site was approached. This was accompanied by a correspondingly intensified activity of all enzymes except succinic dehydrogenase. The osteoprogenitor cells and osteoblasts revealed strong activity of DPNH and TPNH diaphorase, glyceraldehyde 3-phosphate, lactic, dihydrolipoic and malic dehydrogenase, and moderate activity of isocitric and glucose-6-phosphate dehydrogenase (fig. 2) The endosteum was lined by relatively few osteoblasts, which reacted identically to those of the periosteum One or two cell layers deep under the periosteum, young osteocytes revealed a remarkable oxidative enzyme activity (fig. 3) The cytoplasm of the younger osteocytes was filled with diformazan, whereas the older osteocytes exhibited considerably less enzyme activity. No qualitative differences in enzyme pattern were noted among osteoprogenitor cells, osteoblasts and osteocytes.

Close to the fracture sites and at the bone defects themselves the periosteum and endosteum were necrotic and failed to reveal any enzymatic activity (fig. 1) Necrosis of the cortical bone extended for a variable distance from the fracture site. Dead bone was frequently covered by living periosteum which showed evidence of increased osteogenesis (fig. 3) Irregular areas of bone necrosis were also seen at the fracture ends and in isolated bone fragments. The cytoplasm of dead osteocytes did not contain any diformazan. In the areas of bone necrosis, the cells in many Haversian canals maintained some enzyme activity

Seven days

There was a large cellular callus, its bulk consisting of fibroblast-like osteoprogenitor cells and cartilage cells in various stages of differentiation (figs. 4 and 7) The osteoprogenitor cells and young blood vessels spread from the torn ends of the periosteum and endosteum into the space between the fracture ends of the fibula. The osteoprogenitor cells showed marked to moderate activity of DPNH and TPNH diaphorase glyceraldehyde-3-phosphate, lactic dihydrolipoic and malic dehydrogenase (fig. 5) Demonstrable enzymatic activity became stronger as these cells differentiated into chondrocytes, and then gradually decreased as the enlarged cartilage cells underwent degeneration Changes in enzymatic activity associated with cell differentiation were most impressive in the sections demonstrating the localization of isocitric and glucose-6-phosphate dehydrogenase activity These enzymes were not demonstrable in the undifferentiated osteoprogenitor cells, but were quite active in young chondrocytes. Enzyme activity declined as the older cartilage cells became hypertrophic (figs. 4a, 6 and 7) New osteocytes were formed by the osteoprogenitor cells that invaded the cartilaginous ground substance. In some areas, chondroclasts were active in removing the cartilage prior to bone formation The chondroclasts were enzymatically similar to the osteoclasts The latter were seen in large numbers on the surface of the newly formed periosteal and endosteal bone spicules and exhibited strong activity of DPNH and TPNH diaphorase, glyceraldehyde-3-phosphate, lactic, dihydrolipoic, succinic, malic and isocitric dehydrogenase (figs 6, 8 9) Since succinic dehydrogenase activity was hardly demonstrable in osteoblasts and osteocytes, osteoclasts stood out sharply because of their marked succinic dehydrogenase activity (fig 8) Some mononuclear or binuclear cells that exhibited a qualitative enzyme pattern identical with that of the mutinuclear osteoclasts were observed on consecutive sections in the vicinity of the

For the designation of various cell types in growing bone we have used the terminology of Young ('62). Accordingly undifferentiated cells on or near the surface of bone or calcified cartilage were classified as osteoprogenitor cells. These are identical with the spindle and reticulum cells or mesenchyme cells of other authors. The progeny of these cells, osteoblasts, lined the surface of bone or calcified cartilage. Cells derived from osteoblasts and contained within bone lacunae were considered osteocytes. Multinuclear osteoclasts and chondroclasts were multinuclear cells on or near the surface of bone or calcified cartilage, respectively

multinuclear osteoclasts. These mononuclear cells and multinuclear osteoclasts were most conspicuous along the newly formed bone spicules of the anchoring callus (fig 9) Interestingly glucose-6-phosphate dehydrogenase activity was weak in osteoclasts but foreign-body type giant cells and macrophages around fragments of dead bone showed strong activity of this enzyme (fig 7) The Haversian and Volkmann canals were slightly dilated near the fracture site and were transformed into resorption spaces These spaces contained osteoprogenitor cells osteoblasts and numerous osteoclasts that displayed normal enzyme reactions even in areas of bone necrosis at the fracture ends (figs 7 and 10)

Fourteen days

Essentially the same histochemical observations could be made as in the one-week-old fractures. The histologic features of the cartilaginous callus were also similar although more osteoprogenitor cells had differentiated into chondrocytes so that cartilage cells became predominant in the bridging and uniting callus (fig. 11). Relatively few mononuclear or binuclear osteoclasts were present, but a large number of multinuclear osteoclasts with strong dehydrogenase activities could be observed.

Thirty days

Bone union was well established, and remodeling was advanced (fig 12) Considerable osteoblastic activity was seen in the periosteum and in the endosteum (fig. 13) Many osteoblasts were aligned to the walls of the dilated Haversian and Volkmann canals. The periosteum was still thicker than normal, mainly at the fracture site, and showed an increased enzyme activity A few large cartilage cells with marked enzyme activity were seen embedded in the newly formed bone. Small pieces of dead bone were evident in the compact cortical bone and in the spongiosa. Occasionally the necrotic bone was surrounded by osteoclasts which showed characteristically strong enzyme reactions.

DISCUSSION

In our studies, the callus and the sk[illegible] etal tissues near the fracture were t[illegible] source of several interesting observatio[illegible] In normal growing bones, fibroblasts [illegible] the outer periosteal layer were general[illegible] lower in enzyme activity than osteop[illegible] genitor cells of the inner layer (Bal[illegible] et al., '61) When periosteal osteogene[illegible] is stimulated by fracture of the bone sh[illegible] the entire diaphyseal periosteum respo[illegible] rapidly with a remarkable proliferatio[illegible] which becomes most pronounced over the fracture. Concomitantly there is [illegible] striking increase of oxidative enzyme activity in the thickened inner layer. The[illegible] is similar oxidative enzyme activity [illegible] osteoblasts and osteocytes that have be[illegible] incorporated into the osseous ground su[illegible] stance immediately under the periosteu[illegible] Diminution in enzymatic activity is no[illegible] as the young osteocytes mature, but so[illegible] enzyme activity is retained in all liv[illegible] osteocytes. Similar changes have al[illegible] been noted in the course of periost[illegible] osteogenesis in normal bones (Balogh [illegible] al. '61 Balogh, '63) Hence, the depict[illegible] enzyme pattern of appositional bo[illegible] growth following fracture does not dif[illegible] qualitatively from the normal growth pro[illegible] ess. Electron microscopic investigatio[illegible] (Knese and Knoop '58 Dudley and Spi[illegible] '61) have shown that cell maturation fro[illegible] osteoblast through osteocyte involves [illegible] gradual loss of intracytoplasmic orga[illegible] elles. This finding can be correlated wi[illegible] the histochemically demonstrated decrea[illegible] in enzyme activity that accompanies th[illegible] development of osteocytes.

The rate of osteocyte formation is illu[illegible] trated by the large number of young oste[illegible] cytes that appear in the subperiosteal m[illegible] trix within three days of the fractur[illegible] Probably these osteocytes were formed b[illegible] the proliferating periosteum which deve[illegible] oped in response to the fracture becau[illegible] the old cortical bone was necrotic in i[illegible] entire thickness. Evidence to support th[illegible] conclusion comes from recent autoradi[illegible] graphic studies with tritiated thymidin[illegible] Since osteocytes are post-mitotic cells a[illegible] do not synthesize deoxyribonucleic ac[illegible] tritiated thymidine is present only in the[illegible] osteocytes which have been formed fro[illegible] labeled precursor cells. Labeled osteocyt[illegible]

ave been localized in the subperiosteal region of the femur of young rabbits as early as three days after injection of tritiated thymidine (Owen, '63) In necrotic bone, enzyme activity is completely absent in the osteocytes, but viable osteoprogenitor cells, and newly formed osteoblasts and osteoclasts were seen in the periosteum. Cells of these types also filled many dilated Volkmann canals and Haversian canals. The proliferating osteoprogenitor cells in these canals and in the periosteum displayed marked oxidative enzyme activity. The reactive proliferation of the periosteum subsides slowly one month after the fracture there was still an obvious increase in periosteal enzyme activity although bone callus had formed.

Interesting changes take place in the cartilaginous callus when the fibroblast like osteoprogenitor cells become more differentiated. Whereas osteoblasts showed low activity of isocitric and glucose-6-phosphate dehydrogenase a considerable increase in the activity of these (and all other) enzymes could be observed as the osteoprogenitor cells developed into cartilage cells and approached maturity In a later stage, the chondrocytes became hypertrophic and gradually lost their demonstrable enzyme activity. These shifts in enzyme activity were best revealed in slides incubated for the demonstration of isocitric and glucose-6-phosphate dehydrogenase activity inasmuch as it was not possible to localize these enzymes in the osteoprogenitor cells of the callus, but they appeared in the developing cartilage cells and diminished as the chondrocytes underwent degeneration. The development of cartilage cells is associated with an increase in the number of mitochondria, as electron microscopic observations on chondrogenesis (Godman and Porter '60) have clearly shown. Since several of the demonstrated enzymes are mitochondrial, a simultaneous increase of enzyme activity would certainly be expected in the course of chondrogenesis. With further maturation of the cartilage cells oxidative enzyme activities are reduced significantly when the cells become hypertrophic. In keeping with these observations are the degenerative changes and ultimate loss of ultrastructural detail that occurs in hypertrophic cartilage cells (Scott and Pease, '56) Similar striking changes in enzyme activity take place in cartilage cells during normal endochondral ossification (Balogh et al., '61)

All these observations raise the question of the role that these dehydrogenases may play in ossification. Dixon and Perkins ('52) assumed that the relatively high concentration of citrate in the osseous matrix is due to low isocitric dehydrogenase activity in bone More recently however considerable isocitric dehydrogenase activity has been found in bone by biochemical (Van Reen '59 Krane et al. '61) and histochemical (Balogh et al., '61 Balogh, '63) investigations. It is quite possible nevertheless that the citrate content of bone is regulated by isocitric dehydrogenase activity Since glucose-6-phosphate dehydrogenase catalyzes the initial reaction in the hexose monophosphate shunt, the described observations suggest some relationship between the utilization of this metabolic pathway and endochondral ossification.

In 1873 Kölliker suggested that osteoblasts were the precursors of osteoclasts. Support of his theory has been furnished recently by autoradiographic studies with tritiated thymidine It was shown that multinuclear osteoclasts do not arise as a consequence of nuclear division but from the fusion of mononuclear cells of the osteoprogenitor type (Tonna and Cronkite '61; Young, '62) In accord with this concept, tissues originating from the osteoprogenitor cells of the periosteum — the fibrous callus and the periosteal bone spicules — contained many mononuclear and binuclear cells which had an enzyme pattern identical to that of osteoclasts. Mononuclear and binuclear osteoclasts were particularly distinct in sections demonstrating succinic dehydrogenase activity because osteoclasts were the only bone cells that reacted strongly in these preparations. Since these mononuclear and binuclear cells occurred in the general areas of osteoclastic activity and bore all the enzymatic characteristics of the osteoclasts, we consider these cells to be precursors of the multinucleated osteoclasts. It appears, therefore, that metabolic changes in the mononuclear osteoclasts

precede the appearance of the multinuclear cells and also distinguish these cells from the undifferentiated osteoprogenitor cells. Mononuclear or binuclear osteoclasts with strong succinic dehydrogenase activity were also seen in the bones of parathormone treated newborn rats (Walker '61) In 1910 Dubreuil noticed osteoclasts with single nuclei and described the "incredible number of mitochondria in all osteoclasts. His observations were later confirmed by other light microscopic (Chang Hui Ch uan '31; Putschar '31 Pritchard, '52) and electron microscopic (Scott and Pease '56 Dudley and Spiro '61 Gonzales and Karnovsky '61) studies. Hence the unusually rich endowment of osteoclasts in mitochondrial enzymes (Burstone '60 Schajowicz and Cabrini, '60 Balogh '61 '64a '64b Walker '61 Cabrini et al '62) has a morphologic foundation. Foreign body giant cells and macrophages are also present around small fragments of dead bone near the fracture ends (Urist and McLean, 41) In our preparations these cells showed strong activity of various dehydrogenases and diaphorases but they were made especially prominent by virtue of their striking glucose-6-phosphate dehydrogenase activity that was very weak in osteoclasts Thus foreign-body giant cells could be easily distinguished from osteoclasts by virtue of their marked glucose-6-phosphate dehydrogenase activity Marked succinic dehydrogenase activity was noted in the foreign-body giant cells and osteoclasts. Strong succinic dehydrogenase activity in foreign-body giant cells has been observed by others too (Baker and Klapper '61 Cabrini et al. '62) Phagocytosis stimulates the hexose monophosphate pathway (Sbarra and Karnovsky '59) and therefore the histochemical demonstration of marked glucose-6-phosphate dehydrogenase activity in macrophages and foreign-body giant cells may be related to their phagocytic nature. Similar histochemical observations have been made on macrophages in other organs (Rubinstein and Smith, '62) The inability to demonstrate strong activity of this enzyme in osteoclasts however does not imply that they are not capable to phagocytize.

The enzyme histochemical data we have presented are in agreement with the concept that bone regeneration is essentially a rapid recapitulation of normal bone growth Although the techniques employed are only roughly quantitative, the histochemical method critically applied can provide new data on the complex cellular responses observed in fracture healing, a problem not easily approached by conventional biochemical procedures.

LITERATURE CITED

Baker B L., and Z. F Klapper 1961 Oxidative enzymes in the foreign body giant cell. J Histochem. Cytochem., 9 713–714.

Balogh, K., Jr. 1962 Decalcification with versene for histochemical study of oxidative enzyme systems. J Histochem. Cytochem 10 [illegible]

——— 1963 Histochemical study of oxidative enzyme systems in teeth and peridental tissues J Dent. Res., 42: 1457–1468.

——— 1964 Further observations on oxidative enzyme activities in decalcified bone and teeth. J Histochem Cytochem 12 [illegible]

——— 1964 Dihydrolipoic dehydrogenase activity: A step in formation of acyl-Coenzyme A, demonstrated histochemically J. Histochem. Cytochem., 12: 404–412.

Balogh, K., J H. R. Dudley and R. I Cohen 1961 Oxidative enzyme activity in skeletal cartilage and bone. A histochemical study Lab. Invest 10 839–845.

Bourne, G. H. 1956 Phosphatase and bone. In: The Biochemistry and Physiology of Bone. Academic Press, New York, pp. [illegible]

Burstone, M. S. 1960 Histochemical demonstration of succinic dehydrogenase activity in osteoclasts. Nature, 185 866.

Cabrini, R. L. F Schajowicz and C. Hosu [illegible] Histoenzymologic behavior of the giant cell of foreign body granuloma as compared with the osteoclast. Experientia, 18, 322.

Chang Hui Ch uan 1931 Mitochondria in osteoclasts. Anat. Rec., 49: 397–401.

Dixon, T F and H. R. Perkins 1952 Citric acid and bone metabolism. Biochem J. [illegible] 260–265.

Downs, W G., J and R. M. McKeown [illegible] Histology of healing fractures in rats on [illegible] mal diets. Arch. Surg., 23: 94–107

Dubreuil, G. 1910 Mitochondries des osteoclastes et des cellules de Ranvier. C. R. Soc. Biol. (Paris) 69 71–73.

Dudley R. H., and D. Spiro 1961 The fine structure of bone cells. J. Biophys. Biochem Cytol., 11 627–649.

Enneking, W F 1948 The repair of complete fractures of rat tibias. Anat. Rec., 101 515–538.

Godman, G. C., and K. R. Porter 1960 Chondrogenesis studied with the electron microscope. J Biophys. Biochem. Cytol., 8 719–[illegible]

Gonzales, F and M. J Karnovsky 1961 Electron microscopy of osteoclasts in healing fractures

tion of rat bone. J Biophys. Biochem. Cytol., 9 259–316

...n, A. W and W R. Harris 1958 Repair and transplantation of bone. In: The Biochemistry and Physiology of Bone (ed. by G. H. Bourne) Academic Press, New York, 475–506.

...enbach, S. R and M. J Karnovsky 1961 The histochemical demonstration of glyceraldehyde-3-phosphate dehydrogenase activity J Biophys. Biochem. Cytol., 9 573–581

...se, K. H., and A. M. Knoop 1958 Elektronenoptische Untersuchungen über die periostale Osteogenese. Z. Zellforsch., 48 455–478.

—— 1961 Chondrogenese und Osteogenese. Elektronenoptische und lichtmikroskopische Untersuchungen. Z. Zellforsch., 55 413–468.

...lliker, A. 1873 Die normale Resorption des Knochengewebes und ihre Bedeutung fur die Entstehung der typischen Knochenformen. F C W Vogel, Leipzig. p. 86.

...ne, S. M K. L Shane and M. B. Pyle 1961 Citric acid metabolism in slices and homogenates of cortical bone. In: The Parathyroids: Proceedings of Symposium on Advances in Parathyroid Research held at the Rice Institute (ed by R. O Greep and R. V Talmage) Charles C Thomas, Springfield, Ill. 298–309

...sche, A 1937 Die Zusammenhangstrennungen der Knochen. Die Knochenbrüche, die Bruchheilung und ihre Störungen. In: Handbuch der speziellen Pathologischen Anatomie und Histologie (ed. by O Lubarsch and F Henke) J Springer Berlin. 204–308.

...lipe, G and C Roulller 1951 Die alkalische Phosphatase in der Biologie des Knochengewebes. Histochemische Untersuchungen. Virchows Arch Path. Anat., 321 1–61

...lachlas, M. M K. C. Tsou, E. De Souza, C. S. Cheng and A. M. Seligman 1957 Cytochemical demonstration of succinic dehydrogenase by the use of a new p-nitrophenyl substituted ditetrazole. J. Histochem. Cytochem., 5 420–436.

...lachlas, M M D. G. Walker and A. M. Seligman 1958a A histochemical method for the demonstration of diphosphopyridine nucleotide diaphorase. J Biophys. Biochem. Cytol., 4 29–38.

—— 1958b The histochemical localization of triphosphopyridine nucleotide diaphorase. J Biophys. Biochem. Cytol., 4 467–474

...wen, Maureen 1963 Call population kinetics of an osteogenic tissue. I. J Cell Biol., 19 19–32.

...earse, A G. E. 1960 Histochemistry Theoretical and Applied (Edition 2) Little Brown and Company Boston, p. 536.

Pritchard J J 1952 A cytological and histochemical study of bone and cartilage formation in the rat. J Anat., 86: 259–277

Pritchard, J J and A. J Ruzicka 1950 Comparison of fracture repair in the frog, lizard and rat. J Anat., 84 236–261.

Putscher W 1931 Entwicklung, Wachstum und P thologie der Beckenverbindungen des Menschen mit besonderer Berücksichtigung von Schwangerschaft, Geburt und ihre Folgen. G. Fischer Jena. p. 121

Rubinstein L. J and B Smith 1962 Triphosphopyridine nucleotide (TPN) diaphorase and TPN-dependent dehydrogenase activity of reactive macrophages in tissue necrosis. N ture, 193 895

Sbarra, A. J and M. L. Karnovsky 1959 The biochemical basis of phagocytosis. I. Metabolic changes during the ingestion of particles by polymorphonuclear leukocytes. J Biol. Chem., 234 1355–1362.

Scarpelli, D. G., R. Hess and A. G. E. Pearse 1958 The cytochemical localization of oxidative enzymes. I. Diphosphopyridine nucleotide diaphorase and triphosphopyridine nucleotide diaphorase. J Biophys. Biochem. Cytol 4 747–752

Schajowicz, F and R. L. Cabrini 1960 Histochemical distribution of succinic dehydrogenase in bone and cartilage. Science 131 1043.

Scott, B. L., and D C. Pease 1956 Electron microscopy of the epiphyseal apparatus. Anat. Rec., 126. 465–495.

Tonna, E. A., and E. P Cronkite 1961 The use of tritiated thymidine for the study of the origin of the osteoclast. Nature, 190 459-460

Urist, M. R., and F C. McLean 1941 Calcification and ossification. I Calcification in the callus in healing fractures in normal rats. J. Bone Joint Surg., 23 1 16.

Van Reen R. 1959 Metabolic activity in calcified tissues: Aconitase and isocitric dehydrogenase activities in rabbit and dog femurs. J Biol. Chem., 234 1951–1954

Walker D. G. 1961 Citric acid cycle in osteoblasts and osteoclasts. A histochemical study of normal and parathormone-treated rats. Bull. Hopkins Hosp 108 80–99

Weinmann J P and H. Sicher 1955 Bone and Bones. — Fundamentals of Bone Biology (Edition 2) The C. V Mosby Company St. Louis, 309–337

Young, R. W 1962 Cell proliferation and specialization during endochondral osteogenesis in young rats. J Cell Biol., 14. 354–370

Abbreviations

B, Blood vessel(s)
BM, Bone marrow
C, Cartilage cells
Cort, Cortical bone
E, Endosteum
EP, External layer of periosteum
G, Giant cell(s) of foreign-body type
H, Haversian canal or resorption space
HC, Hypertrophic or older cartilage cells
M, Macrophages
N, Necrotic bone
O, Osteocytes
OB, Osteoblasts
OC, Osteoclasts
OP, Osteoprogenitor cells of periosteum
OPC, Osteoprogenitor cells of callus
P, Periosteum
U, Undecalcified compact bone

PLATE 1

EXPLANATION OF FIGURES

1 DPNH diaphorase. Three-day-old fracture. The markedly thickened periosteum shows strong enzyme activity. Arrows indicate the sites of periosteal tear. Notice the cellular infiltrate among the muscle fibers. × 31

2 TPNH diaphorase. Three days after operation. There is remarkable cell proliferation of osteoprogenitor cells in the periosteum (*OP*). The heavy diformazan deposits in osteoblasts and young osteocytes are in sharp contrast to the lesser enzyme activity of the older bone cells (*Cort*). The external layer of periosteum (*EP*) and the skeletal muscle show interstitial edema. Red and white muscle fibers exhibit severe degeneration and necrosis with loss of enzyme activity. Macrophages with considerable enzyme activity infiltrate the damaged muscle fibers. × 110




B
O
Cort
E

Abbreviations

B Blood vessel( )
BM Bone marrow
C Cartilag cells
Cort, Cortical bone
E, Endosteum
EP External layer of periosteum
G Giant cell( ) of foreign-body type
H Haversian canal or resorption space
HC, Hypertrophic or older cartilage cells
M, Macrophages
N Necrotic bone
O Osteocytes
OB Osteoblasts
OC Osteoclasts
OP Osteoprogenitor cells of periosteum
OPC, Osteoprogenitor cells of callus
P Periosteum
U Undecalcified compact bone

PLATE 1

EXPLANATION OF FIGURES

1 DPNH diaphorase. Three-day-old fracture. The markedly thickened periosteum shows strong enzyme activity Arrows indicate the ends of periosteal tear Notice the cellular infiltrate among the muscle fibers. × 31

2 TPNH diaphorase Three days after operation. There is remarkable cell proliferation of osteoprogenitor cell in the periosteum (*OP*). The heavy diformazan deposits in osteoblasts and young osteocytes are in sharp contrast to the lesser enzyme activity of the older bone cells (*Cort*) The external layer of periosteum (*EP*) and the skeletal muscle show interstitial edema. Red and white muscle fibers exhibit severe degeneration and necrosis with loss of enzyme activity Macrophages with considerable enzyme activity infiltrate the damaged muscle fibers. × 110



N

3

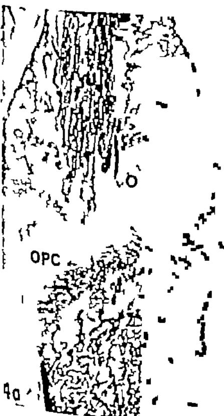




PLATE 3

EXPLANATION OF FIGURES

5 TPNH diaphorase. Callus one week after fracture. Enzyme activity increases as the osteoprogenitor cells (*OPC*) transform into chondrocytes (*C*) and diminishes in areas of cartilage that is being transformed into immature bone. × 105.

6 Isocitric dehydrogenase. One-week-old fracture. The complete spectrum of cell differentiation is seen from left to right. The fibroblast-like osteoprogenitor cells (*OPC*) show no reaction, and enzyme activity becomes distinct only in the cartilage cells (*C*). The older chondrocytes (*HC*) exhibit much less enzyme activity. The very dark cells lining the primitive marrow are strongly reacting osteoclasts (*OC*). Osteoblasts (*OB*) contain less diformazan deposition. × 100


OPC
Cort
C
5

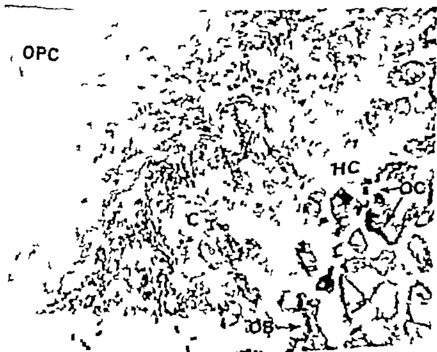
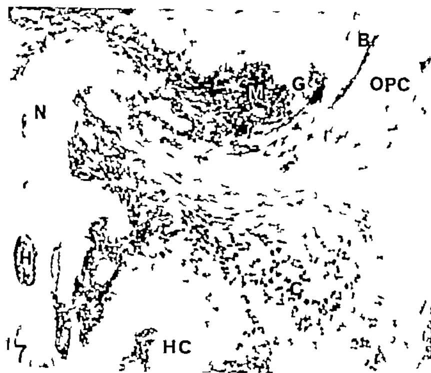

OPC
HC
OC
C
OB

PLATE 4

EXPLANATION OF FIGURES

7 Glucose-6-phosphate dehydrogenase. One week after operation. Macrophages (*M*) and foreign-body-type giant cells (*G*) around debris of dead bone are prominent by virtue of their marked enzyme activity. The callus shows various stages of chondrogenesis similar to those seen in figure 6. × 100.

8 Succinic dehydrogenase. Anchoring callus one week after fracture. Mononuclear and binuclear osteoclasts line the newly formed bone trabeculae and reveal enzyme activity. Osteoblasts (*OB*) and other cells did not react. × 470


B
OPC
G
M
N
H
C
HC
A
7

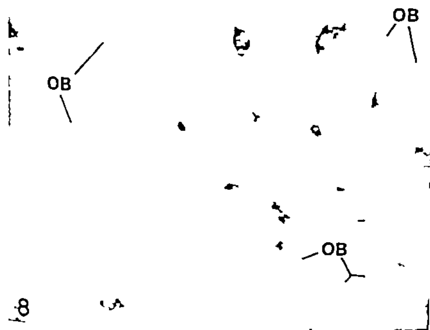

OB
OB
OB
8

PLATE 5

EXPLANATION OF FIGURES

9 Lactic dehydrogenase. One week after fracture. Spicules of newly formed woven bone enclose primitive marrow spaces. The arrows point to mononuclear osteoclasts that show the same intensive reaction as the more obvious multinuclear osteoclasts (*OC*). Most of the bone trabeculae are lined by moderately reacting osteoblasts (*OB*). × 230

10 TPNH diaphorase. One week after operation. The bone near the fracture ends is mostly necrotic (*N*); only few osteocytes (*O*) reveal enzyme activity. The dilated Haversian canals (*H*) have become resorption spaces harboring osteoprogenitor cells, osteoclasts and osteoblasts. Similar osteoprogenitor cells (*OPC*) and osteoclasts (*OC*) are also seen around the dead bone (right upper half). × 140.


OC
OB
OC
O
O
9

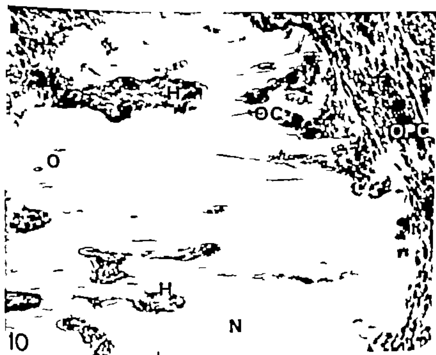
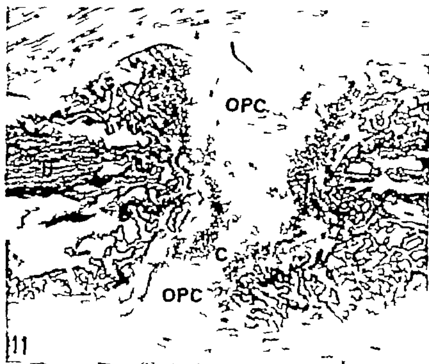

H
OC
OPC
O
H
N
10

PLATE 6

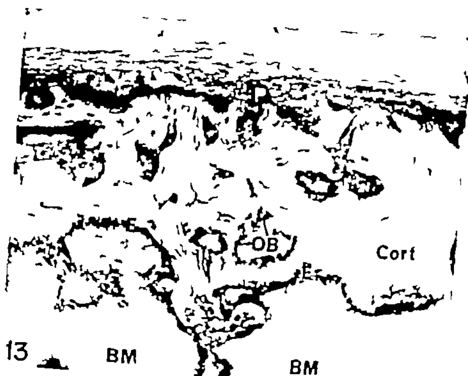
EXPLANATION OF FIGURES

11 Glucose-6-phosphate dehydrogenase Two-week-old fracture. The osteoprogenitor cells (*OPC*) of the bulky cartilaginous callus in the center are practically unreactive but th chondrocytes (*C*) developing from them reveal considerable enzyme activity × 27

12 Lactic dehydrogenase. Four-week-old fracture. The periosteum is thickened and its osteoprogenitor cells are till very active, especially near the point of fracture (arrow) The amount of periosteal callus is greatly reduced but there is a residual endosteal callus in the medullary cavity × 32.


OPC
C
OPC
11


12



13 Isocitric dehydrogenase. Four weeks after fracture. The inner layer of the periosteum is very cellular and reveals considerabl enzyme activity Osteoblasts (*OB*) and strongly reacting osteoclasts line the Haversian canals and the periosteal (*P*) and endosteal (*E*) surface. The cortical bone (*Cort*) i continuous. The pattern of the Haversian canals t the previous fracture site is till irregular but remodeling of the Haversian systems has begun. × 140

The Lymphatic System of *Didelphys azarae* and *Didelphys marsupialis*[1]

GIACOMO AZZALI[2] AND LIBERATO J. A. DI DIO[3]
University of Parma, Italy and Northwestern University, Chicago, Illinois

ABSTRACT The lymphatic system of 45 *Didelphys azarae* and 15 *Didelphys marsupialis*, both species found in Brazil, were studied after injection of Prussian blue suspension and neoprene latex (the latter followed by partial corrosion). The data concern the lymph nodes, the lymphatic networks, vessels and principal trunks. The lymph nodal system in *Didelphys* is less developed (several nodes are missing) than that of the rodents of the same size. In *Didelphys* the posterior cranial mediastinal lymph nodes are well developed; the right node receives the lymph from the stomach and diaphragm through vessels draining the para-esophageal, anterior mediastinal and caudal bronchial nodes, a fact not yet observed in other mammals. Each organ or area has its own lymph nodal station. The posterior para-aortic lymph nodes are almost always absent in the males, while in females only the right one is found. The common iliac lymph nodes are missing and it seems that they are replaced by lymphatic dilatations. Only one lymph node is found for the small intestine and two for the large intestine. The lymphatic networks are simple — 4–5 patches are found in the small intestine and one is constant in the terminal ileum. Other features are the separate drainage of each vaginal cornu and the partial duplication of the thoracic duct.

After the classical work of Mascagni (1787) contributions on the lymphatic system of mammals were made by Edwards (1859), Eisler (1890), McClure and Silvester ('09), Huntington ('11), Silvester ('12), Job ('15), Wood ('24), Baum ('27), Imabe ('30, '31), Ottaviani ('31, '32), Sakamoto ('31), Rouvière ('32), Teshima ('32), Baland ('33), Ottaviani and Cavalli ('33), Zimmermann ('33), Ottaviani ('35), Teshima ('35), Teshima and Kihara ('35), [illegible] ('37), Ottaviani ('37a,b, '39), Endo ('41), Ottaviani ('42 and '50), Hoffmann ('52), Ottaviani and Donini ('53), Michel ('56), Azzali ('58a,b), Azzali and Manfredonia ('59), DiDio, Manfredonia and Ottaviani ('59), Jdanov ('59), Ottaviani, DiDio and Manfredonia ('59), Spira ('62) and others.

We are indebted to Ottaviani for the suggestion of the present investigation which deals with the study of the lymphatic system of Brazilian species of Marsupialia. As far as we know no bibliographical data on a systematic study of the lymphatic system of the Brazilian gambá — *Didelphys azarae* and *Didelphys marsupialis* — were available. The lymph nodes, lymphatic networks, collecting vessels and main trunks in these species will be described in this paper.

MATERIAL AND METHODS

Injection of the lymphatic system was performed in 60 animals (45 specimens of *Didelphys azarae* and 15 of *Didelphys marsupialis*) of both sexes and of various ages. The animals were caught from May to August 1963 in the State of Minas Gerais (Brazil).

In order to inject the superficial lymphatic system, the lymph nodes and the lymphatic vessels of the various organs the following methods were used: (1) Gerota's method consisting of injecting Prussian blue suspension in turpentine oil with glass needles; (2) neoprene injection (40% solution of neoprene latex 842-A in distilled water) according to the technique of Ottaviani ('54).

The organs which had been injected with neoprene after fixation in 10% formalin solution, were submitted to 15% HCl for partial corrosion, then examined

---

[1] The research was aided by a grant from the Consiglio Nazionale delle Ricerche of the Republic of Italy.

[2] Associate Professor of Anatomy at the University of Parma Medical School, Italy (Prof. Dr. Gaetano Ottaviani). Visiting Professor of Anatomy ('63) of the University of Minas Gerais Medical School, [illegible], Brazil, with travel grant from the [illegible] Foundation.

[3] Professor of Anatomy at Northwestern University Medical, Dental and Graduate Schools, Chicago, [illegible]. Former Chairman and Professor of [illegible], University of Minas Gerais Medical School.

and photographed under the Zeiss binocular microscope

The description of the lymphatic system follows the well known Ottaviani's classification namely I lymph nodes II lymphatic networks and vessels III principal lymphatic trunks The structure will be named after Ottaviani's nomencla ture their dimensions and the distances are approximate and given in cm and in mm.

RESULTS

I — *Lymph nodes*

Lymph nodes of the head and neck

Submandibular lymph node (diagram A, nr 1) *Bilateral, ovoid, 1 5 cm long 1 cm* wide slightly flattened is located at the level of the angle of the mandible on the masseter and digastric muscles. It is re lated to the external jugular vein and to the submandibular gland.

It receives collecting vessels from the lymphatic networks of the superior and inferior lips masseter and mylohyoid muscles, mucosa of the oral vestibule and the skin of the suprahyoid region and nose

In two specimens of male *Didelphys azarae* there was a variation of course and termination of two collecting vessels which after having been originated in the subcutaneous lymphatic network of the ...prahyoid region ended in the auriculo-...rotid lymph node.

Auriculoparotid lymph node (diagram A, 2) Bilateral small rounded with a ...iameter 0 6 cm long, is situated lateral ... the external jugular vein at the level of ...he ventral part of the attachment of the ...uricle in the angle formed by the caudal ...ole of the parotid gland and the ventro-...ateral margin of the sternocleidomastoid ...t is related ventrally with the platysma and medially with the lateral aspect of the external jugular vein. In some instances *it was embedded in the parenchyma of the* parotid gland

It receives 4–5 collecting vessels formed at the level of the caudal third of the au ricle. They drain the subcutaneous lymphatic network of both the ventral and dorsal aspects of the auricle

Deep cervical lymph node (diagram A, 6) Paired ovoid, with a major axis 1 cm long, ventral to the prevertebral muscles lateral to the neurovascular bundle of the neck. It is related to the dorsomedial contour of the sternocleidomastoid muscle and to the ventral aspect of the m. longus colli.

At the level of its cranial pole, which corresponds to the cricoid cartilage, it receives 4–5 collecting vessels from the lymphatic networks of the radix linguae, the oral mucosa and one vessel from the thyroid gland.

From its caudal pole 2–3 small collecting vessels take origin and after a very short course they merge in one medium caliber vessel, which runs caudalward close to the lateral aspect of the cervical neurovascular bundle. It crosses, in the *first part of its course,* the deep surface of the m. omohyoideus then reaches the supraclavicular region. Here it fuses, constituting one large collecting trunk (jugular trunk) on the right side with the efferent collecting vessel from the submandibular lymph node and on the left with the efferent collecting vessels of the submandibular and superficial cervical lymph nodes.

Superficial cervical lymph node (diagram A 3) Paired, ovoid, major axis 0 5 cm long, located in the dorsolateral deep portion of the supraclavicular region, close to the ventral aspect of the cords of the brachial plexus. As *tributaries* it has 2–3 collecting vessels from the auriculo-parotid lymph node.

A large collecting vessel *originates* from the anterolateral aspect of the caudal pole of the left-sided node and passes medially in relation to the cranial margin of the subclavian vein it then passes dorsally to the internal jugular vein, where the latter splits to form a ring around the clavicle. This collecting vessel receives those originating from the deep cervical and the sub

Diagram A The lymphatic system of *Didelphys azarae* Head, neck, cranial portion of the cranial limb, thorax and proximal portion of the cranial limb. Ventral view 1 Submandibular lymph node (l.n.); 2, Auriculoparotid l.n.; 3, Superficial cervical l.n.; 4 Superficial axillary l.n.; 5, Deep axillary l.n.; 6, Deep cervical l.n.; 7 Posterior cranial mediastinal l.n.; 8 Posterior middle mediastinal l.n.; ad, Subcutaneous abdominothoracic lymphatic collecting vessels; c, Efferent collecting vessel from the anterior mediastinal l.n.; d, Thoracic duct; g, Jugular trunk (tr); pe, Efferent collecting vessel from the para-esophageal l. ; Subclavian tr

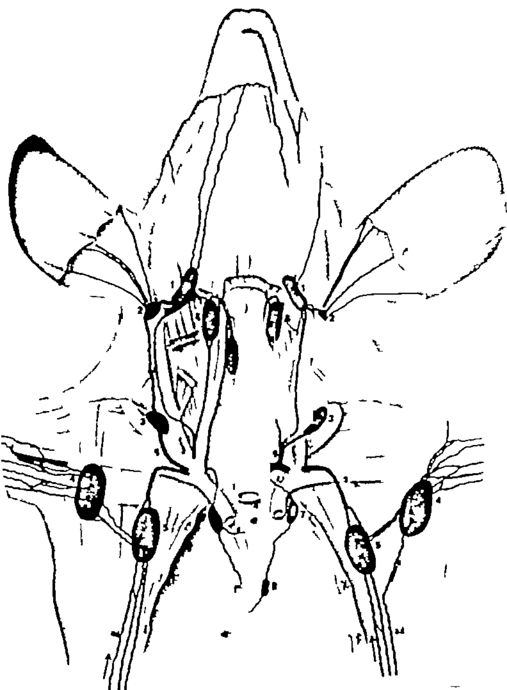


Diagram A

first part of the right subclavian artery and joins the collecting vessel from the right lymph node forming a single large collecting vessel. The latter in its oblique cranialward course presents close relations with the ventrolateral aspect of the right subclavian artery crosses the right brachiocephalic vein and having reached the apex of the thorax terminates in the right posterior cranial mediastinal lymph node

Both lymph nodes receive collecting vessels originating in the subepicardial networks.

Posterior cranial mediastinal lymph node Paired oval, 0 7 cm long and 0 3 cm wide. On the left the node (diagram A, 7) is located on the ventral aspect of the thoracic portion of the m. longus colli, it is related ventrally to the dorsal aspect of the left brachiocephalic vein and medially with the left contour of the first portion of the thoracic aorta. From the ventral aspect of the cranial pole of the lymph node a fine valved collecting vessel takes origin; it crosses the first portion of the brachiocephalic vein near the jugulosubclavian confluence then follows cranialward the course of the thoracic duct and terminates in it just before the duct describes its cranially convex curve. The lymph node receives a collecting vessel from the posterior middle mediastinal lymph node (diagram A 8)

The right-sided node (diagram A, 7 diagram B 1; diagram C 3 diagram D 1) s on the ventral aspect of the lateral ortion of the m longus colli, and on the inner surface of both the first intercostal space and the first two ribs. Its cranial pole is related to the ventrolateral aspect of the right brachiocephalic vein It receives collecting vessels from the anterior mediastinal lymph nodes from the para-esophageal and from the caudal bronchial lymph node and sometimes from the thoracic duct.

From the cranial pole of the node a large valved collecting vessel arises which after a 2–3 mm cranialward course behind the right brachiocephalic vein at the level of the supraclavicular region ends in the dorsal aspect of the right venous jugulosubclavian confluence.

Posterior middle mediastinal lymph node (diagram A 8) Single (often in large adult animals there are two) oval, major axis 0 6–0.8 cm long, situated in an area between the ventrocranial margin of the arch of the azygos vein (to run to the right side) and the dorsal aspect of the left brachiocephalic vein.

From the cranial pole of the node (or of the cranial node when there are two), sometimes two collecting vessels are given off: the lateral one, after a course 0.5 cm long directed cranially and laterally ends in the ventral aspect of the middle portion of the left posterior cranial mediastinal lymph node. The medial vessel accompanies cranially the ductus thoracicus and joins it 3–4 mm before its curve to terminate in the jugulosubclavian venous confluence.

It receives collecting vessels from the lymphatic networks of the lung, occasionally a fine vessel from the thoracic duct and very rarely (one animal) one from the para-esophageal node.

Bronchial lymph nodes. Two, oval, major axis 0.6 cm long, being distinguished in cranial and caudal. The cranial bronchial lymph node lies on the ventrolateral aspect of the trachea, just before its bifurcation Collecting vessels from the lymphatic networks of the trachea, bronchi and parenchyma of both lungs lead to it. It gives off a collecting vessel which ends in the posterior middle mediastinal lymph node

The caudal bronchial lymph node is located just caudally to the tracheal bifurcation and is related dorsally with the ventral aspect of the esophagus. It receives collecting vessels from the lymphatic networks of the ventral portion of the diaphragm and from the left lung.

Visceral lymph nodes of the abdomen and pelvis

Gastric lymph nodes Two, at the level of the cardiac part and along the lesser curvature near the pyloric part.

Diagram C The lymphatic system of *Didelphys azarae* Dorsal wall of the trunk in ventral view 1 Left anterior mediastinal l.n.; 2, Right anterior mediastinal l.n.; 3, Posterior cranial mediastinal l.n.; 4 Anterior para-aortic l.n.; 5, Posterior para-aortic l.n.; 6, Vesical l.n.; C, Cisterna chyli; dt, Thoracic duct; L, Lymphatic collecting vessels from the uterus; L, Lymphatic collecting vessels from the ovary; L, Lumbar

Diagram C

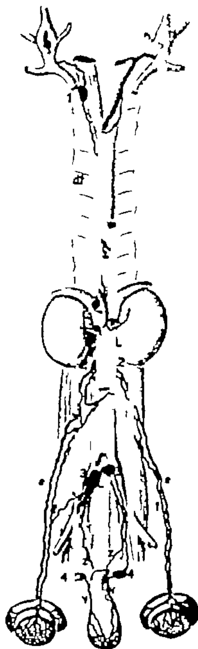


Diagram D The lymphatic system of *Dudel phys anorae* Dorsal wall of the trunk in ventral view 1 Posterior *cranial mediastinal Ln* 2, Anterior para-aortic ll nn 3 Common iliac lymph tic dilatations 4 Vesical Ln.; C, cisterna hyll dt, Thoracic duct Lymphatic collecting vessels from the testis f Lymphatic collectin vessels from the epididymis L, Lumba tr V Lymphatic collecting vessels from the urinary bladder Z, Lymphatic collecting vessels from the rectum and tail.

Cardial lymph node (diagram E, 1) Single sometimes duplicate oval, 0.5 cm long and 0 2 cm wide. In large adult animals it can be larger It is related to the left aspect of the abdominal portion of the esophagus and the cranial margin of the fundus of the stomach.

Collecting vessels from the lymphatic networks of the ventral and dorsal aspects of the cardial part, of the fundus and of the body of the stomach drain to the cardial lymph node.

One collecting vessel extends from it, running on the ventrolateral aspect of the esophagus to the para-esophageal lymph node (diagram E, pa)

Pyloric lymph node (diagram E. 2) Smaller than the preceding one round 0 2–0 4 cm in diameter it is located on the lesser curvature close to the pylorus. Sometimes it is found in a groove between the pylorus and the first part of the duodenum In front the node is related to the blood vessels of the lesser curvature and behind to the ventral aspect of the cranial portion of the head of the pancreas

It has afferent collecting vessels from the lymphatic networks of both ventral and dorsal aspects of the pyloric part, from a portion of the gastric body and from the pancreatic head.

A few collecting vessels fuse in one large vessel which empties into the lymph node of the head of the pancreas

Lymph nodes of the pancreas There are 3–4 and according to their situation are distinguished in lymph nodes of the head of the body and of the tail of the pancreas.

Lymph node of the caput pancreatis (diagram E, 3) It is usually single (sometimes 2–3 small nodes are found) round 0 7 cm in diameter Its cranial pole is in contact with the hepatic surface. In front the node has relations with the dorsocranial aspect of the cranial portion of the pancreatic head with the dorsal contour of the gastroduodenal blood vessels, with the inferior vena cava and with the dorsal contour of the terminal portion of the ductus choledochus.

The node receives collecting vessels draining the lymphatic networks of the first part of the duodenum of the gall bladder of the fibrous connective tissue of the hepatic hilus and a large vessel from the pyloric lymph node.

From the node leave several fine collecting vessels which, after a short distance, form by fusion the large pancreatico-duodenal trunk.

Lymph node of the corpus pancreatis (diagram E, 4) Single oval, major axis 0 7 cm long located at the level of the cranial aspect of the body of the pancreas. It is related closely to the lienal vessels. Its dorsal aspect is in contact with the ventral contour of the inferior vena cava, after the latter has received the left renal vein.

The node receives as a tributary one collecting vessel from the lymph node of the tail of the pancreas.

Lymph node of the cauda pancreatis (diagram E, 5) Smaller than the preceding ones, round, 0 4 cm in diameter, lies in a pit of the tail of the pancreas In front it is related to the dorsal aspect of the body of the stomach and, laterally to the hilus of the spleen.

Its afferent collecting vessels drain the lymphatic networks of the spleen, of the greater curvature of the stomach, and of the body and tail of the pancreas

An efferent collecting vessel takes origin from the medial contour of the node and after 2 cm of its course, directed to the median plane close to the lienal artery, empties *into the* lymph node of the body of the pancreas.

Mesenteric lymph node (diagram E, 6). Single large node 2–3 cm long and 0.7 cm wide is prominent on both aspects of the mesentery Its convex surface presents a few transverse sulci which seem to indicate the boundaries of portions of the lymph node this fact would bring to mind the possibility of union and fusion of several lymph nodes which further in the evolution would be presented separately

Diagram E The lymphatic system of Didelphys azarae Abdominal viscera (some displaced) in ventral view 1 Cardial l n ; 2, Pyloric l n ; 3 L.n. of the caput pancreatis; 4 L.n. of the corpus pancreatis; 5, L.n. of the cauda pancreatis; 6, Mesenteric l.n.; 7 Cecocolic l.n ; 8, Colic l.n.; c, Efferent collecting vessel from the cecocolic [illegible] a, Afferent collecting vessel from the [illegible] l.n.; m, Principal mesenteric [illegible]; p, Folliculi lymphatici aggregati (Peyer patch); pa, Afferent collecting vessel from the para-esophageal l [illegible]



Diagram E

The node is situated at the mesenteric root and is related to the superior mesenteric artery where the latter gives off the intestinal branches

It receives numerous collecting vessels derived from the superficial and deep net works of the jejunum and ileum: these vessels run in the mesentery and their course is independent from that of the blood vessels

Cecocolic lymph node (diagram E, 7) Single round, 0 7 cm in diameter located on the ventromedial aspect of the mesenteric lymph node It receives collecting vessels from the cecum and ascending colon.

Colic lymph node (diagram E, 8) As a rule it is single round, 0 7 cm in diameter situated in the central portion of the mesocolon. It receives collecting vessels from the lymphatic networks of the transverse descending and sigmoid colon. At its cranial pole a collecting vessel takes origin closely related to the blood vessels it is directed lateromedially and leads to the left anterior para-aortic lymph node (diagrams E, c)

In large adult animals is found frequently another colic lymph node much smaller 0.2 cm in diameter located in the mesocolon, 4–5 mm apart from the preceding to which it is connected by 1–2 fine collecting vessels.

Vesical lymph node (diagram C 6 and D 4) Paired round 0 3 cm in diameter lies on the lateral aspect of the rectum. It is related to the tendon of the m. psoas laterally and to the vesical blood vessels cranially

It receives collecting vessels from the lymphatic network of the urinary bladder of the dorsal aspect of the horns of the uterus and of the vagina.

The node sends vessels to the common iliac lymph nodes and when these are absent, to the lymphatic iliac dilatations.

Parietal lymph nodes of the abdomen and pelvis

Anterior para-aortic lymph nodes (diagram C 4 and D 2) Paired, oval major axis 1 cm long. In male animals the nodes are symmetrical, 1 cm below the level of the caudal pole of the kidney in females they are asymmetrical the right node being cranial relatively to the left one. The lymph nodes lie on the ventral aspect of the m psoas and their medial aspect have relations with the abdominal aorta and inferior vena cava.

The left node has as tributaries the collecting vessels from the colic lymph node, from the networks of the testis and epididymis and the lymphatic trunk of the common iliac lymphatic dilatation of the same side in males. In females it receives vessels from the networks of the ovary uterine tubes and ventral aspect of the uterine horns.

The right node receives collecting vessels from the lymphatic networks of the ovary of the uterine tubes and the lymphatic trunk of the posterior para-aortic lymph node.

Posterior para-aortic lymph node (diagram C 5) Single in female animals absent in males It is round, 0.6–0 8 cm in diameter more frequently on the right side, located on the lateral contour of the inferior vena cava at the level of the common iliac veins confluence. It rests on the ventromedial aspect of the m. psoas usually covered by a large amount of fat

It receives collecting vessels from the right lymphatic networks of the uterine tubes of the ventral aspect of the uterine horn and body from the right sided vesical lymph node and from the deep networks of the posterior limb.

In some animals the node is absent also on the right and at its corresponding level can be observed a more or less dense meshwork of fine collecting vessels, which originate from the tubal and uterine lymphatic networks. From the meshwork rise 2 efferent collecting vessels which terminate in the anterior para-aortic lymph node

Common iliac lymph nodes (diagram D 3) Frequently absent. Only in a few males it has been possible to observe on the ventromedial aspect of the common iliac veins two small round dilatations (common iliac dilatations) which receive collecting vessels from the deep lymphatic networks of the penis and of the seminal vesicles and the efferent vessel from the vesical lymph node

From the mentioned dilatations two large lymphatic trunks take origin which

have a cranialward course and end in the anterior para aortic lymph nodes.

Lymph nodes of the posterior limbs

No subpubic, ischial or popliteal lymph nodes were present.

Inguinal lymph node (diagram F 1) Paired, oval, 1 cm in diameter embedded in abundant connective tissue located at the mid-portion of the inguinal groove.

It receives collecting vessels from the lymphatic networks of the skin of the foot, leg thigh and lumbar region from the marsupial pouch mammary glands per.. and scrotum.

Efferent vessels leave its cranial pole and after a few mm fuse in 2–3 collecting vessels, which have a medium caliber (subcutaneous collecting vessels of the abdomen and thorax) The latter run in the tela subcutanea of the ventrolateral wall of the abdomen and thorax and end usually in the deep axillary lymph node (diagram A, 5)

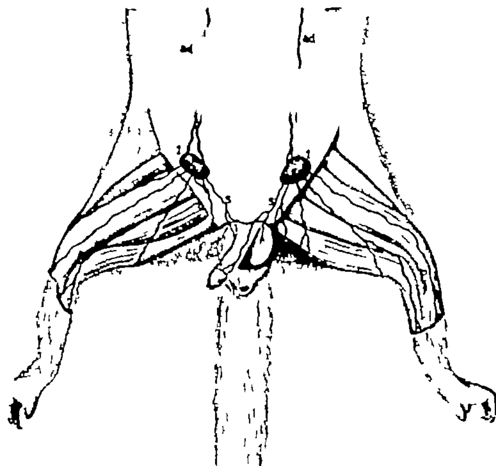


Diagram F The lymphatic system of Didelphys azarae Caudal portion of the ventral abdominal wall, posterior limbs and tail in ventral view 1 Inguinal l.n. ad, Subcutaneous abdominothoracic collecting vessels p Subcutaneous collecting vessels of the posterior limb; s, Subcutaneous collecting vessels from the scrotum and penis.

II — Lymphatic networks and vessels

Lymphatic vessels of the head and neck

Lymphatic vessels of the ear From the subcutaneous network of the ventral and dorsal aspects of the auricle this network has small polygonal meshes and it gives off at the level of the mid-third of the auricle, 3–4 collecting vessels which reach the bottom of the auricle and terminate in the auriculoparotid lymph node

Lymphatic vessels of the nose and upper lip They are easily injected and from the subcutaneous network, which shows nar row meshes take origin 4–5 medium caliber collecting vessels. The latter are di rected craniocaudally until the angle of the mandible where they end in the submandibular lymph node.

Lymphatic vessels of the lower lip and chin From a dense and large lymphatic network rise several collecting vessels, which run in the subcutaneous tissue of the supra and infra hyoid regions, reach the angle of the mandible and terminate in the submandibular lymph node.

Lymphatic vessels of the tongue and oral cavity From the rich submucous lymph atic network numerous collecting vessels originate and they fuse at the level of the root of the tongue both on the right and on the left, forming 2–3 vessels on each side The latter at the level of the larynx, end in the deep cervical lymph node.

Lymphatic vessels of the thyroid gland. The lymphatic networks are easily injected even if the gland is small. The vessels of the middle portion of each thyroid lobe drain to 2–3 fine collecting vessels which merge after a short distance in one medi um caliber collecting vessel. The latter runs cranially and has relations with the lateral aspect of the trachea and the thy roid cartilage then describes a curve cranially convex in a frontal plane and terminates in the cranial pole of the deep cervical lymph node

Lymphatic vessels of the anterior limb

Fine and numerous superficial lymphatic collecting vessels drain the networks of the ventral aspect of the digits and cranial extremity The mentioned vessels ex change anastomoses in their course in the tela subcutanea of the medial aspect of the forearm and arm and fuse in the axillary region, constituting 4–5 collecting vessels of larger caliber After a few mm they end in the superficial axillary lymph node, which receives also the collecting vessels from the subcutaneous networks of the shoulder and nuchal regions.

Originating in the lymphatic networks of the muscles fasciae, tendons and joints and following usually the direction of the blood vessels the deep lymphatic collecting vessels reach the cavum axillae and end in the deep axillary lymph node.

Lymphatic vessels of the thorax

Lymphatic vessels of the heart. The subepicardiac lymphatic network is made up by large and often dilated vessels which show anastomoses with each other thus constituting polygonal and rectangular meshes which are very narrow at the cardiac apex. From the lymphatic network of the right ventricle originate a few collecting vessels which, on the right margin at the level of the coronary groove merge in one large vessel. This runs in that groove until the medial margin of the right auricle then is directed cranially keeping its relation to the ventral aspect of the ascending aorta. At the level of the aortic arch the collecting vessel runs on the ven- tral aspect of the brachiocephalic trun then follows the ventromedial aspect of t right subclavian artery and terminat after 1 cm course in the right anter mediastinal lymph node (diagram C, 1

From the lymphatic networks of the ca diac apex and left ventricle originate c lecting vessels which merge at the level the sulcus coronarius, in one large lymp atic vessel. This follows at first the cau margin of the left auricle, and then margin finally crossing the co medial margin finally crossing the co vexity of the pulmonary artery After b coming related to the ventral and later aspect of the brachiocephalic trunk a left common carotid artery it leads to t left anterior mediastinal lymph node (di gram C 1)

In a few specimens of *Didelphys mars pialis* the left cranial mediastinal node wa absent and the corresponding tributary co lecting vessel drained the lymph to th posterior middle mediastinal node.

Lymphatic vessels of the lung. It ha been difficult to inject the subpleural ne

work as a whole. The lymph collecting vessels of each lung terminate in the cranial bronchial lymph node

Lymphatic vessels of the diaphragm. The lymph drainage of the cranial surface of the muscular portion is done by medium caliber lymphatic vessels oriented according to the direction of the muscular fascicles. The vessels are united by numerous delicate anastomoses limiting narrow rectangular meshes. The lymphatic network of the tendinous portion presents polygonal or quadrangular meshes and its vessels show small caliber (fig. 1)

On the left from the lateral and dorsal portions of the cranial aspect of the diaphragm, collecting vessels take origin. At the level of the esophageal opening they fuse with those draining the contralateral ... ls and a large lymph vessel is ... This vessel runs cranialward on the left aspect of the esophagus and ends ... the para-esophageal lymph node (dia... B 2)

The lymphatic network of the ventral intermediate (muscular and tendinous) ... ons drains into 5–6 collecting vessels ... in the area between the inferior ... cava and the esophagus merge in ... one lymphatic vessel. This runs ... ward on the right ventrolateral as... of the esophagus and empties in the ... bronchial lymph node (diagram B ...). On the very peripheral part of the ... ntioned network a few collecting vessels ... origin. The latter (diagram B ...) run ... lward on the inner surface of the ... closely related to the internal ... (mammary) vessels, and lead to ... e sternal lymph nodes.

...atic vessels of the abdomen and pelvis

Lymphatic vessels of the stomach. The ... muscular network shows large polygonal meshes. From the mentioned network of the ventral and dorsal aspects of the cardiac part of the fundus and of the body of the stomach 3–5 collecting vessels are formed. After a short distance they empty into the cardial lymph node

Collecting vessels are given off from the superficial and deep lymphatic networks of the pyloric part, and they open into the pyloric lymph node at the cranial margin of the lesser curvature.

From the greater curvature take origin 2–3 collecting vessels, which run for a short distance in the gastrolineal ligament and terminate in the lymph node of the cauda pancreatis.

Lymphatic vessels of the duodenum. The subserous-muscular network is formed by fine lymphatic vessels which display a longitudinal orientation (parallel to the long axis of the organ) These vessels anastomose and limit mostly rectangular meshes (fig 2)

The submucous network has lymphatic vessels with larger diameter these are intermingled and limit rounded or polygonal meshes (fig. 3) while the mucous network shows narrower vessels and smaller meshes.

From the precollecting vessels of the submucous and subserous-muscular networks originate a few collecting vessels which after a short course on the ventral aspect of the caput pancreatis empty into the lymph node of the head of the pancreas.

Lymphatic vessels of the jejunum-ileum. The subserous-muscular network has the same angio-architecture as the duodenal one the submucous network has larger meshes limited by vessels with less varicosities and with smooth surfaces (fig 4) In the tunica mucosa a lymphatic network is observed, with dense round meshes, limited by finer vessels (fig. 5)

The collecting vessels which originate from the mentioned networks, particularly from the submucous one run in the mesentery without relation to the blood vessels and at the level of the root of the mesentery end in the large mesenteric lymph node or central lymph node of the mesentery

In the small intestine a few aggregated lymphatic follicles, or Peyer's patches (diagram E, p) are present Their number does not exceed 4–5 They have mostly a variable distribution in the small intestine but a patch resulted constant at the level of the ileocecocolic junction Actually it was found in all the specimens examined and it could be named aggregated lymphatic follicles of the terminal ileum A plastic image of the lymphatic circulation

in a patch is represented in figure 6: besides the more or less dilated lymphatic vessels of a certain diameter surrounding the round meshes which contain the lymphonodular tissue are well shown the larger vessels limiting and separating at the periphery the area of the patch from the submucous lymphatic network.

Lymphatic vessels of the cecum and colon. The subserous-muscular network is made up of medium caliber lymphatic vessels which anastomose with each other and surround quadrangular and rectangular meshes. The latter are subdivided into smaller areas by very fine lymphatic vessels (fig 7)

The rete submucosa has narrow meshes bound by large lymphatic vessels whose surface is globular or varicose, in close relation to the blood vessels (fig 8) On the other hand the rete mucosa is formed by a very delicate lymphatic network with meshes showing variable outlines. From the superficial and deep lymphatic networks of the cecum take origin a few collecting vessels which run in its free contour cross in front of the ileocecocolic sphincter (ileocecal valve or ileal papilla) and run between the laminae of the mesentery (diagram E e) without following the blood vessels, to terminate in the cecocolic lymph node (diagram E, 7)

The subserous-muscular and submucous networks of the transverse, descending and sigmoid colon give off collecting vessels which after having reached their free aspect, follow the large blood vessels run lateromedially toward the root of the mesentery where they empty in the colic lymph node (diagram E 8)

Lymphatic vessels of the ovary There is a dense lymphatic network with polygonal meshes surrounding the organ. This network, at the level of the hilus of the ovary is made up of vessels with a larger caliber which are interlaced as a plexus. From the latter usually take origin 2–3 collecting vessels which are directed cranially in close relation with the ovarian artery and then end in the ventral aspect of the caudal pole of the anterior para-aortic lymph node (diagram C g)

Lymphatic vessels of the uterus (diagram C) From the very dense superficial network, showing polygonal or round meshes of the body of the uterus, the cornua and the uterine tubes, take origin many large vessels which at the level of the free edges of the organ make up a rich plexus. This gives off collecting vessels which drain the lymph to the anterior and posterior para-aortic lymph nodes. The course of the mentioned collecting vessels differs according to the side the vessels draining the lymph from the network of the ventral aspect of the right uterine horn and tube run cranialward, in intimate relation with the common and external ili vessels and with the tendon of the psoas and ultimately lead to the rig posterior para aortic lymph node. On the other hand, the left collecting vessels, aft having run on the ventral aspect of th psoas major and minor and having cross ventrally the ureter terminate in th caudal pole of the homolateral anterio para aortic lymph node.

The lymphatic collecting vessels, whi originate from the networks of the dors aspect of the cornua and corpus uteri, fu in one large vessel. This is directed dors caudally and empties into the vesic lymph node (diagram C 6)

Lymphatic vessels of the vagina. Th lymphatic network of each vaginal corn is drained by a collecting vessel whi leads to the homolateral vesical lymp node.

Lymphatic vessels of the testis and epi didymis (diagram D Ve f) From th lymphatic networks of the epididymis ta origin several large vessels which get the way on the free border of the organ. The vessels merge in one collecting lymphati vessel on each side, which follows the spermatic blood vessels in the abdominal cavity and leads, accompanied by the effer ent ones of the testis, to the ipsilateral anterior para-aortic lymph node At the level of the mid portion of the pelvic cavity the right collecting vessel frequently gives off to a fine lymphatic collateral branch. This fuses with the deep collecting vessels of the penis and of the bladder and after a short course (1 cm long) ends in the common iliac dilatation on the same side

From the testicular superficial network formed by large vessels limiting broad poly gonal meshes originate many precollectors and collecting vessels which after a few

mis merge at first in two large vessels and later in only one for each side. The latter is directed cranially follows the spermatic vessels and the efferent one from the epididymis in the inguinal canal and reaches the abdominal cavity Then it runs on the abundant fat tissue covering the m. psoas and the iliac vessels, and with a latero-medial course opens in the homolateral anterior para-aortic lymph node.

Very frequently in *Didelphys marsupialis* the collecting vessels from the left testis and epididymis do not empty in the homolateral anterior para-aortic lymph node at the level of the aortic bifurcation all of them end in the right anterior para aortic lymph node. The left para-aortic node receives only the lymph from the transverse descending and sigmoid colon.

Lymphatic vessels of the urinary bladder The superficial network is formed of large vessels limiting broad meshes. The network gives off collecting vessels which on the median plane merge on the dorsal aspect of the caudal portion of the bladder giving origin to one vessel on each side (diagram D V) and leading shortly thereafter to the ipsilateral vesical lymph node.

Lymphatic vessels of the posterior limb

From the lymphatic networks of the toes sole, and skin of the leg take origin 3–5 small collecting vessels, which run on the medial aspect of the thigh to terminate in the inguinal lymph node

The deep collecting lymphatic vessels of the leg and thigh, following the blood vessels, reach the abdominal cavity and drain into the anterior para-aortic lymph node of the same side

III — Principal lymphatic trunks

Jugular trunk (diagram A, g) It has a different constitution and course according the side.

The right trunk is formed by the fusion the efferent vessels from the submandib- and deep cervical lymph nodes. The union occurs in the supraclavicular region the level of the caudal border of the m. ... The trunk is related to the ...eral aspect of the internal jugular vein leads to the dilatation of the venous jugulosubclavian confluence just before the opening of the internal jugular vein.

The left trunk is made up of the ... of three efferent vessels from the deep ... superficial cervical and submandibu... lymph nodes The trunk, so formed, run toward the median plane and after havin crossed in front of the internal jugular vein and m. scalenus anterior drains to the cranial convexity of the curve described by the thoracic duct, in the supraclavicular region, before the duct opens in the venous jugulosubclavian confluence.

Subclavian trunk (diagram A, s) The large lymphatic vessels which emerge from the cranial pole of the deep axillary lymph node fuse after a short time and constitute the subclavian lymphatic trunk. This is directed obliquely toward the surface and at the level of the medial ⅓ of the subclavian vein becomes horizontal. Then it runs for a distance of 6–7 mm on the ventrocranial aspect of the mentioned vein and ends in the jugulosubclavian venous confluence.

Hepatoduodenopancreatic trunk. It originates from the ventromedial aspect of the lymph node of the caput pancreatis runs dorsally to the pancreatic parenchyma where it becomes related to the ventromedial aspect of the portal vein and then goes deeply toward the median plane In its course it follows the inferior vena cava then describes a slight curve and on the median plane opens into the left dilatation of the cisterna chyli.

Pancreatic trunk. It is 3 mm long and originates from the lymph node of the caput pancreatis. With a horizontal direction, it runs ventrodorsally and ends in the cisterna chyli.

Mesenteric trunk (diagram E, m) It begins by the convergence of short and large vessels leaving the mesenteric and cecocolic lymph nodes. It is very large 2–3 cm long and ascends obliquely in a ventrodorsal direction. After having crossed the mesenteric vein, it passes dorsally to the most cranial portion of the head of the pancreas It is then related for 2–3 mm with the medial contour of the inferior vena cava and leads to the ventral aspect of the right dilatation of the cisterna chyli.

In a few cases, the trunk is duplicated and both trunks after 1–2 cm drain in a

large lymphatic dilatation, which has a diameter of 1 cm There are two large efferent vessels from the dilatation and they discharge lymph independently The short one leads to the right dilatation and the long one to the left dilatation of the cisterna chyli.

Lumbar trunk (diagram C 1 and D L) From the cranial pole of the anterior para aortic lymph nodes leave two large trunks (right and left) 1 cm long They run laterally to the abdominal aorta, dorsally to the inferior vena cava medially to the m. psoas and after an ascending straight course empty in the caudal part of the dilatations of the cisterna chyli.

Cisterna chyli (diagram C C and D C) It is made up of two large sacciform dilatations 1 cm long, usually located laterally to the aorta between the medial crura of the diaphragm The lymphatic dilatations (the right one is larger) are united by an anastomotic vessel, which can be replaced sometimes by a net of 3–4 large vessels surrounding partially the ventral aspect of the aorta.

The ventral aspect of the right dilatation receives the mesenteric and the lumbar trunks of the same side while the left dilatation receives the hepatoduodenopancreatic and lumbar trunks.

Thoracic duct (diagrams A, C D) Very frequently it shows morphologic variations and the most common type is illustrated in diagram C The thoracic duct is formed by the fusion of two large efferent vessels which are originated from the two dilatations of the cisterna chyli at the level of the 12 V T From this level it runs cranially closely related to the lateral aspect of the aorta and esophagus At the level of the 3–4 V T the duct crosses dorsally to the esophagus goes to its left continues ascending and at the level of the aortic arch becomes related with the medial part of the posterior middle mediastinal lymph node (to which it sometimes sends a fine vessel) Then it rests on the ventral aspect of the thoracic portion of the m longus colli where it is related to the dorsal aspect of the left brachiocephalic vein. As a rule, after having overtaken the cranial aspect of the aortic arch the ductus thoracicus bifurcates and it remains duplicated until the apertura thoracis cranialis, at which level it becomes again a single large lymphatic trunk. In the cervical region, the ductus thoracicus rests on the ventral aspect of the m. longus colli, reaches the supraclavicular fossa, where it describes a cranially convex arch, directed dorsoventrally; after 2–3 mm it opens in the dorsal aspect of the venous jugulosubclavian confluence

In a few animals the thoracic duct has been found to be duplicated from its origin until it reaches the level of the 6–7 V.T After this level it became a single trunk by a short anastomotic vessel which communicates the large left vessel (terminating in a blind sac) with the right one (diagram D dt)

Another feature of variability of the thoracic duct is usually shown in the species *Didelphys marsupialis* each of the two lymphatic trunks which form the ductus thoracicus originates from the fusion of large vessels given off by the right and left dilatations of the cisterna chyli but terminates in a different manner While the right trunk ends in the venous jugulosubclavian confluence, the left trunk, after having been united to the right one by anastomosing branches empties at the level of the third to fourth costovertebral joint in the posterior middle mediastinal lymph node.

DISCUSSION AND CONCLUSIONS

From the qualitative and quantitative distribution of the superficial and deep lymph nodes of both studied species of *Didelphys* (*azarae* and *marsupialis*) we are led to make several remarks. If the lymph nodal system of *Didelphys azarae* is compared to that of the same-sized rodents it is possible to state that the system of the former is less developed and that many lymph nodes stations are missing, for instance the popliteal, epitrochlear and common iliac lymph nodes confirming Wood's general data on the opossum.

In *Didelphys* the posterior cranial mediastinal lymph nodes are well developed. Very interesting is the particular behavior of the right of the mentioned nodes, which receives the lymph from the stomach and diaphragm through the efferent collector

vessels from the para-esophageal, anterior mediastinal and caudal bronchial lymph nodes. Actually this fact was not yet observed in other mammals.

Another important feature is the absence of the direct flow of lymph from the organs to the blood circulatory system to the thoracic duct or to the cisterna chyli. So there is always a lymph nodal station between each organ and the blood vascular system each territory has its own lymph nodal filtrating station.

A different distribution of the abdominal parietal (anterior and posterior para-aortic) lymph nodes was correlated to the sex of the animals. As a matter of fact the posterior para-aortic lymph nodes are almost always absent in the males. They are usually single in the females where only the right lymph node is found.

The common iliac lymph nodes were missing and in the cranial portion of the pelvic cavity two small round lymphatic dilatations were observed constantly in the males. These dilatations seemed to play the role of lymph nodes as far as afferent and efferent vessels were concerned. The dilatations receive collecting lymphatic vessels from the networks of pelvic structures and send large collecting vessels to the anterior para-aortic lymph nodes.

It was interesting to see only one large lymph node for the drainage of the jejunum-ileum and two distinct lymph nodes for the large intestine being one for the cecum and ascending colon and the other for the transverse, descending and sigmoid colons. The different direction of the efferent collecting vessels from the lymph nodes which drain the colons accounts for the mixture in the trunk of the lymph coming from the networks of the cecum and colon ascending with that coming from the small intestine. This fact happens also in the mesentericocolic lymphatic plexus of the *Xenarthra*.

Several remarks should be emphasized as far as the lymphatic networks are concerned (a) the simple texture of the superficial and deep networks of the various organs (b) the similarity between the sub-serous-muscular and submucous networks of the colon in *Didelphys* and the networks of the colon in *Testudo graeca* (Azzali, 58a) (c) the presence in the jejunum-ileum of 4–5 folliculi lymphatici aggregati (Peyer's patches) which are not found in the *Xenarthra* notwithstanding the latter are zoologically more evolved animals (d) the constant presence of the lymph patch of the terminal ileum, at the level of the ileal papilla ("ileocecal valve")

The lymphatic networks observed in the thyroid gland showed dispositions which plainly confirm Ottaviani's and Rossi's ('33) accurate descriptions.

The pattern of the lymphatic network of the vagina is quite different from that found in other mammals indeed, each vaginal cornu has its own network draining to one collecting vessel which leads to the vesical lymph node of the corresponding side.

The mesenteric collecting vessels show an independent course in relation to the blood vessels which is consistent with Ottaviani's observations in the horse sheep and ox.

The smallness of the inguinal lymph vessels observed by Wood in the *Didelphys virginiana* was also a feature of the same vessels found in the Brazilian species just studied.

At its termination (which is the last portion to develop in the opossum according to Zimmermann) the thoracic duct's disposition corresponds to a certain extent to that observed by McClure and Silvester in *Didelphys virginiana* (opossum) on the left side as far as the jugulosubclavian district is concerned The partial duplication of the thoracic duct in both species of *Didelphys* without showing the total duplication which is typical in birds, reminds us of the disposition mentioned by Edwards and Owen (apud Edwards) in the kangaroo and may underline a feature of the Marsupialia. The fact that the same configuration has been found in the *Xenarthra* and also in zoologically more evolved mammals (carnivores primates man) where it is variable, increases the value of the concept of Pensa ('08–'09) Indeed according to him the single trunk of the ductus thoracicus, normally found in man is the perfecting expression a certain background of which can be found in the ontogenesis as well as in the phylogenesis.

ACKNOWLEDGMENTS

We are indebted to Doctor James C Hampton, Professor and Chairman of the Department of Anatomy Northwestern University Medical School, for having kindly supported the publication of this paper

LITERATURE CITED

Azzali, G. 1958a Ricerche sul sistema linfatico di piccoli grossi Cheloni. Ateneo Parmense 29(*Suppl. 4*): 145–175.

——— 1958b Il sistem linfatico dell'Hamster (*Cricetus auratus*) Atti Accad. Fisiocritici Siena, Serie XIII, 5 341–361

Azzali, G., and M. Manfredonia 1959 Il sistema linfatico del Papio (*Comopithecus hamadryas*) Ateneo Parmense, 30 (*Suppl. 3*) 106–151.

Balassy J L. 1933 Untersuchungen über die Lymphgefässe des Kaninchens. Külom, az. összehasonlitó élettan kärtan Köréböl. (Hung.) 26 1–22.

Baum, H. 1927 Die Lymphgefässe des Euters der Haustiere (Rind, Pferd, Schwein, Hund) Dtsch. tierärztl. Wschr., Hannover 35 413–415.

Di Dio, L. J A., M. Manfredonia and G. Ottaviani 1959 Il sistema linfatico di Callithrix penicillata. Ateneo Parmense 30 (*Suppl. 4*): 5–30.

Edwards, H. Milne 1859 Leçons sur la Physiologie et l'Anatomie comparée de l'homme et des animaux. Paris, 4 447–492.

Egehøj J 1937 Lymphgefässsystem des Schweines. Zschr Fleisch. u. Milchyg., Berlin, 47 293–298, 336–333.

Eisler P 1890 Das Gefäss- und periphere Nervensystem des Gorilla. Halle, Tausch und Grosse.

Endo, M. 1941 Die Lymphgefässsystem von Macacus rhesus. Kaibô Z., 17 206–225

offmann, G. 1952 Lymphknoten des syrischen Goldhamsters Monatsch. Vet. Med., Leipzig, 7 191

Huntington, G S. 1911 The anatomy and development of the systemic lymphatic vessels in the domestic cat. Mem. of the Wistar Inst. of Anat. and Biol., nr 1.

Jdanov D A. 1959 Anatomie du canal thoracique et des principaux collecteurs lymphatiques du tronc chez l'homme. Acta Anat., 37 20–47

Job, T T 1915 The adult anatomy of the lymphatic system in the common rat (*Epimys norvegicus*) Anat. Rec., 9 447–458

Manabe, S. 1930–31 Studien über das Lymphgefässsystem der Katze. Kaibô Z., Tokyo, 3 620–649.

Mascagni, P 1787 Vasorum lymphaticorum corporis humani Historia et Ichonographia. Ex Typographia Pazzini-Carli, Siena, 1–138

McClure C. F W and C F Silvester 1909 A comparative study of the lymphaticovenous communication in adult mammals Anat. Rec., 3 534–541.

Michel, G. 1956 Beitrag zur Anatomie und Topographie der Lymphknoten des syrischen Goldhamsters. Zbl. Vet Med Berlin-Hamburg, 3 705–714.

Ottaviani, G. 1931 Il sistema linfatico del Coniglio. Arch. Ist. Bioch. Ital., 1 3–30.

——— 1932 Ricerche comparative sui linfonodi, sui tronchi collettori linfatici e sulle vie linfatiche dell'intestino tenue dell'intestino crasso ricerche comparative sul tronco intestinale. Arch. Ital. Anat. Embr 30. 190–431.

——— 1935 Contributi al sistema linfatico dei Roditori. P II Sciurus italicus — Arctomys marmotta. Atti Ist. Ven. Sci. Lett. ed Art. 94 885–891

——— 1937 Contributi al sistema linfatico dei Roditori. P III Myoxus glis Muscardinus avellanarius. Atti Accad. Agr. Sc. Lett. di Verona 15 129–162.

——— 1937b Contributi al sistema linfatico dei Roditori. P IV Mus decumanus, Mus rattus (var alb.) Mus musculus. Gen. Arvicola (*Microtus arvalis*) Arch. Ist. Bioch. Ital., (3) 2–30.

——— 1939 Il sistema linfatico della Nutria (*Myopotamus coypus*) P V Atti Ist. Ven Sc Lett. ed Arti, 98 297–331

——— 1942 Il sistema linfatico della Cavia (*Cavia cobaya*) P VI dei contributi al sistema linfatico dei Roditori. Arch. Ist. Bioch Ital. (1) 3–22.

——— 1950 Il sistema linfatico del Capibara (*Hydrochoerus capibara*) P VIII Arch. Zool Ital., 35 361–410.

——— 1954 L'uso del neoprene nella ricerca dei vasi linfatici. Ateneo Parmense 25 109

Ottaviani, G and M. Cavalli 1933 Contributo all'anatomia del sistema linfatico del Gatto. La Nuova Veterin., 11 5–72.

Ottaviani, G., and L Donini 1953 Il sistema linfatico della Talpa (*Talpa europaea*). Arch Zool. Ital., 38 419–440.

Ottaviani, G., L. J A. DiDio and M. Manfredonia 1959 Prime osservazioni biometriche sul sistema linfatico di alcune scimmie. Ateneo Parmense, 30- 643–647

Owen art. Marsupialia. Todd' Cyclop of Anat and Physiol., t. III, p. 305, apud Edwards.

Pensa, A. 1908–09 Studio sulla morfologia sulla topografia della cysterna lyph e del ductus thoracicus nell'Uomo in altri Mammiferi. Ricerche Lab. Anat. Norm Roma, 14 109–142

Rossi, F 1933 Ricerche comparative sui vasi collettori linfatici della ghiandola mammaria. Morph Jahrb., 73 13–33.

Rouvière, H 1932 Anatomie des lymphatiques de l'homme. Paris Ed. Masson.

Sakamoto S 1931 Über das Lymphgefässsystem des Kaninchens und Meerschweinchens Trans Jap path. Soc., 21 550–564

Silvester C. F 1912 On the presence of permanent communications between the lymphatic and the venous system at the level of the renal veins in adult South American monkeys Am J Anat. 12 447–472.

Spira, A. 1962 Die Lymphknotengruppe (Lymphocentra) bei den Saugern ein Homologisierungsversuch. Anat. Anz 111 294–364

Teshima, G. 1932 Untersuchungen über den Ductus thoracicus der Japaner Kaibô Z 5 773.

—— 1935 Beiträge zur Anatomie des Lymphgefässsystem des Macacus rhesus. Fol. Anat. Jap. 13 [illegible].

Tokima, C. and T. Kihara 1935 Lymphgefässsystem des Schimpansen. Fol. Anat. Jap. 13 [illegible].

Wood, G. N. 1924 The lymphatics of the opossum. Anat. Rec., 27 192–193 (abs.)

Zimmermann, A. A. 1933 On the development of the lymphatic system in opossum (*Didelphys virginiana*) Anat. Rec., 55 (4 suppl.) 42–43 (abs.)

PLATE 1

EXPLANATION OF FIGURES

1 Diaphragm of *Didelphys azarae* Lymphatic network (neoprene injected) of the cranial surface of the muscular and tendinous portions of the diaphragm. × 16.

2 Subserous-muscular lymphatic network (neoprene injected) of the duodenum of *Didelphys azarae* × 16.

3 Duodenum of *Didelphys azarae* submucous lymphatic network (neoprene injected) with lymphatic vessels showing irregular contour in close relation to blood vessels. × 10

4 Submucous lymphatic network (neoprene injected) of the small intestine of *Didelphys marsupialis*. × 16.

5 Mucous lymphatic network (neoprene injected) of the small intestine of *Didelphys marsupialis* seen from the inner aspect. Large lymphatic vessels of the submucous network are seen in the background. × 16.

6 Small intestine of *Didelphys azarae* Plastic image (by injection of neoprene followed by corrosion) of the lymphatic circulation in folliculi lymphatici aggregati (Peyer patch) × 10.

7 Colon of *Didelphys azarae* S bserous-muscular lymphatic network (neoprene injected) × 25.

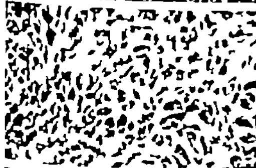
8 Colon of *Didelphys azarae* Submucous lymphatic network (neoprene injected) characterized by large varicose lymph tic vessels, which are interlaced, limiting narrow and irregular meshes. In the upper portion and in the center of the picture, through few meshes of the submucous network, can be seen the fine lymphatic vessels of the mucous network. × 16.

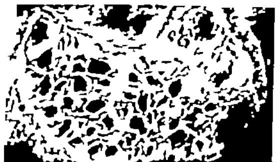




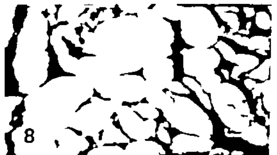









7


8

The Fine Structure of the Supramedullary Neurons of the Puffer with Special Reference to Endocellular and Pericellular Capillaries [1]

Y. NAKAJIMA, G. D. PAPPAS AND M. V. L. BENNETT
Departments of Anatomy and Neurology, College of Physicians and Surgeons, Columbia University, New York, New York

ABSTRACT Many capillaries are embedded in the cytoplasm of large supramedullary neurons (about 200 to 300 μ in diameter). Fewer such capillaries are seen in the smaller neurons (about 80 to 100 μ in diameter). The neuron clusters remain unstained after vital staining with trypan blue indicating presence of the blood-brain barrier. Electron microscopic studies show that the capillary lumen is lined by non-fenestrated endothelial cells, pericytes, and continuous basement membrane. Glial cell processes consisting mostly of astrocytes abut onto the capillary basement membrane separating the capillary from the neuron. The continuous glial investment around blood vessels m y play role in maintenance of the blood-brain barrier. The nucleus in supramedullary cells is roughly circular and contains one large and several small nucleoli. The perikaryon contains neurofilaments, diffusely distributed elements of endoplasmic reticulum, clusters of RNP granules, Golgi complex, mitochondria, multivesicular bodies, and inclusion bodies; but is devoid of elementary neurosecretory granules. The cell body of the neuron is entirely covered by glial cells, often with processes which deeply indent the soma surface. Neither synapses nor arborizing dendrites are found on the cell body.

In many teleost fishes clusters of cells known as supramedullary neurons occur on the dorsal surface of the medula oblongata and extend over the spinal cord (See Kappers, Huber and Crosby '36.) In some species these neurons may attain a diameter exceeding 200 μ. They were first described by Fritsch (1886) in *Lophius piscatorius*. Recently Hughes ('57) found similar neurons in a larval amphibian. The function of these neurons is still a matter of conjecture. Kappers, Huber and Crosby ('36) and Hughes ('57) considered them to be primary sensory neurons. However recent electrophysiological studies (Bennett, Crain and Grundfest, '59a, '59b; Bennett, '60) revealed many peculiarities about these neurons; e.g. (1) they are excited synaptically probably through synapses located on the axons; (2) they send efferent impulses out the dorsal roots, and (3) they are normally active synchronously. On the basis of these factors, it was concluded that the neurons were not sensory but rather have an as yet unknown effector function.

A structural peculiarity of the supramedullary neurons which can be seen with the light microscope is the intimate relationship between the individual cells and the blood vessels. A few capillaries appear to be embedded deep in the cytoplasm of the neurons and many others closely surround the periphery of the cell body. Such vessels are known as endocellular and pericellular capillaries respectively. Fritsch (1886) first described endocellular capillaries in the supramedullary neurons of *Lophius piscatorius* and they were also observed in *Orthagoriscus mola* by Burr ('28). Recently Scharrer ('37, '54) reported that the supramedullary neurons in the puffer have capillaries which penetrate into the cytoplasm. Such endocellular capillaries were also described in the neurosecretory cells in the hypothalamus (Collin, '31; Scharrer and Scharrer, '40) in the teleost caudal neurosecretory neurons, (Bern and Takasugi, '62) in the giant motor neurons of the electric cat fish of *Malapterurus electricus* (Fritsch, 1887) in a pyramidal cell of the motor area in the human brain (Scharrer, '37) and in the facial motor neurons of the rabbit (Cammermeyer

[1] Supported in part by research grants NB-03214 and NB-03448 of the National Institutes of Health, and a grant from the Life Insurance Medical Research Fund and by grant AFOSR-330.

'63) Because the intimate relationship between blood vessels and the supramedullary neurons is somewhat similar to that of neurosecretory cells Scharrer ('54) suggested that the supramedullary neurons are secretory Ishibashi ('62) investigated their staining properties in the Japanese puffer He concluded that these neurons might have a secretory function because many graules were found in the perikaryon which were stained with Gomori's chrome alum hematoxylin.

We have studied with the electron microscope the supramedullary cells and the closely apposed vessels in several species of puffer In addition, vital staining techniques have been employed to establish the presence of a blood-brain barrier. Although many inclusion bodies were found in the cell body and axon, no morphological evidence of elementary neurosecretory granules was noted (Sano and Knoop, '59; Afzelius and Friedberg, '63)

MATERIALS AND METHODS

Adult Atlantic puffer *Spheriodes maculatus* about 10 to 20 cm in length small young Atlantic puffer about 2 to 3 cm in length, and African fresh water puffers about 2 to 4 cm in length were used in this study

Vital staining with trypan blue

Five African fresh-water puffers were injected subcutaneously daily for five days with 0 1 ml of 1% trypan blue aqueous solution. Three adult Atlantic puffers were similarly injected daily with 1 0 ml of the same solution for 2 or 3 days. Three young Atlantic puffers were similarly treated with 0 1 ml of the solution for two days The fish were killed 1 to 3 days after the last injection and fixed in 10% buffered formalin, usually by perfusion.

Microscopy

In the small Atlantic and African puffers, fixation was done by a modification of the perfusion method of Palay et al. ('62) The *conus arteriosus* was canulated and a brief flush of Ringer's solution at room temperature was followed by cold 1 or 2% osmium tetroxide in phosphate buffer approximately 1 ml gm body weight. Several African fresh-water puffers were also perfused with sodium permanganate (Rosenbluth '63) In the case of adult Atlantic puffers 1% osmium tetroxide buffered with phosphate or collidin (Bennett and Luft, '59) was applied directly to the exposed neurons. Specimens were dehydrated in a graded series of ethanol, run through two changes of propylene oxide and embedded in Epon according to Luft's method ('61)

Blocks were sectioned with glass knives on a Porter-Blum microtome. The sections were stained in a saturated solution of uranyl acetate or in lead hydroxide (Karnovsky '61) or lead citrate (Reynolds, '63) and examined with an RCA-EMU 3C electron microscope.

Contiguous thick sections (1 μ) were cut and stained with toluidine blue or with Mallory's Azur II methylene blue according to Richardson, Jarett and Finke ('60)

RESULTS

Vital staining with trypan blue

Following fixation, the brains of animals injected with trypan blue were examined with a dissecting microscope. In contrast to the marked blue color of adjacent muscle bone and dura, the brains of all animals remained unstained and normal in appearance. The choroid plexus, the hypophysis and the cauda equina were stained, however The urophysis was faintly stained in several cases. The supramedullary neurons always remained unstained indicating presence of the blood-brain barrier

Structure of supramedullary neurons

The supramedullary clusters of the puffer are located immediately behind the cerebellum over the medulla oblongata and the anterior portion of the spinal cord (figs. 1a and 1b) These neurons are spherical or ovoid and their diameters measure about 200 to 300 μ for the adult Atlantic puffer 80 to 120 μ for the small young Atlantic puffer and 80 to 150 μ for the African fresh-water puffer

Relationship between the neurons and blood vessels

The supramedullary neurons are richly supplied by capillaries. In one section of a supramedullary neuron of the adult Atlantic puffer many endocellular capillaries

can be seen (fig. 2) These capillaries are confined primarily to the peripheral region of the perikaryon. In addition to the endocellular capillaries many pericellular capillaries are also present around the cells (fig. 2) In the small young Atlantic puffer and in the African fresh-water puffer only a few of the endocellular capillaries are found although many pericellular capillaries are present (fig. 3)

With the light microscope, only the larger capillaries appear to be ensheathed by glial processes but most are apparently devoid of surrounding glial elements i.e. the capillary endothelium appears to be in direct contact with the perikaryon of the neurons (figs. 2 and 3) However with the electron microscope (figs. 4–9) all the capillaries are found to be completely surrounded by processes of glial cells. There are one (figs. 5 and 6) to several layers (figs. 7 and 8) of glial cell processes of varying thickness between the neuron and the capillary Except for the basement membrane no other connective tissue element or space is found around the capillaries. These glial cells which are best described as astrocytes contain distinct intracellular fibrillae (fig. 7) In addition, there are granules about 200 to 400 A in diameter which stain well with lead hydroxide (figs. 4, 5 7 and 8) but faintly with uranyl acetate (figs. 6 and 9) and which therefore are probably glycogen (Revel, Napolitano and Fawcett, '60) Desmosomes are sometimes found where adjacent glial processes are in apposition (fig. 7) Regions where the gap between the apposing membranes is completely occluded are frequently seen between glial processes which cover the supramedullary neurons (fig. 10) (Gray '61 Robertson, Bodenheimer and Stage '63) However we rarely encountered such junctions between the glial cells which abut upon the basement membrane of the endocellular and pericellular capillaries.

Some of the glial cells sheathing the capillaries do not appear to be astrocytes. Occasional glial cells are found (figs. 4 and 8) which have moderately dense cytoplasm resembling that of the neuron, and which do not contain any filamentous structures (figs. 5 and 8) The cells may be identified as oligodendrocytes (Schultz, Maynard, and Pease '57)

The capillaries consist of a rather thin basement membrane and of variably flattened endothelial cells forming a continuous layer without fenestration (figs. 4–8). The *zonulae occludentes* (Farquhar and Palade '63) are always present at the junction of the endothelial cells with desmosome structures frequently intervening between two such areas (fig. 6)

The basement membrane appears as a continuous coat of moderately dense material about 150 to 350 A in thickness between the endothelial cells and glia. Donahue and Pappas ('61) reported that in the capillaries of the cerebral cortex there is a difference in the thickness and in the density of the basement membrane between the adult and immature rats. No such differences were noted between adult and young Atlantic puffers however The total thickness of the *lamina densa* and the clear area around it, i.e. from endothelial plasma membrane to glial plasma membrane varies from 600 to 800 A (figs. 5–8)

The nucleus of the supramedullary neuron is large — about 100 µ to 150 µ in diameter in adult Atlantic puffers and about 70 µ in small Atlantic and African fresh water puffers (figs. 2 and 3) The nucleus has a roughly circular outline with numerous indentations of the nuclear envelope (figs. 2 and 3) The lobulate and multiple nuclei, which were reported as one of the structural peculiarities in the neurosecretory neurons (Scharrer and Scharrer '40 Afzelius and Friedberg '63) are not present in the nuclei of these supramedullary cells. However the irregular shape of nucleus is observed in the supramedullary neurons of Sargassum fish *Histrio histrio* (Nakajima, Pappas and Bennett, in preparation) The nucleus contains a large prominent nucleolus about 20 to 40 µ in diameter and small nucleoli about 3 to 6 µ in diameter (figs. 2 and 3)

The cytoplasm of the perikaryon appears relatively dense and contains fine filaments. Endoplasmic reticulum whose membranes are often associated with RNP granules is widely distributed appearing condensed in some places and scattered in others. This distribution pattern of

endoplasmic reticulum is similar to that in neurons of the superficial neocortex of the cat (Pappas and Purpura '61) but is different from that of neurosecretory neurons (Palay '60 Afzelius and Friedberg, '63) Numerous RNP granules are sometimes found in rosettes throughout the cytoplasm. Sub-surface cisternae of the endoplasmic reticulum (Pappas and Purpura '61 Rosenbluth, '62) are occasionally seen (fig. 10)

Many Golgi bodies are present in the perikaryon (figs. 4 7 9 10 and 13) They consist of several arrays of cisternae and *numerous small vesicles about 500 to 900* A in diameter

The perikaryon contains multivesicular bodies (figs. 6 8 and 13) and other membrane-bounded inclusion bodies resembling lysosomes (Novikoff '61) (figs 4 5 7 9–13) Some of these inclusion bodies appear homogeneously granular; others contain irregular membraneous components. However the dense granules which have been described in neurosecretory cells as the elementary neurosecretory granules (Sano and Knoop '59 Palay '60; Murakani '62; Afzelius and Friedberg, '63) are not present in the supramedullary neuron.

Mitochondria are present in moderate numbers and are generally rod-like containing numerous cristae.

There are no synapses on the cell body of the supramedullary neuron as it is entirely ensheathed by glial cells (figs. 9 10 and 13)

Invaginations of the glial cell processes into the perikaryon are freqently seen (figs 6 9 10 and 12) Sometimes the neuronal plasma membrane doubles up forming a mesaxon-like structure which travels through the perikaryon in places sheathing the deeply invaginated glial processes Along such mesaxon-like structures tight junctions are observed (fig. 11) In figure 12, a myelinated nerve fiber is found invaginated deeply into the neuron of the small young Atlantic puffer

In addition to such mesaxon-like structures chains of vesicles are frequently found just beneath the surface in the osmium tetroxide-fixed specimens (fig. 7) However in sodium permanganate-fixed materials such vesicles are absent (fig. 13) The same difference between osmium tetroxide and permanganate fixed neurons were observed in sympathetic ganglia by Rosenbluth ('63)

The supramedullary neurons are monopolar and a large unmyelinated axon (fig. 3) leaves the cell body and branches at varying distances away (Bennett et al., '59a) There is no dendritic arborization except for very fine cytoplasmic extensions (figs. 9 and 10) which interdigitate with the complicated invaginations of the glial cells. The axon contains longitudinally-oriented filaments, elongated mitochondria and elements of the endoplasmic reticulum. Inclusion bodies similar to those found in the cell body are frequently seen in the axon. Synapses are present on the axon and the apposing membranes of adjacent axons are sometimes fused (maculi occludens) suggesting that such close contact spots are electrotonic junctions (Bennett, Nakajima and Pappas, in preparation)

DISCUSSION

It is well known that some acid aniline dyes which bind to protein such as trypan blue, as well as numerous other substances do not enter most regions of the brain, a finding which led to the concept of the blood-brain barrier In the present study we were not able to stain the supramedullary neurons with trypan blue suggesting the presence of the blood-brain barrier between these neurons and the capillaries. A number of neural structures are known to be stained by these dyes including the neurohypophysis, the pineal body the area postrema, the choroid plexus, the supraoptic crest, and the intercolumnar tubercle (Wislocki and Leduc, '52 Wislocki and King, '36) The neurosecretory neurons in the hypothalamus contain trypan blue granules subsequent to the dye injection (Leonhardt, '55 Clara, '55; Ortmann Takahashi and Miyawaki, '56 Murakami and Ban, '56) The blood-brain barrier is presumably absent in these regions.

With the electron microscope some (Dempsey and Wislocki, '55; Maynard Schultz, and Pease, '57; Donahue and Pappas, '61; and Wolff '63) observed that, where the blood-brain barrier exists the capillaries were characterized by the

presence of a nonfenestrated endothelial wall, a continuous basement membrane, and a continuous pericapillary investment formed mainly by the processes of astrocytes without large intervening pericapillary spaces On the other hand, Dempsey and Wislocki ('55) and Van Breemen and Clemente ('55) reported that in four of the areas where the blood-brain barrier was absent, there was a loose pericapillary space consisting primarily of connective tissue elements. In the neurohypophysis fenestration within the endothelium was described by Palay ('57) In the neurosecretory neurons of the hypothalamus, Palay ('60) and Murakami ('62) observed an immediate contact of the perikaryon with the basement membrane of the capillaries without any intervening connective tissue space or glial processes.

The relationship between capillaries and supramedullary neurons is similar to that found in the regions of the central nervous system where the blood-brain barrier exists. There is always a complete pericapillary investment of glial elements. This relation holds even though the capillaries actually penetrate the cell bodies of the supramedullary neurons. These observations support the concept of De Robertis and Gerschenfeld ('61) that astrocytic processes form the blood-brain barrier.

Many inclusion bodies are observed in the perikaryon and axon of the supramedullary neuron of the puffer The same characteristic feature is observed also in the supramedullary neurons of saragassum fish *Histrio histrio* these inclusion bodies diffusely disseminate in the perikaryon, accumulate in the axon hillock, and also are found in the axon where they are larger than that in the perikaryon (Nakajima, Pappas and Bennett; in preparation) In the cytoplasm of the supramedullary neurons of the puffer Ishibashi ('62) demonstrated the existance of the chrome alum hematoxylin positive granules, and suggested that neurosecretory activity occurs there. We did not find the elementary neurosecretory granules in the supramedullary neurons with the electron microscope. On the other hand the elementary neurosecretory granules are present in the caudal neurosecretory neurons of the same fish (unpublished observation, Nakajima, Pappas and Bennett) In the neurosecretory neurons of the hypothalamus of the goldfish Palay ('60) described two sizes of droplets in the cytoplasm. The smaller ones, have a diameter of about 0 1 µ, corresponding to elementary neurosecretory granules. They were believed to be formed in the Golgi complex and contain the neurosecretory material. The larger ones were apparently derived from multivesicular bodies and were thought to be concerned with intracellular metabolic events and not to contain secretory material. The large droplets correspond to the material stained by chrome alum hematoxylin. Recently Osinchack ('63) reported the presence of acid phosphatase activity in the large granules (0 4 to 1 0 µ) of the neurosecretory neurons of the rat, whereas the smaller granules resembling the elementary neurosecretory granules, were generally devoid of the active enzyme It is reasonable to suggest that inclusion bodies present in the supramedullary neurons (figs. 4 5 9 and 13) correspond to the large droplets of Palay ('60) and Osinchack ('63)

The supramedullary axons terminate in the skin rather than in a neurohaemal organ near the neuroaxis (Bennett — unpublished) This site of termination also suggests that the cells do not have a neurosecretory function.

The reason for the extraordinarily rich vascularization which characterizes supramedullary neurons is not clear In the absence of the metabolic needs of a neurosecretory function their huge size is implicated. In this connection it should be noted that small neurons have few endocellular capillaries, whereas the larger ones have many In the giant motor neurons of the electric catfish *Malapterurus electricus* the same relationship between size of the neuron and numbers of the intracellular capillaries exists (Fritsch, 1887; Nakajima, Pappas and Bennett unpublished data) Thus it is reasonable to suppose that as the neurons grow the pericellular capillaries in the smaller neurons of the young puffer are surrounded by the growing neuronal cytoplasm and are gradually engulfed in the cell body The spherical shape of the neurons may

also be another important factor — there being a minimal surface-to-volume ratio Although the Mauthner cells in the teleost fish measure 500 μ to over 1000 μ in length, they have a cylindrical shape of only about 30 μ to 60 μ in diameter and in fact endocellular capillaries are apparently not present (Bodian '37 Otsuka, '62 and Robertson et al. '64)

LITERATURE CITED

Afzelius B., and G. Friedberg 1963 The fine structure of the caudal neurosecretory system in *Raia batis*. Z. Zellforsch, 59 289–308.

Bennett, H. S., and J H. Luft 1959 S-Collidine as a basis for buffering fixatives. J Biophysic. and Biochem. Cytol., 6 113–115.

Bennett, M. V L. 1960 Electrical connections between supramedullary neurons. Fed. Proc., 19 282.

Bennett, M. V L., S. M. Crain and H. Grundfest 1959a Electrophysiology of supramedullary neurons in *Spheroides maculatus*. I. Orthodromic and antidromic responses. J Gen. Physiol., 43 159–188.

——— 1959b Electrophysiology of supramedullary neurons in *Spheroides maculatus*. III. Organization of the supramedullary neurons. J Gen. Physiol., 43 221–250.

Bern, H. A. and N Takasugi 1962 The caudal neurosecretory system of fishes. Gen. com. Endocr., 2: 96–110.

Bodian, D. 1937 The structure of the vertebrate synapse. A study of the axon endings on Mauthner's cell and neighboring centers in the goldfish. J Comp. Neur., 68 117–159.

Burr H. S 1928 The central nervous system of *Orthagoriscus mola*. J Com. Neur 45 33–128

Cammermeyer J 1963 Intraneuronal capillary Anat. Rec., *143* 415–421.

Clara, M. 1955 Beiträge zur Morphobiologie des nucleus supraopticus und nucleus paraventricularis. Anat. Anz., 102 66–68

Collin, R. 1931 Sur une disposition peri-et endo cellulaire remarquable des capillaries sanguins dans le tuber cinereum chez le cobaye. C. R. Soc. Biol. (Paris) *107* 713–715.

De Robertis, E and H M Gerschenfeld 1961 Submicroscopic morphology and function of glial cells. In: International Review of Neurobiology ed. C. C. Pfeiffer and J R. Smythies, Vol. 3 1–65. Academic Press, N Y

Dempsey E. W and G. B Wislocki 1955 An electron microscope study of the blood-brain barrier in the rat, employing silver nitrate as vital stain. J Biophys. and Biochem. Cytol., *1* 45–256.

Donahue, S., and G. D. Pappas 1961 The fine structure of capillaries in the cerebral cortex of the rat at various stages of development. Am. J Anat., *108* 331–347

Farquhar, M. G., and G. E. Palade 1963 Junctional complexes in various epithelia. J Cell Biol., *17* 375–412.

Fritsch, G. 1886 Ueber einige bemerkenswerthe Elemente des Centralnervensystems von *Lophius piscatorius* L. Arch. mikr. Anat., 27 13–31

——— 1887 Die electrische Fische I. Malopterurus. Veit & Co., Leipzig

Gray E. G. 1961 Ultrastructure of synapses of the cerebral cortex and of certain specializations of neuroglial membranes. In: Electron Microscopy in Anatomy ed. J. D. Boyd, F. R. Johnson, and J D. Lever 54–73. Edward Arnold and Co., London.

Hughes, A. 1957 The development of the primary sensory system in *Xenopus laevis* (Daudin) J Anat., *91* 323–337

Ishibashi, T 1963 CH-positive granules in supramedullary nerve cells of puffer. Zoological M gazine, *71* 183–186.

Kappers, C. U A., G. C. Huber and E. C. Crosby 1936 The Comparative Anatomy of the Nervous System of Vertebrates. The MacMillan Co., New York.

Karnovsky M. J 1961 Simple methods for staining with lead" at high pH in electron microscopy J Biophysic. and Biochem. Cytol., *11* 729–732.

Leonhardt, H. 1965 Die Neurohypophyse als Resorptionsorgan. Acta Neuroveg 27 ...

Luft, J H. 1961 Improvements in epoxy resin embedding methods. J. Biophys. and Biochem. Cytol., *9* 409–414.

Maynard, E. A., R. L. Schultz and D. C. Pease 1957 Electron microscopy of the vascular bed of rat cerebral cortex. Am. J. Anat., 100 409–433.

Murakami, M. 1962 Elektronenmikroskopische Untersuchung der neurosekretorischen Zellen im Hypothalamus der Maus. Z. Zellforsch. *56* 277–299.

Murakami, M. and F Seo 1956 Über die Vitalfarbung der neurosekretorischen Zellen im Hypothalamus des Gecko Japonicus Kurume Med. J 3 129–132.

Novikoff A. B. 1961 Lysosomes and related particles. In: The Cell, ed. J Brachet and A. E. Mirsky Vol. 2: 423–488, Academic Press, New York and London.

Osinchak, J. 1963 Acid phosphatase activity and the identity of intracellular granules in neurosecretory cells of the rat. J. Cell Biol. *19* 54A.

Otsuka, N 1962 Histologisch-entwicklungsgeschichtliche Untersuchungen an Mauthnerschen Zellen von Fischen. Z. Zellforsch. 58 ...

Otsuka, N S Takahashi and K. Miyazaki 1956 Uber den Befund der Vitalfarbung im Hypothalamus-Hypophysensystem. Arch. E. Jap., *11* 11 21

Palay S. L. 1957 The fine structure of the neurohypophysis. In Progress in Neurobiology Vol. 2, Ultrastructure and cellular chemistry of neural tissue, ed. H. Waelsch 31–49 Hoeber N. Y

—— 1960 The fine structure of secretory neurons in the preoptic nucleus of the goldfish (*Carassius auratus*) Anat. Rec., *138* 417–443.
...ley S. L., S. H. McGee-Russell, S. Gordon, J and M. A. Grillo 1962 Fixation of neural tissues for electron microscopy by perfusion with solutions of osmium tetroxide. J Cell Biol 12: 385–410.
...ppas, G. D and D. P Purpura 1961 Fine structure of dendrites in the superficial neocortical neuropil. Exptl. Neural., *4* 507–530.
... J. P L. Napolitano and D. W Fawcett 1960 Identification of glycogen in electron micrographs of thin tissue sections. J Biophys. and Biochem. Cytol., *8* 575–589.
...ynolds, E. S. 1963 The use of lead citrate at high pH as an electron-opaque stain in electron microscopy J Cell Biol., *17* 208–212.
...chardson, K. C., L. Jarett and E. H. Finke 1960 Embedding in epoxy resins for ultrathin sectioning in electron microscopy Stain Tech *35*: 313–323.
...bertson, J D T S. Bodenheimer and D. E. Stage 1963 The ultrastructure of Mauthner cell synapses and nodes in goldfish brains. J Cell Biol., *19*. 159–199.
...senbluth, J. 1962 Subsurface cisterns and their relationship to the neural plasma membrane. J. Cell. Biol., *13* 405–421
—— 1963 Contrast between osmium-fixed and permanganate-fixed toad spinal ganglia. J. Cell Biol., *16*: 143–157
...no, Y and A. Knoop 1959 Electronenmikroskopische Untersuchungen am kaudalen neurosekretorischen System von *Tinca vulgaris* Z. Zellforsch. *49* 464–492.
Scharrer E. A 1937 Gefass und Nervenzelle, Ztschr fd. d. ges. Neurol. u. Psychiat., *159* 93–101.
—— 1954 Functional organization of the brain. In Neuropharmacology Transactions of the First Conference ed. H. A. Abramson: 90–106, The Josiah Macy J Foundation, N. Y
Scharrer E. A. and B Scharrer 1940 Secretory cells within the hypothalamus, Assoc. Res. Nerv Ment. Dis., *20* 170–244.
Scharrer E. A., S. L. Palay and R. G. Nilges 1945 Neurosecretion, VIII, The nissl substance in secreting nerve cells. Anat. Rec., *92*: 23–31.
Schultz, R. L., E. A. Maynard and D C. Pease 1957 Electron microscopy of neurons and neuroglia of cerebral cortex and corpus callosum. Am. J Anat., *100* 369–408.
Van Breemen, V L., and C. D. Clemente 1955 Silver deposition in the central nervous system and the hematopoietic barrier studied with the electron microscope. J Biophys. and Biochem. Cytol., *1* 161–166.
Wislocki, G. B., and L. S. King 1936 The permeability of the hypophysis and hypothalamus to vital dyes, with study of the hypophyseal vascular supply Am. J Anat., *58* 421–471
Wislocki, G. B., and E. H. Leduc 1952 Vital staining of the hematoencephalic barrier by silver nitrate and trypan blue, and cytological comparisons of the neurohypophysis, pineal body area postrema, intercolumnartubercle and supraoptic crest. J Comp. Neur *96* 371–410.
Wolff, J 1963 Beitrage zur Ultrastruktur der Kapillaren in der normalen Grosshirnrinde. Z. Zellforsch., *60* 409–431.

PLATE 1

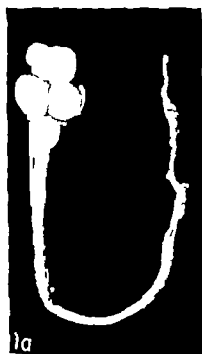
EXPLANATION OF FIGURES

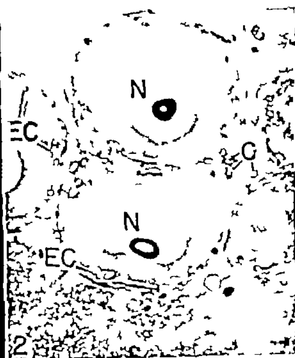
1a Dorsal view of the whole brain and spinal cord of an adult Atlantic puffer. × 2.2.

1b Higher magnification of the medulla oblongata and spinal cord; the large supramedullary neurons are noted (arrow) × 7.0.

2 A light micrograph of 1 μ thick section of adult Atlantic puffer supramedullary neurons. It shows the nuclei (N) with very dense nucleoli, and many endocellular (EC) and pericellular capillaries (C). Mallory' Azure II methylen blue stain. × 160.

3 A light micrograph of 1 μ thick section of dorsal spinal cord of African fresh-water puffer. The supramedullary neurons lie on the dorsal surface covered by thin pial membrane (P) under which many capillaries (C) are found. Endocellular capillaries and many pericellular capillaries can be found in this figure. The axon (A) runs ventrally in the dorsal fissure. The nucleus (N) of these cells contains many very dense nucleoli of various sizes. Toluidine blue stain. × 320.


1a


N
N
EC
EC
C
2


1b

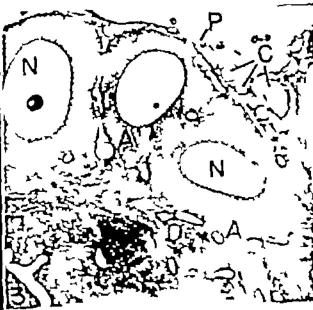

P
C
N
N
A
A
3

PLATE 2

EXPLANATION OF FIGURE

4 A low power electronmicrograph of an adult Atlantic puffer supramedullary neuron showing two endocellular capillaries (EC) and pericellular capillary (C) The capillary wall is made up of the endothelial cell pericytes, and basement membrane. The capillaries are completely surrounded by glial cell processes (G) × 7,500.

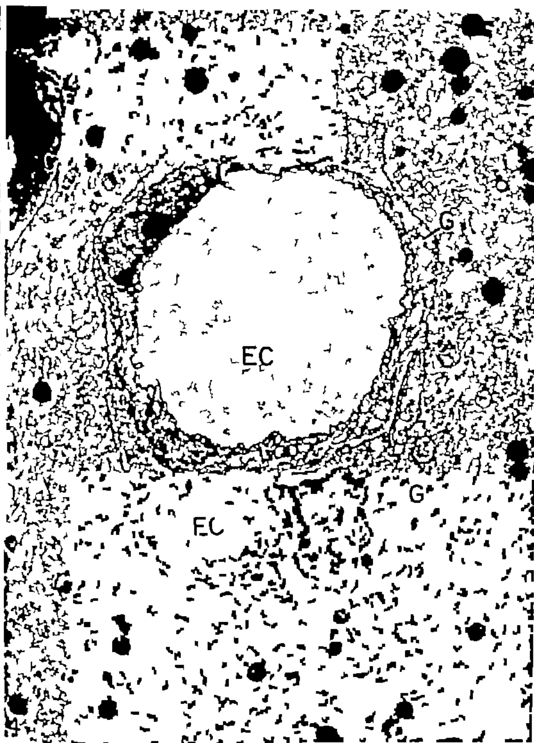

G
EC
G
EC

PLATE 3

EXPLAN TION O FIGURES

5 P rt of an endocell lar capillary of an African fresh-water puffer supramed llary neuron. The capillary i ensheathed by layer of glial (astrocyte) processes (G) The capill ry wall consists of a continuou basement membrane (BM) endothelial cell (E) and some pericyte processes (P) The cytoplasm of the supramedullary cell is abundant with mitochondria (M) clusters of RNP particles, and granular inclusion bodies (IB) × 17,000.

6 A portion of an endocell lar capillary A glial process (G) separates the neuron from the capillary The boundary between glial and neuronal elements is sometimes irregular Apposing endothelial membranes form tight j nction (zonula occludens) and desmosome (arrow) × 20,000

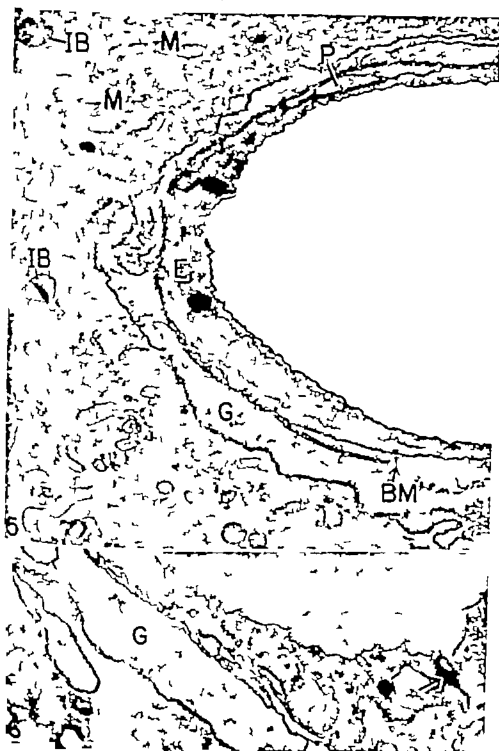

IB
M
M
P
IB
E
G
BM
5
G
6

PLATE 4

EXPLANATION OF FIGURES

7 Part of an endocellular capillary in an African fresh-water puffer. Several layers of glial (astrocyte) processes which contain intracellular fibrils (F) can be seen between the capillary and the neuron. A desmosome (D) is present t the junction of the astrocyte processes. A row of vesicles (V) can be seen in the supramedullary neuron near the glial processes. When permanganate is used as a fixative (see fig. 13) a continuous membrane infolding is found in this area rather than rows of vesicles. Osmium tetroxide-fixed, lead citrate-stained. × 20,000.

8 Part of pericellular capillary of an African fresh-water puffer supramedullary neuron. Occasionally glial processes (G2) contain granular inclusion bodies and no fibrils. S ch processes resemble those of oligodendrocytes. Usually processes of astrocytes surround these capillaries, as shown in figures 5 6 and 7 Osmium tetroxide-fixed, lead citrate-stained. × 13,500.


F
F
D
7


G
8

PLATE 5

EXPLANATION O FIGURE

9 Low power electronmicrograph of the supramedullary neuron (N) of an adult African fresh-water puffer showing an endocellular capillary (EC) t the upper left. The neuron is covered mainly by astrocyte processes. Not complicated glial invaginations into the neuron (G) and the fine extensions of the neuron (N^1) The irregular neuronal processes fold into each other sometimes resulting profiles of neuronal cytoplasm from the same cell bounded by two membranes which ppear as inclusion bodies ( ) (See also fig 11.) × 8,000.


EC
G
G
N
G
G
N
19

PLATE 6

EXPLAN TION O FIGURES

10 Portion of the cell body of an African fresh-water puffer supramedullary neuron, containing mitochondria (M) and Golgi clusters (C). Note the subsurface cisternae (SC) (SC_1) and the fine extensions of the neuronal processes. The neuron is covered by astrocytes (G). Occluded gap between glia processes (arrow) can be seen. Osmium tetroxide-fixed, lead citrate-stained. × 25,000.

11 Infolding of a neuronal process into apparently its own cell body. In some areas (t arrows) the apposing cell membranes are fused and the extracellular space is occluded. Desmosome (D) can also be found in this section. Osmium tetroxide-fixed, uranyl acetate-stained. × 31,000


G
SG
M
L
D
Sch
G
M
L
C
10
D
D
D
11



12 Portion of the cell body of a small Atlantic puffer supramedullary neuron. Note the very deeply invaginated myelinated axon (A) and numerous glial processes (G). An occluded gap between apposing neuronal membranes of the invagination can be seen at arrow. Osmium tetroxide-fixed, uranyl acetate-stained. × 18,500



13 Portion of the perikaryon of an African fresh-water puffer supramedullary neuron fixed with sodium permanganate. Note the folding of the neuron membrane (arrow) and absence of the chains of vesicles t the cell surface. The cytoplasm of the neuron contains mitochondria (M) endoplasmic reticulum (ER) Golgi clusters (GC) multivesicular bodies (MB) and inclusion bodies (IB) are also labeled. 17,000.

The Ultrastructure of Unilaminar Follicles of the Hamster Ovary

D. LOUISE ODOR
Department of Anatomy, Bowman Gray School of Medicine, Winston-Salem, North Carolina

ABSTRACT Unilaminar follicles consisting of primary oocytes surrounded by a single granulosal layer, composed either of flattened, cuboidal or columnar cells, have been studied with the electron microscope in normal prepubertal hamsters. The most striking feature of the oocyte cytoplasm is the occurrence of the mitochondria in small groups with a dense intermitochondrial substance lying between the individual mitochondria. This substance is composed mainly of very small vesicles with a dense profile and a light center. Some of the mitochondria do not appear to have a limiting membrane, their matrices being seemingly continuous with, and similar in structure to, the intermitochondrial substance. In the younger oocytes the Golgi complex is diffuse and has numerous small vesicles. The nucleoli of the young oocytes are large and complex. They consist of a lighter area, predominantly of small particulate elements, and of darker regions, mainly with fine fibrillar components. The initial steps in the formation of the zona pellucida take place in follicles with a single layer of cuboidal granulosa cells. By the time the oocyte is surrounded by a single layer of columnar granulosa cells, a continuous zona pellucida within which lies oocyte microvilli and granulosa cell processes is present.

This study is part of a larger investigation of the effects of exogenous gonadotropins on the ovaries of prepubertal hamsters. In contrast to the normal 15-day-old rat ovary in which there are a number of small vesicular follicles, many of which are undergoing atresia, the hamster of this age has a more immature ovary. There are no follicles with antra and atretic follicles are very infrequently observed. Many unilaminar follicles are present with either a single flattened, cuboidal, or columnar layer of granulosa cells. The largest of the monovular follicles have approximately 4 to 6 layers of follicular cells. Polyovular follicles are numerous. The ovaries of hamsters up to 21 days of age do not appear to respond to the injection of exogenous gonadotropins as far as advancement of follicular development and subsequent ovulation are concerned (Bodemer, Rumery and Blandau, '59). It is important to gain information about the ultrastructure of the unstimulated prepubertal ovary before attempting to judge the effect of hormonal injections. This paper thus deals with a study on the ultrastructure of unilaminar follicles of normal 14 to 15-day-old immature hamsters.

METHODS [1,2]

One ovary of each of nine hamsters, 14 to 15 days old, was processed for electron microscopy and the other for light microscopy. The hamsters were lightly anesthetized with ether, the tissue for electron microscopy was removed and placed in a drop of cold 2% osmic acid adjusted to pH 7.4 with veronal acetate buffer. Under the dissecting microscope the ovary was cut with a razor blade into small pieces which were then immersed in the fixative for one to one and one half hours and dehydrated in a graded series of ethanol. The tissue was embedded in either Epon or Araldite, the latter being more satisfactory. Thin sections cut on the Porter-Blum Ultratome were mounted on grids coated with a parlodion film stabilized with carbon. They were stained with a 2% solution of uranyl acetate or with a lead hydroxide or lead citrate solution. An RCA-EMU-3F electron microscope was used, the electron micrographs being taken

[1] The helpful suggestions and interest of Dr. Richard J. Blandau during this study are greatly appreciated. The technical assistance of Mrs. Gloria Crumbliss and the preparation of the photographic prints by Mr. Roy Hasaki are gratefully acknowledged.

[2] This study was supported by grant HD-00008 from the National Institutes of Health, United States Department of Health, Education and Welfare.

at initial magnifications between approximately 1 700 and 23 000 diameters and subsequently photographically enlarged. The second ovary was prepared for light microscopy The ovaries of two animals were fixed in Zenker formol, processed in the usual way embedded in paraffin sectioned serially and stained with Weigert's iron hematoxylin and eosin. The second ovary of the remaining hamsters was fixed in cold picric acid formol solution, processed embedded in paraffin and sectioned serially These were stained by the periodic-acid-Schiff (PAS) method for the demonstration of glycogen or other polysaccharides. Using this method of fixation, intracellular migration of PAS positive material occurred. To avoid this artefact both ovaries of four additional hamsters were quenched in isopentane cooled with liquid nitrogen They were then placed in cold picric acid-formol solution at − 10 C for seven days dehydrated, embedded in paraffin and stained by the PAS technique

OBSERVATIONS

Light microscopy

In the hamsters studied, the smaller unilaminar follicles lie primarily beneath the germinal epithelium and also near the mesovarium. They are either incompletely r completely surrounded by flattened anulosa cells The oocytes when stained with iron hematoxylin have large nuclei, generally with 2 or 3 nucleoli. The nucleoli have an irregular outline usually lie close to the nuclear membrane and have central regions which stain more lightly than the periphery When sections are stained by the PAS method the small oocytes have a moderate number of PAS positive granules in their cytoplasm and their granulosa cells are not stained but they do rest upon a strongly PAS positive basement membrane After diastase treatment most of the ooplasmic granules disappear but a diffuse pink staining is visible and the basement membrane remains strongly PAS positive This is taken to indicate the presence of a moderate amount of glycogen in the ooplasm.

As the oocyte enlarges and as the granulosa cells become cuboidal and then columnar the growing unilaminar follicles are located internal to the smaller ones. The oocytes of these generally have the same structure as that in the smaller follicles. In the oocytes encompassed by a layer of columnar granulosa cells a thin PAS positive line, not entirely lost with diastase treatment, appears between these cells and the oocyte indicating the presence of the newly forming zona pellucida.

Electron microscopy

Structure of primary oocytes in unilaminar follicles

Ooplasm. Relatively low power views of follicles with flattened (fig 1) cuboidal (fig 4) and columnar (fig. 7) granulosa cells show some of the characteristic structures of the ooplasm at these three phases Other figures give more detailed images.

The most striking feature is the predominant occurrence of mitochondria in small groups with an electron dense substance between the individual mitochondria (figs. 1 7 8) In some oocytes a few of the mitochondria are scattered singly in the cytoplasm (fig 19) Groups of mitochondria with the intermitochondrial material are seen at higher magnifications in figures 10a, 10b 11 13 and 14 In these figures the substance between the mitochondria appears to consist mainly of small vesicular elements with a dense fairly thick profile and a less dense central core Some indistinct tubular or fibrillar components may be seen also (figs. 11 13 14) In the latter figures it is to be noted that the matrices of some of the mitochondria contain vesicular elements similar to those of the intermitochondrial substance. It has not been possible to determine the origin of this intermitochondrial material in the hamster oocytes, for no formative stages have been detected. In both figures 11 and 13 some mitochondria have the characteristic double limiting membrane However in other cases mitochondria with at least a few cristae but lacking the double outer membrane are present and their matrices appear continuous with the intermitochondrial substance Whether this is simply a question of the plane of section through these mitochondria or whether they are contributing to or are receiving materials from the intermitochondrial substance cannot be de-

cided on purely morphologic grounds Since this image occurs so frequently it is not believed to be due to the plane of sectioning. Most of the oocyte mitochondria are slightly oval and have only a few cristae extending obliquely across the organelle. Another interesting feature of some of the mitochondria is shown especially well in figure 10a in the mitochondrion labeled "1 The mitochondrial matrix is quite electron-lucent and there are three outpouchings or blebs, continuous with the matrix, present on the lower border of the mitochondrion. The limiting membrane appears single there A similar image is seen in the upper left mitochondrion in figure 14 The arrow in figure 1 indicates an irregular structure which is believed to be a swollen mitochondrion due to the presence of cristae and of adjacent intermitochondrial substance. A somewhat elongated protrusion is in continuity with the contents of this body Such blebs may form some of the smooth surfaced vesicles of the cytoplasm In figures 10a and 10b irregular bodies, labeled "2 and "3 are present with some outpocketings. There is a possibility also that these two bodies may have originated from mitochondria and contribute to the formation of some of the vesicular elements present in the ooplasm.

In oocytes surrounded by flat or cuboidal granulosa cells the next most prominent ooplasmic component is the Golgi complex, which is quite variable in pattern. In some sections (fig. 15) the narrow smooth-surfaced membranous elements are quite numerous. Associated with them are many vesicles which vary in size and have smooth surfaces. The enclosed spaces in both membranous and vesicular elements are of variable electron density many being moderately dense (fig 15) but some quite electron-lucent. A somewhat different organization of Golgi components is shown in figure 16 Relatively few membranous elements are seen. The many vesicles present vary in size and in density of their contents. There are no large vacuoles associated with the Golgi complex as is so commonly seen in secretory cells. The relationship of Golgi elements to other ooplasmic structures is not constant. A rather diffuse area of Golgi components is seen at low magnification in figures 4 and 19 In the follicles enclosed by a layer of columnar cells the Golgi elements were seen infrequently and, when present were more dispersed than at earlier stages (fig. 8) From the images observed it may be that the Golgi complex contributes many of the numerous smooth-surfaced vesicles to the ooplasm.

Infrequently multivesicular bodies are present either as single units or in small groups of the units (figs. 7 17) If single the body consists of a vacuole whose membrane encloses a space containing a few small vesicles and outside of which are other similar vesicles. When the multivesicular bodies are aggregated the enclosing membrane of some of the vacuoles is not always intact and more numerous vesicles surround the vacuoles than in the case of single units

Membranous elements of the granular endoplasmic reticulum are usually small, with only a few attached ribosomes, and are not very prominent (figs. 13 3 9) The intracavitary contents often have a moderate density Groups of free ribosomes are scattered in the ooplasm (figs. 8 11 12) Although light microscopy of PAS stained primary oocytes indicates the presence of ooplasmic glycogen, it was not possible to identify glycogen granules in electron microscope sections perhaps due to the limited amount present.

Some oocytes have several additional kinds of cytoplasmic bodies. One type quite commonly observed is very electron dense (figs. 4 7) and under higher magnification appears multilaminar in structure resembling myelin figures described in other cell types. They do not seem to be associated with other indications of early atresia. Figures 8 and 12 show another structure (↑) found in some oocytes. It varies in size has no limiting membrane and appears to consist of very small vesicular and granular elements which are irregularly arranged. Although less dense this structure resembles the intermitochondrial substance somewhat. This body may be some kind of nutritive storage material, but it is not similar to the mature yolk platelets seen in non-mammalian vertebrate or invertebrate oocytes.

Nucleus A typical oocyte nucleus is shown in figure 1 and details of nuclear structures are visible in other figures. The nuclear envelope consists of an inner and outer membrane (figs 11 1) and when cut tangentially has circular profiles representing nuclear pores (fig. 15) A prominent and complex nucleolus is often observed, especially in the earlier stages of follicular growth (figs 1 18–20) Most commonly these appear to have two parts a larger moderately dense area surrounded by irregularly arranged more dense projections The lighter area (figs 18 19 20a, 20b) shows rather regularly arranged dense granules with some very fine fibrils between them The dense projections (figs. 20a, 20c) appear to consist of fibrillar elements mainly In other oocytes the nucleolus has a somewhat different appearance being quite dense throughout, though the two general areas can usually be distinguished (figs. 5 6) The nucleoplasm (fig 20a) contains thin threadlike elements with scattered attached granules the dispersed chromatin In some nuclei (figs. 5 6) chromatin material is condensed and rests on the inner membrane of the nuclear envelope, adjacent to a dense nucleolus.

Structure of the granulosa cells and early formation of the zona pellucida

The pattern of formation of the zona pellucida in the oocyte of the hamster follows closely that previously observed in other mammalian oocytes. In the earliest unilaminar follicles the oocyte is surrounded first incompletely and then completely by a layer of flat granulosa cells. The plasma membranes of both the oocyte and the granulosa cells are relatively smooth and in close apposition to one another (figs. 1 9) some contact points being desmosome-like in structure When the granulosa cells become cuboidal very small cytoplasmic processes appear in isolated areas between the oocyte and granulosa cells while in other regions close contact is still maintained (fig 4) Then a space develops at separate sites around the periphery between the oocyte and the granulosa cells. Oocyte microvilli and larger granulosa cell processes appear in these spaces, with a slightly dense zona pellucida substance accumulating between the cellular processes. Eventually in follicles having a single layer of columnar granulosa cells (figs. 7 8) the oocyte and granulosa cells are usually separated by the substance of the zona pellucida around the entire periphery of the oocyte. In the follicle shown in figure 7 the zona pellucida is approximately one-third the width it attains in large follicles with antra.

The ultrastructure of the granulosa cells at different stages of follicular development is of interest, since some of the older light microscopy literature reports changes in intracellular position of various organelles, especially the Golgi complex. The elongated nuclei of the flat granulosa cells occupy much of the cellular volume with most of the organelles lying to either side of it, without any preferential organization of the various types. One may note scattered mitochondria, many small vesicular elements including some granular endoplasmic reticulum and small groups of free ribosomes (fig. 1) The Golgi complex consists of narrow membranous elements with associated small vesicles. Of interest, since the follicle at this stage is not believed to be active in steroid production, is the common occurrence of irregularly shaped lipid bodies (fig. 1) As the granulosa cells become cuboidal (figs. 4 9 2) the nuclei become less elongated and often show small identations. Some of the cytoplasmic elements come to lie above, as well as to either side of the nucleus (fig. 9) Some of the mitochondria are elongated and have a more dense matrix and more irregularly arranged cristae than the mitochondria of the adjacent oocyte. Small elements of the granular endoplasmic reticulum, with moderately dense contents, are scattered in the cytoplasm. Two areas containing Golgi elements are present. In figure 4 irregularly shaped lipid droplets with a dense periphery are present to one side of the nucleus. As the granulosa cells become columnar the nucleus lies more basally, is irregularly oval in shape and contains some areas more dense than the rest of the nucleoplasm (fig 7) In figure 3 many of the cytoplasmic organelles lie above or slightly

one side of the nucleus. The mitochondria are more numerous in the supranuclear area and are predominantly oval in shape. The membranous and vesicular Golgi elements have a few moderately sized vacuoles associated with them. Occasional multivesicular bodies are present (figs. 3, 7) Lipid bodies are now found located more basally than previously The cytoplasm and the processes of the granulosa cells lying immediately adjacent to the substance of the zona pellucida (↑) are often of low electron density and contain none of the larger cytoplasmic structures (figs. 7 8 3 2) In the largest unilaminar follicles observed there was no recognizable theca present external to the basement membrane.

DISCUSSION

Oocyte Although the fine structure of the primary oocyte in the unilaminar follicles of the ovary of the prepubertal hamster is similar to that seen in other mammals and lower vertebrates there are significant differences.

Mitochondria. The mitochondria are the most striking ooplasmic organelles when compared to other species where young primary oocytes have been studied (mouse, Yamada et al., '57 guinea pig, Anderson and Beams '60 rabbit, Blanchette '61; and rat, Sotelo '59 Sotelo and Porter '59 Odor '60 and Franchi and Mandl, '62) In contrast to other species most of the mitochondria of the hamster oocyte are aggregated into small groups having a dense vesicular substance lying between them. This intermitochondrial material often appears to merge with the matrices of some of the mitochondria, whose limiting membranes are not visible. For the mammals the rabbit oocyte (Blanchette, '61) is the only one in which anything resembling this pattern was noted. In this animal the mitochondria are stated to be in close association with cytoplasmic vacuoles and "irregular lipid inclusions. Since the sections were relatively thick it is possible that the "lipid inclusions might have an undetected fine structure Even so the mitochondria are not as obviously aggregated and do not seem bound by intermitochondrial material as in the hamster.

It is of interest that a morphologically similar substance is present in electron micrographs of some oocytes of lower vertebrates which are in the process of forming yolk granules or platelets. Ornstein ('56) in thick sections of young oocytes of the frog, *Rana clamitans* noted dense material in the cytoplasm which appeared to be continuous with the nuclear pores and which then became closely associated with mitochondria, as if the nucleus and mitochondria were cooperatively responsible for the production of the dense masses. In the same species Miller ('62) reported that material passes through the nuclear pores condenses into short dense cylinders approximately 200 A to 400 A from the outer membrane of the nucleus. These cylinders and the pores have the same diameter and the extruded substance is somewhat similar in structure to the fibrous nucleolar component. The cylinders coalesce to form fairly large masses of material, usually associated with mitochondria A less extensive aggregation of dense material occurs in the oocytes of *Triturus viridescens* In the clawed toad, *Xenopus* an electron dense material is believed to be extruded from the nucleus by way of the nuclear pores to form "intermitochondrial cement (Balinsky and Devis, '63)

The dense material described in the papers mentioned above appears quite similar to that in the hamster oocyte but in the latter there is no indication of extrusion of nuclear material However the intermitochondrial substance may receive soluble nuclear substances which are incorporated into it; it may be a product of mitochondrial or other cytoplasmic activity or it may furnish raw materials for the formation of new mitochondria André ('62) in an electron microscopic study of rat spermatogonia describes and illustrates groups of mitochondria and intermitochondrial substance strikingly similar to those observed in this study He notes that the envelopes of some of the mitochondria were invisible with an apparent continuity between the mitochondrial matrix and the intermitochondrial substance He also describes either continuity or contiguity of the mitochondrial envelope with sacs of endoplasmic reticulum The intermito-

chondrial material is stated to be a dense amorphous substance There is thus a distinct similarity between the male and female germ cells of the rat and hamster in this particular feature. Rat oocytes on the other hand do not show these structural relationships (Odor '60) On the basis of both the literature and his ultrastructural studies André hypothesizes that rosettes of ribosomes take part in the formation of the intermitochondrial substance which in turn furnishes material for the *de novo* formation of mitochondria. He does not believe that divisions of existing mitochondria in the spermatogonia occur frequently enough to account for the twenty-fold increase in mitochondrial material but the process presumably is induced by pre-existing mitochondria. Novikoff ('61) reviewed the literature also and discusses the possibilities of *de novo* formation of mitochondria but he does not believe there is a clear substantiation of any of the hypotheses Lee ('64) studied mitochondrial formation by electron microscopy in various cell types obtained from adult rabbits and neonatal and adult rats with or without experimental treatments The sequence in the formation of mitochondria appears to him to be (1) the aggregation of dense granules smaller and less electron dense than ribosomes, (2) the formation of a limiting membrane at the periphery of the aggregates thus becoming granular dense bodies (3) the differentiation of central granules into paired lamellae or tubules before or after the appearance of two dense layers of the limiting membrane The transitional forms are much more numerous in growing animals in adult tissues with frequent mitoses or under certain pathological changes In addition he described four types of self-duplication of mitochondria. However again one is relying solely on morphology and reconstructing a dynamic picture from an essentially static one

Our morphologic data on the ultrastructure of hamster oocytes alone do not allow us to draw definitive conclusions about the origin of mitochondria or the function of the intermitochondrial substance One may postulate however that groups of mitochondria are formed by successive divisions of pre-existing mitochondria with some of the raw materials coming from the intermitochondrial substance. The mitochondrial groups do appear larger and the intermitochondrial substance less in amount in the unilaminar follicles with a columnar granulosal layer than in the younger follicles.

Mitochondria have been implicated in yolk formation in a number of species. In some, the yolk precursor is noted in crystalline form inside clearly recognizable mitochondria (*Rana pipiens* Ward, '63) In others it is believed that mitochondria undergo structural changes and are transformed into protein yolk granules (*Xenopus laevis* Balinsky and Devis, '63 *Planorbis corneus* Favard and Carasso, '58). In *Rana pipiens* a fatty yolk is said to arise from fragmentation of mitochondria

Some mitochondria of the hamster oocytes have outpouchings or blebs on their surfaces. Whether these blebs form ooplasmic vesicles in any appreciable quantities or participate in the formation of the dense intermitochondrial substance is unknown. They may even represent artefacts resulting from tissue preparation André observed very similar images in rat spermatogonia He believes this tends to show that the membranes of the endoplasmic reticulum contribute to the formation of the mitochondrial membranes. Another similarity was noted in large human oocytes in multilaminar follicles (Wartenberg and Stegner '60) where mitochondria are illustrated in close contact with vesicles but no direct continuity exists between the mitochondria and the adjacent vesicles Lee ('64) noted a close spatial relationship between mitochondria and granular endoplasmic reticulum in some of the cell types he studied.

Golgi complex. In immature oocytes in the rat mouse guinea pig and rabbit the Golgi complex is large and lies in a close juxtanuclear position (Sotelo, '59 Sotelo and Porter '59 Odor '60 Franchi and Mandl, '62 Yamada et al., '57; Anderson and Beams, '60 Blanchette '61) It consists of smooth-surfaced membranous elements associated with numerous small vesicles located in a rather restricted area In the more mature oocytes the large Golgi complex fragments into smaller units often lying adjacent to the plasma mem-

brane. In the immature hamster oocyte the Golgi apparatus is not seen as a compact, circumscribed structure but rather its elements are more diffusely arranged. In illustrations of most immature mammalian oocytes, with the possible exception of the rabbit (Blanchette, '61) the membranous elements are in less curved formations and the vesicular elements are less numerous.

Multivesicular bodies In hamster oocytes of unilaminar follicles, multivesicular bodies are found as single units and in groups. This is in accordance with observations in other mammals. Generally in oogonia or immature oocytes single units are most frequently observed. Groups of multivesicular bodies are more common in the mature primary and secondary oocytes and in the fertilized or segmenting eggs (Yamada et al., '57 Sotelo and Porter '59 Odor '60 Franchi and Mandl '62 Izquierdo and Vial, '62 Anderson and Beams, '60 Wartenberg and Stegner '60). Multivesicular bodies are also observed in the oocytes of the toad, *Xenopus* and are thought by Balinsky and Devis ('63) to be derived from mitochondria but no transitional forms have been described. In this species it is stated, through not illustrated that multivesicular bodies form secondary peripheral yolk and pigment granules. Since these structures have been observed in numerous cell types other than oocytes, it appears likely that a more generalized function, as yet not clearly understood, is carried out by these bodies. They have been considered by some to be a type of lysosome.

Endoplasmic reticulum and ribosomes It is generally agreed that membranous or cisternal, granular endoplasmic reticulum is sparsely distributed in immature primary oocytes of mammals (Sotelo and Porter '59 Merker '61 Blanchette '61; Franchi and Mandl '62 Odor '60 Anderson and Beams, '60) This element is more often observed in the hamster than in rat oocytes of comparable developmental stages (Odor '60) but it would not be considered a prominent cytoplasmic component. Sotelo and Porter ('59) state that in the rat a differentiation of the granular endoplasmic reticulum begins early in the 2-cell stage It is interesting to note that in the crayfish oocyte (Beams and Kessel, '63) granular endoplasmic reticulum cisternae are numerous, are continuous with the agranular endoplasmic reticulum and contain within their cavities dense granules 400 A to 600 A in diameter These granules are believed to be subsequently transformed into protein yolk.

Small dense particles, presumably ribosomes, are found in the cytoplasm of the rat oocyte (Sotelo and Porter '59; Odor 60 Franchi and Mandl, '62) In the hamster oocytes, small groups of dense particles similar in size to those attached to the membranous granular endoplasmic reticulum of the surrounding follicle cells are noted scattered rather sparsely in the ooplasm. In sections stained with lead salts it is difficult to determine whether any of the dense particles are glycogen, although the PAS-stained sections observed with the light microscope show the presence of glycogen in the oocyte.

Nucleus The nucleoli present in the nucleus of the hamster oocytes at this stage of development are interesting. Their complexity and size are greater than nucleoli of other ovarian cells. The nucleoli are composed of a less dense, granular part and a more dense, peripheral component which appears to be tubular or fibrillar in nature. Oocyte nucleoli of two amphibian species also exhibit two different structural components one relatively dense and fibrous and the other less compact and granular In all *Rana* oocytes as well as in *Triturus* eggs, the granular part is centrally located (Miller '62) The oocyte in the rat unilaminar follicles, as described by Sotelo ('59) has a large nucleolus It consists of a convoluted thread the nucleolonema, which is made up of very dense granular material. Sotelo and Porter ('59) state that many rat ovarian oocyte nucleoli have a thick dense rim and a less dense center In mature oocytes the rim is composed of a structureless part with small dense granules embedded in it and the center consists of a homogeneous substance of low density In rat oogonia and in oocytes in the dictyate stage the nucleolus consists of a coarse network of finely particulate material (Franchi and Mandl, '62) Although not mentioned the

electron micrographs of the nucleoli show some areas to be more dense than others. In the guinea pig oocyte (Anderson and Beams '60) the nucleolus is said to consist of dense granules arranged in a reticular fashion Parsons ('62) states that in mouse oocytes, up to the stage where there is a single layer of cuboidal follicle cells the nucleolus appears reticulated and has several components The larger part consists of 100 Å microfibrils and is not as dense as the nucleolonema, which seems to contain transverse or oblique sections of coiled fibrils, 60 Å to 100 Å in diameter After the onset of zona pellucida formation the nucleoli either round up or assume a polygonal shape, the coils of the nucleolonema become very dense and the less dense areas disappear In nearly mature mouse oocytes the nucleolus is in an almost completely condensed state Although this description of the nucleolus of the mouse oocyte is somewhat similar to that of the hamster the illustrations of the nucleoli of the two animals are different. However in the older oocytes of both animals the nucleolus becomes more condensed

The nucleoli of the root meristematic cells of *Vicia faba* have two components 150 Å wide granules arranged in threadlike patterns and fibrils 80 Å to 100 Å in diameter (Lafontaine and Chouinard '63) In contrast to the hamster oocyte nucleolus, the area containing these two elements in the root cells are of about equal density and are not arranged as in the oocyte. In cultured Ehrlich ascites tumor cells Mundkur ('64) reports both fibrillar (60 Å to 100 Å in diameter) and particulate (125 Å wide) elements. In these and some other types of cancer cells there is some perinucleolar chromatin associated with the nucleolus (Swift, '63 Mundkur '64 Bernhard and Granboulan '63). Chromatin is occasionally noted near the more condensed nucleoli of the hamster oocytes.

Zona pellucida formation. Although Van Beneden in 1880 reported that in the bat oocyte the formation of the zona pellucida was initiated in unilaminar follicles most of the light microscopy literature described its earliest development as occurring in bi or trilaminar follicles in mammals. The early stages in zona formation have not been studied as extensively as the later phases in multilaminar follicles. In the present study of the hamster material of the zona appears discontinuously around the periphery of the oocyte in unilaminar follicles. The discontinuity of the early zona formation was noted by light microscopy by Mjassojedoff ('23) and has been reported in electron microscope studies for the mouse rabbit and rat (Yamada et al. '57 '60 Chiquoine, '59 '60 Trujillo-Cenóz and Sotelo '59 Merker '61 Odor '59 '60) The pattern of zona formation appears essentially the same in the hamster as in these other three species.

Electron microscope studies on the zona pellucida in more mature mammalian ovarian follicles are more numerous (rabbit, Trujillo-Cenóz and Sotelo, '59 Blanchette, '61 Merker '61; mouse, Yamada et al. '57 Chiquoine '60 rat, Sotelo and Porter '59; Odor '60 Björkman, '62, guinea pig, Anderson and Beams, '60 human Wartenberg and Stegner '60 Stegner and Wartenberg '61) In the hamster there are many microvilli extending from the oocyte into the zona pellucida in the late unilaminar stage at the time when the granulosa layer has become columnar. Less numerous but larger and more irregular granulosa cell processes course obliquely through the zona to terminate on the oocyte plasma membrane or on microvilli. Conclusions about the cellular origin of the substance of the zona are not much more definite than those previously noted (Odor '60) The histochemical studies of Stegner and Wartenberg ('61) do provide some additional evidence for the participation of both the oocyte and granulosa cells in this process.

Ultrastructure of granulosa cells. Relatively little attention has been paid to the submicroscopic structure of the granulosa cells of the unilaminar follicles. It is not always clear from the literature whether the follicle cells being discussed are of uni- or multilaminar follicles. The cytologic changes which accompany the formation of the original of columnar cells from the flat cells has been described in this study The large and numerous lipid droplets present in all stages of development of unilaminar follicles are of interest. The number of mitochondria elements of the granulo

endoplasmic reticulum, ribosomes and Golgi components increases with growth of the cell. The lipid droplets, granular endoplasmic reticulum and ribosomes are more prominent in the granulosa cells than in the oocyte, while the Golgi complex is more highly developed in the latter in the phase before zona pellucida formation, desmosome-like attachments and the presence of lipid bodies similar to those in the hamster have been noted in the mouse, guinea pig and rat (Chiquoine '60 Anderson and Beams '60 Björkman, '62). In the mouse, abundant Golgi membranes, mitochondria and vesicles are reported, and in the guinea pig the granular endoplasmic reticulum is said to be highly organized and abundant. In the hamster as in other species studied, the significance of the large lipid droplets in the granulosa cells is unknown. In the cuboidal and columnar cells, the Golgi complex is located next to the zona pellucida or to the side of the nucleus, but there are no large vacuoles with visible secretory material associated with it. The granular endoplasmic reticulum and free ribosomes as in other species, are abundant and are distributed throughout the cytoplasm.

LITERATURE CITED

Anderson, E., and H. W Beams 1960 Cytological observations on the fine structure of the guinea pig ovary with special reference t the oogonium, primary oocyte and associated follicle cells. J Ultrastruc. Res., 3 432–446.

André, J 1962 Contribution à la connaissance du chondriome. Etude de ses modifications ultrastructurales pendant la spermatogénèse. J. Ultrastruc. Res., Supple. 3: 1–185

Balinsky, B. L. and R. J Devis 1963 Origin and differentiation of cytoplasmic structures in the oocytes of *Xenopus laevis*. Acta Embryol. Morphol. Exper., 6: 55–108.

Beams, H. W and R. G. Kessel 1963 Electron microscope studies on developing crayfish oocytes with special reference to the origin of yolk. J. Cell Biol., 18 621–649.

Bernhard, W and N Granboulan 1963 The fine structure of the cancer cell nucleus. Exper. Cell Res., Supple 9 19–53.

Björkman, N 1962 A study of the ultrastructure of the granulosa cells of the rat ovary Acta Anat., 51 125–147

Blanchette, E. J 1961 A study of the fine structure of the rabbit primary oocyte. J Ultrastruc. Res., 5 349–363.

Bodemer C. W R. E. Rumery and R. J Blandau 1959 Studies on induced ovulation in the intact immature hamster Fert. and Steril 10 350–360.

Chiquoine, A. D. 1959 Electron microscopic observation on the developmental cytology of the mammalian ovum. Anat. Rec., 133 258–259

——— 1960 The development of the zona pellucida of the mammalian ovum. Am. J Anat., 106 149–169

Favard, P and N Carasso 1958 Origine et ultrastructure des plaquettes vitellines de la Planorbe Arch d'Anat. Micr 47 211–234

Franchi, L. L., and A. M. Mandl 1962 The ultrastructure of oogonia and oocytes in the foetal and neonatal rat. Proc. Roy Soc., B 157 99–114.

Izquierdo, L., and J D. Vial 1962 Electron microscope observations on the early development of the rat. Zeit. f Zellforsch. u. Mikr Anat., 56: 157–179

Lafontaine, J G., and L. A. Chouinard 1963 A correlated light and electron microscope study of the nucleolar material during mitosis in *Vicia faba*. J Cell Biol., 17 167–201.

Lee, J C. 1964 Electron microscopic observations on the formation of mitochondria J Roy Micr Soc., 83 229–238.

Marker H. J 1961 Elektronenmikroskopische Untersuchungen über die Bildung der Zona pellucida in den Follikeln des Kaninchenovars Zeit. f Zellforsch u. Mikr Anat 54 677–688.

Miller O. L. 1962 Studies on the ultrastructure and metabolism of nucleoli in amphibian oocytes. *Electron microscopy* 2: NN-8. Fifth International Congress for Electron Microscopy Academic Press, N Y

Mjassojedoff, S. W 1923 Zur Frage über die Struktur des Eifollikels bei den Säugetieren. Arch. Mikr Anat., 97 72–135.

Mundkur, B 1964 Submicroscopic cytochemical organization of interphase nuclei revealed by protein reagents and gallocyanin-chromalum A Study of Ehrlich ascites cells. Zeit. f Zellforsch. u. Mikr. Anat., 63 69–90.

Novikoff A. B 1961 Mitochondria (chondriosomes). In: The Cell, 2: 299–421. Ed. J Brachet and A. E. Mirsky Academic Press, N Y

Odor D. L. 1959 Electron microscopic observations on developing ovarian and unfertilized tubal ova of the rat. Anat. Rec 133 433.

——— 1960 Electron microscopic studies on ovarian oocytes and unfertilized tubal ov in the rat. J Biophysic. Biochem. Cytol 7 567 574

Ornstein, L. 1956 Mitochondrial and nuclear interaction. J Biophysic Biochem. Cytol., 2, (Suppl.) 351–352.

Parsons, D F 1962 An lectron microscope study of radiation damage in the mouse oocyte J Cell Biol 14 31–48.

Sotelo, J R. 1959 An electron microscope study on the cytoplasmic and nuclear components of rat primary oocytes. Zeit. f Zellforsch. Mikr Anat 50 749–765.

Sotelo, J R., and K. R. Porter 1959 An electron microscope tudy of rat ovum. J Biophysic. Biochem. Cytol 5 327–342.

Stegner H. E., and H. Wartenberg 1961 Elektronenmikroskopische und histotopochemische Untersuchungen über Struktur und Bildung

der Zona pellucida menschlichen Eizellen. Zeit. f. Zellforsch. u. Mikr. Anat., 53 702–713.

Swift, H. 1963 Cytochemical studies on nuclear fine structure. Exper. Cell Res., Suppl. 9 54–67

Trujillo-Cenóz, O., and J R. Sotelo 1959 Relationships of the ovular surface with follicle cells and origin of the zona pellucida in rabbit oocytes. J Biophysic. Biochem. Cytol., 5 347–350.

Van Beneden, E. 1880 Contribution à la connaissance de l'ovaire des mammifères. L ovaire de Vespertilo murinus et du Rhinolophus ferrum-equinum. Arch. Biol., 1: 475–550.

Ward, R. T 1962 The origin of protein and fatty yolk in *Rana pipiens*. II. Electron microscopical and cytochemical observations of young and mature oocytes. *J. Cell Biol.*, 14 309–341

Wartenberg, H., and H. E. Stegner 1960 Über die elektronenmikroskopische Feinstruktur des menschlichen Ovarialeies. Zeit. f. Zellforsch. u. Mikr. Anat., 52: 450–474.

Yamada, E., T Muta, A. Motomura and H Koga 1957 The fine structure of the oocyte in the mouse ovary studied with electron microscope Kurume Med. J 4 148–171.

ADDENDUM

During preparation of this paper an article ppeared in J Cell Biol., 21 397–427 entitled "Studies on guinea pig oocytes. I. Electron microscopic observations on the development of cytoplasmic organelles in oocytes of primordial and primary follicles, by E. C. Adams and A. T Hertig. In primary oocytes they described mitochondria aggregated around some dense granular material and stated that some of these mitochondria have incomplete peripheral membranes and cristae. These observations are very similar to those reported here.

PLATES

Abbreviations

BM, basement membrane
CC, condensed chromatin
ER, endoplasmic reticulum
G Golgi complex
GC, granulosa cell
GER, granular endoplasmic reticulum
GN granulosa cell nucleus
GP granulosa cell process
IM, intermitochondrial substance
L, lipid droplet
M, mitochondrion ( )
ML, multilaminar body
MV microvilli
MVB multivesicular body
NL, nucleolus
ON oocyte nucleus
OP oocyte cytoplasm
R, ribosomes
ZP zona pellucida

PLATE 1

EXPLANATION OF FIGURES

1 Part of follicle in which the oocyte is surrounded by one layer of flat granulosa cells. The plasma membranes of the oocyte and granulosa cells lie in close contact. Of particular interest in the oocyte nucleus is the large complex nucleolus with lighter central region and on either side more dense, irregular area. The mitochondria characteristically lie in groups and have some electron dense intermitochondrial substance. Parts of two granulosa cells show irregularly shaped lipid bodies and scattered mitochondria. × 10,300. Araldite. Lead hydroxide.

2 Area of f llicle in which zona pellucida formation has begun. A single layer of cuboidal or columnar granulosa cells surrounds the oocyte. The granulosa cell seen above is separated from the oocyte by the substance of the forming zona pellucida, oocyte microvilli being visible. The lower granulosa cell is still partly in close contact with the oocyte plasma membrane though in two small areas some zona pellucida material and a few oocyte microvilli are present. × 5,040. Araldite. Lead citrate

3 This oocyte is surrounded by one layer of columnar granulosa cells. In the area shown, as well as in other regions around the periphery of the oocyte, zona pellucida material is forming. However this does not occur synchronously around the whole periphery of the oocyte. T the far right the granulosa cell, with a lipid body mitochondria, endoplasmic reticulum and multivesicular body is *still in direct contact with the oocyte and* small desmosome-like contact area is present. There is space between the granulosa cells and the oocyte in the remaining area. The space contains some slightly electron dense material in which several granulosa cell processes and oocyte microvilli are visible. The organelles of the granulosa cells are quite typical of this stage. Their mitochondria and granular endoplasmic reticulum are scattered throughout the cytoplasm. The rather small Golgi complex lies either to one side of, or above and slightly to one side of the nucleus. As in the cell to the left the cytoplasm immediately adjacent (↑) to the zona pellucida contains none of the larger cytoplasmic organelles. × 18,030. Araldite Lead hydroxide.


ZP
OPs
ZP
GC
L
MVR
GRR
MV
ZP
GP

PLATE 2

EXPLANATION OF FIGURES

4 This follicle shows the very beginning of zona pellucida formation, the oocyte being surrounded by layer of cuboidal granulosa cells. Between the arrows the plasma membranes of the oocyte and granulosa cells are directly in contact, partly in desmosome-like form. In the other areas small processes are present between the adjacent structures, this being the earliest evidence of beginning zona pellucida formation observed. In the granulosa cell three irregularly shaped lipid droplets and scattered cytoplasmic organelles may be noted. Numerous mitochondria, rather diffusely arranged Golgi complex, many vesicles and three very dense multilaminar bodies are visible in the ooplasm. × 15,400 Araldite. Lead hydroxide.

5 Area of oocyte nucleus showing a very dense nucleolus. The regions around the light spaces are somewhat more dense than the remainder and probably are similar to the peripheral areas in figures 18 through 20. Granules are quite well seen to the right of the larger light space. The material lying adjacent to the nuclear membrane is structurally different and represents a site of chromatin condensation. × 30,250. Araldite. Lead hydroxide.

6 Part of the nucleus of an oocyte surrounded by one layer of cuboidal granulosa cells. Here again the whole nucleolus is very dense. The part above is somewhat less dense than the darker more irregularly arranged parts, contains both granules and fibrils and is similar to the light central area in figures 18 through 20. The moderately dense material represents condensed chromatin material. × 28,125. Epon. Lead hydroxide

B
ML





PLATE 3

EXPLANATION OF FIGURES

7 Low power micrograph of part of follicle whose oocyte is surrounded by single layer of columnar granulosa cells, resting on a basement membrane. Although not shown in the electron micrograph no theca was present. Approximately one-third the mature width of the zona pellucida has formed, this being the greatest diameter seen in the unilaminar follicles. Present in the ooplasm are some multivesicular bodies, numerous vesicular and granular elements, several very dense multilaminar bodies and clusters of mitochondria, between which be an electron dense intermitochondrial substance. The oocyte plasma membrane has formed many slender microvilli extending for variable distances into the zona. Many irregular nd larger granulosa cell processes are seen mainly near the outer edge of the zona. The basal region of the middle granulosa cell ha some lipid inclusions. × 5,670. Araldite. Uranyl acetate.

8 Part of the periphery of the same follicle as in figure 7 but to one side of the area shown there. The mitochondria remain in clusters with dense intermitochondrial substance but the clusters are larger and the intermitochondrial substance less in amount than in earlier stages. Also to be noted are few Golgi membranous elements, some granular endoplasmic reticulum numerous groups of ribosomes and small, rather light body similar to larger ones seen i other oocytes. The oocyte microvilli and few granulosa cell processes are present in the zona. × 16 160 Araldit Uranyl acetate

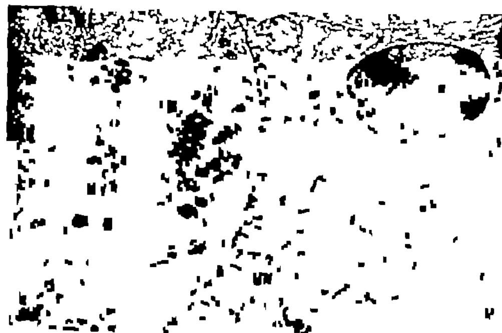


PLATE 3

EXPLANATION OF FIGURES

7 Low power micrograph of part of follicle whose oocyte is surrounded by a single layer of columnar granulosa cells resting on basement membrane. Although not shown in the electron micrograph no theca was present. Approximately one-third the mature width of the zona pellucida has formed, this being the greatest diameter seen in the unilaminar follicles. Present in the ooplasm are some multivesicular bodies, numerous vesicular and granular elements, several very dense multilaminar bodies and clusters of mitochondria, between which lie an electron dense intermitochondrial substance. The oocyte plasma membrane has formed many slender microvilli extending for variable distances into the zona. Many irregular and larger granulosa cell processes are seen mainly near the outer edge of the zona. The basal region of the middle granulosa cell has some lipid inclusions. × 5,670. Araldite. Uranyl acetate.

8 Part of the periphery of the same follicl in figure 7 but to one side of the area shown there. The mitochondria remain in clusters with a dense intermitochondrial substance but the clusters are larger and the intermitochondrial substance less in amount than in earlier stages. Also to be noted are few Golgi membranous elements, some granular endoplasmic reticulum, numerous groups of ribosomes and small, rather light body similar to larger ones seen in other oocytes. The oocyte microvilli and few granulosa cell processes are present in the zona. × 16,160 Araldite. Uranyl acetate


IM
M
OP
GER
B
YGN
9
GER
IM
M
M
IM
ER
M
10a
OPC
ER
OP
M
10b

PLATE 5

EXPLANATION OF FIGURES

11 An area of an oocyte around which lay layer of flat granulosa cells. The group f mitochondria has considerable amount of intermitochondrial substance. The latter appears to consist of an unorganized mass of vesicles nd possibly some fibrils. Similar vesicles are present in the mitochondrial matrix. The two mitochondria to the left have a typical double outer membrane and relatively few cristae. While cristae are visible in the remaining mitochondria the outer membranes are incomplete or lacking Whether this appearance is due to the plane of sectioning or due to an intimate relationship of the intermitochondrial substance to the mitochondria cannot be determined on morphological basis alone. However this is frequent picture in oocytes of unilaminar follicles. Another interesting structure is the membrane formation (↑) in contact with the outer nuclear membrane. A few ribosomes are attached to the most external membrane lying next to the ooplasm. × 70,870. Araldite. Lead citrate.

12 An enlargement of a light body lying in the ooplasm which is larger but of the same structure as that seen in figure 8. There is no limiting membrane and it appears to consist of very small vesicles, granules and fibrils. These components are different from the dark ribosomes lying adjacent to this inclusion body This structure may represent some kind of protein storage product. × 41,220 Epon. Uranyl acetate

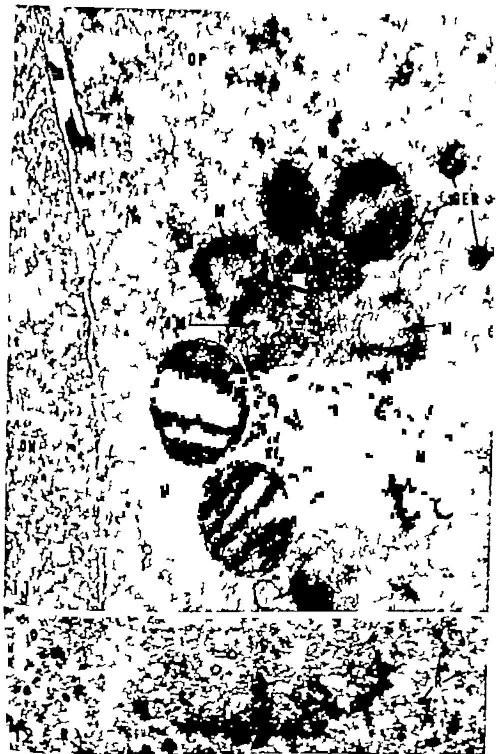

OP
M
SER
M
M
M
M
M

PLATE 6

EXPLANATION FIGURES

13 Area of ooplasm showing group of mitochondria with the inter mitochondrial substance. Most of the mitochondria have a double outer limiting membrane. One of them (?) appears to be in the process f dividing into two, as indicated by the middle constricted area. The very small vesicles f the material between the mitochondria is shown well. × 70,870. Araldite. Lead citrate

14 A small group of ooplasmic mitochondria at high magnification. The vesicular and possible tubular or fibrillar constituents of the intermitochondrial substance are well seen. The mitochondrion at the upper left has an outpouching enclosed in a single membrane instead of the normal double membrane The granulosa cells lay in flattened layer around this oocyte. × 92,560. Araldite Lead citrate


M
GER
R
14

PLATE 7

EXPLANATION OF FIGURES

15 An area of the oocyte of follicle with flat granulosa cells. The nuclear membrane is sectioned tangentially so some circular outlines of nuclear "pores" are visible. The remainder of the field consists mainly of elements of the Golgi complex, showing the rather variable arrangements of the components. One notes some closely packed membranous element and numerous vesicles of arying size none very large. × 24,240. Araldite. Lead citrate.

16 Area of the ooplasm showing another type f arrangement of the Golgi complex. In this one there are fewer membranous elements and more vesicular forms than in figure 15 Also there is a greater range of size of the vesicles. Some have moderately electron dense contents, while some f the larger ones ppear electron-lucent. A layer of flat granulosa cells lay around this oocyt The mitochondrion indicated by the arrow has an outpouching of its membrane × 36,200 Araldite. Lead citrate.

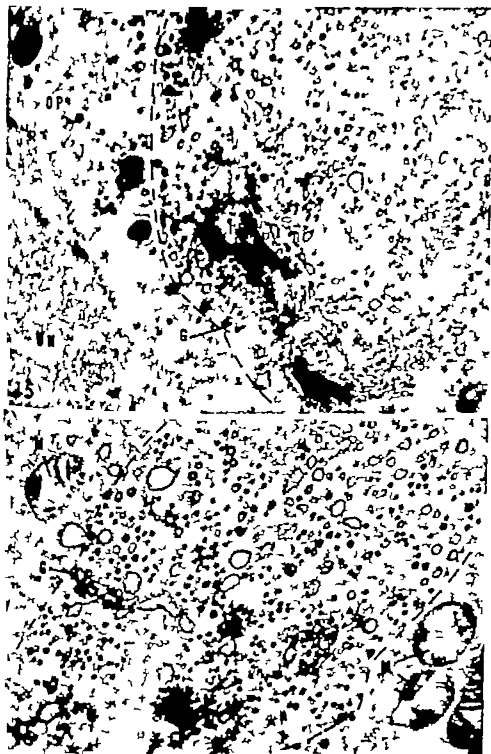

OP
G
G

PLATE 8

EXPLANATION OF FIGURES

17 This group of multivesicular bodies, consisting of few larger vacuoles and many small vesicles, was observed in the cytoplasm of an oocyte enclosed by flat granulosa cells. Below are two typical mitochondria, some intermitochondrial ubstance and changing mitochondrion (↑) with pale matrix and an outpouching in continuity with the matrix. × 32,320. Araldite. Lead citrate.

18–19 Parts of oocytes from follicles with flat granulosa cells. A complex nucleolus is visible in both nuclei. The bulk of the nucleolus is less dense than the peripheral irregular regions and is composed primarily of distinct small dense granules, arranged linearly in places. These granules are similar in appearance to the ribosomes seen in the surrounding ooplasm. The peripherally located, more dense nucleolar areas ppear to contain fine closely packed fibrils and few granular or vesicular structures. In the ooplasm of both oocytes mitochondria typical of these cells are seen. In figure 19 part of Golgi complex lies adjacent to the nuclear membrane. Figure 18, × 30,250. Figure 19 × 20,200 Araldit Lead citrate



DN
DP
ML
18

DN
DP
ML
M
19

PLATE 9

EXPLAN TION O FIGURE

20 Nucleus of oocyte in follicle with a flat granulosa cell layer The large nucleolus consists, as in figures 18 and 19 of a large central area and an irregular dense peripheral region. At this higher magnification the structure of these two areas may be better visualized. Figure 20b is a portion of the lighter central area nd hows the dense granules. Some of the larger granules may be composites of 2 to 4 smaller granules. A few very small vesicular forms and very fine fibrils lying between the granules re visible I figure 20c the predominance f fibrillar structures with fewer granules, may be noted The nucleoplasm (20a) around the nucleolus shows fine irregular fibril with a few granules attached t some of them these elements representing the chromatin. Figure 20a, × 48 400. Figures 20b and × 96,800. Araldite. Lead citrate


20a
OP

An Electron Microscope Study of the Development of the Somatic Muscle of the Chick Embryo [1]

D. A. DESSOUKY AND RICHARD G. HIBBS
Department of Anatomy, Tulane University School of Medicine, New Orleans, Louisiana

ABSTRACT Somites 16 through 18 were obtained from chick embryos from 36 hours to 15 days incubation, and prepared for both light and electron microscopy. It was found that the myoblasts in the early stages increase in size and become elongated. Myofilaments of two types are first discernible in the peripheral cytoplasm in the 32 somite stage. Those of one type are about 100 Å in diameter and are probably myosin while the others are approximately 70 Å and are believed to be actin. These filaments are organized into bundles (myofibrils) which are from the first striated. Throughout later development recognizable myofibrils are present; alongside are found numerous myofilament bundles in all stages of development indicating continuous myofibril formation. Smooth-surfaced vesicles and tubules become the main constituent of the sarcoplasmic reticulum. Free ribosomes numerous at first, take up positions around the developing filament bundles and decrease in number as the myofilaments are formed. At the time of appearance of the first myofilaments glycogen granules become visible in the sarcoplasm and increase rapidly in number. The mitochondria become arranged between the developing myofibrils.

The differentiating skeletal muscle fiber has been extensively studied by many early investigators, although their findings have not always been in agreement. Controversies have arisen involving such basic features of skeletal muscle development as the multicellular versus the unicellular origin of the muscle fiber, the appearance of striation, the role of the different cytoplasmic organelles in the differentiation of the muscle fiber, etc., which have not yet been resolved.

The literature on the subject is confusing, and an attempt at impartial assessment of it leads to two conclusions. First, it is apparent that the material used in many instances has been insufficient in amount, and the available histological techniques have been inadequate for a solution of the problem. Second, it is now apparent that this is an area of research for which the light microscope has been inadequate. The resolving power of the instrument is too low for the visualization of such minute structures as the developing myofibril. Investigators have therefore had to rely largely on tissue-staining properties and, frequently, on their own imagination to identify cell membranes, cytoplasmic filaments and other fine structures which could barely be detected in their histological preparations. Because of inadequate techniques and instruments, many of the early theories could not be proved or refuted, and by the middle of the present century interest in skeletal muscle differentiation began to decline.

The introduction of electron microscopy into cytological research, together with the recent advances in light microscopic techniques such as tissue culture and radioautographic techniques, have reawakened the interest of cytologists in these unsolved problems of skeletal muscle differentiation. The advances in biochemical techniques and the correlation between the morphology and the biochemistry of various cellular constituents have increased our knowledge of the processes leading to cell differentiation and development.

In the present work, the process of skeletal muscle differentiation in the chick embryo has been studied, combining light and electron microscopy. An attempt has been made to determine the changes occurring in the mesodermal cells of the myotomes during their differentiation into the definitive muscle fiber.

[1] This work was supported by N.I.H. Grant 5T1-GM-783 and U.S.P.H.S. Grant H2490 and Career development award 1-K3-GM 18-281-03.
Present address: Department of Anatomy, Georgetown University School of Medicine and Dentistry, Washington, D. C.

MATERIALS AND METHODS

Fertilized chicken eggs were incubated at 103 F for periods of 36 hours to 15 days. The age of the embryos was determined by their somite number until the fourth day of incubation After this stage incubation time alone was used.

Embryos from the following stages were used

16 somite stage	(approximately 36 hours)
20 somite stage	(approximately 48 hours)
26 somite stage	(approximately 60 hours)
32 somite tage	(pproximately 72 hours)
36 somite stage	(approxim tely 78 hours)
40 somite tage	(approxim tely 84 hours)
42 to 44 somites	(approximately 96 hours)
5 day stage	
6 d y stage	
7 day stage	
10 day stage	
15 d y stage	

The embryos were removed from the eggs and dissected in warm Ringer s solu tion One-half of the embryo was used for electron microscopy and the other half for light microscopy In the early stages whole embryos were used for light microscopy For electron microscopy somites 16–18 were in each case fixed in cold (1 C) phosphate-buffered 1% osmium tetroxide (Millonig '62) dehydrated rapidly in graded alcohols and embedded in a cardolite-maraglas mixture (Freeman and Spurlock, 62)

The blocks were sectioned with a Porter Blum *Ultramicrotome* at approximately 0 05 µ using glass knives The sections were mounted unsupported on 300–400 mesh copper grids Some sections were stained with lead hydroxide (Dalton '60) An RCA EMU 3 C electron microscope was used for examining the sections

Tissues for light microscopy were fixed in Bouin s solution, embedded in paraffin and sectioned at 6 µ. The sections were stained with Heidenhain iron hematoxylin and counter-stained with van Gieson stain

OBSERVATIONS

16 somite stage (approx 36 hours)

Light microscopy (fig 1) The somites consisted of masses of closely packed elongated cells whose cytoplasm appears mottled and the cell membranes were difficult to discern. The nuclei were oval in shape and centrally located in the cell Some nuclei showed some clumping of chromatin, while others were vesicular in appearance. Each nucleus contained one or more prominent nucleoli. Mitotic figures were occasionally encountered.

Electron microscopy The cell membranes of the myoblasts were discontinuous in some areas, being replaced by rows of small vesicles (fig. 5) The endoplasmic reticulum consisted of a few smooth surfaced vesicles, and of membranous profiles studded with ribosomes. The cytoplasm also contained numerous small clusters of free ribosomes.

Mitochondria of various shapes were present in moderate numbers and were randomly distributed throughout the cytoplasm Their average diameter was 1.3 µ

The nuclei were limited by double membranes and contained numerous, evenly dispersed chromatin granules. One or more nucleoli were present in each nucleus

The Golgi material consisted of flattened vesicles and of vacuoles of various sizes located near the nuclear poles (fig. 5).

No filaments were discernible in the cytoplasm at this stage

20 somite stage (approx 48 hours)

Light microscopy (fig 2) The somite cells of this stage were larger than those of the 16 somite stage but showed no other remarkable changes.

Electron microscopy The cells at this stage were similar to those of the 16 somite stage However the mitochondria were present in somewhat greater numbers and the endoplasmic reticulum was more prominent (fig 6)

26 somite stage (approx 60 hours)

Light microscopy (fig 3). The myotome plate was first recognizable at this stage The myoblasts were elongated and closely applied to each other The cytoplasm was more abundant than in the previous stage and the cell membranes were still difficult to discern. The nuclei were larger and more elongated than those of the previous stage and were vesicular in appearance and the nuclear membranes were well defined Mitotic figures were seldom encountered

Electron microscopy The cell membranes were convoluted and the cyto-

plasmic membrane of each myoblast interdigitated with those of its neighbors (fig 8) The cytoplasmic membranes were discontinuous in places and the gaps were bridged by rows of small vesicles (fig 7)

The sarcoplasmic reticulum consisted of numerous vesicles of various shapes and sizes, mainly of the smooth-surfaced variety. Clusters of free ribosomes were present throughout the cytoplasm (fig 8)

The mitochondria were randomly distributed throughout the cytoplasm and were found either singly or in small clusters. They were similar in shape and size to those of the previous stage. The Golgi apparatus appeared unaltered.

32 somite stage (approx. 72 hours)

Light microscopy (fig. 4) The myoblasts were oriented parallel to the long axis of the embryo The cytoplasm was abundant and contained a number of rod-shaped bodies, some of which were sharply angulated. With iron hematoxylin these bodies stained a deep brown in contrast to the diffuse yellow color of the rest of the cytoplasm.

Electron microscopy The sarcoplasmic reticulum consisted of vesicles of various sizes most of them larger than those encountered in the previous stages. Many of these vesicles were located near the cell membrane and were often in direct contact with it Clusters of free ribosomes were present throughout the cytoplasm.

Small bundles of filaments varying in diameter from 0 15 to 0 4 μ were present in the peripheral cytoplasm, some of them closely applied to the cell membranes (fig 9). Some of these filament bundles were crossed by dense lines somewhat resembling Z bands (figs. 10–12) Each of the filaments composing these bundles measured 60 Å to 70 Å in diameter

Bundles, consisting of filaments of about 100 Å diameter and those consisting of both sizes of filaments were encountered in the peripheral cytoplasm also (figs. 10–12) None of these bundles show any cross-striation. Single filaments of various diameters were also present in the cytoplasm (figs 9 10)

Glycogen particles in varying numbers were distributed throughout the cytoplasm (figs 9 12) They appear as electron dense granules 150 Å to 500 Å in diameter arranged singly or in groups. They were larger and more electron dense than the ribosomes

Cells of a different variety were encountered in association with the myoblasts at this stage They possessed cytoplasmic processes and contained a large amount of rough-surfaced endoplasmic reticulum and numerous clusters of free ribosomes (fig 13) No myofilaments or glycogen granules were seen in these cells

36 somite stage (fig 14)

The light microscopic preparations were indistinguishable from those of the previous stage.

Electron microscopy Filament bundles were more numerous and of larger diameter than earlier (fig 18) In some instances bundles of filaments could be traced through one or more sarcomeres. The Z, A and I bands were often discernible although they were not uniform in appearance The Z bands consisted of minute filaments smaller in size than the thin filaments just described which appear as tiny granules when seen in cross section (figs 19 20) The I bands consisted of filaments 60 Å to 70 Å in diameter which continued into the adjacent A bands where they interdigitated with the 100 Å filaments (fig 19) Some of these bundles were acutely angulated at the level of the Z bands.

Flattened vesicles of sarcoplasmic reticulum were often seen in close association with and paralleling the Z bands (figs. 18 19) Golgi vesicles were present at the nuclear poles.

40 somite stage (approx 84 hours)

Light microscopy (fig. 15) The cytoplasm of the myoblasts contained larger numbers of wavy dark-staining fibrils up to 2 μ in length Most of these fibrils were located in the peripheral part of the cell The cytoplasm, especially that near the nucleus was homogenous and light staining The nuclei were oriented parallel to the long axis of the myoblast, and occasionally two or more nuclei were seen in one cell No mitotic figures were observed

Electron microscopy Vesicles of sarcoplasmic reticulum were present through-

out the cytoplasm but these vesicles were larger and fewer in number than in earlier stages. Many of these vesicles were in relation to and flattened in a plane parallel to the Z bands as in the *previous stage*.

Clusters of ribosomes were found throughout the cytoplasm, *especially* around the developing fibrils (fig. 22).

More filament bundles were present than in the previous stage. Some bundles were less than one sarcomere in length while others were in the form of myofibrils of three or more sarcomeres. These myofibrils varied in diameter from 0.2 μ to 0.4 μ and the sarcomeres varied from 1 μ to 1.6 μ in length. Both 70 Å and 100 Å filaments were prominent. Single short filaments were *still* encountered free in the cytoplasm. Most of the mitochondria were more centrally located although some were found between the developing myofibrils (figs. 21, 22).

96 hour stage

Light microscopy (fig. 16). Recognizable muscle fibers were present at this stage, and were oriented parallel to each other and to the long axis of the embryo. A number of myofibrils occupied the peripheral area of each fiber. Lighter staining, small myofibrils were encountered deeper in the fiber. A few cells containing small dense nuclei were present between the muscle fibers.

Electron microscopy. The myofibrils were longer and less wavy than in the previous stages and could sometimes be traced through several sarcomeres (fig. 23).

The sarcoplasm near the nucleus and between the myofibrils contained accumulations of ribosomes, glycogen granules, sarcoplasmic reticulum and mitochondria (figs. 23, 24).

A longitudinally arranged component of the sarcoplasmic reticulum consisting of irregularly outlined vesicles, was located between the myofibrils (fig. 23); a transverse component consisting of small vesicles and anastomosing tubules was found close to or passing across the myofibrils at the level of the Z bands (fig. 24).

5 days

Light microscopy (fig. 17). Many myofibrils were present in each of the muscle fibers. Small cells of irregular outline were located in the spaces between the muscle fibers. Their nuclei could be easily distinguished from those of the muscle fibers by their smaller size and greater density.

Electron microscopy. The myofibrils were larger in diameter than those of the previous stage. They were peripherally located and occupied a greater portion of the cytoplasm. The sarcomeres, especially those of the large myofibrils, were of more constant length (about 1.4 μ) and the Z, A and I bands were more clearly visible (fig. 25).

The other cytoplasmic elements and the nuclei were similar to those in the previous stage.

The interstitial cells possess more cytoplasmic processes and contain greater quantities of ribosome-studded endoplasmic reticulum. They were characterized by an absence of cytoplasmic filaments and glycogen granules.

6 days

Light microscopy (fig. 26). The most striking feature observed at this stage was the presence of visible transverse striations in some of the myofibrils. These myofibrils consisted of alternate dark and light segments, possibly representing primitive A and I bands. Muscle fibers containing several nuclei were frequently encountered.

Electron microscopy. Many myofibrils of uniform diameter were present in each muscle fiber. Between the myofibrils were clusters of ribosomes and glycogen granules, varying in number from one area to another. Large accumulations of mitochondria, ribosomes and glycogen granules were also found at the nuclear pole in the center of the muscle fiber and immediately under the sarcolemma (figs. 31, 3.)

7, 10 and 15 days

Light microscopy (figs. 27, 28, 29 and 30). During this period, the number of myofibrils continued to increase and the striations became more regular until at 15 days incubation the muscle fibers resembled those of the adult.

Rows of small cells with dark-staining nuclei resembling fibroblasts were present in the interstitial spaces between the muscle fibers.

Electron microscopy (figs. 33 34 35 36 and 37) The myofibrils became less wavy and more regularly oriented. The spaces between the myofibrils, in which were found clusters of ribosomes, glycogen granules, and mitochondria, decreased in size as the myofibrils encroached upon them. Filaments making up the myofibrils increased in number and became more closely packed as the myofibrils grew in diameter. The H and M bands became more distinct and all of the myofibrils of each muscle fiber became transversely aligned so that the various striations could be traced across the entire fiber

Almost no change was detected in the Golgi apparatus during this period.

The interstitial cells elongated and became more closely applied to the muscle fibers (figs. 36, 37) They sent long thin cytoplasmic processes between the muscle fibers.

DISCUSSION

Origin of myofilaments

Some authors (Meves, '09 Duesberg '10 and Naville '22) believed that mitochondria transform directly into myofibrils. Weed ('36) however found a change in the staining properties of mitochondria at the time of appearance of the myofibrils but she did not find a direct transformation of mitochondria into myofibrils. Conklin ('31) found that myoblasts could still produce myofibrils after the removal of mitochondria by centrifugation.

No direct transformation of mitochondria into myofibrils has been observed in this study although mitochondria have been seen to line up in rows between the developing myofibrils. This is in agreement with the findings of van Breemen ('52) Frost ('54) Hibbs ('56) Meyer and Queiroga ('59) and Allbrook ('62) in their electron microscope studies on the developing skeletal muscle. Since this occurs at the time the myofibrils are first becoming visible by electron microscopy it is probably a passive alignment; the mitochondria are simply pushed aside to make room for the developing myofibrils so that they become mechanically oriented with their long axes parallel to those of the myofibrils. This could easily have been mistaken for evidence of direct transformation by many investigators, since the myofibrils at this stage are not visible with the light microscope The mitochondria, however may be indirectly involved by providing the energy needed for the synthesis of myofilaments. It is known that mitochondria are the site of oxidative phosphorylation reactions in which energy stores are built up.

The nuclei of the developing muscle fibers have been observed by MacCallum (1898) Cameron ('17) Naville ('22) Katznelson ('34) Weed ('36) and others to increase gradually in size and come to occupy a central position in the fiber They are characterized by their evenly dispersed chromatin and prominent nucleoli. These features have been correlated by Weed and other light microscopists with the appearance of the first myofibrils No such correlation can be made on the basis of the present observations. No evidence of direct transformation of nuclear or nucleolar material (Franz, 15 and Cameron, 17) or centriolar material (Wolbach, '28) into myofibrils has been found in this study

Other investigators believed that myofibrils arise from cytoplasmic granules which become aligned in rows parallel to the long axis of the cell and fuse (Godlewski, '02 McGill, '07 Weed, '36 and Moscona, '55)

Weed ('36) believed that the myofibrils arise at the expense of certain cytoplasmic granules which are distinguishable from mitochondria. Suggesting that the myofibrils are produced in a way similar to that by which secretory materials are elaborated she compared the developing muscle cells to secretory cells on the basis of their large nuclei and prominent nucleoli. In muscle however the products are not eliminated from the cell as in the case of glandular cells but are retained as part of the cell. She did not exclude however the possible involvement of mitochondria in fibrillogenesis since they change in shape, staining reactions and number as the myofibrils appear Moscona ('55) also believed that the myoblasts contain cytoplasmic granules 0 8–2.2 μ in diameter which consist of RNA and polysaccharides and differ from mitochondria in their staining reactions. He stated that these granules de-

creased in number and became smaller as the myofibrils appeared.

The only cytoplasmic granules observed in the present study were ribosomes (Palade, '55 and Siekevitz and Palade, '58) and glycogen granules (Fawcett and Selby '58 and Bergman, '60) both of which are too small to be resolved by the light microscope and thus cannot be the granules seen by these earlier investigators However the myofilament bundles de scribed above in the early myoblasts are *large enough to be seen with the light* microscope. Therefore, the granules re ported by early investigators to line up in rows as the early myofibrils appear could be such myofilament bundles. However the possibility also exists that these granules were mitochondria. Another possibility is that these granules were masses of ribosomes which could have arisen by the clumping action of the fixatives used in preparation of the tissue.

Heidenhain (11) proposed that myofibrils arise from submicroscopic particles that come together to form fibrils which can be resolved by the microscope. Van Breemen ('52) supported Heidenhain's view and proposed that the filaments are formed by a condensation of cytoplasmic material, and later aggregate to form loose bundles. Polymerization of submicroscopic elements has been suggested also by Porter ('54) from his electron microscope studies on the amphibian myoblast. Godman's observations ('57) on regenerating adult muscles *in vivo* led him to suppose that the fibrils originate from pre-existing submicroscopic protofibrils which gradually aggregate into cables of sufficient size to be visible microscopically Hibbs ('56) found that the myofibrils arise from the aggregation of fine myofilaments which seem to be synthesized in the cytoplasm in an unknown manner

The large nuclei, prominent nucleoli, *abundant free ribosomes* and *smooth* surfaced ER indicate that the myoblasts are actively involved in protein synthesis The use of radioactive isotopes to trace protein formation has demonstrated that newly *synthesized proteins first appear in* association with the ribosomes. Siekevitz and Palade ('58 '60) suggested that proteinaceous enzymes produced by the pancreatic acinar cells are synthesized on the ribonucleoprotein particles attached to the endoplasmic reticulum and move through the channels of the reticulum into the Golgi complex where the zymogen granules are formed. This hypothesis has been partly confirmed by radioautography (Caro, '61) *Actively growing cells in the act of* synthesizing intracellular protein, however contain more free ribosomes than glandular cells and less granular endoplasmic reticulum (Slautterback and Fawcett, '59). *The present study shows that free ribo*somes are abundant in the cytoplasm of the myoblasts before the myofilaments appear Later they become oriented pref
entially around the developing myofib
and in close proximity to the newly form
myofilaments. As the number of myofi
ments increases, the number of free ri
somes decreases, so that in advanc
stages of development they are found o
at the nuclear poles and under the sar
lemma while the rest of the sarcoplasm
almost devoid of ribosomes. Bergm
('62) believed that a dense variety of R
granules (70 A to 250 A in diameter) a
present near the A bands and are respon
ble for myosin filament synthesis while
less dense variety (70 A to 189 A) a
found near the I bands and are responsib
for the synthesis of actin filaments. In t
present study ribosomes of different siz
and densities were seen in relation to th
developing myofilaments but no relatio
ship between their density or size and th
type of myofilament in their vicinity wa
noted. Other electron microscopists (Sh
and Ikemoto '57 Siro and Kobayashi, '60
Edward and Challice '58 Allbrook, '62
Hay '63 and Shafiq '63) stressed th
close association between the ribosome
and the developing myofilaments and th
possibility that ribosomes are directly in
volved in myofilament synthesis. The pres
ent observations show that there is a posi
tional relation between the free ribosome
and the myofilaments and suggest that the
myofilaments are synthesized at the ex
pense of the ribosomes.

Formation of myofibrils

Hibbs ('56) stated that in cardiac mus
cle, myofilaments running in various di
rections in the cytoplasm aggregate to

form loosely arranged wavy bundles Those bundles from their first appearance are associated with Z band material which may act as a binding material to hold the myofilaments together They later become more straight and are recognizable as myofibrils Bergman ('62) states "Independent foci of synthesis of A and I band material were observed in the longitudinal plane, in the form of portions of separate myofilaments. This early stage appeared to be followed by the sequential synthesis and registration of the myofilaments to form A and I bands. Subsequently myofibrils appeared to be formed by the synthesis of additional myofilaments in both the longitudinal and transverse planes.

Hay ('63) on the other hand, stated that the first detectable filaments synthesized in the cytoplasm of myoblasts are not necessarily present as organized myofibrils, but may be scattered throughout the cytoplasm. She also stated that the initial stage of myofibril formation may in some cases consist of a coalescence of the disorganized clumps of myofilaments and Z bands in longitudinal array to form primitive sarcomeres of variable length

In light microscopic preparations rod-shaped bodies and angulated fibrils are seen in the cytoplasm of early myoblast. This is followed shortly by the appearance of long wavy myofibrils, which vary in length and in diameter The fact that the first formed myofibrils are wavy in light microscope sections of 6 μ in thickness may explain the presence of separate short bundles of filaments in the much thinner section prepared for electron microscopy since in sections 0 03–0 05 μ in thickness such myofibrils would not be found in the plane of section for any great distance. From these observations it is suggested that the short myofilament bundles are in fact parts of long myofibrils following undulating courses within the cells.

There has been considerable disagreement as to the sequence of appearance of the various types of myofilaments. Porter ('54) found that actin filaments appear before myosin filaments Siro and Ikemoto ('57) and Siro and Kobayashi ('60) believed that one type of filament appeared before the other They did not mention however which type appeared first. Ferris ('59) described the simultaneous appearance of thick and thin filaments in developing chick muscle Lindner ('61) is also of the opinion that actin and myosin filaments appear simultaneously in developing chick hearts. Bergman ('62) in studies on rat skeletal muscle and Hay ('63) in studies on salamander skeletal muscle were in agreement with this concept.

The present study indicates that both thick (myosin) and thin (actin) filaments are synthesized simultaneously in their definitive positions in the myofibrils. New myofilaments are later synthesized and added to the existing bundles increasing their diameters. At the same time the filaments increase in length and become more closely applied to each other This is for the most part in agreement with the conclusions of Hibbs in his studies on developing chick myocardium and Bergman in studies on the development of rat skeletal muscle

The process by which the myofibrils increase in number has been a subject of controversy for many years. The view of Heidenhain ('13) Godlewski ('02) Eycleshymer ('04) McGill ('07) Duesberg ('10) Naville ('22) Katznelson ('34) Weed ('36) van Breemen ('52) and others is that the myofibrils increase in number by longitudinal splitting Hibbs ('56) believed that new myofibrils are synthesized from cytoplasmic elements in the same way as the first. The present study favors the latter idea.

There has been a great deal of disagreement also as to the time and sequence of the appearance of the various striations Some investigators believed that striations were present in the cytoplasm before any fibrils were formed (Cameron, '17; Lewis '19 and Naville '22) Others, however were of the opinion that the appearance of striations is concomitant with the appearance of myofibrils (MacCallum 1898; and Wieman, '06) The opinion held by many workers among whom were Bardeen ('00) Godlewski ('02) Duesberg ('10) Weed ('36) and Holtzer ('60) was that the first myofibrils were homogenous and only later in development did cross-striations appear Siro and Ikemoto ('57) believed that the Z band is formed before the ap-

pearance of the myofilaments and that the A and I bands appear later Hibbs ('56) believed that the Z band appears concurrently with or shortly after the first bundles, followed by the laying down of the A substance. The Z, A and I bands were believed by Schulze ('61 and '62) to appear simultaneously followed later by H and M bands while Bergman ('62) and Hay ('63) believed that all bands appear at the same time.

It is now known that striation or banding is due to the characteristic distribution of the different types of filaments which make up the myofibrils (Hanson and Huxley '53a, b Hanson, '56 Huxley '53 '57; and Huxley and Hanson, '54 '59) The A bands consist of both thick and thin filaments the I bands of only thin filaments and the Z bands of extremely fine filaments, several of which are attached to each I band filament at its point of contact with the Z band (Knappeis and Carlsen, '62) These striations are by their very nature necessarily present as soon as the filaments are organized into myofibrils. There can be no stage in which unstriated myofibrils exist as described by Bergman ('62) and others.

MacCallum (1898) and Wieman ('06) stated that the Z and A bands are formed from the cytoreticulum. This cytoreticulum referred to by early workers on the basis of light microscopic studies is not to be confused with the endoplasmic reticulum seen in electron microscopic preparations. The cytoreticulum consists of a meshwork of cytoplasmic strands visible in light microscopic preparations. Its electron microscopic counterpart is not known but it possibly consists of a combination of myofilaments and other cytoplasmic proteins which have become clumped together during tissue preparation into strands large enough to be seen with the light microscope

The M bands were visible in our preparation only after five days incubation. The M band which appears as a dense line bisecting the H band consists of localized thickenings of the myosin filaments. It was not possible from this study to determine the nature of the M bands. Whether they are actual thickenings of the myosin filaments or localized accumulations of some other material on these filaments was not discernible

The way which the striations of adjacent myofibrils become aligned transversely is not known, but the transverse component of the sarcoplasmic reticulum by its continuity across the entire muscle fiber may play a role in binding the adjacent myofibrils together at the level of the Z bands.

Mitochondria

Mitochondria of various shapes and sizes were observed in the myoblasts of all stages. The number of mitochondria increases rapidly at first. Later after the myoblasts have increased in size the number of mitochondria increases more slowly. They seem to be closely associated with myofilament synthesis since they are preferentially located in those areas where the myofilaments are being formed. Later, however they lie adjacent to and between the myofibrils either singly or in small groups becoming passively oriented with their long axes parallel to the myofibrils between which they are located. No prominent structural changes have been observed in the mitochondria from one stage to another and it is believed that mitochondria play only an indirect role in the myofibril synthesis. This is in agreement with Bergman's findings in his study on rat skeletal muscle.

The Sarcoplasmic reticulum

Prominent changes were observed in the sarcoplasmic reticulum during muscle differentiation. In the early stages of development, the sarcoplasmic reticulum consists of smooth-surfaced vesicles together with a few ribosome-studded membranous profiles scattered throughout the sarcoplasm. There is a gradual increase in the smooth sarcoplasmic reticulum with a decrease in the number of the ribosome-studded vesicles. As the first myofilament bundles appear some of the smooth-walled vesicles come into close approximation to the Z bands where some of them become flattened and appear as tubular profiles passing across the myofibrils. As the number of the myofibrils increases, rows of elongated vesicles are observed paralleling the myofibrils. These vesicles become more and more elongated as the myofibrils

proach each other thus, a longitudinal component of interconnected flattened vesicles as well as a transverse component is present early in the developing muscle fiber. As transverse alignment of the myofibrils becomes apparent, the transverse component of the reticulum can be seen to better advantage passing across several myofibrils to the sarcolemma. This arrangement of the two components of sarcoplasmic reticulum is similar to that described in adult skeletal muscle by Porter ('58 '61) Edwards et al. ('56) Bennett ('55, '56 '58) Porter and Palade ('57) Nelson and Benson ('63) and others.

Other cytoplasmic structures

The appearance of glycogen granules in late myoblasts has been described by Bergman ('62) Shafiq ('63) and Hay ('63) In the present study glycogen granules could be seen in the early myoblasts. They were distributed irregularly throughout the sarcoplasm at first, but later became situated between the myofibrils, at the nuclear poles and under the sarcolemma in association with mitochondria and ribosomes The significance of the presence of glycogen granules in early myoblasts which are not yet capable of contraction is unknown.

Golgi material has been observed consistently in one or more locations around the nucleus. No changes in its structure or distribution which can be correlated with the progressive developmental events occurring during muscle differentiation were observed. Thus the role of the Golgi complex in the process of skeletal muscle development is still completely unknown.

Multinucleation

Many investigators working with fixed tissue preparations (Remak, 1845; Bardeen, '00 Naville, '22 and Weed, '36) and with tissue culture preparations (Chevremont, 40 Pogogeff and Murray '46, and Godman, '55 '57) believed that multinucleation was produced by some sort of nuclear division without subsequent cytoplasmic division. Another group of investigators believed that the multinuclear skeletal muscle fiber was the result of fusion of a number of early myoblasts. Among those were Schwann (1838) Heidenhain (1899 '11) and Eycleshymer ('04) working with fixed tissue preparation; and Lash et al ('57) Holtzer ('60) Konigsberg et al. ('60) Capers ('60) and Stockdale and Holtzer ('61) working with tissue culture preparations. Further evidence in support of the multicellular or fusion theory of multinucleation came from radioautographic studies on skeletal muscle regeneration by Bintliff and Walker ('60) and from electron microscope studies on the developing skeletal muscle by Hay ('61 '63) Bergman ('62) and Shafiq ('63)

In this study the plasma membranes of the early myoblasts were discontinuous in some areas but well-defined in others The regions of discontinuity were occupied by rows of small vesicles. Later in development vesicles gradually decrease in number until they are encountered only in the least differentiated cells. It appears that the cytoplasmic membranes break up into vesicles which later disappear leaving cytoplasmic continuity between adjacent cells. This may account for the multinucleation of the mature muscle fibers. These observations and findings agree with those of Bergman ('62) Hay ('63) and Shafiq ('63)

Interstitial cells

The cells described here as interstitial cells appear fairly early in development and are closely associated with the myoblasts. They can be distinguished from myoblasts by their irregular boundaries and their greater content of rough-surfaced endoplasmic reticulum They increase in number as development progresses and are located between the developing muscle fibers. Because of their mesodermal origin, their position in relation to the muscle fibers and their morphology it seems likely that these cells are embryonic fibroblasts. These cells have been described by Bergman ('62) and Hay ('63) without comment as to their eventual fate

LITERATURE CITED

Allbrook, D. 1962 An electron microscopic study of regenerating muscle. J Anat. (Lond.) 96 137–152.

Bardeen, C. R. 1900 The development of the musculature of the body wall of the pig, including its histogenesis and its relations to the myotomes and to the skeletal and nervous apparatus. Johns Hopkins Hosp. Rep., 9 367–399.

pearance of the myofilaments and that the A and I bands appear later Hibbs ('56) believed that the Z band appears concurrently with or shortly after the first bundles, followed by the laying down of the A substance. The Z, A and I bands were believed by Schulze ('61 and '62) to appear simultaneously followed later by H and M bands while Bergman ('62) and Hay ('63) believed that all bands appear at the same time

It is now known that striation or banding is due to the characteristic distribution of the different types of filaments which make up the myofibrils (Hanson and Huxley '53a b; Hanson, '56 Huxley '53 '57; and Huxley and Hanson, '54 '59) The A bands consist of both thick and thin filaments the I bands of only thin filaments, and the Z bands of extremely fine filaments, several of which are attached to each I band filament at its point of contact with the Z band (Knappeis and Carlsen, '62) These striations are by their very nature necessarily present as soon as the filaments are organized into myofibrils. There can be no stage in which unstriated myofibrils exist as described by Bergman ('62) and others

MacCallum (1898) and Wieman ('06) stated that the Z and A bands are formed from the cytoreticulum. This cytoreticulum referred to by early workers on the basis of light microscopic studies is not to be confused with the endoplasmic reticulum seen in electron microscopic preparations. The cytoreticulum consists of a meshwork of cytoplasmic strands visible in light microscopic preparations. Its electron microscopic counterpart is not known but it possibly consists of a combination of myofilaments and other cytoplasmic proteins which have become clumped together during tissue preparation into strands large enough to be seen with the light microscope

The M bands were visible in our preparation only after five days incubation. The M band which appears as a dense line bisecting the H band consists of localized thickenings of the myosin filaments. It was not possible from this study to determine the nature of the M bands. Whether they are actual thickenings of the myosin filaments or localized accumulations of some other material on these filaments was not discernible.

The way which the striations of adjacent myofibrils become aligned transversely is not known but the transverse
of the sarcoplasmic reticulum by its continuity across the entire muscle fiber may play a role in binding the adjacent myofibrils together at the level of the Z bands.

Mitochondria

Mitochondria of various shapes and sizes were observed in the myoblasts of all stages. The number of mitochondria increases rapidly at first. Later after the myoblasts have increased in size, the number of mitochondria increases more slow They seem to be closely associated with myofilament synthesis since they are preferentially located in those areas where the myofilaments are being formed. Later, however they lie adjacent to and between the myofibrils either singly or in small groups becoming passively oriented with their long axes parallel to the myofibrils between which they are located. No prominent structural changes have been observed in the mitochondria from one stage to another and it is believed that mitochondria play only an indirect role in the myofibril synthesis. This is in agreement with Bergman's findings in his study on rat skeletal muscle

The Sarcoplasmic reticulum

Prominent changes were observed in the sarcoplasmic reticulum during muscle differentiation. In the early stages of development, the sarcoplasmic reticulum consists of smooth-surfaced vesicles together with a few ribosome-studded membranous profiles scattered throughout the sarcoplasm There is a gradual increase in the smooth sarcoplasmic reticulum with a decrease in the number of the ribosome-studded vesicles. As the first myofilament bundles appear some of the smooth-walled vesicles come into close approximation to the Z bands where some of them become flattened and appear as tubular profiles passing across the myofibrils. As the number of the myofibrils increases rows of elongated vesicles are observed paralleling the myofibrils. These vesicles become more and more elongated as the myofibrils ap

—— 1957 The double array of filaments in cross-striated muscle. J Biophys. Biochem. Cytol., 3 631–648.

Huxley H. E. and J. Hanson 1954 Changes in the cross-striations of muscle during contraction and stretch and their structural interpretation. Nature 173 973–976.

—— 1959 The structural basis of the contraction mechanism in striated muscle. Ann. N.Y. Acad. Sc., 81 403–408.

Knappeis, G. G., and F. Carlsen 1962 The ultrastructure of the Z disc in skeletal muscle. J Cell Biol., 13 323–335.

Konigsberg, I. R. N. McElvain, M. Tootle and H. Herrmann 1960 The dissociability of deoxyribonucleic acid synthesis from the development of multinuclearity of muscle cells in culture. J. Biophys. Biochem. Cytol., 8 333–343.

Lash, J., H. Holtzer and H. Swift 1957 Regeneration of mature skeletal muscle. Anat. Rec., 128 679–693.

Lewis, M. R. 1919 The development of cross-striations in the heart muscle of the chick embryo. Bull. Johns Hopkins Hosp., 30 176–181

Lindner, E. 1960 Myofibrils in the early development of chick embryo hearts as observed with the electron microscope. Anat. Rec., 136 234–235.

MacCallum, J. B. 1898 On the histogenesis of the striated muscle fiber and the growth of the human sartorius muscle. Johns Hopkins Hosp. Bull., 9 208–215.

McGill, C. 1907 The histogenesis of smooth muscle in the alimentary canal and respiratory tract of the pig. Internat. Mschr. Anat. u. Physiol. 24 209–245.

—— 1910 The early histogenesis of striated muscle in the oesophagus of the pig and the dogfish. Anat. Rec., 4 23–47

Meves, F 1909 Über Neubildung quergestreifter Muskelfasern nach Beobachtungen am Hühnerembryo. Anat. Anz., 34 161–165.

Meyer, H., and L. T. Queiroga 1959 An electron microscope study of embryonic heart muscle cells grown in tissue culture. J Biophys. Biochem. Cytol., 6 169–170.

Millonig, C. 1962 Further observations on a phosphate buffer for osmium tetroxide solutions in fixation. In: Fifth International Congress for Electron Microscopy Academic Press, Inc., New York, p. 8.

Moscona, A. 1963 Cytoplasmic granules in myogenic cells. Exp. Cell Res., 9 377–380

Naville, A. 1922 Histogenèse et régénération du muscle chez les Anoures. Arch. de Biol., 32 37–171.

Nelson, D. A., and E. S. Benson 1963 On the ultrastructural constituents of the transverse tubular system of rabbit and human myocardial cells. J Cell Biol., 16 297–313.

Palade, G. E. 1955 A small particulate component of the cytoplasm. J Biophys. Biochem. Cytol., 1 59–68.

Pogogeff, I. A., and M. R. Murray 1946 Form and behavior of adult mammalian skeletal muscle in vitro. Anat. Rec., 95 321–335.

Porter K. R. 1956 The sarcoplasmic reticulum in muscle cells of Amblystoma larvae. J Biophys. Biochem. Cytol., 2 (suppl.): 163–170.

—— 1961 The sarcoplasmic reticulum. Its recent history and present status. J Biophys. Biochem. Cytol., 10 (suppl.) 219–226.

Porter K. R., and G. E. Palade 1957 Studies on the endoplasmic reticulum. III. Its form and distribution in striated muscle cells. J Biophys. Biochem. Cytol 3 269–300.

Remak, R. 1845 Uber die Entwicklung der Muskelprimitivbundel. Frorieps Neue Notizen, 35 305–308.

Schulze, W 1962 Electronen mikroscopische untersuchung des embryonalen Hundeherz muskels. Z. mikr Anat. Forsch 68 721

Schwann, T 1847 Microscopical Researches into the Accordance in the Structure and Growth of Animals and Plants. Translated from the German by H. Smith, C. London and J Adlard, printers.

Shafiq S. A. 1963 Electron microscopic studies on the indirect flight muscles of Drosophila melanogaster II. Differentiation of myofibrils. J Cell Biol 17 363–373.

Siekevitz, P and G. E. Palade 1958 A cytochemical study on the pancreas of the guinea pig. III. In vivo incorporation of leucine-1-C^{14} into the proteins of cell fractions. J Biophys Biochem. Cytol., 4 557–566

—— 1960 A cytochemical study on the pancreas of the guinea pig V In vivo incorporation of leucine-1-C^{14} into the chymotripsinogen of various cell fractions. J Biophys. Biochem. Cytol., 7 619–630.

Siro K., and N Ikemoto 1957 Electron microscopy of myogenesis in the Earthworm, Eisenia foetida. Biol. J Takayama Univ 3 239–247

Siro K., and T Kobayashi 1960 Electron microscopic study of the cardiac myogenesis. Biol. J Okayama Univ 6 (1/2) 53–60.

Slautterback, D B., and D. Fawcett 1959 The development of the cnidoblasts of Hydra. An electron microscopic study of cell differentiation. J Biophys. Biochem. Cytol., 5 441–452.

Stockdale, F and H. Holtzer 1961 DNA synthesis and myogenesis. Exp. Cell Res., 24 508–520.

Weed, I. G. 1936 Cytological studies of developing muscle with special reference to myofibrils, mitochondria, Golgi material and nuclei Z. Zellforsch., 25 516–540.

Wieman, H. L. 1906 The relation between the cytoreticulum and the fibril bundles in the heart muscle cell of the chick. Am. J Anat., 6: 191–205.

Wolbach, S. B. 1927 Centrioles and the histogenesis of the myofibril in tumors of striated muscle origin. Anat Rec., 37 255–273

The light micrographs were taken at an initial magnification of $\times 500$ and the electron micrographs t $\times 3{,}500$–$\times 12{,}000$ and were photographically enlarged as required. The following code of labeling was followed throughout:

A, Thin actin filaments	M, Mitochondria
a, A band	m, M Band
ER R, Rough endoplasmic reticulum	MF Myofibril
ER-S, Smooth endoplasmic *reticulum*	Mn, Thick myosin filaments
G Golgi	My Myofilament
Gl, glycogen	*N Nucleus*
h, H band	Nu, Nucleolus
i, I band	R, Ribosomes
	Z, Z band

PLATE 1

EXPLANATION OF FIGURES

1 A transverse section of a somite from a 16 somite embryo as seen with the light microscope. Note the closely packed cells around the myocele, with their centrally located nuclei and prominent nucleoli. $\times 2{,}000$.

2 A transverse section of somite from 20 somite embryo. Note the mottled cytoplasm, $\times 2{,}000$.

3 A section of the myotome plate of 26 somite embryo. Note the developing myoblasts (arrow) with their indistinct cell boundaries. $\times 2{,}000$

4 A section of the myotome of 32 somite embryo. Note the rod-shaped bodies which give the cytoplasm striated appearance (arrows) $\times 2{,}000$.

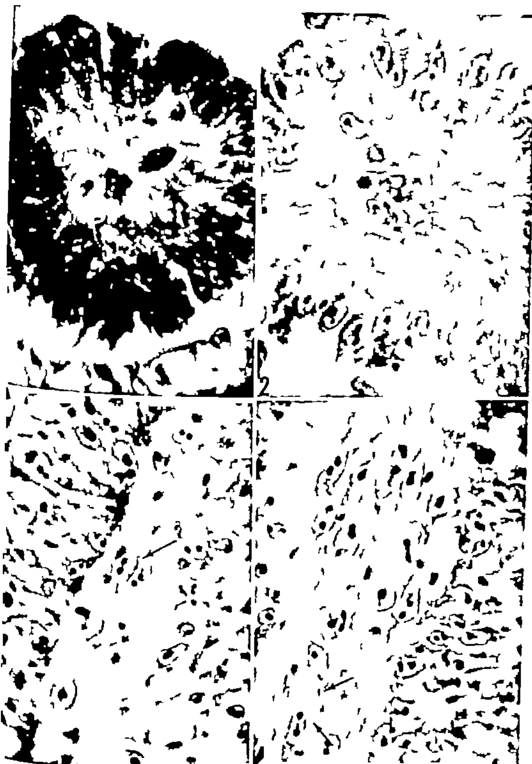

2

PLATE 2

EXPLANATION OF FIGURE

5 An electron micrograph of a number f somite cells from a 18 somite embryo. Note the discontinuities in the plasma membranes which are bridged by rows of small vesicles (arrows) and the close approximation of the cells. × 13,500.



PLATE 3

EXPLANATION OF FIGURE

6 An electron micrograph of a group of myoblasts from a 20 somite embryo. Note the typical Golgi zones (arrows) at the nuclear poles. × 24,000.


N
M
G

PLATE 4

EXPLANATION OF FIGURES

7 A section through a myotome of 26 somite embryo. Note the vesiculation of the plasma membranes and the numerous circular profiles of smooth surfaced endoplasmic reticulum. × 14,000.

8 A section through myotome of 26 somite embryo at higher magnification. Note the interdigitation of adjacent cytoplasmic membranes (arrows) and the abundant endoplasmic reticulum × 19,500.


ER
S
M
R

PLATE 5

EXPLANATION OF FIGURES

9 A section showing parts of adjacent myoblasts of a 33 somite embryo. Note the myofilament bundles especially near to the plasma membranes, some of which are crossed by Z bands (arrows). Single filaments are scattered in other area of cytoplasm, × 14,500.

10 A part of the previon figure t a higher magnification. Note the presence of bundles of thick filaments (Mn) bundles of thin filaments (A) and bundles of mixed filaments, × 28,000.

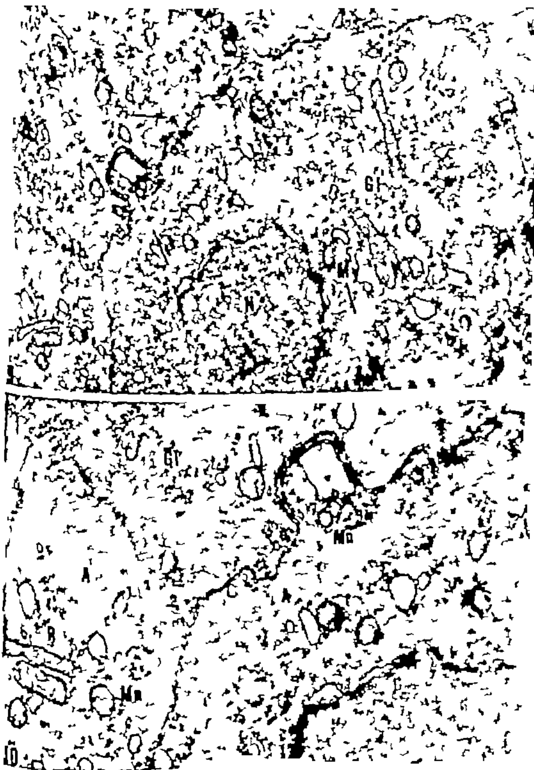

Gl
M
N
Gl
Mo
Ds
A
B
Mo
10

PLATE 6

EXPLANATION OF FIGURES

11 A section of part of a myoblast of 32 somite embryo howing bundles of thick and of thin myofilaments and large sarcoplasmic reticulum vesicles near the cell membrane × 30 000.

12 Parts of adjacent myoblasts of a 32 somite embryo containing thin and thick myofilament bundles and smooth-surfaced sarcoplasmic reticulum profiles, × 34,000

13 A section through the myotome of 32 somite embryo showing part of two early myoblasts and an interstitial cell (arrow) Note the bsence of myofilament bundles and glycogen granules in the inter titial cell, × 11,000.

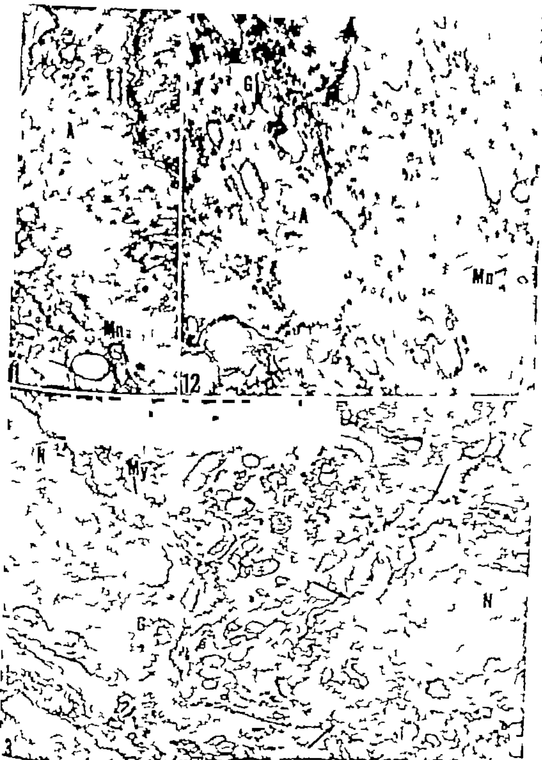

G
A
A
Mn
Mn
11
12
N
My
N
G
13

PLATE 7

EXPLANATION OF FIGURES

14 A section through myotome of 38 somite embryo. Note the abundant cytoplasm, and the large size and vesicular appearance of the nuclei. The cell boundaries are indistinct, × 2,000.

15 A section through myotome of a 40 somite embryo. Note that the nuclei are elongated in direction parallel to the long axis of the myoblast, × 2,000.

16 A section showing a number of myoblasts of a 96-hour embryo. Note the parallel arrangement of the fibers and the long myofibrils in the peripheral cytoplasm. A few small cells with small darker staining nuclei are seen between the fibers (arrows) × 2,000.

17 A section through group of muscle fibers of five day embryo. Note th presence of numerous myofibrils of various lengths and diameters, × 2,000.


14
15
17

PLATE 8

EXPLANATION OF FIGURE

18 A section through group of myoblasts of 36 somite embryo. Note the peripherally located myofilament bundles which run in various directions. The central part of the cells is occupied by clusters of ribosomes, glycogen granules and mitochondria. Flattened vesicles of the endoplasmic reticulum are seen in association with some Z bands (arrow) × 9 600.

19 A section through a myoblast of 36 somite embryo. Note the presence of a myofibril of two sarcomeres which is angulated at the Z band. Note also the flattened vesicles of endoplasmic reticulum situated across the Z band (arrow) Ribosomes and glycogen granules are scattered throughout the central cytoplasm and around the myofilament bundles, × 25,500.

20 A section through part of a myoblast of 38 somite embryo showing an obliquely cut Z band (arrow) Note the presence of transversely cut filaments, × 22,000.

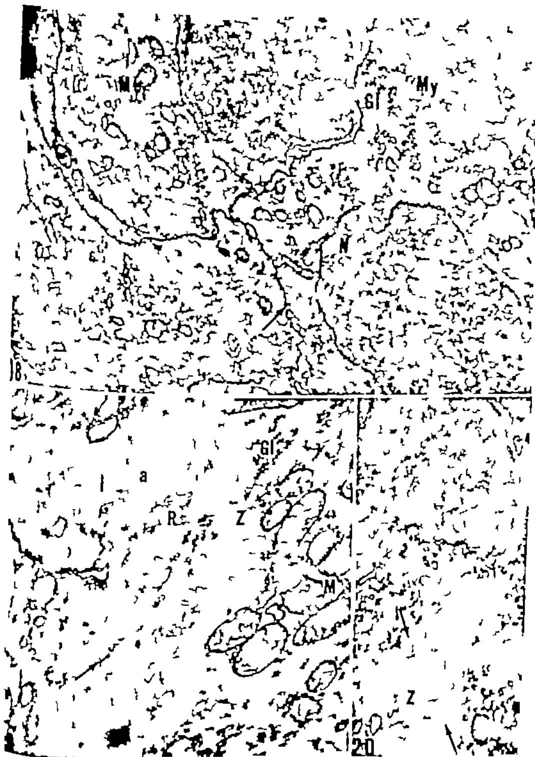

M
My
Gl
N
18
Gl
a
R
Z
M
Z
20

PLATE 9

EXPLANATION OF FIGURES

21 A section of a myoblast of 40 somite embryo. Note the peripheral position of the myofilament bundles pushing the other cytoplasmic constituents more centrally Golgi material is seen near an irregularly shaped nucleus with a nucleolus, × 12,900

22 A section of a myoblast from 40 somite embryo showing myofibril and a number of myofilament bundles encroaching on the central part of the cytoplasm. Large vesicles of smooth endoplasmic reticulum are seen scattered throughout the cytoplasm. Note the transverse component of the endoplasmic reticulum djacent to the Z bands (arrow) × 24,000

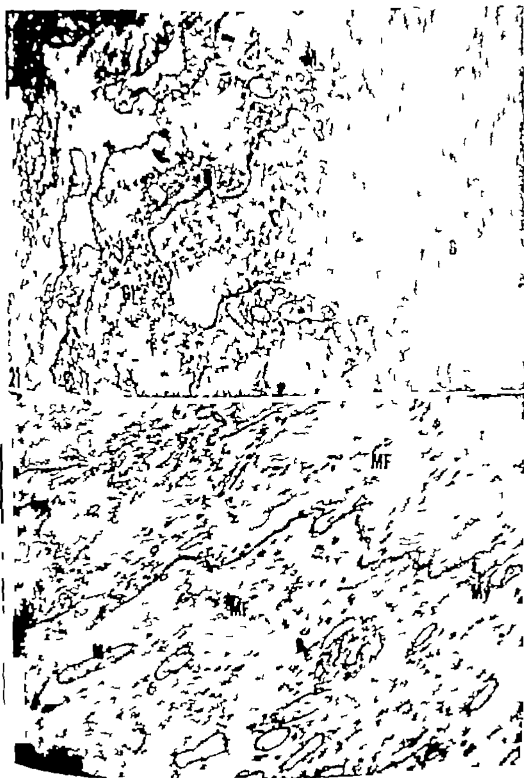

S
GF
21
MF
MF
MF

PLATE 10

EXPLANATION OF FIGURES

23 A section of a muscle fiber of a 96-hour embryo showing three nuclear masses and number of long slender myofibrils. Note the longitudinal arrangement of the sarcoplasmic reticulum between the myofibrils, × 15,500.

24 A section through a part of muscle fiber of a 96-hour embryo. Note longitudinal component of the sarcoplasmic reticulum between the myofibrils, and the transverse component (arrows) paralleling the Z bands. Clusters of ribosomes and glycogen granules can be seen between the myofibrils, × 24,000.


G
R
ER
S
MF
N
MF
R

PLATE 11

EXPLANATION OF FIGURE

25 A section through number of muscle fibers from five-day embryo. Note the well-developed myofibrils with typical striations. Golgi material can be seen at th nuclear pole (arrow) × 20,000.

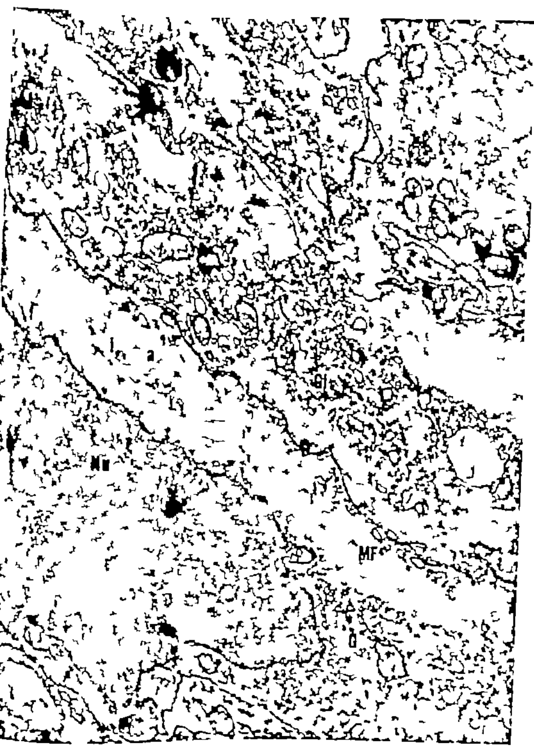

a
Gl
Mi
MF

PLATE 12

EXPLANATION F FIGURES

26 A light microscope section through developing muscle of a six-day embryo. Note the large number of myofibrils in each muscle fiber. A few of the myofibrils show alternate dark and light segments while the majority appear non-striated. Small nuclei are seen between the muscle fibers, × 2,000.

27 A section through developing muscle of a seven-day embryo. Note the parallel arrangement of the fibers, each containing number of myobrils. Note also that in many of the myofibrils striations are visible × 2,000.

28 A section through the developing muscle of ten-day embryo. Note the large number f striated myofibrils together with some on which striations cannot be seen Many small nuclei of interstitial cells an be seen (arrows) × 2,000.

29 A section through developing m scle of a 15-day embryo. Note the large size of the fibers which are filled completely with striated myofibrils. Small oval nuclei of interstitial cells are closely pplied to the muscle fibers (arrows) × 2,000.

30 A transverse section through developing muscle of 15-day embryo. Note the arrangement of the fibers in small groups. Note the myofibrils t the periphery of the fibers, × 2,000.

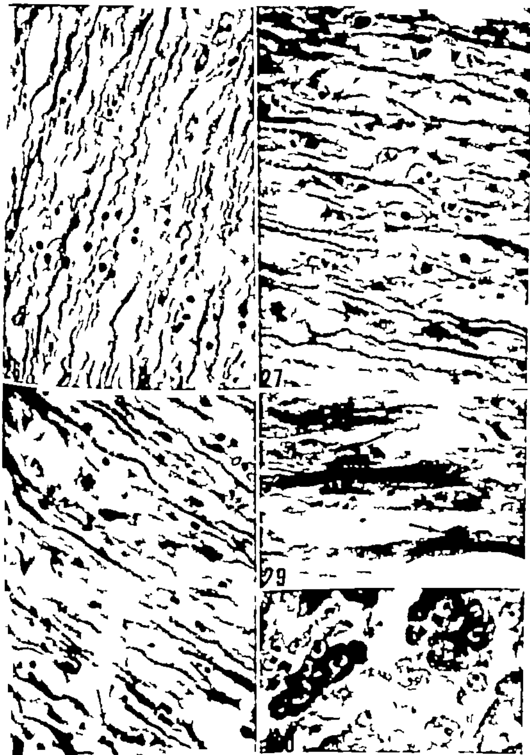

26
27
29

PLATE 13

EXPLANATION OF FIGURES

31 A section through a muscle fiber from six-day embryo. Note the presence of myofibrils in different st ges of development which are separated by varying amounts of sarcoplasm, clusters of ribosomes, glycogen granules and mitochondria × 10,250.

32 A section through developing muscle m t ix-d y embryo. Note the large accumulations of free ribosomes, glycoge granules and mitochondria in the central part of the fiber × 25,000


MF
G
1
M
MF
Gl
1
2

PLATE 14

EXPLANATION OF FIGURE

33 A section through developing muscle of a seven-day embryo. Note the large number of myofibrils in transverse alignment. Longitudinal and transverse components of the sarcoplasmic reticulum can be seen. × 22,000.

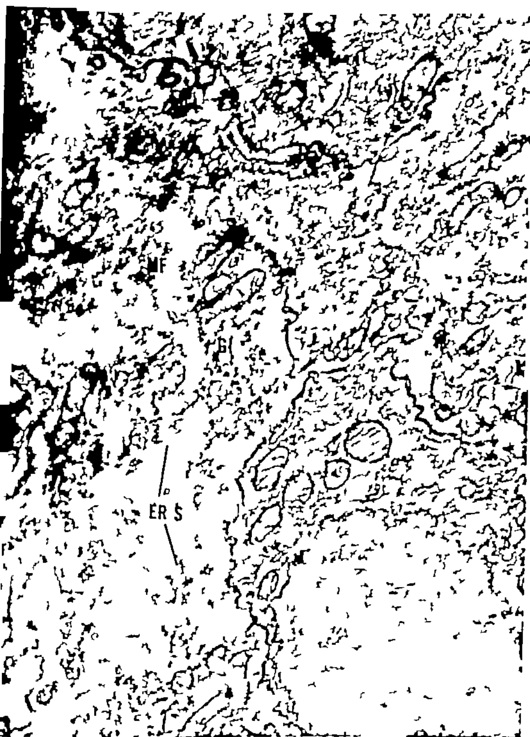

MF
BI
ER S

PLATE 15

EXPLANATION OF FIGURES

34 An oblique section through developing muscle of ten-day embryo. Note that the myofibrils are straight and of uniform diameter. Many of them are in transverse alignment. Small interstitial cells and their cytoplasmic processes can be seen in th spaces between the muscle fibers (arrows) × 8,900.

35 A longitudinal section through developing muscle of a ten-day embryo showing the same features as in the previous figure together with number of nuclear masses closely adjacent t each other × 8,600.


34
R
ER S.
N
Nu

PLATE 16

EXPLANATION OF FIGURES

36 A section through developing muscle of 15-day embryo. Note the large number of myofibrils and the presence of Z, A, I, H and M bands. Parts of Golgi material and accumulations of sarcoplasm are seen at the nuclear pole. Parts of two interstitial cells and their cytoplasmic processes are closely applied to the fiber (arrows). × 9,500.

37 A section through developing muscle of a 15-day embryo. The fibers are packed with myofibrils and surrounded by interstitial cells (arrows). × 9,400.


M
R
Gl
G
Mf
ER S
M

The Fine Structure of Bat Spermatozoa [1]

DON W. FAWCETT AND SUSUMU ITO
Department of Anatomy, Harvard Medical School, Boston, Massachusetts

ABSTRACT The fine structure of epididymal spermatozoa of *Myotis lucifugus* and *Eptesicus fuscus* is described. Caudal to the acrosomal cap in both species, thin intermediate layer is described as uniting the plasmalemma to the outer leaf of the nuclear envelope. Although this layer does not form a separate cap-like structure, it evidently corresponds to the "post nuclear cap" of light microscopists. A redundant portion of the nuclear envelope turns away from the condensed chromatin and continues caudad into the neck region where it forms pair of concentric membrane systems on either side of the connecting piece. Two flattened mitochondria are closely applied to the dorsal and ventral aspects of the connecting piece.

The sperm tails in the two species are generally similar except for the shape and distribution of mitochondria in the middle-piece and the thickness of the fibrous sheath of the principal piece. A unique arrangement of the mitochondria in *Myotis* makes it possible to determine the orientation of the plane of the central pair of flagellar fibrils in relation to the transverse axis of the flattened head and hence to deduce the probable plane of bending movements of the tail. Cortical and medullary zones are distinguished in the outer dense fibers of the flagellum and fibers 9, 1, 5, and 6 are consistently larger than the others. A set of slender satellite fibers are closely related to the inner aspect of the nine large outer fibers. Additional structural details of the axial filament complex are described, especially the cross-sectional configuration of the subfibrils in the doublets and their mode of termination in the end-piece. N secondary fibers" or mid fiber" were found.

Since the axial filament complex of mammalian sperm tails is not continuous with basal body as in other flagella, it is suggested that the connecting piece is centriolar derivative and may be the functional equivalent of a basal body for both the axial complex and the outer dense fibers.

Comparisons are made of bat sperm tails and those of other mammalian species and the ultrastructure and arrangements of tail components are discussed in relation to the current concepts of sperm locomotion.

Chiropteran sperm were well studied by several able cytologists in the latter part of the Nineteenth Century. Eimer (1874) described the sperm of several Vespertilionid bats and his observations were confirmed and extended to other families by Ballowitz (1891). When Retzius in his extensive comparative studies of sperm structure, turned his attention to this group in 1906 he remarked that his predecessors had explored bat sperm so thoroughly that little remained for him to add. The same might be said today if we were limited to light microscopy but the electron microscope has made it possible to observe in the sperm of *Myotis lucifugus* and *Eptesicus fuscus* several structural features not described heretofore. The sperm of both conform in most respects to the common mammalian pattern but they differ somewhat in relative size arrangement and symmetry of the tail components.

In other mammalian species it has been difficult to determine the topographical relation between the asymmetrical pattern of sperm tail fibrils and the orientation of the head. In *Myotis* a unique organization of the mitochondrial sheath provides landmarks from which it can be determined that the line through the central pair of flagellar fibrils is perpendicular to the transverse axis of the dorsoventrally flattened head. This orientation is entirely consistent with cinematographic observations indicating that the tail movements in mammalian spermatozoa are mainly in the plane coinciding with the transverse axis of the head (Gray '58).

The most conspicuous differences among the sperm of related species of rodents are usually in the shape of the head. It has

[1] Research supported by grant RG 6729 from the National Institutes of Health, United States Public Health Service.

been inferred from this that the structural requirements for sperm locomotion permit little variation in the flagellar components. The observations recorded here demonstrate that sperm of closely related bat species may have similar head structure but exhibit distinctive differences in the organization of the middle-piece; in the degree of development of the fibrous sheath and in the symmetry of outer longitudinal fibers. Detailed cinematographic analysis of sperm locomotion in these species might shed additional light upon the respective contributions of the several components to tail movements.

MATERIALS AND METHODS

Male specimens of the little brown bat, Myotis lucifugus and of *Eptesicus fuscus* were collected during the fall, winter and spring in northern New Jersey or western Massachusetts Their epididymides were fixed for 1 5 to 2 hours by immersion in ice cold 1% or 1.3% osmium tetroxide maintained at pH 7 6 to 7 8 with veronal acetate or collidine buffers. Rapid dehydration was accomplished by a brief exposure to ice cold 70 and 80% ethanol followed by longer periods in 95% and absolute alcohol. A few blocks of tissues were embedded in a mixture of butyl and methyl methacrylate (8 2) with added uranyl nitrate (50 mg per 100 ml) but the majority of tissues were embedded in Epon 812 according to the procedure recommended by Luft ('61) Sections were cut with glass knives on a Porter Blum microtome. Methacrylate sections were supported on carbon-coated celloidin-covered grids Epon sections were picked up on 200 mesh grids without a supporting celloidin or formvar film To improve contrast, all sections were stained with lead hydroxide as recommended by Watson ('58) or by the lead citrate method of Reynolds ('63) Electron micrographs were made on an RCA EMU-3E or Siemens Elmiskop I electron microscope

Observations by phase contrast microscopy

The head of the sperm of both species of bats studied, is spatulate when viewed on the flat (fig 1) and cuneiform when seen edge on. It is quite homogeneous in density and the limits of the acrosome cannot be clearly resolved. The truncated caudal end of the head is joined to the middle-piece by a constricted neck region which is particularly obvious in *Myotis* sperm because of the unusual thickness of its middle piece In *Eptesicus* the middle-piece is thinner and the neck is accordingly less conspicuous. In both species the middle-piece is long in proportion to the tot length of the spermatozoon. Faint tran verse striations and a slight scalloping c its lateral contours suggest the presenc of a very regular helical mitochondri sheath. The phase contrast images do nc permit enumeration of its gyres. Th middle-piece tapers slightly to its junctic with the principal piece which, in *Myoti* is considerably thicker than that of roden sperm. The terminal piece of the tail i short and relatively slender

In a free swimming spermatozoon, th absence of any fixed orientation leaves u without obvious and generally acceptabl criteria for application of the commo terms descriptive of surfaces (dorsal ven tral, lateral) or of planes of section (sag ittal, frontal) In both of the species con sidered here the flattening of the sperm head introduces an asymmetry that is read ily visible with either the light or the elec tron microscope. In the description which follows we will arbitrarily assign the terms of direction and designate the planes of section with respect to the shape of the head. The broad faces which it normally presents in dried smears will be designated dorsal and ventral surfaces. In cross section the outline of the flattened head is an ellipse with a shorter *dorsoventral* axis (xx in fig. 18) and a longer *transverse* axis

For purposes of description many investigators divide the spermatozoon into three principal regions, the head, *middle-piece* and tail. According to this view the *middle-piece* is defined as that region of the flagellum between the proximal centriole and the annulus. The tail then begins at the end of the mitochondrial sheath. In our view the [illegible] flagellum that has regarded as [illegible] highly evolved flagellum [illegible] acquired certain additional motor elements and specialized sheaths. Its axial filament complex [illegible] of other flagella should have [illegible] centriole or [illegible] triole derivative [illegible] its base. It seems to be [illegible] to consider the tail and to serve no useful purpose [illegible] here the tail beginning well above the flagellum [illegible] mitochondrial sheath [illegible] filaments emerge from the [illegible] centriole [illegible] prefer to regard the sperm tail as [illegible] axial filament complex which originates at the [illegible] pole of the nucleus. Therefore in this paper the spermatozoon is considered to have two principal regions, the head and the tail. The tail is subdivided into four regions, the neck, *middle piece*, *principal piece* and *end piece*

(yy in fig. 18) A midline longitudinal section coinciding with the dorsoventral axis will be referred to as a *sagittal section*. A longitudinal section perpendicular to this coinciding with the transverse axis of the ellipse will be called a *frontal section*. *Anterior* will be in the direction toward the tip of the acrosome and *posterior* will be toward the tip of the tail.

Electron microscopic observations

The head. In frontal section, the sperm head has a smooth rounded anterior edge and roughly parallel lateral margins (figs. 2 and 4). When cut sagittally it appears wedge-shaped, being thicker at base and gradually tapering to a slender tip (fig. 3). The degree of dorsoventral flattening is greater toward the tip than near the base. Therefore in transverse sections at successive levels from base to tip the dorsoventral axis of the elliptical cross-section becomes shorter while the transverse axis remains about the same (fig. 18 A, B and C). The nucleus takes up nearly all of the head and is extremely dense and homogeneous throughout except for occasional small cavities or nuclear vacuoles 70 to 100 mμ in diameter. These are variable in number and location (figs. 3, 4 and 16). The thin anterior edge of the nucleus is surmounted by a small crescentic acrosome best seen in sagittal sections. It is thinner in *Myotis* (fig. 3) than *Eptesicus* (fig. 27). While the bulk of the acrosome is localized in this crescentic structure at the tip of the sperm head it can be seen to extend in a thinner layer back to the posterior margin of the head-cap (see arrows fig. 3). The acrosomal substance is homogeneous but differs in its density with the method of fixation employed. It completely fills the membranous head-cap and thus covers the anterior two-thirds of the nucleus. The inner aspect of the cap is closely applied to the outer membrane of the condensed nucleus except at the tip where an infolding of the inner membrane of the head-cap bounds a minute space between the anterior edge of the nucleus and the under surface of the acrosomal cap. This subacrosomal space is slightly larger in *Eptesicus* (fig. 27) than in *Myotis* (figs. 3 and 16). It appears empty in both species and would not merit the attention given it here were it not for the fact that a dense structure called the apical body has been observed in this space in the sperm of other species notably the rabbit (Hadek, '63; Bedford, '64). Furthermore an important function in fertilization has been attributed to a component of invertebrate spermatozoa that occupies a corresponding location (Kaye, '62; Colwin and Colwin, '64). In the bat sperm described here the subacrosomal space is very small and does not appear to have any dense contents that could appropriately be designated an apical body. It seems unlikely that this structure has a significant function in fertilization in this species.

Caudal to the posterior margin of the head-cap in the region where a post-nuclear cap was described by light microscopists the plasmalemma is attached to the outermost membrane of the nuclear envelope by a specialized intermediate layer. In longitudinal section (fig. 33) this layer appears as a line about 50 A thick and of somewhat lower density than the membranes on either side of it. In transverse sections of the head the intermediate layer has a distinctive periodic structure (figs. 32 and 34). In this plane it seems to be a corrugated sheet appearing in section as a series of short lines inclined at angles in alternate directions. From the angulations that recur at about 200 A intervals along the zig-zag course of this layer short lines extend alternately outward to the plasmalemma and inward to the nuclear envelope. The short projections of the corrugated intermediate layer seem to be continuous with the outer dense leaflet of the neighboring unit membranes. The complex thus formed by the two membranes and the thin intermediate layer connecting them, bears a superficial resemblance to a septate desmosome but is more elaborate in its structure. This unusual differentiation is probably responsible for the argyrophilia of this region which was the basis for descriptions of a post-nuclear cap. This term no longer seems appropriate however because the exceedingly thin, corrugated intermediate layer does not appear to be an entity distinct from the cell membrane and nuclear envelope it connects, and it does not the caudal or implantation

sperm head. It would seem to be merely a device for maintaining cohesion between the membranous coverings of the sperm nucleus.

The neck. The relations of components in the neck of the mammalian spermatozoon are complex and difficult to visualize in three dimensions from the study of thin sections. In consequence, this region has been less thoroughly described than others. The nine longitudinal fibers that form an outer row around the axial filament complex in the middle-piece, are continuous in the neck region with nine segmented columns that together comprise the *connecting piece by which the tail is attached to* the head (figs. 4 20 and 22) The longitudinal elements of the connecting piece are dense like the coarse fibers which end *in them but they are interrupted at regular* intervals of 50 to 60 mu by narrow transverse bands of relatively low density This results in the familiar segmented or cross-*banded appearance that is characteristic of* the connecting piece of all mammalian spermatozoa thus far examined. Although nine distinct columns are identifiable in the distal part of the connecting piece, two groups of columns on either side of the sagittal plane corresponding respectively to fibers 5 and 6 on one side and 9 1 2 on the other coalesce anteriorly so that the number of elements is reduced to six (figs. 23 and 24) There may be further fusion among these just before their insertion into the implantation site in the base of the nucleus, but the details of this have not been worked out. In frontal sections (figs. 4 and 22) the expanded proximal portion of the wall of the connecting piece on one side is triangular in shape with its base uppermost and applied to the nucleus. The cylindrical proximal centriole rests with one end against the oblique inner surface *of this portion of the wall of the connecting* piece. The long axis of the centriole is thus inclined at an angle of 45 to the long axis of the flagellum and is in a plane corresponding to the long transverse axis of the flattened head (fig 22) In sagittal sections (figs. 3 and 20) the centriole is seen more-or-less on end but it never presents a distinct image because of its oblique orientation with respect to this plane of section. This centriole seems to be the only one that persists, as such, the mature spermatozoon. The second c distal centriole that was forming the *basal body* of the developin flagellum is no longer identifiable in th mature sperm. Thus instead of being co tinuous with the wall of a centriole-lik basal body the nine doublets of the filament complex lose their identity in th neck, apparently merging with the inne aspect of the columns of the connectin piece (figs. 4 and 23) *The central pair o single fibrils continues beyond the anterio termination of the doublets to a poin very near the proximal centriole (figs. 2 and 24)*

The neck of the spermatozoon is com monly defined as the region between th head and the first gyre of the mitochon *drial helix of the middle-piece.* Mitochon dria are usually thought to be absent fro *this segment of the spermatozoon.* In th bat, however two small mitochondria, th *are not part of the middle-piece helix,* ar regularly *found* in the neck. They ar roughly triangular in surface view (fig 21) and are flattened against the dorsal and ventral aspects of the neck with their an terior margins extending into the cleft be tween the wall of the connecting piece and the implantation fossa in the base of the nucleus (Mi₁ and Mi₂, fig. 3) They are so closely applied to the base of the flagellum that small *folds of the outer mitochondrial* membrane occasionally penetrate between *the longitudinal columns of the connecting* piece and extend *into its interior* (see fig 24) In *frontal* sections small circular profiles are seen in the neck which evi dently represent sections through small *lateral projections* from the base of thes two mitochondria.

A novel feature of the neck region that has not received much attention heretofore *is a redundant portion of the nuclear enve lope that forms a scroll-like mass of mem* branes in the groove between the base of the nucleus and the first turn of the mito chondrial helix (Ms, fig 4) The mem branes within these *concentric systems* are paired and where they enter and leave the scroll their continuity with the nuclear envelope can be clearly traced (see ar *arrows fig. 4 and fig. 25) The intervening* portion of the condensed nucleus has no

closely applied covering membrane. The membranous scrolls do not completely encircle the neck but are found mainly on its two sides, and are therefore seen most clearly in longitudinal sections in the frontal plane. In cross-sections of the neck (figs. 23 and 24) it can be seen that the connecting piece is covered dorsally and ventrally by the two mitochondria and laterally by the scrolls of redundant nuclear envelope. We have observed in other mammalian spermatozoa a similar deflection of the nuclear membrane from the base of the condensed nucleus and the formation of a fold of excess membrane extending back into the neck region but a scroll-like configuration of the membranes has so far been seen only in the two species of bat described here.

The mitochondrial sheath of the middle-piece

The arrangement of mitochondria in the middle-piece differs significantly in the two species studied. In *Eptesicus* as in other mammalian species elongated cylindrical mitochondria are wound helically around the longitudinal fibers comprising the core of the flagellum and their end-to-end junctions are randomly distributed along the course of the helix (figs. 25 28 30). In *Myotis* all of the mitochondria with the exception of the two in the neck are extremely uniform in size. They are flattened anteroposteriorly and have a broad crescentic form when seen in transverse sections of the middle-piece (figs. 10 and 11). Their arrangement is such that each turn of the flat helix is made up of just two mitochondria whose end-to-end junctions are directly opposite on the dorsal and ventral aspects of the middle-piece (figs. 10 and 11) In transverse sections, it is clear that a line joining these opposite junctions nearly coincides with the line through the central pair of fibrils in the axial filament complex (fig 11) In sections passing tangential to the dorsal or ventral surface of the middle-piece (fig 5) it can be seen that the end-to-end junctions of the pairs of mitochondria in successive turns of the helix, are in line along its entire length. Such a precise ordering of the mitochondria with respect to the dorso-ventral plane of the flagellum has not been reported in any other mammalian spermatozoon. The significance of this finding is not entirely clear but it is noteworthy that the flattened semilunar form of the mitochondria makes the middle-piece in the sperm of *Myotis* exceptionally thick. A broad mitochondrial sheath might well offer considerable resistance to the bending movements of the flagellum. If we assume that the tail movements are mainly planar it would not be unreasonable to speculate that somewhat greater flexibility might result from having the mitochondrial junctions aligned in the plane perpendicular to the direction of the bending movements.

As a consequence of the regular occurrence of two mitochondria in the neck and two in each turn of the helix it has been possible, in favorable sections that include the full length of the mid-piece to count the gyres and thus to estimate quite accurately the total number of mitochondria in the spermatozoon. In a small sample this number proved to fall within the rather narrow range of 114 to 120

In several animal species the mitochondria have been reported to undergo a peculiar sequence of changes in the course of spermatid differentiation that results in an atypical internal structure in the mitochondria of the mature sperm. The clefts within the cristae open up to delimit large clear spaces and there is a concurrent condensation of the matrix. The intracristal spaces come to be more capacious than the intercristal space and are occupied by material of low density which has been termed the pseudomatrix" (André '62) These alterations do not appear to occur in bat spermatozoa. The mitochondria have a homogeneous matrix of considerable density lacking the granules that are a prominent component of the mitochondria of many other cell types. The cristae are of normal thickness but irregularly oriented and more likely to be parallel than perpendicular to the limiting membranes of the organelle.

Cytoplasmic droplet. Bat sperm are capable of survival over the winter in the female reproductive tract. They might therefore be expected to have a greater storage of endogenous substrates than sperm of other species. Such does pear to be the case. The plasma

is closely applied to the mitochondrial sheath for most of its length leaving very little cytoplasmic matrix. In *Myotis* occasional small vesicles found between the mitochondria and the surface membrane are presumed to be isolated remnants of the endoplasmic reticulum of the spermatids. In the corresponding location in sperm of *Eptesicus* there are numerous small tubules 200–300 A in diameter oriented circumferentially and therefore usually seen as circular profiles in longitudinal sections (figs. 25 and 30) It is not clear whether these are attenuated elements of the reticulum or persisting microtubules of the manchette which surrounded the developing mitochondrial sheath late in spermiogenesis during the stage of spermatid elongation.

Epididymal sperm have a prominent rounded mass of cytoplasm the *cytoplasmic droplet* or *middle piece bead* projecting laterally from the caudal end of the middle piece This sizable remnant of spermatid cytoplasm contains numerous smooth-surfaced tubular and vesicular elements that are probably derivatives of the endoplasmic reticulum or possibly of the Golgi complex. The cytoplasmic matrix of the droplet is of very low density and devoid of free ribosomes, glycogen or lipid inclusions (figs 6 7 25) It has often been suggested that the middle-piece bead might be a site of accumulation and storage of endogenous substrates to provide for the survival of the sperm during their passage through the epididymis and possibly to sustain their motility after ejaculation. This view is not supported by our observations since there is nothing in the fine structure of the cytoplasmic droplet to suggest that it is anything more than a transient and functionless remnant left behind when the excess spermatid cytoplasm is pinched off to form the *residual bodies of Regaud*.

The annulus At the junction of the middle piece and principal piece is the structure formerly called the *ring centriole* or *Jensen's ring* (Jensen 1887) In longitudinal sections it is represented by two triangular profiles on either side of the tail just distal to the last mitochondrion (figs. 7 and 26) It is slightly smaller in cross-sectional area in *Eptesicus* than in *Myotis* but it is otherwise similar The dense triangular sections of the ring have their apex directed inward and their base against the plasma membrane In general, the cell membrane of the tail has an irregular undulant course and does not closely conform to the contours of the underlying structures. However the membrane is invariably closely applied and apparently firmly adherent to the outer rim of the annulus (fig. 7) This ring arises in close relation to the distal centriole of the early spermatid soon after formation of the simple primary flagellum, and later in development it migrates caudally to its definitive position at the end of the middle-piece. Because of its origin, the classical cytologists considered it to be a centriole of unusual shape The electron microscope however reveals nothing in its fine structure that would justify perpetuation of this concept. It seems advisable, therefore to abandon the term ring centriole and simply refer to this structure as the *annulus* Its functional significance is unknown but its proximity to the circumferential elements of the fibrous sheath and its similarity to the latter in density and fine structure suggest that the annulus may be involved in the formation of the fibrous sheath of the principal piece Consistent with this speculation is the observation that a typical annulus is not found in those animal species whose spermatozoa have no fibrous sheath.

The fibrous sheath The sheath of the principal piece formerly called the "tail helix" or spiral sheath was described by light microscopists as a continuous fiber wound in a tight coil around the axial filaments of the tail. This interpretation has been perpetuated by some electron microscopists despite abundant evidence for a more complex structure. In earlier papers (Fawcett '58 Telkka et al. '61) we have denied the existence of a continuous helical fiber and instead have described the fibrous sheath as being made up of a large number of circumferentially oriented stays or ribs that pass halfway around the axial filament complex. At both ends, the successive fibers or ribs are held together longitudinally by their fusion with two longitudinal columns. In the common laboratory rodents the expanded ends of the ribs and

the longitudinal columns to which they attach, form conspicuous thickenings of the dorsal and ventral aspects of the sheath, such that the cross-section of the tail is elliptical in outline.

The fibrous sheath of bat sperm is similar in its general organization to that of rodent sperm but differs in certain details. In *Myotis* the sheath is exceptionally thick near the middle-piece tapering gradually to more usual dimensions at the caudal end of the principal piece. At its anterior end the sheath appears, in transverse sections, as a broad ring of uniform thickness (fig 12) There are no noticeable dorsal and ventral thickenings such as are seen in other species but in the corresponding location there are two radially oriented bands of greater density opposite fibers 3 and 8 of the axial filament complex (figs. 12 and 31) Although these are relatively small compared to their counterpart in other species it is clear that they represent sites of longitudinal connections between successive half rings of the sheath and thus correspond to the longitudinal columns in the sperm tails of other mammalian species.

At high magnification a substructure is discernible in the circumferential elements of the fibrous sheath consisting of closely compacted parallel filaments embedded in a dense matrix. In transverse sections through the proximal part of the sheath in *Myotis* crescentic clefts of varying length are observed in the rings of the sheath (see arrows, fig 17) The presence of these slit-like discontinuities in the broad rings gives rise in longitudinal sections (Upper part of fig. 8) to the spurious appearance of more than one layer of concentric circumferential elements However study of both transverse and longitudinal sections makes it evident that the sheath is actually composed of a single layer of closely-spaced, ribbon-like semicircular bands or ribs that attach to the dorsal and ventral longitudinal columns. Near the middle-piece, these are broad, flat and interrupted by narrow slits (fig 8) Farther posteriorly the slender discontinuities disappear and the fibers gradually become narrower in their radial dimension while maintaining approximately the same anteroposterior thickness (fig. 9) Instead of being compared to a simple coil spring or helical wrapping as has been the practice in the past, the three-dimensional configuration of the fibrous sheath might better be likened to a column of closely spaced, flat half washers spot-welded together along opposite sides. Both analogies, however are oversimplifications because neither takes into account the fact that the encircling bands are neither gyres of a simple helix nor separate rings but can be shown to branch in both the radial and circumferential directions. The branching of the fibers along their length is demonstrable in tangential sections of the tail which show frequent bifurcations and anastomoses between successive circumferential elements of the sheath (lower part of fig. 8 and fig 29) A splitting of the fibers in a radial direction is evident from the frequent occurrence of V and Y shaped cross-sectional profiles in longitudinal sections of the tail (figs. 9 and 29)

In *Eptesicus* sperm, the principal piece is much more slender than in *Myotis* and the difference resides mainly in the radial dimensions of the circumferential elements of the sheath (compare figs. 26 and 28 with 7 8 12, and 17) In *Eptesicus* these are relatively narrow and change little in thickness along the length of the principal piece

Outer dense fibers In the bat, as in other mammalian species, the nine coarse fibers that form an outer row around the axial filament complex are all of approximately the same shape and cross-sectional area near the neck (fig. 19) but farther back in the middle-piece they exhibit marked individual differences in thickness and cross-sectional outline (figs 11 14 and 30) In most of the species studied heretofore fibers 1 5 and 6 are distinctly larger than the others (Bradfield, '55 Telkka et al. '61) The remaining fibers can be grouped in pairs of similar size and shape occupying corresponding positions on either side of a line passing through fiber 1 and midway between 5 and 6. Such a line divides the cross-section into symmetrical dorsal and ventral halves. Fiber 2 is usually like 9 3 resembles 8 and 4 matches 7 In bat sperm these relations do not hold. In both species studied here there are four larger fibers instead of the

usual three. This is most evident in *Myotis* (figs 11 and 12) but is also true of *Eptesicus* (fig. 20) The numbers of these four fibers are 9 and 1 5 and 6. With this unusual arrangement, no axis of dorso-ventral symmetry can be drawn through fiber 1 and between the central pair Neither can the remaining five fibers be paired according to their size and shape. The arrangement of the components thus appears completely asymmetrical.

In the anterior part of the middle-piece the coarse outer fibers are large and separated an appreciable distance from the axial filament complex. They taper gradually in their course through the middle piece. The slender terminal portion of numbers 9 1 5 and 6 in the principal piece are reduced to 40 mμ or less in diameter and are fused to the corresponding fibrils of the axial complex where they form rounded or fan-shaped projections from the outer aspect of the doublets (fig 31) One of the arguments formerly raised against the suggestion that the outer dense fibers are tensile elements was based upon the misapprehension that they ended blindly in the principal piece. Since it has now been shown in the bat and several other mammalian species that these fibers are attached at their caudal ends to the corresponding doublets of the axial bundle this argument no longer holds. Instead the observed attachments of the outer fibers would argue in favor of their functioning as accessory contractile elements.

No filamentous substructure has been resolved in the outer fibers. Their interior is very dense and homogeneous but in favorable preparations a thin cortical layer of lower density can be seen (fig. 30) This layer is generally limited to the convex outer surface of the fibers Associated with their inner aspect is another component which has been overlooked or misinterpreted in earlier descriptions of sperm structure In *Myotis* two or three small punctate profiles ~ 150 A in diameter are found near the inner surface of each coarse fiber (see at arrows fig 15) These might be interpreted either as small granules or as cross-sections of longitudinally oriented fine filaments. They have been difficult to identify in longitudinal sections in this species. They are much better developed in *Eptesicus* (see fig. 30) where multiple dense profiles 150 to 200 A in diameter are clustered around the inner aspect of each coarse fiber These vary in size and are irregularly angular in cross-section (fig. 30). Their arrangement seems more haphazard than that of other components of the flagellum. In the corresponding location in longitudinal sections of the middle-piece, one can identify linear markings (fig. 25, at arrows) which suggest that the punctate profiles seen in transverse sections of the middle-piece are cross-sections of additional longitudinal fibers of undetermined length. They decrease in number along the length of the middle-piece and near its caudal end only a few such fibers can be found, usually quite closely applied to the inner surface of the coarse fibers (fig. 23, at arrows) Similar structures are present in other mammalian species. They probably reach their greatest development in the marsupials where the dense outer fibers are at a considerable distance from the axial filament complex but are connected to it by radial dense lines called "laminae" by Cleland and Rothschild ('59) Upon re-examination of their figures it seems likely that the laminae in the bandicoot are formed by alignment of fibrous elements similar to those described here. There is at present no basis for speculation as to their chemical nature or their possible function in tail movements.

The axial filament complex. The internal bundle of nine peripheral and two central fibrils forming the core of the bat sperm tail conforms closely to the descriptions of the axial filament complex of cilia, flagella, and sperm tails in other species (Fawcett, '58 '61) The two central fibrils are circular in transverse section, about 250 A in diameter and 350 A center to center They have a dense rim about 45 A thick and a less dense interior and therefore appear to be tubular The presence of an open lumen has not been established, however The nine outer doublets are composed of two subfibrils which are designated A and B in accord with the terminology proposed for protozoan flagella by Gibbons and Grimstone ('60). Subfibril A is slightly smaller. It lies slightly closer to the center of the cilium and its center appears denser than that of subfibril B In

published diagrams of cross-sections of flagella, the doublets are commonly depicted as two apposed oval profiles which together have a figure-of-eight configuration. If the doublet were formed by fusion of two independent tubular elements, the septum of the figure-of-eight might be expected to be straight and approximately double the thickness of the wall of the two fused subfibrils. Actually it is slightly curved and of about the same thickness as other portions of the dense wall. The doublet thus appears instead to be made up of one tubular element with a circular cross-section (subfibril A) to which is joined a tubule with an incomplete wall having a C-shaped cross-section (subfibril B). As a consequence of this construction the interior of subfibril A is typically circular in cross-section while the interior of subfibril B is crescentic. This difference in outline of the two subfibrils is probably present in the doublets of bat sperm tails (fig. 31) but is often obscured by the density of the interior of subfibril A and by the broad attachment of the associated coarse fiber to its outer aspect. In simple sperm flagella of other species in which the relationships can be visualized more clearly as in the sperm tail of the guppy (fig. 31 inset) dark subfibril A is circular in section while subfibril B is distinctly crescentic. A similar configuration is also evident if one examines the corresponding structures in the triplet fibrils of centrioles or basal bodies. There too the center of subfibril A is circular while that of subfibrils B and C is crescentic. It seems likely that this difference in shape of the subfibrils is of widespread if not universal occurrence in centrioles and the proximal portions of flagella. True figure-of-eight profiles also occur in some species particularly in the distal parts of the flagellum.

Subfibril A bears two short diverging arms that project diagonally from its wall toward the next doublet as described by others (Afzelius '59 Gibbons '61; André '61) The outermost arm which is invariably present, is about 40 A thick and 120 A long. It not only projects outward from the wall but appears also to extend inward traversing the center of the subfibril diagonally to terminate in the opposite wall which forms the septum of the doublet. The other arm, directed toward the center of the flagellum is inconstant, its limits are seldom clearly defined and it cannot be traced into the interior of the subfibril. In cilia doublets 5 and 6 are said to be joined by a bridge formed by the B subfibril of 6 bearing arms that extend counter-clock wise to meet the arms on the subfibril A of 5 (Gibbons '61) An additional connection extending from the center of the bridge to the ciliary membrane has also been described. In the sperm tails of the species described here no arms were found on B subfibrils and no evidence was found of a link between doublets 5 and 6

A pattern of faint linear densities observed in the matrix of the axial filament complex is interpreted as a system of connections between the various fibrils. These indistinct and often discontinuous markings include a short straight link between the central fibrils and a pair of curving lines that form an arc on either side between corresponding points on the circumference of these two fibrils. Nine radial densities extend to subfibril A of each doublet from the central fibrils themselves, or from the arcs connecting them (Fawcett, '62) In descriptions of the cilia of ctenophores (Afzelius, '61) and molluscs (Gibbons, '61) a sheath is reported to surround the center pair of fibrils a slender midfiber" is said to be situated between the central pair and nine secondary fibers are placed midway along the radial links between the central and outer fibrils. We are unable to make out a sheath around the central pair of fibrils or to establish to our satisfaction the reality of the mid-fiber or the nine secondary fibers described by Gibbons ('61) It is possible that our methods of specimen preparation have simply failed to preserve them. It seems equally likely however that the poorly defined densities interpreted by Gibbons ('61) and Afzelius ('61) as additional fibers are not longitudinally continuous structures that play an essential role in flagellar motion and they may therefore be subject to considerable variation from species to species.

A slender radial link is found extending from subfibril A of doublets 3 and 8 to th apex of two wedge-shaped d of the surrounding fibrous

represent transverse sections of the longitudinal connections between successive circumferential elements of the sheath (fig. 31). Neither fibrils 3 and 8 nor the dorsal and ventral longitudinal columns of the sheath are directly in the sagittal plane of the tail, but are so disposed that lines drawn from the center of the flagellum through fibrils 3 and 8 and the respective longitudinal columns of the sheath, make an angle of about 160 and divide the cross-section into two unequal sectors. The smaller of the two contains fibrils 9, 1 and 2 while the larger contains 4, 5, 6 and 7. Doublets 9, 1, 5 and 6 bear fan-shaped projections that represent the terminal portions of the outer coarse fibers. Similar but smaller radial projections are present on doublets 2, 4 and 7. Near the end of this segment of the tail, attached terminal portions of the outer fibers end and the doublets beyond this point resemble those of simple flagella.

Near the tip of the terminal piece of the bat spermatozoon the connecting linear densities and the arms on the doublets disappear and the arrangement of fibrils becomes disordered. The doublets are also reduced to single fibrils (compare figs. 14 and 15). It is not certain which of the two subfibrils terminates first but an indication of their mode of termination is shown in the upper part of figure 17. The dense wall of one member of each doublet has become detached at one end from its partner and has opened up to form a curving tail on the circular cross-section of the intact subfibril. The figure-of-eight cross-section is thus converted into a figure-of-nine. It is assumed that a short distance farther along this free portion of the wall is lost and the remaining subfibril continues (fig. 15a).

Investigators have long been uncertain as to whether the fibrils of cilia and flagella are tubules, as their cross-sectional appearance would suggest, or whether they are solid structures with a dense outer layer and a less dense interior. This opening up of the wall of subfibril B to leave a free edge is consistent with the view that the fibrils are tubular rather than solid structures and also tends to support the interpretation that subfibril B is a tubule with an incomplete wall fused at its edges to the wall of subfibril A.

DISCUSSION

Head. Electron microscopic studies have greatly clarified the relations of the structural components of the sperm head but we are left with a heritage of multiple terms from light microscopy that are no longer accurately descriptive. Their continued use without redefinition tends to perpetuate outmoded structural concepts. "Galea capitis," "head-cap" and acrosome for example are all used in the current literature with little regard for their exact meaning in relation to electron microscopic findings. *Acrosome* is the term that was originally applied to the granule observed by Lenhossek (1898) within a clear "vacuole" in the idiosome of the spermatid. Confusion in usage later developed owing to differences of opinion as to the respective contributions of the granule and the vacuole to the head coverings of the mature sperm. The *head cap* or *galea capitis* was usually regarded as a thin membranous structure distinct from the acrosome but overlying it and covering the anterior portion of the nucleus. Electron microscopic studies have now shown in a number of mammalian species that both the limiting membrane of the vesicle (Lenhossek's "vacuole") and the acrosomal granule itself contribute to the formation of a single head covering in the mature sperm (Burgos and Fawcett, '55; Fawcett, '58). The closed, membrane-limited vesicle spreads over the anterior pole of the spermatid nucleus and defines the limits of the future head cap. The substance of the acrosomal granule in its interior then becomes redistributed so that it ultimately occupies all of the space within the confines of the membrane bounding the head cap. It has l ur practice to ... n this type ... refer to the closed ... as the *head-cap* and ... *acrosome*. The two ... fulness in descri... components at ... differentiation ... mammalian s... and the head ... term such as ... well, provide

shaped structure so designated consists of an amorphous component enclosed in a continuous membrane.

The head cap of the bat spermatozoa described here presents no unusual features. The acrosomal substance occupies an inconspicuous thickening along the crescentic anterior margin of the head and extends in a thinner layer back over the anterior two-thirds of the nucleus. The cap is very closely applied to the nucleus everywhere except at the tip where there is a small recess between its inner surface and the thin apical margin of the nucleus. The term *apical body* has been applied by other authors to a dense content of this space (Hadek, '63 Bedford, '64) This body is reported to persist in rabbit spermatozoa penetrating the zona pellucida even though the acrosomal substance has mostly disappeared at this stage. This has been interpreted as an indication that the apical body is a relatively stable structure. It has been suggested (Bedford '64) that it may prove to be homologous with the rod or perforatorium which is said to occupy a corresponding site between the acrosome cap and nuclear envelope in various rodent species (Clermont et al '55 Austin and Bishop, '58) Our failure to find a dense material in the subacrosomal space in bat spermatozoa is interpreted to mean that the apical body is either not developed in this species or is not sufficiently stable to resist extraction during the specimen preparation procedures employed here The latter alternative seems somewhat unlikely inasmuch as the general preservation of fine structure achieved in the present investigation compares favorably with that of studies on other species in which an apical body has been described. Although a small subacrosomal space occurs in a number of species the findings to date do not seem to establish the so-called apical body as a common component of mammalian sperm nor does the evidence thus far presented warrant assigning to this structure an important role in fertilization.

In early electron microscopic studies of cat human, and guinea pig spermatozoa we failed to find any formed component between the plasma membrane and the nuclear envelope caudal to the posterior margin of the head cap (Burgos and Fawcett, '55) The existence of a *post nuclear cap* in these species was therefore denied (Fawcett, '58) Other authors have since described in this location in boar (Nicander and Bane '62) and bull sperm (Saacke and Almquist, '64) a thin layer of dense amorphous material without any membranous cover of its own. Nicander and Bane noted that this layer has a strong affinity for phosphotungstic acid and concluded that it corresponds to the *post nuclear cap* which light microscopists demonstrated in preparations stained with silver salts. In the present study of bat spermatozoa the tenuous intermediate layer observed between the plasmalemma and the nuclear membrane is not amorphous, as previously described but exhibits a complex periodic structure when seen in transverse sections of the head. This layer appears to be fixed to the membranes on either side and is tentatively interpreted as a specialization for maintenance of the close cohesion of the membranous coverings of the posterior third of the nucleus. It has been noted by other authors that the relationship of the plasma membrane with the post-nuclear cap differs from its relationship with other parts of the head The apparent attachment of the plasmalemma to the outer leaf of the nuclear envelope via the intermediate layer that corresponds to the post nuclear cap may well account for the frequent observation (Bedford '64) that the cell membrane remains in close apposition to the posterior part of the nucleus even though it loosens and balloons out from the acrosome region

Although the intermediate layer probably corresponds to the argyrophilic component described earlier by light microscopists as the *post nuclear cap* we adhere to the position that the term is quite inappropriate. It implies the existence of a substantial cap-like structure comparable to the head-cap. Actually this layer in bat sperm is thinner than a unit membrane. Since its processes are apparently continuous with the dense leaflets of the adjacent membranes, there is some doubt as to whether it should be regarded as an independent structure Furthermore it is not cap-like since it does not extend over the base of the nucleus but appears to terminate at its posterior margin. There seems

to us no reason to perpetuate the term *post nuclear cap*

The neck. The neck of mammalian spermatozoa has received less attention than other regions because of its complexity and its variable appearance in different planes of section. Certain features common to most species are beginning to emerge, however. The segmented columns that comprise the *connecting piece* have a cross-banded structure consisting of broad dense segments separated by narrow light bands. The appearance of cross-striation in these structures is not like that of collagen, in that, the light bands are marked by conspicuous notches or grooves on the surface as though solid dense segments were separated by clefts occupied by material of lower density. Phosphotungstic acid penetrates into these clefts and deeply stains their contents while the broad dense segments are not stained (Nicander and Bane, '62). The segmented columns on either side of the connecting piece coalesce near the head to form stout articular structures or *capitella* that vary somewhat in number and configuration in different species. The *capitellum* resulting from fusion of the segmented columns of one side is larger than the other and is characteristically expanded at its upper end, so that in longitudinal sections it is triangular with its base occupying about half of the *implantation fossa*. The proximal centriole is parallel to the flat plane of the head and is oriented at an angle of 45° to the axis of the tail with one end resting against the sloping inner surface of the *capitellum*. These general relationships described here for the bat, appear to hold also for the boar (Nicander and Bane '62) and bull (Saacke and Almquist '64) and probably for most other mammalian species.

Mitochondria have usually been thought to occur only in the middle-piece but their presence in the neck region may prove to be more common in mammalian sperm than suspected heretofore. In both species of bats studied, two mitochondria have invariably been found on the dorsal and ventral aspects of the neck with their thin anterior margins extending up into the angle between the connecting piece and the rim of the implantation fossa. Their intimate relationship to the connecting piece suggests the possibility that they may be essential to the function of this region possibly providing energy for the initiation of the wave movements.

A puzzling feature of the organization of the mature mammalian sperm flagellum is the absence of a longitudinally oriented centriolar structure at the base of its axial filament complex. In other motile cilia and flagella the nine doublets are continuous at their base with triplet fibers in the wall of a centriole-like basal body. There is abundant evidence that the basal body of epithelial and protozoan cilia is essential for motility and serves as the site of initiation of the beat. The tails of sperm of lower forms that have a simple 9 + 2 flagellum, have a typical basal body. The loss of a basal body in mammalian sperm appears to have been associated with the development of the segmented connecting piece and the outer dense fibers. Since it appears unlikely that the obliquely placed *proximal centriole* which is not in contact with the axial filaments could serve as a kinetic center for their movements, it seems reasonable to attribute this function to the *connecting piece* and to consider it to be a modified centriole. The mitochondria of the neck would then be strategically placed to serve as an energy source for a kinetic function of the connecting piece. Whether the contiguous coarse outer fibers are tensile elements directly activated by impulses generated in the connecting piece or are accessory structures involved in the generation and/or propagation of the impulse along the proximal part of the tail are questions that remain to be elucidated.

The presence of a fold of redundant nuclear membrane extending from the base of the nucleus into the neck region appears to be another common feature of mammalian spermatozoa. It has recently been described in boar sperm (Nicander and Bane '62) and we have seen it in the guinea pig and several other species. The prominent scroll of concentric double membranes described here in the neck region of bat sperm is the most extensive elaboration of the excess nuclear envelope thus far described. Considering the marked diminution in volume of the spermatid nucleus during its condensation and modelling to the final shape of the mature

sperm head, it is not surprising that there is an excess of nuclear envelope. It is somewhat unexpected, however that it is retained instead of being resorbed or otherwise eliminated. Its persistence in the mature sperm raises the question as to whether this redundant membrane is reincorporated into the nuclear envelope after fertilization when the sperm head enlarges to form the male pronucleus.

Middle-piece The arrangement of mitochondria in the middle-piece of *Eptesicus* is similar to that described in other mammalian species, the mitochondria being disposed in a helix with their tapering ends overlapping or abutting end-to-end. The contacts of successive mitochondria appear to occur at random along the helical course of the mitochondrial sheath and there are no surface landmarks that provide any clues to the orientation of the components of the axial filament complex in the interior of the middle-piece. The arrangement of mitochondria in the middle-piece of *Myotis* sperm, on the other hand, appears to be unique. There are just two mitochondria to each turn of the sheath and their end-to-end junctions in successive turns are aligned on opposite sides of the middle-piece for its entire length. Since these lines coincide with the plane of the central pair of fibrils in the axial filament complex, they provide a surface landmark that bears a constant relation to the orientation of the tail components. Therefore in oblique sections through the head and middle-piece we were able to relate the orientation of the tail components to the principal axes of the sperm head (Fawcett, '62). Arbitrarily defining the broad faces of the head as dorsal and ventral, the line of junctions of the mitochondria was shown to run down the dorsal and ventral aspects of the middle-piece. It could be inferred from this that the plane of the central pair of filaments in the tail is perpendicular to the transverse axis of the head.

In spermatozoa of most mammalian species no attainable plane of section will permit one clearly to visualize the central pair of fibrils and determine the orientation of the head of the same spermatozoon. Therefore, in species other than the bat, the orientation of the tail components with respect to the head is not known. Anberg ('37) in his diagram of the human sperm and Cleland and Rothschild ('59) for the bandicoot, depict an orientation that differs by 90 from that reported here. In their view the line drawn through the centers of the central pair of fibrils corresponds to the transverse axis of the head and divides the tail into dorsal and ventral halves. The morphological evidence upon which this interpretation is based is not clear and such an orientation is difficult to bring into accord with results of cinematographic studies on swimming bull sperm. Such observations have shown that the waves propagated down the tail are essentially two-dimensional and the plane of the waves is clearly in the transverse axis since during rotation of the sperm as a whole a thin linear optical envelope of the tail is invariably associated with flat views of the head (Gray '55 '58) The unique and constant arrangement of the mitochondria in relation to the orientation of the internal tail components of *Myotis* sperm has made it possible to obtain the first direct evidence that the plane of the central pair of fibrils is perpendicular to the transverse axis of the head. From what is known of the orientation of the central pair in relation to the direction of movement in cilia and flagella (Fawcett and Porter '54 Gibbons '61) this is the orientation that would be expected if the plane of the waves in sperm tails is to coincide with the transverse axis of the head as demonstrated by the cinematographic studies of Gray ('58)

The reasons for the unusual width of the mitochondria in the sperm of *Myotis* and for their unique arrangement are not obvious. One may speculate however that closely apposed broad mitochondria would increase considerably the resistance of the middle-piece to bending. Given mitochondria of this configuration, somewhat greater flexibility might result from having their end-to-end junctions located on the axis of bending. What forces in the developing spermatid might be responsible for establishing this precise arrangement is far from clear

The outer row of nine coarse fibers around the axial filament complex which is characteristic of mammalian spermato-

zoa is also found in certain birds molluscs and insects. Although it is commonly assumed that these fibers are accessory tensile elements their chemical nature is still undermined and their contractility has yet to be established. These fibers are usually associated with a well developed mitochondrial sheath and the suggestion has been advanced that the additional set of longitudinal fibers has evolved to overcome the greater resistance to bending offered by a long and relatively thick middle-piece It can be argued with equal cogency how ever that the mitochondrial sheath has developed to meet the energy requirements for contraction of the outer coarse fibers. Marine invertebrates fish and other groups with external fertilization have spermatozoa with only one or two mitochondria at the base of a simple flagellum consisting of the $9 + 2$ complex alone. It is evident that such sperm tails like protozoan flagella, do not require the close proximity of mitochondria to the fibrils for vigorous motility However in gastropods insects and mammals having internal fertilization, nine outer fibers have been added to give the $9 + 9 + 2$ pattern. Such sperm invariably have an extensive middle-piece. Perhaps it can be inferred from this that the presence of the outer coarse fibers makes necessary the development of a long mitochondrial sheath. The very intimate topographical relation of the mitochondria to the outer fibers also suggests that the two are functionally related

Near the head the outer fibers are similar in cross-sectional outline and area but farther along the middle-piece individual and characteristic differences appear In the majority of species fibers 1 5 and 6 are larger than the others. Assuming that these fibers are tensile elements contribut ing to tail movements the presence of two fibers on one side of the tail and only one on the other has been interpreted as an indication of a predominance of power on one side which might result in a more rapid and effective stroke in one direction. Bat spermatozoa are exceptional in having four larger fibers (9 and 1 5 and 6) instead of the usual three In species with three large fibers there is a concentration of power on one side but the tensile elements are distributed symmetrically with respect to the axis passing through fibril 1 and between the central pair of fibrils. With the arrangement in the bat, the power is evidently more nearly equal on the two sides but its direction of application would seem to be oblique with respect to the dorsoventral axis of the tail. In the light of these differences in arrangement of coarse fibers cinematographic studies comparing the pattern of tail movements of bat spermatozoa with those of other mammals might throw additional light upon the role of the outer coarse fibers in sperm tail movements.

The present paper is among the first to draw attention to dense punctate profiles of irregular and variable shape clustered around the inner aspect of each coarse outer fiber These have either been disregarded by previous authors as artifacts resulting from inadequate fixation of the cortex of the coarse fibers or have been interpreted as anastomosing bridges between adjacent coarse fibers (Nicander and Bane '62) It now appears that neither of these interpretations is correct. These structures are present to varying degree in sperm of most mammalian species but are confined to the anterior portion of the middle-piece where the coarse fibers are separated some distance from the corresponding doublets. They decrease in number farther posterior in the middle-piece and are usually absent in the principal-piece where the slender continuations of the coarse fibers are fused to the doublets of the axial filament complex. They are apparently a normal constituent of the mammalian spermatozoon and are believed to be homologous with the filamentous units comprising the connecting laminae described by Cleland and Rothschild in the spermatozoa of the marsupial Perameles nasuta and observed by ourselves in the American opossum Didelphys virginiana In these marsupial sperm certain of the outer coarse fibers are displaced a very considerable distance outward from the axial filament complex. They are connected with the corresponding doublet by a series of structures arranged about 50 A apart, in rows and embedded in an amorphous matrix. The components of these so called connecting laminae were described as obliquely oriented filaments 400

to 250 A in diameter In cross-sections of the tail they appeared as granules or short rods. It was speculated that these laminar arrays of filaments served to maintain an essential contact between the outer fibers and their corresponding doublets either for purposes of conduction or for mechanical integration of the movements of the two sets of fibers. We have little doubt that the 200 to 250 A punctate profiles associated with the coarse fibers, in cross-sections of the sperm of bat, bull, boar and other mammals, are homologous with the filamentous components of the connecting laminae in marsupial sperm, but their irregular distribution and apparent disorder lends no support to the view that they establish connections between the outer and inner fibers of the tail. It is possible however that reconstruction from serial transverse or longitudinal sections will clarify their relations to neighboring structures. In the meantime we can offer no suggestion as to their functional significance

LITERATURE CITED

Afzelius, B. 1959 Electron microscopy of the sperm tail results obtained with new fixative. J Biophys. and Biochem. Cytol., 5 269–278.

——— 1961 The fine structure of the cilia from ctenophore swimming plates. J Biophys. and Biochem. Cytol, 9 383–394.

Anberg, A. 1957 The ultrastructure of the human spermatozoon. Acta obstet. gynec Scand., 36 Suppl. 2, 1–133.

André J. 1961 Sur quelques détails nouvellement connus de l'ultrastructure des organites vibratiles. J Ultrastruct. Res. 5 86–108.

——— 1962 Contribution à la connaissance du chondriome. Etude de ses modifications ultrastructurales pendant la spermatogénèse. J. Ultrastruct. Res., Suppl 3 1 185

Austin, C. R., and M. W H. Bishop 1958 Some features of the acrosome and perforatorium in mammalian spermatozoa. Proc. Roy Soc. B., 149 234

Ballowitz, E. 1891 Weitere Beobachtungen ber den feineren Bau der Saugethierspermatozoen. Ztschr. f wissensch. Zoologie 52 217 292.

Bedford, H. M. 1964 Fine structure of the sperm head in ejaculate and uterine spermatozoa of the rabbit. J Reprod and Fertil. 7 221–228.

Blom, E., and A. Birch-Andersen 1961 An apical body in the galea capitis of the normal bull sperm. Nature 190 1127

Bloom, G., and L. Nicander 1961 On the structure and development of the protoplasmic droplet of spermatozoa. Zeitsch f Zellforsch 55 833–844.

Burgos, M. H., and D W F awcett 1955 Studies on the fine structure of the mammalian testis. I. Differentiation of the spermatids in the t. J Biophys. and Biochem. Cytol., 1 28 –300

Bradfield, J R. G. 1955 Fibre patterns in animal flagella and cilia. In 9th Symposium of the Society for Experimental Biology on Fibrous Proteins and their Biological Significance, pp. 306–334 Academic Press New York.

Challice C. E. 1953 Electron microscope studies of spermiogenesis in some rodents. J Roy Micr. Soc., 73 115–127

Cleland K. W and Lord Rothschild 1959 The bandicoot spermatozoon An electron microscope study of the tail. Proc. Roy Soc. B 150 24–42.

Clermont, Y E. Einberg, C. P Leblond and S. Wagner 1955 The perforatorium — an extension of the nuclear envelope of the rat spermatozoon. Anat. Rec., 121 1.

Colwin, A. L., and L. H. Colwin 1964 Role of gamete membranes in fertilization. In Cellular Membranes in Development (Michael Locke, ed.) Academic Press, pp. 233–280

Eimer T 1874 Untersuchungen über den B u und die Bewegung der Samenfaden. Verhandl. der physikal.-medicin. Gesellsch. zu Würzburg., (N.F) 6 93–136.

F awcett, D W 1958 The structure of the mammalian spermatozoon. Int. Rev Cytol., 7 195–235

——— 1961 Cilia and flagella. In The Cell (J Brachet and A. E Mirsky eds.) Academic Press, New York, Vol. 2, pp. 217–297

——— 1962 Sperm tail structure in relation to the mechanism of movement. In Sperm Motility (D. Bishop ed.) A.A.A.S Washington, D C.

F awcett, D W and K. R. Porter 1954 A study of the fine structure of ciliated epithelia. J Morph., 94 221–281

Gibbes, H. 1879 On the structure of the vertebrate spermatozoon. Q J Micros Sci., 19 487–491

Gibbons, I. R. 1961 The relationship between the fine structure and direction of beat in gill cilia of lamellibranch mollusc. J Biophys. and Biochem. Cytol., 11 179–206.

Gibbons, I. R., and A. V Grimstone 1960 On flagellar structure in certain flagellates. J Biophys and Biochem. Cytol., 7 697–716.

Gray J 1955 The movement of sea-urchin spermatozoa. J Exp. Biol., 32 775–801

——— 1958 The movement of the spermatozoa of the bull J Exp. Biol., 35: 96–108

Hadek, R 1963 Study on the fine structure of the rabbit sperm head. J Ultrastructure Res 9 110–122.

Jensen, O S. 1887 Untersuchungen über die Samenkörper der Sä gethiere Vögel und Amphibien. I. Sä gethiere Arch. Mikr Anat., 30 379–425.

Karnovsky M. J 1961 Simple methods for staining with lead" t high pH in electron microscopy J Biophys. and Biochem. Cytol 11 729.

Kaye J S. 1962 Acrosome formation in the house cricket. J Cell Biol., 12 411–431

Lenhossek, M. 1898 Untersuchungen über Spermatogenese. Arch. f. mikros Anat., 51 215–318.

Luft, J H. 1961 Improvements in epoxy resin embedding methods. J Biophys. and Biochem. Cytol., 9 409–414.

Nicander L., and A. Bane 1962 Fine structure of boar spermatozoa. Zeitschr f. Zellforsch., 57 390–405.

Retzius, G 1906 Die Spermien der Marsupialier. Biol. Untersuch. (N.F) 13 77–88.

——— 1906 Die Spermien der Vespertilionen. Biol. Untersuch. (N.F) 13 91–95.

Reynolds, E. S. 1963 The use of lead citrate at high pH as an electron opaque stain in electron microscopy J Cell Biol., 17 208–212.

Saacke, R. G., and J O. Almquist 1964 Ultrastructure of bovine spermatozoa. I. The head of normal ejaculated sperm. Am. J Anat., 115 143–162.

——— 1964 Ultrastructure of bovine spermatozoa. II. The neck and tail of normal ejaculated sperm. Am. J. Anat., 115 163–184.

Telkka, A., D W Fawcett and A. K. Christensen 1961 Further observations on the structure of the sperm tail. Anat. Rec., 141 231–245.

Watson, M. L. 1958 Staining of tissue sections for electron microscopy with heavy metals. II. Application of solutions containing lead and barium. J Biophys. and Biochem. Cytol., 11 729

PLATE 1

EXPLANATION OF FIGURES

1 Phase contrast photomicrograph of spermatozoa of *Myotis lucifugus*, illustrating the spatulate form of the head, the distinct neck segment and the unusually thick middle-piece and principal-piece. 4,500 ×

2 Electron micrograph of a frontal section of the anterior portion of *Myotis* sperm. Around this favorably sectioned spermatozoon are subtangential sections of the curving middle or principal pieces of several others. 18,000 ×

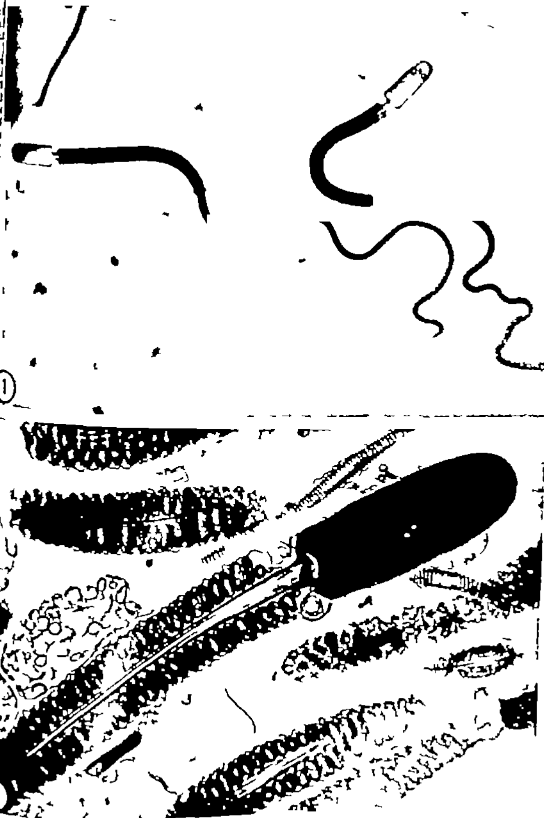


PLATE 2

EXPLANATION OF FIGURES

3 A sagittal section of sperm head of *Myotis*. Sectioned in the dorso-ventral axis, the head lanceolate, tapering to thin point. The nucleus which takes up nearly all of the head is homogeneous and very dense *throughout except for one or two small clear vacuoles* (V) The anterior two third of the nucleus is covered by membranous head cap (Hc) that encloses the acrosome (Ac) The bulk of the acrosomal material is concentrated t the tip but it also extends backward in a thin layer between the outer and inner membranes of the head cap to its posterior margin (indicated by arrows)

A concavity in the base of the head is the *implantation fossa* the site of attachment of the flagellum. The outer coarse fibers of the flagellum (Cf) exhibit no periodic structure in the middle-piece but have a distinct cross-banded ppearance in the neck region where they coalesce to form the *connecting piec* (Cp) which surrounds an bliquely oriented centriole (Ce)

Two mitochondria (Mi 1 and Mi 2) in the neck are flattened against the dorsal and ventral aspects of the connecting piece and extend anteriorly to the rim of the implantation fossa. Magnification 46,000 ×

4 A frontal section of the head. In this plane th head is broad and spatulate with rounded tip and slightly convex lateral contours. In the original micrograph the limits of the nucleus and of the crescentic crosome could be distinguished by slight density difference. An interrupted white line has been drawn along their line of *junction*.

At the posterior rim of the head lateral to the margin of the implantation fossa, a redundant portion of the nuclear envelope is reflected from the surface of the condensed chromatin, and forms membranous scroll (Ms) on either side of the neck.

The continuity of the outer coarse fibers (Cf) of the mid piece *with the segmented connecting piece* (Cp) is clearly visible here On one side the connecting piece is expanded anteriorly to form a triangular lement with its base occupying bout half of the implantation fossa. M gnification 46,000 ×

Ac
Hc
Va
Mi1
Cp
Ce
Mi2
Cf
3
Ac
Ms
Cp
Cf
Mi
4

PLATE 3

EXPLANATION OF FIGURE

5 A subtangential section of a segment of the middle piece of a *Myotis* spermatozoon corresponding to that indicated by the rectangle on the inset. The mitochondria are flattened anteroposteriorly and arranged in a flat helix in which there are two mitochondria to each gyre. The end-to-end junctions of the mitochondria in successive gyres are in line along the dorsal and ventral aspects of the middle-piece for its entire length. The mitochondria do not show the condensation of the matrix and the opening of the cristae to form light "pseudomatrix" such as has been described for a number of other mammalian species. Magnification 96,000 ×

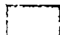


PLATE 4

EXPLANATION OF FIGURE

6 A longitudinal section of a segment from the middle piece of *Myotis* sperm such as that indicated on the inset. The mitochondria are very uniform in size and precisely aligned in close proximity to the outer longitudinal fibers of the flagellum. The cristae in their interior are long and irregular in their orientation but tend to be arranged parallel rather than perpendicular to the outer limiting membrane. At the lower right f the figure is portion of the cytoplasmic droplet of neighboring spermatozoon, containing persisting canalicular lements of endoplasmic reticulum, devoid of associated ribosomes. Magnification 96,000 ×

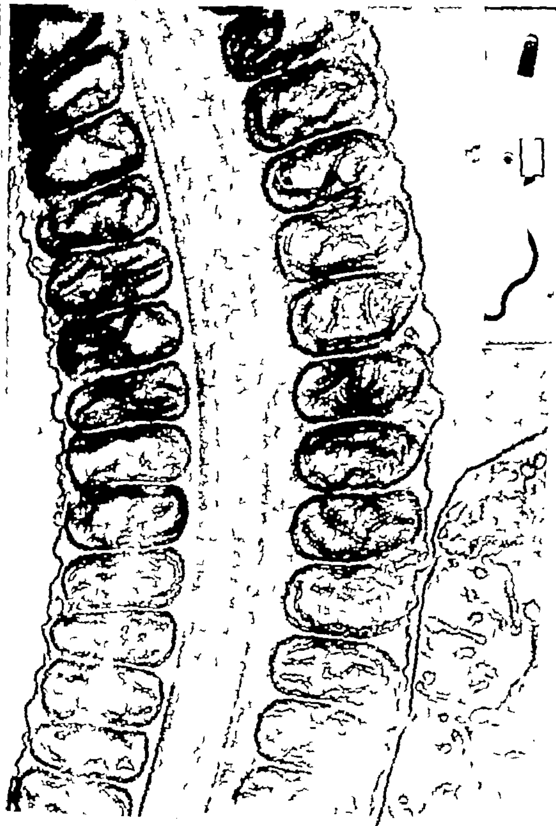


PLATE 5

EXPLANATION OF FIGURE

7 A longitudinal section of the junction of the middle and principal piece of a *Myotis* spermatozoon (for orientation see inset)

In the upper half of the figure the axial bundle of longitudinal fibers in the middle piece is flanked by cross-sections f the encircling mitochondria (Mi) The mitochondria are not as broad or as flattened they are in the anterior portion of the middle piece In the lower half of the figure the axial filament complex is flanked by cross-section of the circumferential strands of the fibrous sheath (F) The bilateral triangular dense areas t the junction of the mitochondrial nd fibrous sheaths (An) are cross-sections f the annulus, which was formerly called Jensen ring or the ring centriole. At the upper right is portion of the cytoplasmic droplet (Pd) or middle-piece bead which is characteristically located at the caudal end of the long middle piece in epididymal perm tozoa. Magnification 105,000 ×


MT
Pd
An
An
Fs
Fs

PLATE 6

EXPLANATION OF FIGURES

8 A section through the distal end of the middle piece the annulus, and the first portion of the principal piece (see inset) The cross sectioned elements of the fibrous sheath show discontinuities that correspond t the slender clefts in the circumferential fibers as seen in transverse sections of the tail (see t arrows in fig. 17) In the lower part of this figure where the plane of section passes tangential to the tail, several examples of bifurcation of the circumferential fibers of the sheath can be seen Magnification 68,000 ×

9 A longitudinal section of a sperm principal piece at level some distance caudal t the segment illustrated in figure 8. Here the circumferential fibers are narrower in their radial dimension and do not show the discontinuities present in the first portion of the sheath. The fibers in this region tend to be paired with the two members joined at their outer margin so that they ppear U or V shaped in transverse section. The limiting membrane of the tail is not closely adherent t the fibrous sheath but appears wrinkled and loose fitting. Magnification 75,000 ×

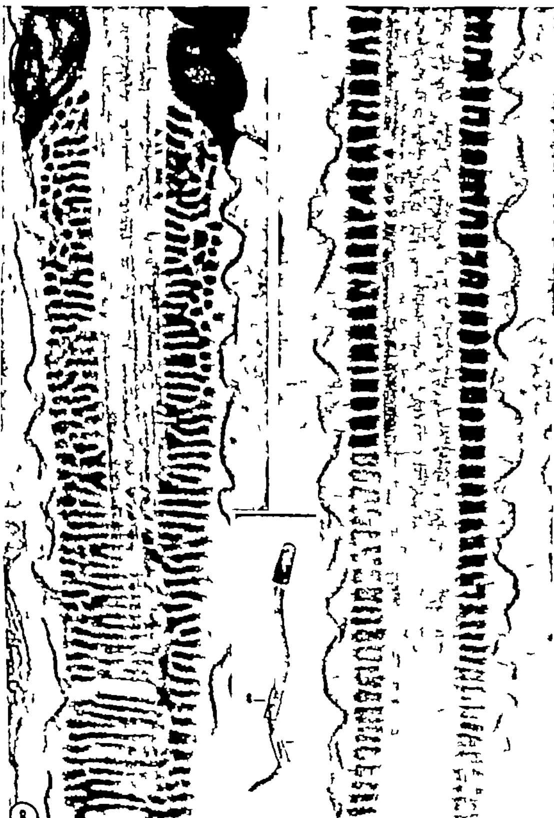


PLATE 7

EXPLANATION OF FIGURE

10 A relatively low magnification electron micrograph of an area in the lumen of the ductus epididymidis in *Myotis lucifugus* illustrating numerous spermatozoa cut transversely t various levels. For the reader interested in following the changing appearance of cross sections of the sperm at different levels along the tail, certain of the cross sections in this field have been numbered from 1 to 11 to indicate their relative position in sequence from the neck region to the tip of the end-piece. The approximate levels are also indicated on the inset. Numbers 1 t 4 are in the mid piece 5 to 10 show the grad al taper of the principal piece and the narrowing of the end-piece before termination of any of the fibers of the axial filament complex. Notice in all of the transverse sections through the mid piece that the points of end-to-end junction of the two mitochondria are pproximately on a line passing through the central pair of fibers in the axial filament complex. Magnification about 30,000 ×


1
2
3
4
5
6
7
8
9
10
11
5
7
8
10
6
2
11
1
9
4
3
10

PLATE 8

EXPLANATION OF FIGURES

11 A transverse section through the mid-piece (see inset) showing the appearance of the axial filament complex, the outer row of dense fibers and the typical arrangment of the ends of the two mitochondria on the line through the centers of the central pair of fibrils. Subfibril A in each of the nine doublets in the axial complex has dense interior and bears a pair of short diverging arms that project toward the next fiber. Subfibril B has dense rim and a light interior. Four of the coarse dense fibers of the outer row numbers 9 1 5 and 6, are distinctly larger than the others. This is an unusual feature of bat sperm. In most mammalian species studied to date, only numbers 1 5 and 6 are unusually large. Magnification 140,000 ×

12 A transverse section through the upper part of the principal piece (approximate level indicated on the inset) The circumferential elements of the fibrous sheath at this level are broad ribbon-like fibers that form a wide ring of uniform thickness around the axial filament complex. Two denser bands that cross the ring opposite fibers 3 and 8 represent the sites of longitudinal connection between the successive rings of the sheath.

The outer dense fibers at this level are reduced in number and size. Numbers 9 1 5 and 6 are about the size of the corresponding doublet to which they are attached. Numbers 2 and 7 are only about half as large and 4 3 and 8 seem to have terminated at higher level. Magnification 140 000 ×

PLATE 9

EXPLANATION OF FIGURES

13 Transverse sections near the posterior end f the principal piece. The outer dense fibers are not represented at this level and the fibrous sheath is considerably thinner The two spermatozoa shown here evidently are positioned with their heads in opposite directions since in th section at the left, the arms on the doublets project counter clockwise as they do when viewed from tip-to-base whereas in the one on the right, they point clockwise as they do when viewed from base-to-tip. Magnification 90,000 ×

14 Transverse sections through the terminal piece of one sperm (a) and the mid-piece of another (b) The latter shows nothing that has not already been illustrated in figure 11 In the section ( ) near the tip of the end-piece subfibrils A and B are still present in the doublets but the arms are no longer discernible on subfibril A. The central pair of fibrils are farther part than usual and in the interfibrillar matrix the pattern of densities linking the various fibers is less conspicuous than in the main part of the tail. Magnification 100,000 ×

15 Transverse section through the terminal portion of the end piece (a) and the anterior part of the mid-piece (b) Very near the tip of the tail one member of each doublet terminates before the other The manner in which it terminates is illustrated in figure 17

In the anterior part of the mid-piece (b) the outer coarse fibers are farther removed from the corresponding doublets than they are more posteriorly They have homogeneou dense interior and thin cortical layer of slightly lower density A number of punctate densities interpreted as cross sections of slender filaments (see at arrows) are commonly associated with the inner spect of the coarse fibers. Magnification 100,000 ×


13


14
a
15b
14b
13


15
a

PLATE 10

EXPLANATION O FIGURES

16 A sagittal section of the sperm head (in the xx axis of A in fig. 18). The head cap is bounded by amooth continuous membrane which is clearly visible in this micrograph owing to the relatively low density of the acrosome. The inner membrane of the head cap is closely pplied t the nuclear envelope except t the tip of the nucleus where an invagination of the membrane bounds a narrow subacrosomal space (Sa) The plasma membrane does not follow the contours of the underlying structures of the head but appears loose and irregularly wrinkled. 45,000 ×

17 In the upper part of the figure is transverse section through the region at the tip of the sperm tail where the double fibrils of the axial filament complex are pparently being reduced to single fibrils by an opening up f one member of each figure-of-eight cross-sectional profile t form figure-of-nine The fibrils are also losing their precise arrangement. The central pair of fibrils remain essentially altered.

In the lower half of the figure is a cross-section at the beginning of the principal piece. The narrow clefts (at the arrows) in the broad, flat, circumferential fibers of the sheath correspond to the radial discontin ities seen in longitudi al sections (figs. 7 and 8) 90,000 ×

18 Sections t three different levels of the sperm head. A is transverse section in the posterior third f the head showing its plump lliptical profile with the m jor (yy) and minor (xx) axes indicated B and C are slightly oblique sections in the anterior third of the head. The minor axi of the cross section shortens as the head tapers and becomes more flattened at the tip. 30,000 ×

19 A cross section through the first portion of the middle-piece. At this level, the size differences among the coarse outer fibers are negligible but they become marked at points f rther along the middle-piece The development of these differences can be followed by examining figures 19 15 nd 11 in that sequence. 120,000 ×

Sa

15

17

C

B

A

x

y

18

6 7 8 5 9 4 1 3 2

19

PLATE 11

EXPLANATION OF FIGURES

20 A longitudinal section through portions of the head, neck and middle-piece f a *Myotis* spermatozoon. The plane of the section is slightly oblique. The cross-banded or segmented connecting piece (Cp) is seen to be continuous with the coarse outer longitudinal fibers of the mid-piece. The outer fibrils of the axial filament complex terminate in or near two poorly defined dense masses on either side of the interior of the connecting piece. The central pair of fibrils extends into the connecting piece beyond the termination of the other fibrils. The dense mas lodged in the expanded upper end of the connecting piece is an obliquely cut centriole (Ce)

It has been postulated that the fibers in the core of the sperm tail may have a slow spiral course. A long segment of the middle-piece has been included in this figure to illustrate the absence of any suggestion of torsion of the longitudinal fibers over the span of several microns shown here. 36,000 ×

21 The plane of section illustrated here is slightly oblique so that it passes tangential to the head and through one of the two exceptional mitochondria (Mi) that re oriented longitudinally on the dorsal and ventral aspects of the connecting piece. These mitochondria are also shown in figure 3 cut in plane perpendicular t that shown here. 40,000 ×

22 A frontal section through the flattened head. The separation of the connecting piece from the concavity in the base of the head is artifactitious. The section is instructive however because it coincides with the long axis of the proximal centriole (Ce) which is set t an angle of 45 to the axis of the tail and perpendicular t an expanded upper portion of the segmented wall f the connecting piece Owing to the peculiar orientation of this centriole sections revealing the nine identifying triplet fibrils in its wall are encountered only in rare sections t an angle of bout 45 to the long axis of the spermatozoon. 38,000 ×

23 A transverse section t the lower end of the neck region at the level indicated by the interrupted line on figure "0. The central pair of fibrils is all that can be identified of the axial filament complex. They are flanked by two dense masses of granular material which seem to be the sites of termination of the other fibril The connecting piece is made up of six or seven components of irregular cross-sectional hape These are more ariable in their form nd les orderly in their arrangement than the dense outer fibers f the mid piece with which they are continuous. 54,000 ×

24 An additional example of cros section through the lower end of the connecting piece The variability of this complex structure is indicated by the fact that the number of longitudinal lements in it wall smaller here than in figure 23. I this case also portion of mitochondrion (t arrow) is inaln ted between two of the longitudinal omponents of the connecting piece and project int its interior 52,000


Nu
Ce
Cp
20


Nu
21


Nu
Ce
C
22


M
23


Ms
24

PLATE 12

EXPLANATION OF FIGURES

25 Longitudinal section through the neck and middle-piece of a spermatozoon of *Eptesicus fuscus*. The general organization of the spermatozoon is similar to that of *Myotis* except for the form and arrangement of mitochondria in the middlepiece. The mitochondria are smaller, more variable in diameter and not flattened antero-posteriorly (compare with figures 6 and 20). Small circular profiles (Mt) between the mitochondria and the plasma membrane may be persisting microtubular elements of the caudal sheath. Between the dense outer fibers (Of) and the axial filament complex (Af) are linear profiles (see at arrows) that represent the filaments which are seen in cross-sections as punctate profiles clustered around the inner aspect of the outer coarse fibers (see at arrows figs. 15 and 30). The two arrows at the upper right indicate the points where the excess nuclear envelope is reflected from the condensed chromatin to form a scroll of membranes in the neck region. 70,000 ×

26 The distal part of the middle-piece and proximal portion of the principal piece of *Eptesicus* spermatozoon. The fibrous sheath is thinner than in *Myotis* and shows no clefts in its circumferential fibers. 70,000 ×

Mt
Af
Of
25
26

PLATE 13

EXPLANATION OF FIGURES

27 Sagittal section of the tip of the sperm head in *Eptesicus* The acrosome is somewhat thicker than in *Myotis* and the subacrosomal space is slightly larger Otherwise the sperm heads of the two species are quit similar 65,000 ×

28 Cross sections through the middle-piece (below) and principal piece (above) of *Eptesicus* sperm. Both the mitochondrial and fibrous sheaths are thinner than those of *Myotis* at corresponding le h. 90,000 ×

29 Longitudinal sections of the principal piece in *Eptesicus* sperm. The sperm at the right has been sectioned tangential t the fibrous sheath Several examples of branching of its circumferential elements are indicated by arrows. This is further visual evidence gainst the persistent belief that this sheath is simple helical wrapping. 60,000 ×

30 Cross section through the proximal portion of the middle-piece of an *Eptesicus* sperm. The thin cortical layer on the outer coarse fibers is clearly shown. Between these coarse fibers and the doublets of the axial filament complex are irregular punctat profiles (at arrows) that are interpreted as cross sections f longitudinally oriented filament (see also fig 25) 90,000 ×

27

28

29

30

PLATE 14

EXPLANATION OF FIGURES

31 A highly magnified cross section through the principal piece of an *Eptesicus* sperm to illustrate the details of the axial filament complex. Each doublet fibril consists of two subfibrils. Subfibril A bears two arms which project obliquely toward the next doublet. The outermost arm is more clearly and regularly visible and it seems to extend back into the interior of subfibril A which consequently has a dark interior. Subfibril B lacks arms and has a clear center. A fan shaped dense structure projecting outward from the wall of each doublet is the slender continuation of the outer coarse fibers of the middle piece. Numbers 9 1 5 and 6 are larger than the others.

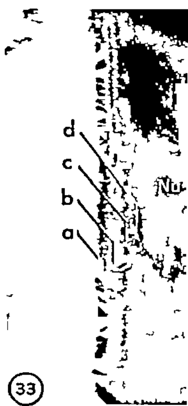
Although details of the shape of the two subfibrils is difficult to resolve clearly it appears that subfibril A is circular in section and that the wall of subfibril B is incomplete and C shaped joining the convex wall of A in such w y as to make the lumen of subfibril B crescentic rather than round. Such is clearly the case in the doublet in the inset which are from sperm tails of *Lebistes reticulatus*.

The triangular dense areas in the fibrous sheath opposite fibrils 3 and 8 are sections of the longitudinal columns that run along the dorsal and ventral aspects of the sheath. They are not in the plane of the central pair of fibrils, but lines from the center of the flagellum through doublet 3 and 8 and the corresponding thickening of the sheath make an ngle of 160 and divide the cross section into two unequal sectors. 300,000 ×

32 and 34 Transverse sections of the c udal third of the sperm head of *Myotis* at high magnification to show the relations of the head coverings. *The dense lines designatd by letters in figure 34* are respectively the plasma membrane ( ) an intermediate layer corresponding to the "post-nuclear cap of lassical cytologists (b) the outer leaf of the nuclear envelope ( ) and the inner leaf of the nuclear envelope (d) In figure 32 the relation of the tenuous intermediate l yer t the unit membranes on either side of it is interpreted in the inset. This thin layer appears to have periodic ridges that extend alter nately to one membrane then to the other Approximately 300,000 ×

33 A longitudinal section through the same region of the head. The same layers seen in transverse sections are identifiable but no periodic structure of the intermediate layer (b) is evident in this plane of section. Approximately 300,000 ×


a
32


d
c
b
a
Nu
33


a
b
c
d
34

Studies on the Thymus of the Mammal

XIV HISTOLOGY AND HISTOCHEMISTRY OF EMBRYONIC AND EARLY POSTNATAL THYMUSES OF C57BL/6 AND AKR STRAIN MICE [1]

CHRISTIANNA SMITH

Department of Biological Sciences Mount Holyoke College South H dley Massachusetts

ABSTRACT Thymuses of mice of the C57Bl/6 and AKR strains from ten-day-old embryos through one day after birth were studied histologically and histochemically New evidence is presented of the penetration of the endodermal epithelium of the third pharyngeal pouch of ten-day-old embryos by basophilic lymphoblasts.

Both alkaline and acid phosphatases showed different distributions in the thymuses of the two strains at 12 and 13 days. By 15 and 16 days, alkaline phosphatase activity in thymuses of the C57Bl/6 strain was peripheral; in thymuses of AKR mice, it was present throughout the lobes. In the C57Bl/6 lobes, little acid phosphatase activity was observed; however in the AKR thymuses, activity was strong and was located especially in the cortex. The characteristic patterns of enzymatic ctivities of the postnatal thymuses were well established at 17–18 days. Prenatally the medullae of the thymuses of both strains contained esterase-rich inclusion cells and epithelial reticular cells which occurred singly or as nests of cells. The inclusion cells also possessed alkaline phosphatase activity It is suggested that these cells may contain the precursors of the humoral factor( ) of the thymus. The thymuses were also studied after treatment with the periodic acid-Schiff technique for glycogen and the procedure for showing sites of adenosine triphosphatase activity

Although there have been many studies on the embryology of the thymus they have for the most part neglected changes in the chemical properties of the differentiating thymic cells. In the present report, there has been an attempt not only to reinvestigate the origin of the thymic lymphocyte but also to examine histochemical aspects of the transformation of the epithelial pouch into its definitive post natal structures. In addition a comparative study has been made of the developing thymuses of C57Bl 6 and AKR strains of mice, since previous work (Smith '61) showed that there are differences in alka line and acid phosphatase activities in thymuses of these two strains

It was found that cells differing morphologically from the epithelial cells and interpreted as lymphoblasts were present in the epithelium of the third pouch of the 10- and 11-day-old embryos Differences between the two strains in the patterns of alkaline and acid phosphatase activities were found as early as 12–13 days. The suggestion i made that the medullary inclusion cells and the epithelial reticular cells may be the thymic elements responsible for the humoral factor now attributed to the thymus (Metcalf, '56 Osoba and Miller '63 Law Trainin Levey and Barth, '64)

MATERIALS AND METHODS

Fetal mice from 10–19 days of age, newborn and one-day-old postnatal mice of the C57Bl/6 and AKR strains of mice were used in this study Also studied were a few litters from lines 25 and 55 of the Mount Holyoke College stock (courtesy Dr K F Stein) The ages of the mice were determined mostly by the presence of a vaginal plug (day 0) observed after mating during the night or for more accurate timing of the early stages, during a short morning period Body lengths were recorded and were used for timing by reference to Gruneberg tables ('43) when

[1] Thi investigation was supported by research grant CA-01358 from he Nation l Cancer Institute National Institutes of H alth, U S Public Health Service
The author is indebted to Carol C. Cole and Judith H Myers for technical ssistance

vaginal plugs were not observed The lengths within a given litter were alike or nearly so although in a few litters a range of 4 mm was found with an occasional runt or long fetus Because of this there is some overlapping of total lengths in this consideration of the ontogeny of the thymus Observations were also correlated with the descriptions and models of the developing pharynx of the mouse by Crişan ('35) In 10- and 11-day-old fetal mice pharyngeal complexes two, three, and four were compared; at 12 and 13 days the parathyroid-thymic rudiment was followed in later stages only the thymus was examined

The pregnant mice were killed by cervical dislocation and dissected on a table kept cold with ice Material from embryos or newly born mice from 90 litters was frozen on dry ice and stored in a freezer at −18 C Whole embryos were used if they were 12 days old or younger Between 14 and 17 days of age the thoracic regions were cut and at 18 days and older the thymuses were isolated and sectioned. Fresh frozen sections were cut in a cryostat at −18 C dried in front of a fan for a half hour and stored no longer than three hours at 4 C before continuing with the various technical procedures With the younger embryos best results were obtained if sections were cut at 15 μ with the older the routine thickness was 10 μ. For cellular detail thinner sections were needed

Standard methods were employed for the demonstration of sites of enzymatic activity but certain modifications were necessary with the embryonic material. Unless otherwise noted all sections were fixed in 10% buffered formalin for 30 minutes at 4 C Sites of activity of two enzymes alkaline phosphatase and nonspecific esterase were studied in all thymuses The technique of Pearse ('53) modified by Padykula ('55) for the demonstration of *nonspecific esterase* activity was chosen The incubation time in the substrate was lengthened to 40 minutes so that sites of weak activity could be seen more clearly The azo dye method of McKay Hertig Adams, and Danziger ('53) for determining the presence of *alkaline phosphatase* was regularly employed. Incubation at 4°C was one hour Gomori's glycerophosphate-cobalt sulfide method ('52) modified by Padykula and Herman ('55) was also often used to demonstrate *alkaline phosphatase* and routinely for *adenosine triphosphatase* activity sections for the latter techniques were not fixed. As the appearance of adenosine triphosphatase activity in the developing thymus was so gradual and weak, an incubation of 20–40 minutes was necessary To show sites of *acid phosphatase* activity sections were incubated in glycerophosphate-lead sulfide substrate (Gomori, after Lillie '48) The usual two hour incubation period was lengthened to three hours for embryonic thymuses of C57Bl/6 mice and decreased to one hour for those of the AKR strain because of differences in the degree of acid phosphatase activity Toward the end of the study Barka's azo-dye method ('60) was also tried with unfixed sections and proved superior for cellular detail. Also with unfixed sections sites of *leucine aminopeptidase* activity in developing parathyroid glands were brought out with the methods of Nachlas Crawford, and Seligman ('57) The *periodic acid-Schiff* technique was successfully employed with frozen sections postfixed in ice cold Rossman's fluid. May-Grunwald Giemsa solutions (Jacobson and Webb, '52) were used on sections postfixed in Carnoy's solution. Some sections prepared for studies of enzymatic activity were counterstained with safranin but most were not.

Control sections for the enzymatic reactions were inactivated by immersion in boiling water for five minutes or the substrate was omitted from the incubating solution. In the periodic acid Schiff method control sections were digested in several changes of saliva for a period of one hour

In some of the youngest stages only one technique was applied to an embryo but in the majority successive slides of alternate serial sections were treated with the different techniques In this way the properties of given areas blood vessels or cells could be compared Beginning with the 15-day-old fetuses a number of techniques were applied to a series of slides on which several sections had been mounted thus

the last section of one slide could then be read with the first of the next.

For paraffin embedding, thymuses were fixed in Rossman's fluid for the periodic acid-Schiff techniques and in Helly's and Bouin's fluids for subsequent staining with the May-Grunwald-Giemsa procedure

Suspensions of thymic cells and imprints were made from 18-day-old fetuses. Thymuses from the fetuses of one litter were pooled and minced in serum from the blood of the mother Streaks of suspended cells were then made with a camel's hair brush on slides and dried rapidly This material and imprints were treated with the techniques for demonstrating alkaline phosphatase or nonspecific esterase activity or stained with May-Grunwald-Giemsa's solutions. A suspension of thymic cells from a newborn AKR mouse was also made and the preparations were stained with Barka's azo dye technique for acid phosphatase activity

OBSERVATIONS

Histology

10- and 11-day-old embryos In embryos of both strains 4–7 mm long average 5 1 mm the second, third and fourth pouches opened into the pharynx. The second and third pouches maintained their attachment to the ectoderm for the most part but the fourth did not. Of the 37 examined, in only one animal, 6 5 mm long was there a fourth pouch with a well developed cord of cells uniting it to the ectoderm. The two sides were usually at the same stage of development but this was not always so This dissimilarity is well shown in Crisan's model of the pharynx of a 9–10-day-old embryo in which the cervical duct is intact on one side and not on the other (fig. 11 '35)

At ten days of age embryos 4 mm long, the epithelium of the third pouch (the parathyroid-thymic anlage) varied from one layer near the pharynx to two or more layers toward the periphery If two layered or more the surface wing-shaped cells had processes which extended around basal fusiform cells In fixed material stained in May Grunwald-Giemsa solutions this parathyroid-thymic complex could be easily differentiated from the second and fourth pouches by the strong basophilia of the epithelial cells toward the lumen and the smooth appearance of the lining cells (figs 1 2) The strongest basophilia occurred usually toward the base of the pouch. Epithelial cells with typical nuclei (sharply defined spherical or oval nucleolus delicate nuclear membrane scant amount of chromatin) are seen in the upper wall of the pouch (fig. 2) and in the basal epithelial cells (fig. 7) Nuclear characteristics are more clear cut in material fixed in Bouin's (fig. 7) than in Helly's solution (fig. 2) The nuclei of the pouch epithelium resemble closely those of the epithelial reticular cells of the postnatal thymus (Downey 48) In other regions, as in some parts of the lower wall in figure 2 it was difficult to classify the nuclei.

The epithelium was in general sharply delimited from the surrounding mesenchyme (figs. 1 2) but there were areas where this was not so (fig. 2 indicated by horizontal arrows) Even when the outline of the pouch was sharp occasional cells could be seen bridging the line between epithelium and mesenchyme (figs. 2, 2a 3) These bridging cells were identified as basophilic lymphoblasts They possessed nuclei with a typically large, irregular central nucleolus and basophilic cytoplasm (figs. 2 2a, 3) These nuclei are similar to those described by Ohno and Kinosita ('56) who showed in rat lymphoblasts that this characteristic irregular central body was composed of a Feulgen negative nucleolus surrounded by three double stranded Feulgen positive threads attached to it and radiating from it

Evidence of migration of these lymphoblasts into the epithelium was indicated by the following shapes of the cells and their nuclei (1) the "handmirror" type with a rounded or pointed cap of cytoplasm directed toward the lumen a round or oval nucleus within the epithelium (figs. 2 2a 3) and a basophilic tail that extended straight out into the mesenchyme (figs 2 2a 3) or that was more or less parallel to the under surface of the epithelium (figs 5 6) and (2) less often, an elongated worm-like or corkscrew shaped nucleus The latter type gave no hint as to direction of migration The handmirror

type of lymphoblasts with extended tails was relatively scarce as few tails were in the same plane as the nucleus within the epithelium Many cells with stumps of tails within the epithelium (fig 4) were found and isolated sections of tails could be seen just under the epithelium in the mesenchyme Figure 7 demonstrates lymphoblasts which have been incorporated into the epithelium and have lifted up the basal layer of typical epithelial cells The nucleus of the lower cell shows the characteristic lymphoblastic structure Similar basophilic lymphoblasts were often found in the mesenchyme adjacent to the pouch (figs 1 2 4 6) and their forms indicated that many were fixed while in motion. Mitoses were numerous toward the surface of the epithelium (fig 2) which is the usual position for dividing cells in columnar epithelium some were present basally or at the junction of the epithelium and the mesenchyme (fig 11)

Macrophages could be seen within or on the surface of the epithelium of the second third and fourth pouches These loaded phagocytes were more numerous in the proximal and distal regions They were filled with Feulgen positive granular debris which could be seen as scattered granules throughout the epithelium.

12–14-day-old embryos At 12–14 days of age 50 embryos averaging 9 3 mm in length (range 7–11 mm) were studied. This period is one of transition in structure and form The thymic anlage of the AKR strain mouse was usually more advanced in its development than that of the C57Bl 6 In embryos 8 mm or less in length the parathyroid thymic complex might still possess endodermal (fig 11 C57Bl 6) and ectodermal connections but in those about 9 mm long these ducts had mostly disappeared Macrophages were associated with remnants of the connections At 12 days the thymic rudiment was somewhat V-shaped with short arms and a thick apex In 13–14-day-old embryos the rudiments were larger and more elongate

In the preparations stained with May Grunwald-Giemsa basophilic lymphoblasts with large irregular nuclei could be found singly or in nests of [illegible] three cells within the epithelium An occasional handmirror shaped lymphoblast could be seen with its cell body within the epithelium and its tail in the mesenchyme (fig. 6) As the walls of the third pouch thickened in embryos of this age group a gradual increase in strongly basophilic lymphoblasts took place until they were numerous throughout the anlage (arrows, fig 12 AKR 12 days old 8 mm long) The basophilic wing-shaped cells that formerly lined the lumen were now scattered (fig 12) At this same time a fairly wide cellular capsule enclosed the thymus in contrast to the few cells around the parathyroid and thyroid glands (fig. 12) This capsule of oval and round cells looked as though it were being incorporated into the thymus in regions of a hilus or in some tangential sections at the base of the rudiment However the outline of the thymic anlagen was for the most part clear-cut

15–18-day-old embryos The growth of the thymuses in the 15–16- and 17–18-day old groups was accompanied by the appearance of postnatal characteristics The 15–16-day-old embryos averaged 14 1 mm in length (range 12.5–16 mm); the 1 18-day-old 17 5 mm (range 15–19 mm) Lymphocytes with intensely stained basophilic cytoplasm were more abundant in the developing cortex than in the medulla Epithelial reticular cells could be distinguished in both cortex and medulla. In the thymus of the 18-day-old mice the characteristic subcapsular zone of cells, larger and paler than the rest of the cortex had differentiated. In these thymuses the typical thymic vascular pattern with arched cortical capillaries was seen Lobulation of the surface had occurred and the capsule had lost the cellularity of earlier stages

19 days prenatal–1 day postnatal mice As growth continued through the perinatal period (19-day embryo new born one day old) the morphology of the thymus was essentially the same as that described for the 15–18-day old embryos.

In the adult, the thymus of the AKR strain of mouse is larger than that of the C57Bl 6 (Smith '61) and this difference was evident in the embryonic thymuses of the two strains

Histochemistry
Alkaline phosphatase

10–11-day-old embryos With the alkaline phosphatase techniques, the third pouch was more reactive than the second and the fourth. As frontal sections were followed from the ventral to the dorsal side, a strong reaction appeared in the ventral portion of the pouch and again dorsally particularly in the anterior wall near the opening into the pharynx. The faintly colored cells of the opening of the pouch to the pharynx (a continuation of the lining of that part of the pharynx) were sharply delimited from the rest of the highly reactive parathyroid-thymic anlage (fig. 8)

12–14-day-old embryos With this technique a difference appeared in the thymic lobes between C57Bl/6 and AKR strains at 12 days of age. In general, in the embryonic thymuses of the C57Bl/6 strain, the body (the thickened apex of the V) and particularly its lateral cells, was the most reactive (fig. 13) Even though the pouch was less reactive dorsally and medially in most cases, the blackened cells in that region were sharply delimited from the negative epithelium of the pharyngobranchial duct (fig. 14 arrows) In the thymic pouch of the AKR strain, the strongest reaction was usually in the head, directed toward the periphery (fig. 15) In both strains, the cytoplasm of all cells in the most reactive areas possessed alkaline phosphatase activity; the enzyme occurred in the lymphocytes, around the nucleus of the epithelial cell, and in the processes of the mesenchymal reticular cell. In the 14-day-old embryo the mesenchymal cells were the most reactive and were often arranged parallel to and a short distance away from the outer surface as seen in figure 21 Nonreactive macrophages were occasionally present within the epithelium of the pouch.

15–18-day-old embryos. At these ages, clear-cut differences were present between the thymuses of the C57Bl/6 and AKR strains of mice with the alkaline phosphatase techniques. As most lymphocytes of the C57Bl/6 thymus were negative the thymus was ivory in color under low power after treatment with the azo dye technique except for an uneven reactive outer zone of blackened mesenchymal reticular cells and large lymphocytes (figs. 24 28 30) This zone varied in width and in intensity of reaction not only among thymuses from different animals but between the two lobes of one thymus. In general, the anterior dorsal border was most reactive.

In the AKR thymus however there were so many positive reticular cells and lymphocytes that with the azo dye technique it appeared grey in color (figs. 25 29 31) There were more of these phosphatase rich cells in the cortex than in the medulla. These show clearly in figure 26 a photomicrograph of a thymus of a 16-day-old embryo (beta glycerophosphate-cobalt sulfide method) and in figure 31 (18-day-old thymus, azo dye technique) As in the C57Bl/6 thymus some anterior dorsal lobules were more intensely reactive than any other region of the lobes.

The extent of the medulla in both strains was indicated by the presence of blackened medullary arteries and strongly reactive inclusion cells occurring singly or in nests with less reactive mesenchymal reticular cells and the least reactive epithelial cells. The examination of suspensions and imprints confirmed the difference in alkaline phosphatase activity in the thymic lymphocytes of the two strains.

19 days prenatal–1 day postnatal mice In this group the postnatal enzymic characteristics of the thymuses of the two strains became well established In the C57Bl/6 thymus, the cortex was mostly inactive except for scattered reticular cells and the endothelium of the arched cortical capillaries; in the cortex of AKR thymuses in addition to the reactive arterial endothelium, reticular cells and lymphocytes were positive. However in the AKR thymus, distinctive strongly reactive focal areas in the medulla which characterize the adult thymus had not yet developed the medullae of both strains appeared as described in the 15–18-day-old group.

Nonspecific esterase

10–11-day-old embryos In general, the second third and fourth pouches resembled each other in regard to degree of esterase activity although if any variation occurred, the third pouch was the most active The reactive cells were the wing

shaped cells lining the lumen and those which were located near the pharynx possessed the greatest activity (figs. 9 10) With this technique, reactive macrophages loaded with debris were seen clearly within the epithelium and on the mesenchymal surface of the three pouches.

12–14-day-old embryos In this group the most deeply stained region was the body of the pouch (fig. 16) There were no obvious variations due to strain of mice With the occlusion of the lumen, the derivatives of the wing-shaped or stellate epithelial cells were grouped centrally (fig 17) or were present toward the center of the lobe as single cells or as small groups or nests of cells (fig 18) These epithelial cells were now differentiated into two kinds One type the strongly reactive inclusion cell, was an ovoid or roundish cell distinguished by an eccentric nucleus, round or oval nucleolus and coarse round, *blackened cytoplasmic inclusions on one side only of the nucleus* (figs. 19 22) The other the epithelial reticular cell was an irregularly shaped cell with fine, negative granules in extensive reactive cytoplasmic processes (figs 19 22 23) These cells varied in degree of activity many were highly reactive. Capillaries were differentiated at 14 days but only occasional reactive cells abutted their walls. Less reactive mesenchymal cells and/or macrophages might be components of the nests (fig 23)

15–18-day-old embryos As in the 12–14-day-old embryos no differences due to strain were observed with this technique Highly reactive single cells and groups of inclusion and epithelial reticular cells were concentrated in the medulla often near the corticomedullary line (fig. 32) A reconstruction of six sections indicated that, as in the adult, these dense nests of cells ran through a number of sections. In the older thymuses of this group slightly reactive mesenchymal and epithelial reticular cells began to appear in the cortex. The cytoplasm of lymphocytes sometimes contained a few dye granules Reactive cysts were present.

Suspensions of cells treated to show sites of esterase activity were made from fetal thymuses of both C57Bl/6 and AKR strains of mice as had been done with postnatal thymuses (Smith '64) Variations in degree of activity among cells showed more clearly in these preparations than in the frozen sections. Some lymphocytes of all sizes possessed esterase activity in the cytoplasm. Reactive small and large *macrophages contained one or more phag*ocytosed cells. Inclusion cells were strongly reactive Single reticular cells varied in depth of stain from pale (probably cortical cells) to dark (probably medullary cells) Nests of reticular cells inclusion cells and macrophages varied in size from small groups (three cells) to large balls.

19 days prenatal–1 day postnatal mice The pattern of esterase activity developed in the 15–18-day-old embryos became that of the postnatal thymus, with more activity concentrated in the medulla than in the cortex. From one thymus to another the lymphocytes showed a wide range of activity

Acid phosphatase

12–14-day-old embryos During this period, a difference in acid phosphatase activity between the two strains became established In the thymic rudiments of the C57Bl/6 embryos, little activity was present and most of that occurred in the macrophages. In contrast, the thymic anlagen of the AKR strain of mice were the most active organs in their area (fig. 30)

15 days prenatal–1 day postnatal mice The adult distribution of acid phosphatase activity was established at 15–16 days These characteristics were low activity in the medulla of the C57Bl/6 thymus and a high activity in the *cortex* of the AKR strain mouse (fig. 33, 19-day-old mouse). In the C57Bl/6 thymus, the reactive medullary cells were mostly macrophages and mesenchymal *reticular* cells. In the AKR thymus, the positive cells included some medium sized and large lymphocytes, mesenchymal reticular cells with extensive cytoplasmic processes and macrophages Epithelial reticular cells were unstained or only slightly so. Cellular types were best seen with the azo dye technique A suspension of cells from a newborn mouse stained with Barka's azo dye technique confirmed the observations made on the frozen sections.

Adenosine triphosphatase

15–18-day-old embryos Vascular adenosine triphosphatase activity became evident in this age group in both strains in the interlobular and medullary arteries arterial capillaries and some arched cortical capillaries. Of the 18 embryos examined, 17–18 days old, only one possessed reactive endothelium in the medullary veins. The blood vessels in the mediastinal connective tissue were reactive prior to any activity in the thymus.

19 days prenatal–1 day postnatal mice In this age group the endothelium of all thymic blood vessels had high adenosine triphosphatase activity

Periodic acid-Schiff reaction

10–11-day-old embryos With the periodic acid-Schiff technique glycogen was present in two locations in pouches of embryos 6.5 mm long both C57Bl/6 and AKR strains (1) in the endoderm continuous with that of the reactive pharynx, and (2) in the anterior dorsal wall, the first evidence of the differentiation of the parathyroid glands.

12–14-day-old embryos. In embryos of both strains of mice measuring 7 5 mm and 8 mm long, well defined proliferations of parathyroid cells in the anterior dorsal wall of the pouches near the attachment to the pharynx contained glycogen These cells were comparable to ones active with the esterase and leucine aminopeptidase techniques. In a litter of four AKR embryos 14 days of age two possessed not only anterior dorsal reactive cells but also well stained medullary cells the other two contained less obvious scattered reactive cells throughout the lobes. The C57Bl/6 thymuses at this age were mostly negative Differences such as these have made it difficult, in some instances, to draw general conclusions. There was no well defined capsule of reticular fibers

15–18-day-old embryos In this age group the anterior dorsal border of the thymic lobes in both strains was populated with reticular cells and lymphocytes with glycogen in them this border was a site also of alkaline phosphatase activity Within the medulla, mesenchymal and epithelial reticular cells, both as single cells and as groups contained glycogen (fig 2") Lymphocytes lacked glycogen except in the subcapsular zone In these sections of the thorax, the thymus was the least reactive structure.

19 days prenatal–1 day postnatal mice At 19 days a distinct change occurred in the amount of glycogen in the thymus Many of the small cortical lymphocytes, but not the larger lymphocytes of the subcapsular zone contained glycogen the lymphocytes of the medulla were negative. Glycogen-containing reticular cells continued to be present in the medulla.

Leucine aminopeptidase

12–14-day-old embryos In the third pouch complex, leucine aminopeptidase activity was localized in the anlagen of the parathyroid glands of embryos 12 days of age and older The thymic rudiments were negative and continued to be in the thymuses of the older embryos and postnatal mice investigated in this study

Cervical vesicle

Well formed and distinct cervical vesicles or their remnants were followed in 11-day-old embryos through newborn mice. In general, the cervical vesicle was closely applied to the head of the third pouch rarely did it seem to be an integral part of it. The epithelial cells of the cervical vesicle were not basophilic when stained with May-Grunwald-Giemsa as were those of the third pouch. After the techniques for demonstrating alkaline phosphatase and esterase activities the vesicles were in general either negative or weakly reactive. Some or all of the vesicle was reactive with the periodic acid-Schiff technique as was the cervical sinus from which it was derived; in the anterior dorsal tips of the older thymuses (16-day-newborn) the cervical vesicles remained as cysts with reactive cells or as nests of cells. These remnants of the cervical vesicle extended into the peripheral connective tissue as cellular cords.

DISCUSSION

Morphological correlations

An understanding of the morphogenesis of the thymus of the mouse can best be obtained from Crisan's "Die Entwicklung

des thyreo-parathyreo-thymischen Systems der weissen Maus ('35). This important report presents a detailed description of the development of these pharyngeal derivatives with pictures of models from the 3–4-day-old stage through 13–14 days. Crişan noted marked variations in crown-rump length not only between embryos of the same age in different litters but also among individuals of the same litter. Because of these variations the data presented in this report include both the age and crown-rump length. Strain variations in size are also present. In the adult, the thymus of the AKR strain of mouse is larger than that of the C57Bl/6 (Smith, '61) and this difference in size has been shown to be also a fetal characteristic.

Crişan described the thymic anlage as possessing two main parts (1) a tail from which the main body of the thymus develops as an endodermal derivative of the third pouch a head partly endodermal from the lateral half of the dorsal diverticulum and partly ectodermal from the medial end of the cervical duct and the cervical vesicle. Crişan noted in his observations of the 16- and 17-day stage the presence of a remnant of the lumen of the cervical vesicle which was lined with flat or cuboidal epithelium at the anterior end of one lobe At 18 days he mentioned only the existence of cysts in the anterior third of the thymus. In our material the remnants of the inner end of the cervical duct and cervical vesicle were still present in the 19-day and newborn thymuses and were distinct from the thymic cells. From the present study there is no clear evidence of a contribution by the ectodermal cells to the thymic parenchyma.

Origin of thymic lymphocytes

The origin of thymic lymphocytes has been the subject of much investigation over a long period of years (Hammar '36, brief review by Auerbach '61) The question is simply are thymic lymphocytes mesenchymal lymphoid cells which have invaded the pouch epithelium or are they epithelial cells which have differentiated *in situ?*

In an experimental approach to the problem Auerbach ('60 '61) presented data to support the concept of the epithelial origin of thymic lymphocytes. Auerbach explanted 12 and 12½-day-old thymuses of mice (BALB/C × C3H) which had been treated with trypsin to remove the layers of mesenchymal cells surrounding the lobes. From his experimental work, he concluded that " the epithelial component of the rudiment is capable of forming the lymphoidal tissue of the thymus, and that neither migrating cells of the host, n[illegible] thymic mesoderm, nor generalized mese[illegible]chyme contributes significantly to th[illegible] initial lymphoidal cell population of th[illegible] mouse thymus ('61 p. 337)

Our work, on the other hand, support[illegible] that of Maximow ('09) who concluded from a comparative study of rabbit, rat mouse, guinea pig, and cat material, that mesenchymal lymphocytes infiltrated the epithelial anlage of the thymus. Maximow found the mouse thymus less favorable than that of the rat or rabbit for study because of the slight difference between the basophilia of the epithelium and the lymphocytes. The similarity in depth of stain of the cytoplasm in these two types of cells is demonstrated in our figures 2–6.

Observations made in our study of the embryonic thymus *in situ* suggest that the 12 and 12½-day-old thymuses which Auerbach used as explants already possessed lymphocytes which had migrated earlier from the mesenchyme into the epithelium. Evidence has been presented that basophilic lymphoblasts migrated into the endodermal epithelium of the third pouch in 10- and 11-day-old embryos (figs. 2–5) At this time the pouches were still open to the pharynx and were connected to the ectoderm.

The evidence supporting the conclusion that lymphoid cells found in the epithelium of the thymic anlage had migrated from the mesenchyme were (1) the presence of handmirror shaped lymphoblasts bridging the epitheliomesenchymal border and ( ) the existence of lymphoblasts in the subepithelial mesenchyme. The evidence gains support from observations made on the motion of cells in tissue culture in which one of the phases of lymphocytic movement is this so-called "handmirror" stage with the nucleus ahead. In 1945, DeBruyn described the migration of lymphocytes in tissue culture as consisting of two phases

(1) a polarized phase with an active anterior pseudopodial area and a passive posterior tail (the handmirror form) (2) a depolarized phase with pseudopodia arising continuously from a rounded cell body The anterior cap with motile pseudopodia had been described previously by Rich, Wintrobe and Lewis ('39) In our material the anterior cap is seen in figures 2 and 4 A review of the movement of lymphocytes has been made by Trowell ('64) in which he concluded that lymphocytes crawl through the meshwork of a plasma clot by a predominantly worm-like motion, with transitory handmirror forms and examination of sections suggests that this is the way they normally migrate through tissues, especially through layers of epithelium."

Although the handmirror shape is a form often seen during the movement of lymphocytes, Marchesi and Gowans ('64) have portrayed lymphocytes with a forward extension of cytoplasm and no posterior tail migrating into the lymph node from its postcapillary veins.

The origin of the thymic mesenchymal reticular cell may be related to the origin of the lymphocyte According to Sundberg ('60) lymphocytes may enlarge and become indistinguishable from mesenchymal reticular cells. These cells may also enter the anlage later with the ingrowth of the capillaries.

Cytochemcial aspects of thymic differentiation

One of the few cytochemical studies of the developing thymus is that of Milaire ('59) who investigated the pharyngeal region of embryonic mice from eight through eleven and one-half days of age as part of a larger study of cephalogenesis. His techniques included the periodic acid-Schiff for glycogen pyronin-methyl green for DNA and RNA, and Gomori's metal-salt method for alkaline phosphatase in paraffin sections. Milaire noted that the successive evaginations of five visceral pouches were accompanied by the conspicuous development within the cells first of glycogen and RNA and secondly of alkaline phosphatase activity He described the presence of RNA particularly in the apical pole of the cells a region which in our material was most strongly basophilic in the cells of the third pouch. The ectoderm covering the arches and lining the cervical sinus was also positive for these three chemical components. According to Milaire at eleven and eleven and one-half days, there was little evidence of activity in the endoderm and in the ectoderm there was almost none. We found, between 10 and 12 days, that glycogen varied in amount in the cells of the cervical sinus and was consistently present in the parathyroid anlage. During this period, also alkaline phosphatase activity did not decrease but a difference in pattern occurred in the distribution of active cells which was characteristic for the thymic rudiments of C57Bl/6 and AKR strains of mice

It has been shown in histochemical studies of the postnatal thymus of C57Bl/6 and AKR strains (Smith Wharton, and Gerhardt, '58 Smith, '61 '64) that these strains differ in the distribution of alkaline and acid phosphatase in the mesenchymal components but that both possess nests of esterase rich epithelial cells in the medulla and medullary inclusion cells (also epithelial in origin) reactive with the techniques for alkaline phosphatase and nonspecific esterase activities. The present study demonstrates that these characteristics appear in the embryo

The differentiation of the adult pattern of cells reactive with the techniques for the demonstration of alkaline phosphatase activity is established in 15-day embryos. As noted by Smith ('64) the thymus of the C57Bl/6 mouse (and its close relatives C57Br/J C57L/J and C58/J) is characterized by no activity in the lymphocytes, some in the cytoplasm of the mesenchymal reticular cells some around the nucleus of the epithelial reticular cells and strongly reactive inclusion cells. In contrast, most cells in the cortex and medulla of the AKR thymus (and many other thymuses from strains of mice from the Jackson Laboratory) are reactive. The strongly reactive focal areas in the medulla which are however distinct characteristics of the adult thymus of the AKR strain, had not appeared at one day of age

The present study corroborates that of McAlpine ('55) who noted increased alkaline phosphatase activity in the subcapsu-

lar zone of the cortex of the rat thymus particularly at the cranial pole. McAlpine concluded that the greater activity was associated with the formation of the large thymocytes characteristic of the outer cortical zone

In both strains of mice beginning with the thirteenth day the peripheral distribution of sites of alkaline phosphatase activity in the reticular cells and lymphocytes is paralleled to a fairly marked degree by cells containing glycogen after staining with P.A.S solutions. This distribution of glycogen was noted also by Smith and Waldron ('50) in their study of glycogen in fetal thymuses of C57Bl/6 mice Single cells and cell nest with glycogen in them were present in the medulla. In both strains glycogen appeared in the small cortical lymphocytes by the nineteenth day and according to Smith and Thomas ('50) was contained in about one-third of the cortical small lymphocytes through the fourteenth day after birth. The presence of glycogen in these small thymic lymphocytes suggests that it may be important in the energy requirements of thymic function during this period An outer zone of medium and large sized lymphocytes and reticular cells developed at the 17–18-day-old stage The lymphocytes of this zone did not contain glycogen Kaplan ('61) noted this outer zone in one day-old C57Bl mice its decrease by ten days and its loss at 20–30 days. He believed that the immature cells of this subcapsular zone were particularly susceptible to the strain C57Bl lymphoma agent.

Evidence of secreting and phagocytic activity in the thymus

Two interesting derivatives of the epithelial anlage of the third pouch have been traced in the embryonic thymic medulla One cell type is rich in esterase activity and contains fine seed like unstained cytoplasmic granules Similar cells but less reactive are found in the cortex. The other the inclusion cell strongly reactive with the techniques for esterase and alkaline phosphatase possesses coarse cytoplasmic granules or inclusions which have blackened surfaces and are embedded in highly reactive cytoplasmic ground substance (Smith, '61) These inclusion cells were first described by Ito in 1959 in the hamster thymus and were called oval cells by Smith in 1961 in the mouse thymus Ito's prior designation has been adopted. If the thymus secretes a humoral factor (Metcalf '56; Osoba and Miller '63 Law Trainin Levey and Barth, '64) these reactive cells could be the source of the secretion. In his discussion of the electron microscopy of the thymus Clark ('63, '64) noted that the thymic epithelial cells contained two types of inclusions that might be considered secretory The electron micrograph of one type of cell which contained cytoplasmic vacuoles with amorphous contents resembles the inclusion cell. The second type of cell contained small dense granules but Clark noted that similar granules were also present in macrophages and endothelial cells and therefore might not be secretory

The presence of macrophages loaded with phagocytosed cellular debris throughout the embryonic life of the thymus should be noted as an example of the constant removal of cells during growth Furthermore little is known about the differentiation of phagocytes during the fetal existence of the mammal. The current study presents morphological evidence of the presence of phagocytes in the epithelium and on the surface of the pharyngeal pouches as early as ten days.

LITERATURE CITED

Auerbach, R. 1960 Morphogenetic interactions in the development of the mouse thymus gland Develop Biol., 2. 271 284.

——— 1961 Experimental analysis of the origin of cell types in the development of the mouse thymus. Develop. Biol 3 336–354

Barka, T 1960 A simple azo-dye method for histochemical demonstration of acid phosphatase Nature 187 248–249.

Clark, S. L., Jr. 1963 The thymus in mice of strain 129/J studied with the electron microscope. Am. J Anat., 112 1–34

——— 1964 Electron microscopy of the thymus in mice of strain 129 J In The Thymus in Immunobiology (R. A. Good and A. E. Gabrielsen, eds.). Chapt. 2, 85–93 P al B Hoeber Inc New York.

Crisan C. 1935 Die Entwicklung des thyreo-parathyreo-thymischen Systems der Weissen Maus. Z. Anat. Entwicklungsgeschichte 104 327–358.

DeBruyn, P P H. 1945 The motion of the migrating cells in tissue cultures of lymph nodes. Anat. Rec 93 295–315.

Downey H. 1948 Cytology of rabbit thymus and regeneration of its thymocytes after irradiation; with some notes on the human thymus. Blood, 3 1315–1341
Gomori, G. 1952 Microscopic Histochemistry Univ Chicago Press, Chicago.
Grueneberg, H. 1943 The development of some external features in mouse embryos. J Hered., 34 89–92.
Hammar, J. A. 1936 Die normal-morphologische Thymusforschung. Barth, Leipzig.
Ito, T 1959 Über einschlusshaltige Zellen im Thymus des Goldhamsters. Z. Zellforsch., 49 739–747
Jacobson, W and M. Webb 1952 The two types of nucleoproteins during mitosis. Exptl. Cell Research, 3 163–183.
Kaplan, H. S. 1961 The role of cell differentiation as determinant of susceptibility to virus carcinogenesis. Cancer Research 21 981–983
Law L. W N Trainin, R. H. Levey and W F Barth 1964 Humoral thymic factor in mice: further evidence. Science, 143 1049–1051
Lillie, R. D 1948 Histopathologic Technic and Practical Histochemistry The Blakiston Co., Inc., New York.
McAlpine, R. J 1955 Alkaline glycerophosphatase in the developing thyroid parathyroid, and thymus of the albino rat. Am. J Anat., 96 191–227
McKay D. G., A. T Hertig, E. C. Adams and S. Danziger 1953 Histochemical observations on the germ cells of human embryos. Anat. Rec., 117 201 219
Marchesi, V T and J L. Gowans 1964 The migration of lymphocytes through the endothelium of venules in lymph nodes: an electron microscope study Proc. Roy Soc. series B 159 283–290.
Maximow A. 1909 Untersuchen über Blut und Bindegewebe II. Über die Histogenese der Thymus bei Säugertieren. Arch. für mikro. Anat. und Entwick., 74 525–621
Metcalf D 1956 The thymic origin of the plasma lymphocytosis stimulating factor Brit. J. Cancer, 10 442–457
Milaire, J 1959 Prédifférentiation cytochimique de diverses ébauches cephaliques chez l'Embryon de Souris. Arch. de Biol., 70 587–730.
Nachlas, M. M., D T Crawford and A. M Seligman 1957 The histochemical demonstration of leucine aminopeptidase. J Histochem. and Cytochem., 5 264–278
Ohno, S., and R. Kinosita 1956 On the nucleolus-associated chromatin. Exp Cell Research, 10 66–70.
Osoba, D., and J F A. P Miller 1963 Evidence for humoral thymus factor responsible for the maturation of immunological faculty Nature 199 653–654
Padykula, H. A. 1965 Personal communication.
Padykula, H A., and E. Herman 1955 Factors affecting the activity of adenosine triphosphatase and other phosphatases as measured by histochemical techniques. J Histochem. and Cytochem., 3: 161 169
Pearse, A. G. E. 1953 Histochemistry Little Brown and Co., Boston.
Rich, A. R., M. M. Wintrobe and M. R. Lewis 1939 The differentiation of myeloblasts from lymphoblasts by manner of locomotion. Johns H. Hos. Bul., 65 291–327
Smith, C., and F C. Thomas 1950 Studies on the thymus of the mammal. III. Glycogen in the cortical cells of the thymus. Anat. Rec., 106: 17–36
Smith, C and M. J Waldron 1950 Glycogen in the thymus of the fetal mouse. Anat. Rec., 108 113 (Abstract)
Smith, C., T J Wharton and A. M. Gerhardt 1958 Studies on the thymus of the mammal. XI. Histochemical studies of thymus, spleen and lymph node in normal and irradiated mice Anat. Rec., 131 369–384.
Smith, C. 1961 Studies on the thymus of the mammal. XII. Histochemistry of the thymuses of C57Bl/6 and AKR strain mice. J N t. Cancer Inst., 26 389–401.
——— 1964 Microscopic anatomy of the thymus. In: The Thymus in Immunobiology (R. A. Good and A. E. Gabrielsen, eds.) Chapt. 3, 71–84 Paul B. Hoeber Inc., New York.
Sundberg, R. D. 1960 Lymphocytes origin, structure and interrelationships. In: The Lymphocyte and Lymphocytic Tissue (J Rebuck, ed.) pp. 1 21. Paul B Hoeber Inc New York.
Trowell, O A. 1964 The Biology of Cells and Tissues in Culture Vol. 2, Chapt. 2. Academic Press, New York.

EXPLANATION OF FIGURES

1 *11 days AKR, May-Grunwald-Giemsa, 6 μ, longitudinal section.* The third and fourth pharyngeal pouches (3 4) are seen between the third and fourth aortic arches (3a, 4a). The third pouch is lined by smooth columnar epithelium. In the lumen of the fourth pouch, droplets of secretion are present. da, dorsal aorta; l, basophilic lymphoblasts in the mesenchyme. × 210.

2 *11 days, AKR, May-Grunwald-Giemsa, 6 μ.* A section of the third pharyngeal pouch shows lymphoblasts (le) with nuclei within the epithelium ( ) On the left, the lymphoblast (le) has a handmirror shape; its nucleus within the epithelium has the typical large, irregular nucleolus of a lymphoblast, and its basophilic tail is in the mesenchyme (see fig. 2a) Toward the right, two lymphoblasts, one (le) with the nucleus in the epithelium is joined to one in the mesenchyme (l) by a cytoplasmic bridge (b) The round nucleoli of the nuclei of the epithelial cells (e) are best seen in the upper border of the lumen. A clear-cut epithelio-mesenchymal line shows at the basal surface of the upper epithelial layer In the lower border there is a region (indicated by horizontal arrows) where the epithelial boundary is lost. The two labeled lymphoblasts (l) below the epithelium show radiating pseudopods indicative of the depolarized phase of movement. The smooth contour of the lining cells is evident. × 840.

2a This is the same section as figure 2. The lymphoblast at the left is shown at a higher magnification. The defect in the section makes it possible to see better the forward cytoplasmic cap. × 2,100.

3 *11 days AKR, May-Grunwald-Giemsa, 6 μ.* Two lymphoblasts (le) are seen with nuclei in the epithelium. These nuclei have nucleoli typical of lymphoblasts. The basophilic tails (arrows) extend into the mesenchyme. × 2,100.

4 *11 days, AKR, May-Grunwald-Giemsa, 6 μ.* The edge of the wall of the third pouch (3) possesses a lymphoblast (le) with the basophilic tail within the epithelium. The middle mesenchymal lymphoblast (l) has a strongly basophilic tail with a filamentous process and an anterior filmy cap which hardly shows in the photograph. × 2,100.

5 *10 days C57Bl/6 May-Grunwald-Giemsa, 6 μ.* A lymphoblast within the epithelium (le) is seen with a strongly basophilic tail extending from it parallel to the basal border of the epithelium (arrows). Many are found in this position. *At* this focus the irregularity of the nucleolus is not evident. At its right is another cell (nucleus indistinct) with a basophilic tail within the epithelium. × 2,100.

6 *12 days, C57Bl/6, May-Grunwald-Giemsa, 7 μ.* Another lymphoblast (le) can be seen with its nucleus within the epithelium and with its tail (arrows) parallel to the basal edge of the epithelium. Below it is another lymphblast with a narrow rim of basophilic cytoplasm. × 2,100.

7 *10 days C57Bl/6, May-Grunwald-Giemsa, 8 μ.* Lymphoblasts (le) have indented the basal layer of the epithelium of the third pouch, lifting up the epithelial cells (e). Typical epithelial nuclei (e) with spherical or oval nucleoli and little chromatic network are evident. Below are epithelial cells of the cervical vesicle separated in this section from the third pouch by a thin layer of mesenchyme. The irregular nucleolus and chromatic network of the nucleus of the lower lymphoblast contrast sharply with the structure of the epithelial nucleus. The nucleus × 2,100. of the upper lymphoblast is twisted and is cut in cross section at one end.

8 *11 days C57Bl/6, alkaline phosphatase activity azo dye method, 15 μ, longitudinal section.* This frozen section of the third pouch near the opening to the pharynx shows faintly reactive ductus pharyngobranchialis (dpb) continuous with the negative or slightly reactive pharyngeal epithelium (pe) The epithelium lining the lumen of the pouch is highly reactive. × 135.

9 *11 days C57Bl/6 esterase activity Pearse procedure 15 μ, longitudinal section.* This section is from the same embryo photographed for figure 8 but it is not adjacent to it. The slender lumen is bordered by highly reactive cells, most deeply colored in the wall toward the third aortic arch and at the base. × 135.

10 *11 days C57Bl/6, esterase activity Pearse procedure 15 μ, frontal section.* This is a frozen section of the third pouch toward the periphery. Most of the activity is localized in wing-shaped cells which border the lumen, particularly toward the upper or pharyngeal end. × 210.

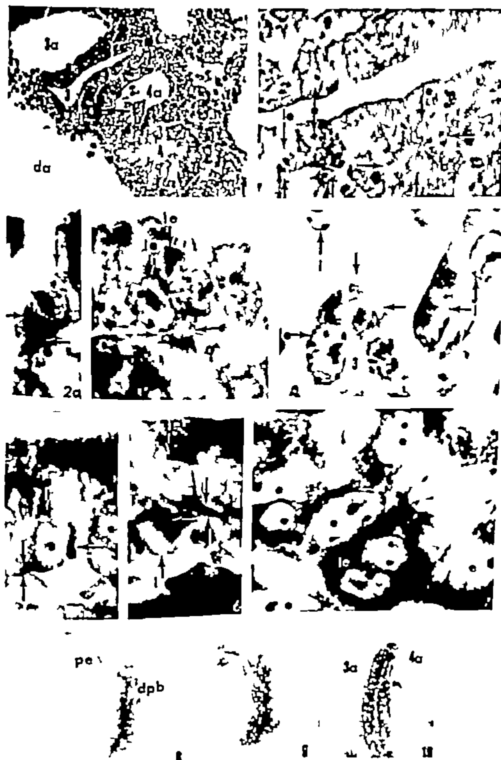

3a
4a
da
le
2a
le
pe
dpb
3a
4a
8
9
10

PLATE 2

EXPLANATION OF FIGURES

In plates 2, 3 and 4 alkaline phosphatase activity is shown by the azo dye method (except where noted) acid phosphatase by the metal-salt technique and nonspecific esterase by the Pearse procedure, in frozen sections cut in the cryostat.

11 *12 days C57Bl/6 May-Grunwald-Giemsa 7 μ longitudinal section.* The third pouch (3) open into the pharynx. The epithelium is basophilic toward the lumen and its surface is smooth. One mitosis (arrow) is t the junction of the epithelium and the mesenchyme. The fourth pouch (4) does not have deeply basophilic lining cells is paler than the third and possesses small, indistinct droplets of secretion. l, lymphocytes in the mesenchyme. × 210.

12 *12 days AKR, May-Grunwald-Giemsa 10 μ, frontal ection* This section of the thymus, parathyroid (Pt) and thyroid (T) glands has been chosen to show the greater width of the cellular capsule around the thymus. Single basophilic lymphoblasts and groups of them (arrows) can be seen within the thymus. Also, epithelial cells (er) are present with basophilic cytoplasm. These can be distinguished by their nuclei, t a higher magnification. × 210.

13 *12 days C57Bl/6 alkaline phosphatase activity 15 μ frontal section.* A har acteristic distribution of strongly reactiv cells can be seen in the lateral region of the body of the thymic rudiment and less reactive ones in the head (h) and inner part of the cervical duct (cd) The most reactive cells are stellate reticular cell with cytoplasmic processes. × 105.

14 *13 days C57Bl/6 alkaline phosphatase activity 10 μ longitudinal section* This section of an older thymic lobe hows ites of enzymatic activity in the body of the thymus, harply delimited from an unreactive anterior portion toward the pharynx (arrow) This section can be compared with figure 8. × 105

15 *13 days AKR, lkaline phosphatase activity 15 μ, frontal section.* The head (h) and the lateral extension of the thymic anlage is much more reactiv than the posterior part of the body × 105.

16 *13 days AKR esterase activity 15 μ, frontal section.* This section is adjacent t the one photographed in figure 15 The body of the anlage is more reactiv with this technique than with that for alkaline phosphatase activity Groups of highly reactive epithelial cells are indicated by arrows. The head (h) is much les reactive than the body × 105

17 *13 days AKR, esterase activity 10 μ, front l section* I thi section groups of strongly reactiv epithelial reticular cells are prominent in the medial region of the thymic lobe. Groups of cells and single cells (arrows) throughout the body of the lobe are more deeply colored than the m jority of cells. The upper portion of the thymic anlage, which still possesses lume is the less reactiv head Cells of the parathyroid gland (Pt) are also slightly reactiv × 210.

18 *13 days AKR, esterase activity 15 μ, f ontal section.* I this thymic lobe the more trongly reactive cells are in groups and indicate the position of the medulla Some single cells are more deeply stained than others (arrows) The rims of all other cells how some activity × 210.

19 *12 day AKR esterase activity 15 μ.* A strongly reactiv inclusion cell (ic) is shown with w ll defined nucleu and oval nucleolus rimmed with granules indicativ of its epithelial character The cytopla m is highly reactive and contains indistinct coarse granules or incl sions on one side of the nucleus These inclusions may possess reacti surfaces. The reactive cytoplasm of other epithelial cell (er) contains fine negativ granules and rrounds the nucleus This group of cells is at the posterior end of central longated cord similar to that seen in figure 17 840

20 *13 days AKR acid phosphatase activity 15 μ, frontal section.* The thymic anlage in hi strain is the most re ctive organ in it immediate region. 210


11
12
13
14
15
16
17
18
19
20
Pt
T
ek
cd
h
t
Lf

PLATE 3

EXPLANATION OF FIGURES

21 *14 days C57Bl/6 alkaline phosphatase activity 15 µ.* This section was chosen to show the peripherally arranged highly reactiv mesenchymal reticular cells surrounded by lymphocytes with scattered granules in the cytoplasm. The arrows are directed toward the nuclei of three reticular cells. × 840.

22 *14 days line 25 esterase activity 15 µ.* This section shows the contrast in group of cells between the strongly reactive inclusion cell (ic) in the center of the photograph and the other medullary epithelial cells (er) with fine unstained granules in a reactive ground substance. × 840.

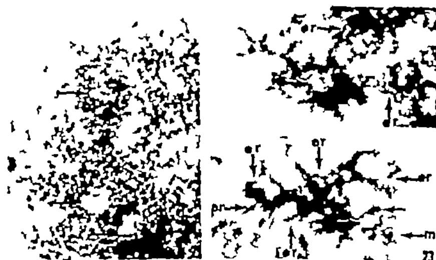
23 *14 days, line 25 esterase activity 15 µ.* This is an example of nest of epithelial reticular cells (er) in which the small, unstained granules can be seen within the blackened cytoplasm. Among the 15 cells of this group is less reactive macrophage (m) with inclusions (arrows) × 840.

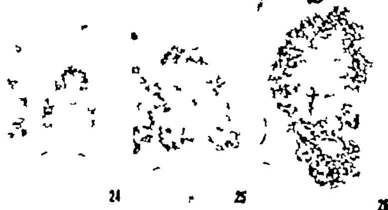
4 *15 days C57Bl/6 alkaline phosphatase activity 10 µ, frontal section.* This photograph and th ones following should be compared for differences in size and in sites of enzymatic activity in the thymuses of the two strains of mice A peripheral arrangement of blackened reticular cells and large lymphocytes is typical of the C57Bl/6 thymus in later embryonic lif in contrast to the generally unreactive lymphocytes in the rest of the thymus. Some cells of the medulla are slightly stained. × 42.

25 *15 days AKR, lkaline phosphatase activity 10 µ frontal section.* The generalized distribution of reactive cell is seen throughout the thymus with increased density in the lobulated outer zone. Almost all of the cells of the cortex are reactive but in the medulla, reactive reticular cells alone or these cells and surrounding lymphocytes are separated by areas of unreactive cells. × 42.

26 *16 days AKR, alkaline phosphatase activity glycerophosphate 15 µ, longitudinal section.* The greater activity of the cortex with its scattered reactiv reticular cells is in sharp contrast to the les reactive medulla. × 42.

27 *16 days, C57Bl/6 PAS frozen section, 10 µ.* A group of two epithelial reticular cells and a possible mesenchymal cell t the left in the medulla are stained with the periodic cid-Schiff technique for glycogen. Small, uncolored granules in the cytoplasm are outlined by glycogen. × 840.


er
er
er
er
er
pr
m
[er]
23


24
25
26

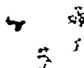

27

PLATE 4

EXPLANATION OF FIGURES

28 *17 days C57Bl/6 alkaline phosphatase activity 10 μ frontal section.* The C57Bl/6 thymus has increased greatly in volume (compare with fig. 24) but it is much smaller than that of the AKR strain, figure 29. The differences noted between the strains in the 15-day-old thymuses are even more evident. The pattern of activity in the outer zone of the cortex is influenced by the lobulation of the surface and by the presence of the radial cortical capillaries. The most deeply stained cells are mesenchymal reticular cells. The corticomedullary line is not evident. ma, medullary artery; c arterial capillary × 42.

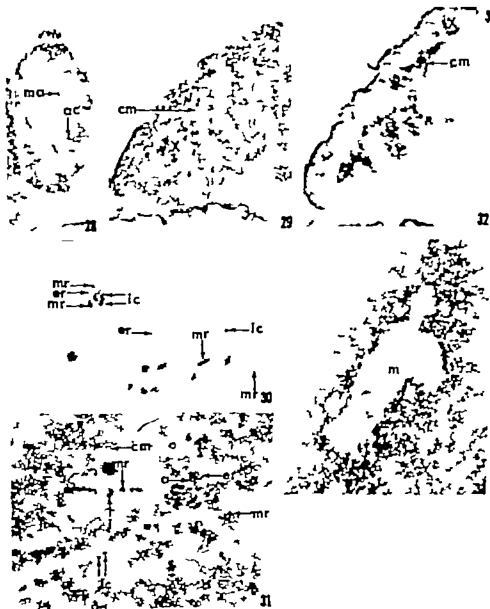
29 *17 days, AKR, alkalin phosphatase activity 10 μ, frontal section.* The great activity of both reticular cells and lymphocytes in the cortex and medulla is in triking contrast to the littl seen in the C57Bl/6 thymus, figure 28. The uneven appearance is due to the reacti clusters of mesenchymal cells and lymphocytes separated by less reactive or negative areas. cm, corticomedullary line; X, groups of reactive cells which include blackened inclusion cells and less reactive mes enchymal and epithelial cells. × 42.

30 *18 days C57Bl/6 alkaline phosphatase activity 10 μ, frontal section.* The post-natal characteristics of the C57Bl/6 thymu are now attained. These include slight activity beneath the capsule which later disappears, and the presence of unreactive lymphocytes. In the medulla are scattered nests of reactive inclusion cells, mesenchymal and epithelial reticular cells and an occasional cross section of a medullary artery N cortical medullary line is evident. er slightly reactive epithelial reticular cell mr more re ctive mesenchymal reticular cell; ic black ened inclusion cell. × 105

31 *18 days AKR lkaline phosphatase ctivity 10 μ, frontal section.* The uneven ppearance of the more reactive cortex and less reactive medulla of the AKR thymus is due t clusters of or single reacti reticular cells and large lympho-cytes separated by areas of reactive and sometimes unreacti smaller lymph-ocytes. Within the medulla are highly reactive inclusion cells (ic) less reacti mesenchymal reticular cells (mr) nd epithelial reticular cells (er) and sections f arteries (a) cm corticomedullary line; X; group of large lymphocytes and mesenchymal reticular cells. × 105.

32 *17 day AKR terase activity 10 μ, frontal section.* This section is from the same embryonic thymus as the one photographed in figure 29, but it is not adja-cent t it. It shows the characteristic distribution f nests of deeply stained in lusion and ep thelial reticular cells and single cells in the medulla and, as some-times occurs, at the corticomedullary line The medulla is typically more reactive than the cortex with this technique The neven appearance of the corte is due to scattered slightly reactive reticular cells. X, reactive cell in the region of branched blood essel. 42.

33 *19 days AKR acid phosphatase activity 10 μ, frontal section.* The postnatal pattern of th distribution of ell reactive with acid phosphatase technique in this train is distinctive The highly reactive cortex is sh rply defined from the almost unreactive medulla by an inner cortical zone crowded with reacti cells cortex m medulla × 105


ma
ac
cm
cm
mr
er
mr
lc
er
mr
lc
mr
cm
mr
er
mr
m
30
31

A Study of Salivary Glands of Rats Injected with Actinomycin D [1,2]

HEUN T JHEE, SEONG S. HAN AND JAMES K. AVERY

The University of Michigan School of Dentistry Ann Arbor Michigan and Y nsei University Medical School, Seoul, Korea

ABSTRACT   A study has been made of the salivary glands of the rat following an injection of sublethal dose of actinomycin D Body weights and weights of the parotid and submandibular glands showed significant decreases during the first 7 to 14 d ys. The loss in weight was the greatest in the parotid gland.

Histological and cytological observations indicated that the changes in secretory cells occurred in the following order: (1) beginning of nuclear pyknosis with rapid decrease in number and size of nuclei by 24 hours after the injection; (2) advanced stages of nuclear pyknosis with concomitant decrease in cytoplasmic basophilia and granules by day 3; (3) apparent vacuolization and rarification of cytoplasm by day 7; (4) beginning of nucleolar and nuclear recovery by day 10; and (5) complete cytoplasmic recovery by the end of experiment as evidenced by the return of basophilia and disappearance of vacuoles.

Paralleling the weight changes, cytological damages were greater in the parotid than in the submandibular acini. This was thought to be related to differences in nature of secretory products by the two organs. A decrease in number and pronounced irregularity in size of the granules in salivary ducts of the submandibular gland were observed but t a later time than the above mentioned changes in the acini. The significance of these changes has been discussed in light of the recently gained knowledge on the biosynthesis of nucleic acids and proteins as related to the chemical mechanism of actinomycin D in the inhibition of m-RNA synthesis.

Since the isolation of actinomycin D from *Streptomyces parvullus* (Manaker et al. '54) its potent cytostatic effects have been widely recognized and numer ous reports have already appeared describing the effects of it and related compounds on embryonic tissues (Tuchmann-Duplessis and Mercier Parot '58, '59 and '60 and Denis, '63) various tumors (Gregory et al. '56 Boric et al '57 and '58 Oota et al. '57 Plummer and Walker '58; and Awa, '61) and other normal tissues (Hack mann, '54 Friederici, '55 and Bierling '60) Meanwhile the chemical mechanisms of actinomycin in inducing cytostatic effects have been clarified to a large extent and experiments have proven that the drug can be used as an excellent analytic tool for studies of the biosynthesis of proteins especially of the role played by messenger RNA (m-RNA) in this process (Kirk, '60 Reich et al. '61 and '62 Goldberg and Rabinowitz, '62; Harbers and Mueller '62 Kahan et al., '63 Meritz, '63 Paul and Struthers '63 Perry '63 and Strachelin et al., '63) A survey of these articles and others illuminates the following (1) m-RNA as well as soluble and ribosomal RNA is produced in the nucleus; (2) m-RNA combines with the ribosomes which are held together in the form of polyribosomes; (3) compared to other types of RNA, the turnover of m-RNA is relatively fast and (4) the production of the m-RNA can be inhibited by actinomycin D which combines specifically with DNA resulting in the blockage of DNA-dependent RNA poly merase activity

With respect to the digestive glands synthesizing proteineous enzymes for secretion an insult imposed by the administration of actinomycin D would seriously affect the functioning of the gland which in turn would be reflected in its structure In a preliminary communication we have described the weight changes and cytology of rat parotid and submandibular glands following a single injection of a sublethal

---

[1] Based in part on thesis for the degree of the Doctor of Medical Sciences in Anatomy Yonsei University Seoul.

[2] Supported by grant from U S P H S (D-1620-3).

Present address Yonsei University Medical School, Seoul, Korea.

dose of actinomycin D (Jhee and Han '64). The present article represents the final report of the complete study.

MATERIALS AND METHODS

Experimental design. Twenty-eight adult male Sprague-Dawley rats were used. Of these 21 received an intraperitoneal injection of 75 μg actinomycin D dissolved in 0.5 ml of saline. In a previous dose-lethality study it was found that the dose used produced a pronounced effect on the body weight at the end of three weeks while maintaining over 85% survival in adult male Sprague-Dawley rats weighing about 350 gm. The remaining seven rats served as controls and were injected with the same volume of saline alone. Animals were fed *ad libitum* with regular laboratory rat chows. Following injection three of the experimental and one of the control rats were sacrificed on days 1, 3, 5, 7, 10, 14 and 21. Each rat was weighed at the beginning of the experiment and at the time of sacrifice and the average body weight of the experimental animals was subjected to statistical analysis.

Histological procedures. Upon sacrifice, the right parotid and submandibular gland were dissected out and weighed. Small pieces of the gland were fixed in Bouin's solution and in Zenker formol, double-embedded in parlodion-paraffin and sectioned at 6 μ.

All sections were routinely stained with hematoxylin and eosin. In addition the following staining procedures were employed for observing different aspects as indicated: Unna Pappenheim's methyl green-pyronin for changes in nucleic acid contents, PAS-azure II for RNA content and cytoplasmic granules, aldehyde fuchsin-Masson for the general appearance of the parotid gland, and mucicarmin-hematoxylin and PAS-alcian blue for cytology of the submandibular gland.

The nucleoli to nuclei ratio. In order to obtain a quantitative estimate of the nucleolar changes of the secretory cells the ratio of the number of nucleoli to that of nuclei was studied in the following manner. Methyl green-pyronin stained sections of the parotid gland from blocs fixed in Zenker formol were used. Under oil immersion nuclear counts were made in random areas. From each gland at least 1,500 or more nuclei of acinar cells were counted. Of these the number of nuclei which contained nucleoli was recorded separately. The nucleoli to nuclei ratio (No/N) was obtained as follows.

$$No/N = \frac{\text{No. of nuclei containing nucleoli}}{\text{Number of nuclei}} \times 100$$

RESULTS AND OBSERVATIONS

Weight changes

Body weights. Figure 1 records the changes in average body weight of rats receiving an intraperitoneal injection of 75 μg actinomycin D. A gradual and linear decrease was observed through the first two weeks followed by a partial recovery on day 21. The control rats kept growing at the rate indicated.

Glandular weights. The changes in weight of the right parotid and submandibular glands are shown in figure 2. Of the two glands the parotid suffered a greater and more rapid loss of weight. By 24 hours the average glandular weight was less than 60% of the control value. As was true with body weight the lowest point was obtained on day 14 when the glandular weight decreased to less than 50% of the control. Again, by the end of the experiment the weight showed a significant recovery. The high value obtained on day 7 is not consistent with changes in body and other organ weights.

As expected from the nature of secretory products the weight of the submandibular gland was less affected than that of the parotid. The decrease was more gradual and did not drop as much as the latter. The low point was observed on day 10 and a moderate recovery was seen by the second week.

Histological and cytological changes of the parotid

The first sign of degeneration was the appearance of focalized areas of nuclear pyknosis in the parenchyme. Such lesion was recognized as early as 24 hours after injection and became progressively larger through the first ten days (figs. 3 and 4). Despite the progressive damage some of the acini maintained a near normal appearance. A reversal of degenerative

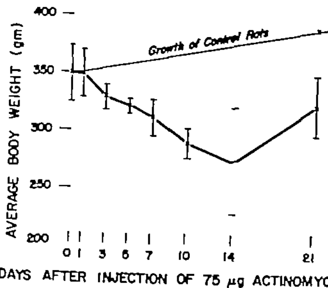


Fig. 1 The change in body weight of rats injected with actinomycin D as compared with the growth of control rats.

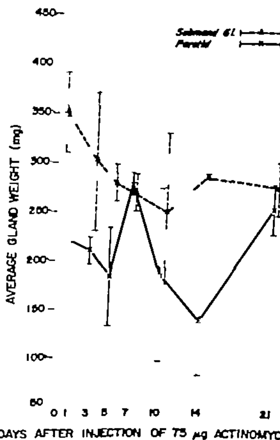


Fig. 2 The change in weight of right parotid and submandibular glands in rats injected with actinomycin D. Note the precipitous drop of the parotid weights, whereas the submandibular weights appear to parallel the changes of total body weights.

changes was noted by day 14 and, by the end of the third week, the gland recovered an essentially normal appearance (fig. 5).

Acinar cells. Secretory cells of the parotid acini became somewhat smaller compared to those of the control (figs. 6, 7 and 8). The selective pyknosis of nuclei of acinar cells was apparent 24 hours following the injection and became extensive by day 3 (figs. 7 and 11). The nucleus of such cells was smaller than control and had an irregular wrinkled outline. The nucleoplasm has lost the typical vesicularity and becomes increasingly condensed (figs. 11, 12 and 13). By day 7 the nucleus was so dense that only by means of differential staining could the presence or absence of the nucleoli be determined. Elsewhere the progressive rarification of the cytoplasm was notable in the affected cells (fig. 13). It seemed to result from a combination of the decrease in number of secretory granules and the gradual loss of cytoplasmic basophilia. On day 7 many cells were completely devoid of basal striations (figs. 12 and 13).

Within the rarified cytoplasm small vacuoles were present, which grew in number and size (figs. 8 and 12). They were most numerous on day 7 and were often located adjacent to the nucleus. Sometimes their increase in size appeared to be facilitated by the coalescence of smaller vacuoles (fig. 12). In some cells the entire cytoplasm was clear and what seemed to be cytoplasmic aggregates were scattered throughout the otherwise empty-looking cytoplasm (fig. 13). Nuclei in such cells were barely recognized as a large clump adhering to the basal plasma membrane.

On day 10 changes indicating the nuclear recovery were noted in many acinar cells. The contour of nuclei became rounded and the vesicular appearance returned. Nucleoli grew larger and more prominent. By day 14 nuclei in most acinar cells were indistinguishable from those of the control (figs. 6, 9, 10 and 14). A slight recovery of the basal basophilia of acinar cells was observed on day 14 and, by day 21, many acini presented a near-normal picture. The only difference between an acinus of a control rat and that of a 21-day animal of the experimental group was the relatively small number of secretory granules observed in the latter group (fig. 14).

The appearance of ducts. All ducts of the parotid were essentially not affected. Throughout the experiment cells of the intercalated, striated and excretory ducts appeared normal. However a difference was noted in the content of these ducts

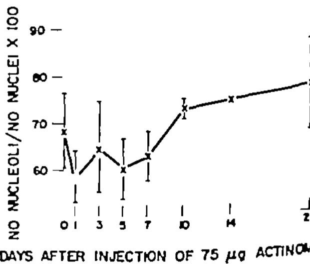


Fig. 18 The change in nucleocytoplasmic ratio of acinar cells of the parotid. A sharp drop on day 1 is followed by gradual recovery which preceded that of body and glandular weights.

during the early period. Twenty four hours after the injection large masses of stainable materials were present in all portions of the duct system (figs. 15 and 16) This could be stained with eosin after Zenker formol fixation as well as other cytoplasmic stains. The eosinophilic materials were cleared by day 3 (fig. 17) The cells of the interacinar connective tissue remained unaltered.

Changes in number of nucleoli. To ascertain the results of microscopic observation of nucleolar changes in quantitative terms, the nucleoli to nuclei ratio was studied in the manner previously described. This was considered important especially because of the fact that, during the early period of the experiment, there was a considerable variation in number of the affected cells from area to area of the same gland. Figure 18 summarizes the efforts of quantitation. Although the initial drop of the ratio during the first 24 hours was similar to weight changes of the gland, it remained basically unchanged during the first week and, by day 10 a significant increase was observed. Since the histological picture of acinar cells was progressively degenerating during this period and the glandular weight kept dropping, the early quantitative recovery of nucleoli, independent and ahead of other cytoplasmic changes, might be important. This is in agreement with the histological finding in which the nucleolar recovery was seen to proceed that of the nuclear structure and cytoplasmic basophilia.

Histological changes of the submandibular gland

Acinar cells The basic quality of alterations produced in the submandibular gland was similar to what was observed in the parotid The degree and extent of damage however was considerably less in comparison to those of the parotid. The nuclear pyknosis was moderate and the ergastoplasm appeared to persist, although a significant decrease was apparent (figs. 19 and 20) A fairly large number of vacuoles were evident by day 7 As was true in the case of the parotid, an early nuclear recovery was followed by the return of cytoplasmic normalcy namely the disappearance of vacuoles and a rise of basophilia.

As revealed by mucicarmin-hematoxylin staining the mucoprotein content in acinar cells was notably decreased during the initial phase and did not regain the staining intensity observable in control rats.

Ducts Of the extensive duct system only the granulated portion of the striated duct appeared affected. Compared to changes observed in acinar cells the effect was rather slow The ducts remained unchanged during the first 3 days when the cytoplasm was undergoing a rapid degeneration (fig 21) On day 5 a decrease in number of the granules was observed in some specimens and by day 7 depletion of the granules was evident in many cells (fig. 22) The granules that were still present assumed irregular size and distribution. The basal striation appeared somewhat less distinct than in the controls. Occasionally wrinkling of the nuclear membrane was observed in such cells.

DISCUSSION

Glandular weights. It is significant that an early precipitous drop in weight was observed only in the parotid gland, which produces a purely proteineous secretion. The average rate of turnover of m-RNA in parotid gland cells is not known. However the rapidity of its turnover has been shown by various experiments using actinomycin (Levinthal et al. '62 and Staehelin et al. '63) For instance 50 to 80% of the ribosome-associated m RNA breaks down within 4 to 8 hours after injection of actinomycin D which specifically inhibits the nucleus-dependent RNA polymerase activity Since it has been established that the polyribosomal activities are dependent on the continued availability of the nucleus-produced m-RNA (Nirenberg and Matthaei, '61; and Rich et al., '63) the early and specific reduction of parotid weights might be taken as indicative of the arrested synthesis of digestive enzymes by the gland due to blockade of m-RNA

The relatively slow drop in weight of the submandibular gland might be related to the nature of secretory products or the rate of enzyme synthesis by the gland.

It is known that, although the acinar cells of the submandibular gland have a distinctly different structure from that of the ordinary mucus-secreting cells the cells seem to secrete glycoproteins and acid mucopolysaccharides (Baker et al. '64) Thus the result of our weight studies supports the general contention that the elaboration of glycoproteins and acid mucopolysaccharides is less dependent upon m-RNA activities than protein biosynthesis

The cytology of parotid cells The sequence of cellular changes observed in this study appears to reflect faithfully the biochemical events occurring in the affected cell. Thus the early pyknosis of nuclei supports the concept that the cells indeed have suffered the initial insult to nuclei which would have stopped the production of m-RNA The latter in turn would have prevented the formation of new polyribosomes which at the light microscopic level, might be reflected as a decrease in basophilia as well as a secondary drop in number of secretory granules Both of these changes have followed the nuclear pyknosis.

The interesting and dramatic changes in nucleolar morphology following actinomycin D administration have been recently demonstrated by Schoefl ('64) in his electron microscopic studies of cultured kidney cells. Although whether or not the same sort of changes occurs in vivo in acinar cells of the parotid gland cannot be determined with the light microscope the rapid drop within 24 hours of the nucleoli to nuclei ratio along with histological observations might be taken as evidence for the specific effect of the drug on the nucleolar structure On the basis of quantitative data on the nucleolar behavior it could be said that the direct effect on the nucleoli is with the dose used an immediate one which lasts for the first seven days and that a full recovery is gained by the tenth day It is significant that the nucleolar regeneration was evident even before the first sign of cytoplasmic recovery could be recognized since such sequence of changes would suggest that cytoplasmic regeneration might indeed be dependent upon the nuclear recovery

Although the nature of vacuolization and rarification of the cytoplasm cannot be visualized with clarity in light microscope observations it has been pointed out that the ultrastructural sequence of cytoplasmic vacuolization may be similar in cells affected by different toxic agents (Lafontaine and Allard, '64) The ultrastructural aspects of the cytoplasmic vacuolization in glandular cells with impaired protein synthesis have been described by Herman and Fitzgerald, ('62) who in a study of degenerating pancreas after ethionine administration described the widening of endoplasmic reticulum and development of fine and coarse vacuoles containing granular disoriented membranes along with other changes such as decrease in ribosomes associated with the endoplasmic reticulum.

The accumulation of eosinophilic mass in the duct system during the initial phase of response might be related to the alteration of the flow rate of the nature of secretory products, or of the functioning of ducts themselves. No apparent changes were observed in the structure of duct cells although it might be possible that certain functional changes have been produced and have not been detected by the techniques employed here

The submandibular gland. As mentioned previously the nature of secretory products by the rat submandibular gland has been described as being composed of glycoproteins and acid mucopolysaccharides (Baker et al., '64) Baker et al. have also described that, after hypophysectomy a procedure known to affect many protein secretory cells, the effects on cells of the submandibular gland were similar to what was observed in the parotid, although the latter was affected to a greater extent. No demonstrable changes were observed in the sublingual a pure mucous gland. In our study also no basic qualitative differences between structural effects on acinar cells of the parotid and those of submandibular cells were found and, therefore reflects the involvement of both organs in protein synthesis. Thus the difference in severity of damage between the glands might be taken as an indication of the degree of their relative importance

Much discussion has been made on the nature and physiological significance of the granulated salivary ducts of the rodent submandibular gland (Junqueira et al., '49 Sreebny et al. '55 and '57 Baker '58 Raynaud, '60 and '64 Tamarin et al., '63 Baker et al. '64 Juiqueira, '64; Levi-Montelcini and Angeletti, '64 Screebny and Meyer '64 and Scott and Pease, '64) A review of these permits the following summary on the matter the granulated salivary duct might be producing a good portion of protease and a nerve growth factor there is a sexual dimorphism which is dependent upon male sex hormones the ultrastructure of the duct cells suggests that they are qualified for active fluid transport in large amount, as well as for the synthesis of proteins and experimental alterations of acinar structure such as produced by the use of isoproterenol, do not affect the duct cells, indicating the independence of the latter from acini. The slow effect of actinomycin D on the granulated segment of salivary ducts adds to the evidence that duct cells are different in their function from cells of the acinus. Only as the total glandular weight approached its bottom did the number of PAS positive granules show a measurable decrease As to the reason why the methyl green-pyronin staining brings out the PAS positive granules as well no explanation is sought at this time. It should be added, however that the staining was not abolished by prior application of ribonucleases which removed cytoplasmic basophilia.

LITERATURE CITED

Awa, A. 1961 Cytological effect of chemicals on tumors. XI. Effects of thio-TEPA and actinomycin-C. on normal and neoplastic cells in vitro Gann., 52: 49–55.

Baker B. L. 1958 Restoration of involuted zymogenic cells in hypophysectomized rats by replacement therapy Anat. Rec., 131 389-404

Baker B L., H. W Clapp Jr. and J A. Light 1964 Hormonal influences on the cytology and physiology of salivary glands. In: Salivary Glands and Their Secretions. International Series of Monographs on Oral Biology Ed. Sreebny and Meyer Pergamon Press, pp. 63–81

Bierling, R. 1960 The effect of actinomycine on human tissue in vitro. Zschr Krebsforsch., 63 519–522.

Boric, F S. Ivankovic and N Seemayer 1957 Effect of actinomycin C. on transplantable lymphosarcoma of mice. Zschr. Krebsforsch., 62: 239–241

Boric, F N Seemayer and S. Ivankovic 1957 Research on the effect of actinomycin C. on the Yoshida sarcoma of rats. Zschr. Krebsforsch., 62: 242–243.

Denis, H. 1963 Effects of actinomycin on neural differentiation of the ectoblast in the amphibian embryo. Exp. Cell Res 30 613-615.

Friederici, L. 1955 Studies on the effect of actinomycin C. (Sanamycin) on rabbit blood and hemopoietic organs and on bone marrow cultures. Zschr. Krebsforsch., 60 653–663.

Goldberg, I. H., and M. Rabinowitz 1962 Actinomycin D. inhibition of deoxyribonucleic acid dependent synthesis of ribonucleic acid. Science, 136 315–316.

Gregory F J L N Pugh, T Hata and R. Thielen 1956 The effect of actinomycin D on experimental ascitic tumors in the mouse. Cancer Res., 16 985–987

Hackmann, C. 1954 Studies of the effect of Sanamycin (actinomycin C.) on animal organs: Spleen, thymus, lymph nodes, adrenal glands and reproductive glands. Zschr Krebsforsch., 60: 250–268.

Habers, E., and W Mueller 1962 On the inhibition of RNA synthesis by actinomycin. Biochem. Biophys. Res. Commun., 7 107–110

Herman, L., and P J Fitzgerald 1962 The degenerative changes in pancreatic acinar cells caused by DL-ethionine. J Cell Biol., 12 277–296.

Jhee, H. T and S. S. Han 1964 Effects of actinomycin D on salivary glands of the rat. Life Sciences, in press.

Junqueira, L. C. U 1964 Studies on the physiology of rat and mouse submaxillary glands. III. On the function of the striated ducts of the mammalian salivary glands. In: Salivary Glands and Their Secretion, International Series of Monographs on Oral Biology Ed. Sreebny and Meyer Pergamon Press, pp. 123–128.

Junqueira, L. C. U A. F yer M. Rabinovitch and L. Frankenthal 1949 Biochemical and histochemical observations on the sexual dimorphism of mice submaxillary glands. J Cell. and Comp. Physiol., 34 129–158.

Kahan, E., F M. Kahan and J Hurwitz 1963 The role of deoxyribonucleic acid in ribonucleic acid synthesis. VI. Specificity of action of actinomycin D. J Biol. Chem., 238 2491 2497

Kirk, J M. 1960 The mode of action of actinomycin D. Biochem. Biophys. Acta, 42 167 169

Lafontaine, J C., and C. Allard 1964 A light and electron microscope study of the morphological changes induced in rat liver cells by the azo dye 2 ME-DAB. J Cell Biol., 22 143–172.

Levi-Montalcini, R., and P U Angeletti 1961 Hormonal control of the NGF content in the

submaxillary glands of mice. In Salivary Glands and Their Secretions, International Series of Monographs on Oral Biology Ed. Sreebny and Meyer Pergamon Press pp. 129–141

Levinthal, C., A. Keynan and A. Higa 1962 Messenger RNA turnover and protein synthesis in B subtilis inhibited by actinomycin D Proc. Nat. Acad. Sci. U S., 48 1631–1638.

Manaker R. A., F J Gregory L C. Vining and S. A. Waksman 1954–1955 Antibiotics Ann., 853–857

Merits, I. 1963 Actinomycin inhibition of RNA synthesis in rat liver Biochem. Biophys Res. Commun., 10 245–259

Nirenberg, M. W., and H. Matthaei 1961 The dependence of cell-free protein synthesis in E. Coli upon naturally occurring or synthetic polyribonucleotides. Proc. N t. Acad. Sci. U S 47 1588–1602.

Oota K., A. Nishibori and N Takahashi 1957 Experimental study on the oncostatic activity of actinomycin J I. Histological findings of therapeutic effects on Ehrlich mouse ascites carcinoma in the ddN strain mice. J Antibiotics, Ser. A. Tokyo, 10: 48–55.

P ul, J and M. G. Struthers 1963 Actinomycin D-resistant RNA synthesis in animal cells. Biochem. Biophys. Res. Commun., 11 135–139

Perry R. P 1963 Selective effects of actinomycin D on the intracellular distribution of RNA synthesis in tissue culture cells. Exp Cell Res., 29 400–406.

Plummer J and D G. Walker 1958 Effect of actinomycin D on tissue cultures of normal and neoplastic cells. J N t. Cancer Inst., 21 263–278.

Raynaud, J 1960 Control hormonal de la glande sous-maxillaire de la souris. Bull. Biol. de France et de Belgique, 94 400–523. Thèse.

Reich, E., R. M. Franklin, A. J Shatkin and E. L. Tatum 1961 Effect of actinomycin D on cellular nucleic acid synthesis and virus production. Science, 134 556–557

——— 1962 Action of actinomycin D on animal cells and viruses. Proc Nat. Acad. Sci. U S., 48 1238–1245.

Rich, A., and H. M. Goodman 1963 Mechanism of polyribosome action during protein synthesis. Nature (London) 199: 318–322.

Rich, A., and J R. Warner 1963 A multiple ribosomal structure in protein synthesis. Proc. N t. Acad. Sci. U.S.A., 49 122–129.

Schoefl, G. I. 1964 The effect of actinomycin D. on the fine structure of the nucleolus J Ultrastr Res., 10 224–243.

Scott, B L., and D. C. Pease 1964 Electron microscopy of induced changes in the salivary glands of the rat. In Salivary Glands and Their Secretions, International Series of Monographs on Oral Biology Ed. Sreebny and Meyer, Pergamon Press, pp. 13–44.

Sreebny L. M., and J Meyer 1964 Hormones, inanition and salivary glands. In Salivary Glands and Their Secretions, International Series of Monographs on Oral Biology Ed. Sreebny and Meyer Pergamon Press, pp 63–103.

Sreebny L. M., J Meyer E. Bachem and J P Weinmann 1955 Postnatal changes in proteolytic activity and in the morphology of the submaxillary gland in male and female albino rats. Growth, 19 57–74.

——— 1957 Restoration of enzymatic activity in the submaxillary gland of the hypophysectomized albino rat. Endocrinol., 60 200–204

Staehelin, T F O Wettstein and H. Noll 1963 Breakdown of rat-liver ergosomes in vivo after actinomycin inhibition of messenger RNA synthesis. Science, 140: 180–183.

Tamarin, A., B Wanamaker and L. M Sreebny 1963 The effect of inanition on the submandibular salivary glands and exocrine pancreas of the rat in mucous secretions Ann. N Y Acad. Sci 109 609–624.

Tuchman-Duplessis, H., and L. Mercier-Parot 1958 The teratogenic activity of actinomycin D in rats. C. R. Acad. Sci 247 2200–2202

——— 1959 Production of various malformations by administrations of actinomycin D to pregnant rats. C. R. Soc. Biol 153 338–339

——— 1960 Influence of actinomycin D on gestation and fetal development in the rabbit C. R. Soc. Biol., 154 914–916.

PLATE 1

EXPLANATION OF FIGURES

3 A survey micrograph of the right parotid gland from control rat. Cells of acini have large and round nuclei with prominent nucleoli. Approximately × 336. Fixed in Bouin fixative and stained with hematoxylin and eosin.

4 A survey micrograph of the right parotid gland from a rat sacrificed seven days after injection. An extensive nuclear pyknosis is observed. Approximately × 336. Fixed in Bouin fixative and stained with hematoxylin and eosin

5 A urvey micrograph of the right parotid gland from a rat sacrificed 21 days after injection Note the similarity in ppearance of acinar cells to those seen in figure 3. Approximately × 336. Fixed in Bouin fixative and stained with hematoxylin and eosin.

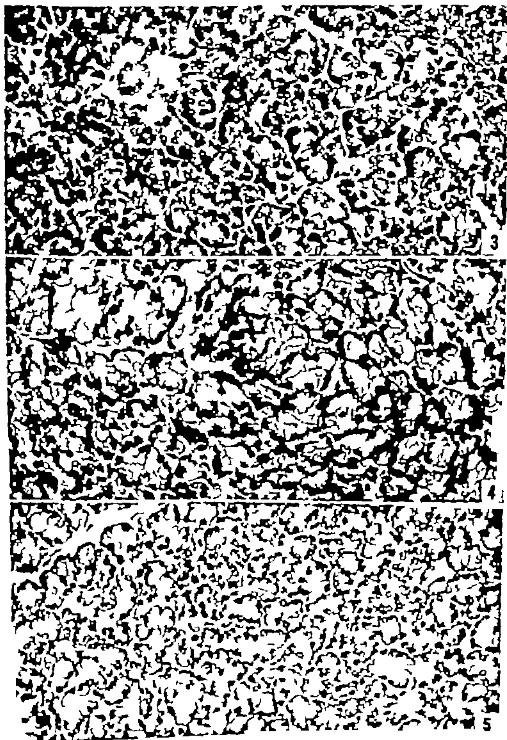

3
4
5

PLATE 2

EXPLANATION O FIGURES

6 A portion of the right parotid gland from a control rat. The acini are well-defined with cells showing a clear erg stoplasm and rounded nuclei. Approximately × 840 Fixed in Bouin s sol tion and stained with hematoxylin and eosin.

7 A portion f the right parotid gland from a rat sacrificed three days after injection. Note the selective wrinkling of nucleoplasm in acinar cells. Myoepithelial cells, and cells f the duct and interstitial connective tissue appear relatively unaffected. Approximately × 840. Fixed in Bouin solution and stained with hematoxylin and eosin.


6
7

PLATE 3

EXPLANATION OF FIGURES

8 A portion of the right parotid gland from an animal sacrificed seven days after the injection. Numerous cytoplasmic vacuoles of varying sizes are seen in many acinar cells. Approximately × 840. Fixed in Bouin fixative and stained with hematoxylin and eosin.

9 A portion of the right parotid gland from a rat sacrificed 21 days after the injection. The structure of acinar cells closely resembles that of the control (see fig. 6) Approximately × 840. Fixed in Bouin solution and stained with hematoxylin od eosin.


8
9

PLATE 4

EXPLANATION O FIGURES

10 A portion of the parotid acinus from a control rat. The nucleus of secretory cell is large and vesicular Prominent nucleoli are present. Approximately × 2,100. Fixed in Zenker-formol and stained with PAS-azure II.

11 A parotid acinus from a rat sacrificed three da) after the injection. The nuclear contour is irregular and the n cleoplasm hyperchromatic. Note the clumped appearance of basal basophilia and degranulation f the apical cytoplasm. Approximat ly × 2,100. Fixed in Zenker-formol nd stained with PAS-azure II.

12 An acinus of the parotid gland from rat sacrificed seven d ys fter the injection The nuclear pyknosis is further advanced. The cytopla m contains vacuoles f various sizes. Their appearance suggests that large acuole (V) might be formed by the coalescence of number of smaller ones. Approximately × 2,100. Fixed in Zenker formol nd stained with PAS-azure II.

13 A portion of the parotid acinus from rat sacrificed seven days after the injection. N granules are visible and the cytoplasm ppears to form filamentous aggregates creating clea regions in between the l mped masses. Appro imately × 2,100 Fixed in Zenker-formol nd stained with PAS-azure II.

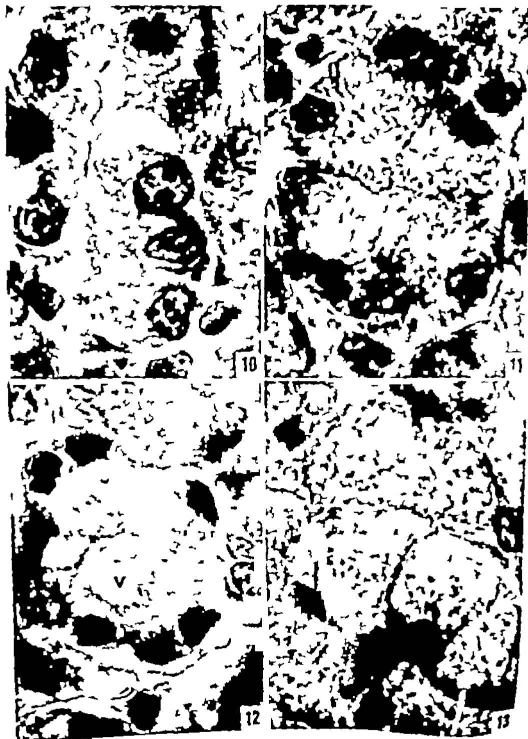

10
11
V
12
13

PLATE 8

EXPLANATION OF FIGURES

14 An acinus f the parotid gland from a rat sacrificed 21 days after the injection. The nucleus has become larg and round again and resumed its typical vesicularity The ergastoplasmic region is strongly basophilic. The only difference between cells of this group and those of the control is the degranul ted appearance of the apical cytoplasm. Approximately × 2,100. Fixed in Zenker formol and stained with PAS-azure II.

15 A salivary duct of the parotid gland from control rat. Approximately × 840 Fixed in Zenker-formol and stained with hematoxylin and eosin.

16 Salivary ducts f the parotid gland from a rat 24 hours after the injection. Note the presence of dense materials within the lumina. Approximately × 840 Fixed in Zenker-formol nd tained with hematoxylin and eosin.

17 Salivary ducts of the parotid gland from a rat three days fter the injection. The dense materials seen in figure 16 h ve disappeared and duct cells present an essentially normal ppearance Approximately × 840 Fixed in Zenker formol and stained with hematoxylin and eosin.

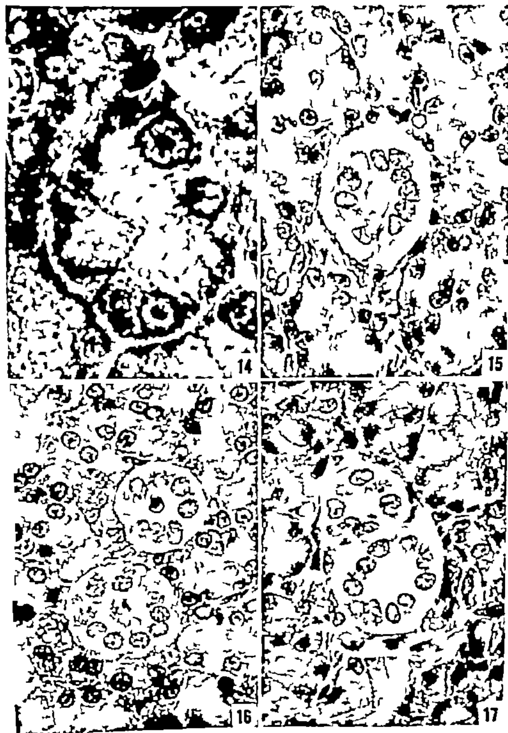

14
15
16
17

PLATE 6

EXPLANATION OF FIGURES

19 A portion of the subm ndibular gland from rat seven d ys after the injection. Despite the extensive acuolization of the cytoplasm the nuclear pyknosis is not as severe as in the comparable parotid section (fig. 8) Approximately $\times$ 840 Fixed in Zenker-formol and stained with PAS-azure II.

20 A portion of the submandibular gland from control rat. Approximately $\times$ 840. Fixed in Bouin fixative and stained with nuclear min-hem toxylin.


19
20
21

PLATE 7

EXPLANATION OF FIGURES

21 Granulated sali ary ducts of the submandibular gland from a rat three days after the injection. The PAS positive granules which are tained here with methyl green-pyronin are as n merous as in the control. Approximately × 840 Fixed in Zenker-formol and stained with methyl green and pyronin.

22 Granulated salivary duct of the submandibular gland from a rat seven days after the injection. The granules are reduced in number and irregular in size Approximately × 840. Fixed in Zenker-formol and tained with methyl green and pyronin.

21

22

O

P

R

S